Check for updates

TISSUE ENGINEERING: PART A
Volume 32, Numbers 23 and 24, 2026
Mary Ann Liebert, A Part of Sage
© The Author(s)
DOI: 10.1177/19373341261488537

2026 TERMIS-AM Conference
New Orleans, Louisiana
November 15-18, 2026



ABSTRACTS (BY NUMBER)

These are the abstracts as submitted through the website. Last minute changes, title and presenting changes are not always reflected in this file.

ORAL PRESENTATION ABSTRACTS

Session 1
3D Printing Advances in Musculoskeletal Tissue Engineering

11-15-2026 @1:00 PM - 2:30 PM

OP-002 - Human 3D Skeletal Muscle Platform for Evaluating Dexmedetomidine-Mediated Attenuation of Local Anesthetic-Induced Myotoxicity

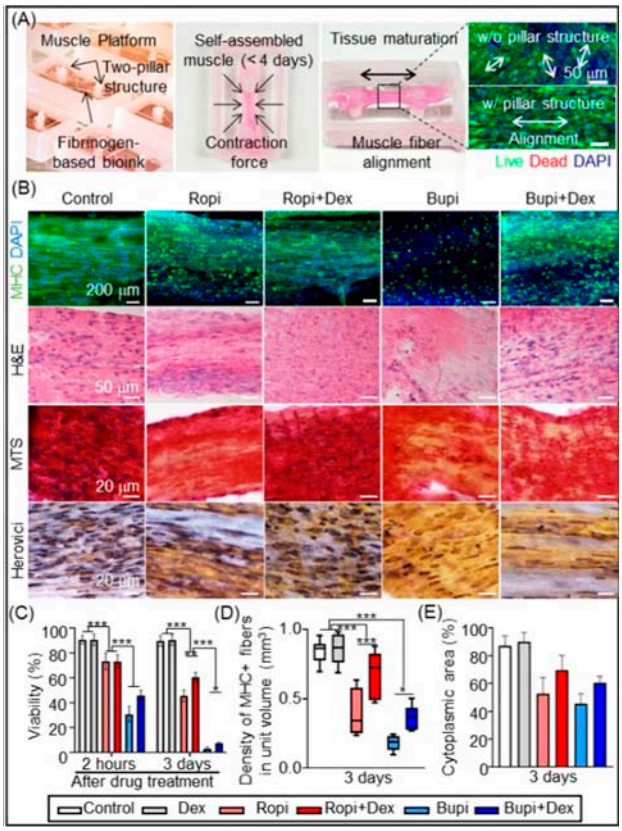
Wonwoo Jeong[1], Hoon Choi[2], Min Suk Chae[2], Hyung Mook Lee[3], Sang Jin Lee[1]

[1]*Wake Forest Institute for Regenerative Medicine, Winston-Salem, United States of America*
[2]*Seoul St. Mary's Hospital, Anesthesiology And Pain Medicine, Seoul, Korea, Republic of*
[3]*Seoul St. Mary's Hospital, Anesthesiology And Pain Medicine, Seoul, United States of America*

Purpose/Objectives: Long-acting local anesthetics (LAs) are widely used for peripheral nerve blocks and multimodal postoperative analgesia, often with adjuvants to prolong block duration and reduce opioid use. However, LA-induced myotoxicity has been reported after peripheral nerve catheters, femoral nerve blocks, and orbital blocks. These injuries involve muscle damages, but they remain clinically under-recognized as symptoms overlap with postoperative pain or weakness. Conventional two-dimensional assays cannot reproduce aligned muscle architecture or tissue-level damage. Therefore, New Approach Methodologies (NAMs) are needed to evaluate clinically used perioperative drug combinations using clinically-relevant readouts.

Methodology: We developed a human 3D skeletal muscle platform to test LA-induced injury and dexmedetomidine-mediated protection. Primary human skeletal muscle cells were encapsulated in fibrinogen-gelatin hydrogels within polycaprolactone two-pillar chambers. Pillar-guided compaction promoted uniaxial alignment during 7 days of differentiation. Fabrication parameters were optimized by varying cell density and fibrinogen concentration. Mature constructs were treated with 0.5% bupivacaine or 0.5% ropivacaine for 2 hours with or without dexmedetomidine. Medium was replaced to mimic clinical vascular washout. Myotoxicity was assessed using multifactorial readouts that captured cytocompatibility, myosin heavy chain (MHC)-positive fiber after tissue clearing, and histopathology.

Results: Engineered tissues self-assembled into aligned, multinucleated MHC-positive fibers **(Fig.A)**. LA treatment induced drug-specific myotoxicity, and bupivacaine caused greater injury than ropivacaine **(Fig.B)**. Dexmedetomidine attenuated acute and delayed injury, improving viability in bupivacaine-treated tissues by 1.48-fold at 2 hours and 2.62-fold by day 3 **(Fig.C)**. Structural imaging showed partial preservation of fiber alignment, fiber length, cytoplasmic integrity, and MHC-positive architecture **(Fig.D)**. Histology further resolved tissue-level injury. Hematoxylin and eosin staining showed nuclear loss and reduced eosinophilic cytoplasm, Masson's trichrome showed decreased actin-positive muscle fraction, and Herovici staining showed collagen depletion **(Fig.E)**. Dexmedetomidine preserved cytoplasmic area, actin-positive fiber area, and collagen retention.



Conclusion/Significance: This human 3D skeletal muscle NAM provides a standardized platform for evaluating clinically used LA-adjuvant strategies. By capturing drug-specific myotoxicity, delayed injury, and dexmedetomidine-mediated protection through tissue-level readouts, this model supports human-relevant musculoskeletal pharmacotoxicology before animal testing. Its modular pillar-guided design also provides a foundation for sensory neuron integration and electrical pulse stimulation to model neuromuscular signaling and activity-dependent recovery.

OP-003 - Investigation of effects of decellularized bone ECM content on 3D-printed scaffold properties and osteogenic potential

Vasiliki Kolliopoulos[1], Sadhana Chari[1], Ana Letca[2], Priya Kumar[1], Ellena Jeon[1], Zina Helal[1], Marissa Perez[1], Udayabhanu Jammalamadaka[1], Antonios Mikos[1]

[1]*Rice University, Bioengineering, Houston, United States of America*
[2]*Rice University, Biosciences, Houston, United States of America*

Purpose/Objectives: Tissue-derived decellularized extracellular matrix (dECM) biomaterials have emerged as an exciting platform for the development of tissue-mimicking materials, as they retain key biomolecular constituents of the tissue. This inherent complexity of the materials' composition and structure can be harnessed to design and fabricate clinically relevant biomaterials. Demineralized

bone matrix (DBM) is a clinically used dECM and has shown great promise in inducing osteogenesis and bone formation. However, DBM is achieved through harsh acid exposure that dissolves the mineral phase, lysing cells and removing cellular debris, which concurrently has detrimental effects on other biomolecules. Furthermore, DBM can lead to tissue collapse in large defects due to its rapid degradation rate and lack of a mineral phase. There is a critical need to develop a dECM material that maintains native biological signals.

Methodology: We have developed a first-of-its-kind bone decellularization protocol that results in a significant reduction in DNA content while maintaining minerals, collagens, and glycosaminoglycans. We fabricated colloidal composite 3D-printable inks using dECM and gelatin nanoparticles (GNPs) at different GNP:bdECM ratios (67:33 and 50:50) based on previously established procedures. We have thoroughly characterized the composition of each material, including total collagen, sulfated glycosaminoglycan, and mineral content. We conducted swelling and degradation studies of the scaffold groups in PBS and in PBS with collagenase to simulate physiological conditions and investigate the effect of composition on scaffold stability and evaluated osteogenic potential of mesenchymal stem cells over 21 days of culture.

Results: The developed decellularization protocol resulted in the maintenance of collagens and GAGs while also maintaining ~50% of the native mineral. bdECM scaffolds demonstrated dose-dependent effects as a function of bdECM content in swelling, degradation, and mineralization. Higher bdECM content resulted in decreases swelling and increase degradation rates, while lower bdECM content resulted in greater cell proliferation and significantly greater mineral formation compared to an unseeded control.

Conclusion/Significance: This work directly addressed challenges in the field with printing high dECM content materials by resulting in printable inks with upwards of 40 wt/v%. Furthermore, these data provide new insights into the effect of ECM constituents on osteogenesis and a new bone-mimicking biomaterial platform with translatable potential.

Session 2
Emerging Bioengineering and GENE-BASED Strategies for Wound Healing and Tissue Regeneration

11-15-2026 @ 1:00 PM - 2:30 PM

OP-005 - Fabrication of a CRISPR–Cas9/HIF-1α-Deliverable Tissue-Engineered Vascular Graft and Mechanistic Study of Vascular Regeneration

Yuan Chi[1,2], Jinfei Hou[2], Qingfang Zhao[2]

[1]*Zhejiang University, Hangzhou, China*
[2]*the First Affiliated Hospital, Zhejiang University School of Medicine, Hangzhou, Hangzhou, China*

Purpose/Objectives: Small-diameter vascular grafts remain in persistent clinical demand, however, current small-diameter vascular tissue engineering is limited by two major barriers: insufficient post-implant endothelialization and restricted in situ functionalization strategies. We aimed to construct an organic hydrogel-based small-diameter tissue-engineered vascular graft (TEVG) with robust anti-fatigue mechanical performance and to functionalize it through nanoparticle-enabled delivery of a CRISPR–Cas9/HIF-1α module for sustained local bioactivity after implantation.ar remodeling.

Methodology: Candidate sgRNAs against upstream regulators of HIF-1α stability were rationally designed, screened, and subsequently complexed with Cas9 to generate functional ribonucleoprotein (RNP) complexes.RNPs were loaded into nanoparticles and integrated into a photocrosslinkable hydrogel TEVG to enable site-confined sustained release. Material characterization included gelation behavior, rheological properties, swelling performance, release kinetics, and compliance-related mechanical testing under cyclic loading. In vitro assays evaluated endothelial cell viability, migration, tube formation, intracellular ROS, and polarization-related responses. In vivo efficacy was assessed in a New Zealand White rabbit carotid interposition model, with predefined endpoints including patency, Doppler flow, luminal endothelial coverage, neotissue organization, and inflammatory remodeling. Perigraft tissues were further analyzed by RT–qPCR, immunoblotting, and pathway-level transcriptomics.

Results: Nanoparticle integration did not compromise TEVG structural integrity or cyclic anti-fatigue performance, and compliance-related mechanics remained stable compared with unloaded grafts. In vitro, the CRISPR-loaded TEVG enhanced endothelial migration and angiogenic behavior. In the rabbit carotid model, treated grafts exhibited higher patency and more stable Doppler flow, together with more continuous luminal endothelialization, improved neotissue organization, and attenuated inflammatory remodeling. Molecular profiling supported activation of HIF-1α-associated pro-angiogenic and redox-adaptive programs in peri-graft tissues.

Conclusion/Significance: A nanoparticle-enabled CRISPR–Cas9/HIF-1α hydrogel TEVG can preserve implant-relevant mechanical reliability while improving endothelialization quality and early in vivo remodeling. This platform provides a mechanistically defined and translationally relevant strategy for next-generation small-diameter vascular grafts.

OP-006 - Precision EV Engineering: CRISPR-Interference Tailoring of iPSC-Derived Extracellular Vesicles Toward Antifibrotic Cardiac Repair

Yiran Li[1], Kaiyue Zhang[1], Yiping Wu[1], Joseph Sun[1], Nicole Rosas[1], Lamia Chowdhury[2], Yilan Hu[1], Sharon Fleischer[1], Bohao Liu[1], Roberta Lock[1], Ke Cheng[1], Gordana Vunjak-Novakovic[1]

[1]*Columbia University, Biomedical Engineering, New York, United States of America*
[2]*Barnard College, Biology, New York, United States of America*

Purpose/Objectives: Induced pluripotent stem cell-derived extracellular vesicles (iPSC-EVs) have emerged as promising cell-free therapeutics for regenerative medicine, yet their pleiotropic and context-dependent miRNA cargo can produce divergent biological effects across tissues and cell populations, limiting their utility as precision therapeutics. Current EV engineering strategies primarily rely on exogenous cargo loading or transient pathway modulation and lack programmable control over endogenous EV regulatory composition. Here, we demonstrate that CRISPR interference (CRISPRi) enables tunable reprogramming of iPSC-EV miRNA cargo at the producer-cell level, establishing a modular framework for precision EV engineering.

Methodology: Using miRTalk, a computational framework for predicting functional EV miRNA–target interactions, we identified the miR-302/367 cluster as a candidate regulator of fibrosis-associated signaling following myocardial infarction. To suppress miR-302/367 expression, we generated sg-302 iPSCs expressing a doxycycline-inducible dCas9-KRAB CRISPRi construct targeting the miR-302/367 locus and isolated EVs using tangential flow filtration and ultracentrifugation. Functional validation was performed in TGF-β-stimulated primary cardiac fibroblasts and a murine left anterior descending ligation model with intramyocardial EV delivery and serial echocardiographic assessment.

Results: CRISPRi-mediated repression of miR-302 enabled stable reprogramming of iPSC-EV cargo composition (a). Small RNA sequencing confirmed >85% depletion of miR-302 family members and coordinated remodeling of the EV miRNA landscape toward an antifibrotic state, including enrichment of let-7g-5p and miR-145-5p (b). Engineered EVs significantly reduced fibroblast activation, collagen deposition, and profibrotic gene expression *in vitro*, including α-SMA (0.61-fold) and COL1A1 (0.80-fold), while decreasing soluble collagen secretion by 71.2% (c–e). *In vivo*, sg-302 EVs reduced post-infarction scar area from 40.31% to 18.52%, suppressed myofibroblast infiltration, and preserved cardiac function following myocardial infarction (f,g).

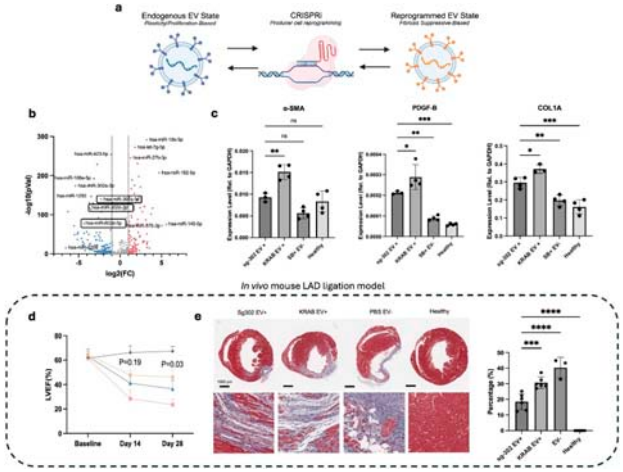


Figure 1: (a) CRISPRi-mediated engineering of miR-302-targeted iPSC-EVs. (b) Small RNA sequencing demonstrating EV cargo reprogramming toward an antifibrotic regulatory state. (c) Engineered EVs suppress fibroblast activation and collagen deposition in vitro. Intramyocardial delivery of sg-302 EVs (d) preserves cardiac function *in vivo* and (e) attenuates post-infarction fibrosis.

Conclusion/Significance: These findings establish CRISPRi as a programmable strategy for tailoring EV therapeutics without exogenous cargo loading. By enabling stable and systems-level reprogramming of endogenous EV cargo, this platform provides a generalizable framework for designing context-specific EV therapeutics tailored to distinct pathological and regenerative microenvironments.

Session 3
Harnessing the Power of Microgravity to Accelerate Breakthroughs in Regenerative Medicine

11-15-2026 @ 1:00 PM - 2:30 PM

OP-010 - Passive Multi-Organ-on-a-Chip Biotwins to Enable Digital Twins for Spaceflight and Earth

Sylvain Costes[1], Sara Rothrock[2]

[1]*University of Pittsburgh, School Of Medicine, Trivedi Institute For Space And Global Biomedicine, Pittsburgh, United States of America*
[2]*Department of Bioengineering, Swanson School of Engineering, University of Pittsburgh, Pittsburgh, United States of America*

Purpose/Objectives: Understanding human physiological responses to complex environmental stressors, such as microgravity, radiation, high CO2 levels, remains a major challenge for spaceflight and translational medicine. Traditional animal models and single-organ in-vitro systems are poorly suited to capture integrated human responses or operate under spaceflight constraints. The objective of this work is to introduce a triplet framework linking human data, passive multi-organ-on-a-chip (OoC) biotwins, and knowledge-graph–driven digital twins to enable scalable, mechanistic, and non-animal experimentation applicable to both space and Earth-based medicine.

Methodology: We are developing a passive multi-organ-on-a-chip platform composed of interconnected human organoids representing key physiological systems. Unlike conventional OoC systems relying on pumps and electronics, this design uses organoid-intrinsic forces, such as contractility and engineered geometry, to enable directional flow, nutrient exchange, and mechanical coupling. This simplicity allows long-duration operation and compatibility with spaceflight. Biological outputs from the biotwin, including multi-omics profiles, imaging, and functional readouts, are integrated with human cohort data (e.g., biospecimens, clinical and wearable data) into a knowledge graph (KG). The KG formalizes relationships across in-vivo and in-vitro data streams and serves as the computational backbone for constructing and iteratively refining digital twins.

Results: To this day, the Trivedi Institute for Space and Global Biomedicine is in its first year and as such, most of this work will remain at the conceptual level by the time this conference will take place. However, we anticipate showing how this framework will define how passive OoC biotwins can function as experimentally accessible intermediaries between human physiology and digital twin models. The approach explicitly supports New Approach Methodologies (NAMs) by reducing reliance on animal testing while enabling integrated, multi-organ assessment. The passive design removes major barriers to space deployment and facilitates standardized data generation across gravity environments for computational modeling.

Conclusion/Significance: By unifying passive multi-organ-on-a-chip systems with knowledge-graph-based digital twins, this triplet framework offers a scalable strategy for predictive modeling, biomedical risk assessment, and translational discovery. The approach is broadly relevant to tissue engineering, organs-on-chips, AI-enabled modeling, and precision medicine, with applications spanning spaceflight, regenerative medicine, and remote healthcare.

OP-011 - System for Testing Impact of Both Simulated Microgravity and Perfusion on Endothelial Cells

Abby Houghton[1], Emma Angelo[1], Samantha Shortal[1], Danny Carlos[2], Jeffrey Richards[3], Ye Zhang[4], Chris Bashur[5]

[1]*Florida Institute of Technology, Biomedical Engineering, Melbourne, United States of America*
[2]*Bennett Aerospace, Lasso Ii, Kennedy Space Center, United States of America*
[3]*Aetos Systems, Inc., Lasso Ii, Kennedy Space Center, United States of America*
[4]*NASA, Utilization And Life Sciences Office, Kennedy Space Center, United States of America*
[5]*Florida Tech, Chemistry And Chemical Engineering, Melbourne, United States of America*

Purpose/Objectives: It is known that microgravity can lead to endothelial cell (EC) dysfunction and that EC function depends on blood flow-applied shear stress. However, new systems need to be developed to enable investigation of the relative importance of each stimulus. Thus, we developed and validated a system to simultaneously study the impact of simulated microgravity and perfusion on ECs within hydrogel channels. This system is being used to determine EC growth and phenotype when microgravity is simulated.

Methodology: Custom flow chambers and reservoirs were developed (OnShape®) and 3-D printed. Channels mimicking blood vessels were prepared within 1-ethyl-3-(3-dimethylanimopropyl)carbodiimide (EDC) crosslinked gelatin hydrogels. A leakproof perfusion system was assembled by combining with micro-peristaltic pumps and tubing. This system was contained within a custom 3-D printed box that mounts on a random positioning machine (RPM). The system was validated, including testing with GFP^+ human umbilical vein ECs (HUVECs) seeded within the channel at 3 million cells/mL. Simulated microgravity was performed for 72h prior to imaging (stereoscope, confocal) and RT-PCR.

Results: The channels diameters decreased after processing to 1.04±0.12µm. Pumps were calibrated at 2.6mL/min, but this rate increased with voltage adjustments. For the average channel diameter, the calculated wall shear stress (3.9dynes/cm^2) was within the range for capillaries. Adjusting channel diameter and/or flow rate can provide the 10dynes/cm^2 in small arteries. Finite element simulations (Comsol®) demonstrated that local changes (e.g., partial channel collapse) can greatly impact shear stress and pressure. For cell studies, the RPM achieved g levels <0.025 within 1h. Confluent EC coverage inside most channels was observed initially and after 3 days of microgravity. The cells were not highly spread, but channel perfusion is expected to improve spreading. We are currently testing VE-cadherin expression and other EC responses to microgravity vs. no microgravity.

Conclusion/Significance: The system was developed and validated under simulated microgravity and shear stress conditions found in astronauts. The results also show promise since the ECs remained viable over 3 days and presented a cobblestone-like

morphology. We are in currently systematically testing the impact of microgravity on ECs with this system. Overall, this study will aid in understanding how microgravity influences astronauts' vascular health.

OP-012 - Engineered Skeletal Muscle Tissues Under Real and Simulated Microgravity Reveal Multi-Scale Dysfunction and Therapeutic Rescue

Beu Oropeza, Jaesang Kim, Ngan Huang

Stanford University, Palo Alto, United States of America

Purpose/Objectives: Skeletal muscle atrophy induced by microgravity remains a major challenge for long-duration spaceflight and represents a clinically relevant model of muscle degeneration. Although current countermeasures provide only partial protection, there remains a need for physiologically relevant in vitro systems capable of mechanistic investigation and therapeutic screening under altered mechanical loading conditions.

Methodology: Engineered skeletal muscle tissues were generated using aligned collagen-based scaffolds designed to mimic native muscle architecture and promote myotube organization. Myogenic cells cultured on these constructs were exposed to simulated microgravity and compared to 1G controls. Morphological and functional analyses were performed to assess myogenesis, tissue alignment, and contractile capacity. A targeted pharmacologic screening approach was implemented to evaluate candidate therapeutic interventions. RNA sequencing was subsequently performed across experimental groups to characterize transcriptomic responses associated with simulated microgravity and therapeutic rescue. A smaller scale version of these experiments was done on the International Space Station, to determine the effects seen under real microgravity strain. Fluorescent imaging and RNA sequencing analysis was performed on the tissues upon their return.

Results: Both the simulated microgravity and real microgravity significantly impaired skeletal muscle tissue formation, resulting in reduced myotube formation, decreased cellular alignment, and altered fiber morphology relative to 1G controls. These structural abnormalities were accompanied by diminished functional performance of engineered tissues. Pharmacologic intervention partially restored myotube formation and improved tissue organization under simulated microgravity conditions. Transcriptomic analyses revealed broad dysregulation of pathways associated with myogenesis, extracellular matrix remodeling, mechanotransduction, and catabolic signaling. Drug-treated groups demonstrated partial normalization of these molecular signatures, correlating with phenotypic recovery observed at the tissue level.

Conclusion/Significance: This study demonstrates the utility of biofabricated skeletal muscle tissues as a translational platform for modeling microgravity-induced degeneration and evaluating therapeutic countermeasures. Integration of structural, functional, and transcriptomic analyses enables multi-scale interrogation of muscle biology in altered mechanical environments. Beyond spaceflight applications, this engineered platform may serve as a scalable model for investigating muscle-wasting diseases on Earth and advancing regenerative medicine strategies.

Session 4
Quantitative Non-Invasive Imaging for Regulatory-Ready Engineered Tissues and human-Relevant Models

11-15-2026 @ 1:00 PM - 2:30 PM

OP-013 - Ex Vivo Liver Oxygen Imaging for Optimization of Preservation Window

Irene Canavesi[1], Casie Pandexter[2], Boris Epel[1], Basak Uygun[2], Mrignayani Kotecha[1]

[1]*O2M Technologies, Chicago, United States of America*
[2]*Massachusetts General Hospital, Harvard Medical School, Center For Engineering In Medicine And Surgery, Boston, United States of America*

Purpose/Objectives: Orthotopic organ transplantation remains the only viable method for treating end-stage organ diseases. Current preservation times for whole organs are limited to only a few hours of storage, resulting in inefficient use of available critical organs. To address these limitations, advanced preservation strategies, such as ex vivo machine perfusion with oxygenated media show promise in extending preservation times. However, progress in preservation technologies will be meaningful only if accompanied by equally robust, reliable, and non-invasive approaches for assessing organ viability and function. Trityl-OXO71-based electron paramagnetic resonance oxygen imaging (EPROI) is the only method that provides non-invasive three-dimensional (3D) partial oxygen pressure (pO_2) maps, to assess cells, tissue, and organ viability.

Methodology: The goal of this study was to investigate how whole-organ pO_2 imaging can assist to organ preservation technologies. We performed ex vivo mouse liver pO_2 imaging for three groups of livers (n = 4): fresh, 48-hours-post-static-cold-storage (48h-SCS), and 72 hours-post-SCS (72h-SCS). The pO_2 measurements were performed with JIVA-25® (O2M Technologies). The experiment included 90 minutes of pO_2 imaging while perfusing the livers with 100% oxygenated media, 1 hour of warm ischemia (WI), then another 90 minutes of pO_2 imaging again with 100% oxygenated perfusion media.

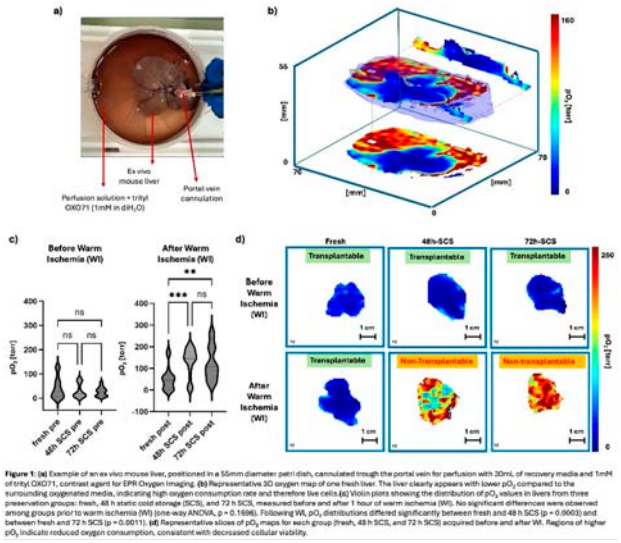


Figure 1: (a) Example of an ex vivo mouse liver, positioned in a 55mm diameter petri dish, cannulated trough the portal vein for perfusion with 30mL of recovery media and 1mM of trityl OX071, contrast agent for EPR Oxygen imaging. (b) Representative 3D oxygen map of one fresh liver. The liver clearly appears with lower pO_2 compared to the surrounding oxygenated media, indicating high oxygen consumption rate and therefore live cells.(c) Violin plots showing the distribution of pO_2 values in livers from three preservation groups: fresh, 48 h static cold storage (SCS), and 72 h SCS, measured before and after 1 hour of warm ischemia (WI). No significant differences were observed among groups prior to warm ischemia (WI) (one-way ANOVA, $p = 0.1696$). Following WI, pO_2 distributions differed significantly between fresh and 48 h SCS ($p = 0.0003$) and between fresh and 72 h SCS ($p = 0.0011$). (d) Representative slices of pO_2 maps for each group (fresh, 48 h SCS, and 72 h SCS) acquired before and after WI. Regions of higher pO_2 indicate reduced oxygen consumption, consistent with decreased cellular viability.

Results: A statistical difference between pre- and post-WI pO_2 was found for 48h-SCS and 72h-SCS groups (p-value < 0.0001), but not for fresh livers. A statistical difference after WI between fresh-48h-SCS and fresh-72h-SCS, suggests that the 48h-SCS and 72h-SCS groups did not survive the WI time. The voxel-wise analysis demonstrated that more than 30% of voxels in the livers were hypoxic (pO_2 < 10 torr) during pre-WI time for the three groups indicating an exposure to hypoxic stress before transplantation. The oxygen consumption rate for 48 h-SCS and 72 h-SCS groups decreased as these livers became non-viable.

Conclusion/Significance: This is the first study, to the best of our knowledge, where whole ex-vivo organ oxygen imaging is utilized to assess organ viability for transplantation. The real-time oxygen consumption rate assessment of whole organ is a novel aspect of EPROI, not available through any other method. The success of organ preservation technologies will save countless lives via successful transplantation.

OP-014 - AI-Based Segmentation in Organoid Culture Plates Enables Robust High-Throughput Screening With Reduced Experimental Variability

Douglas Kondro[1], Santiago Campuzano[1], Selena Cen[1], Aaron Ang[1], Michael Hiatt[1], Allen Eaves[1,2], Sharon Louis[1], Ryan Conder[1]

[1]*STEMCELL Technologies Inc., Vancouver, Canada*
[2]*Terry Fox Laboratory, Bc Cancer, Vancouver, Canada*

Purpose/Objectives: Organoids offer a complex in vitro physiologically-relevant disease model that when scaled could be

used for drug screening and diagnostic applications. However, high-throughput adoption is hindered by high levels of culture variability in combination with the lack of generic image analysis tools, capable of addressing the nuances of culture complexity and suboptimal image quality. To address these limitations, we developed an automatable workflow to generate high-quality intestinal and hepatic organoid cultures and images for consistent downstream analysis.

Methodology: Intestinal and hepatic cells derived organoids were cultured separately in 10 µL Matrigel® domes using manual or automated (Hamilton STARlet) workflows in standard 96-well plates or in 96-well Organoid Culture Plates (OC Plates; STEMCELL Technologies). Brightfield whole-well images were analyzed using a cloud-based AI segmentation tool. Drug response was tested using forskolin-induced swelling (FIS) assays and EGFR inhibitor gefitinib titrations (0.001 - 10 µM). Drug effects were assessed by measuring total culture area and CellTiter-Glo® 3D viability assays.

Results: OC Plates reduced the occurrence of culture failures by 10 – 20% and improved the overall image quality (n = 128), which eliminated the need to exclude edge wells or failed wells. In manually seeded cultures, OC Plates reduced the coefficient of variation (CV) by 51% in intestinal and 58% in hepatic cultures over five passages (n = 10). Automation further reduced variability as automatically maintained cultures in OC Plates had a 59% lower CV than those in standard plates (8.75% vs. 23.02%, respectively). In FIS assays, organoids cultured in OC Plates exhibited a more robust response to forskolin, with a 16% greater increase in size (137 ± 8.5%) compared to traditional 96-well domes (118 ± 8.8%). In gefitinib-based drug screening assays, OC Plates produced an IC_{50} of 0.46 ± 0.08 µM, comparable to 0.39 ± 0.09 µM obtained with traditional domes ($p \leq 0.05$, n = 3).

Conclusion/Significance: Organoid Culture Plates significantly enhance organoid culture workflows by improving image quality while reducing experimental variability and failure rates. Automation amplifies these benefits. Together, these advances support larger-scale organoid experiments for use in high-throughput drug or toxicity screening programs with lower variability while maintaining consistent assay outcomes.

OP-015 - Continuous Viscoelasticity Measurement of Cell Spheroids via Microfluidic Electrical Aspiration

Heyi Chen[1], Jacob Brown[2], Aaron Urban[1], Ge Zhang[3], Jiang Zhe[1]

[1]*University of Akron, Department of Mechanical Engineering, Akron, United States of America*
[2]*University of Akron, Biomedical Engineering, Akron, United States of America*
[3]*The University of Akron, Department of Biomedical Engineering, Akron, United States of America*

Purpose/Objectives: Measurement of viscoelastic characteristics of cells cultured in 3D is critical to study many biological processes including tissue and organ growth. We present a unique electrical aspiration method to measure the viscoelastic properties of cell spheroids. A microfluidic sensor was created to demonstrate this method. Unlike the traditional optical aspiration, the aspiration of the cell spheroids is monitored via dynamic electrical resistance changes of a symmetrical microfluidic aspiration channel.

Methodology: A multilyer microfluidic aspiration device was designed to enable a symetrical aspiration channel that is sandwiched by two gold planar electrodes. As a cell spheroid aspires into the channel, we measure the relative resistance change of the microchannel $\Delta R(t)$. Since aspiration length $L(t)$ is a result of $\Delta R(t)$, $L(t)$ can be also be determined. Using a linear half-space model to fit the aspiration length $L(t)$ of the sample, G_0, the instantaneous shear modulus, α_1, a unitless viscoelastic parameter, and τ, the creep time constant can be determined through the linear half-space model. Using additional relations, shear moduli (G_∞), instantaneous and equilibrium elastic moduli (E_∞, E_0), the apparent viscosity (μ) can be calculated.

Results: We first used the microfluidic device to measure the viscoelastic properties of biological tissues derived from calfskin and porcine left ventricular myocardium. The equilibrium elastic modulus and creep time constants were measured to be 148.1-±24.1kPa and 76.7±3.5seconds and 64.5±7.7kPa and 31.4±2.7seconds respectively, which matched well with reported data. Next, hMSCs spheroids cultured for 3 days and 7 days were measured. The equilibrium elasticity (E_∞) of the spheroids was estimated to be 851.3±12.4Pa and 836.7±10.3Pa, apparent viscosity µ of the hMSCs spheroids was estimated to be 36583.4±14085.7Pa•s and 9726.7±7050.8Pa•s for 3-day and 7-day samples respectively. E_∞ and µ decreased significantly from day 3 to 7, likely from changes in MSC behavior within the 3D spheroids.

Conclusion/Significance: We proved the electrical aspiration method enables fast, optical free, continuous viscoelasticity measurements of 3D cell culture models in flow conditions. Compared to existing technologies this method can provide a high throughput, material tolerant, low-cost characterization of 3D cell culture models for investigating mechanobiology, tissue development and repair, and the discovery of new biomarkers for disease diagnosis.

OP-016 - Defining Dosing Framework for Sustained Intracellular Delivery using Extraction-Free Hydrogel Nanoparticle Emulsions

Ruth Guallpa, Marcella Vaicik

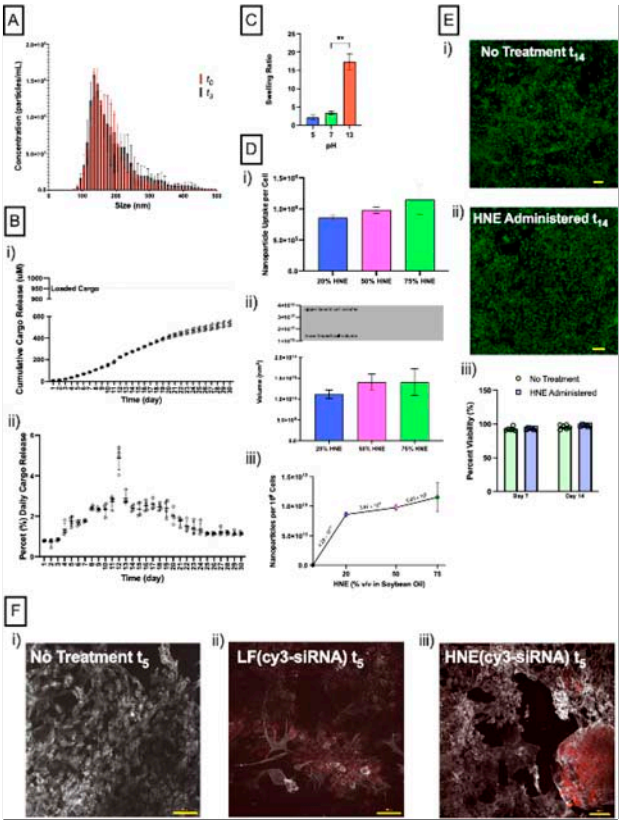
Illinois Institute of Technology, Biomedical Engineering, Chicago, United States of America

Purpose/Objectives: Regulating cellular function benefits from delivery systems that sustain intracellular therapeutic availability without repeated dosing or post-synthesis particle extraction. We established a cytocompatible, extraction-free Hydrogel Nanoparticle Emulsion (HNE), linking cargo loading, release kinetics, and administered dose to intracellular nanoparticle delivery.

Methodology: Poly(ethylene glycol) diacrylate (PEGDA)-based HNEs were synthesized by inverse miniemulsion polymerization. Particle diameter was measured at year 0 (t_0) and 3 (t_3) by nanoparticle tracking analysis (NTA). Fluorescein disodium salt release was monitored for 30 days. Swelling at pH 5, 7, and 13 tested acidic endosomal stability and alkaline degradation. 3T3-L1 preadipocytes received 20%, 50%, or 75% HNE; lysates were analyzed by NTA to estimate internalized nanoparticles per cell. Cytocompatibility was assessed by live/dead staining. Cy3-labeled small interfering RNA (Cy3-siRNA) delivery was compared qualitatively with Lipofectamine (LF).

Results: HNEs maintained stable nanoscale distributions from t_0 to t_3, with diameters of 178.7 ± 9.9 nm and 185.6 ± 14.8 nm and polydispersity index (PDI) <0.2. Fluorescein release persisted for 30 days, reaching 56.3 ± 2.6% of loaded cargo. Swelling did not differ significantly between pH 5 and 7, suggesting hydrogel mesh stability under acidic endosomal conditions; pH 13, included as degradation positive control, significantly increased swelling. Lysate analysis indicated approximately 10^6 internalized nanoparticles/cell. Increasing HNE administration concentration yielded diminishing uptake gains, suggesting an endocytic threshold to guide siRNA loading. HNE-treated cells maintained viability comparable to untreated controls through day 14 (t_{14}). Cy3-siRNA signal was detectable on day 5 (t_5) after HNE administration. Figure 1. (A)HNE size distribution. (B) (i)Cumulative and (ii)daily fluorescein release. (C)Swelling after 0.5 h at 37 °C in pH 5, 7, or 13. (D) (i)Nanoparticles per cell, (ii)internalized nanoparticle volume versus literature cell-volume bounds, and (iii)uptake-rate versus HNE content. (E)Live (green)/dead (red) images after (i)no treatment or (ii)HNE treatment; (iii)viability. (F)Images after (i)no treatment, (ii)LF(cy3-siRNA) administration, and (iii)HNE(cy3-siRNA) administration. Scale bar = 100µm.

Conclusion/Significance: Extraction-free HNEs are stable, cytocompatible platforms for sustained intracellular delivery, allowing quantitative estimation of intracellular cargo dose from administered nanoparticle concentration. By linking long-term release behavior with cellular nanoparticle uptake, this framework establishes a rational basis for designing dose-guided therapeutic delivery strategies that regulate cell function over time.



OP-017 - Enhanced Soft Tissue Contrast in Micro–Computed Tomography (μCT) Enables Three-Dimensional (3D) Reconstruction of Equine Hoof Laminae

Thi Hong Tham Phan, Mandi J. Lopez

Louisiana State University, School of Veterinary Medicine, Veterinary Clinical Sciences, Baton Rouge, United States of America

Purpose/Objectives: Hoof laminitis causes irreversible tissue damage and impaired mobility in horses. Visualization of hoof soft laminar tissues is limited by low intrinsic contrast, limiting the development of three-dimensional hoof tissue models as templates for bioprinted organoids. This study was aimed at optimizing staining protocols for high-contrast micro-computed tomography (μCT) imaging of equine hoof laminae.

Methodology: Laminae from normal and laminitic hoof tissue were collected postmortem. Tissue sections were fixed in 10% formalin, 4% paraformaldehyde with graded ethanol, or 70% ethanol. Samples were stained with Lugol's solution (I2KI), phosphotungstic acid (PTA), or sequential I2KI followed by PTA. Staining was qualitatively evaluated based on detailed microstructure and quantitatively assessed using grayscale intensity on μCT images. Optimized protocols were then applied to samples, and laminar microstructural dimensions were measured.

Results: I2KI had superior tissue penetration but lower contrast, whereas PTA provided higher contrast with poor penetration. Sequential I2KI followed by PTA staining had the best contrast and structural fidelity. In normal tissue, this approach combined with 70% ethanol fixation enabled clear μCT imaging. In laminitic tissue, however, it caused oversaturation and structural distortion, potentially due to poor tissue condition. Formalin fixation with sequential staining resolved these issues.

Conclusion/Significance: Two fixation–staining protocols preserved morphological features and enabled accurate three-dimensional reconstruction of normal and laminitic laminae, providing the first clear μCT-based visualization of equine hoof laminae for organoid-based studies and expanding applications for soft tissue imaging.

Session 10
Advances in Decellularization and Recellularization of Complex Tissues

11-15-2026 @ 2:30 PM - 4:00 PM

OP-019 - Development of new a method for the ready-to-use preservation of a human Acellular Dermal Matrix

Valeria Purpura[1], Francesco Vinelli[1], Elena Bondioli[1], Paola Minghetti[1], Stefano Palo[1], Matilde Tschon[2], Francesca Becherini[3], Francesca Scarpellini[3], Davide Melandri[1]

[1]*AUSL Romagna, Burn Center And Skin Tissue Establishment, Cesena, Italy*
[2]*Rizzoli Orthopedic Institute, Surgical Sciences And Technologies, Bologna, Italy*
[3]*AUSL Romagna, O.u. Pathological Anatomy, Cesena, Italy*

Purpose/Objectives: The Acellular Dermal Matrices derived from human dermis (hADMs) are widely used as a reconstructive approach in the field of Regenerative Medicine. The Emilia Romagna Regional (ERR) Skin Tissue establishment previously developed and patented a method of decellularization (PTC/IB2008/002753) able to produce a hADM that is widely distributed as permanent dressing for several clinical fields such as breast surgery, orthopedics, dermatology, plastic and reconstructive surgery, ophthalmology, dentistry. To date, cryopreservation is the method used by ERR Skin Tissue Establishment to store hADM for its ability to maintain good tissue properties over time. However, the thawing of cryopreserved hADM is always performed before distribution and its clinical use is ensured until 3 days reducing, in turn, a wide-ranging distribution. With the aim to enhance hADM use even outside Italy we decided to develop a new method for its ready-to-use preservation based on tissue storage at room temperature in a solution, patented by us, in which tissue is maintained until its clinical use. In this way, we provide to clinicians a tissue packaged and used only if required.

Methodology: We described our outcomes in terms of cytotoxicity, bioactivity, *in vitro* colonization and morphological, microbiological, histological, biochemical and biomechanical properties of hADM preserved for 1 year in these new ready-to-use modality.

Results: Our results show how hADM in solution maintains good morphological, structural, biochemical and biomechanical properties compared to cryopreserved hADM. Moreover, no microbial and/or fungal contamination was identified in all samples up to 1 year. No cytotoxic effects were also identified, and cells maintain their ability to repopulate hADM when stored in solution until 1 year, also maintaining growth factor's release similar to control. Thus, our results make this preservation method potentially suitable for clinical purposes.

Conclusion/Significance: Taking into account the biological results obtained, we can conclude that the proposed ready-to-use new modality of hADM preservation in solution at room temperature appears to be a safe and effective method to maintain tissue properties for clinical use, reducing costs of its production and expanding the possibility to satisfy clinical requests even outside Italy. This work was funded by the Italian Ministry of Health. Project Code: RF-2021-12372260.

OP-020 - 3D in vitro organ-specific model of vaginal fibroblasts for pelvic organ prolapse repair

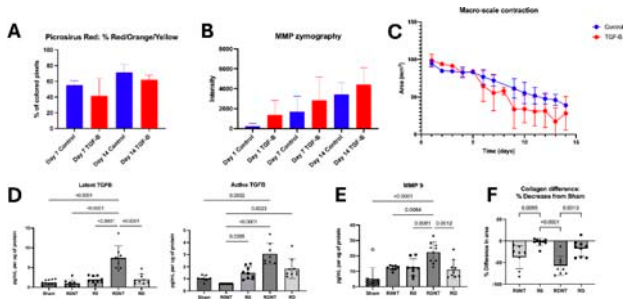
Marrisa Therriault[1,2], Temitope Obisesan[3,4], Bryan Brown[4], Pamela Moalli[1,2,4]

[1]*Magee Womens Research Institute, Pittsburgh, United States of America*
[2]*University of Pittsburgh, Obgyn, Pittsburgh, United States of America*
[3]*University of Pittsburgh, Magee Womens Research Institute, Pittsburgh, United States of America*
[4]*University of Pittsburgh, Bioengineering, Pittsburgh, United States of America*

Purpose/Objectives: Polypropylene mesh augmented pelvic organ prolapse surgery is associated with complications including pain, fibrosis, and mesh exposure. Prior in vivo studies by our lab demonstrated that mesh deformation and increased mesh burden drive a maladaptive remodeling response characterized by macrophage activation, elevated TGF-β signaling, matrix disorganization, and myofibroblast accumulation. However, the specific contribution of vaginal fibroblast mechanobiology to these remodeling pathways remains incompletely understood. We therefore developed a three-dimensional (3D) in vitro model to isolate and characterize vaginal fibroblast responses to polypropylene mesh under conditions relevant to POP repair.

Methodology: Hydrogels derived from decellularized nulliparous porcine vaginal extracellular matrix (ECM) were seeded with primary human vaginal fibroblasts (HVFs). Restorelle® polypropylene mesh was incorporated into the constructs to generate gel–mesh complexes that were cultured for 14 days in the presence or absence of transforming growth factor-beta 1 (TGF-β1). Constructs were assessed longitudinally for macroscopic contraction, matrix metalloproteinase (MMP) activity, and collagen remodeling. Collagen organization and maturity were quantified using picrosirius red polarization imaging.

Results: Polarized picrosirius red imaging demonstrated reduced deposition of mature collagen fibers in TGF-β1-treated constructs, indicating impaired matrix organization and persistence of an immature remodeling phenotype (Figure-1A, p=0.01). TGF-β1 stimulation induced a pro-remodeling phenotype characterized by increased construct contraction (Figure-1C, p<0.001) and elevated pro- and active-MMP2 expression across all time points (Figure-1B, p=0.01). By Day 14, TGF-β1-treated gel–mesh complexes demonstrated greater contraction compared to untreated controls, consistent with enhanced fibroblast activation and matrix remodeling. These findings parallel prior in vivo observations in which increased mesh burden and maladaptive remodeling were associated with elevated TGF-β signaling (Figure 1D), increased matrix degradation (Figure 1E), and deposition of disorganized extracellular matrix (Figure 1F).



Conclusion/Significance: This study establishes a biomimetic 3D vaginal fibroblast platform that recapitulates key features of the maladaptive host response to polypropylene mesh in vivo. By isolating fibroblast-driven remodeling within an organ-specific ECM environment, this model provides a mechanistically relevant system to study mechanotransduction, fibroblast activation, and matrix remodeling following mesh implantation. The platform may enable the development and screening of next-generation biomaterials and targeted biologic therapies aimed at mitigating fibrosis, improving tissue integration, and enhancing healing outcomes following POP repair.

OP-021 - Alpha-Gal Elimination in Bovine Pericardium-Derived Collagen Bioinks: A Path to Clinical Translation

Vanessa Worsfold, Lisa Blackett, Terance Hart

Maverick Biomaterials, Dubbo, Australia

Purpose/Objectives: The advancement of tissue engineering increasingly relies on xenogeneic collagen-based biomaterials due to their ability to mimic the native extracellular matrix (ECM) and undergo *in vivo* remodelling. However, clinical translation is often hindered by the presence of immunogenic antigens, particularly the galactose-alpha-1,3-galactose (alpha-gal) epitope. While humans naturally produce high titres of anti-alpha-gal antibodies, current bioprosthetic materials frequently retain residual epitopes that trigger inflammation and late-stage calcification, compromising long-term device safety. Standard decellularization protocols are frequently insufficient for the complete removal of these epitopes or inadvertently damage the ECM structural integrity.

Methodology: This study reports the characterization and performance of a novel atelocollagen bioink, derived from bovine pericardium and designed specifically for bioprinting applications. To eliminate xeno-antigens, a multi-step decellularization and purification protocol was engineered. Effective removal of the alpha-gal antigen was confirmed using a high-sensitivity immunohistochemistry (IHC) technique, meeting the stringent requirements set by regulatory authorities.

Results: As an alpha-gal free formulation, the 18 mg/mL bioink is pH-neutral, endotoxin free and optimized to support high-resolution constructs with natural fibrillogenesis. Biological evaluation confirmed that the biomimetic environment supports fundamental cellular behaviours, including adhesion and proliferation, with cell viability exceeding 95% post-printing. Rheological characterisation confirmed suitability for extrusion-based bioprinting, with pronounced shear-thinning behaviour (n = 0.201) and a viscosity drop ratio of 336x. Temperature sweep analysis confirmed thermally driven fibrillogenesis around 30-32°C, with a post-gelation storage modulus of ∼650 Pa, matching or exceeding commercial reference materials at higher concentrations

Conclusion/Significance: By addressing these biocompatibility risks through sophisticated engineering controls, this study provides a practical approach for the development of safe, repeatable, and effective tissue-engineered products, demonstrating a clear pathway for the translation of advanced bioprinted constructs into the clinical landscape.

OP-022 - Laminin Exposure and ERK Activation Underlie Improved Recellularization of Stretch-Conditioned Lung Scaffolds

Shiyuan Bian[1,2], Ethan Chen[2], Tom Waddell[2,3,4], Golnaz Karoubi[1,2,5]

[1]*University of Toronto, Department of Laboratory Medicine And Pathobiology, Toronto, Canada*
[2]*University Health Network, Latner Thoracic Research Laboratories, Toronto, Canada*
[3]*University of Toronto, Institute Of Biomedical Engineering, Toronto, Canada*
[4]*University of Toronto, Institute Of Medical Sciences, Toronto, Canada*
[5]*University of Toronto, Department of Mechanical and Industrial Engineering, Toronto, Canada*

Purpose/Objectives: Lung transplantation currently remains the only life-saving treatment for end-stage lung disease, but donor shortages contribute to high waitlist mortality. Bioengineered lungs generated by recellularizing acellular scaffolds represent a promising alternative. In our previous study, cyclic stretch preconditioning of decellularized mouse lung scaffolds improved alveolar type II (ATII) cell attachment, viability, proliferation, and coverage, while increasing extracellular signal-regulated kinase (ERK) activation. However, the mechanisms underlying these effects remain unclear. This study investigated whether cyclic stretch alters extracellular matrix (ECM) protein exposure within the scaffold and examined the role of ERK signaling in regulating ATII cell function.

Methodology: A Negative Pressure Wet Ventilation System was used to apply cyclic stretch to decellularized mouse lungs. Scaffolds were cultured for 5 days under either perfusion-only conditions or perfusion with moderate cyclic stretch (0.3mL tidal volume, 16 breaths/min). Changes in ECM protein exposure were assessed through histological and biochemical analyses. Primary human ATII cells, cultured with or without the ERK inhibitor PD0325901 (1μM), were seeded onto non-ventilated and pre-ventilated precision-cut lung slices (PCLSs). Initial attachment was evaluated at 2, 6, and 12 hours, integrin α3 and α6 expression at 24 hours, and

cell coverage, viability, proliferation, and mechanotransduction signaling over 5 days.

Results: Moderate cyclic stretch preserved alveolar architecture and overall ECM protein content while increasing laminin exposure in specific scaffold regions by approximately fivefold. Compared with perfusion-only controls, preconditioned scaffolds increased expression of the laminin-binding integrin subunits α3 and α6 in ATII cells by approximately 1.5-fold. Relative to ERK-inhibited cells, untreated ATII cells on preconditioned scaffolds showed greater attachment at 12 hours (+20%±13%), coverage (+34%± 21%), viability (+29%±17%), and proliferation (+68%±22%). No significant differences were observed at the 2- or 6-hour attachment time points. ERK inhibition abolished the improvements in coverage, viability, and proliferation, producing outcomes comparable to perfusion-only controls ($p>0.05$).

Conclusion/Significance: Moderate cyclic stretch preconditioning enhances laminin exposure while preserving scaffold integrity, promoting epithelial cell attachment, survival, and proliferation through integrin-associated ERK signaling. These findings provide mechanistic insight into how mechanical preconditioning improves lung scaffold recellularization and support its use as a strategy to enhance the development of bioengineered lungs for regenerative medicine and transplantation.

Session 11
Advancing Women's Health Through Inclusive Innovation

11-16-2026 @ 8:00 AM - 9:30 AM

OP-025 - An acellular ECM hydrogel mitigates atrophy and fibrosis of the rat pelvic floor muscles consequent to birth injury

Bianca Pena[1,2], Khushi Diwakar[3], Marianna Alperin[2,4], Karen Christman[1,2,5]

[1]*UC San Diego, Shu Chien-gene Lay Department of Bioengineering, San Diego, United States of America*
[2]*Sanford Consortium for Regenerative Medicine, La Jolla, United States of America*
[3]*UC San Diego, Biological Sciences, San Diego, United States of America*
[4]*UC San Diego, Obstetrics, Gynecology, and Reproductive Sciences, San Diego, United States of America*
[5]*Sanford Stem Cell Institute, San Diego, United States of America*

Purpose/Objectives: Pelvic floor muscle (PFM) injury and dysfunction consequent to birth injury is a key risk factor for pelvic floor disorders that negatively impact ~30% of women worldwide. Despite high prevalence and significant morbidity, effective strategies to prevent or treat the maladaptive recovery of PFMs are scarce. We have previously demonstrated that an acellular skeletal muscle ECM hydrogel (SKM) can promote constructive remodeling, modulate the immune response, and prevent atrophy and fibrosis in a non-pregnant simulated birth injury (SBI) rat model. We thus aimed to determine if SKM would mitigate PFM atrophy and fibrosis in a translationally relevant pregnant/postpartum rat model.

Methodology: Late-pregnant Sprague-Dawley rats underwent SBI via vaginal balloon distention ~2 days before parturition. Postpartum animals were randomly assigned to either 1) SBI; 2) SBI+saline; 3) SBI+SKM groups. SKM/saline was injected directly into PFMs either immediately or 4-weeks postpartum to determine efficacy at two clinically relevant time points of prevention and treatment of pathological PFM alterations consequent to birth injury. PFMs were harvested at 4 or 8 weeks post SBI, snap frozen, and cryosectioned. Muscle cross-sections were incubated with anti-laminin and anti-collagen I antibodies for quantification of fiber area and collagen content, respectively.

Results: Immediate postpartum injection of SKM increased fiber size compared to SBI and SBI+saline animals and significantly decreased collagen content compared to SBI animals (Figure 1A-C). Delayed injection of SKM increased fiber size compared to SBI and SBI+saline animals (Figure 1D-E). The delayed SKM injection also significantly decreased collagen content compared to SBI (Figure 1F).

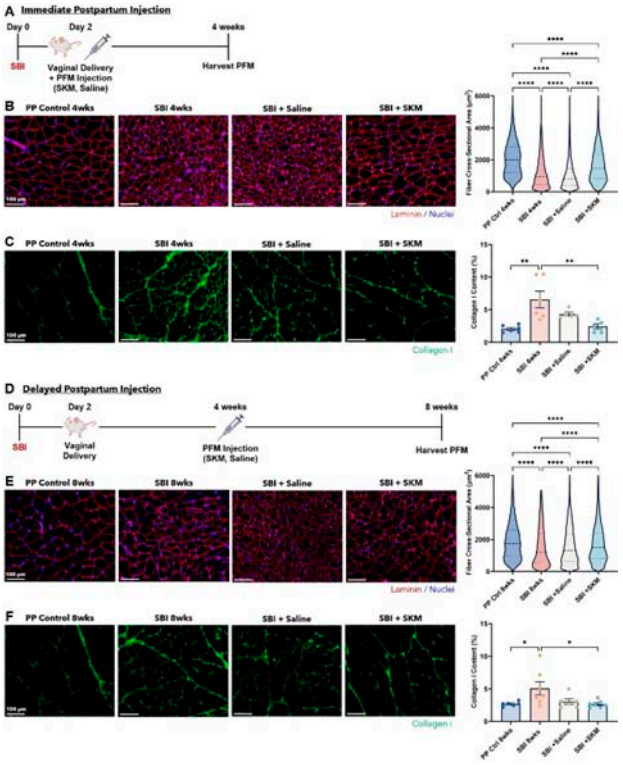


Figure 1. (A-C) Immediate postpartum injection and (D-F) Delayed postpartum injection of SKM/saline. (B, E) Laminin and nuclei-stained cross sections with quantification of fiber cross-sectional area; median + IQR; Kruskal-Wallis. (C, F) Collagen-I stained cross sections with quantification of collagen content; mean ± SEM; one-way ANOVA. Postpartum (PP) controls are used for comparison. N=5-7/group. *P<0.05,**P<0.01,****P<0.0001.

Conclusion/Significance: SKM prevents PFM atrophy and fibrosis when administered immediately or 4-weeks postpartum. This work demonstrates therapeutic potential of this low-cost intervention in women following vaginal delivery in the relevant postpartum period.

OP-026 - Isogenic Sex-Specific Engineered Cardiac Tissues Enable Modeling of Divergent Human Cardiac Physiology

Yiran Li[1], Lamia Chowdhury[2], Sharon Fleischer[1], Roberta Lock[1], Ke Cheng[1], Gordana Vunjak-Novakovic[1]

[1]*Columbia University, Biomedical Engineering, New York, United States of America*
[2]*Barnard College, Biology, New York, United States of America*

Purpose/Objectives: Cardiovascular disease exhibits profound sex differences in prevalence, progression, and therapeutic response, yet most preclinical cardiac models fail to incorporate sex as a biological variable. A major barrier is the lack of physiologically relevant *in vitro* systems integrating genetics and hormonal signaling to recapitulate male and female human myocardium. While 2D cultures lack tissue-level architecture and animal models incompletely capture human sex-specific biology, engineered cardiac tissues (ECTs) provide a more physiologically and translationally relevant platform. Here, we engineered an isogenic sex-specific cardiac tissue platform using induced pluripotent stem cell (iPSC) lines derived from a single Klinefelter syndrome (XXY) donor, enabling chromosomal sorting into genetically matched XX and XY lines differing only in sex chromosome complement.

Methodology: Six isogenic iPSC clones (3 XX, 3 XY) were differentiated into cardiomyocytes (iCMs) and cardiac fibroblasts (iCFs). To eliminate confounding estrogenic signaling, iCMs were maintained in hormone-free B27 lacking progesterone and phenol red during hormone treatment. XX iCMs were treated with estradiol (E2, 10 nM) and/or progesterone (P4, 30 nM), while XY iCMs

received dihydrotestosterone (DHT, 10 nM) for 7 days. Sex-specific ECTs were fabricated on the milliPillar platform using physiologically informed cellular compositions. Baseline physiology and hormone responsiveness were assessed by qRT-PCR, western blotting, and contractile analysis.

Results: At baseline in hormone-free B27, XY iCMs exhibited higher spontaneous beating rates than XX iCMs, whereas XX iCMs showed prolonged contract90 and shorter tau, consistent with known sex differences in cardiac electrophysiology. Hormone treatment robustly activated expected sex hormone signaling pathways, with E2 upregulating EGR1 and GPER1, progesterone increasing EGR1 and PGRMC, and DHT elevating AR and FKBP5 expression. Functionally, DHT-treated XY iCMs exhibited shortened contract90, whereas hormone-treated XX iCMs demonstrated prolonged relax90, recapitulating sex-divergent contractile phenotypes.

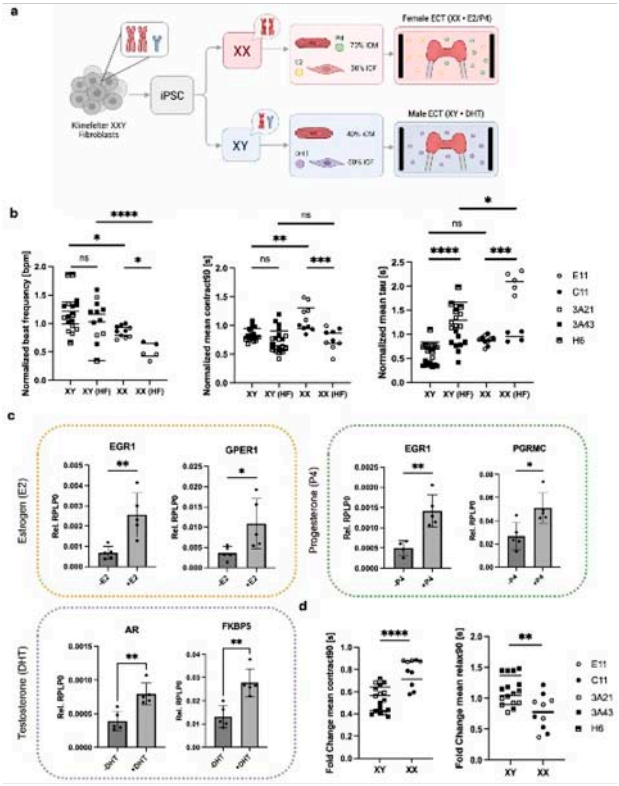


Figure: (a) Isogenic ECT fabrication schematic. (b) Baseline contractility in regular vs hormone free media (HF). (c) Hormone receptor qRT-PCR after 7-day treatment. (d) Contractile function in hormone-treated XX vs. XY iCMs.

Conclusion/Significance: This work establishes, to our knowledge, the first isogenic sex-specific 3D human ECT platform for modeling divergent cardiac physiology. Ongoing studies leverage these ECTs to model sex-dependent doxorubicin cardiotoxicity and identify sex-specific therapeutic strategies for precision cardiovascular medicine.

OP-027 - Optimizing in vitro Culture of Ovarian Cells for Biomaterial-based Estrogen Restoration Therapies

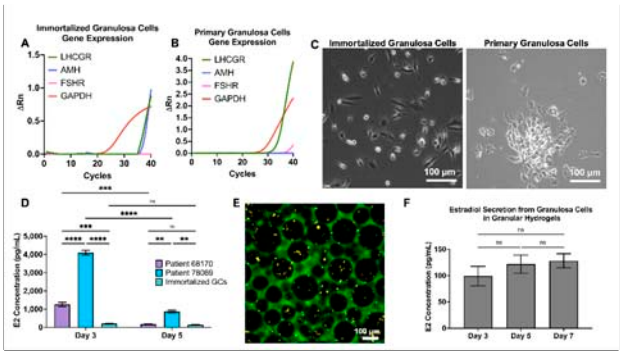
Natasha Claxton[1], Arieana Talavera[1], Isabella Cabrera[1], Lindsay Wells[2], Mykel Green[1]

[1]*Tulane University, Biomedical Engineering, New Orleans, United States of America*
[2]*Audubon Fertility, New Orleans, United States of America*

Purpose/Objectives: Loss of estrogen during menopause contributes to hormonal imbalance, disrupted folliculogenesis, infertility, cardiovascular disease, and metabolic dysfunction. Age-associated estrogen decline is partially driven by depletion and dysfunction of ovarian granulosa cells (GCs), the primary producers of estradiol. Although hormone replacement therapy alleviates menopausal symptoms, it does not restore endogenous ovarian endocrine function. Regenerative approaches integrating cell-based therapies with engineered biomaterials may enable localized and tunable hormone restoration. We hypothesized that recreating key mechanical and biochemical features of the ovarian microenvironment would enhance GC survival and endocrine function. Here, we compared endocrine phenotype and estradiol secretion between immortalized and primary human GCs encapsulated in tunable granular hydrogels.

Methodology: Primary GCs were isolated from discarded follicular fluid obtained from patients undergoing in vitro fertilization procedures. A polyethylene glycol (PEG)-based granular hydrogel system was developed to independently tune matrix viscoelasticity and biochemical composition to support GC survival and endocrine function. Matrix stiffness, follicular fluid-derived components, and culture medium formulation were evaluated for effects on GC viability, proliferation, and estradiol secretion using enzyme-linked immunosorbent assay (ELISA). Quantitative polymerase chain reaction (qPCR) was used to assess expression of granulosa cell endocrine markers, including luteinizing hormone/choriogonadotropin receptor (LHCGR), anti-müllerian hormone (AMH), and follicle-stimulating hormone receptor (FSHR).

Results: Immortalized human GCs expressed LHCGR and AMH, but not FSHR, whereas primary human GCs expressed higher levels of LHCGR and FSHR (Fig. 1A-B). Both GC populations proliferated and exhibited morphological changes after 48 hours in specialized GC medium (Fig. 1C). Primary GCs secreted higher estradiol levels than immortalized GCs on extracellular matrix-coated substrates (Fig. 1D). PEG-based granular hydrogels supported GC encapsulation and longitudinal assessment of endocrine function over 1 week in culture (Fig. 1E-F). Figure Legend: Characterization of immortalized and primary granulosa cells, including ovarian marker expression, morphology, estradiol secretion, and encapsulation within PEG-based granular hydrogels.



Conclusion/Significance: Collectively, these findings demonstrate phenotypic and endocrine differences between immortalized and primary human GCs and establish a biomaterial platform for investigating ovarian endocrine restoration. These studies support development of engineered ovarian microenvironments for localized therapies targeting menopause-associated estrogen loss.

Session 12
Complex Data Sets and AI Applications in Term

11-16-2026 @ 8:00 AM - 9:30 AM

OP-030 - CRISPR-EpiGEM: Deep Learning CRISPR Screens for Data-Driven Epigenetic Editing

Alexander Arteaga, Josh Graham, Tomas Gonzalez Fernandez

Lehigh University, Bioengineering, Bethlehem, United States of America

Purpose/Objectives: DNA methylation (DNAm) is a key epigenetic regulator of stem cell fate. CRISPR-based tools such as CRISPR-off enable stable, heritable gene silencing through targeted methylation; however, identifying which CpG sites drive therapeutically relevant

phenotypic changes remains a major challenge. We developed CRISPR-EpiGEM, a contrastive variational autoencoder platform that learns cell-type-specific DNAm representations to predict CpG editing targets for directed stem cell reprogramming.

Methodology: CRISPR-EpiGEM integrates a Linformer-based CpG attention module, a multi-layer perceptron encoder-decoder, and three combined loss functions (reconstruction, KL divergence, contrastive) to encode biologically meaningful latent DNAm representations. The model was trained on publicly available Gene Expression Omnibus datasets from human mesenchymal stromal cells (MSCs), adipocytes, chondrocytes, and osteocytes. Latent space perturbations were used to identify CpG sites whose methylation editing could reprogram MSCs toward adipogenesis. CRISPRoff mRNA was transcribed *in vitro* and delivered to primary MSCs via RALA, a cell-penetrating peptide nanoparticle system. Transfection efficiency was quantified by flow cytometry, and cytotoxicity was assessed via Alamar Blue assay.

Results: Training and validation loss curves showed smooth convergence with minimal overfitting (Fig. 1B–C). UMAP visualization revealed well-defined cell-type clusters (Fig. 1D–F), with strong K-means performance: training silhouette score 0.867/ARI 1.000, validation 0.846/ARI 0.944, and unseen test set 0.737/ARI 0.918, confirming generalizability. Latent space perturbation nominated CpG sites in *VASN* and *INHBA*, known anti-adipogenic genes, as top CRISPRoff targets. Gene ontology of the top 150 targets enriched for fatty acid metabolism pathways. RALA-mediated CRISPRoff delivery achieved 35.23±2.23% transfection efficiency in primary MSCs with no significant cytotoxicity (Fig. 1G).

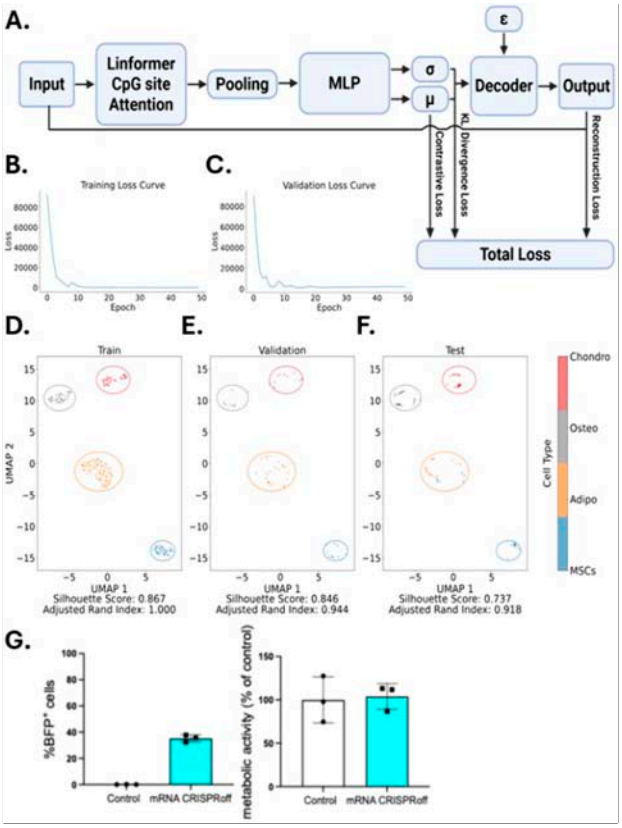


Figure 1. CRISPR-EpiGEM framework (A), training loss (B), validation loss (C), training UMAP (D), validation UMAP (E), test UMAP (F), and CRISPRoff transfection efficiency and cytotoxicity (G).

Conclusion/Significance: CRISPR-EpiGEM provides a causal, data-driven framework linking DNAm patterns to cell phenotype. By integrating deep learning with CRISPR epigenetic editing, this platform enables *in silico* identification of targetable CpG sites to guide stem cell fate. Successful CRISPRoff delivery validates translational feasibility. Ongoing work will confirm adipogenic induction through DNAm editing of nominated targets, establishing CRISPR-EpiGEM as a foundation for precision epigenomic engineering in regenerative medicine.

OP-031 - A Causal Cardiac Digital Twin Predicts Late-stage Phenotype from Early Embryonic Signaling

Jonghyeuk Han[1], May Wang[2], Michael Davis[2]

[1]*Emory University, Atlanta, United States of America*
[2]*Emory University, Department of Biomedical Engineering, Atlanta, United States of America*

Purpose/Objectives: Engineering a developing heart requires knowing which signals to deliver, when, and to which lineage; the target moves. Between E12.5 and E18.5, the mouse left ventricle rewires its cell–cell communication, and the signaling state at one stage is not the one a later stage will face. Any model, or any rationally designed cardiac model, built on an early window must predict into a signaling space it has never seen. Here, we investigate whether double machine learning prioritized causal features can improve cardiac twin predictabilty and explanability for the future traits.

Methodology: Using lineage-resolved scRNA-seq from the developing mouse left ventricle E12.5–E18.5 (GSE193346), where 43 of 702 ligand features turn on and 18 turn off across the window, we benchmarked thirteen neural-network architectures on forward (early→late) versus backward extrapolation of echocardiographic traits. Double Machine Learning (DML) estimated a standardized causal effect θ for each of 7,020 ligand→trait connections; permutation-FDR control and leave-one-timepoint-out stability filters prioritized 30 edges, all surviving E-value sensitivity analysis above the strongest measured covariate. This sparse causal pathway was convexly blended with a neural network model under a tunable ratio α, with linear-branch weights initialized at DML estimates so the prior contributes both structure and magnitude.

Results: Signaling composition in the left ventricle reorganized progressively across E12.5–E18.5: 43 of 702 lineage-resolved ligand features turned on and only 18 turned off. All 13 architectures degraded when predicting forward in developmental time (mean $\Delta R^2 = 0.40$ versus backward), indicating that early-stage signaling input alone is insufficient to specify late-stage ventricular phenotype. A 30-edge causal prior closed a 0.13–0.54 R^2 gap across four neural-network families, restored per-trait R^2 above 0.85 where the unstructured baseline failed, and reduced per-trait variability ∼2.7-fold. A mask-size sweep ($K \in \{30, 50, 70, 100\}$) confirmed that performance was governed by edge identity rather than sparsity. The recovered ligands (BMP2, POSTN, FN1 anchoring cardiomyocyte and fibroblast-like compartments) are the molecules already employed to drive chamber growth and matrix remodeling in cardiac tissues.

Conclusion/Significance: A causally identified signaling backbone enables predictable, explainable cardiac digital twins for congenital heart disease and signaling-aware design of engineered tissues.

Session 13
Musculoskeletal Microphysiological Systems and New Alternative Models: Development to Application

11-16-2026 @ 8:00 AM - 9:30 AM

OP-033 - Injury-Driven Spatial Regulation of FAP-Mediated Adipogenesis in Engineered Skeletal Muscle

David Leyton Cifuentes[1], Christopher Rathbone[1,2]

[1]*University of Texas at San Antonio, Department of Biomedical Engineering, San Antonio, United States of America*
[2]*UTSA-UTHSA, Joint Graduate Program In Biomedical Engineering, San Antonio, United States of America*

Purpose/Objectives: Fibro-adipogenic progenitors (FAPs) are involved in adipose infiltration during skeletal muscle regeneration; however, the extent to which adipogenic conditions and local injury-associated factors influence FAP responses remains incompletely understood. This study evaluates spatial patterns of adipogenic and myogenic responses in tissue-engineered skeletal muscle (TE-SkM) following injury under distinct culture conditions.

Methodology: TE-SkM constructs were generated by co-culturing satellite cells (SCs) and FAPs isolated from rat skeletal muscle. FAPs were purified by negative selection ($CD31^-/CD45^-/VCAM1^-$) and

positive selection ($SCA1^+/PDGFR\alpha^+$), while SCs were isolated via $VCAM1^+$ selection using MACS. Cells were combined at a concentration of 2.5×10^6 cells/mL, with FAPs comprising 0% or 25% of the total cell population. Cells were embedded in fibrin hydrogels (~5.7 mg/mL) and seeded into custom PDMS molds. Constructs were injured at day 18 and maintained under myogenic (MM) or adipogenic (AM1 and AM2) conditions until day 25. Constructs were then stained for lipid accumulation (BODIPY), FAP localization (PDGFRα), cytoskeletal organization (F-actin), and nuclei (DAPI). Confocal imaging was used to compare injured and non-injured regions.

Results: Preliminary qualitative comparisons revealed distinct spatial and condition-dependent patterns of adipogenic differentiation. Lipid accumulation was observed under AM1 and AM2 conditions, predominantly in non-injured regions, and was reduced at the injury site, in some cases minimal or absent. Under MM, little to no lipid accumulation was observed. The $PDGFR\alpha^+$ signal was enriched in the injury region across conditions, suggesting FAP migration and/or activation within the injury region.

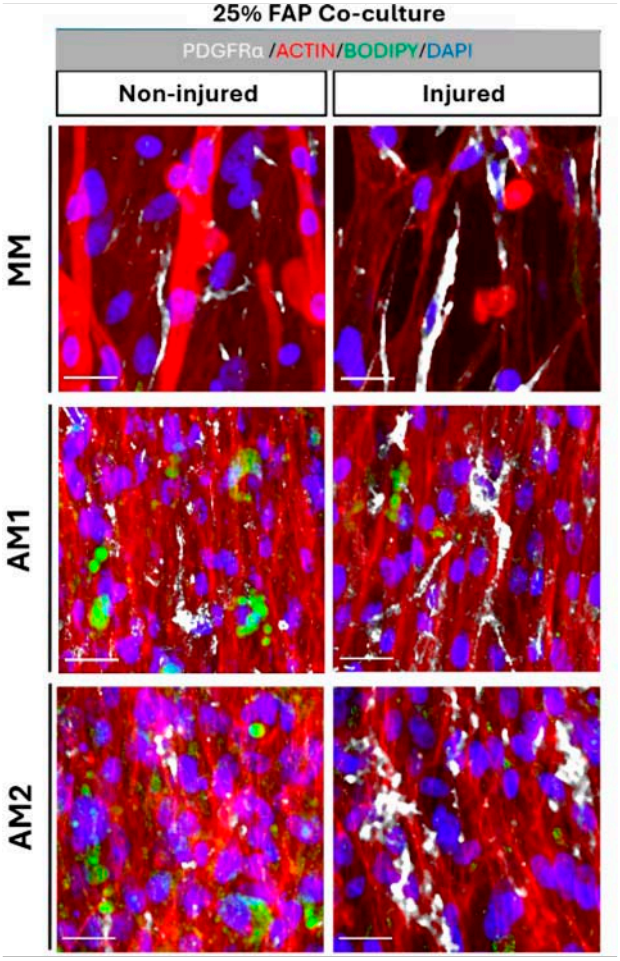


Figure 1. Representative confocal images of TE-SkM co-cultures (75% SCs, 25% FAPs) under myogenic (MM), white adipogenic (AM1), and browning (AM2) conditions. Images were acquired from injured and non-injured regions. BODIPY (green), PDGFRα (white), F-actin (red), and DAPI (blue) are shown. Scale bars = 25 μm.

Conclusion/Significance: These findings suggest that FAP-driven adipogenesis in TE-SkM is spatially and condition-dependent. Adipogenic differentiation appears reduced at the injury site, even under pro-adipogenic conditions, while features consistent with myogenic remodeling are enriched in this region. This work highlights the importance of local and spatial regulation of progenitor cell fate and provides insight into strategies to control pathological fat accumulation in engineered muscle systems.

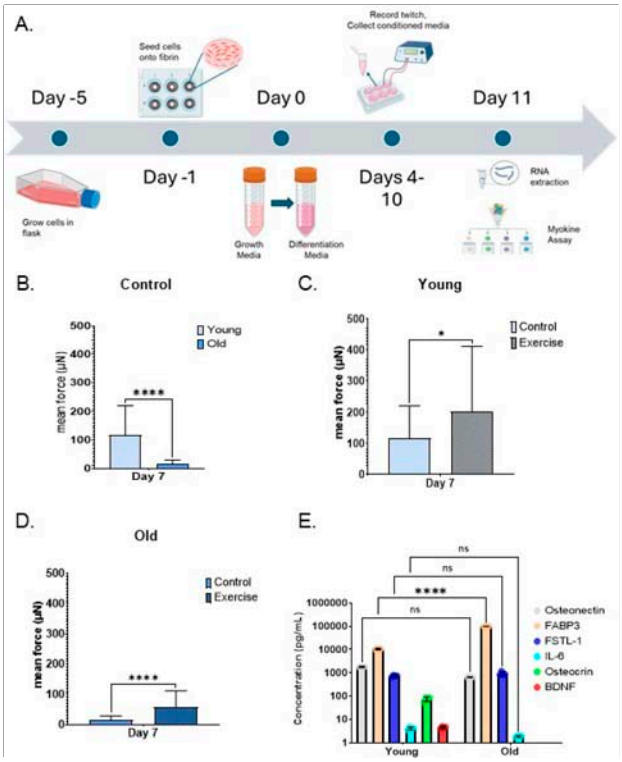
OP-035 - Human primary skeletal muscle-derived in vitro models to study human aging

Brandon Rios, Ritu Raman, Isabella Weiner

Massachusetts Institute of Technology, Mechanical Engineering, Cambridge, United States of America

Purpose/Objectives: Age-associated skeletal muscle decline (sarcopenia) contributes significantly to frailty, mobility loss, and reduced quality of life, yet current preclinical models fail to capture multiscale adaptation during human muscle aging. Here, we developed a primary human skeletal muscle microphysiological system to evaluate how young and aging muscle differentially adapt to therapeutic regimen (exercise-mimetic electrical stimulation) across tissue, cellular, and molecular scales.

Methodology: Primary human myoblasts obtained from 3 young (29–35 years) and 3 old (65–67 years) donors were differentiated on fibrin hydrogels, yielding contractile muscles. Tissues were subjected to exercise-mimetic electrical stimulation (30 min/day) for 7 days starting on day 4. Conditioned media collected at days 7 and 10 were analyzed using the Luminex FLEXMAP platform to quantify muscle secreted factors (myokines). Bulk RNA sequencing was performed to characterize transcriptomic responses to donor age and treatment conditions.



Results: At baseline, engineered muscles from older donors generated significantly lower contractile force compared to younger donors (14.1 μN vs. 117 μN, $p < 0.0001$, panel B). Chronic electrical stimulation significantly improved force production in aged tissues (>310% increase; 14.1 μN to 57.9 μN, $p < 0.0001$, panel D), demonstrating the adaptive capacity of aging muscle. Secretome analysis revealed age-dependent differences in myokine responses, including significantly elevated FABP3 in old compared to young, while young also showed the presence of Ostecrin and BDNF (panel E).Transcriptomic analysis further demonstrated that donor age was the dominant determinant of global gene expression. Gene set enrichment analysis of biological processes revealed young donors at baseline upregulate gene sets associated with oxidative metabolism, contractile apparatus maintenance, and myogenic differentiation, while old donors upregulate gene sets associated with ER stress, protein glycosylation, and secretory pathway dysfunction. In progress work seeks to use machine

learning tools to map how treatment impacts old muscles' biological age from bulk RNA sequencing data.

Conclusion/Significance: This work establishes a human primary cell-derived microphysiological muscle platform capable of integrating functional, secretomic, and transcriptomic readouts to study aging muscle biology. Importantly, the platform preserves donor-specific molecular identity while remaining responsive to therapeutic intervention, supporting its utility for mechanistic studies and preclinical screening of anti-sarcopenic therapies.

OP-037 - Modelling Tumor-Induced Cachexia: Unraveling Cellular and Molecular Drivers of Muscle Atrophy and Adipose Lipolysis to Inform Improved Therapies

Rita Lima-Sousa, Aike Sijtsma, Lucília Silva, Rui Reis, David Caballero

University of Minho, 3b´s Research Group, I3bs, Barco, Guimaraes, Portugal

Purpose/Objectives: Tumor-induced cachexia (TiC) is a multifactorial metabolic syndrome characterized by involuntary weight loss, muscle wasting, adipose tissue depletion, and systemic inflammation, affecting ~80% of patients with advanced malignancies, and markedly worsening treatment tolerance and survival. Despite substantial clinical and preclinical efforts, no approved pharmacological therapy exists for treating and reversing TiC, underscoring the need to define actionable mechanisms that connect tumor biology to peripheral tissue remodeling. Emerging evidence implicates tumor-derived extracellular vesicles (EVs) as long-range effectors of cachexia, delivering bioactive cargo that can reprogram skeletal muscle (SM) and adipose tissue (AT). However, how tumor origin and associated EV molecular signatures shape the incidence and severity of cachectic phenotypes remains insufficiently resolved. Here, we hypothesized that tumor cells remotely modulate SM and AT catabolism through EV-mediated signaling, and that EV cargo composition differs by tumor origin in ways that associate with cachexia severity.

Methodology: To test this, we established a novel in vitro model of TiC integrating both SM and AT, the latter typically overlooked in TiC preclinical modeling, using an indirect co-culture platform enabling EV-mediated communication. This system combined SM/AT cell models with cancer cells representing malignancies with distinct cachexia prevalence. We additionally performed EV molecular profiling to identify tumor-type-specific cargo signatures and evaluated the therapeutic potential of mesenchymal stromal/stem cell (MSC) secretome by assessing its capacity to promote tissue recovery after exposure to tumor-derived factors.

Results: Across conditions, we observed tumor-origin-dependent differences in the magnitude of myotube atrophy and lipolytic responses, consistent with differential cachexia-like remodeling. EV molecular profiling revealed distinct cargo signatures associated with each tumor type, supporting a link between tumor origin, EV composition, and downstream catabolic phenotypes. Importantly, treatment with MSC secretome promoted tissue recovery, partially rescuing cachexia-like alterations in SM and AT following exposure to tumor-derived factors.

Conclusion/Significance: Collectively, this work provides a mechanistically grounded preclinical framework to interrogate tumor-specific cachectic drivers, nominates EV cargo features as candidate biomarkers and therapeutic targets for tumor-tailored early detection and intervention in TiC, and supports MSC-derived secretome as a promising regenerative strategy to counteract TiC-associated peripheral tissue wasting.

Session 14
Engineering Dynamic Microenvironments to Direct Cell Signaling, Stem Cell Fate, and Function

11-16-2026 @ 8:00 AM - 9:30 AM

OP-038 - Engineering a Tunable Hydrogel Microenvironment to Regulate TNBC Invasion and Signaling

Anju Rana Magar, Hossein Tavana

The University of Akron, Biomedical Engineering, Akron, United States of America

Purpose/Objectives: Extracellular matrix (ECM) stiffening and hepatocyte growth factor (HGF) signaling are important regulators of breast cancer progression. HGF activates the MET receptor tyrosine kinase pathway, promoting tumor invasion and metastasis. However, the combined effects of ECM mechanics and HGF–MET signaling remain poorly understood. The objective of this study was to develop a tunable collagen–alginate hybrid hydrogel model and investigate how matrix stiffness and HGF regulate triple-negative breast cancer (TNBC) invasion and associated signaling pathways.

Methodology: Hybrid hydrogels composed of collagen (3 mg/mL) and alginate (5 mg/mL) were fabricated, and stiffness was tuned by varying $CaCl_2$ concentration (5 or 30 mM), which crosslinks alginate while maintaining constant matrix composition. Hydrogels were characterized by atomic force microscopy (AFM) and scanning electron microscopy (SEM). SUM159 TNBC spheroids were encapsulated alone, with normal human mammary fibroblasts (HMFs), or with HGF-expressing HMFs with or without crizotinib, a MET inhibitor. Invasion was quantified from confocal images, and signaling pathways were evaluated by RT-qPCR and Western blotting.

Results: AFM confirmed soft (~0.5 kPa, 5 mM $CaCl_2$) and stiff (~7 kPa, 30 mM $CaCl_2$) hydrogels spanning the stiffness range of breast tumors. SEM images showed reduced and more uniform pore size in stiffer hydrogels. Increased matrix stiffness significantly promoted TNBC spheroid invasion and was associated with a reduced p-YAP/t-YAP ratio, increased vimentin and N-cadherin expression, and upregulation of invasion and matrix remodeling-associated genes (CTGF, FN1, ITGA5, ITGB1, MMP9, and LOX). Co-culture with normal HMFs reduced spheroid invasion relative to tumor-only controls, whereas HGF-expressing HMFs induced the greatest invasive response. Western blot analysis revealed MET phosphorylation exclusively in HGF-expressing HMF conditions, accompanied by activation of downstream ERK signaling. Crizotinib significantly reduced invasion and inhibited MET and ERK phosphorylation, confirming involvement of the HGF–MET signaling axis in regulating TNBC invasion.

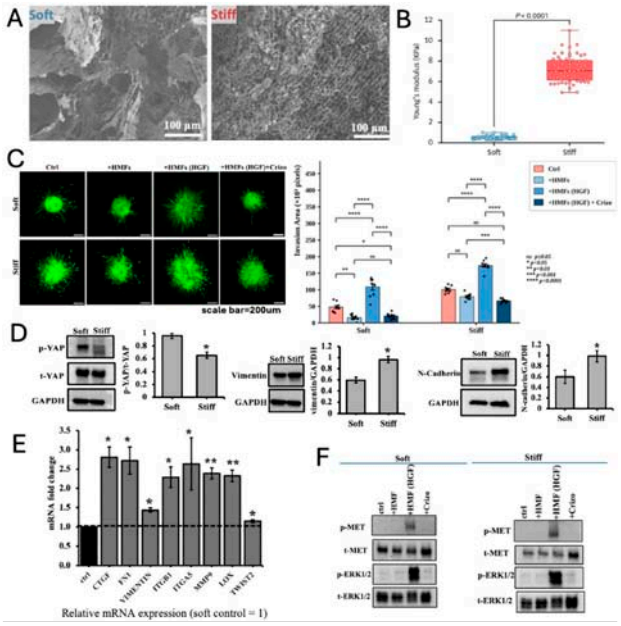


Figure: (A–B) Hydrogel characterization. (C) TNBC invasion. (D–F) Molecular analysis by Western blot and RT-qPCR.

Conclusion/Significance: Increased matrix stiffness and HGF signaling enhanced TNBC invasiveness through distinct mechanotransduction and MET/ERK signaling mechanisms. This tunable collagen–alginate hydrogel platform enables independent control of mechanical and biochemical cues, providing a controlled system for investigating breast cancer progression and evaluating targeted therapeutic strategies.

OP-039 - Electrical Stimulation Device for Soft Material Platforms with Electrically Conductive Additives and its Effects on Schwann Cell Morphology and Functions

Kylie Schmitz[1], Michael Borovich[2], Geyou Ao[1], Megan Jack[3,4], Liqun Ning[2]

[1]*Cleveland State University, Chemical and Biomedical Engineering, Cleveland, United States of America*
[2]*Cleveland State University, Mechanical Engineering, Cleveland, United States of America*
[3]*Cleveland Clinic, Neurosurgery, Cleveland, United States of America*
[4]*Lerner Research Institute, Cleveland Clinic, Neurosciences, Cleveland, United States of America*

Purpose/Objectives: Peripheral nerve (PN) injuries affect millions, leading to pain, loss of sensory and motor function, and reduced quality of life. Electrical stimulation (ES) has been explored as a therapeutic technique in PN injuries to improve regeneration and function of the repaired nerve. However, in vitro ES studies often require expensive, highly specialized equipment, which can limit the accessibility of related research. Additionally, while numerous studies have investigated the effects of ES on nerve regeneration, the direct effects of some electrically conductive additives, in conjunction with ES, on neural cell functions are not fully understood.

Methodology: In this study, we developed and verified cost-effective electrical impedance spectroscopy (EIS) and ES setups, which can be utilized in sterile conditions for in vitro therapeutic studies on soft substrates. In addition, we performed ES experiments on electrically conductive hydrogel substrates to determine the impact of ES on Schwann cells (SCs), a major neural cell type involved in PN regeneration after injury. SC alignment and protein expression were quantified via immunostaining to determine cell morphology and functions using different electrically conductive additives with and without ES.

Results: The novel EIS and ES systems allowed for in vitro assessments of SC behavior on hydrogel-based substrates without cell disruption or sample damage. Gelatin methacrylate (gelMA)-based substrates with electrically conductive additives provided platforms for enhanced SC activity, with specific cell functions depending on the additive used. DNA-wrapped single-walled carbon nanotubes (SWCNTs) led to aligned SC networks when ES was applied, mimicking the bands of Büngner, which are present in the native regenerating nerve environment. However, incorporating poly(3,4-ethylenedioxythiophene) polystyrene sulfonate (PEDOT:PSS) in conjunction with ES led to increased S100β expression in SCs without significantly impacting alignment.

Conclusion/Significance: This study provides a novel platform for in vitro EIS and ES experiments, enabling more cost-effective studies in tissue engineering and regenerative medicine applications. By evaluating the effects of ES on SCs seeded on multiple gelMA-based substrates, it was found that the specific changes in cell behavior are highly dependent on the additive type. Thus, electrically conductive additives should be carefully selected based on the desired outcomes of scaffolds in the context of PN regeneration.

OP-041 - Collagen-mediated cell-matrix interaction modifies TGFβ1-induced nucleation of SMAD3 in primary human vaginal fibroblasts

Joshua Montano[1], Rikki Rooklin[2], Amanda Artsen[3], Pamela Moalli[3,4]

[1]*University of Pittsburgh School of Medicine, Department of Pharmacology and Chemical Biology, Lothrop St, United States of America*
[2]*University of Pittsburgh, Bioengineering, Pittsburgh, United States of America*
[3]*Magee Womens Research Institute, Pittsburgh, United States of America*
[4]*University of Pittsburgh, Obgyn, Pittsburgh, United States of America*

Purpose/Objectives: Mechanoregulation of the TGF-β1/SMAD3 signaling pathway has been defined in dermal and renal fibroblasts but remains poorly understood in the human vagina. Defining mechanotransduction pathways in human vaginal fibroblasts (HVFs) is highly relevant to vaginal wound healing, fibrosis, biomaterial integration, and the development of regenerative therapies for pelvic reconstructive surgery. We hypothesized that substrate mechanics modulate TGF-β1 signaling through ROCK-dependent regulation of SMAD3 intracellular trafficking.

Methodology: Primary HVFs were cultured on glass or collagen-coated substrates and stimulated with TGF-β1 in the presence or absence of ROCK inhibitor Y-27632 (ROCKi). SMAD3 localization was quantified using immunofluorescent imaging and image analysis to assess absolute nuclear SMAD3 localization (NuSMAD3) and % partition of nucleated SMAD3 over both nucleated and cytosolic compartments. Substrate-dependent differences in SMAD3 partitioning were compared across experimental conditions using one-way ANOVA to define the contribution of substrate mechanics and cytoskeletal tension to TGF-β1 mechanotransduction.

Results: TGF-β1 stimulation increased NuSMAD3 on both substrates, consistent with profibrotic signaling. ROCK inhibition significantly reduced NuSMAD3 on both glass and collagen, supporting a role for ROCK-mediated cytoskeletal tension in NuSMAD3. However, substrate-dependent differences emerged in intracellular SMAD3 partitioning. On glass, ROCK inhibition reduced the nucleated SMAD3 %, whereas on collagen-coated substrates the nucleated SMAD3 % paradoxically increased despite reduced NuSMAD3. These findings suggest that collagen-mediated cell–matrix interactions alter cytoplasmic SMAD3 retention or trafficking, independent of ROCK-dependent mechanotransduction. Collectively, the data indicates that substrate mechanics influence TGF-β1 signaling both through regulation of nuclear translocation and sequestration of intracellular SMAD3. Fig 1. Confocal imaging of SMAD3 nucleation in HVFs. Fig 1a. Merge overlay of SMAD3 (FITC), vimentin (Cy5), and Hoechst stain (DAPI) and SMAD3. Fig 1b. Quantification of mean fluorescent intensity of the FITC channel across culture and treatment conditions.

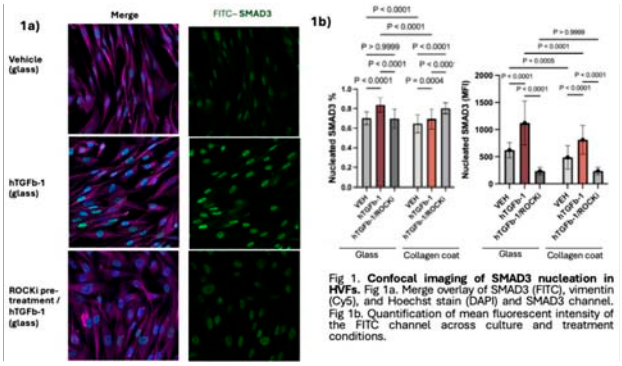


Fig 1. **Confocal imaging of SMAD3 nucleation in HVFs.** Fig 1a. Merge overlay of SMAD3 (FITC), vimentin (Cy5), and Hoechst stain (DAPI) and SMAD3 channel. Fig 1b. Quantification of mean fluorescent intensity of the FITC channel across culture and treatment conditions.

Conclusion/Significance: TGF-β1-induced SMAD3 signaling in HVFs is strongly influenced by substrate mechanics. While ROCK-mediated cytoskeletal tension contributes to SMAD3 nuclear localization, collagen-coated substrates partially preserve SMAD3 nuclear partitioning despite ROCK inhibition, suggesting the presence of compensatory matrix-dependent signaling mechanisms. These findings identify cell-matrix interaction as an important regulator of vaginal fibroblast mechanotransduction, providing new insight into pathways that contribute to fibrosis and biomaterial response in the female pelvic floor.

OP-042 - Degradation-related geometrical changes in 3D-printed PLGA microsphere scaffolds enhance spontaneous osteogenesis

Roland Klar[1], James Cox[2], Naren Raja[2], Houssam Bouloussa[3], Stefan Lohfeld[2]

[1]*University of the Witwatersrand, School of Clinical Medicine, Department of Internal Medicine, Johannesburg, Gauteng, South Africa*
[2]*University of Missouri-Kansas City School of Dentistry, Oral and Craniofacial Sciences, Kansas City, United States of America*

[3]*University of Missouri-Kansas City, School of Medicine, Orthopedic Surgery, Kansas City, United States of America*

Purpose/Objectives: Microsphere-based scaffolds are increasingly investigated in tissue engineering because of their capacity to generate controlled micro- and macroporous architectures. Previously, we demonstrated that 3D-printed poly(lactic-co-glycolic acid) (PLGA) microsphere scaffolds induced spontaneous de novo bone formation within a murine calvarial model without the addition of exogenous osteogenic growth factors. Larger microspheres supported superior osteogenesis, suggesting that scaffold geometry and degradation-associated topographical changes may play an important role in the induction process. The aim of the present study was therefore to determine whether 300 μm diameter PLGA microsphere scaffolds further enhance bone formation and whether degradation-induced geometrical alterations may contribute to the observed osteoinductive response.

Methodology: PLGA microspheres with an average diameter of 300 μm were generated using a Büchi Encapsulator system and processed into scaffolds utilizing the 3D-MultiCompositional Microsphere-Adaptive Printing (3D-McMap) technique. Scaffolds were implanted into critical-sized calvarial defects in TOPGAL mice and compared to previously generated 200 μm microsphere scaffolds. Bone formation was evaluated longitudinally by in vivo micro-computed tomography (μCT) over 60 days. In parallel, microsphere degradation behavior and associated topographical alterations were assessed in vitro over the same time period.

Results: The 300 μm PLGA microsphere scaffolds induced significantly greater bone formation than the previously investigated 200 μm scaffolds. In vitro degradation analyses demonstrated progressive geometrical alterations of the microsphere surfaces, including concavity-like indentations and topographical restructuring during hydrolytic degradation. These degradation-associated architectural changes temporally corresponded with increasing osteogenesis observed within the implantation sites. The findings suggest that degradation-mediated topographical modifications may contribute to the spontaneous osteoinductive response by generating dynamic geometrical and mechanical cues within the scaffold microenvironment.

Conclusion/Significance: The present study further supports the concept that scaffold geometry and degradation-associated topographical evolution are important contributors to osteogenic tissue responses. The results indicate that microsphere-based PLGA scaffolds may generate intrinsic architectural cues capable of supporting spontaneous bone formation without exogenous bioactive factor supplementation. These findings highlight the importance of temporospatial scaffold design and degradation behavior in regenerative biomaterial strategies for bone tissue engineering.

Session 17
Biofabrication of Spatial Gradients and Complex Interfaces

11-16-2026 @ 8:00 AM - 9:30 AM

OP-046 - Hybrid Biofabrication Approach for Engineering Spatially Graded Tissue Constructs

Marco Domingos, Stephen Richardson, Fraser Shields

The University of Manchester, Manchester, United Kingdom

Purpose/Objectives: The meniscus is a spatially heterogeneous fibrocartilaginous tissue with region-specific structural, mechanical and biological properties essential for joint function. Current repair strategies fail to restore this complexity, often leading to degeneration and osteoarthritis (OA). A major challenge in meniscus tissue engineering is the recreation of spatial gradients and functional interfaces. This study aims to develop a hybrid biofabrication approach combining melt electrowriting (MEW) and microvalve-based inkjet bioprinting to engineer meniscus constructs with controlled architectural, mechanical, and cellular gradients.

Methodology: MEW was used to fabricate aligned polycaprolactone (PCL) microfibre scaffolds with tunable geometries, forming microchamber networks. Process parameters were optimised using a design of experiments (DoE) approach to control fibre diameter and spacing. Microvalve bioprinting enabled precise deposition of alginate-based bioinks containing human mesenchymal stem cells (MSCs) within these microchambers, allowing spatial patterning of cellular gradients. Hybrid constructs with varying fibre architectures were cultured under chondrogenic conditions, with and without dynamic mechanical stimulation. Scaffold morphology, mechanical properties, and cell viability were assessed using SEM, mechanical testing, and fluorescence imaging. Matrix formation and differentiation were evaluated via qPCR, histology, immunohistochemistry, and biochemical assays.

Results: MEW enabled the fabrication of highly organised fibre architectures with controllable microchamber dimensions, directly influencing scaffold biomechanical response. Bioprinting enabled precise spatial deposition of bioinks with high cell viability, resulting in the formation of defined cellular gradients. Scaffold architecture had a dominant effect on chondrogenesis; constructs with larger microchamber spacing (800 μm) under static conditions exhibited enhanced chondrogenesis, likely driven by scaffold contraction over time, which increased local cell density and provided mechanical feedback to encapsulated cells. In contrast, dynamic mechanical stimulation reduced chondrogenic differentiation while increasing scaffold stiffness.

Conclusion/Significance: This study introduces a hybrid biofabrication platform for engineering functionally graded meniscus constructs with controlled spatial organisation. By integrating MEW and inkjet bioprinting, both mechanical and biological gradients can be tailored to guide tissue development. Importantly, scaffold architecture and cell-matrix interactions were found to play a dominant role in regulating chondrogenesis, outweighing the effects of mechanical stimulation. This approach provides a promising strategy for meniscus regeneration and offers a broader platform for engineering complex tissues with hierarchical organisation and spatial heterogeneity.

OP-047 - 3D Bioprinted PAH Vascular Platform Reveals Altered Mechanosensing in BMPR2 Deficiency

Naghmeh Abbasi[1,2], Yi-Yin Tai[2], Poorya Esmaili Bambizi[3], Antonio Pereiratavares[2,4], Sara Trbojevic[5], Vinay Abhyankar[3], Stephen Y Chan[1,2], Daniel Shiwarski[1,2,6]

[1]*University of Pittsburgh, Department of Medicine, Pittsburgh, United States of America*
[2]*Vascular Medicine Institute, University of Pittsburgh Medical Centre, Pittsburgh, United States of America*
[3]*Rochester Institute of Technology, Department of Biomedical Engineering, Rochester, United States of America*
[4]*University of Pittsburgh, Department of Bioengineering, Pittsburgh, United States of America*
[5]*Center for Craniofacial Regeneration, University of Pittsburgh, Dentistry, Pittsburgh, United States of America*
[6]*Department of Bioengineering, University of Pittsburgh, Department of Bioengineering, Pittsburgh, United States of America*

Purpose/Objectives: Pulmonary arterial hypertension (PAH) is characterized by extracellular matrix remodeling, arterial stiffening, and dysregulated mechanotransduction that collectively drive vascular remodeling. Although BMPR2 dysfunction and matrix stiffening are established contributors, current in vitro models fail to recapitulate the spatial mechanical heterogeneity and architectural remodeling of diseased pulmonary arteries. This study aimed to engineer a biomimetic vascular platform reproducing localized stiffness gradients, structural anisotropy, and PAH-relevant mechanobiological responses.

Methodology: A stereolithography-based multi-material bioprinting strategy was developed using GelMA–PEGDA hydrogels combined with grayscale photomask-guided DLP to generate scaffolds with tunable stiffness heterogeneity and aligned microarchitectures. Mechanical properties were systematically tuned via methacrylation degree, photoinitiator concentration, grayscale exposure, and PEGDA reinforcement. Spatially patterned stiffness gradients within the scaffolds were confirmed using nanoindentation measurements. Healthy pulmonary arterial smooth muscle cells (PASMCs) and BMPR2 knockdown PASMCs were cultured on seven mechanically

distinct scaffold groups to investigate YAP1-mediated mechanotransduction responses.

Results: The engineered constructs exhibited controlled stiffness gradients ranging from healthy-like (~4–5 kPa) to PAH-like (~15–28 kPa) conditions while maintaining high print fidelity (Figure 1A-C). Healthy PASMCs responded primarily to bulk stiffness, showing pronounced YAP1 nuclear translocation in uniformly stiff scaffolds (Figure 1D). In contrast, BMPR2-deficient PASMCs exhibited enhanced sensitivity to spatial mechanical heterogeneity and microarchitectural cues (Figure 1D). Grayscale-patterned heterogeneous scaffolds significantly increased YAP1 nuclear localization and upregulated mechanosensitive genes including CYR61 and CTGF compared with homogeneous constructs (Figure 1D). Spatial mapping further demonstrated region-dependent YAP activation governed by local stiffness distribution, scaffold geometry, and alignment (Figure 1D).

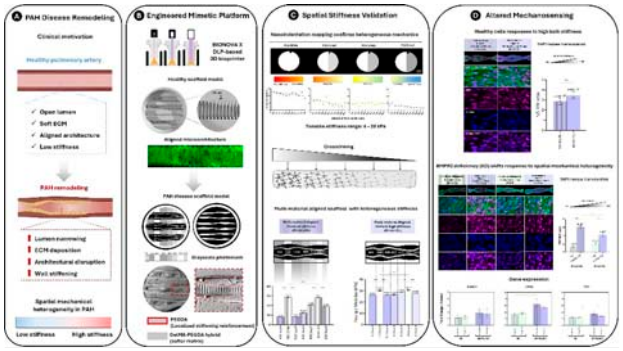


Figure 1. Multi-material bioprinted vascular platform for PAH modeling: (A) schematic of vascular remodeling in healthy vs PAH; (B) GelMA–PEGDA DLP bioprinting workflow with grayscale patterning; (C) nanoindentation-based stiffness mapping of heterogeneous scaffolds; (D) YAP1 localization and mechanosensitive gene expression in healthy and BMPR2-deficient PASMCs cultured on mechanically distinct scaffolds.

Conclusion/Significance: Overall, this platform integrates multi-material bioprinting, grayscale-mediated stiffness patterning, and BMPR2 deficiency to model PAH mechanobiology in a single system. These findings reveal that BMPR2 loss shifts mechanosensing from global stiffness perception toward spatially resolved mechanical microenvironments, providing mechanistic insight into PAH progression and enabling a scalable platform for disease modeling and therapeutic screening.

OP-048 - Establishing Intercellular Spatial Gradients via Dynamic Nanopore Microfluidic Targeted Electroporation for In Situ Disease Models

Emily Mccorkle, Cheyenne Meeks, Claire Oshima, Albert Liu, Sasha Cai Lesher-Pérez

University of Michigan, Ann Arbor, United States of America

Purpose/Objectives: A hallmark of various diseases, such as cardiovascular arrhythmias, cancer, and neurogenerative disorders is heterogeneously dysregulated gene expression in a subpopulation of cells. While current methods can build heterogeneous cell populations to model these diseases, they largely require that cellular modifications occur first before tissue construction, taking a "transfection-then pattern" approach. However, this process does not emulate pathophysiological progression that usually affects a subpopulation within a tissue. Additionally, subsequent cellular modifications are difficult in predetermined methods. Our work addresses these limitations by developing a new dynamic spatiotemporal transfection method for *in situ* tissue modification that uses nanopore electroporation (NanoEP). NanoEP utilizes an insulated nanoporous substrate, which localizes an electric field to temporarily open pores along the cell membrane in contact with the substrate to deliver macromolecules into cells. By developing a microfluidic system integrated with NanoEP, we established a technology platform, **Dy**namic **Na**nopore **Mi**crofluidic **T**argeted **E**lectroporation (DyNaMiTE), to create bespoke tissues through controlled patterning of the transfection cargo delivery.

Methodology: The DyNaMiTE system consists of a five-layered microfluidic device made from polydimethylsiloxane (PDMS) with the middle three layers containing cells, a nanoporous polycarbonate track-etched substrate, and a cargo delivery solution that are sandwiched between the top and bottom indium tin oxide-based electrodes (**Fig 1a**). Parallel flow streams of distinct cargoes are inputted in the bottom channel in the simplest configuration (y-channel). By leveraging the size scale and fluid characteristics of a low Reynolds number (laminar flow) and a high Peclet number (minimal diffusion), discrete and predictable spatial patterns can be generated.

Results: We used fluorescently labelled proteins, bovine serum albumin (BSA) Alexa Fluor™ 488 and 647, to characterize the flow dependency of patterned transfection into HT1080 cells during NanoEP at 20 V, 20 Hz, 1 ms pulse widths for 10 s (**Fig 1b**). By increasing the flow rate, we showed an increase in the intercellular fluorescence gradient steepness.

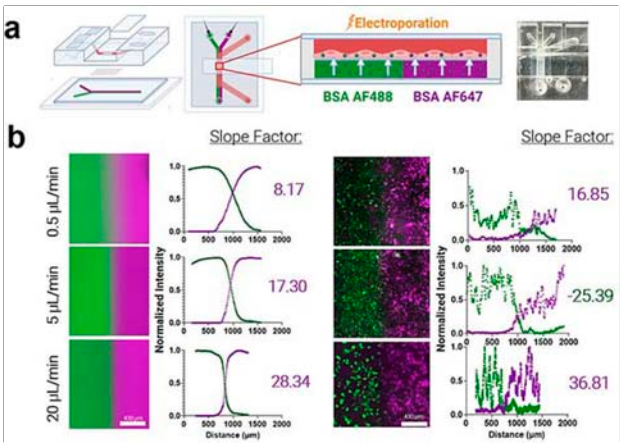


Fig 1. a) Schematic of and fully fabricated dynamic device for active flow in NanoEP. **b)** Line profiles of fluorescence intensity for cargo and cell population.

Conclusion/Significance: This characterization of DyNaMiTE has laid the foundation for gene and other cargo delivery for functional tissue modification.

OP-049 - Developing 3D extrusion bioprinted models with dynamic stiffness gradients to probe hematopoietic stem cell behavior

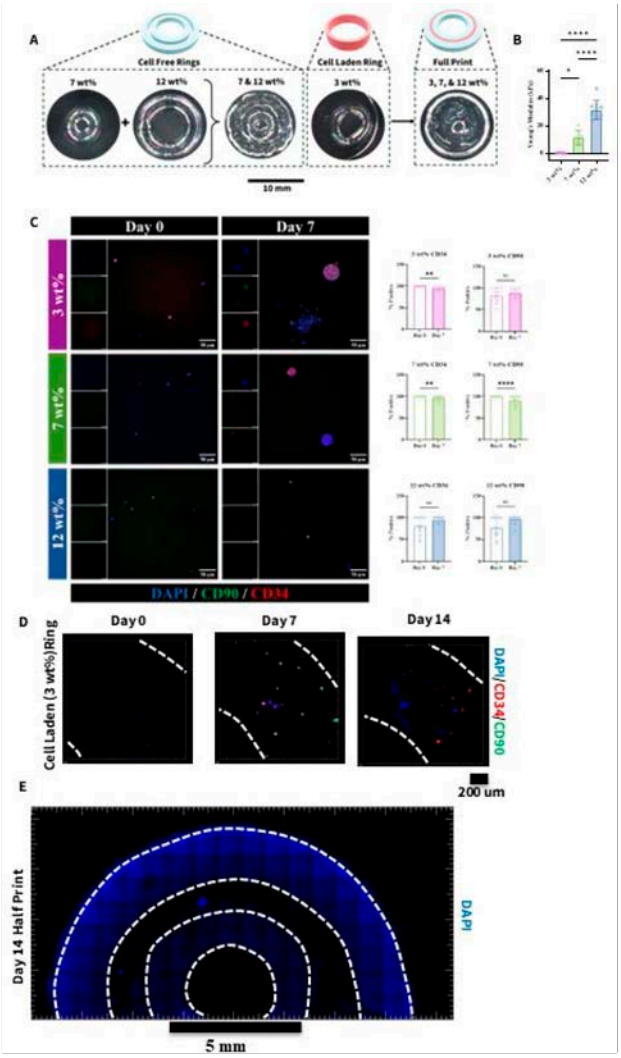
Deshea Chasko[1], Patrick Hall[1], Salem Bassi[1], Paul Dalton[1], Luiz Bertassoni[2], Gabriella Lindberg[1]

[1]*University of Oregon, Department of Bioengineering, Phil And Penny Knight Campus for Accelerating Scientific Impact, Eugene, United States of America*
[2]*Oregon Health and Science University, Department of Biomedical Engineering, Portland, United States of America*

Purpose/Objectives: CD34+ hematopoietic stem cell (HSC) transplants are a life-saving treatment for hematological malignancies. However, obtaining sufficient HSCs from patient bone marrow (BM) remains a major clinical challenge. Native BM contains spatially heterogenous stiffness niches, including endosteal (>35kPa), perivascular (2-20kPa), and central (0.1-1kPa) regions that regulate HSC fate. Despite this, the role of BM stiffness gradients on HSC behavior remains poorly understood due to the predominance of 2D systems and lack of biofabricated models capable of recapitulating BM complexity. Our objective is to develop 3D bioprinted BM models with tunable stiffnesses to investigate stiffness-dependent changes on HSC fate.

Methodology: Gelatin methacryloyl (GelMA) hydrogels at 3, 7, and 12wt% were fabricated and characterized using photorheology, sol fraction, and compressive loading. Cell viability, DNA content, and morphology of HSCs were assessed for up to 14 days, while immunohistochemistry (IHC) evaluated percentage positive of HSC markers (CD34, CD90, CD38, and CD44).

Results: Mechanical characterization demonstrated tunable hydrogel properties, with storage modulus increasing from 48±12 Pa (3wt%) to 13,539±1,284 Pa (12wt%) and mesh size decreasing as wt% increased. Young's Moduli recapitulated native central (0.16±0.5236kPa), perivascular (11.08±5.253kPa), and endosteal (31.48±6.868kPa) niches. HSC viability was initially high across all conditions (>83%, day 0), but significantly decreased in stiffer hydrogels (51%, 12wt%). DNA quantification revealed a ∼6.6 fold increase in the 3wt% condition, with a decrease in the 12wt%. IHC demonstrated time-dependent reductions in percentage of cells expressing CD34 and CD90 across 3 and 7wt%. Softer matrices promoted HSC clustering and expansion, while stiffer matrices resulted in dispersed morphology and increased cell death. **Fig.1:** A. Process for printing BM models. B. Young's Moduli. C. IHC staining of DAPI, CD34, and CD90 with percentage positive cells of each condition. D. IHC of cell laden bioprinted ring. E. DAPI staining of HSCs in the bioprinted construct.



Conclusion/Significance: Stiffness regulates HSC survival, proliferation, and morphology, with softer matrices supporting HSC expansion and clustering behavior. 3D bioprinting enables spatial control of physiologically relevant BM stiffnesses and provides a versatile tool for investigating HSC behavior. This approach will improve our understanding of HSC behavior in the BM and inform strategies of *ex vivo*expansion and personalized therapies.

Session 18
From in Silico Design to Precision Recovery: AI and Biofabrication in Tissue Regeneration

11-16-2026 @ 1:30 PM - 3:00 PM

OP-052 - AI-Driven Closed Loop Control of Cell Concentration Gradients in Bioprinted Tissues

Giannka Picache[1], Ferdows Afghah[1], Giovanni Zanderigo[2], Ritu Raman[3,4]

[1]*Massachusetts Institute of Technology, Cambridge, United States of America*
[2]*Politecnico di Milano, Milano, Italy*
[3]*MIT, Mechanical Engineering, Boston, United States of America*
[4]*Massachusetts Institute of Technology, Mechanical Engineering, Cambridge, United States of America*

Purpose/Objectives: 3D extrusion bioprinting aims to generate patient-specific tissues, but the same print file rarely produces the same printed tissue twice. Bioink extrudability changes with small environmental variations in temperature and humidity, yielding inconsistent filament geometries. Cells settle within bioinks during long duration prints, causing cell distribution to vary within the filament and between consecutive layers *(Figure 1A).* Regional differences in cell density gradients in printed tissues can have a significant negative impact on cell viability, differentiation capacity, and function. Pre-print calibration of bioinks cannot address this problem because extrusion variability evolves over time.

Methodology: We have previously demonstrated that in-situ imaging of bioprinted tissues enables adapting print parameters (pressure, velocity) to control filament geometry, but these methods do not monitor cell distribution within prints. Here, we present an in-situ computer vision-based closed-loop printing platform that monitors cell distribution in real-time during biomaterial extrusion and automatically adjusts mixing speed to ensure uniform cell distribution within a print *(Figure 1B).*

Results: C2C12 myoblasts in various bioinks were extruded into a support bath on a commercially available and open-source bioprinter, fitted with a compact low-cost USB microscope aimed at the deposition zone *(Figure 1C).* A real-time video processing pipeline counted, located, and quantified distribution of cells within a printed filament *(Figure 1D).* The coefficient of variation (CoV), a metric used to quantify cell uniformity and distribution, was used as the error signal for a PID/Bang-Bang controller driving an in-situ bioink mixing device. We compared prints with mixing held constant (open-loop) against prints with active mixing (closed-loop) and tracked per-frame CoV throughout. Results demonstrated that closed-loop control increased the overall cellular homogeneity and viability of the printed tissue.

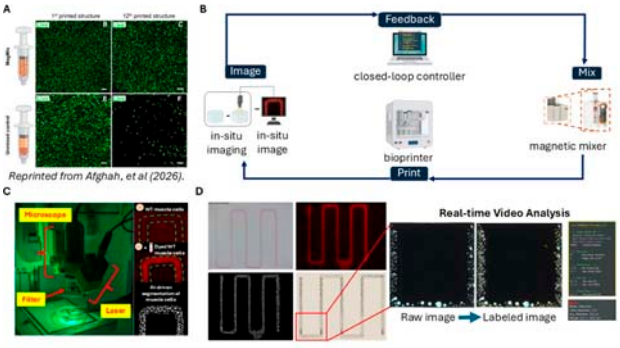


Figure 1. A) Mixed and unmixed bioprints show decreasing homogeneity over time. B) Closed loop control integrated with in-situ monitoring and active mixing. C) Fluorescent monitoring system, C2C12 imaging, and AI thresholding. D) Multimodal filament imaging and cell density video analysis pipeline.

Conclusion/Significance: Closing the loop with a relatively affordable microscope and open-source computer vision pipeline removes one of the largest sources of print-to-print variability in extrusion bioprinting, enabling future applications in disease modeling and regenerative medicine.

OP-053 - Multimodal Deep Learning for Cross-Species Assessment of Skeletal Muscle Injury: Integrating Histological Imaging with Quantitative Morphometric Features

Isaac Nkrumah[1], Amelia Ridolfo[2], Carlos Alejandro Formoso Godoy[2], Koyal Garg[2], Jie Hou[3]

[1]*Saint Louis University, Computer Science, Saint Louis, United States of America*
[2]*Saint Louis University, Biomedical Engineering, Saint Louis, United States of America*
[3]*Michigan State University, Computational Mathematics, Science And Engineering, East Lansing, United States of America*

Purpose/Objectives: Accurate assessment of skeletal muscle injury remains a significant challenge in clinical practice, as current histological evaluation methods are largely manual, subjective, and difficult to standardize across institutions. Quantitative morphometric measures, such as myofiber cross-sectional area (CSA) and fiber count, are established indicators of muscle health; however, they are rarely integrated into automated classification pipelines in a principled manner. This work aims to develop a unified deep learning framework that combines histological image analysis with quantitative morphometric features to enable objective, standardized, and scalable assessment of muscle injury status.

Methodology: We present a multimodal deep learning framework that combines patch-level histological image analysis with slide-level morphometric features, specifically average myofiber CSA and fiber count, to classify muscle injury status across multiple tasks: uninjured vs. injured tissue, poor vs. very poor recovery outcomes, and multiclass classification of uninjured, poor, and very poor states. A ResNet backbone extracts spatial features from image patches, while a lightweight multilayer perceptron (MLP) projects morphometric measurements into a shared embedding space. The two representations are fused through late feature concatenation and passed to a classification head, enabling the model to jointly leverage tissue appearance and structural morphometry. The model was trained on whole slide images (WSIs) from a rodent Volumetric Muscle Loss (VML) model and subsequently applied, without retraining, to human muscle biopsies from patients following anterior cruciate ligament reconstruction (ACLR), directly evaluating cross-species generalizability. Patch-level predictions were aggregated to the WSI level and evaluated using accuracy, F1-score, and ROC-AUC metrics.

Results: Preliminary results demonstrate that integrating morphometric features with image-based representations improves classification performance compared to image-only approaches across the evaluated tasks (uninjured vs. injured, poor vs. very poor recovery, and multiclass classification). Furthermore, models trained on rat tissue data demonstrated the ability to generalize to human tissue without retraining, retaining meaningful discriminative capability across species when applied to ACLR patient biopsies.

Conclusion/Significance: This work establishes a scalable and translatable framework for objective muscle health assessment, demonstrating that the principled fusion of histological imagery and quantitative morphometry enhances classification performance while supporting cross-species generalization. The framework has potential applications in muscle injury evaluation, recovery monitoring, and regenerative medicine.

Session 19
Fetal and Pediatric Tissue Engineering and Regenerative Medicine

11-16-2026 @ 1:30 PM - 3:00 PM

OP-056 - Aligning Predicted Biological Dysregulation with Tendon Material Property Deficits Following Fetal Immobility

Ivy Vien[1], Aniket Jana[1], Paige Ruschke[1], Chia-Lung Wu[2], Catherine Kuo[1,3]

[1]*University of Maryland, Fischell Department of Bioengineering, College Park, United States of America*
[2]*University of Rochester, Department of Orthopaedics and Rehabilitation, Rochester, United States of America*
[3]*University of Maryland, Department of Orthopaedics, Baltimore, United States of America*

Purpose/Objectives: Fetal immobility is associated with common and debilitating musculoskeletal birth disorders (e.g., clubfoot, arthrogryposis), affecting up to 1 in 100 live births. Current surgical and physical therapeutic approaches, which manipulate joints into more normal positions, are associated with high recurrence rates of deformity due to persistently abnormal tendon material properties. Here, we hypothesized that fetal immobility dysregulates extracellular matrix composition and organization that contribute to tendon material properties. Our goal is to determine potential mechanisms by which immobility alters tendon formation, to inform development of therapies that restore tendon material properties.

Methodology: Flaccid and rigid immobility were induced in chick embryos from days(d) 13-17 (vehicle treatments for normal). At d17, Achilles tendons were harvested for tensile testing, RNA-sequencing, histology (picrosirius red/Alcian blue/Mallory's trichrome staining with brightfield or polarized microscopy), and cell adhesion assays. One-way ANOVA with Tukey's post hoc analyzed differences between groups. DESeq2 determined differentially expressed genes (DEGs) (|log2-fold-change|≥1, FDR<0.05). DAVID was used for gene ontology (GO) analysis.

Results: Immobility inhibited elastic modulus and ultimate strength (**Fig. 1a**), but not ultimate strain. Flaccid and rigid immobility similarly dysregulated 251 genes and 168 biological processes (**Fig. 1b**). Surprisingly, collagen content, organization, and maturity (**Fig. 1c**) were not affected by immobility despite altered collagen-related GO terms. Although 'chondrocyte differentiation' was upregulated, glycosaminoglycan content was unaffected, suggesting lack of chondrogenesis (**Fig. 1d**). Blood vessel density was higher with immobility (**Fig. 1e**), which was interesting considering 'negative regulation of vasculature development' was upregulated. Immobility also dysregulated genes associated with stress fibers, which regulate focal adhesions. Interestingly, immobility appeared to lead to more adherent cells.

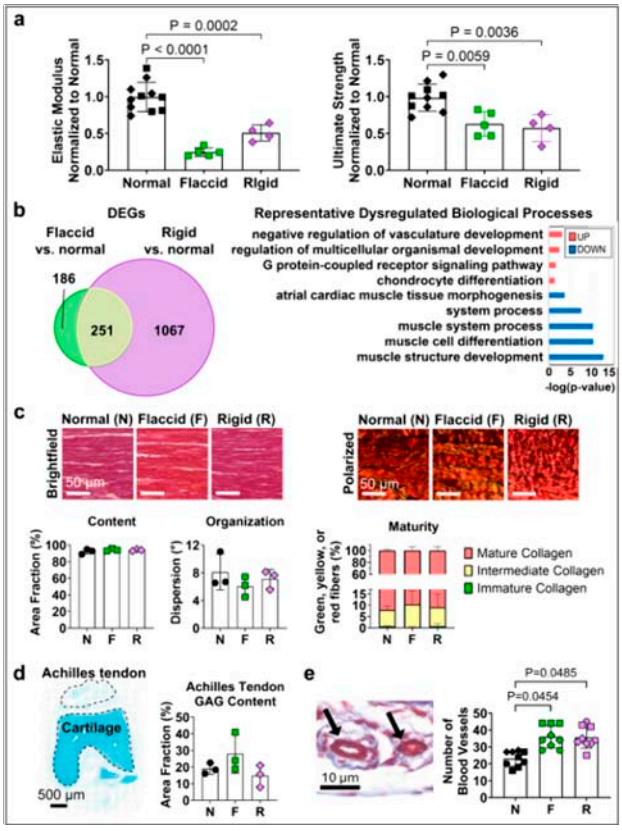


Fig. 1: a) Tendon elastic modulus and ultimate strength. **b**) Number of DEGs and dysregulated biological processes with immobility. **c**) Collagen content, organization, and maturity analyzed in

picrosirius red-stained longitudinal sections. **d**) Glycosaminoglycan content analyzed in Alcian blue-stained transverse sections. **e**) Blood vessels in Mallory's trichrome-stained transverse sections. Mean±SD shown; p<0.05 considered significant.

Conclusion/Significance: Ongoing studies are building on these data to identify and validate specific mechanisms by which fetal immobility dysregulates tendon development, which could inform development of more effective therapies for abnormal tendons involved in musculoskeletal birth disorders.

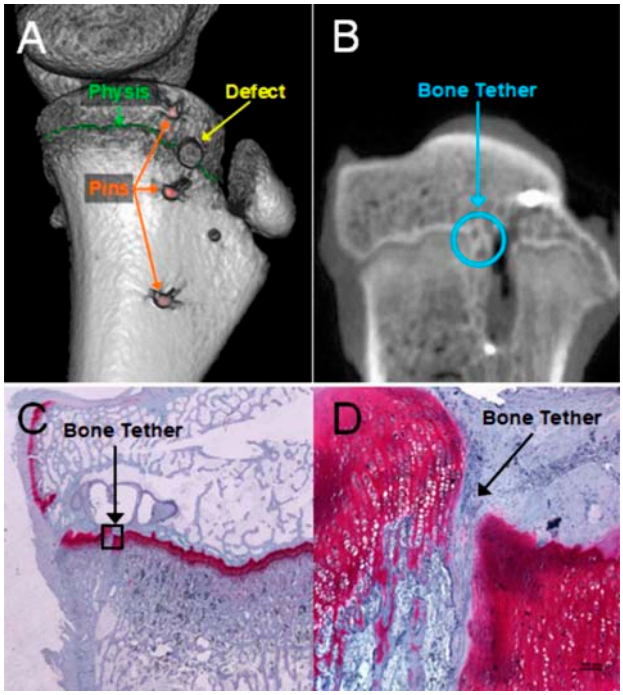
OP-114 - Treatment of Physeal Defects in Goats with an Anti-mineralizing Chondrogenic Interpositional Hydrogel

Juan Taboas[1], Jingming Chen[2]

[1]*University of Pittsburgh, Oral And Craniofacial Sciences, Pittsburgh, United States of America*
[2]*University of Pittsburgh, Biomedical Engineering, Pittsburgh, United States of America*

Purpose/Objectives: Growth plate (physeal) fracture is a common pediatric orthopedic injury (35% prevalence in 10 to 15-year-olds). Fractures that cross or crush the physis yield bone tethers across it that cause growth arrest, biomechanical problems, and predisposition to osteoarthritis. To restore growth, tethers are surgically excised and the void filled with interpositional materials to prevent tether reformation. Current materials are inadequate and have low success rates (15%-40%). We have developed a chondrogenic hydrogel (PGH) that inhibits osteogenesis by bone marrow-derived stromal cells (MSCs) and that inhibits mineralization by hypertrophic chondrocytes, reverting them to an anabolic chondrogenic state. Here, we investigated PGH as an interpositional material for physeal defects in juvenile goats.

Methodology: The PGH (8% w/v) was comprised of methacrylated gelatin, heparin, and poly(ethylene glycol) with photoinitiator and 10 ug/ml TGF-B1. Autologous MSCs were harvested from Spanish Boer goats (3-month-old females, n=8), expanded, and encapsulated at 30x10^6 cells/ml. Bilateral medio-lateral defects (n=16) were drilled into the proximal tibia. Three implants were tested: homogenous hydrogel as above (n=4), tri-layered hydrogel (parathyroid hormone at one edge and triiodothyronine opposite, n=9), and untreated controls (n=3). Fiduciary k-wires were inserted to track growth. After 3-months growth, terminal CTs and histochemical staining was used to determine percentages of fat and bone within the defect, amount of chondrogenesis in the hydrogel, the thickness and number of tethers spanning the physis, and disposition of the MSCs.



Results: The untreated defects contained more bone content (53±7.0%) compared to the tri-layered (18±12%, p=0.0125) and homogeneous (26±12%, p=0.09) treated defects, while the latter contained more fat (38±25% and 35±17%) than the untreated defects (3.6±3.62%). Defects primarily through the epiphysis showed significantly more fat (68±17%) compared to those through the physis (39±19%, p=0.0076) or the metaphysis (35±26%, p=0.0241). Tethers did not disrupt growth (no significant differences in number or thickness between treatments, Figure B-D).

Conclusion/Significance: The mineralization resistant PGH hydrogel decreased but did not prevent bone tether volume in physeal defects. Our novel model suggested surgical approaches creating greater void in the epiphysis may favor fat formation and decrease tether impact on growth. However, no feasible model exists with similar growth rates to humans.

Session 20
Development of Stimuli-Responsive Implants for Musculoskeletal Tissue Engineering

11-16-2026 @ 1:30 PM - 3:00 PM

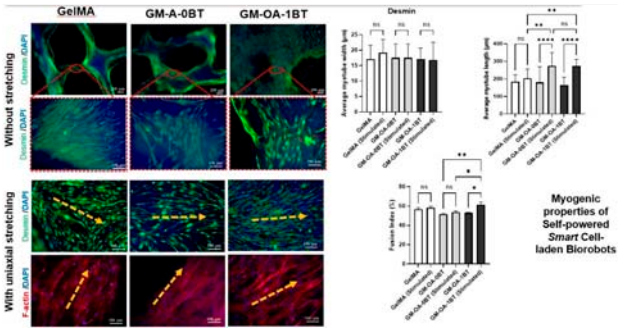
OP-057 - A Mechanoelectrically Instructive 4D Bioprinted Piezoelectric Platform for Skeletal Muscle Tissue Engineering

Prabaha Sikder, Surendrasingh Sonaye

Cleveland State University, Mechanical Engineering, Cleveland, United States of America

Purpose/Objectives: Volumetric muscle loss (VML) is a severe skeletal muscle injury in which extensive tissue loss overwhelms the body's intrinsic regenerative capacity, and current treatment strategies remain inadequate for restoring fully functional muscle. While 3D bioprinted cell-laden scaffolds have shown promise for skeletal muscle tissue engineering, most constructs remain biologically static after fabrication and lack the ability to provide dynamic cues that regulate muscle development over time. The objective of this study was to develop a dynamic 4D bioprinted, cell-laden piezoelectric construct capable of generating localized mechanoelectrical cues through deformation-induced piezoelectricity to support skeletal muscle growth and maturation.

Methodology: GelMA–oxidized alginate (GM–OA) bioinks containing polyethylene glycol-modified barium titanate (BT) nanoparticles were formulated at varying concentrations to generate printable electroactive hydrogel composites. Rheological analyses were performed to assess viscoelasticity, shear-thinning behavior, and extrusion suitability. Printing parameters were optimized by varying temperature and speed to fabricate high-resolution constructs. Cell-free and cell-laden constructs were then bioprinted and crosslinked. Physicochemical characterization was conducted using FTIR and XRD, while scaffold morphology was evaluated by SEM. Swelling, degradation, compressive properties, and cyclic deformation-induced electrical output were measured to assess scaffold stability, biomechanics, and electroactivity. Cytocompatibility was evaluated using live/dead staining, confocal imaging, and Alamar Blue assays.



Results: The GM–OA–BT bioinks exhibited favorable viscoelasticity and strong shear-thinning behavior, enabling high-resolution

extrusion bioprinting of cell-laden constructs. FTIR and XRD confirmed successful incorporation and structural preservation of crystalline BT within the hydrogel network. BT addition improved scaffold stability by reducing swelling and slowing degradation, while intermediate BT loading provided the most favorable compressive properties within a range relevant to native skeletal muscle. Under cyclic compression, BT-containing scaffolds generated measurable voltage in a concentration-dependent manner, confirming deformation-induced piezoelectricity. Importantly, BT incorporation did not adversely affect cell viability or metabolic activity, and viable cells were distributed throughout the constructs.

Conclusion/Significance: These findings establish, to the best of our knowledge, the first 4D bioprinted cell-laden piezoelectric platform for skeletal muscle tissue engineering. This approach offers a new strategy for providing localized, wireless bioelectrical cues and holds promise for VML regeneration, in vitro muscle models, and pharmaceutical testing.

OP-058 - Multifunctional 3D-Printed Mesoporous Calcium-Aluminosilicate Scaffolds Enable Rapid Hemostasis and Heterogeneous Activation of Endogenous TGF-β1 for Bone Regeneration

Chun Xu

The University of Sydney, Sydney, Australia

Purpose/Objectives: Large bone defects remain difficult to treat because current biomaterials primarily provide structural support and often rely on exogenous growth factors to stimulate regeneration, which are associated with high costs, safety concerns, and limited clinical translation. We hypothesized that multifunctional mesoporous calcium-aluminosilicate nanoparticles (MCANs) can be engineered to simultaneously promote rapid hemostasis and activate endogenous latent TGF-β1 through nano-bio interfacial interactions, thereby initiating regenerative cascades without exogenous biologics. The objective of this study was to develop bioactive MCAN-based 3D-printed scaffolds and evaluate their ability to harness endogenous regenerative mechanisms to enhance bone repair in clinically relevant preclinical models.

Methodology: MCANs possessing hierarchical mesoporosity and tunable calcium-aluminosilicate compositions were synthesized and incorporated into extrusion-based 3D-printed porous scaffolds. Physicochemical properties, ion release profiles, blood-material interactions, and growth factor activation were characterized. Hemostatic performance and endogenous TGF-β1 activation were evaluated through coagulation assays, protein analyses, and cell-based mechanistic studies. Osteogenic activity was assessed using mesenchymal stromal cells, while regenerative efficacy was validated in clinically relevant preclinical bone defect models.

Results: The engineered scaffolds exhibited interconnected macroporous architectures suitable for tissue ingrowth while preserving the high surface area and bioactivity of MCANs. Upon implantation, the scaffolds rapidly initiated clot formation and stabilized the early wound environment. Mechanistically, MCANs induced heterogeneous activation of endogenous latent TGF-β1 through nano-bio interfacial interactions and controlled ionic dissolution, leading to activation of downstream Smad signaling pathways. This biomaterial-driven activation enhanced endogenous cell recruitment, osteogenic differentiation, matrix deposition, and vascularized tissue formation. Importantly, the 3D-printed scaffolds demonstrated robust bone regeneration in preclinical models, achieving accelerated defect bridging, enhanced bone volume, and superior tissue integration compared with current clinical benchmark materials.

Conclusion/Significance: We present a translational biomaterial strategy that combines advanced 3D printing with bioactive mesoporous calcium-aluminosilicate nanotechnology to harness the body's intrinsic regenerative potential. By integrating rapid hemostasis with localized activation of endogenous TGF-β1, these multifunctional scaffolds eliminate the need for exogenous growth factor delivery while promoting robust bone repair. This platform offers a clinically scalable approach for the treatment of large bone defects and represents a new paradigm for endogenous regenerative engineering.

OP-059 - Engineering a Stimuli-Responsive 3D-Printed Biomaterial for Localized, Proteolytic Enzyme-Triggered Delivery of Therapeutics

Chiebuka Okpara[1], Juliana Magarelli[1], Zachary Weiser[1], Josh Graham[1], E. Thomas Pashuck[1], Lesley Chow[1,2], Tomas Gonzalez Fernandez[1]

[1]*Lehigh University, Bioengineering, Bethlehem, United States of America*
[2]*Lehigh University, Materials Science And Engineering, Bethlehem, United States of America*

Purpose/Objectives: Osteoarthritis (OA) is characterized by recurrent flare-ups driven by fluctuating temporal profiles of proteolytic enzymes, which sustains inflammation-induced degradation of the cartilage matrix. Intra-articular injections of anti-inflammatory therapeutics (e.g. dexamethasone; Dex) can reduce inflammation, but typically results in rapid clearance and systemic biodistribution, leading to increased risk of tissue toxicity. Biomaterial-based technologies have therefore been developed for controlled, localized drug delivery. However, current scaffold-based delivery systems rely on passive release mechanisms, which lack the temporal precision needed to synchronize therapeutic action with OA flare-ups. To address this challenge, **our objectives are (1) to engineer an enzyme-responsive biomaterial that selectively releases a model drug in response to a proteolytic environment and (2) to verify bioactivity of a drug-peptide conjugate.**

Methodology: *Biomaterial fabrication*: Cyanine-3 (Cy3) (model drug) tethered to an enzyme-sensitive peptide (Cy3-KRVKR-RLLMETGGGC) was synthesized using solid-phase peptide synthesis techniques and reacted with poly(caprolactone) (PCL) diol and *p*-Maleimidophenyl isocyanate to produce Cy3-conjugate. Inks containing PCL and Cy3-conjugate in hexafluoroisopropanol were solvent-cast 3D-printed into scaffolds. *Release kinetics*: Scaffolds were incubated in a collagenase solution for 10 days. Cy3 release was quantified by measuring fluorescence of the solution. *Cell culture*: Dex was tethered to the cleaved fragment of the enzyme-sensitive peptide (Dex-KRVKRRL; Dex-pep) to assess bioactivity of the modified Dex. MSCs were cultured in macrophage-conditioned media or chondrogenic media containing 100-500 nM Dex-pep. The samples were harvested for biochemical analysis or fixed for histology. Macrophages were polarized towards a pro- or anti-inflammatory phenotype then stimulated with 100-300 nM Dex-pep to assess immunomodulatory effects with flow cytometry.

Results: Fluorophore release studies demonstrated sustained Cy3 release from Cy3-conjugate scaffolds in response to collagenase. Cy3 physisorbed to the scaffolds released rapidly and non-specifically in both collagenase-rich and collagenase-absent conditions. Dex-pep at 300 nM reduced caspase-3/7 activity in MSCs exposed to macrophage-conditioned media, supported MSC chondrogenesis, and decreased both intra- and extracellular inflammatory macrophage markers similarly to 100 nM unmodified Dex.

Conclusion/Significance: This platform leverages the elevated protease activity characteristic of OA flares to achieve selective, enzyme-responsive therapeutic delivery. Dex-pep retained its pharmacological activity, underscoring the potential of this system to provide on-demand release of drug-loaded biomaterials for anti-inflammatory applications.

OP-060 - Spatial Regulation of Cell Contractile Force-Driven 4D Bioprinting via siRNA Delivery

Kaelyn L. Gasvoda[1], Aixiang Ding[1,2], Cong Truc Huynh[1,2], Oju Jeon[1,2], Alexandria Sterenberga[1], Eben Alsberg[1,2,3]

[1]*University of Illinois Chicago, Biomedical Engineering, Chicago, United States of America*
[2]*Jesse Brown Veterans Affairs Medical Center, Chicago, United States of America*
[3]*University of Illinois Chicago, Orthopaedic Surgery, Pharmacology And Regenerative Medicine, and Mechanical & Industrial Engineering, Chicago, United States of America*

Purpose/Objectives: Four-dimensional (4D) bioprinting enables the fabrication of dynamic tissue constructs capable of programmed

shape transformations over time. Previously, cell contractile force (CCF)-driven tissue morphing has been achieved through actin cytoskeleton-mediated cellular contraction. However, strategies to precisely regulate cellular force generation within bioprinted constructs remain limited. This study aimed to develop a spatially controlled, self-actuating 4D construct platform whereby cell contractility and tissue morphing are modulated through locally patterned RNA interference molecule (RNAi) delivery within printable hydrogels.

Methodology: Human mesenchymal stem cells (hMSCs) were encapsulated within oxidized and methacrylated alginate/gelatin methacryloyl (OMAGM) bioinks containing siRNA complexes targeting LIM domain kinase 1 (LIMK1), a key regulator of actin polymerization in the Rho/ROCK signaling pathway. Constructs were fabricated via extrusion bioprinting followed by photocrosslinking. The rheological, swelling, and degradation properties of the hydrogels were characterized. siRNA delivery efficiency and bioactivity were initially evaluated using red fluorescent protein (RFP)-expressing reporter cells. Spatial patterning of siRNA presentation was further developed to enable localized regulation of gene expression within encapsulated cells. Cytoskeletal organization, cell contractility, and shape-morphing behaviors of the printed constructs were subsequently assessed.

Results: OMAGM hydrogels exhibited predominantly elastic behavior and supported sustained siRNA delivery in both bulk and spatially patterned constructs. Efficient gene knockdown of RFP expression in encapsulated hMSCs confirmed preservation of siRNA bioactivity within the hydrogel system. LIMK1 silencing reduced filamentous actin (F-actin) formation and suppressed hMSC-mediated contractile forces, resulting in tunable and spatially controlled morphing of the bioprinted constructs. Moreover, spatial regulation of LIMK1 expression enabled coordinated, region-specific deformation for the formation of complex architectures. Collectively, integration of RNAi within the 4D bioprinting platform enabled programmable construct deformation through modulation of cellular mechanobiology.

Conclusion/Significance: This study presents a self-actuating RNAi-mediated 4D bioprinting strategy for programmable tissue morphogenesis. By combining siRNA delivery with cell-responsive biomaterials, this platform provides a versatile approach for dynamically regulating tissue architecture and may enable the engineering of complex tissues with spatially controlled maturation and function.

WITHDRAWN

OP-061

WITHDRAWN

Session 21
Cardiovascular, Angiogenesis, Blood (General Session)

11-16-2026 @ 1:30 PM - 3:00 PM

OP-062 - Microparticle-Based UPI Peptide Delivery to Promote Vascular Graft Endothelialization

Sunita George[1], Fatemeh Goodarzinia[1], Cyrah Pinnock[1], Shirin Changizi[1], Hong Chen[2], Chris Bashur[3]

[1]*Florida Tech, Biomedical Engineering, Melbourne, United States of America*
[2]*Boston Children's Hospital, Boston, United States of America*
[3]*Florida Tech, Melbourne, United States of America*

Purpose/Objectives: Tissue-engineered vascular grafts (TEVGs) are promising alternatives for peripheral artery bypass, but limited endothelialization and graft stenosis remain as challenges. UPI peptides disrupt epsin–VEGFR2 interactions and enhance endothelial cell proliferation; however, sustained and localized delivery is required for long-term graft success. This study aims to develop microparticle-based delivery systems using different luminal coatings and evaluate their effects on endothelialization and graft remodeling.

Methodology: Poly(DL-lactide-co-glycolide)(PLGA) microparticles encapsulating UPI peptides (2 mg/g polymer) were fabricated

via water/oil/water double emulsion, with scrambled peptide and water-loaded controls. Microparticles were characterized by SEM and Micro BCA assay. Microparticles were incorporated into gelatin and fibrinogen luminal coatings within electrospun polycaprolactone(PCL) conduits. Coating thickness was measured using optical coherence microscopy.(OCM), and morphology was assessed by SEM and cryo-SEM. *In vitro* endothelialization was evaluated using GFP^+ human umbilical vein endothelial cells (HUVECs). *In vivo*performance was assessed via rat aortic grafting over 4 weeks with ultrasound and histological analyses. Significance was determined using one-way ANOVA with Tukey.

Results: Microparticle diameters were below capillary size (6.7±2.0 μm). FITC-tagged UPI peptides confirmed encapsulation. UPI exhibited sustained release over 5 days, followed by continued lower-level release. Microparticles were uniformly incorporated into luminal coatings without delamination, producing smooth surfaces. OCM showed consistent coating thicknesses, with 20-gauge needles yielding the most uniform gelatin coatings (30.05±1.76 μm). *In vitro* studies demonstrated increased HUVEC attachment and spreading for UPI-gelatin vs. uncoated samples, with VE-cadherin also present (n=3). *In vivo*, UPI-microparticle-loaded grafts remained 100% patent after 4 weeks (n=3) with no stenosis. Crosslinked gelatin-coated grafts showed limited remodeling, whereas fibrinogen-coated grafts demonstrated increased tissue infiltration, suggesting improved remodeling, and a consistent luminal cell layer. Further histological and immunofluorescence analyses are ongoing.

Conclusion/Significance: This study demonstrates that sustained UPI peptide delivery can be achieved using microparticle-embedded luminal coatings. *In vitro* results demonstrate that UPI-containing coatings support endothelial cell attachment. In *vivo* results demonstrate patency at 4 weeks for UPI-microparticle-loaded grafts, but also that the coating material carrying the peptide are important parameters for endothelialization and graft remodeling. This long-term delivery strategy with fibrinogen coatings shows promise for future use in the clinic where endothelialization occurs over an extended timeframe.

OP-063 - Targeted Hybrid Nanoparticles and Injectable Hydrogels for microRNA-Mediated Cardiac Reprogramming

Letizia Nicoletti[1,2], Camilla Paoletti[1], Martina Coletto[1], Francesco Schiavone[1], Giovanni Paolo Stola[1,2], Alessandra Introvaia[3], Gerardina Ruocco[1], Elena Marcello[1], Gabriella Balestra[3], Alice Zoso[1], Clara Mattu[1], Valeria Chiono[1,2]

[1]*Politecnico di Torino, Department of Mechanical And Aerospace Engineering, Torino, Italy*
[2]*PoliRNA Srl, Torino, Italy*
[3]*Politecnico di Torino, Department of Electronics And Telecommunication, Torino, Italy*

Purpose/Objectives: Heart failure remains a leading cause of morbidity and mortality worldwide due to the limited regenerative capacity of the adult myocardium after infarction. Direct reprogramming of cardiac fibroblasts (CFs) into induced cardiomyocytes using a combination of microRNAs (miRcombo: miR-1, miR-133, miR-208, and miR-499) represents a promising regenerative strategy. However, the clinical translation of miRcombo is hindered by the lack of safe and efficient delivery systems. This study aimed to develop a targeted platform for localized miRcombo-mediated cardiac reprogramming.

Methodology: Patented hybrid nanoparticles (NPs) comprising a lipoplex core and a polymeric shell were produced by nanoprecipitation. Surface functionalization through click chemistry enabled conjugation of CF-targeting ligands, generating functionalized nanoparticles (F-NPs). NPs and F-NPs loaded with negative control miRNA, miR-1, miRcombo, or Cy5-labelled siRNA were characterized for physicochemical properties, loading efficiency, cytocompatibility, cellular uptake, and transfection efficiency. To enhance local retention and sustained release, F-NPs were incorporated into injectable self-healing hydrogels based on alginate dialdehyde/gelatin-carbohydrazide. Hydrogel rheological properties, degradation kinetics, and release profiles were evaluated. The therapeutic performance of the developed platform was assessed in CF/induced pluripotent stem cell-derived cardiomyocyte co-cultures, 3D human cardiac scar models, and a mouse model of myocardial infarction.

Results: F-NPs exhibited diameters of 150–200 nm, negative surface charge, approximately 99% miRNA loading efficiency, and excellent biocompatibility. Functionalization significantly enhanced CF uptake and transfection compared with non-targeted NPs, as confirmed in CF/induced pluripotent stem cell-derived cardiomyocyte co-cultures. Among the tested formulations, alginate dialdehyde/gelatin-carbohydrazide 30/70 hydrogels showed biomimetic stiffness, stability for up to 21 days, and sustained miRNA release for over 15 days. In 3D human cardiac scar models, F-NPs loaded with miR-1 or miRcombo achieved enhanced transfection and cardiac reprogramming efficiency compared with non-targeted NPs. In a mouse myocardial infarction model, F-NPs/miRcombo accumulated in the injured myocardium and promoted significant functional recovery at 30 and 60 days after treatment.

Conclusion/Significance: The combination of CF-targeted hybrid nanoparticles and injectable self-healing hydrogels provides an effective platform for localized miRNA delivery and cardiac reprogramming. By enhancing therapeutic retention, sustained release, and cell-specific targeting, this approach supports myocardial regeneration and offers strong translational potential for the treatment of ischemic heart disease and heart failure.

OP-065 - Click-Functionalized MSC-Derived Extracellular Vesicles on Silk Fibroin: A Strategy for Improving Vascular Cell Biocompatibility in Small-Diameter Graft Engineering

Kiran Mcloughlin[1], Amanda Pellegrino[2], Ellen Otto[3], Charlie Ren[3], Phil Campbell[3], Justin Weinbaum[2], David Vorp[2]

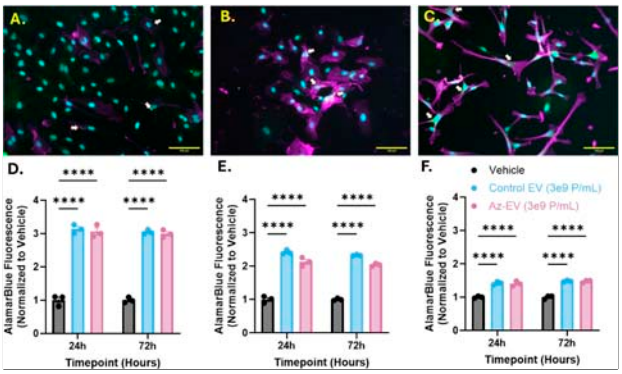
[1]*University of Pittsburgh, Bioengineering, Pittsburgh, United Kingdom*
[2]*University of Pittsburgh, Bioengineering, Pittsburgh, United States of America*
[3]*Carnegie Mellon University, Biomedical Engineering, Pittsburgh, United States of America*

Purpose/Objectives: Coronary artery disease (CAD) accounts for approximately 610,000 deaths annually in the US. Tissue-engineered vascular grafts (TEVGs) are bioengineered blood vessels that can replace autologous grafts currently used for CAD, which are not ideal for various reasons. We previously reported a silk-based TEVG containing MSC-derived extracellular vesicles (EVs) which increased patency efficiency in a rat aortic interposition graft model than blank or parent cell-seeded controls. Click chemistry has emerged as a potential strategy to immobilize EVs to the surface of biomaterials, improving their retention and bioactivity. We hypothesize that click-binding EVs to a silk TEVG will enhance vascular-relevant cell population bioactivity that could potentially improve TEVG remodeling and regeneration.

Methodology: EVs were stained with CellTrackerRed and cultured with human coronary artery endothelial cells (hCAECs), endothelial colony forming cells (hECFCs), and smooth muscle cells (hSMCs) for 6 hours, before fixing and staining cells with phalloidin and DAPI to determine EV internalization. For silk film experiments, Azido (Az)-labelled EVs were "clicked" to dibenzocycloooctyne (DBCO)-labelled bombyx mori silk films. Proliferation of hCAECs, hECFCs and SMCs in response to Az-EV-DBCO silk films was measured using AlamarBlue plate reader assay to determine proliferation of cells compared to vehicle/non-Az-EV loaded silk. Adhesion of seeded cells to Az-EV-DBCO silk was determined by fixation after one hour and staining with DAPI/phalloidin to quantify number of cells and cytoplasmic spreading, respectively.

Results: EVs were internalized by all cells within 6 hours. Proliferation, adhesion, and cytoplasmic spreading of all cells were significantly increased in the presence of both control-EVs and Az-EVs compared to vehicle controls, with no significant differences between EV groups. **Enhancement of vascular cells in**

response to MSC-derived EVs. (A) EVs were internalized by hCAECs, (B) hECFCs and (C) hSMCs after 6 hours of culture. (D) EV-loaded silk induced significant increases in proliferation after 24 and 72h of culture in hCAECs, (E) hECFCs and (F) hSMCs at 1e9 and 3e9 P/mL EVs.



Conclusion/Significance: Vascular-relevant cell populations are enhanced in both control-EV and Az-EV loaded DBCO-silk. Future studies will investigate the interactive mechanisms of cells in response to EV-DBCO silk and its regenerative capabilities in *in vivo* models.

OP-066 - Localized mRNA Delivery from Aligned Collagen Scaffolds for Treatment of Limb Ischemia

Jisoo Shin[1], Ngan Huang[2]

[1]*Stanford University, Stanford, United States of America*
[2]*Stanford University, Department of Cardiothoracic Surgery, Stanford, United States of America*

Purpose/Objectives: Peripheral artery disease (PAD) is characterized by impaired vascular perfusion, tissue loss, and skeletal muscle degeneration, and remains a major cause of limb amputation. Growth factor therapies are limited by rapid clearance, poor spatial control, and safety concerns with integrating gene delivery. Chemically modified mRNA (mmRNA) offers transient, non-integrating protein expression, but effective local retention remains challenging. The objective is to develope aligned nanofibrillar collagen scaffolds as a biomimetic platform for localized delivery of pro-myogenic insulin-like growth factor-1 (IGF-1) mmRNA to promote ischemic muscle regeneration.

Methodology: As an initial reporter system, green fluorescence protein (GFP) mmRNA was used to evaluate carrier performance, scaffold loading efficiency, and temporal reporter expression profiles. To improve retention on collagen scaffolds, ionizable LNPs were modified with the cationic lipid DOTAP to increase positive surface charge and enhance electrostatic association with negatively charged collagen. GFP mmRNA-LNPs were loaded onto aligned collagen scaffolds by adsorption, and loading efficiency was quantified. Human coronary artery endothelial cells (HCAECs) were then seeded directly onto LNP-loaded collagen scaffolds to assess scaffold-associated transfection efficiency, cell compatibility, and GFP expression over time.

Results: Initial Lipofectamine-mediated GFP mmRNA delivery produced high transfection efficiency at early time points, but reporter expression declined over several days, supporting the need for a sustained local delivery platform. Near-neutral LNPs showed limited association with collagen scaffolds, motivating a charge-engineering strategy to improve scaffold retention. DOTAP modification increased LNP loading onto collagen scaffolds compared with unmodified LNPs. Importantly, HCAECs seeded directly onto DOTAP-modified LNP-loaded scaffolds maintained GFP reporter expression for over one week, supporting the functional bioactivity of scaffold-associated LNPs after loading. Qualitative imaging showed no obvious scaffold-associated cytotoxicity.

Conclusion/Significance: These results demonstrate that charge engineering can improve LNP retention and functional bioactivity on aligned collagen scaffolds. This strategy provides a foundation for localized therapeutic mmRNA delivery, including future IGF-1 mmRNA delivery, to promote ischemic tissue regeneration in PAD.

Session 22
Emerging Advances in Microphysiological Platforms to Study Disease

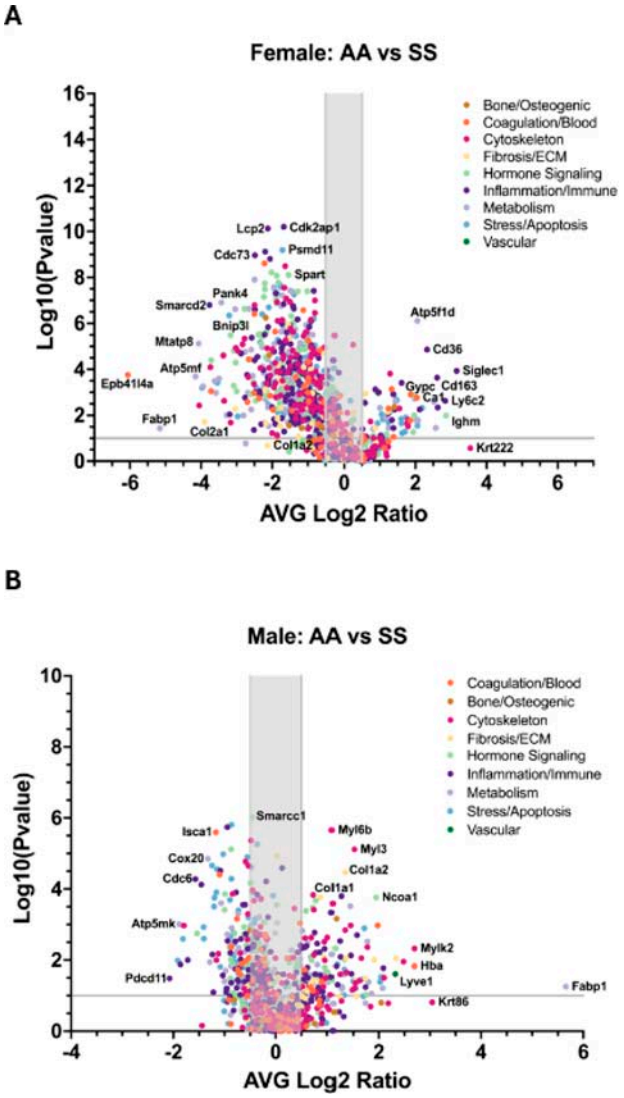
11-16-2026 @ 1:30 PM - 3:00 PM

OP-070 - Engineering the Bone Marrow Perivascular Niche for In Vitro Studies of Sickle Cell Disease

Arielle Efotte, Natasha Claxton, Mykel Green

Tulane University, Biomedical Engineering, New Orleans, United States of America

Purpose/Objectives: The bone marrow is a dynamic and complex tissue responsible for hematopoietic stem cell (HSC) maintenance and hematopoiesis, specifically within the perivascular niche[1]. In sickle cell disease (SCD), this microenvironment is disrupted, leading to impaired erythropoiesis, chronic inflammation that contributes to hematopoietic stem cell (HSC) dysregulation[2]. While animal models have provided important insights, they often do not reproduce human specific cell, matrix, and stressor interactions that are central to SCD. This gap has increased interest in non-animal models that can capture key features of the human marrow niche for



mechanistic studies. Here, we establish a vasculogenic hydrogel of polyethylene glycol (PEG), utilizing primary cells from Townes mice for vessel formation and mass spectroscopy data to inform our hydrogel design.

Methodology: Polyethylene glycol (PEG) and collagen hydrogels are co-encapsulated with primary bone marrow endothelial cells (BMECs) and bone marrow mesenchymal stromal cells (BMSCs) from sickled Townes mice. In parallel, a human bone marrow aligned condition is implemented using human BMECs and BMSCs. Hydrogel fabrication methods are adapted from Byrne et al. and Jansen et al. Viability is assessed using LIVE DEAD staining. Hydrogel mechanics are evaluated by rheometry, and vascular morphometrics including vessel length, diameter, and lumen-like features are quantified via ImageJ. Mass spectroscopy of AA, SS, and AS genotype Townes mice are used to inform protein and cytokine composition for the syngthetic gel. To recapitulate sickled marrow biomechanics, rheometric methods are used for obtaining healthy and sickled marrow moduli.

Results: Results are obtained from mass spectroscopy anaylsis of the bone marrow of female and male Townes mice of AA and SS genotypes. There are significant differences in up and down regulated genes, where female Townes mice showcase more gene expression downregulation as compard to the males. ECM genes like collagen type 1 alpha 2 (Col1a2) are shown to be upregulated in male SS models, yet downregulated in female SS.

Conclusion/Significance: Results from our preliminary mass spec data show significant sex dimorphisms between male and female bone marrow genetic composition. These results motivate our overall research goal of creating tunable vascular hydrogels that recapitulate the healthy and sickled bone marrow for SCD therapeutic studies.

Session 23
Tissue Engineering and Regenerative Medicine for Upper Airway Restoration

11-16-2026 @ 1:30 PM - 3:00 PM

OP-071 - Spatial Transcriptomic Mapping of Vocal Fold Epithelial–Fibroblast Interfaces Reveals Candidate Cellular Niches Relevant to Mucosal Tissue Engineering

Michelle Bretl[1,2], Elliot Xie[3], Christina Kendziorski[3], Susan Thibeault[1,2]

[1]*University of Wisconsin-Madison, Otolaryngology-head And Neck Surgery, Madison, United States of America*
[2]*University of Wisconsin-Madison, Communication Sciences And Disorders, Madison, United States of America*
[3]*University of Wisconsin-Madison, Biostatistics And Medical Informatics, Madison, United States of America*

Purpose/Objectives: Vocal fold (VF) structure and function are unlike any other tissue in the body, presenting significant challenges in laryngological tissue engineering. VF mucosa requires specialized cellular and extracellular matrix (ECM) organization to withstand vibratory mechanical stress and environmental irritants. Investigating VF tissue dynamics in health and injury repair is critical to advancing upper airway tissue engineering and regenerative medicine. In this study, we used high-definition spatial RNA sequencing (spRNAseq) to characterize VF cell niches within healthy and injured murine laryngeal tissue.

Methodology: Adult mice underwent VF injury via mechanical brush, and laryngeal dissection occurred at six post-injury timepoints: 12-hour, 24-hour, 3-day, 7-day, 14-day, 21-day. SpRNAseq of control and VF-injured coronal larynx sections was performed using 10X Genomics Visium HD CytAssist. Spatially resolved clustering identified diverse epithelial and fibroblast-associated transcriptional states.

Results: Distinct epithelial subclusters demonstrated transcription consistent with basal repair, differentiated suprabasal, and inflammatory states (**Fig1**). A basal repair subcluster exhibited co-expression of canonical basal epithelial markers together with fibroblast-associated genes, suggesting a partial epithelial-mesenchymal repair niche localized to epithelial-lamina propria (LP) interface. In contrast, differentiated epithelial populations demonstrated gene expression enriched for barrier restoration and epithelial maturation. Most notably, a unique epithelial repair population at 24-hour and 3-day timepoints was characterized by inflammatory/remodeling-associated gene expression consistent with wound-edge epithelium undergoing re-epithelialization. Within stromal compartments, we identified activated ECM-remodeling fibroblast populations, revelaing specialized states required for critical biomechanical ECM restoration. Inflammatory fibroblast subclusters at early wound healing timepoints suggested acute immunoresponsive repair niches. Interestingly, several spatially organized fibroelastic niches localized to epithelial–LP interface were present across both healthy and injured tissues, representing intrinsic features of VF architecture rather than transient injury states alone.

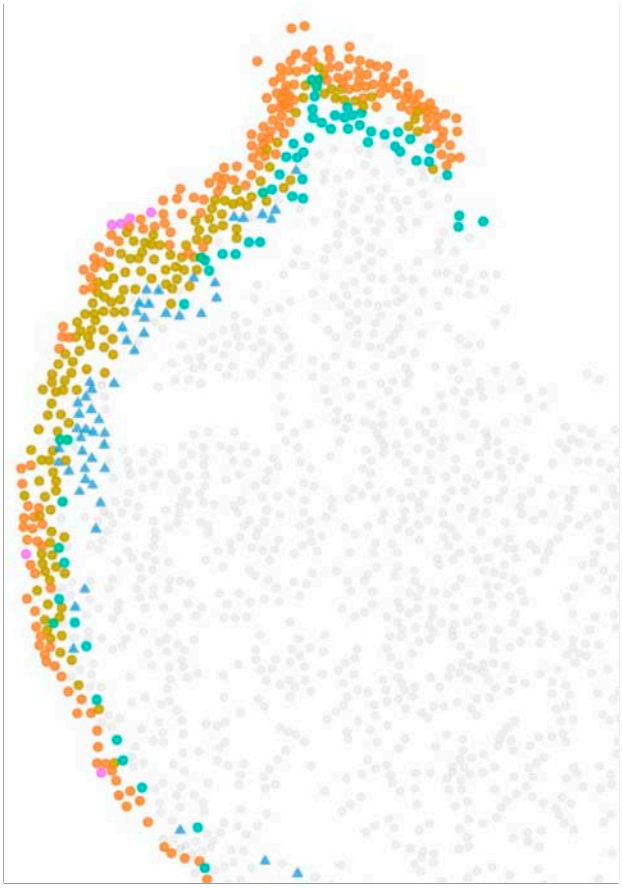


Fig1. VF epithelial cell clusters (circles) at 3-day post-injury reveal wound-edge (pink), suprabasal (orange), thickened basal (gold), and epithelial-mesenchymal repair (aqua) niches, with adjacent activated fibroblast populations (blue triangles).

Conclusion/Significance: These findings demonstrate that VF health and repair involve coordinated spatially organized microdomains extending beyond traditional cell-type classifications. Identification of stable epithelial-LP interface niches, epithelial repair response populations, and specialized matrix-remodeling fibroblast states may inform VF tissue engineering strategies designed to recapitulate native mucosal architecture, epithelial-ECM interactions, and vibratory tissue mechanics.

OP-072 - Tunicate-Inspired Carboxymethyl Cellulose Hydrogel Filler for Treating Age-Associated Vocal Fold Atrophy

Sang-Yoon Han[1], Seong Keun Kwon[2], Jeon Seong[3]

[1]*Hanyang university, Department of Otolaryngology-head And Neck Surgery, College Of Medicine, Hanyang University, Seoul, Korea., Seoul, Korea, Republic of*
[2]*Seoul National University, Seoul, Korea, Republic of*
[3]*Biomedical Research Institute, Seoul National University Hospital, Department of Otorhinolaryngology-head And Neck Surgery, Seoul, Korea, Republic of*

Purpose/Objectives: For the treatment of dysphonia and aspiration induced by presbylaryngis, injection laryngoplasty is widely conducted. Here, the feasibility of carboxymethyl cellulose hydrogel modified with pyrogallol (CMC-PG) is checked for injection laryngoplasty.

Methodology: CMC-PG was synthesized by conjugating 5′-hydroxydopamine to a carboxymethylcellulose backbone via EDC/NHS chemistry. The hydrogel was characterized by ^{1}H NMR and UV-vis spectroscopy. Injectability was assessed using a universal testing machine, and mechanical properties were evaluated by rheometry and tensile testing. Drug release profiles of bFGF and BSA were measured under physiological conditions over 5 weeks. Biocompatibility was confirmed in vitro using human vocal fold fibroblasts (Live/Dead and MTT assays) and in vivo via subcutaneous injection in mice. For the vocal fold rejuvenation study, CMC-PG with or without bFGF was injected into the vocal folds of 22-month-old aged rats under endoscopic guidance. After one month, histological analyses (H&E, Alcian blue, Masson's trichrome, immunofluorescence) and ex vivo phonation testing were performed to assess structural and functional restoration.

Results: CMC-PG hydrogel, combining mechanical bulking effects with sustained bFGF delivery, offers a promising alternative to conventional vocal fold fillers. Its favorable injectability, biocompatibility, and regenerative potential support its clinical translation as an effective injectable filler for presbylaryngis.

Conclusion/Significance: CMC-PG hydrogel demonstrated superior injectability, mechanical stability, tissue adhesiveness, and sustained bFGF release compared to a commercial vocal fold filler. In an aged rat model, bFGF-loaded CMC-PG hydrogel effectively restored the lamina propria and muscle layer, reduced interstitial fibrosis, enhanced angiogenesis, and modulated immune responses. Functional evaluation confirmed improved vocal fold vibration and glottal closure. These results suggest that CMC-PG hydrogel has strong clinical potential as an injectable filler for the treatment of presbylaryngis.

OP-074 - Differential Wound Healing Potential of Tonsil Parenchymal and Epithelial Mesenchymal Stromal Cell-Derived Exosomes in Chemotherapy-Induced Oral Mucositis

Haesang Park, Harry Jung

Hallym University, Chuncheon, Korea, Republic of

Purpose/Objectives: The biological characteristics of mesenchymal stromal cells (MSCs) and their exosomes can vary depending on the tissue layer of origin, potentially influencing their regenerative capacity. This study aimed to determine whether exosomes derived from epithelial (TE-MSCs) and parenchymal (TP-MSCs) layers of human tonsils exhibit distinct therapeutic effects in oral mucositis (OM).

Methodology: MSCs were isolated from the epithelial (TE-MSCs) and parenchymal (TP-MSCs) layers of human tonsils. Exosomes were characterized and tested for regenerative and anti-inflammatory effects in vitro and in a 5-FU-induced OM hamster model.

Results: Both TP-MSCs and TE-MSCs exhibited typical MSC phenotypes and multipotency comparable to BMSCs. Transcriptomic profiling revealed distinct layer-specific features, with TE-MSCs enriched in developmental and morphogenetic pathways. TE-MSC-derived exosomes (TE-MSC-Exo) showed enhanced wound closure, downregulation of IL-1β and TNF-α, and selective induction of HGF and ICAM-1 expression. In vivo, TE-MSC-Exo treatment resulted in the smallest mean wound size and most complete re-epithelialization among experimental groups.

Conclusion/Significance: Exosomes derived from tonsil MSCs effectively promote epithelial regeneration in OM, with TE-MSC-Exo exhibiting enhanced therapeutic potential. These findings highlight the importance of MSC layer origin in defining exosome function and suggest that TE-MSC-Exo may serve as a promising platform for exosome-based mucosal repair therapies.

OP-075 - Complementary Methods for the Production of Porous Polymeric Scaffolds for Laryngotracheal Reconstruction

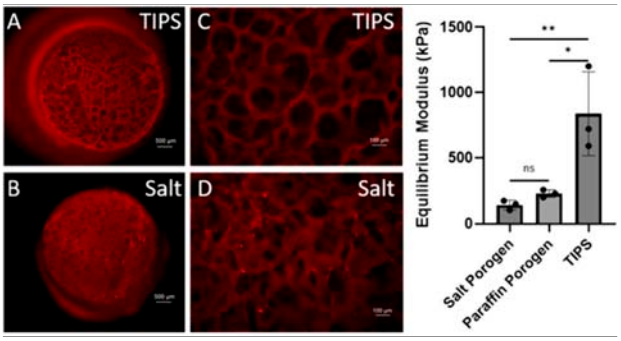
Matthew Pellicore[1], Federico Testa[1], Vincenzo La Carrubba[2], Riccardo Gottardi[1]

[1]*Children's Hospital of Philadelphia, Philadelphia, United States of America*
[2]*Universita di Palermo, Palermo, Italy*

Purpose/Objectives: Pediatric laryngotracheal reconstruction (LTR) for the treatment of subglottic stenosis (SGS) has a high failure rate which can be attributed in part to insufficient cartilage autograft quality or quantity. We seek to address this by developing polymeric tissue scaffolds made of poly(l-lactide) (PLLA) using two complementary methods: porogen leaching and thermally induced phase separation (TIPS). These approaches generate scaffolds with controlled pore sizes and mechanical properties, which influence cell behavior and clinical utility, respectively. Our objective is to produce scaffolds that promote chondrogenesis and have sufficient mechanical properties to ensure airway patency after LTR.

Methodology: Paraffin and salt (NaCl) porogens were prepared by processing large particles and sieving. Porogens were mixed with 5% PLLA in dioxane and frozen. Solvent was removed by lyophilization, and porogens were removed using appropriate solvents – d-limonene and water for paraffin and salt, respectively. TIPS was performed on 4% PLLA solutions in an 87/13 dioxane/water solvent mixture with a thermal history characterized by a long hold at 32C. Scaffolds were recovered by lyophilization. Mechanical testing was performed on a custom compression testing device, and equilibrium moduli were calculated.

Results: Stable, porous PLLA scaffolds were generated with pores ranging from ~75-200 μm (Fig. 1A-D), a size range which we have previously demonstrated promotes chondrogenesis *in vitro*. Equilibrium moduli of TIPS scaffolds (837 ± 321 kPa) approached that of mature hyaline cartilage, while equilibrium moduli of salt and paraffin porogen scaffolds (144 ± 37 kPa and 231 ± 29 kPa) were similar to those of immature cartilage.



Conclusion/Significance: We present complementary methods for the production of biocompatible scaffolds with tunable geometries and mechanical properties. TIPS generates PLLA scaffolds with superior mechanical properties, while porogen leaching gives superior control over pore size and structure. As it is still unknown which of these characteristics will best predict success in LTR, we will continue to investigate both methods of scaffold production. These scaffolds may find use in the treatment of SGS as components in engineered alternatives to autologous cartilage grafts used in LTR.

Session 25
Sex Hormone Influence on Tissue Engineering and Regenerative Medicine

11-16-2026 @ 3:05 PM - 4:35 PM

OP-078 - Age- and Sex-Specific Cartilage Matrix Responses to Physiologic 17β-Estradiol in a Human Joint Microphysiological System

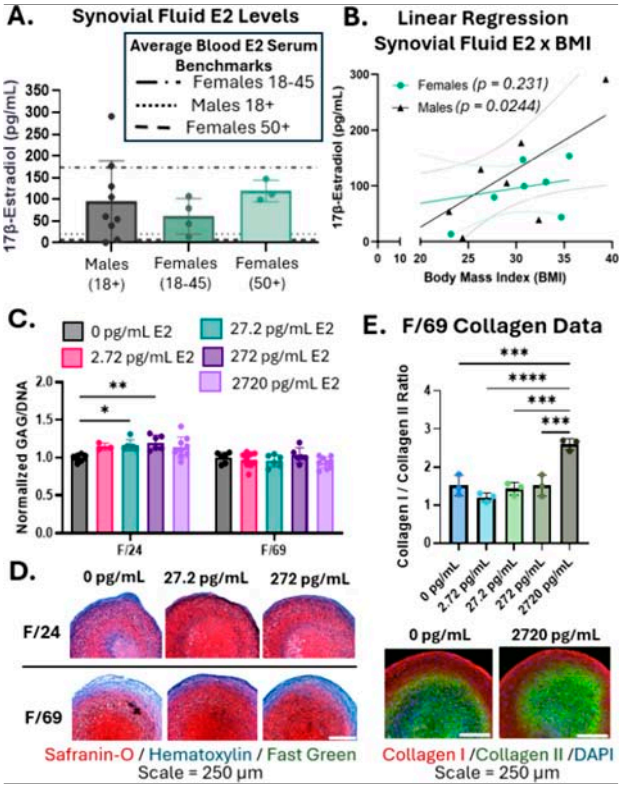
Cora Ferguson[1], Sophia Foerster[1], Nataliia Shchotkina[1], Mira Schoeberlein[2], Brad Wilkins[2], Nick Willett[1], Gabriella Lindberg[1]

[1]*University of Oregon, Bioengineering, Eugene, United States of America*
[2]*University of Oregon, Human Physiology, Eugene, United States of America*

Purpose/Objectives: Osteoarthritis (OA) affects over 500 million adults globally, with females 50+ experiencing a 1.3-fold higher incidence than age-matched males. Emerging evidence suggests that estrogen signaling contributes to cartilage extracellular matrix (ECM) homeostasis; however, the mechanisms underlying sex-based OA risk remain poorly understood. This gap is partly driven by the limited characterization of physiologic 17β-estradiol (E2) concentrations within synovial fluid (SF), hindering the development of hormone-relevant in vitro models for studying cartilage biology. Our objective was to quantify E2 concentrations in SF and evaluate the sex- and age-specific effects of E2 on cartilage development in a human microphysiological system (MPS). *We hypothesized that aging in female patients is associated with reduced synovial fluid E2 concentrations and diminished E2-mediated cartilage ECM formation.*

Methodology: SF and articular chondrocytes were harvested from human subjects during routine orthopedic procedures. SF E2 concentrations were quantified by ELISA (n = 16). Cartilage spheroids were cultured across physiologic and supraphysiologic E2 conditions (0 – 2720 pg/mL) for 4 weeks. Cartilage ECM integrity was assessed through spheroid size, biochemical assays (DNA, glycosaminoglycans; GAGs), histology (GAGs, collagen I/II), and mechanical testing. Statistical analyses were performed using one-way ANOVA with Tukey's post hoc testing.

Results: SF E2 levels did not differ significantly among males (18+), younger females (18-45), and older females (50+), but exceeded previously established blood serum E2 benchmarks for males and older females (Fig. 1A). SF E2 positively correlated with BMI in male donors, but not female donors, suggesting sex-specific local regulation of joint hormone levels (Fig 1B). Cartilage spheroids were generated from 4 donors: F/24, F/25, F/69, M/53. F/24 exhibited significantly increased GAG deposition under physiologic and high physiologic E2 exposure, whereas all other donors demonstrated attenuated hormone responsiveness (Fig 1 C-D). In contrast, supraphysiologic E2 exposure increased collagen I deposition in F/69, consistent with fibrocartilaginous matrix formation (Fig. 1E).



Conclusion/Significance: These findings demonstrate that SF E2 concentrations differ from conventional systemic benchmarks and drive donor-specific cartilage ECM responses in a human MPS. This work establishes foundational parameters for physiologically relevant hormone modeling in musculoskeletal tissues and highlights the need for patient-specific approaches to studying sex-based OA mechanisms and therapeutic design.

OP-079 - Estrogens in Traditional Cell Culture Media Influence Human Mesenchymal Stromal Cell (hMSC) Processes and Differentiation in a Sex-Biased Manner

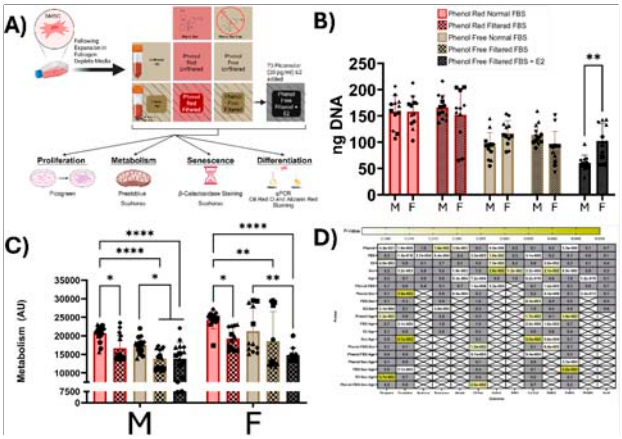
Jenny Robinson, John Bradford

University of Washington, Seattle, United States of America

Purpose/Objectives: Estrogens are global regulators of cellular signaling pathways, impacting fundamental processes that are essential for tissue remodeling and homeostasis. Traditional cell culture media contains estrogen-mimetic compounds, including phenol red and endogenous estrogen in fetal bovine serum (FBS). However, the potential of these compounds to bias in vitro studies, particularly when considering sex as a biological variable, remains unclear. Human mesenchymal stromal cells (hMSCs) have immense potential for cell-based regenerative therapies. Herein, we investigate the effects of these estrogen-mimetic compounds on male and female hMSC metabolism, proliferation, senescence, and differentiation. We hypothesized that estrogen-like compounds would increase metabolism and proliferation in a sex-based manner.

Methodology: Human mesenchymal stem cells from 4 male (19-22 years) and 4 female (19-23 years) donors were assessed. Cells were expanded in estrogen-free media (no phenol red, charcoal dextran filtered FBS) and then exposed to respective media conditions (with or without phenol, normal or filtered FBS) with a group dosed with 20 pg/mL E2 (**Fig 1A**). Proliferation (Picogreen), metabolism (Prestoblue and Seahorse XF analysis) and senescence-like phenotype (β-Galactosidase staining) was assessed. Impact of media component on differentiation capacity was assessed via trilineage differentiation assessed with alcian blue (chondrogenic), oil red o (adipogenic), and alizarin red (osteogenic) stains. Lastly, qPCR was used to determine pre-differentiation lineage commitment using lineage specific proteins and transcription factors.

Results: Overall, phenol red significantly increased proliferation (**Fig 1B**) and normal, unfiltered FBS significantly increased the oxidative metabolism (**Fig 1C**) in both male and female hMSCs. Notably, dosing with estrogen at the levels found in FBS did not recover most of the hMSC metrics tested. The notable outcomes that were significantly impacted by sex for the overall analysis include proliferation, metabolism, senescence, osteogenic differentiation, adipogenic differentiation, and gene expression for Col1a1, ESR1, Col10a1, RUNX2, FABP4, and PPARγ. Sex specific outcomes were seen across most outcomes as determined by linear model analysis (**Fig 1D**).



Conclusion/Significance: Overall, these findings reveal the sex-biased effects of estrogen and estrogen-mimetic compounds in

traditional culture media, underscoring a current gap in considering sex as a biological variable in cell therapy and tissue engineering research and manufacturing.

OP-080 - Developing Self-Assembled Myometrial Tissue Constructs with Embedded Spheroids for Modeling Intramural Uterine Fibroids

Kiran Tremblay, Isabella Palit, Arthur Clark, Catherine Whittington

Worcester Polytechnic Institute, Biomedical Engineering, Worcester, United States of America

Purpose/Objectives: Uterine fibroids are benign tumors that form in the uterus of over 77% of women over the age of 50, are associated with a healthcare cost of over $40 billion annually, and produce symptoms ranging from amenorrhea to infertility. Yet there is a gap in understanding how interactions between fibroids and surrounding uterine tissue affect fibroid pathophysiology and treatment response, prompting a need for new in vitro uterine fibroid models that can replicate these relevant effects. In this project, we establish a self-assembled smooth muscle ring model of the myometrium (uterine muscle layer) capable of supporting integrated spheroids for future hormone and treatment testing.

Methodology: Human uterine smooth muscle cells (HUtSMC; ATCC) were added to a ring-shaped agarose mold and cultured within control media and media supplemented with macromolecular crowders (Ficoll 70, 400). Cells self-assembled into ring-shaped tissue constructs (7 days), then were analyzed to determine effects of crowders on ring mechanical properties (tensile testing), collagen production (Masson's trichrome), and hormone receptor expression (immunohistochemistry). HUtSMC spheroids were formed using an agarose mold and combined with HUtSMC into ring molds, resulting in rings self-assembling around the spheroids.

Results: Showed that HUtSMC within tissue rings organized radially in control and crowder media. However, adding crowders did not significantly alter ultimate tensile strength, elastic modulus, or collagen:smooth muscle ratios, which was unexpected given that prior 2D results showed significantly more collagen production in crowder-cultured HUtSMC. Immunohistochemical analysis revealed disperse estrogen receptor alpha and beta expression and edge-localized progesterone receptor alpha, consistent with native myometrium. Preliminary studies showed successful embedding of HUtSMC spheroids in tissue rings, with qualitative differences in cell organization in the ring (radial) vs. embedded spheroid (disorganized) and no impact on ring stability.

Conclusion/Significance: This research establishes HUtSMC self-assembled rings as a myometrial model suitable for creating a future in vitro model of intramural fibroids. Hormone expression results demonstrate tissue rings can model native myometrial tissues, and macromolecular crowders are not needed to maintain ring integrity. Rings also support spheroid integration which is important for future work with embedded fibroid spheroids that will investigate how fibroid-myometrium interactions regulate fibroid growth and treatment response.

OP-081 - Sex-Specific Differences in Flow-Mediated Arterial Stiffening in Atherosclerotic Murine Femoral Arteries

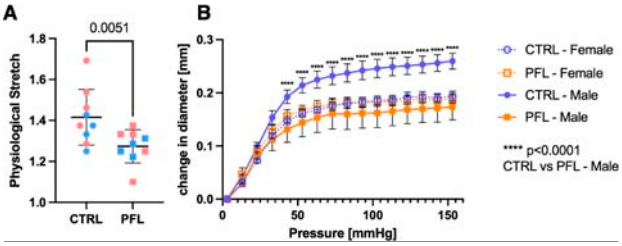
Gloriani Sánchez Marrero[1], Fujie Zhao[2], Rudolph Gleason[3], Luke Brewster[2]

[1]*Georgia Institute of Technology, Wallace H. Coulter Department of Biomedical Engineering, Atlanta, United States of America*
[2]*University of Cincinnati, Division Of Vascular Surgery, Uc College Of Medicine, Cincinnati, United States of America*
[3]*Georgia Institute of Technology, Woodruff School Of Mechanical Engineering, Atlanta, United States of America*

Purpose/Objectives: Arterial stiffening is an age-related modifiable process associated with increased cardiovascular disease risk. Arterial stiffening presents clinically in a sex-dependent manner with women having a 10-year delayed onset and 2-3-fold increased mortality when compared to men. Post-menopausal women are disproportionately affected by arterial stiffening and its associated effects. Two hallmarks of peripheral artery disease (PAD) include disturbed blood flow (d-flow) and arterial stiffening. Our research group recently proposed a murine model that mimics the PAD environment of d-flow in muscular arteries. The objective of this study is to characterize flow-mediated atherosclerotic arterial stiffening in our PAD model and uncover sex-specific differences in this process. Understanding sex-differences in arterial stiffening and PAD will inform treatment options.

Methodology: Five male and five female S129 23-week-old mice underwent partial femoral artery ligation (PFL) surgery one week after induction of atherogenic profile by PCSK9 infection and high fat diet. Six weeks post-PFL surgery, the FAs were harvested. During FA dissection, physiological stretch was measured as the ratio of *in vivo* to *ex vivo* length. FAs were subjected to cylindrical biaxial testing to identify differences in axial and circumferential stiffening.

Results: Atherosclerotic stenosis at the 6-week endpoint was confirmed following dissection. Physiological stretch decreased in the PFL side when compared to the control side (Panel A). Moreover, there was increased circumferential stiffening in the PFL artery when compared to *in situ* control in the male cohort only (Panel B). **PFL surgery in atherosclerotic mice promotes atherosclerotic growth and remodeling in a sex-specific manner. (A)** Physiological stretch of the control and PFL femoral artery 6 weeks after PFL surgery. Statistical significance was assessed with a Student's paired t-test at all timepoints. **(B)** Diameter changes with respect to initial diameter of the control and PFL femoral artery 6 weeks after PFL. Statistical significance was assessed with a two-way repeated measures ANOVA.



Conclusion/Significance: PFL surgery in atherosclerotic mice promotes active growth and remodeling in the left FA as evidenced by atherosclerotic plaque growth, decrease in physiological stretch, and increased circumferential stiffening. Ongoing work aims to delineate the role of sex chromosomes and sex hormones on these sex-specific differences in arterial stiffening.

Session 27
Advanced Biomaterials for Controlled Drug Release and Immune Modulation

11-16-2026 @ 3:05 PM - 4:35 PM

OP-085 - Valency Control of Immune Ligands for Tunable Immune Responses

Maria Coronel, Nicole Racca, John-Paul Pham, Jinhua Sun

University of Michigan, Bme, Ann Arbor, United States of America

Purpose/Objectives: Autoimmune diseases frequently arise from dysregulated immune signaling, where the balance between T cell activation and tolerance is disrupted. Programmed cell death protein 1 (PD-1) is a central inhibitory checkpoint receptor, yet how the integration of receptor engagement signals dictates tolerance versus anergy remains poorly understood. Here, we engineer valency-controlled PD-1 agonist proteins to selectively enhance the duration and amplitude of PD-1 signaling as a strategy for restoring immune tolerance.

Methodology: De novo fusion proteins were designed to engage murine and human PD-1 at the PD-L1 binding interface and incorporate a SpyTag domain for bioorthogonal conjugation to coiled-coil scaffolds bearing SpyCatcher, for precise valency control. Receptor

clustering was confirmed by mass spectrometry and biophysical characterization. PD-1 engagement was validated in NF-κB reporter cell lines, and Jurkat cells by phosphor flow cytometry and live-cell imaging. Functional outcomes were evaluated in primary T cell cultures for induced regulatory T cell (iTreg) induction and in an in vitro model of transplant rejection. In vivo efficacy was tested in prediabetic female NOD mice by intraperitoneal injection, with immune mechanism characterized by multiplexed immunophenotyping.

Results: Scaffolds generated a stable tetrameric PD-1 agonist that did not aggregate, as confirmed by multiple orthogonal methods. Compared to the monomeric format, the tetramer induced SHP-2 phosphorylation in a significantly higher proportion of cells (Figure 1A). This enhanced proximal signaling suppressed downstream NF-κB activation, confirming that valency amplifies the amplitude of inhibitory signals through the canonical SHP-2 axis. Functionally, the tetramer reduced the proliferation of activated T cells (Figure 1B-C). This anergy bias was consistent across both murine and human primary T cell cultures, supporting cross-species translational relevance. In NOD mice, intraperitoneal administration of the tetrameric fusion protein significantly delayed spontaneous diabetes onset to a degree comparable to current standard-of-care immunotherapeutics in this model (Figure 1 D-E). Multiplexed immunophenotyping revealed selective targeting of autoreactive T cell populations driving disease (Figure 1F), with a corresponding decrease in pathogenic clones in the pancreatic lymph nodes but not systemically, distinguishing the mechanism of action from broad immunosuppression.

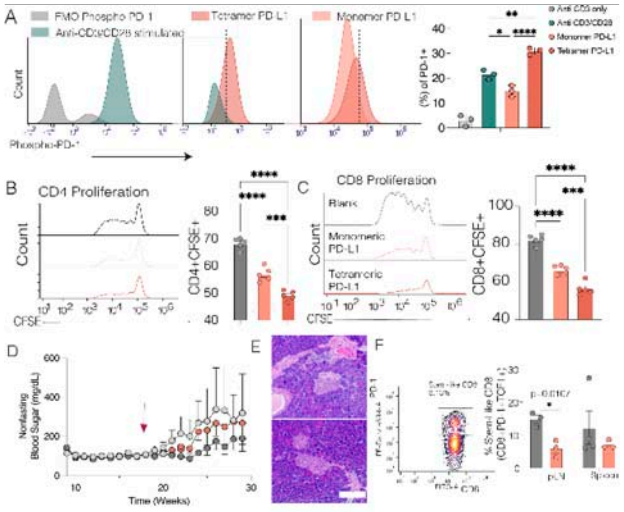


Figure 1. Engineered PD-1 protein binders in tetrameric form skew receptor triggering towards anergy. A) Detection of PD-1 receptor ligation in vitro through receptor engagement by stimulated Jurkat cells after 1 hrs of stimulation with anti-CD3 and anti-CD28 antibodies (green) versus monomeric PD-L1 salmon, or tetrameric PD-L1 (coral). (left) MFI, mean fluorescence intensity compared to fluorescent minus one control. (right) Frequency of phosphor PD-1 signal in PD-1 positive Jurkats post stimulation. B-C) Tetrameric PD-L1 presentation suppresses T cell proliferation in vitro after 72 hrs of culture in the presence of ConA. Histograms representing CFSE fluorescence shifts over time for controls in the absence of PD-L1 protein (blank) or in the presence of monomeric PD-L1 (salmon) or equimolar amounts of the tetrameric protein (coral). Quantification of CFSE+ dilution for both T helper (CD4) and cytotoxic T cell proliferation (CD8) after 72 hours. D) NOD mice at 16 weeks of age received 5 intraperitoneal injections of 5 µg/kg isotype control (n=3, grey), anti-CD3 (n=4, black), or tetrameric-PD-L1 (n=3, coral). Diabetes incidence was monitored for 15 weeks post-treatment. E) H&E staining of pancreatic tissue to evaluate insulitis grade. Islets of Langerhans appear as light purple structures, with infiltrating T cells visible as small, dense dark purple cells. Scale bar 100 µm. F) Representative TCF-1 expression profile on CD8 cells in the pLNs of treated mice at take down. The frequency of CD8 cells expressing stemness marker (TCF-1) and inhibitory checkpoint (PD-1) was quantified by flow cytometry. Data is presented as mean ± s.d. One-way ANOVA was used to compare all groups. P <0.05 (*), p<0.005 (**), p <0.0005 (***), p <0.0001 (****).

Conclusion/Significance: Herein, valency is shown as a tunable parameter for engineering immunotherapeutics, with direct implications for new designer therapies.

OP-086 - Injectable Biodegradable Implantable Matrices For Prolonged Anti-VEGF Delivery: Toward Minimally Invasive Retinal Treatments

Husam Younes[1,2], Hana Kdavil[2], Sandi Ali-Adib[2], Ali Al-Kinani[3], Raid Alany[3]

[1]*American University in Baghdad, College Of Pharmacy, Baghdad, Iraq*
[2]*Qatar University, Tissue Engineering And Nanopharmacueticals Research Laboratory, Doha, Qatar*
[3]*Kingston University London, Pharmacy Department, London, United Kingdom*

Purpose/Objectives: Retinal neovascular disorders, including diabetic retinopathy (DR) and age-related macular degeneration (AMD), are predominantly driven by vascular endothelial growth factor (VEGF) and require frequent intravitreal anti-VEGF injections. This imposes a significant clinical and patient burden and increases the risk of complications. The objective of this study was to develop and evaluate an injectable biodegradable elastomeric implant capable of providing sustained intraocular delivery of sunitinib, thereby reducing dosing frequency while maintaining therapeutic efficacy.

Methodology: Biodegradable elastomeric implants were fabricated using poly(diol-tricarballylate) (PDT/POT) polymeric networks via thermal crosslinking. Sunitinib was incorporated using solvent casting or direct mixing approaches. The implants were systematically characterized for physicochemical properties, drug–polymer interactions, and in vitro release kinetics. Cytocompatibility was assessed using ARPE-19 retinal pigment epithelial cells. In vivo pharmacokinetics and ocular tolerability were evaluated following intravitreal administration in rabbit models, with monitoring for inflammation, hemorrhage, and drug distribution in the vitreous humor.

Results: The developed implants demonstrated sustained, pH-stable drug release over 222 days, following Higuchi diffusion-controlled kinetics, without an initial burst release. Drug loading influenced release profiles, with higher loading (1000 µg) yielding increased release rates. In vitro studies confirmed preservation of ARPE-19 cell viability and reduced apoptosis relative to free drug exposure. In vivo evaluation indicated excellent ocular tolerability, with no evidence of inflammation or vitreous hemorrhage. Therapeutically relevant sunitinib concentrations were maintained in the vitreous humor for more than six weeks.

Conclusion/Significance: This study establishes a clinically relevant biodegradable implant platform for long-acting intraocular delivery of anti-angiogenic agents. The system offers a minimally invasive alternative to repeated intravitreal injections, with the potential to improve patient compliance, reduce treatment burden, and enhance therapeutic outcomes in chronic retinal diseases. These findings support further translational development of elastomer-based sustained delivery systems for ophthalmic applications.

OP-087 - Backpack-activated Natural Killer Cell Immunotherapy for Glioblastoma Treatment

Zerin Khan, Samir Mitragotri

Harvard University, Harvard John A. Paulson School Of Engineering And Applied Sciences, Boston, United States of America

Purpose/Objectives: Glioblastoma (GBM) is the most malignant type of primary brain cancer in adults. Even after surgery and chemoradiotherapy, residual GBM cells form secondary tumors and lead to median survival times of 15 months. The blood-brain-barrier hinders transport of drugs, while GBM cells secrete immunosuppressive factors that polarize immune cells to an anti-inflammatory, pro-tumor phenotype contributing to therapy resistance in the immunosuppressive tumor microenvironment (TME). Immune cells face difficulty in eradicating the tumor due to low persistence and exhaustion. To address these challenges, we developed polymeric micropatches adhering to the surface of natural killer (NK) cells to continuously activate their pro-inflammatory, anti-tumor phenotype. Activated NK cells directly lyse cancer cells without prior antigen priming, and we investigate backpack-carrying NK–GBM interactions using 3D, physiologically relevant *in vitro* platforms recapitulating the GBM TME and acquire mechanistic insights into this novel GBM immunotherapy.

Methodology: We adapted our previously established protocol with soft lithography, spin-coating, and microcontact printing to develop 8 µm poly(lactide-co-glycolic) acid (PLGA) microparticle backpacks (Figure 1A). Functionalizing backpacks with NK receptor targeting antibodies (CD45 and hNKp30) allowed them to attach to the surface of human NK-92 cells (Figure 1B).

Results: Characterization with flow cytometry revealed 80% high binding efficiencies and quantitative confocal microscopy indicated an average of four backpacks attached per NK cell (Figure 1 C,D). Compared to NK cells alone, backpack-bound NK cells were

significantly more cytotoxic to human U-251 GBM cells, and their cytotoxicity against GBM can be tuned further in a dose-dependent manner. We developed physiologically relevant, 3D *in vitro* models of the GBM TME comprising brain-mimicking collagen hydrogels embedded with GBM spheroids (U-251 cells or patient-derived BT-89 cells) and NK-92 cells with and without backpacks. Confocal microscope imaging of GBM-NK interactions revealed backpack-carrying NK cells can invade through collagen and infiltrate GBM spheroids (Figure 1E).

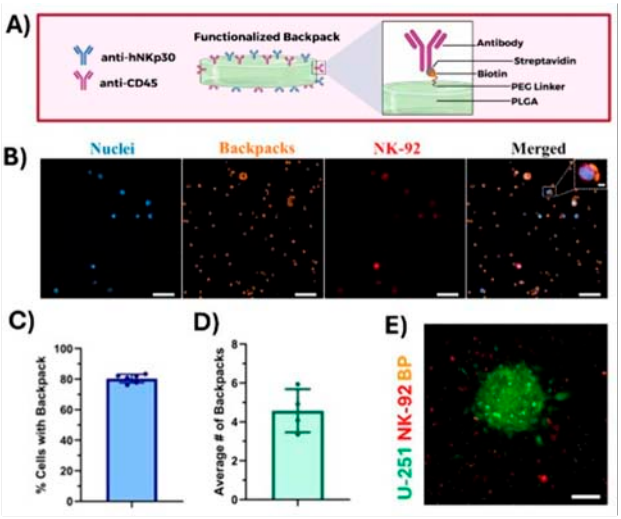


Figure 1. Backpack-mediated NK cell therapy against GBM. (A) Schematic overview. (B) Representative confocal microscope image. (C) Backpack adhesion. (D) Backpack distribution. (E) 3D in vitro platform.

Conclusion/Significance: Further molecular/biophysical profiling in this platform will be performed for mechanistic insights into GBM responses to NK-backpack immunotherapy and contribute to understanding and overcoming GBM immunotherapy treatment resistances.

OP-088 - Complement-Preserving DAMP-Enriched Adsorbed Protein Layers Enhance Macrophage Inflammatory Response to Biomaterials

Meghan Vanbuuren, Lindsay Fitzpatrick

Queen's University, Department of Chemical Engineering, Kingston, Canada

Purpose/Objectives: The foreign body reaction (FBR) is an immune response to implanted biomaterials, driven in part by macrophage responses to biomaterial-adsorbed protein layers. These layers may contain plasma and complement proteins, and damage-associated molecular patterns (DAMPs), all of which can regulate macrophage activation. However, many in vitro biomaterial models rely on serum, which lacks key plasma proteins or EDTA plasma, which inhibits complement activation, potentially underestimating inflammatory signaling at biomaterial surfaces. Both serum and EDTA plasma also lack injury-associated DAMPs. This study aimed to develop a physiologically relevant protein adsorption model that combines complement-preserving bivalirudin plasma with fibroblast lysate-derived DAMPs.

Methodology: Human blood was collected to prepare bivalirudin plasma, which preserves complement activity, and EDTA plasma, which inhibits complement activity. Complement activation potential was assessed by incubating plasma with zymosan A for 1 hour and measuring C3a and C5b-9 concentrations by ELISA. Primary human fibroblast lysate was generated by three freeze-thaw cycles and added to plasma at 10% w/w to create DAMP-enriched plasma samples. Adsorbed protein layers were formed on bivalirudin or EDTA plasma, with and without a 10% lysate spike. Primary human macrophages were cultured on these adsorbates for 24 hours, and pro-inflammatory cytokine secretion (TNF-α, IL-6) was quantified by ELISA.

Results: Bivalirudin plasma retained higher complement activation potential, as demonstrated by increased C3a and C5b-9 levels following zymosan A stimulation when compared to EDTA plasma. Macrophages cultured on adsorbed protein layers derived from bivalirudin plasma with a 10% lysate spike exhibited enhanced pro-inflammatory cytokine secretion compared to EDTA plasma counterparts, supporting a role for both complement activity and DAMP-enriched adsorbed proteins in macrophage activation.

Conclusion/Significance: This complement-preserving, DAMP-enriched protein adsorption model improves the physiological relevance of in vitro macrophage-biomaterial studies. By integrating complement activity and damage-associated molecular cues, this platform can help define molecular mechanisms that drive biomaterial-associated inflammation and fibrous encapsulation, supporting the development of biomaterials with improved long-term performance.

Session 28
Nanotechnology-Driven Strategies for Inflammatory Modulation in Term Applications

11-16-2026 @ 3:05 PM - 4:35 PM

OP-089 - Microfluidic Engineering of Nanocarriers for Inflammatory Modulation

Sara Gimondi[1,2], Daniel Mendanha[1,2], Carlos Guimarães[1,2], Rui Reis[1,2], Helena Ferreira[2], Nuno Neves[1,2]

[1]*3B's Research Group, I3bs – Research Institute on Biomaterials, Biodegradables and Biomimetics, University of Minho, Headquarters of The European Institute of Excellence On Tissue Engineering and Regenerative Medicine, Barco Gmr, Portugal*
[2]*ICVS/3B's, Pt Government Associate Laboratory, Braga/GMR, Portugal*

Purpose/Objectives: Traditional nanoparticle (NP) synthesis methods often present poor reproducibility, limited scalability, and insufficient control over physicochemical properties of the resulting nanocarriers. Microfluidic technology offers a powerful alternative, enabling rapid, precise, and tunable NP fabrication. Here, we demonstrate the versatility of a herringbone-architecture microfluidic platform for the synthesis of polymeric, polysaccharide-based, and lipidic NPs, and their potential for inflammation-targeted drug delivery.

Methodology: A passive microfluidic device with herringbone rib channel architecture was used to promote rapid mixing of up to three fluid streams on a millisecond timescale (Figure 1A). At low flow rates, laminar flow reduces diffusion distances, while higher flow rates induce chaotic advection, enhancing mixing efficiency. This design enables controlled and reproducible NP formation through precise interactions between precursors. Poly(lactic-co-glycolic acid) (PLGA) and lipids were dissolved in acetone and ethanol, respectively. To produce the polysaccharide NPs, chitosan was dissolved in acetic acid 1% (v/v), and hyaluronic acid was dissolved in water.

Results: Microfluidic-driven polymeric NPs with diameters of 30, 50, and 70 nm were successfully synthesized, characterized, and evaluated for drug delivery performance. Notably, 30 nm NPs exhibited the highest cellular uptake and achieved efficacy comparable to free diclofenac (DCF) in reducing macrophage PGE_2 production under inflammatory conditions, highlighting enhanced delivery efficiency (Figure 1B). Microfluidic synthesis was further adapted for high-molecular-weight polysaccharides, yielding smaller and more homogeneous NPs with improved modulation of pro-inflammatory cytokines than the ones produced by the conventional method. For large unilamellar vesicles (LUVs), microfluidic synthesisenabled their production 4-times faster than the conventional thin-film hydration followed by extrusion (Figure 1C), enabling a simplified single-step strategy. This approach facilitated efficient encapsulation of docosahexaenoic acid (DHA), significantly enhancing its therapeutic efficacy in glioblastoma models. DHA-loaded liposomes exhibited

efficient cellular internalization and superior anti-inflammatory activity compared to free DHA, significantly downregulating IL-6, IL-1β, TNFα, NF-κB, and STAT-1 expression, while reducing cytokine secretion in macrophage and glioblastoma cells (Figure 1D).

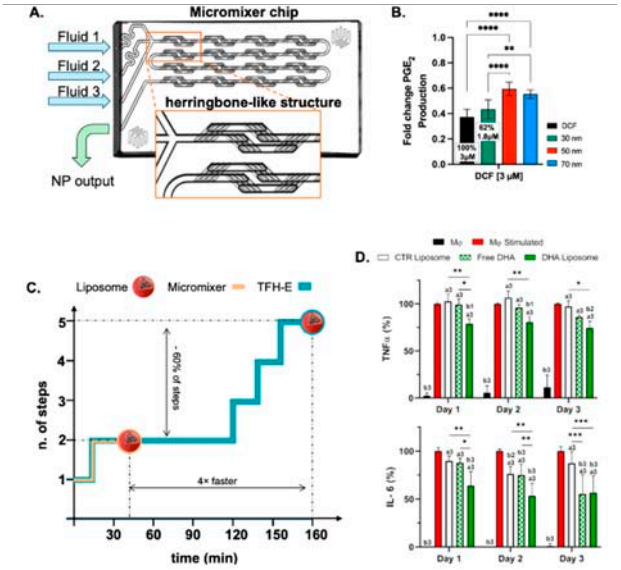


Figure 1. ***(A)*** *Passive micromixer device design.* ***(B)*** *PGE2 production in LPS-activated macrophages after treatment with 30, 50, and 70 nm NPs loaded with DCF, compared to free DCF.* ***(C)*** *Comparison of microfluidic-enhanced liposome synthesis vs. conventional thin-film hydration followed by the extrusion method (THF-E).* ***(D)*** *Secretion of TNFα and IL-6 by macrophages (Mφ) after incubation with free DHA, CTR liposomes, and DHA liposomes.*

Conclusion/Significance: This microfluidic platform enables the reproducible and controlled production of diverse, immunomodulatory nanocarriers with precise physicochemical tuning. By linking nanoscale design to inflammatory modulation, it represents a versatile and relevant strategy to enhance therapeutic outcomes in regenerative medicine.

OP-090 - Mitochondria-based delivery enables intracellular NAD^+ restoration and metabolic functional recovery

Fang Tang[1], Pei Zhu[2], Aurea Del Carmen[1], Brandon Applewhite[1], Merilyn Li[3], Anne Victoria Sefen[3], Bowen Wang[4], Bin Jiang[1,3,4]

[1]*Northwestern University, Querrey Simpson Institute Of Regenerative Engineering, Chicago, United States of America*
[2]*Feinberg School of Medicine, Department of Biochemistry And Molecular Genetics, Chicago, United Kingdom*
[3]*Northwestern University, Department of Biomedical Engineering, Chicago, United States of America*
[4]*Northwestern University, Department of Surgery, Chicago, United States of America*

Purpose/Objectives: Nicotinamide adenine dinucleotide (NAD^+) depletion is increasingly recognized as a hallmark of aging and numerous pathological conditions. Current NAD^+ restoration strategies primarily rely on precursor supplementation, which depends on multistep, enzyme-mediated salvage pathways that often limit conversion efficiency and intracellular bioavailability. Here, we propose an engineered mitochondrial delivery strategy for intracellular NAD^+ restoration and metabolic functional recovery. This approach combines two synergistic advantages: (i) direct delivery to the intracellular NAD^+ pool, and (ii) enhancement of mitochondrial resistance to oxidative stress within NAD^+-depleted microenvironments.

Methodology: Mitochondria were isolated from human induced pluripotent stem cell-derived mesenchymal stem cells (iPSC-MSCs) engineered with the mitochondria-specific redox-sensitive reporter mito-roGFP. Isolated mitochondria were co-incubated with NAD^+, followed by centrifugation to remove free NAD^+, generating NAD^+-loaded mitochondria (NAD^+@Mito). Mitochondria with and without NAD^+ loading were characterized for mitochondrial NAD^+ content, size distribution by dynamic light scattering (DLS), and oxidative stress response using confocal imaging of mito-roGFP under H_2O_2 challenge. Diabetic patient-derived endothelial cells (DAECs) were treated with 0.1 mM H_2O_2 to establish an oxidative stress-induced NAD^+ depletion model and subsequently incubated with unloaded mitochondria (+Mito) or NAD^+-loaded mitochondria (+NAD^+@Mito).

Results: NAD^+ was successfully loaded into isolated mitochondria, increasing mitochondrial NAD^+ content by approximately 1,000-fold. DLS analysis confirmed that mitochondrial morphology remained after NAD^+ loading. NAD^+ loading attenuated H_2O_2-induced mitochondrial oxidative stress, as demonstrated by reduced mito-roGFP oxidation ratios compared with unloaded mitochondria. Fluorescence imaging confirmed efficient cellular uptake of NAD^+-loaded mitochondria by DAECs, resulting in significantly higher intracellular NAD^+ levels relative to mitochondria alone. Collectively, these findings suggest that NAD^+-loaded mitochondria retain functional metabolic activity following transplantation and improve intracellular redox homeostasis under oxidative stress conditions.

Conclusion/Significance: This work establishes engineered mitochondria as a metabolically active intracellular NAD^+ delivery platform and highlights the broader potential of organelle-based systems for therapeutic delivery of bioactive metabolites and metabolic regulators.

OP-091 - Micropuncture enhances the angiogenic potential of exosomes through stress-adaptive immunomodulatory signaling

Jazzmyn Dawes[1], Emily Bianchini[2], Maryam Abdelaal[1], Neekita Jikaria[1], Ji Ho Park[1], Mohammad Hossein Asgardoon[1], Mary Landmesser[1], Dino Ravnic[1]

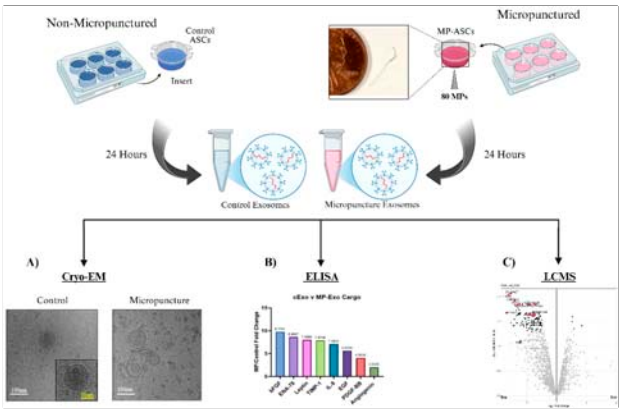
[1]*Penn State College of Medicine, Surgery, Hershey, United States of America*
[2]*Penn State College of Medicine, Cell & Biological Systems, Hershey, United States of America*

Purpose/Objectives: Ischemia is a major cause of morbidity and mortality worldwide. Few pro-angiogenic therapies have found clinical translation, and thus, alternative therapies are warranted. Exosomes are an emerging acellular therapeutic strategy for tissue repair, but little is known about rendering them pro-angiogenic. Our recently developed surgical approach, micropuncture (MP), can be used to trigger immune cell recruitment for targeted angiogenesis. It is unknown what role exosomes play in this process. We hypothesize that MP triggers the development of pro-angiogenic exosomes.

Methodology: Human adipose-derived stem cells (ASC) were isolated from patients undergoing lipectomy, then expanded in culture. ASCs ($1x10^5$) were seeded onto a semi-permeable membrane within a 6-well plate. 80 MPs were delivered into each well using a 60 μm-diameter needle. Cells without MP served as a control. At 24 hours, control (cExo) and MP (MP-Exo) exosomes were retrieved from the supernatant via ultracentrifugation or immunomagnetic bead isolation and quantified with nanoparticle tracking analysis (NTA). Exosome morphology was assessed using cryo-Transmission Electron Microscopy (Cryo-TEM). Exosome cargo was evaluated with ELISA microarrays and Liquid Chromatography Mass Spectrometry (LCMS).

Results: NTA showed that the average diameter of MP-Exo (174 nm) was slightly larger than cExo (173 nm). Cryo-TEM demonstrated that MP enhanced exosome release from ASCs ($p < 0.001$). It also appeared that MP-Exo had variable morphologies, including double-membraned, multilayered, and MVB-like vesicles compared to the uniformly round cExo (Figure 1A). LCMS highlighted the upregulation of ECM remodelers (PLOD2 p=0.02, COLGALT1 p=0.01), calcium signaling regulators (ITPR3 p=0.02, ATP2B1 p=0.02) stress-adaptative proteins (HYOU1 p=0.01), and immu-

nomodulatory signals (C1QBP p=0.01) within MP-Exo (Figure 1C). ELISA of MP-Exo cargo corroborated this with increased levels of pro-angiogenic, immunomodulatory factors such as b-FGF (FC 9.77), EGF (FC 5.5), IL-8 (FC 7.1), ENA-78 (FC 8.6), and PDGF-BB (FC 4.2) (Figure 1B).



Conclusion/Significance: Current pharmacologics for treating ischemia rely on conventional approaches that address symptoms rather than promote angiogenesis. Our data suggest that MP enhances the release of pro-angiogenic exosomes through cargo modification and stress-adaptive mechanisms. This information will allow for a better mechanistic understanding of MP that can be leveraged to develop novel nanotherapeutics to promote angiogenesis.

OP-092 - Lignin-Derived Carbon Dots Promote Wound Healing in an In Vivo Porcine Model of Full-Thickness Excisional Skin Defect

Eli Christoph[1], Nikolaos Zaharas[1], Steven Newby[1], Chiara Hampton[2], Madhu Dhar[1]

[1]*University of Tennessee, Tissue Engineering And Regenerative Medicine, Large Animal Clinical Sciences, College Of Veterinary Medicine, Knoxville, United States of America*
[2]*University of Tennessee, Large Animal Clinical Sciences, College Of Veterinary Medicine, Knoxville, United States of America*

Purpose/Objectives: Our lab has investigated lignin-derived carbon dots (LCDs) for cell and tissue engineering applications. This pilot study's objective was to investigate the effects of LCDs on wound healing for full-thickness excisional skin defects in pigs.

Methodology: LCDs were synthesized, characterized and ultrasonically dispersed onto film-casted, polyethyleneimine-treated (75:25) poly(lactic-co-glycolic) scaffolds at 700 mg/mL in nanopure water. Six juvenile gilts were assigned to receive six 4 cm diameter, full-thickness excisional defects. Each treatment (undoped LCDs, nitrogen-doped LCDs, and scaffold without LCDs as control) was randomly assigned to one of three wound pairs per gilt. Gilts were anesthetized, 4cm-diameter dermal excisions performed, and treatments applied onto wound beds. Wounds were covered with a 4 layer-bandage post-operatively and this was changed every 3 days for one week, then once every 7 days, when wounds were measured. Adverse reactions were monitored and recorded. Gilts were humanely sacrificed after 28 days post-operatively, and skin encompassing original defect areas was harvested and preserved. Mean wound area was determined by calculating granulation tissue surface area using FIJI (ImageJ). One-way ANOVA and Tukey post hoc tests were used to test significance of differences in mean ± SD wound area between treatments. Immunohistochemistry (IHC) was performed to evaluate CD206 expression, cell count and epidermal thickness using Masson's Trichome (MT) and H&E staining.

Results:

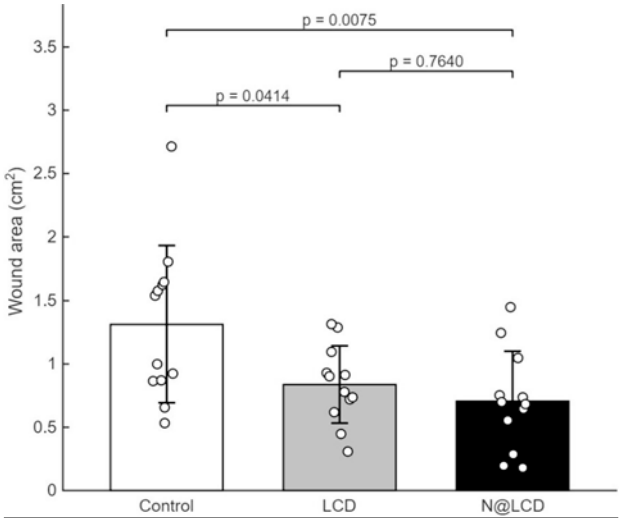


Figure 1: Wound area per treatment group quantification 28 days post-operatively. All gilts displayed healthy activity without adverse reactions to scaffolds. Computational analysis determined that at 28 days, undoped (p=0.041) and nitrogen-doped (p=0.008) LCDs treatment significantly reduced wound area compared to the control treatment (Figure 1). LCD treated wounds exhibited elevated CD206 %positive cells (mean difference to control: 6.1% and 6.3%) and total cell count (average difference to control: 319 and 376). LCD groups also demonstrated epidermis thickness ratios closer 1 than controls (control: 0.79; undoped LCD: 1.00; N@LCD: 0.98).

Conclusion/Significance: Treatment of full-thickness skin defects with LCDs reduced wound area and enhanced closure by 28 days. Tissue staining/analysis revealed elevated CD206 expression, cell count, and epidermal thickness in response to LCDs. This pilot study is a foundational step for progressing LCDs toward large animal models for translational clinical applications.

OP-093 - Developing Dexamethasone-Loaded Chitosomes for Vocal Fold Aerosolized Drug Delivery

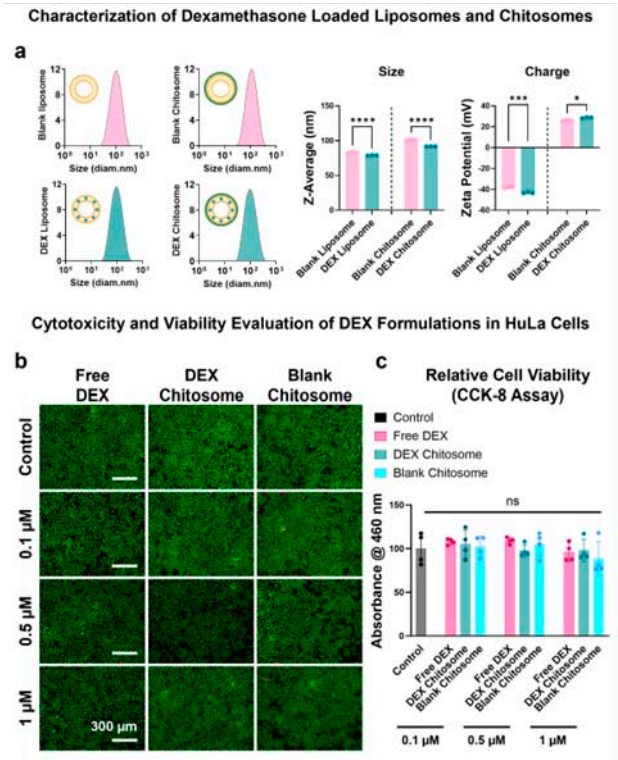
Samjhana Thapa[1], Guojun Chen[1], Nicole Li-Jessen[1,2]

[1]*McGill University, Biomedical Engineering, Montreal, Canada*
[2]*McGill University, Otolaryngology, Communication Sciences and Disorders, Montreal, Canada*

Purpose/Objectives: Human vocal folds (VF) in the upper airway control daily speech, breathing, and swallowing. Severe VF injuries such as scarring are treated by invasive intralaryngeal injection, an approach with limited drug bioavailability and airway safety risks. Aerosolized dexamethasone (DEX) is an attractive alternative for anti-fibrotic therapy. However, bare liquid DEX has reduced potency and short residence on airway mucus. Chitosan-coated liposomes (chitosomes) carry a positive surface charge that binds the negatively charged mucus layer and prolongs local drug exposure. This study aimed to develop DEX-loaded chitosomes and evaluate their physicochemical properties and biocompatibility *in vitro*.

Methodology: DEX-loaded liposomes were synthesized via one-step ethanol injection and coated with chitosan to yield positively charged DEX-chitosomes. Cytotoxicity was evaluated in human immortalized laryngeal epithelial (HuLa) cells. Cells were treated with free DEX or blank/DEX-chitosomes at concentrations ranging from 0.1 μM to 1 μM. Following a 72-hour incubation, cell toxicity and viability were evaluated via LIVE/DEAD and Cell Counting Kit-8 (CCK-8) assay.

Results: DEX encapsulation efficiency was 40±0.9% and loading capacity was 5.8±0.1%. Upon DEX loading, liposome size decreased from 83.5±0.8 to 78.9±0.5 nm. Chitosan coating (0.08 mg/mL) inverted the charge from −38.5±0.8 to +26.4±0.6 mV (blank chitosome) and from -43.2±0.7 to +28.7±0.5 mV (DEX-chitosomes). Concurrently, hydrodynamic sizes increased to 101.6±0.8 nm (blank chitosomes) and 91.9±0.1 nm (DEX-chitosomes). HuLa cells exhibited no significant cytotoxicity after a 72-hour exposure to DEX formulations. Cells remained viable and proliferated up to 0.5 μM, with a non-significant reduction at 1 μM **(Figure 1)**. **Figure 1. Nanoparticle characterization and cytotoxicity evaluation.** (a) Size and zeta potential measured with Malvern Zetasizer (n= 4) (b) Fluorescence images of LIVE/DEAD staining (green: live cells; red: dead cells) and (c) Relative viability quantified by CCK-8 at 72-hour post-treatment (n=4). Data is presented as mean ± SD.



Conclusion/Significance: Liposomes achieved a high DEX payload, and subsequent chitosan coating produced mucoadhesive surface charge without compromising laryngeal epithelial viability. This outcome met the first requirement towards aerosolized VF drug delivery. DEX-chitosomes formulation is currently being optimized for aerosol formation, deposition, and cellular uptake, prior to evaluating its antifibrotic efficacy in human-relevant 3D injured VF models.

Session 31
Biofabrication Technologies for Organoid Engineering

11-16-2026 @ 3:05 PM - 4:35 PM

OP-094 - A Glycocalyx-Mediated Macromolecular Assembly Platform for Organoid Engineering and Regenerative Tissue Repair

Xu Han, Colin Bishop, Anthony Atala

Wake Forest Univeristy, Wake Forest Institute of Regenerative Medicine, WINSTON SALEM, United States of America

Purpose/Objectives: Current regenerative therapies and biomaterial systems inadequately coordinate epithelial repair, extracellular matrix (ECM) remodeling, and tissue maturation. This study investigated ProteuSol®, a glycocalyx-directed polysaccharide cocktail designed to enhance regenerative signaling through integrin-mediated mechanotransduction. We hypothesized that ProteuSol interacts with heparan sulfate proteoglycans at the cell surface to reorganize receptor architecture and activate integrin–FAK signaling pathways that coordinate epithelial maturation and ECM remodeling. The objectives were to: (1) investigate glycocalyx-dependent mechanistic signaling; (2) evaluate tissue organization in organoids; (3) assess epithelial barrier enhancement in retinal pigment epithelial (RPE) tissues; and (4) determine regenerative efficacy in vivo using a murine wound-healing model.

Methodology: Glycocalyx-dependent signaling was evaluated through heparan sulfate inhibition, immunofluorescence staining, and analysis of integrin-associated focal adhesion kinase (FAK) activation. Skin organoids were generated using scaffold-free self-assembly methods and analyzed for epithelial stratification, ECM deposition, and tissue organization. Liver organoids were evaluated for hepatocyte maturation, stromal organization, and endothelial distribution. RPE tissues were analyzed for transepithelial electrical resistance (TEER) and ZO-1 tight junction organization. RNA sequencing and pathway enrichment analyses were performed to identify mechanotransduction-associated signaling pathways. In vivo regenerative potential was evaluated using a murine wound-healing model.

Results: ProteuSol induced robust glycocalyx-mediated mechanotransduction and enhanced tissue maturation across multiple regenerative systems. Mechanistic studies demonstrated activation of integrin-associated signaling and increased focal adhesion organization through heparan sulfate–dependent interactions. In RPE tissues, ProteuSol significantly increased TEER (50%) and enhanced ZO-1 organization. Skin organoids exhibited accelerated self-organization, enhanced epithelial stratification, and increased collagen deposition. Transcriptomic analyses demonstrated enrichment of integrin signaling, focal adhesion, and ECM remodeling pathways, with integrin β1 identified as a central signaling hub. Liver organoids showed enhanced albumin expression. In vivo, ProteuSol accelerated wound closure and promoted improved epithelial regeneration and collagen ultrastructure.

Conclusion/Significance: ProteuSol represents a glycocalyx-directed regenerative engineering platform that enhances tissue organization through integrin-mediated mechanotransduction rather than passive macromolecular crowding alone. Across mechanistic cellular studies, organoid systems, RPE tissues, and in vivo wound healing, the polysaccharide cocktail consistently promoted epithelial maturation, ECM remodeling, and coordinated tissue organization. These findings establish a new paradigm in which glycocalyx-directed macromolecular assembly functions as an active regulator of receptor organization and regenerative signaling.

OP-095 - Engineering Lumenized hiPSCs for Scalable Generation of Physiologically Relevant Multi-Organ Organoids in a Defined Synthetic Matrix

Xiuzhi Susan Sun

Wake Forest University School of Medicine, Wake Forest Institute Of Regenerative Medicine, Winston Salem, United States of America

Purpose/Objectives: Pluripotent stem cells (PSCs), including embryonic stem cells (ESCs) and human induced pluripotent stem cells (hiPSCs), hold significant potential for generating physiologically relevant organoids. However, this potential remains limited by conventional 2D culture systems and the lack of defined 3D microenvironments that support early morphogenesis. The objective of this study was to engineer lumenized hiPSCs (L-hiPSCs) within a synthetic extracellular matrix-mimetic hydrogel to promote self-organization, accelerate maturation, and enable coordinated multicellular and functional development across all three germ layers.

Methodology: A xeno-free synthetic peptide hydrogel (PGmatrix, PepGel LLC) was optimized to support long-term maintenance and expansion of L-hiPSCs. L-hiPSCs were directly differentiated into organoids without embryoid body formation. Cerebral, cardiac, and hepatic organoids were selected to represent ectodermal,

mesodermal, and endodermal lineages, respectively. Conventional organoid generation methods using 2D-expanded hiPSCs followed by suspension aggregation served as controls, while Matrigel was included as a benchmark matrix.

Results: The optimized hydrogel supported robust L-hiPSC formation with >96% viability and 12–20-fold expansion, depending on cell source and culture duration. Approximately 95% of hiPSCs formed lumenized structures, maintaining an intrinsic naïve-like state during long-term culture (>50 passages). L-hiPSCs generated self-organized organoids across all three germ layers. Cerebral organoids exhibited neurovascular-like complexity, including myelination, blood-brain barrier characteristics, and microglia-associated neuroimmune functions. Cardiac organoids developed multi-chamber architectures with synchronized beating and vascular-like structures. Hepatic organoids displayed physiologically relevant liver functions, including albumin production approaching 90% of primary human hepatocyte levels. Across all organoid types, L-hiPSC-derived organoids demonstrated enhanced structural organization, maturation, and functional performance compared with conventional controls.

Conclusion/Significance: A chemically defined, scalable, and reproducible synthetic peptide hydrogel enabled generation of lumenized hiPSCs and advanced brain, heart, and liver organoids within a fully defined 3D microenvironment. By integrating biomaterials engineering with developmental biology, this platform accelerates organoid maturation and functional complexity, providing human-relevant models for studying organ development, disease modeling, drug discovery, and therapeutic evaluation while advancing New Approach Methodologies (NAMs) as alternatives to animal models.

OP-097 - Rapid Generation of Tissue-Like Human Adipose Organoids

Yuan Wan[1], Jesse Liszewski[1], Austin Scholp[1], Aloysius Klingelhutz[2], Edward Sander[1], James Ankrum[1]

[1]*University of Iowa, Roy J. Carver Department of Biomedical Engineering, Iowa City, United States of America*
[2]*University of Iowa, Department of Immunology And Microbiology, Iowa City, United States of America*

Purpose/Objectives: This study aimed to develop a rapid and physiologically relevant human adipose organoid culture platform capable of achieving rapid lipid droplet enlargement and adipose maturation within 10 days. This is achieved by strategically blocking TGF-β1, adding an insulin sensitizer, and supplying free fatty acids during maturation.

Methodology: Immortalized pre-adipocytes were seeded into agarose micromolds and differentiated using PDM-2 adipogenic medium to generate human adipose organoids. To enhance adipogenic maturation, organoids were cultured with various combinations of 5μM SB431542 (SB), 2μM rosiglitazone (Rosi), and 500μM oleic acid (OA) supplementation during the first 5 days of differentiation, followed by OA treatment alone for an additional 5 days. Lipid accumulation and morphology were assessed by BODIPY and Hoechst staining.

Results: Combined treatment with SB431542, rosiglitazone, and OA produced the greatest enhancement in adipogenic maturation compared to control and single-factor treatment groups. BODIPY staining demonstrated substantially increased lipid accumulation and enlarged lipid droplet formation in optimized adipose organoids. Quantitative analysis revealed increased lipid coverage, elevated upper-percentile lipid droplet area, and a pronounced shift toward larger lipid droplet distributions under combinational treatment conditions. Among all groups, SB431542, rosiglitazone, and OA co-treatment generated adipose organoids with the most mature lipid morphology, including large lipid droplets resembling native white adipose tissue. Notably, this level of lipid droplet enlargement and adipose maturation was achieved within only **10 days**, whereas comparable adipose-like maturation typically requires **several months** in conventional culture systems.

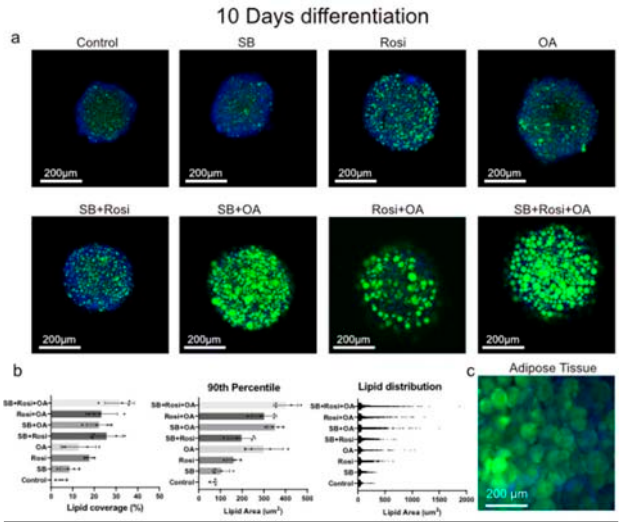


Figure 1. Human adipose organoid maturation can be accelerated through rational supplementation of differentiation media. (a) Representative BODIPY/Hoechst images of organoids treated with SB431542 (SB), rosiglitazone (Rosi), oleic acid (OA), or combinations. (b) Lipid coverage, 90th-percentile lipid area, and lipid size distribution. Scale bars = 200 μm. (c) Native adipose tissue shown as a morphology reference.

Conclusion/Significance: Rational supplementation of adipogenic media with a TGF-β1 inhibitor, insulin sensitizer, and free fatty acid resulted in significantly accelerated maturation of human adipose organoids. These organoids feature enlarged lipid droplets and tissue-like morphology within a culture period that is weeks shorter than previous strategies.

OP-098 - Bioengineered Melanoma-TME Organoids Model Context-Dependent Invasion and Drug Sensitivity Driven by Tumor Genotype and Microenvironmental Factors

Gemma Nomdedeu-Sancho[1], Nicholas Edenhoffer[1], Anastasiya Gorkun-Roeder[1], Anthony Atala[2], Shay Soker[2]

[1]*Wake Forest University School of Medicine, Wake Forest Institute For Regenerative Medicine, Winston-Salem, United States of America*
[2]*Wake Forest Institute for Regenerative Medicine, Winston Salem, United States of America*

Purpose/Objectives: Metastasis remains the main cause of mortality in cutaneous melanoma patients. While targeted and immunotherapies have improved patient survival, treatment resistance remains a major clinical challenge. Besides specific melanoma driver mutations, the tumor microenvironment (TME) critically influences prometastatic behaviors, such as invasion and migration, and represents a vital, yet underexploited, therapeutic target. However, the development of effective TME-directed therapies has been limited by the lack of relevant human in vitro models that capture the dynamic interactions between the tumor and the surrounding stroma.

Methodology: We generated melanoma-TME organoids (mTMEOs) by embedding layered melanoma-skin organoids (mSOs), containing BRAF-mutant, NRAS-mutant, or triple wild-type (TWT) melanoma cell lines, into fibroblast-laden collagen gels mimicking the human dermis. Invasion and cell-association patterns were tracked quantitatively using a custom-built image analysis tool applied to live-cell fluorescence microscopy. To validate the model's utility for drug screening of TME-directed therapies, we blocked tumor-ECM interactions by pharmacologically inhibiting focal adhesion kinase (FAK) with Defactinib.

Results: We found that fibroblasts significantly enhanced melanoma cell migration across all genetic backgrounds by promoting extracellular matrix (ECM) remodeling, though invasion rates varied based on cell-intrinsic properties. Furthermore, stromal fibroblasts altered cell-association behaviors: in BRAF-mutant cells, fibroblasts

restricted proliferation in favor of migration, whereas in NRAS-mutant cells, they promoted cell clustering and facilitated the transition to a collective-like migration mode. FAK inhibition successfully reduced migration in BRAF-mutant and TWT but not in NRAS-mutant lines, consistent with known mechanisms of increased invasiveness upon FAK downregulation in these cells.

Conclusion/Significance: The mTMEO platform effectively recapitulates both cell-intrinsic and TME-mediated mechanisms of tumor invasion and therapeutic response. Ongoing bulk RNA-seq analyses will further elucidate the genetic programs driving TME-induced motility. Ultimately, the rapid assembly and tunability of these organoids make them an ideal platform for high-throughput anti-metastatic drug discovery and testing. Future iterations incorporating patient-derived melanoma and stromal cells will likely provide a powerful tool for personalized oncology.

Session 32
Lymphatic Engineering and Regeneration

11-16-2026 @ 5:05 PM - 6:35 PM

OP-099 - Bio-Hybrid Electro-Osmotic Pumping Platform for Active Lymphatic Rerouting in Lymphedema

Shivesh Anand[1,2], Ande Marini[1,2], Tatiana Zaitseva[3], Michael Paukshto[3], Dung Nguyen[4], Ngan Huang[1,2]

[1]*Stanford University, Department of Cardiothoracic Surgery, Stanford, United States of America*
[2]*Stanford Cardiovascular Institute, Stanford, United States of America*
[3]*Fibralign Corporation, Union City, United States of America*
[4]*Stanford University, Division Of Plastic & Reconstructive Surgery, Palo Alto, United States of America*

Purpose/Objectives: Lymphedema is a progressive condition of the lymphatic system affecting up to 250 million people worldwide. Characterized by protein-rich fluid accumulation from compromised drainage, its current clinical interventions demand high surgical complexity and yield variable success. Existing biomaterials-based strategies rely on passive drainage, frequently failing against adverse pressure gradients. This work develops the first minimally invasive electro-osmotic pumping implant designed to actively reroute excess fluid and promote lymphangiogenesis for functional tissue recovery in lymphedema.

Methodology: Previously reported aligned nanofibrillar collagen scaffolds (BioBridge) were employed. A custom 3D-printed platform characterized bi-directional, voltage-driven flow (0-120 V) during electro-osmosis. Flow velocity and volume were quantified while continuously monitoring resultant currents for physiological safety. Theoretical simulations performed with COMSOL Multiphysics corroborated experimental pressure and velocity. Pre-clinical validation involved fluid transport assessment in explanted mouse tails, followed by subcutaneous rat implantation to compare active pumping against passive capillary flow. *In vivo* fluid dynamics were evaluated via near-infrared imaging and bioimpedance measurements. Finally, a rat hindlimb lymphedema model has been implemented to rigorously assess these novel bio-hybrid electro-osmotic pumps.

Results: BioBridge scaffolds exhibited voltage-dependent fluid transport with reversible directionality determined by electrode polarity (**Figure 1A**). Currents remained below 4 mA across all voltages, yielding flow velocities (20-30 μm/s) consistent with native lymphatic transport. *In silico* modeling corroborated that higher voltage generates requisite electro-osmotic pressure for these velocity gains (**Figure 1B**). Electro-osmotic efficacy was robustly preserved *ex vivo* in mouse tails (**Figure 1C**). *In vivo* near-infrared fluorescence imaging demonstrated uniform dye distribution with active flow over passive capillary control (**Figure 1D**). A rat hindlimb lymphedema model incorporating lymph node resection and X-ray irradiation has been established for translational validation (**Figure 1E**).

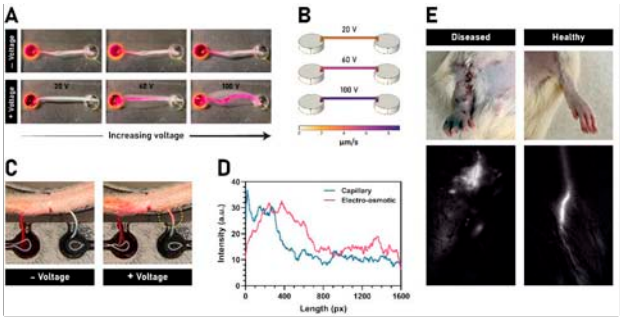


Figure 1. ***(A)*** *Voltage-dependent electro-osmotic flow.* ***(B)*** *In silico predictions.* ***(C)*** *Ex vivo validation in mouse tail.* ***(D)*** *In vivo dye quantification.* ***(E)*** *Successful rat hindlimb lymphedema model.*

Conclusion/Significance: Bio-hybrid electro-osmotic pumps demonstrated reversible, voltage-dependent fluid transport within physiologically safe parameters, consistent with computational predictions. *Ex vivo* and *in vivo* assessments confirmed active electro-osmosis outperforms passive capillary action. Future studies will validate therapeutic efficacy in the rat lymphedema model, combining electrical stimulation with FDA-cleared scaffolds to accelerate tissue recovery.

Session 33
Extracellular Vesicles for Regenerative Medicine, Drug Delivery, and Cell-Free Therapies

11-16-2026 @ 5:05 PM - 6:35 PM

OP-103 - Targeting Age-Associated Breast Cancer Progression Using Matrix-Bound EV-Informed Lipid Nanoparticles

Lauren Hawthorne, Pinar Zorlutuna

University of Notre Dame, Aerospace And Mechanical Engineering, Notre Dame, United States of America

Purpose/Objectives: Aging of the breast extracellular matrix (ECM) contributes to a pro-tumorigenic microenvironment that enhances cancer cell invasion and progression, in part through matrix-bound extracellular vesicles (MBVs) enriched in oncogenic cargo. However, MBV-driven effects across clinically relevant breast cancer subtypes remain poorly defined, and therapeutic strategies targeting these signals are lacking. This study aims to characterize age-dependent MBV function in HR+ and TNBC cells within a humanized age-mimetic platform and develop novel therapeutic lipid nanoparticles (LNPs) for the delivery of MBV-informed miRNAs.

Methodology: Age-mimetic hydrogels are engineered using young and aged human collagen I to recapitulate mammary ECM properties. Mechanical and structural validation was performed, and MBVs were isolated from young and aged ECM and characterized. HR+ and TNBC-derived cells were formed into organoids and encapsulated in hydrogels, followed by MBV treatment to assess viability, proliferation, and invasion. In parallel, LNPs were fabricated and loaded with miRNA mimics identified through machine learning analysis of MBV cargo. Nanoparticles were characterized for size, polydispersity, encapsulation efficiency, and uptake. Functional effects were evaluated in organoid models and compared against young/aged ECM conditions and FDA-approved therapies.

Results: Age mimetic hydrogels successfully recapitulated key mechanical and structural features of mammary ECM, with aged matrices exhibiting altered properties consistent with tissue aging. Aged MBVs promoted increased invasion and proliferation, while young MBVs suppressed malignant phenotypes. miR-loaded LNPs demonstrated efficient loading, stability, and cellular uptake, and delivery reduced cancerous phenotypes. FDA-approved therapeutics showed subtype- and age-dependent efficacy differences.

Conclusion/Significance: This study establishes an age-mimetic hydrogel platform to define the role of MBVs in subtype-specific breast cancer progression. Aged MBVs promote invasive and

proliferative phenotypes, while young MBVs exert protective effects. MBV-informed miR-loaded LNPs provide a strategy to counteract age-associated tumor signaling via miRNA delivery. Together, these findings offer mechanistic insight into ECM aging in breast cancer and support a translational framework for targeting microenvironment-driven disease progression. Evaluation of FDA-approved therapies in aged models further highlights age-dependent treatment responses, supporting improved therapeutic strategies for older patient populations.

OP-104 - Inter-donor Variability of Angiogenic microRNAs in MSC-Derived Extracellular Vesicles May Contribute to Inconsistent Regenerative Outcomes in Critical Limb Ischemia

Shoji Fukuda[1], Tomomi Kusakabe[2], Yoshiki Wada[3], Shinobu Akiyama[1], Masaki Kano[1], Shun Suzuki[1], Toshiki Fujiyoshi[1], Toru Iwahashi[1], Yusuke Shimahara[1]

[1]*Tokyo Medical University Hospital, Department of Cardiovascular Surgery, Tokyo, Japan*
[2]*Tokyo Medical University Hospital, Center For Cell Therapy And Regenerative Medicine, Tokyo, Japan*
[3]*Institute of Science Tokyo, Department of Vascular Surgery, Tokyo, Japan*

Purpose/Objectives: Therapeutic responses to mesenchymal stromal cell (MSC)-based angiogenic therapy for critical limb ischemia (CLI) remain highly variable among patients. We hypothesized that donor-dependent differences in angiogenic microRNAs (miRNAs) within MSC-derived extracellular vesicles (EVs) contribute to variability in regenerative potency.

Methodology: Bone marrow-derived MSCs were cultured, and EV-associated angiogenic miRNAs were analyzed by RT-qPCR. miR-9, miR-105, miR-126, miR-135b, and miR-210 were investigated. In vitro angiogenic activity was evaluated using HUVEC tube formation assays. In vivo therapeutic efficacy was assessed using a murine hindlimb ischemia model with full-field laser perfusion imaging (FLPI).

Results: Among the investigated angiogenic miRNAs, miR-126, miR-135b, and miR-210 were consistently detected in MSC-derived EVs, whereas miR-9 and miR-105 were not detected, suggesting selective miRNA loading into EVs. In CLI-relevant donors aged >60 years, angiogenic miRNA secretion from MSC-derived EVs was lower than in younger donors and demonstrated substantial inter-donor variability, with up to 3-fold differences observed within the elderly group. EVs with higher angiogenic miRNA levels showed stronger pro-angiogenic activity in vitro. In vivo, EVs enriched with angiogenic miRNAs significantly improved perfusion recovery compared with control EVs lacking these miRNAs.

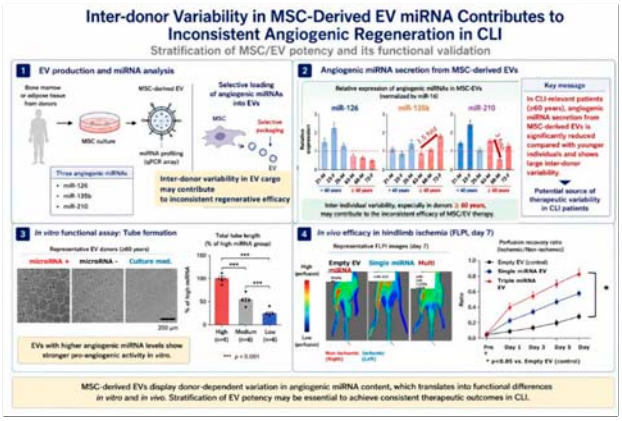


Figure legend: Inter-donor variability in angiogenic miRNA content of MSC-derived EVs contributes to functional differences in vitro and in vivo. Elderly donors relevant to CLI therapy exhibit reduced angiogenic miRNA secretion and marked variability, suggesting a potential source of inconsistent regenerative efficacy.

Conclusion/Significance: Donor-dependent variability in angiogenic miRNA content of MSC-derived EVs may represent an important determinant of regenerative potency and therapeutic inconsistency in CLI. Angiogenic miRNA profiling may support donor stratification, potency assessment, and improved reproducibility of MSC/EV-based regenerative medicine.

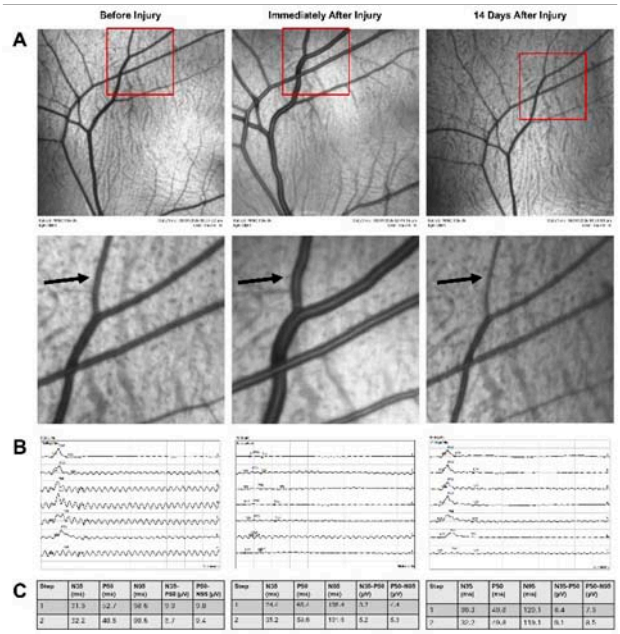
OP-105 - Matrix-Bound Nanovesicle-Mediated Immunomodulation to Protect and Repair Injured Retina and Optic Nerve

Peyton Leyendecker[1,2], Scott Johnson[2,3], Catalina Pineda Molina[2,3], Ethan Rossi[1,4], George Hussey[1,2,3,5]

[1]*University of Pittsburgh Swanson School of Engineering, Department of Bioengineering, Pittsburgh, United States of America*
[2]*McGowan Institute for Regenerative Medicine, Pittsburgh, United States of America*
[3]*University of Pittsburgh School of Medicine, Department of Surgery, Pittsburgh, United States of America*
[4]*University of Pittsburgh School of Medicine, Department of Ophthalmology, Pittsburgh, United States of America*
[5]*University of Pittsburgh School of Medicine, Department of Pathology, Pittsburgh, United States of America*

Purpose/Objectives: Traumatic retinal and optic nerve injury causes irreversible vision loss in warfare, worsened by combat logistic delays (up to 5 days) before specialized microsurgery. During this window, secondary pro-inflammatory cascades often inflict more damage than the initial trauma. This study introduces a portable, off-the-shelf matrix-bound nanovesicle (MBV) therapy for immediate field application to minimize this secondary trauma and preserve visual function.

Methodology: We evaluated MBV efficacy in a porcine model of acute ocular hypertension. Pigs were assigned to injury-only controls or treated with intravitreal injections of low, medium, or high MBV doses and survived for 14 days. Retinal changes were assessed longitudinally via portable fundus photography, scanning laser ophthalmoscopy (SLO), and pattern electroretinography (PERG). Post-mortem evaluations utilized hematoxylin & eosin for retinal architecture, Luxol Fast Blue (LFB) for optic nerve myelination, and immunohistochemistry for retinal ganglion cell (RGC) survival, astrocyte reactivity, axonal integrity, and apoptosis.



Results: Longitudinal SLO and portable fundus imaging showed acute post-injury vasodilation and increased vessel tortuosity across all groups, progressing to marked vasoconstriction by day 14 in

untreated eyes (**Figure 1A**). By day 14, injury-only controls exhibited marked vessel atrophy and increased cup-to-disc (C/D) ratios, indicating structural damage. Conversely, medium and high-dose MBVs prevented vessel constriction, with high-dose eyes maintaining pre-injury C/D baselines. Representative PERG recordings (**Figure 1B**) demonstrated a decrease in wave amplitude (by ~50%) and increased latency (by ~10 ms) immediately following injury (**Figure 1C**). By day 14, untreated eyes exhibited a ~20 ms increase in N95 latency (**Figure 1C**), indicating a highly compromised, slow-response RGC state. Histologically, injury-only eyes displayed architectural disruption and thinning of the ganglion cell layer (GCL). High-dose MBVs preserved retinal architecture, maintaining GCL density and thickness indistinguishable from uninjured controls. Furthermore, untreated injured nerves showed reduced LFB staining, suggesting myelin loss, while high-dose MBVs preserved staining at baseline levels.

Conclusion/Significance: This established porcine model demonstrates that MBV therapy provides promising neuroprotection following ocular trauma. By mitigating secondary injury mechanisms, MBVs preserve retinal vascular health, structural architecture, and optic nerve morphology. These findings support the continued optimization of MBVs as a transformative, field-deployable therapeutic to prevent permanent vision loss in injured service members.

OP-106 - Homing, Remodeling, and Repair: Estradiol-Conditioned MSC-Derived Extracellular Vesicles as a Cell-Free Strategy for Elastic Matrix Restoration in Abdominal Aortic Aneurysm

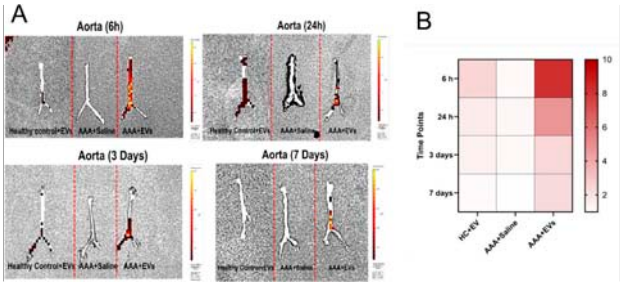
Ali Abba Mutah[1], Anand Ramamurthi[2]

[1]*Lehigh University, Bethlehem PA., Bethlehem, United States of America*
[2]*Lehigh University, Bethlehem PA., Bioengineering, Bethlehem, United States of America*

Purpose/Objectives: Introduction: Abdominal aortic aneurysm (AAAs) is a rupture-prone and fatal localized dilatation of the abdominal aorta due to chronic proteolysis. Current management of AAAs is primarily open surgical or endovascular without a pharmacological option. Clinical prevalence of AAAs is 6-fold higher in males than in pre-menopausal females. Evidence suggests that female sex hormones such as estrogen (17β-estradiol or E2) may reduce AAA formation and rupture. E2-conditioned MSCs showed improved cardioprotective effects vs. untreated MSCs. MSC secretion of extracellular vesicles (EVs) has been shown to mediate these therapeutic effects. Therefore, E2-primed-EVs could render them more protective against disorders like AAAs. We investigated the fate of MSC-EVs in a rat AAA model, critical for evaluating their therapeutic efficacy in vivo and the effects of E2 pre-treatment on vascular remodeling.

Methodology: Methods: EVs were isolated from male, E2-conditioned male and female human bone marrow – MSCs culture using differential ultracentrifugation. Elastase-injured SD rat AAA models were exposed to vehicle (PBS) alone (diseased controls), whereas healthy rats (negative controls) and AAA rats (test) received fluoro-tagged (near infra-red ExoGlow-Vivo dye) EVs, respectively. Fluor-tagged EVs were tracked (6 hours, 24 hours, 72 hours and 7 days) following systemic administration, and major organs were imaged/sequenced for EV presence. To determine the E2 priming effect of generated EVs, elastase-induced rat aneurysmal smooth muscle cells and rat AAA models were treated with EVs from male MSCs, E2-primed male MSCs and female MSCs.

Results: Results and Discussion: Imaging revealed EV uptake at aneurysmal sites within the initial 6-24 h, though retention declined by day 3, through day 7 (Fig.1). qPCR results showed a significantly higher TIMP2 gene expression with EVs from E2-primed male cells compared to the non-primed male, female EVs and the control. Similarly, western blot results show a significantly higher TIMP2 protein with E2-primed male EVs compared to female EVs. Overall, MMP2 gene and protein expressions were significantly lowered with EVs from the treated samples compared to the non-treated.



Conclusion/Significance: This approach, coupled with repeat dosing at weekly intervals, holds potential for maximizing MSC-ENV therapeutic benefits, including elastic matrix restoration and inflammatory modulation, toward a stem cell-inspired, cell-free treatment for AAAs.

Session 34
Scaffolds, Matrices, and Biomaterials (General Session) 1

11-16-2026 @ 5:05 PM - 6:35 PM

OP-107 - Extracellular matrix fragments as microenvironmental regulators of adipogenic and angiogenic processes in a reconstructed human adipose tissue model for tissue engineering applications

Elias Cuartas-Gomez[1,2], Fanny Brunard[1,2], Viviane Séguin[1], Sylvie Ricard-Blum[3], Julie Fradette[1,2]

[1]*CHU de Québec-Université Laval Research Centre, Division Of Regenerative Medicine, Centre De Recherche En Organogénèse Expérimentale De L'université Laval / Loex, Québec, Canada*
[2]*Laval University, Department of Surgery, Québec, Canada*
[3]*Institut de Chimie et Biochimie Moléculaires et Supramoléculaires (ICBMS), Umr 5246 Cnrs Université Lyon 1, Lyon, France*

Purpose/Objectives: Extracellular matrix can release biologically active fragments (matricryptins) displaying activities that may differ from their parent molecules. Periostin (FL-POSTN) is a matricellular protein presenting context-dependent effects during angiogenesis and adipogenesis, processes that are central to successfully engineer microvascularized adipose tissue *in vitro*. However, the impact of the $POSTN_{136-151}$fragment on human adipocyte differentiation and endothelial cell migration remains unexplored. We hypothesize that $POSTN_{136-151}$ i) will not impair lipid accumulation, in contrast to FL-POSTN, during the differentiation of human adipose-derived stromal/stem cells (ASCs) in a biomimetic 3D human reconstructed adipose tissue (hrAT) model, and ii) will promote the migration of human endothelial cells (ECs).

Methodology: Cultures of ASCs (N=3 females, 36.3 ± 1.5 years) were treated in triplicate for 22 days with an adipogenic medium supplemented with 250 µM ascorbic acid, $POSTN_{136-151}$(0.25-1 µM), FL-POSTN (0.6 and 1.2 µM) or endostatin (ES, 1.1 µM), an anti-angiogenic and anti-adipogenic matricryptin of collagen XVIII. Metabolic activity, DNA content and lipid accumulation were evaluated via AlamarBlue™, PicoGreen™ and Oil Red O staining, respectively. VEGF and leptin levels were measured by ELISA assays.

Results: ASC metabolic activity and DNA content were not significantly modified in the supplemented hrATs. FL-POSTN and ES decreased lipid accumulation by 19.5 and 40.8% ($p<0.05$) respectively compared to controls. FL-POSTN and ES anti-adipogenic effects were reported in murine models, but we describe them for the first time in a 3D human AT model. $POSTN_{136-151}$did not significantly ($p>0.05$) alter lipid accumulation. The average lipid droplet size did not differ between each group ($p>0.05$). ES significantly reduced adipocyte-derived leptin and $VEGF_{165}$ secretion by 20.6 and 13.8% respectively ($p<0.05$). FL-POSTN reduced leptin secretion (13.4%, $p<0.05$) but not $VEGF_{165}$, while $POSTN_{136-151}$had no effect. Preliminary data showed that $POSTN_{136-151}$ (0.5 µM)

increased EC migration by 1.2-fold over 24 h, while ES reduced it by 1.3-fold compared to the controls ($p<0.05$). No differences were measured for FL-POSTN.

Conclusion/Significance: These findings reveal that FL-POSTN and ES negatively impact human adipocyte differentiation in a biomimetic AT model, while $POSTN_{136-151}$ preserves adipogenesis and enhances endothelial migration, highlighting the potential of this matricryptin as a microenvironmental regulator for tissue engineering applications.

OP-108 - Extracellular matrix remodeling in women with polypropylene mesh complications: a proteomics approach

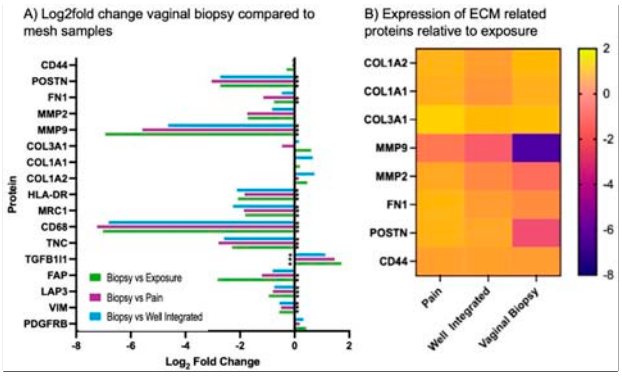
Malini Harinath, Marrisa Therriault, Jordan Head, Tianjiao Chu, Pamela Moalli, Amanda Artsen

Magee Womens Research Institute, Pittsburgh, United States of America

Purpose/Objectives: Polypropylene mesh complications, most commonly manifested as mesh pain and exposure, are characterized by chronic foreign body inflammation, aberrant matrix remodeling, fibrosis, and epithelial failure. However, the extracellular matrix pathways associated with divergent clinical phenotypes remain incompletely defined. This study uses proteomics to compare extracellular matrix (ECM) proteins and remodeling enzymes to identify new targets for mechanistic investigation and therapeutic intervention. We hypothesized that ECM dysregulation would be higher in women with mesh exposure as compared to women with mesh related pain.

Methodology: Samples from women with well-integrated mesh (N=9), mesh exposure through the vaginal epithelium (N=9), mesh-pain (N=10) and 10 control vagina without mesh underwent proteomic analysis. Specimens were lysed, digested, and normalized to 50µg total protein and nano-scale liquid chromatographic tandem mass spectrometry was performed. Forty ECM-related proteins were selected *a priori* for a hypothesis-driven differentially expressed protein analysis.

Results: There were no significant differences in menopausal status or age in patients with well-integrated mesh (62±13 years), pain (49±14 years), or exposure (52±7 years), while control subjects were slightly younger (42±6 years). Twenty *a priori*proteins were identified in the dataset. Eleven were differentially expressed in mesh samples relative to control (adjusted $p<0.05$), including upregulation of CD68, MMP9, tenascin C, and periostin, and down regulation of TGFβ11. Fibroblast activation protein and fibronectin were elevated in exposure and pain but not well-integrated mesh, indicating a differential response in complications. **Figure 1.** (A) Differential expression of ECM proteins in vaginal biopsy controls relative to exposure, pain, and well-integrated mesh. Bars to the left indicate lower levels in controls and upregulation in mesh while bars to the right indicate higher levels in controls and therefore downregulation in mesh samples. (B) Differential expression of ECM proteins in pain, well-integrated mesh, and vaginal biopsy controls relative to exposure.



Conclusion/Significance: Mesh complications were associated with distinct ECM remodeling signatures. Enrichment of matricellular proteins including periostin and tenascin-C suggests persistent injury-associated remodeling, while altered TGFβ1I1 implicates disrupted focal adhesion-mediated TGFβ signaling. These findings identify candidate pathways underlying failed mesh integration and provide mechanistic targets for biomaterial design and therapeutic modulation of the foreign body response.

OP-109 - Matrix stiffness reveals distinct activation and early YAP (Yes-Associated Proteins) nuclear translocation of human vaginal fibroblasts from prolapsed tissues in-vitro

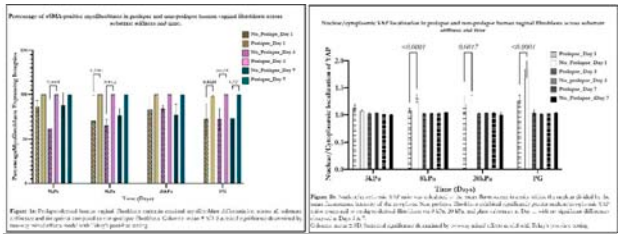
Temitope Obisesan[1], Mya Fulton[1], Pamela Moalli[2]

[1]*University of Pittsburgh, Bioengineering, Pittsburgh, United States of America*
[2]*Magee Womens Research Institute, Pittsburgh, United States of America*

Purpose/Objectives: Fibroblasts mediate vaginal repair through fibroblast-to-myofibroblast transition (FMT) in response to mechanical and biochemical cues. While transient FMT supports normal wound healing, persistent activation promotes fibrosis and aberrant matrix remodeling. Pelvic organ prolapse (POP) is associated with altered tissue biomechanics, suggesting dysregulated mechanotransduction. We hypothesized that increasing substrate stiffness would enhance FMT and mechanotransduction signaling, with prolapse-derived human vaginal fibroblasts (hvfs) exhibiting accelerated myofibroblast differentiation and altered mechanosensitivity.

Methodology: Primary human vaginal fibroblasts (hvfs) were isolated from prolapse and non-prolapse vagina (n=3/ group). Hvfs were seeded onto RGD-functionalized polyacrylamide gels tuned to physiologic (5, 8, and 20 kPa) stiffness levels, with glass serving as a high-stiffness control. Cells were cultured 1, 3, or 7 days. Immunofluorescence staining assessed fibroblast phenotype (vimentin), myofibroblast differentiation (αSMA), integrin α5β1 expression as a myofibroblast mechanosensory receptor, and mechanotransduction through nuclear/cytoplasmic YAP localization. Statistical analysis was performed using a two-way mixed effects model with Tukey's post-hoc testing ($p<0.05$).

Results: At Day 1, non-prolapse hvfs cultured on glass and 8 kPa substrates demonstrated 26% ($p=0.0324$) and 29% ($p=0.009$) fewer myofibroblasts, respectively, compared to prolapse-derived hvfs. By Day 3, between groups, non-prolapse hvfs exhibited reduced myofibroblast differentiation across 5 kPa (38%, $p=0.0004$), 8 kPa (35%, $p=0.001$), and glass substrates (28%, $p=0.0190$). At Day 7, differences persisted only on glass substrates, where non-prolapse hvfs maintained 27% fewer myofibroblasts ($p=0.02$). In contrast, prolapse-derived hvfs maintained a near-complete myofibroblast phenotype across all stiffness conditions and time points (Figure 1A). Integrin α5β1 expression remained elevated in prolapse-derived hvfs, consistent with persistent fibroblast activation. Both groups demonstrated stiffness-dependent YAP nuclear localization at Day 1 (Figure 1B); however, non-prolapse hvfs exhibited greater stiffness-sensitive YAP nuclear translocation on 8 kPa ($p<0.0001$), 20 kPa ($p=0.0017$), and glass substrates ($p<0.0001$). No significant differences in YAP localization were observed by Days 3 or 7.



Conclusion/Significance: While matrix stiffness augmented FMT and mechanotransduction responses in both groups, prolapse-derived hvfs maintained a 100% myofibroblast phenotype across all conditions and demonstrated a significantly reduced

stiffness-sensitive YAP response. These findings suggest impaired mechanoadaptation and constitutive fibroblast activation in prolapse-derived hvfs, supporting a role for dysregulated mechanotransduction in aberrant vaginal tissue remodeling associated with POP.

OP-110 - Extracellular Matrix Hydrogels Derived from Porcine Reproductive Tissues Preserve Tissue-Specific Regenerative Signatures and Modulate Wound Healing

Gustavo Henrique Almeida[1,2], Luan Lima[1], Celso Vitor Calomeno[3], Bianca Candian[4], Leonardo Adolfo Stella[2], Sergio Chammas[2], Durvanei Maria[2]

[1]*Faculty of Veterinary Medicine and Animal Science, University of São Paulo, Pathology, São Paulo, Brazil*
[2]*Butantan Institute, Center Of Development And Innovation - Cdi, São Paulo, Brazil*
[3]*Institute of Biomedical Sciences, University of São Paulo, Microbiology, São Paulo, Brazil*
[4]*State University of Maringá, Biochemistry, Maringá, Brazil*

Purpose/Objectives: To develop and characterize tissue-specific extracellular matrix-derived hydrogels obtained from porcine reproductive organs and evaluate how their distinct ultrastructural, rheological, and proteomic profiles differentially influence cytocompatibility, biocompatibility, and cutaneous wound healing responses in vitro and in vivo.

Methodology: Decellularized extracellular matrices obtained from porcine ovary, ampulla, uterus, and placenta were processed into injectable hydrogels through enzymatic digestion and neutralization. The biomaterials were characterized by scanning electron microscopy, gelation kinetics, ATR-FTIR spectroscopy, rheological analysis, and LC–MS/MS-based proteomics. Cytocompatibility was evaluated in HaCaT and L929 cells using Live/Dead, resazurin, and DAPI/phalloidin assays, while hemocompatibility was assessed by hemolysis testing. In vivo biocompatibility was investigated through subcutaneous implantation in Wistar rats, followed by histopathological analysis. The regenerative potential of the hydrogels was further evaluated in a full-thickness cutaneous wound model in rats through macroscopic and histological analyses.

Results: ECM-derived hydrogels exhibited marked tissue-dependent ultrastructural, rheological, and proteomic differences, demonstrating that the origin of the extracellular matrix directly influenced biomaterial organization and biological behavior. AmpECM and PlaECM hydrogels showed more organized, cohesive, and mechanically stable fibrillar networks, with enhanced viscoelastic properties and rapid gelation kinetics. Proteomic and functional enrichment analyses revealed preservation of tissue-specific extracellular matrix signatures associated with angiogenesis, extracellular matrix remodeling, focal adhesion, integrin-mediated signaling, and cell migration pathways. In vitro assays demonstrated high cytocompatibility and hemocompatibility for all hydrogels, supporting cell viability, adhesion, cytoskeletal organization, and metabolic activity without significant cytotoxic or hemolytic effects. In vivo, the biomaterials exhibited favorable biocompatibility profiles characterized by reduced inflammatory infiltrate and fibrosis, absence of adverse tissue reactions, and improved tissue integration compared to sham controls, supporting their regenerative potential for cutaneous wound healing applications.

Conclusion/Significance: Porcine reproductive tissue-derived ECM hydrogels preserved tissue-specific structural and molecular characteristics after decellularization and hydrogel formation, resulting in distinct biological and regenerative behaviors. Overall, the biomaterials demonstrated favorable physicochemical properties, high cyto- and hemocompatibility, excellent in vivo biocompatibility, and the ability to modulate tissue remodeling responses, supporting their potential as biologically instructive platforms for regenerative medicine and cutaneous wound healing applications.

Session 35
Musculoskeletal (General Session) 1

11-16-2026 @ 5:05 PM - 6:35 PM

OP-113 - Pirfenidone Treatment Compromises Functional Recovery: A Case for Reconsidering Antifibrotic Strategies in Musculoskeletal Injury

Jessica Motherwell[1,2], Ondine Eken[1,2,3], Claudia Hernandez[1,2,4], Christopher Dearth[1,2], Stephen Goldman[1,2]

[1]*Defense Health Agency, Falls Church, United States of America*
[2]*Uniformed Services University of the Health Sciences, Surgery, Bethesda, United States of America*
[3]*The Henry M. Jackson Foundation for the Advancement of Military Medicine, Inc., Bethesda, United States of America*
[4]*C2 Alaska, LLC, San Antonio, United States of America*

Purpose/Objectives: Volumetric muscle loss (VML) injuries result in a permanent loss of functional skeletal muscle that exceeds the endogenous capacity for regeneration. This pathology is characterized by a persistent inflammatory response and transforming growth factor-β1 (TGF-β1) signaling, which drives excessive fibrotic deposition and hinders *de novo* myogenesis. Repurposing FDA-approved antifibrotics, such as nintedanib and pirfenidone, presents a near-term translational strategy to mitigate this VML-induced scarring. However, while nintedanib attenuated fibrosis in a porcine VML model, it also reduced the functional capacity of the injured musculature. Pirfenidone, a more established small molecule with pleiotropic anti-inflammatory and TGF-β1-suppressing properties, has shown efficacy in hepatic and cardiac tissues but remains uncharacterized in skeletal muscle applications. To close this knowledge gap, we investigated whether pirfenidone treatment would mitigate the pro-fibrotic response and facilitate functional skeletal muscle recovery in a clinically relevant porcine model.

Methodology: Yorkshire-cross pigs (n=12) underwent VML injury or sham procedure in the peroneus tertius muscle and were subsequently allocated to pirfenidone treatment or untreated controls. The antifibrotic was administered at the approved clinical dose (2403 mg/day). At the 4-week study endpoint, the affected muscles underwent comprehensive histological, biochemical, transcriptional, and neuromuscular functional assessments.

Results: Transcription profiling demonstrated that pirfenidone downregulated key pro-inflammatory cytokine and chemokine regulators involved in excessive fibrosis, including TNF, CCL3L1, and CCL2. Although pirfenidone treatment failed to reduce total collagen deposition, evidenced by Picrosirius Red quantification and hydroxyproline content, it did result in a less dense collagen fiber architecture by polarized image analysis, suggestive of altered tissue remodeling. However, pirfenidone treatment impaired functional recovery through reduced contractile output and lower weight gain compared to the untreated cohort.

Conclusion/Significance: This work demonstrates that systemic pirfenidone administration failed to meaningfully reduce fibrosis and subsequently worsened muscle function following VML injury, similar to previous studies. The functional deficits and stagnant weight gains observed in this and prior studies underscore a critical knowledge gap regarding the impact of systemic antifibrotics on contractile recovery following VML, necessitating a rigorous re-evaluation of delivery routes, dosages, and administration timelines to ensure that future therapies for fibrotic scarring do not inadvertently hinder the physiological recovery of traumatically injured skeletal muscle.

OP-115 - Advanced Age Delays Functional Recovery Following Composite Bone-Muscle Injury

Austin Ricci, Cynthia Alcazar-Daleo, Joshua Vanderpool, Karina Nakayama

Oregon Health and Sciences University, Biomedical Engineering, Portland, United States of America

Purpose/Objectives: Traumatic musculoskeletal injuries involving bone and muscle require complex surgery and prolonged rehabilitation, often leading to limb salvage or amputation and severe mobility impairments[1]. Exercise improves muscle mass and recovery in young mice after volumetric muscle loss (VML)[2,3] but its effects on multi-tissue injuries in aged musculoskeletal systems, where regenerative capacity and mobility are reduced[4,5], remain unclear. This poses clinical challenges when designing rehabilitative approaches, highlighting the need for targeted regenerative and rehabilitative treatment options tailored to specific age groups. This study aimed to evaluate bone-muscle regeneration and functional recovery after composite tissue injury (CTI) in aged mice and whether exercise accelerates recovery.

Methodology: 16 aged (24–26mo) male C57BL/6 mice underwent CTI (2 mm tibia osteotomy + ~30% TA VML). After 14 days of rehabilitation, 8 mice received running wheels (exercised, EX) and 8 remained in standard cages (non-exercised, NE) for 14 days. Dynamic weight bearing assessed mobility at baseline, d7, d14, d21, and d28. At d28, micro-Computed Tomography measured injured tibia bone volume (BV) and mineral density (BMD) against 3 age-matched control mice (CON), and terminal muscle physiology evaluated contractility and fatigability of injured and contralateral TA.

Results: Daily running distance ranged from 0-865m/d and averaged 357.7±352.3m/d. 3 mice ran <11m/d and are considered to be NE. Injured:uninjured ratio of limb weight bearing recovered to baseline at d14 and was not different between NE and EX. BV ($p<0.001$) and BMD ($p<0.001$) were lower in CTI than CON ($p<0.001$), but not different between NE and EX. CTI reduced muscle force ($p<0.001$) yet was not different between NE and EX in either limb. CTI had greater fatigue resistance ($p<0.001$) and force recovery ($p<0.05$) than uninjured limbs. Figure 1. A). Surgical procedure for CTI. B). Limb weight bearing (left) and LMS (right). Bone volume (left) and mineral density (right). D). Maximum force (left), RFD (middle), and fatigability (right). Data presented as mean ± SD. *injury, #exercise

Conclusion/Significance: Aged mice exhibited persistent deficits in BV, BMD, and muscle force over 28 days, unresponsive to exercise. Exercise exposure varied widely, and activity was lower than in young mice from previous studies. Overall, advanced age delays musculoskeletal recovery following CTI.

OP-116 - FK506-loaded Biosponges Exhibit Sex-Specific Responses in a Rat Volumetric Muscle Loss Model

Jamshid Tadiwala[1], Priya Modi[2], Nishitha Mekala[3], Abigail Mallo[1], Koyal Garg[1]

[1]*School of Science and Engineering, Saint Louis University, Biomedical Engineering, Saint Louis, United States of America*
[2]*College for Public Health and Social Justice, Health Management, Saint Louis, United States of America*
[3]*College of Arts and Sciences, Neuroscience, Saint Louis, United States of America*

Purpose/Objectives: Inflammation persists for several weeks following volumetric muscle loss (VML), defined as the surgical or traumatic loss of muscle tissue, resulting in functional impairment. Heightened inflammation ultimately contributes to extensive fibrosis and loss of limb function. As a result, VML often leads to compromised quality of life, permanent disability, and delayed amputations. To modulate the inflammatory response at the site of trauma, biosponge (BSG) scaffolds were loaded with FK506 (Tacrolimus), an FDA-approved immunosuppressant. To achieve prolonged and sustained FK506 release, electrostatic interactions between gelatin nanoparticles (GNPs) and BSGs were exploited.

Methodology: Positively charged GNPs with or without FK506 were embedded into negatively charged BSGs. VML-injured TA muscles were either treated with blank GNP BSGs or FK506-loaded GNP BSGs (~20 μg FK506 per sponge) (n=4-6/group/time-point). On 7 and 28 days post-injury (dpi), TA muscles were weighed and preserved for histological and biochemical analysis. Gene expression of innate and adaptive inflammatory markers was determined at 7 dpi using an RT2 Profiler PCR array kit. At 14 dpi, all animals received intramuscular injection of either blank GNPs or FK506-loaded GNPs. At 28 dpi, sub-maximal (80 Hz) and peak isometric torque (150 Hz) were determined before euthanasia.

Results: The concentration of FK506 released from biosponges was found to be between 1 and 1.5 μg/ml over 5 days, suggesting consistent availability of the drug at the injury site upon implantation. While females showed significant ($p < 0.05$) upregulation of IL-1b, IL-6, and IL-1a, all inflammatory genes were downregulated in males with FK-506 treatment at 7 dpi. T cells ($CD3^+$) were decreased in males ($p=0.0288$) but not in females ($p=0.0118$) at 7 dpi with FK506 treatment. At 28 dpi, only males exhibited a significant increase in mean myofiber size with a higher percentage of large-sized fibers (>5000 μm^2).

Conclusion/Significance: Collectively, FK506 reduced inflammation in males and promoted myofiber maturation and hypertrophy, whereas similar effects were not observed in females, highlighting sex dependent effects of the drug in VML injuries. Currently, there is no FDA-approved therapy for VML. An acellular bioscaffold therapy with both immunomodulatory and regenerative properties is a promising solution for these injuries.

OP-117 - Scaffolds fabricated using different techniques resemble the structural and compositional properties of osteochondral tissues from different species

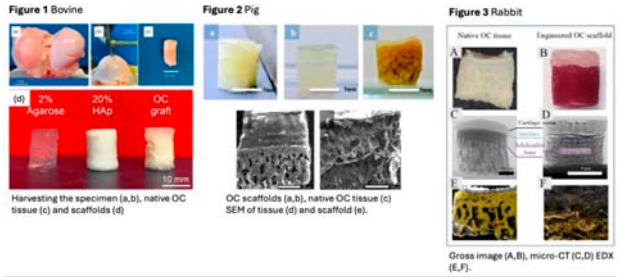
Swera Naz[1], Xiao Zhao[2], Victoria Effanga[1], Albina Abdossova[1], Dilhan Kalyon[2], Cevat Erisken[1]

[1]*Nazarbayev University, Chemical And Materials Engineering, Astana, Kazakhstan*
[2]*Stevens Institute of Technology, Hoboken, United States of America*

Purpose/Objectives: We fabricated tri-layered scaffolds employing different techniques including extrusion, 3D printing and molding using agarose (Ag) and gelatin Methacrylate (GelMA) for the cartilage region; addition of nano-hydroxyapatite (nHAp) to these for bone region; and polycaprolactone (PCL) nanofiber mesh to represent the tidemark. Theobjective was to compare the structural properties of the scaffolds with the native osteochondral (OC) interface harvested from bovine, pig and rabbit.

Methodology: Agarose and Agarose-Hydroxyapatite(HAp) composite-gels were prepared for cartilage and subchondral bone. A twin-screw extruder was used to form OC scaffolds of agarose. GelMA scaffolds were prepared using 3D-printing and molding. A solution of Type B Gelatin was prepared in PBS and methacrylic anhydride was added in drops, allowing reaction to proceed with stirring. The solution was dialyzed for 7 days, lyophilized for 3 days to produce GelMA. GelMA was either printed or molded. In either case an electrospun PCL mesh was placed between cartilage and bone layers. GelMA was cured using Irgacure. To prepare hydrogel for bone region, nHAp was added to GelMA and cured. Compositions were determined using thermogravimetric-analysis, EDX-mapping, and micro-CT. Biomechanical properties were determined upon compression at 0.05mm/s. Migration of osteoblasts through PCL membrane was measured using Live/Dead-assay.

Results: Mineral gradient thickness in the scaffold fabricated using extrusion, 3D printing and molding were 645±6μm*, 151±24μm*, 260±33μm*, respectively. The thickness was determined as 275±3μm for bovine, 250±23μm for pig, and 151μm* for rabbit tissues. Scaffolds fabricated with extrusion, 3D printing and molding had moduli values of 0.04±0.01MPa, 0.07±0.05 MPa, and 0.1±0.08MPa, respectively. It was determined as 2.13±0.55MPa, 1.8 ± 0.1MPa, and 0.6±0.02MPa*, for bovine, pig and rabbit, respectively. All the samples exhibited a viscoelastic behavior ($G' > G''$). Morphological examination revealed a pore size optimized to region-specific functionality (80-180μm in cartilage and 100-350μm in bone). Electrospun PCL mesh had submicron pore sizes (0.2-1.2μm) and fiber diameters (0.1-0.7μm), resembling the native tidemark. *$p<0.05$ Funded by Science Committee of Ministry of Science and Higher Education of Republic of Kazakhstan, Grant-No: AP26195607.



Conclusion/Significance: This study demonstrated methods to create biomimetic grafts that could be used in the regeneration of OC defects, addressing a critical clinical need that affects millions of people globally.

Session 36
Advancing MPS as New Approach Methods (Nams)

11-16-2026 @ 5:05 PM - 6:35 PM

OP-121 - A human placenta barrier model for translational assessment of inflammatory and autoimmune stressors across gestation

Justine Noel[1], Yu-Chi Chen[2], Cristina Acedo[2], Min Jae Song[2], Marc Ferrer-Alegre[2], Kyung Sung[3]

[1]*NIH/FDA, Ncats/cber, Rockville, United States of America*
[2]*National Center For Advancing Translational Sciences, Rockville, United States of America*
[3]*FDA, Silver Spring, United States of America*

Purpose/Objectives: Placental insufficiency is a major driver of adverse pregnancy outcomes, including preeclampsia, intrauterine growth restriction, and preterm birth. Inflammation and maternal autoimmune conditions are key contributors, yet their gestational-stage–specific effects on placental barrier function remain poorly understood due to limitations of conventional in vitro systems. To address this gap, we developed a 96 well 3D bioprinted human placenta barrier model that recapitulates the cellular architecture and functional properties of the maternal–fetal interface across gestation.

Methodology: The objective of this study was to investigate how inflammatory and autoimmune-related stressors differentially affect placental barrier function at distinct stages of pregnancy and to evaluate the utility of this platform for mechanistic studies and translational applications. The model incorporates primary human trophoblasts, endothelial cells, placental fibroblasts, and pericytes organized to reflect early- and late-gestation placental structure. Inflammatory stimulation was induced using bacterial and viral mimetics, while autoimmune-relevant perturbations associated with hyperglycemic conditions, including anti-insulin antibodies, were applied to model clinically relevant maternal environments. Barrier integrity, endocrine function, inflammatory signaling and nutrient transport were assessed using integrated functional and molecular readouts.

Results: The platform revealed clear gestational-stage–dependent responses. Early-gestation models demonstrated adaptive behavior characterized by preserved barrier integrity despite reduced nutrient transport capacity, suggesting compensatory mechanisms that maintain fetal protection under stress. In contrast, late-gestation models exhibited diminished endocrine output, elevated inflammatory signaling, and compromised barrier integrity, consistent with maladaptive placental remodeling associated with adverse pregnancy outcomes. Inflammatory stimulation elicited cytokine profiles resembling those reported in pregnancy-related disorders, including preeclampsia and gestational diabetes mellitus, supporting the physiological and disease-relevant fidelity of the system.

Conclusion/Significance: In conclusion, this bioprinted human placenta barrier model enables controlled investigation of gestational-stage–specific placental responses to inflammatory and autoimmune stressors. Its scalability and physiological fidelity support its use for mechanistic discovery, disease modeling, and screening strategies aimed at improving maternal and fetal health outcomes.

OP-122 - A closed-loop oxygen-controlled microphysiological platform for zonal conditioning of human liver organoids

Ahmed Usaid[1], Noreen Alqadhi[2], Nic Leipzig[1,2]

[1]*University of Akron, Department of Chemical, Biomolecular, and Corrosion Engineering, Akron, United States of America*
[2]*University of Akron, Department of Biomedical Engineering, Akron, United States of America*

Purpose/Objectives: Hepatic zonation organizes phenotypic liver metabolism along a sinusoidal oxygen gradient, from periportal Zone 1 to pericentral Zone 3 (~60-30 mmHg P_{O2}). Conventional organoid culture removes this physiological cue, limiting oxygen-dependent modeling of hepatic function. Here, we aimed to develop a feedback-regulated oxygen-conditioning platform that maintains defined zonal P_{O2} for perfused human liver organoids (HLOs).

Methodology: HLOs were differentiated from IMR90-iPSCs using the STEMdiff Hepatocyte Kit (STEMCELL Tech.) and cultured in an ibidi µ-Slide III 3D perfusion chip. Circulating media passed through a polysulfone hemofilter as a membrane gas exchanger before entering the chip. Outlet P_{O2} was measured using inline OXFLOW oxygen sensors (Firesting), while custom Python control on a Raspberry Pi adjusted gas delivery through an Alicat mass flow controller, and switched between premixed 95% N_2/5% CO_2 (deoxygenation) and compressed air (re-oxygenation) to maintain 30 ± 5 mmHg P_{O2}. To establish oxygen sensitivity, parallel HLOs were cultured statically at ~30 mmHg or normoxia for 10 days and analyzed for albumin, urea (BioAssay Systems), and CYP3A4 activity (Promega).

Results: The feedback system reduced P_{O2}in the media from normoxia (~135 mmHg) to a Zone 3 range within 10 min and maintained 29.6 ± 2.3 mmHg over 30 min runs (mean ± SD, n=3). As a proof of concept, static 30 mmHg culture produced a pericentral-like functional shift: albumin decreased to 0.48 ± 0.03-fold of normoxia ($p<0.0001$), urea decreased to 0.36 ± 0.12-fold ($p<0.01$), and CYP3A4 activity increased 4.37 ± 1.05-fold ($p<0.05$), demonstrating stable oxygen control and HLO responsiveness to Zone 3-like P_{O2}.

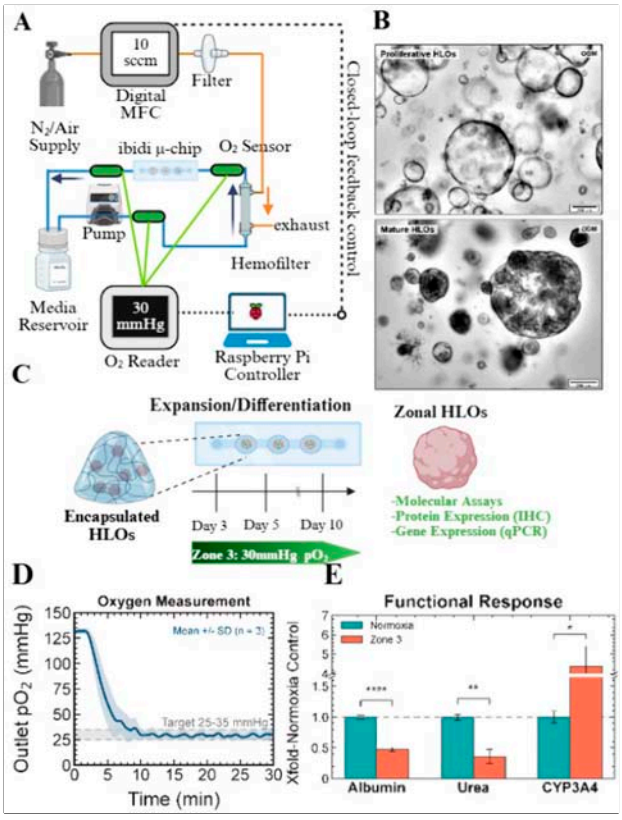


Figure: (A) Closed-loop MPS schematic. (B) HLOs in growth/differentiation media. (C) Experimental workflow. (D) Outlet P_{O2}

stabilization. (E) Functional outputs in static 30 mmHg cultures (student's t-test, *p<0.05; **p<0.01; ****p<0.0001).

Conclusion/Significance: This platform couples real-time P_{O2}sensing with automated gas-flow control, moving liver organoid culture beyond passive hypoxia toward programmable physiological oxygen conditioning. Ongoing work will compare on-chip Zone 1 and Zone 3 perfused culture, with urea and albumin through Days 3-10, and endpoint immunostaining and qPCR for GLUL, CYP2E1, and CYP3A4. Zone-selective drug metabolism (acetaminophen, lidocaine) will validate the platform as a new approach methodology (NAM) for zonal hepatotoxicity testing.

Session 37
Tissue Engineering and Regenerative Medicine in Otolaryngology: Historical Perspectives and Current Challenges

11-16-2026 @ 5:05 PM - 6:35 PM

OP-127 - AdMSC spheroids encapsulating antioxidant hybrid protein carrier for irradiation-damaged salivary gland repair

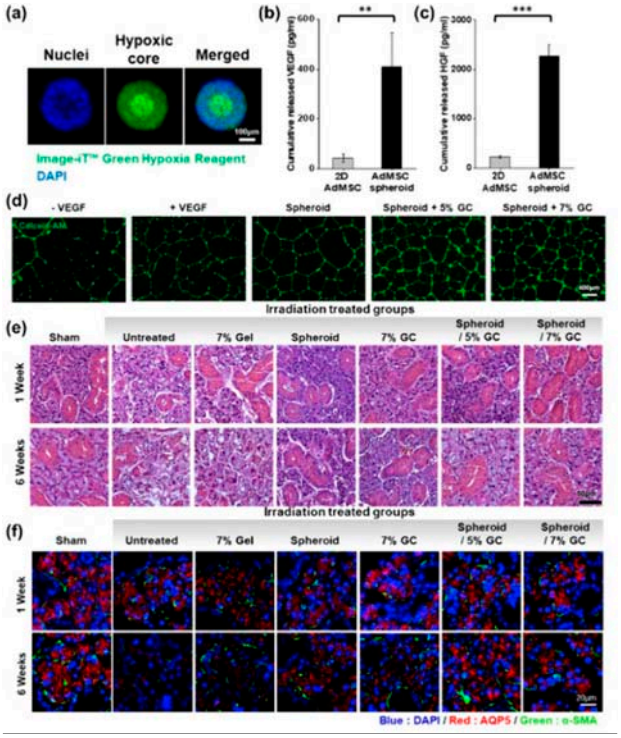
Hyerin Yoo

Seoul National University, Seoul, Korea, Republic of

Purpose/Objectives: Radiation-induced xerostomia is a debilitating salivary gland (SG) dysfunction caused by chronic reactive oxygen species (ROS)-mediated damage, leading to acinar atrophy, fibrosis, and vascular rarefaction with limited treatments. Current options, including artificial saliva and secretagogues, provide only transient symptomatic relief without correcting oxidative injury. This study evaluates the synergistic regenerative potential of antioxidant adipose-derived mesenchymal stem cell (AdMSC) spheroids encapsulated in a glutathione-conjugated gelatin (GC) hydroge for irradiated SG repair.

Methodology: Uniform ∼300 μm AdMSC spheroids were produced in agarose microwells to mimic three-dimensional architecture and encapsulated in GC hydrogels via blue light-mediated di-tyrosine crosslinking. In vitro analyses included ELISA for vascular endothelial growth factor (VEGF) and hepatocyte growth factor (HGF), HUVEC Matrigel tube formation, Annexin V/propidium iodide (PI) flow cytometry for apoptosis in primary SG cells, and M1/M2 polarization in lipopolysaccharide (LPS)-stimulated macrophages. In vivo efficacy was assessed in a 15 Gy SG irradiation mouse model by hematoxylin and eosin (H&E) and Masson's trichrome staining and immunohistochemistry.

Results: AdMSC spheroids exhibited pronounced hypoxic cores (Fig.a) with 2–3-fold higher VEGF/HGF secretion than 2D cultures (p<0.01) (Fig.b,c). GC encapsulation markedly enhanced spheroid viability (>95% live cells at day 7) and paracrine activity. The GC+AdMSC spheroid combination showed superior efficacy over single treatments or 2D AdMSC controls: conditioned media strongly increased HUVEC tube formation (total length +340%, mesh/junction number +280%; p<0.001) (Fig.d) and protected SG cells from H2O2-induced apoptosis (Annexin V/PI, cleaved caspase-3; live cell recovery 78% vs 22% control; p<0.001). Notably, 5 wt% GC-spheroid media induced maximal M2 macrophage polarization (53.3% M2/M1 ratio vs 0.12% LPS control). In vivo, GC+spheroid treatment preserved acinar structures (H&E: acinar integrity 85% vs 32% control) (Fig.e), reduced fibrosis (Masson's trichrome: collagen area −67%), restored acinar/myoepithelial markers (AQP5, α-SMA +3.2-fold) (Fig.f), enhanced angiogenesis (CD31+ vessels +4.1-fold), and decreased oxidative stress/apoptosis markers (8-OHdG/NOX4 −72%, cleaved caspase-3 −81%) versus controls. Result Figure



Conclusion/Significance: GC-encapsulated AdMSC spheroids represent a potent regenerative platform for radiation-damaged SGs by integrating sustained ROS scavenging with hypoxia-boosted angiogenic and immunomodulatory paracrine signaling, surpassing conventional stem cell or antioxidant therapies.

Session 39
Stem Cells & Cell Therapies & Developmental Biology and Cell Signaling (General Session)

11-17-2026 @ 8:00 AM - 9:30 AM

OP-129 - An Agent-Based Simulation Model of Adipose-Derived Stem Cell Differentiation in 3D Physicochemically Tuned Hydrogels for IVD Regeneration

Meghana Munipalle[1], Yin Liu[2], Jianyu Li[1,3,4], Nicole Li-Jessen[5]

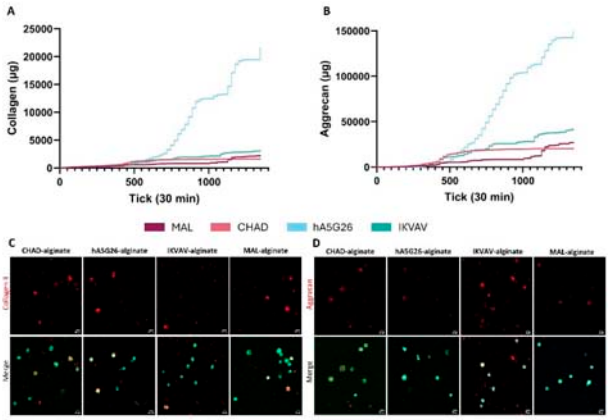
[1]*McGill University, Biomedical Engineering, Montreal, Canada*
[2]*McGill University, School Of Communication Sciences And Disorders, Montreal, Canada*
[3]*McGill University, Mechanical Engineering, Montreal, Canada*
[4]*McGill University, Surgery, Montreal, Canada*
[5]*McGill University, Otolaryngology, Biomedical Engineering, Communication Sciences And Disorders, Montreal, Canada*

Purpose/Objectives: Stem cell-laden hydrogels offer a promising therapeutic strategy for mitigating intervertebral disc (IVD) degeneration. By tuning their physicochemical properties, hydrogels can be engineered to promote tissue-specific regeneration. Computer simulations supplement *in vitro* experiments by providing a mechanistic understanding of cellular dynamics to guide rational, tissue-specific biomaterial designs. While previous computational IVD models relied on mature nucleus pulposus (NP) cells, robust mathematical models describing stem cell discogenic differentiation are lacking. Therefore, we employed 3D agent-based models (ABM) to simulate adipose-derived stem cell (ADSC) differentiation towards NP-like cells in tunable NP-mimicking hydrogels for IVD repair.

Methodology: Agent-rules governing cell behaviors (e.g., cell migration and extracellular matrix (ECM) secretion) were formulated from empirical literature and *in vitro* data. The IVD-ABM was initialized using *in vitro* NP-mimicking viscoelastic alginate hydrogels with stress relaxation time ($\tau_{1/2}$) from ∼100s (fast-relaxing) to

$\sim$1000s (slow-relaxing). Hydrogel viscoelasticity was mathematically represented using the Standard Linear Solid equation. Additionally, the simulation incorporated hydrogels conjugated with NP ECM-specific peptides (hA5G26-, CHAD- and IKVAV) with enhanced viscoelasticity ($\tau_{1/2}$ $\sim$25s) to mimic human non-degenerative NP behavior. Unknown model parameters were optimized using a gradient-free method, and the model was validated against independent empirical datasets. Model uncertainty was quantified by bootstrapping biological outcomes from 10 independent simulation runs.

Results: The ABM simulated 28 days of ADSC discogenic differentiation and ECM secretion. All peptide-conjugated hydrogels exhibited physiological stiffnesses matching native NP tissue (5.39 $\pm$ 2.56 kPa). Among these, hA5G26-alginate reported the highest aggrecan and collagen deposition (**Figure 1**: Preliminary ABM simulations and *in vitro* tests of (A, C) collagen and (B, D) aggrecan deposition during ADSC discogenic differentiation (MAL: maleimide control)). IKVAV-alginate yielded the highest aggrecan-to-collagen ratio ($\sim$13:1), which significantly exceeded the unconjugated alginate ($\sim$3:1) and approached that of healthy NP tissue.



Conclusion/Significance: Incorporation of NP ECM-specific peptides IKVAV or hA5G26 significantly promoted ADSC secretion of NP-like ECM. The enhanced matrix viscoelasticity better replicated healthy native NP tissue behavior compared to the unconjugated alginate. This improvement was reflected in the simulation via increased migration and ECM deposition. Our simulation findings demonstrated how biochemical and viscoelastic properties of hydrogels affected ADSC regenerative efficacy.

OP-130 - GMP-Validated Infrapatellar Fat Pad-Derived Mesenchymal Stem Cells for Orthopedic Cell Therapy: An Intra-Patient Comparison with Bone Marrow MSCs

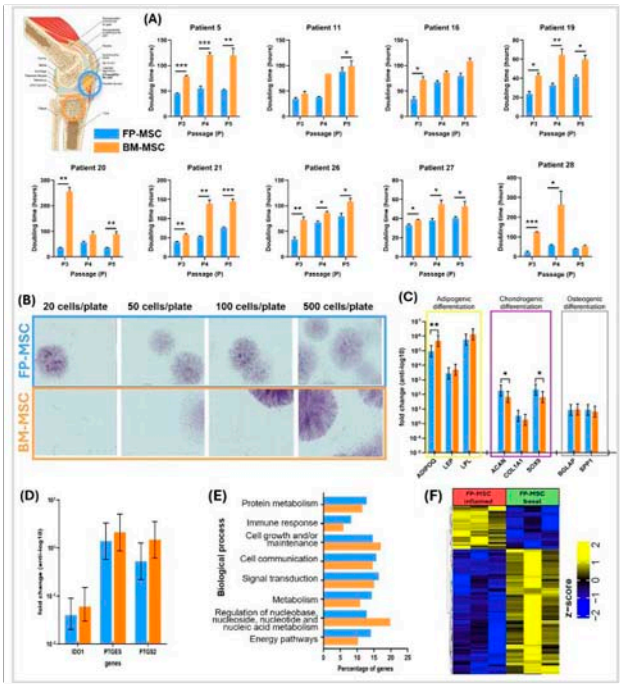
Federica Banche-Niclot[1], Michael Williams[1], Patrick Mcculloch[2], Francesca Taraballi[1]

[1]*Houston Methodist Research Institute, Center For Musculoskeletal Regeneration, Dept. Orthopedics And Sports Medicine, Houston, United States of America*
[2]*Houston Methodist Hospital, Orthopedics And Sports Medicine, Houston, United States of America*

Purpose/Objectives: Mesenchymal stem cells (MSCs) are promising adjuncts for inflammatory orthopedic conditions, able to regulate immune responses and support tissue repair. Bone marrow-derived MSCs (BM-MSCs) remain the reference source, but BM aspiration is invasive and poorly aligned with routine surgical workflows. Infrapatellar fat pad-derived MSCs (FP-MSCs) can instead be isolated from tissue discarded during knee surgery. This intra-patient study compared BM-MSCs and FP-MSCs and established a Good Manufacturing Practices (GMP)-compliant product for clinical translation.

Methodology: Matched BM and FP samples were collected from 10 patients undergoing anterior cruciate ligament (ACL) surgery (IRB protocol n.PRO00038346). MSCs were isolated and expanded under identical conditions, and assessed for proliferation (doubling time), colony-forming capacity, surface marker (flow cytometry), multilineage differentiation, immunomodulatory potential upon inflammation (qRT-PCR), proteomics, and lipidomics. FP-MSCs were then manufactured under GMP-accredited conditions (n=4) and evaluated for viability, sterility, phenotype, cryostability, and post-thaw handling.

Results: Across donors, FP-MSCs showed 2.61-, 2.12-, and 1.59-fold shorter doubling times across P2-P5 passages (Fig.A), greater clonogenicity in 8/9 donors (Fig.B), and comparable MSC immunophenotypic purity to matched BM-MSCs. Gene analysis confirmed multilineage potential in both sources (Fig.C), and comparable immunomodulatory response (Fig.D), including activation of prostaglandin–associated axes (PTGES and PTGS2), consistent with a pro-healing profile. Proteomics revealed shared inflammatory licensing response (Fig.E), with similar induction of STAT1, GBP1, and IDO1. Notably, PTGES was preferentially induced in FP-MSCs, reinforcing the prostaglandin pathway as a source-associated immunomodulatory feature. Lipidomics demonstrated clear separation of basal versus inflamed FP-MSCs (1091 lipid species detected, 151 significantly altered, Fig.F), with selective enrichment of docosahexaenoic acid-containing triacylglycerols, supporting an immunometabolic program linked to resolution-oriented signaling. Under GMP conditions, FP-MSCs achieved $1.15\pm0.27\times10^8$ cells within 17$\pm$3.83 days from 17$\pm$3.82 mL of starting aspirated tissue. FP-MSCs product met release criteria, including viability, sterility, consistent phenotype, >6-month cryostability, and post-thaw viability for up to 4 hours.



Conclusion/Significance: FP-MSCs emerged as a clinically practical, minimally invasive alternative to BM-MSCs for orthopedic cell therapy applications aimed at modulating inflammation and promoting tissue repair. Their regenerative, immunomodulatory, and lipid-associated profile, combined with GMP-compliant manufacturing, led to FDA-authorized clinical trial (IND 30919) for ACL repair. The authors acknowledge the KJCCT group for the GMP support.

OP-131 - Subacromial Bursa-Derived Mesenchymal Stem Cells as an Orthobiologic Strategy for Rotator Cuff Repair: Feasibility and GMP-Compliant Clinical Translation

Federica Banche-Niclot[1], David Armond[2], Patrick Mcculloch[2], Francesca Taraballi[1]

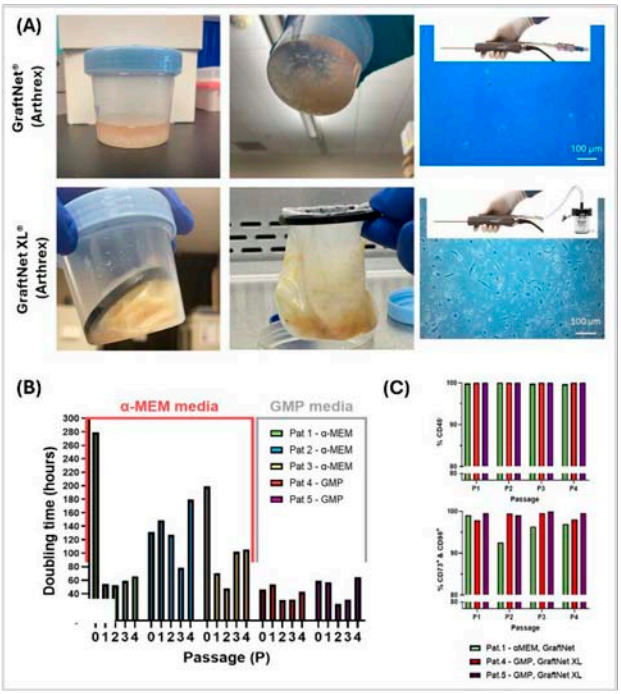
[1]*Houston Methodist Research Institute, Center For Musculoskeletal Regeneration, Dept. Orthopedics And Sports Medicine, Houston, United States of America*

[2]*Houston Methodist Hospital, Orthopedics And Sports Medicine, Houston, United States of America*

Purpose/Objectives: Chronic rotator cuff inflammation from overuse or aging represents a major source of musculoskeletal morbidity, causing persistent pain and progressive functional decline. Mesenchymal stem cell (MSC)-based approaches are promising adjuvant strategies given their immunomodulatory and regenerative properties, but standard bone marrow-derived MSC harvesting is invasive and distant from the injury site. We investigated the feasibility of subacromial bursa-derived MSCs (B-MSCs) as a minimally invasive, anatomically relevant cell source for rotator cuff repair, and developed a Good Manufacturing Practice (GMP)-compliant manufacturing protocol for clinical translation.

Methodology: Subacromial bursal tissues were surgically harvested from ten patients undergoing shoulder arthroscopy using GraftNet® or GraftNet® XL systems (Arthrex) (IRB n. PRO00038346). B-MSCs were isolated via collagenase digestion and expanded in standard α-MEM or GMP-grade media. Proliferation was monitored via doubling time across passages (P0-P4), and MSC identity was confirmed by flow cytometry. GMP manufacturing protocol was developed (n=6), targeting a clinical dose of 50×10^6 cells. Quality control release testing was performed to confirm identity, post-cryopreservation stability, and microbiological safety.

Results: GraftNet® XL system resulted in a 6.6-fold higher initial cell yield at isolation compared to GraftNet® ($2.36\pm0.56\times10^6$ vs $355\pm139\times10^3$ cells, respectively, Fig.A). B-MSCs expanded in GMP-grade media exhibited faster and more consistent proliferation than α-MEM-cultured cells (P0: 84.12±32.93h vs 216.01±57.09h; P4: 42.71±7.57h vs 70.29±33.27h, Fig.B). Characteristic MSC marker expression was retained across P1–P4 under all conditions (Fig.C). GMP manufacturing was successfully completed, with B-MSCs expanding from $5.23\pm0.31\times10^6$ initial cells to $105.10\pm36.12\times10^6$ cells within 16.75±1.5 days from tissue harvest. Final products consistently expressed CD73 (99.74±0.12%), CD90 (99.65±0.13%), and CD105 (99.88 ±0.04%), with low CD45 (1.73±2.14%), CD34 (1.96±1.17%) and HLA-DR (3.02±2.39%), confirming maintained MSC identity. All lots passed safety release testing, and product stability was confirmed up to 4 hours post-thaw, demonstrating stability under clinically relevant handling.



Conclusion/Significance: This study confirms B-MSCs can be reliably isolated, expanded, and manufactured under GMP-compliant conditions. Their anatomical relevance, minimally invasive harvest, and GMP scalability position B-MSCs as a compelling cell therapy for rotator cuff repair. These findings provide the translational foundation for ongoing IND-enabling activities toward clinical evaluation of B-MSCs for shoulder regenerative applications. The authors acknowledge the KJCCT group for GMP support.

OP-134 - Injectable Hydrolytically Degradable PEG Granular Hydrogels for Tunable Stem Cell Delivery

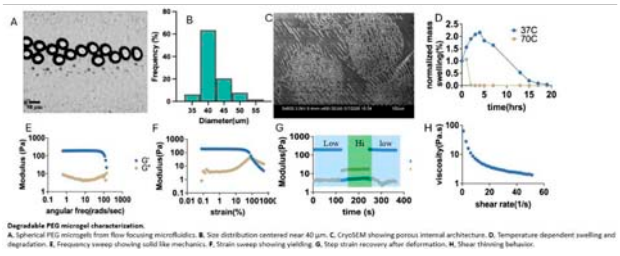
Eferoghene Okakuro[1], Mykel Green[2]

[1]*Tulane University, Biomedical Engineering, New Orleans, United States of America*
[2]*Tulane, Biomedical Engineering, New Orleans, United States of America*

Purpose/Objectives: Hematopoietic stem cell transplantation depends on efficient homing and engraftment within bone marrow niches, yet delivery and post transplant microenvironmental control remain important challenges. Engineered biomaterials offer a potential strategy to better define the local physical and biochemical cues that influence transplanted cell behavior. Granular hydrogels are promising for this purpose because they combine injectability, and microporosity. The purpose of this work is to engineer hydrolytically degradable PEG based granular hydrogels with tunable microgel size, mechanics, and degradation behavior as a foundation for future stem cell delivery applications.

Methodology: Hydrolytically degradable PEG microgels were designed using four arm poly(ethylene glycol) maleimide macromers crosslinked with dithiothreitol through thiol maleimide Michael addition chemistry. Network degradability was incorporated through ester containing thioether linkages to enable hydrolysis dependent remodeling. Flow focusing microfluidic devices were fabricated from polydimethylsiloxane replicas cast from additively manufactured molds for PEG microgel production. PEG precursor and dithiothreitol crosslinker streams were introduced under droplet forming conditions to produce microgels. Microgels were collected, assembled into granular hydrogels, and characterized by optical microscopy, image based particle sizing, mass loss analysis, cryo scanning electron microscopy, and rheology. Degradation behavior was evaluated by monitoring normalized mass over time at 37°C and under accelerated hydrolysis conditions at 70°C. Cryo scanning electron microscopy was used to qualitatively evaluate internal architecture. Granular hydrogel mechanics were assessed using oscillatory frequency sweeps, shear thinning analysis, and step strain recovery measurements.

Results: Flow focusing microfluidics generated spherical PEG microgels with a narrow size distribution. Swelling studies showed temperature dependent behavior, with gels at 37°C exhibiting transient swelling followed by gradual mass loss, while gels at 70°C rapidly lost swollen mass. Rheology confirmed solid like behavior, with storage modulus exceeding loss modulus across the tested frequency range. Strain sweep identified yielding, and step strain recovery showed mechanical recovery after high strain deformation. Steady shear measurements demonstrated shear thinning behavior. Cryo scanning electron microscopy revealed porous internal microgel architecture.



Degradable PEG microgel characterization.
A. Spherical PEG microgels from flow focusing microfluidics. B. Size distribution centered near 40 µm. C. CryoSEM showing porous internal architecture. D. Temperature dependent swelling and degradation. E. Frequency sweep showing solid like mechanics. F. Strain sweep showing yielding. G. Step strain recovery after deformation. H. Shear thinning behavior.

Conclusion/Significance: Degradable granular hydrogel platforms present a tunable foundation for injectable stem cell delivery. Future studies will optimize microgel degradation rate and mechanics to improve cell encapsulation, viability, and microenvironmental support, addressing key barriers in biomaterial mediated transplantation.

Session 41
Dental & Craniofacial (General Session)

11-17-2026 @ 8:00 AM - 9:30 AM

OP-140 - Engineering the temporomandibular joint using cartilage progenitors

Hannah Bonelli[1,2], Cristina Barbella[2,3], Adya Srinivasan[1,2], Dana Ragbirsingh[2], Hagar Kenawy[2], Riccardo Gottardi[1,2,4]

[1]*University of Pennsylvania, Bioengineering, Philadelphia, United States of America*
[2]*Children's Hospital of Pennsylvania, Department of Otolaryngology, Philadelphia, United States of America*
[3]*Brown University, Providence, United States of America*
[4]*The Children's Hospital of Philadelphia, Surgery, Philadelphia, United States of America*

Purpose/Objectives: Juvenile idiopathic arthritis is the most common form of pediatric arthritis, and of that population, up to 96% experience temporomandibular joint osteoarthritis (TMJOA), characterized by degeneration of mandibular cartilage. Unlike other joints, the TMJ can simultaneously function as a hinge joint and a gliding joint, requiring a complex structure which consists of hyaline cartilage (rich in collagen II) covered by fibrocartilage (rich in collagen I). Like other articulating joints, the TMJ is often studied using mice for genetic models and pigs for reparative strategies. However, unlike other articulating joints, very little is known regarding the composition of this distinctive bilayered cartilage. We first need to better understand this complex structure across species to more effectively choose animal models and to develop regenerative approaches.

Methodology: In this work we described changes in matrix organization, glycosaminoglycan (GAG) content, and elastin content in condylar cartilage across species via histology, immunofluorescence, and second harmonic generation. Furthermore, we identified ear cartilage progenitor cells (eCPCs) as a neural crest derived cell source that could be effective for TMJ cartilage repair and is accessible via a minimally invasive procedure. We compared eCPC differentiation to native TMJ cell phenotypes from both the hyaline cartilage (hyaline cartilage chondrocytes, hCCs) and fibrocartilage (fibrochondrocytes, fCCs).

Results: Our results show that condylar cartilage organization (Fig. 1A) and elastin content increase with increasing species size while GAG content decreases (Fig. 1B). Comparison by histology, immunofluorescence, and RT-qPCR of porcine hCCs and fCCs with eCPCs suggests that with distinct, targeted growth factor modulation in the culture medium, eCPCs can be directed to secrete key cartilage components of either TMJ hyaline cartilage or fibrocartilage (Fig. 1C).

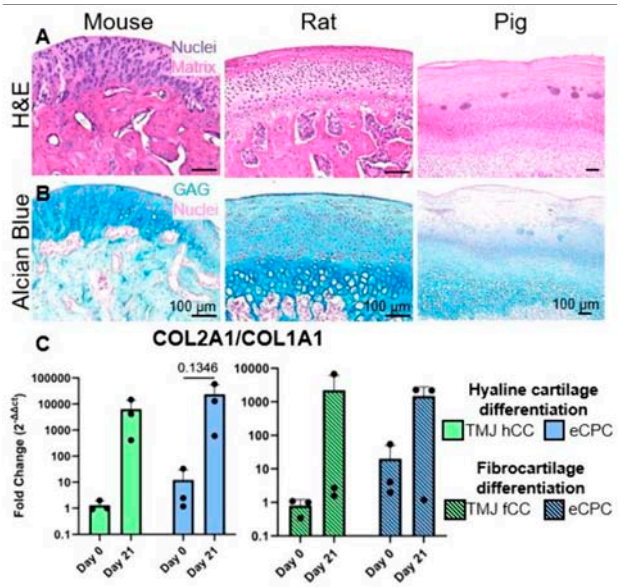


Figure 1. (A) H&E and **(B)** Alcian Blue of TMJ condyles. **(C)** RT-qPCR results for COL2A1/COL1A1 between native TMJ cells and eCPCs. Two-way ANOVA.

Conclusion/Significance: These findings highlight the critical advantage of studying cartilage composition across species to better choose relevant animal models and benchmark cartilage components to assess the efficacy of selected cell sources for TMJOA repair.

Session 42
Strategies for Regeneration of the Nervous System

11-17-2026 @ 8:00 AM - 9:30 AM

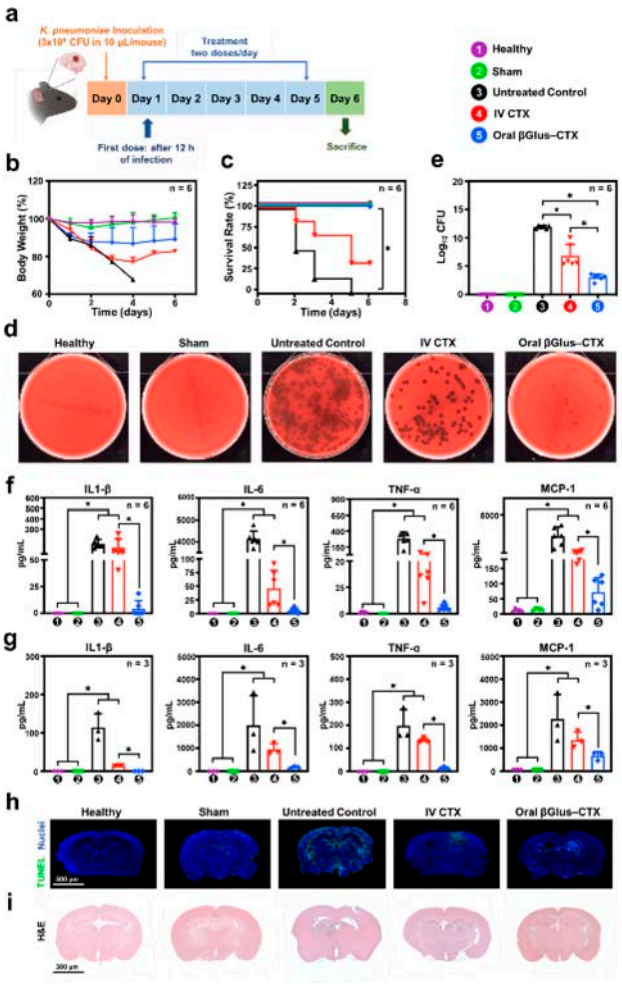
OP-141 - Inflammation-Responsive Macrophage-Mediated Prodrug Nanocarriers for Enhanced Oral Therapy of Bacterial Meningitis

Van Khanh Nguyen[1], Hsing-Wen Sung[1], Jui-To Wang[2]

[1]*National Tsing Hua University, Department of Chemical Engineering, Hsinchu, Taiwan*
[2]*Taipei Veterans General Hospital, Neurological Institute, Department of Neurosurgery, Taipei, Taiwan*

Purpose/Objectives: Effective treatment of bacterial meningitis remains limited by poor blood–brain barrier (BBB) penetration and systemic toxicity associated with high-dose intravenous antibiotics. Here, we developed an orally administered β-glucan-based prodrug nanocarrier designed to exploit immune cell trafficking and inflammation-responsive drug release for targeted antibiotic delivery to infected brain tissue.

Methodology: A reactive oxygen species (ROS)-responsive β-glucan–cefotaxime (βGlus–CTX) prodrug nanoparticle was synthesized through covalent conjugation of cefotaxime to oxidized β-glucan using a thiodiglycolic linker. The nanocarriers were characterized by nuclear magnetic resonance spectroscopy, Fourier-



transform infrared spectroscopy, X-ray diffraction, particle size analysis, and drug release studies under inflammatory ROS conditions. Cellular uptake and immune cell–mediated transport were evaluated in macrophages and intestinal models. In vivo biodistribution, pharmacokinetics, and therapeutic efficacy were investigated in a *Klebsiella pneumoniae*-induced murine meningitis model following oral administration.

Results: The βGlus–CTX nanocarriers exhibited stable nanoscale self-assembly (∼200 nm), sustained gastrointestinal stability, and ROS-triggered cefotaxime release under inflammatory conditions. The nanoparticles demonstrated enhanced macrophage uptake through β-glucan receptor-mediated internalization and promoted immune cell–assisted transport across intestinal and brain barriers. In meningitis-bearing mice, orally administered βGlus–CTX showed significantly enhanced accumulation in inflamed brain tissue compared with untreated controls and healthy mice. Therapeutic treatment markedly reduced bacterial burden and suppressed pro-inflammatory cytokines including IL-1β, TNF-α, IL-6, and MCP-1. Furthermore, the oral nanocarrier significantly improved survival rate, preserved body weight, and reduced histological brain damage compared with conventional intravenous cefotaxime treatment, while maintaining favorable systemic safety profiles.

Conclusion/Significance: This study presents a biomaterial-based oral nanocarrier platform capable of leveraging inflammation-directed immune trafficking for targeted brain delivery. The ROS-responsive β-glucan prodrug system provides a promising non-invasive strategy for treating central nervous system infections and demonstrates the translational potential of immune-interactive nanotechnologies for tissue engineering and regenerative medicine applications.

OP-142 - Development of a scalable in vitro mechanical stimulation platform to study mechanobiology of motor neurons

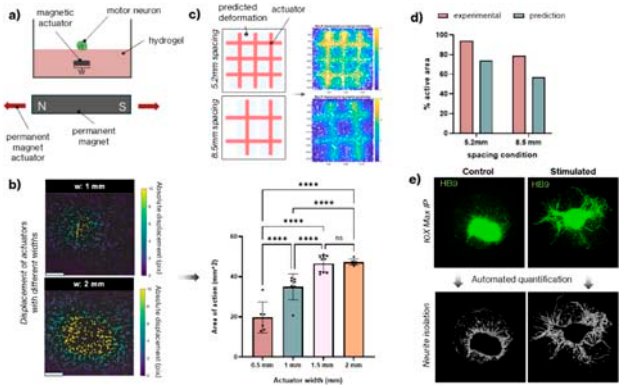
Sonika Kohli, Vesper Evereux, Ritu Raman

MIT, Mechanical Engineering, Boston, United States of America

Purpose/Objectives: Motor neurons can regenerate after small injuries, but severe injuries (>5mm) limit functional recovery. While emerging treatments for nerve injuries, such as nerve guidance conduits, have shown promise, their reliance on passive substrates yields incomplete regeneration. We and others have previously established that motor neurons are mechanosensitive and respond to dynamic mechanical stimulation by increasing the magnitude and rate of axonal outgrowth. However, the biological basis of dynamic mechanical stimulation on axonal regeneration after injury is not known.

Methodology: Embedding magnetic actuators within hydrogels enables non-invasive matrix actuation via external magnetic fields (Fig. 1A-B). Designing Magnetic Matrix Actuation (MagMA) platforms capable of precisely patterning spatiotemporal mechanical cues for cells requires predictive computational models. We have developed a computational model that predicts how single magnetic actuators of varying geometries, as well as arrays of such magnetic actuators, deform the hydrogels in which they are embedded (Fig. 1C-D). This model is used to predict optimized actuator geometries, which are precisely fabricated using a laser cutter prior to empirical testing with hydrogels seeded with motor neurons (differentiated from mouse embryonic stem cells).

Results: Understanding how motor neuron gene expression is modulated by mechanical stimuli requires culturing cells on uniformly actuated hydrogel substrates, enabling reproducible data generation via bulk RNA sequencing. Our computational model predicted an optimized magnetic actuator design that yielded uniform deformation in multi-well plates, which was then empirically validated. Healthy and chemically injured neurons cultured on this optimized platform were stimulated with a range of physiologically-relevant parameters (∼5-15% static stretch and dynamic stretch at 1-4 Hz), showing mechano-responsive changes in morphology (increased axon length and branching) and gene expression (upregulation of axon guidance pathways). Future work leveraging motor neurons with functional knockdowns of mechanosensitive genes will establish the mechanisms underlying observed mechanotransduction (Fig. 1E shows example of this in non-injured case).



Conclusion/Significance: Uncovering how dynamic forces impact healthy and injured motor neurons in vitro will inform new mechano-therapeutic strategies for in vivo testing. Moreover, our scalable and reproducible framework for fabricating non-invasive mechanical stimulation platforms can be adapted for mechanobiology studies in a wide range of other cell types.

OP-143 - Hyaluronic Acid-Alginate Hydrazone Crosslinked Hydrogels Support the Generation and Maturation of V2a Spinal Interneurons

Madison Mclaren[1], Alycia Galindo[2], Alyssa Chi[2,3], Jenna Khachatourian[2,4], Marian Hettiaratchi[2,3,5], Jessica Butts[1,6]

[1]*Rice University, Bioengineering, Houston, United States of America*
[2]*University of Oregon, Phil And Penny Knight Campus For Accelerating Scientific Impact, Eugene, United States of America*
[3]*University of Oregon, Chemistry And Biochemistry, Eugene, United States of America*
[4]*University of Oregon, Human Physiology, Eugene, United States of America*
[5]*University of Oregon, Institute Of Molecular Biology, Eugene, United States of America*
[6]*Rice University, Neuroengineering Initiative, Houston, United States of America*

Purpose/Objectives: Spinal cord injury (SCI) causes severe neuronal degeneration resulting in motor, sensory, and autonomic dysfunction. While hydrogels can deliver cells directly to the injury site, many lack the biochemical signals required to support cell maturation and integration. To address this, we developed an injectable hyaluronic acid-alginate (HA-Alg) hydrogel using dynamic hydrazone crosslinking. This platform is engineered to provide a bioactive environment through the conjugation of extracellular matrix (ECM)-derived peptides, RGD and IKVAV. These peptides provide the necessary binding motifs for neuronal adhesion, facilitating neurite outgrowth essential for functional tissue repair.

Methodology: HA-Alg hydrogels were synthesized by crosslinking adipic acid dihydrazide-functionalized HA with oxidized alginate. HA was additionally modified with norbornene for photoinitiated thiol-ene conjugation of cysteine-terminal RGD (0.43 ± 0.23 mM) or IKVAV (0.38 ± 0.18 mM) peptides. Embedded mouse embryonic stem cell aggregates were cultured for twelve days to assess V2a interneuron viability, differentiation efficiency, and neurite outgrowth.

Results: Embedded V2a viability varied, with neuron-specific IKVAV supporting significantly higher survival (∼70%) than RGD (∼50%) (Fig. 1A-B). Gene expression analysis demonstrated 2- to 4-fold increases in mature neuronal markers (*Mapt*, *Vglut2*) and the post-mitotic V2a marker *Chx10* across conditions, showing successful differentiation despite hydrogel crosslinking and peptide chemistry (Fig. 1C). Interestingly, neurite outgrowth varied across hydrogels. V2a interneurons in unmodified hydrogels remained spherical and confined, whereas RGD or IKVAV functionalization drove extensive neurite outgrowth (Fig. 1D).

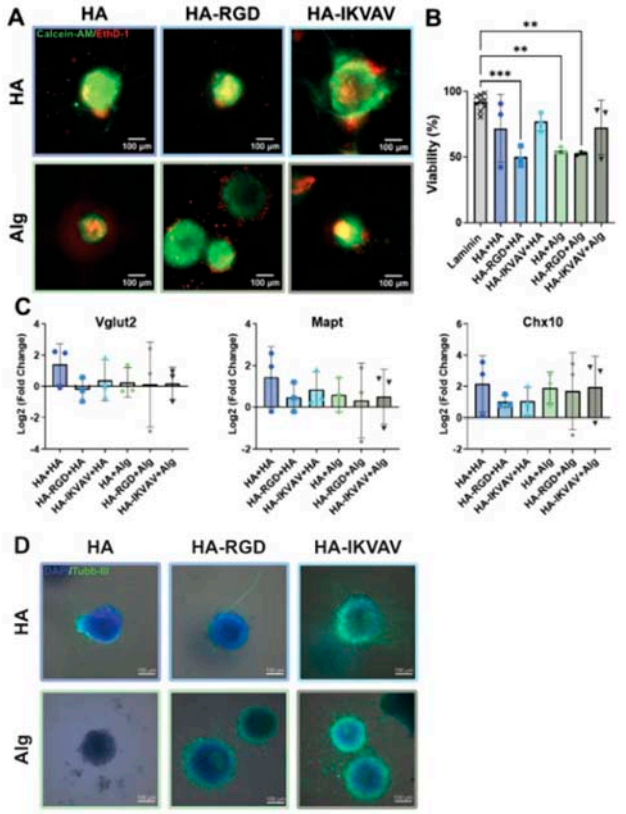


Figure 1. V2a interneuron viability, maturation, and morphology in HA-Alg hydrogels. (A) Day-12 Live(green)/Dead(red) staining of V2a enriched cells. (B) Quantitative viability across hydrogels compared to 2D laminin control. (C) Fold change of mature neuronal (*Vglut2*, *Mapt*) and V2a-interneuron (*Chx10*) expression normalized to 2D laminin control, with no significant difference between hydrogel groups. (D) Tubulin-III (green) immunostaining of neurite extension in peptide-functionalized hydrogels versus non-conjugated controls.

Conclusion/Significance: While a biocompatible matrix supports survival, specific ECM cues are required to drive the functional maturation of transplanted neurons. Dynamic hydrazone chemistry enables minimally invasive delivery, while peptide functionalization overcomes the biological limitations of standard scaffolds. By actively promoting neurite extension, this HA-Alg platform addresses a critical bottleneck in spinal cord repair, offering a strategy to restore connectivity following SCI.

OP-144 - A Tale of Two Hydrogels: Human versus Porcine Peripheral Nerve ECM for Spinal Cord Repair

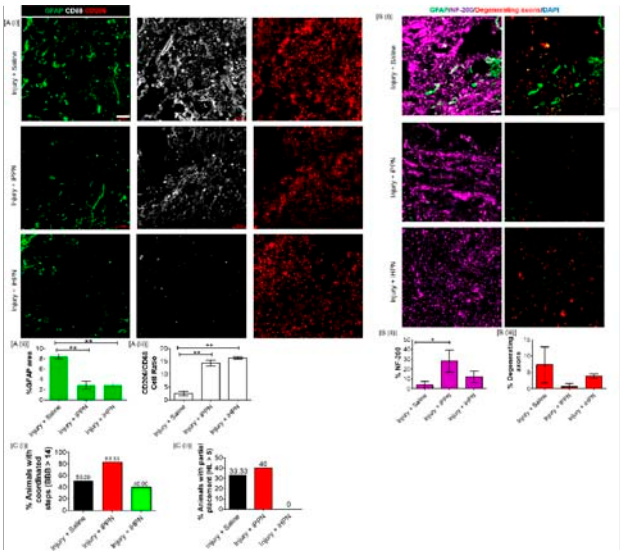
Gopal Agarwal, Abiah Sentic, Leina Owens, Anouska Seal, Sofia Reyes, Christine Schmidt

University of Florida, Biomedical Engineering, GAINESVILLE, United States of America

Purpose/Objectives: Traumatic spinal cord injury (SCI) triggers persistent neuroinflammation and limited regeneration, resulting in poor functional recovery. Here, we compare injectable hydrogels derived from decellularized human (iHPN) and porcine (iPPN) peripheral nerves, which biomimic the mechanical properties of native central nervous system tissue.

Methodology: In a thoracic T9-T11 contused rat spinal cord, iPPN and iHPN were injected within 15 minutes post injury. The animls were monitored for improvement in locomotion using BBB and horizontal ladder score. Post 28 days post injury, the spinal cord was isolated and immunostained for axonal regeneration markers (NF-200, and NF-L), and glial cell reactivity (GFAP, CD206 and CD68).

Results: Following injection, both hydrogels promoted polarization of reactive macrophages toward an anti-inflammatory phenotype and attenuated astrocyte reactivity (Fig. 1A). iPPN demonstrated better neuroprotective efficacy, evidenced by significantly greater neuronal sparing i.e. higher neurofilament-200 (NF-200) area, increased neurite lengths, and improved myelination of spared neurons compared with injury-only controls (Fig. 1B (i, ii and iii)). iPPN and iHPN treated animals exhibited a decrease in degenerating axons percentage area as compared to saline treated animals (Fig. B (iii)). Functionally, iPPN-treated animals exhibited significantly improved locomotor recovery, as assessed by Basso, Beattie, and Bresnahan (BBB) scoring (Fig. 1C (i)) and horizontal ladder performance (Fig. 1C (ii)), compared with both injury-only and iHPN-treated injury controls. Figure 1: A (i) Representative images showing glial cell reactivity at the site of injury post hydrogel treatment. Astrocyte reactivity was determined using GFAP (green); while macrophage polarization ratio was determined using CD206 (anti-inflammatory) and CD68 (inflammatory). A (ii) and A(iii) are bar graph representing %GFAP area and CD206/CD68 ratio respectively. B) (i) A (i) Representative images showing axonal regeneration at the site of injury post hydrogel treatment. NF-200 (magneta) stains mature neurons; degenerating axons were stained by NF-L antibody (shown here red) B (ii), and B(iii) represents the bar graph for percentage of NF-200 and NF-L at the injury site; C) Locomotor recovery assessment was done using C (i) BBB and C(ii) horizontal ladder.



Conclusion/Significance: iPPN shows greater potential over iHPN for treating SCI, with advantages in neuronal sparing and early locomotor recovery, while both iPPN and iHPN modulate inflammation.

OP-145 - A Suture-Free Chitosan-Based Hydrogel Wrap Promotes Functional Recovery After Peripheral Nerve Transection in a Rat Model

Dzana Katana, Daiki Kitano, Alexander Madanat, Kevin Yang, Sihan Hao, Kacey Marra

University of Pittsburgh, Plastic Surgery, Pittsburgh, United States of America

Purpose/Objectives: Peripheral nerve injuries affect millions annually and remain a significant clinical challenge. Epineurial suture repair, the current standard of care, relies on tension-dependent coaptation and is associated with incomplete functional recovery. Biomaterial-based nerve wraps offer a promising suture-free alternative providing structural support at the repair site. This study evaluated sensory, sensorimotor, and histological outcomes following

application of a chitosan-based hydrogel nerve wrap without guide sutures in a Lewis rat sciatic nerve transection model, compared to a cut-and-repair control.

Methodology: Adult Lewis rats underwent complete sciatic nerve transection and received either a rehydrated chitosan-based hydrogel wrap without guide sutures (n=4) or served as cut-and-repair controls. Recovery was assessed at presurgery baseline and weeks 1, 2, and 4 using Von Frey filament testing (mechanical detection threshold), acetone drop test (cold allodynia), and Rat Pincher assessment (sensorimotor response). Within-group comparisons were made against presurgery baseline; between-group comparisons at each timepoint. Nerve and muscle tissues were harvested at week 4 for histological analysis with hematoxylin and eosin and Masson's trichrome staining.

Results: Following an expected post-injury elevation at week 1, Von Frey thresholds progressively declined toward presurgery baseline, indicating sensory recovery. Wrap-treated animals maintained significantly lower thresholds than cut-and-repair controls at weeks 2 and 4 ($p<0.0001$), reflecting better-preserved sensory function (Figure 1). Acetone testing revealed fewer cold-evoked reactions in the wrap group at weeks 1 and 2 ($p<0.05$), with both groups trending toward baseline by week 4. Rat Pincher responses in the wrap group remained stable near presurgery baseline, while cut-and-repair control showed elevated responses at weeks 1 and 2 ($p<0.05$), confirming better-preserved sensorimotor function. Nerve tissue was present and viable; uninjured nerve displayed well-defined fascicular organization, while injured nerve assessment was limited by tissue processing. Muscle sections showed preserved fiber organization with modest collagen deposition, consistent with post-denervation remodeling.

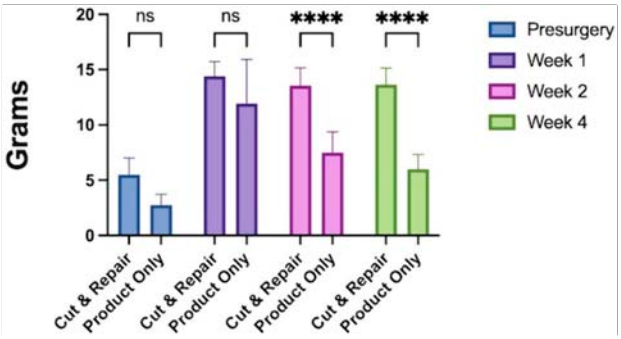


Figure 1. *Von Frey thresholds (grams); wrap-treated vs cut-and-repair. ****p<0.0001. n=4.*

Conclusion/Significance: A suture-free chitosan-based hydrogel nerve wrap demonstrated more favorable sensory and sensorimotor recovery than standard epineurial repair following sciatic nerve transection in Lewis rats. These findings support clinical potential of a simplified suture-free approach to peripheral nerve repair. Larger cohorts and extended follow-up are needed.

Session 43
Respiratory, Urologic & Gastrointestinal (General Session)

11-17-2026 @ 8:00 AM - 9:30 AM

OP-147 - Assessment of Radiation Exposure in Healthy and Lung Cancer-Integrated 3D Airway Organ-Tissue Equivalent (OTE) Microphysiological Systems

Dariya Fischer[1], Beatriz Mateo[2], Sean Murphy[3], Adam Hall[1]

[1]*Wake Forest University School of Medicine, Biomedical Engineering, Winston Salem, United States of America*
[2]*Wake Forest University School of Medicine, Cancer Biology, Winston Salem, United States of America*
[3]*Wake Forest Institute for Regenerative Medicine, Winston Salem, United States of America*

Purpose/Objectives: Radiation-induced lung injury (RILI) remains a major clinical challenge in lung cancer treatment, as the radiosensitivity of healthy lung tissue limits radiotherapy (RT) effectiveness. RILI significantly impairs quality of life, progressing from acute inflammation to irreversible fibrosis, ultimately damaging healthy lung tissue. Adequate countermeasures are lacking and this emphasizes the need for physiologically relevant models to improve understanding of radiation-induced damage and identify selective radioprotectants. Current models lack physiological relevance, and no existing model incorporates both healthy and cancerous cells within the same RT exposure field, which is essential for evaluating radioprotectant selectivity. Here, we employ a 3D airway organ-tissue equivalent (OTE) platform of primary human cells to investigate acute and progressive effects of radiation exposure and integrate cancer cells to enable assessment of differential radiation responses

Methodology: Differentiated airway OTEs were exposed to X-ray doses of 0-20 Gy and evaluated for acute effects including DNA damage and progressive effects including inflammatory response, barrier function decline, loss of epithelial integrity, and onset of fibrotic remodeling over 28 days. PC9 and A549 cells were independently assessed for radiosensitivity, then transduced with mCherry lentivirus to enable identification within the OTEs and later integrated into the OTEs to establish a cancer-integrated airway OTE.

Results: DNA double-strand break staining revealed acute, dose-dependent damage within 2 hours that persisted across the progressive injury phase. Over 28 days, airway OTEs exhibited dose- and time-dependent progressive inflammatory signaling, functional decline in barrier integrity and ciliary activity, and structural deterioration of the epithelial architecture. Coinciding with these changes, increased collagen deposition indicated the onset of fibrotic remodeling. Independently irradiated cancer cells demonstrated pronounced acute dose-dependent damage and when integrated into airway OTEs, formed distinguished tumor-like clusters within the differentiating epithelium.

Conclusion/Significance: Airway OTEs recapitulate the native lung microenvironment through a pseudostratified columnar epithelium, mucociliary differentiation, and a dense stromal layer, providing a physiologically relevant platform for studying RILI and screening radioprotectants. Leveraging this model, we demonstrated that airway OTEs capture the progressive nature of RILI, from acute DNA damage and sustained inflammatory signaling through functional decline and the onset of fibrotic remodeling. The differential radiosensitivity observed between cancer cells and healthy airway epithelium further highlights the potential of this system for evaluating selective radioprotection strategies. Collectively, these findings establish airway OTEs as an enabling technology for improving radiotherapy protocols and identifying selective radioprotective agents, supporting the development of strategies that maximize tumor cell death while protecting healthy tissue.

OP-148 - Best practices for directed differentiation of hiPSCs into lung epithelial cells

Dana Brinson[1,2], Golnaz Karoubi[2,3,4], Tom Waddell[2,5,6]

[1]*University of Toronto, Institute Of Biomedical Engeineering, Toronto, Canada*
[2]*University Health Network, Latner Thoracic Research Laboratories, Toronto, Canada*
[3]*University of Toronto, Laboratory Medicine And Pathobiology, Toronto, Canada*
[4]*University of Toronto, Department of Mechanical And Industrial Engineering, Toronto, Canada*
[5]*University of Toronto, Institute Of Biomedical Engineering, Toronto, Canada*
[6]*University of Toronto, Institute Of Medical Sciences, Toronto, Canada*

Purpose/Objectives: Current protocols for generation of human induced pluripotent stem cell (hiPSC)-derived lung epithelial progenitor cells (LPCs) give heterogeneous results. Reported LPC yields range from 20-90% between batches despite starting with a uniform hiPSC population with exposure to the same differentiation media.

Methodology: Several key parameters may influence success with directed differentiation protocols. These include hiPSC passage

number, initial seeding density, split ratio of definitive endoderm, an optional passage during LPC induction, retinoic acid concentration during LPC induction, the harvesting reagent used to dissociate cells prior to sorting, and the seeding density of LPCs in 3D Matrigel droplets. We assessed the viability and yield of definitive endoderm (DE), LPCs, and distal alveolar epithelial cells by flow cytometry to determine the effects of these parameters.

Results: Our results indicate that passage number (up to a maximum of two months of hiPSC maintenance) does not affect definitive endoderm or LPC yield. Increased initial cell density from 200,000 to 250,000 cells/cm^2 improves DE yield (94.6±7.5% versus 98.8±0.9%) but has no effect on downstream LPC yield. An optional passage during LPC induction increases LPC yield (18.0±13.2% without passaging, versus 47.8±15.5% with a passage on day 8) but may decrease downstream AT2 yield. Increased retinoic acid concentration during LPC induction may increase LPC yield for this hiPSC line, though not significantly (11.3±11.0% with 100 nM retinoic acid, versus 21.1±12.1% for 500 nM retinoic acid). Harvesting LPCs for sorting using accutase yields a greater proportion of LPCs (30.4±16.4%) than trypsin (17.2 + 8.7%). Lastly, decreased seeding density in 3D Matrigel increases the final AT2 yield (11.2±2.9% for 200 cells/

Conclusion/Significance: Further investigation of these parameters in several hiPSC lines, or of other small molecule concentrations will benefit the field. Protocols vary in their media composition and timing, seeding densities, sorting versus not sorting LPCs prior to spheroid culture, and other parameters. Standardization of existing protocols would help improve consistency across labs. Overall, this work aims to provide insight into several parameters which influence hiPSC-derived cell yields.

OP-150 - Controlled decorin delivery from injectable microgels prevents the development of vocal fold fibrosis

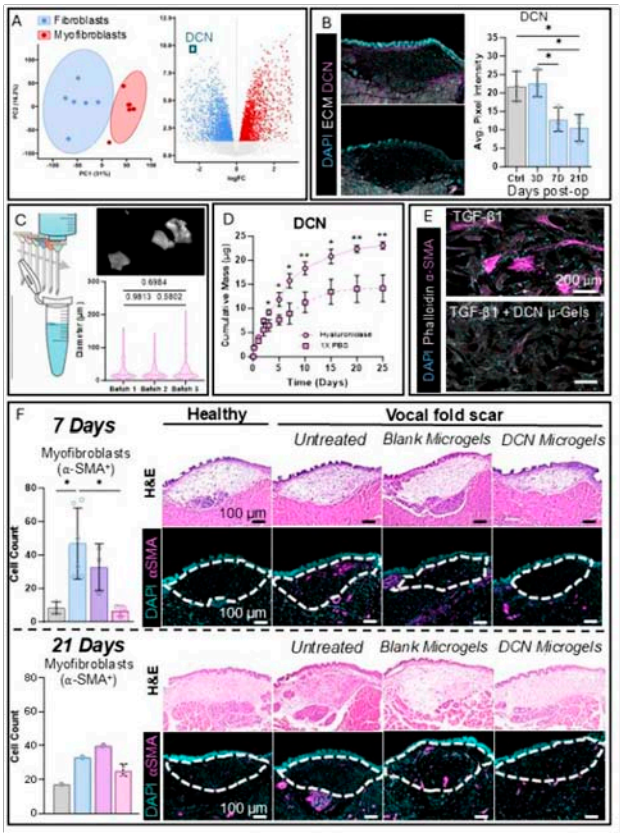
Cayman Matson[1,2], Riccardo Gottardi[1,3], Karen Zur[4,5], Eiman Bandora[6,7], Hannah Oh[1,2], Kendra Mcdaid[8], Matthew Aronson[1,2], Yashna Gupta[1,2], Hannah Bonelli[1,2], Elizabeth Brown[1,2], Ryan Friedman[1,2]

[1]*Children's Hospital of Pennsylvania, Department of Otolaryngology, Philadelphia, United States of America*
[2]*University of Pennsylvania, Bioengineering, Philadelphia, United States of America*
[3]*University of Pennsylvania, Philadelphia, United States of America*
[4]*Children's Hospital of Philadelphia, Otolaryngology, Department of Surgery, Philadelphia, United States of America*
[5]*University of Pennsylvania, Department of Otorhinolaryngology – Head And Neck Surgery, Philadelphia, United States of America*
[6]*Tel Aviv Medical Center, Department of Otolaryngology, Head And Neck Surgery, Tel Aviv, Israel*
[7]*Tel Aviv University, The Gray Faculty of Medical And Health Sciences, Tel Aviv, Israel*
[8]*Children's Hospital of Pennsylvania, Department of Veterinary Resources, Philadelphia, United States of America*

Purpose/Objectives: The vocal folds play a crucial role in speech. Vocal fold (VF) scarring, typically caused by routine procedures like intubation, affects approximately 2-6 million Americans, often causing hoarseness, difficulty breathing, or pain when speaking. Persistent myofibroblast activation after initial wound healing results in scar formation, negatively impacting vocal control and quality. The most common intervention, intracordal steroid injections, only alleviates symptoms, but effects are short-lived and fail to solve the underlying scar tissue buildup. Currently, no treatments provide long-lasting relief nor halt fibrosis progression, highlighting the need for new therapeutics. Here, we have developed a novel hyaluronan microgel platform for sustained release of the antifibrotic proteoglycan decorin (DCN) to prevent development of vocal fold fibrosis.

Methodology: Bulk RNA sequencing was performed on immortalized human VF fibroblasts and myofibroblasts. DCN's depletion was confirmed by IF in scarred rat VFs. DCN-Loaded hyaluronan microgels were fabricated via extrusion fragmentation and characterized. DCN-loaded microgels were suspended in hyaluronidase and PBS to determine release profiles. In vitro, we utilized human VF myofibroblasts to determine released DCN's ability to reduce expression of fibrotic marker αSMA. In vivo, DCN-loaded microgels were injected into a rat model of VF scarring. VF histology after 7 and 21 days was analyzed to determine DCN's anti-fibrotic effects.

Results: A) Bulk RNA-seq indicates DCN is downregulated in immortalized human myofibroblasts. B) DCN is depleted in the lamina propria after injury in a rat model of VF scarring. C) Extrusion fragmentation of hyaluronan gels produce microgels of consistent sizing. D) Release profile of DCN-loaded microgels in PBS and hyaluronidase over 25 days. E) DCN reduces αSMA expression in TGF-ß1 dosed fibroblasts. F) Intracordally injected DCN reduced αSMA expression in scarred rat VFs throughout early and late wound healing.



Conclusion/Significance: DCN is depleted after VF injury, but its restoration can halt the progression of VF fibrosis. Our hyaluronan microgel platform is capable of releasing DCN to the VFs for the entirety of the wound healing process. These results not only elucidate that DCN plays a key role in VF fibrosis but also represent a path towards a novel clinical solution.

OP-151 - Development of a Chorioallantoic Membrane (CAM)-based Angiogenesis Platform for Enhancing Neovascularization in Renal Organoid Constructs

Young Min Ju, Roopa Chalasani, Ingrid Bello, Ji Hyun Kim, John Jackson, Anthony Atala, James Yoo

Wake Forest School of Medicine, Wake Forest Institute For Regenerative Medicine, Winston-Salem, United States of America

Purpose/Objectives: Human renal organoids, derived from renal progenitor or stem cells, possess the ability to self-organize into nephron-like structures and exhibit aspects of kidney development *in vitro*. However, the absence of functional vasculature restricts their maturation and longevity. This study investigated a novel approach to promoting vascularization of human renal organoids

using the chorioallantoic membrane (CAM) model. We hypothesize that supplementation with vascular endothelial growth factor (VEGF) and co-culture with endothelial cells (ECs) would enhance angiogenesis, vessel infiltration, and organoid structural preservation.

Methodology: Human renal organoids were embedded in fibrin hydrogel scaffolds (250 μL, 10 mg/mL) prepared from a stock solution containing 40 mg/mL fibrinogen, 3 U/mL thrombin, and 40 μg/mL aprotinin. Three experimental groups were established: (1) organoids-only, (2) organoids with VEGF, and (3) organoids with VEGF plus endothelial cells (5M cells, MS1). Each scaffold in the VEGF-treated groups was supplemented with 100 ng/scaffold of VEGF. Scaffolds were implanted on the CAM of chick embryos on embryonic day 6, precisely positioned at the intersection of mature blood vessels to maximize host vascular interaction. Constructs were harvested on day 10 post-implantation and analyzed using gross imaging, histology, and immunofluorescence staining to evaluate vascular infiltration, organoid structure, and host–implant interactions. Lectin staining was performed to assess vessel morphology within the scaffold.

Results: The VEGF + MS1 group demonstrated the most favorable outcomes, characterized by larger organoid size, enhanced structural integrity, and robust integration with CAM vasculature, with clear evidence of vessel penetration into the fibrin scaffold. The organoid-only scaffolds remained smaller and exhibited poor survival despite hypoxia-induced angiogenesis. Statistical analysis of the organoid size revealed significant differences among groups ($p = 0.016$) and significant temporal changes *in vitro* ($p = 0.00044$). Immunofluorescence staining confirmed the presence of endothelial, stromal activation, and preservation of organoid-specific markers.

Conclusion/Significance: These results demonstrate that VEGF plays a crucial role in stimulating angiogenesis and maintaining organoid structure. Furthermore, co-existing with endothelial cells facilitates superior vessel–organoid integration and organoid survival. These findings suggest that fibrin hydrogel scaffolds supplemented with VEGF and endothelial cells provide a promising strategy for generating pre-vascularized renal constructs, advancing their potential applications in regenerative medicine.

Session 44
Skin, Wound Healing, and Inflammation (General Session) 1

11-17-2026 @ 8:00 AM - 9:30 AM

OP-153 - Skin Organoids in Bioprinted Skin Implants Facilitate Human-Like Epidermis Formation, Induce Pigmentation and Skin Appendage Development in a Mouse Wound Model

Anastasiya Gorkun-Roeder[1], Kelsey Willson[2], Naresh Mahajan[1], Nicholas Edenhoffer[1], Gemma Nomdedeu-Sancho[1], Shay Soker[3], Anthony Atala[3]

[1]*Wake Forest University School of Medicine, Wake Forest Institute For Regenerative Medicine, Winston-Salem, United States of America*
[2]*Wake Forest Institute for Regenerative Medicine, Biomedical Engineering, Winston-Salem, United States of America*
[3]*Wake Forest Institute for Regenerative Medicine, Winston Salem, United States of America*

Purpose/Objectives: Current cell-based treatments for skin wounds primarily use keratinocytes and fibroblasts, limiting the development of skin appendages. While 3D bioprinting enables rapid fabrication of large skin constructs, these require extended maturation to acquire full regenerative potential. To address these limitations, we developed bioprinted "reorganized skin" constructs composed of six human skin cell types arranged into epidermal, dermal, and hypodermal layers, with pre-formed skin organoids integrated into the dermal compartment to enhance regenerative capacity and accelerate wound healing.

Methodology: Skin organoids were generated by culturing a mixture of six key skin cell types under non-adhesive conditions for 21 days. Using 3D bioprinting, we fabricated two experimental groups of tri-layered skin constructs: (1) reorganized skin, containing 25% cells as pre-cultured organoids in the dermal layer, and (2) bioprinted skin without organoids. Constructs were matured for 7 days and implanted into 2×2 cm full-thickness wounds on athymic nude mice. Control groups included hydrogel-only and untreated wounds. Wound healing and pigmentation were assessed over 90 days using weekly imaging and digital analysis (ImageJ, R). Histological evaluation (H&E, Trichrome, Picrosirius, Melanin staining) and immunohistochemistry were performed, and gene expression analyzed by qPCR.

Results: Reorganized skin constructs accelerated wound closure, reduced contraction, and promoted the formation of human-like rete ridges compared to bioprinted skin lacking organoids. Notably, only reorganized skin constructs supported the development of skin appendages and enabled pigmentation across the wound site. Collagen deposition patterns and gene expression profiles further indicated improved structural and functional regeneration. By day 56, the regenerated tissue exhibited mature features, including hair follicles and glandular structures. Immunohistochemical analysis revealed uptake of human melanosomes by the regenerated murine epidermis, indicating direct melanin deposition, while qPCR demonstrated upregulation of mouse pigmentation-associated genes, suggesting indirect stimulation of melanogenesis.

Conclusion/Significance: Incorporating pre-formed skin organoids into multi-layered bioprinted constructs significantly improves epidermal architecture, pigmentation, and appendage formation, supporting physiological healing in full-thickness wounds. This approach demonstrates valuable potential for clinically translatable skin replacements.

OP-154 - Baricitinib Hydrogels as a Potential Therapeutic for Hidradenitis Suppurativa (HS) via Reduced JAK-STAT Signaling and Sustained Drug Release

Elaine Kim[1], Stephanie Yoon[1], Leo Wang[1,2]

[1]*University of Pennsylvania, Department of Dermatology, Philadelphia, United States of America*
[2]*University of Pennsylvania, Department of Chemical And Biomolecular Engineering, Philadelphia, United States of America*

Purpose/Objectives: Hidradenitis suppurativa (HS) affects 3.3 million people in the U.S. and causes painful, recurring boils and abscesses that can lead to hospitalization and death. One therapeutic target is the JAK-STAT signaling pathway, which contributes to inflammation and immune memory. However, systemic use of JAK inhibitors can lead to side effects, including cardiovascular events and thrombosis. Here, we assess local pharmacokinetics and assess efficacy and safety for use in HS.

Methodology: Baricitinib hydrogels were prepared by combining sterile baricitinib and hyaluronic acid thiol (HA-S) in phosphate-buffered saline (PBS). NSG mice were grafted with human foreskin. Baricitinib hydrogels or controls were injected intradermally. Skin samples were collected at 24 hours and 1 week post-injection for MALDI-MSI (Matrix-Assisted Laser Desorption/Ionization Mass Spectrometry Imaging). For HS studies, hydrogels were injected into 8 mm biopsy punch sections of human HS skin after 24 hours of culture post-collection. Skin samples were cultured for 14 days, and culture media was collected at designated time points for Luminex immunoassays. For safety studies, hydrogels were injected into porcine abdominal skin.

Results: MALDI imaging showed that compared to baricitinib solution, baricitinib hydrogels maintained higher intradermal drug signal over time, indicating sustained and localized drug release (Figure 1A, 1B). Signal was persistent for 7 days. In HS tissue, our results demonstrated reduced inflammatory signaling, including key inflammatory cytokines such as IL-17A, IFN-γ, GM-CSF (Figure 1C), TNF-α, and IL-10 (not shown). Histology showed dose-dependent decreases in inflammatory infiltrate on day 14 post-culture. No evidence of intradermal toxicity was observed at 1, 7, and 14 days after intradermal injection into pig.

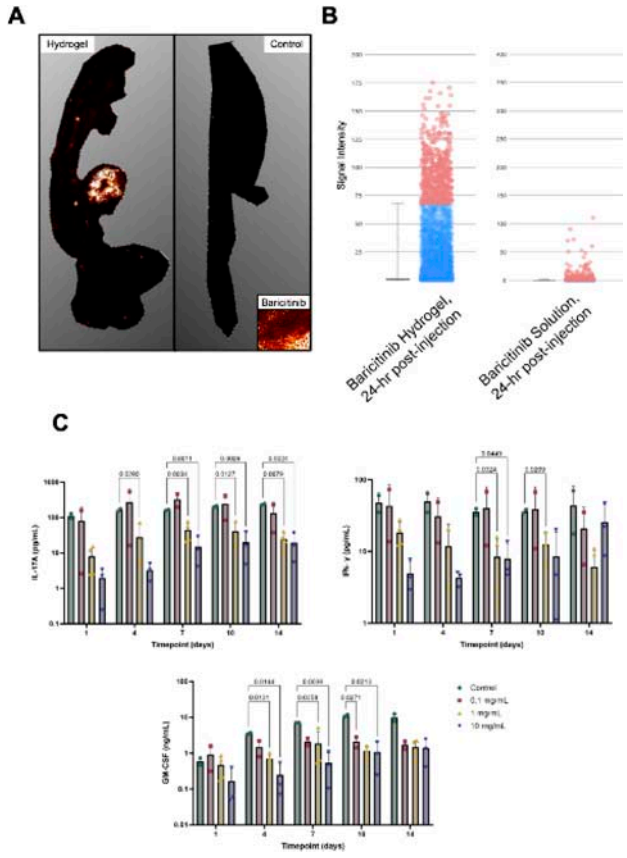


Figure 1. (A) MALDI imaging of xenograft mice skin sections 24 h after intradermal injection of baricitinib hydrogel (10 mg/mL, left) or solution (10 mg/mL, right). (B) Baricitinib signal intensity in MALDI images 24 h following hydrogel (left) or solution (right) injection. (C) IL-17A, IFN-γ, and GM-CSF concentrations in culture media from HS skin.

Conclusion/Significance: This study demonstrates that baricitinib hydrogels localize to human skin, sustain release, and can reduce inflammatory markers in HS skin. Our studies underscore the use of reversible thioimidates to sustain the release of other small molecules in inflammatory diseases.

OP-155 - Enhancing Pro-Regenerative Neutrophil Function Through Mitochondrial Transplantation

Samantha Hall, Evan Main, Gary Bowlin

The University of Memphis, Biomedical Engineering, Memphis, United States of America

Purpose/Objectives: Proper modulation of the acute immune response following biomaterial implantation is critical for tissue regeneration and implant integration. Neutrophils, once viewed as short-lived initiators of inflammation, are now recognized as key regulators of wound healing through their coordination of immune signaling and tissue repair. However, prolonged neutrophil activation induces mitochondrial dysfunction, contributing to oxidative stress and immune dysregulation. Mitochondrial transplantation, the delivery of exogenous mitochondria to recipient cells, has emerged as a promising strategy for restoring metabolic homeostasis and modulating cellular behavior. Although this approach has demonstrated therapeutic potential, its effects on neutrophils and the acute wound healing cascade remain largely unknown. This study investigated the potential of transplanted mitochondria to modulate neutrophils toward tissue regenerative states supporting host-biomaterial integration.

Methodology: Human peripheral blood neutrophils were isolated from healthy donor blood. Mitochondria were isolated from normal adult human dermal fibroblasts (ATCC, PCS-201-012) and delivered to neutrophils following stimulation with 100 nM phorbol 12-myristate 13-acetate (PMA). Confocal microscopy was used to evaluate mitochondrial uptake and neutrophil nuclear morphology. Retention of mitochondrial membrane potential following uptake was assessed using tetramethylrhodamine methyl ester (TMRM) imaging up to 3 hours post-mitochondrial delivery. Intracellular reactive oxygen species (ROS) activity was quantified using a DCFH-DA oxidation assay. Neutrophil secretomes were evaluated using multiplex protein analysis of inflammatory and regenerative proteins.

Results: Confocal imaging demonstrated uptake of exogenous mitochondria by stimulated and unstimulated neutrophils after only 15 minutes of co-incubation. Colocalization between exogenous mitochondria and endogenous neutrophil mitochondrial networks was also observed. TMRM confirmed maintenance of mitochondrial membrane potential up to 3 hours following uptake, indicating promise for preserved metabolic integrity. Multiplex analysis revealed that mitochondria induced significant increases in pro-regenerative factors, FGF-2 and IL-22, and immune-modulatory cytokines, G-CSF and MCP-1, in both stimulated and unstimulated groups. Importantly, mitochondrial uptake did not significantly increase intracellular ROS or pro-inflammatory protein secretion.

Conclusion/Significance: Exogenous mitochondria are internalized by human neutrophils and promote pro-regenerative cytokine expression without upregulating pro-inflammatory mediators. These findings support mitochondrial transplantation as a promising immunomodulatory strategy for tissue repair and regenerative medicine applications.

OP-156 - Adipocyte-Derived Signals Transcriptionally Reprogram the Functional State of Dermal Fibroblasts into a Regeneration-Related Phenotype

Zhenru Wang[1], Austin Scholp[1], Aloysius Klingelhutz[2], James Ankrum[1], Edward Sander[1]

[1]*University of Iowa, Roy J. Carver Department of Biomedical Engineering, Iowa City, United States of America*
[2]*University of Iowa, Department of Immunology And Microbiology, Iowa City, United States of America*

Purpose/Objectives: The purpose of this study was to define how adipocyte conditioned medium (ACM) derived from 3D human adipocyte spheroids shapes fibroblast phenotype and regulates transcriptional programs associated with extracellular matrix (ECM) remodeling. We then compared this response with fibroblast subpopulations identified in single-cell datasets and further connected these transcriptional responses with adipocyte-secreted proteins through ongoing proteomic analysis.

Methodology: Human Dermal Fibroblasts were treated with either ACM or TGF-β1. Bulk RNA-seq was performed to identify differentially expressed genes and ACM-regulated biological pathways. Pathway analysis was used to characterize transcriptional programs related to fibroblast activation and ECM remodeling. ACM-induced transcriptional signatures were then mapped onto published single-cell RNA-seq fibroblast datasets to assess their alignment with regeneration-associated or fibrosis-associated fibroblast states. In parallel, proteomic analysis of ACM is being performed to identify secreted proteins and link them to key pathways identified from the RNA-seq results.

Results: RNA-seq analysis showed that ACM-treated fibroblasts showed a transcriptional profile distinct from canonical TGF-β1 induced fibroblasts. ACM group regulated genes were associated with ECM remodeling and metabolic signaling and related pathways (Fig. A and B). Projections with published single-cell fibroblast populations suggested that ACM-treated fibroblasts show greater similarity to regeneration-associated fibroblast states than to canonical scar-forming fibroblast populations (Fig. C). Together, these results suggest that adipocyte-derived soluble factors may promote a regeneration-associated fibroblast phenotype rather than a fully fibrotic fibroblast state. Ongoing proteomic analysis will help identify candidate secreted proteins in ACM that may correspond to the key transcriptional pathways observed. Fig. **A**. **a)** KEGG and **b)** GO Pathway Enrichment. **B. a)** Expression of collagen genes. **b)** Expression of selected matrix-associated regulatory genes. **C. a)** Fibroblast single-cell subcluster landscape. **b)** Fibroblast subcluster composition across experimental conditions.



Conclusion/Significance: These findings suggest that ACM may direct fibroblasts toward a regeneration-associated phenotype while limiting features of canonical fibrotic activation. By integrating RNA-seq, single-cell comparison, and ACM proteomic analysis, this study aims to identify candidate adipocyte-derived mediators that regulate fibroblast behavior. This work may provide insight into adipose to fibroblast crosstalk in the context of wound healing, tissue repair, and regeneration.

OP-157 - Biofabrication of immunocompetent, vascularized full-thickness skin models incorporating primary human macrophages as drug discovery tools for skin fibrosis diseases

Yi Wei Lim, Yu-Chi Chen, Shayne Frebert, Min Jae Song, Marc Ferrer-Alegre

National Center for Advancing Translational Sciences, Rockville, United States of America

Purpose/Objectives: Scleroderma is an autoimmune disease that causes inflammation and thickening of the skin and connective tissues. This hardening and thickening of tissue are attributed to the excess deposition of extracellular matrix (ECM) such as collagen, a process known as fibrosis. While the exact pathophysiological mechanism of scleroderma is elusive, microvascular injury and vasculopathy are the initial pathological features of this disease. Vasculopathy is hypothesized to trigger inflammation and fibrosis in scleroderma. One of the prominent immune players are M2 macrophages, canonical skin immune subset that supports tissue repair by promoting angiogenesis and tissue remodeling. However, aberrant activation of M2 macrophages can lead to secretion of cytokines and chemokines that activate fibroblasts and drive fibrosis progression. Due to its complex pathophysiological mechanisms, current therapeutics only slow down disease progression but do not cure or reverse existing fibrosis. Current in vitro skin models used in preclinical testing failed to recapitulate cellular and physiological complexity of the skin immune components, while animal models demonstrated large structural and functional differences. Therefore, there is a critical need for the development of immunocompetent 3D skin tissue fibrosis model to study the interplay between different skin-resident immune and non-immune compartments in fibrosis and use it as a preclinical testing platform for therapeutic discovery.

Methodology: Immunocompetent, vascularized full-thickness skin (VFTS) constructs were generated by incorporating M2 macrophages (differentiated from CD14+ peripheral primary human monocytes) with dermal fibroblast, endothelial cells, and pericytes to form the dermal compartment, followed by air-liquid interface (ALI) differentiation of the epidermis in a 96-well transwell format.

Results: We demonstrated that addition of macrophages in VFTS are functional and responds to bacterial and viral stimuli by producing pro- and anti-inflammatory cytokines. To model fibrosis, TGFβ1 treatment led to vasculopathy (reflected by endothelial-GFP intensity) and a significant increase in collagen deposition, a hallmark of scleroderma. We further confirmed that blocking TGFβ signaling with Galunisertib, a TGFβ receptor I inhibitor, prevented TGFβ-induced collagen deposition and vasculopathy.

Conclusion/Significance: We successfully generated a 3D VFTS tissue equivalent with functional macrophages in a 96-well transwell format, providing a high-throughput-compatible drug discovery assay platform for antifibrotic drug screening in skin fibrotic diseases.

OP-158 - Combinatorial Sustained Delivery of VEGF and TGFB2 for Diabetic Wound Healing

Tracey Moyston[1], Parul Katiyar[2], Sumit Singh Verma[2], Sagar Dhoble[3], Kanhaiya Singh[2], Steven Little[3]

[1]*University of Pittsburgh, Bioengineering, Pittsburgh, United States of America*
[2]*University of Pittsburgh, Department of Surgery, PITTSBURGH, United States of America*
[3]*University of Pittsburgh, Department of Chemical Engineering, PITTSBURGH, United States of America*

Purpose/Objectives: Diabetic foot ulcers (DFU) carry a 20% amputation rate and are typically ischemic with delayed healing. Vascular endothelial growth factor (VEGF) has been explored to increase angiogenesis and improve healing however, VEGF alone has limited success in producing stable blood vessels and healing DFU. Studies show that combination therapy with VEGF could improve healing. Transforming growth factor beta2 (TGFβ2) is promising for combination therapy as it has been shown to increase mural cell migration and collagen deposition for vessel maturation and wound remodeling. This work delivers a combination of VEGF and TGFβ2 in a diabetic wound model to improve healing. Poly(lactic-co-glycolic) acid microparticles (PLGA MPs) were tuned for sustained release of VEGF and TGFβ2 in the wounds.

Methodology: TGFβ2 and VEGF were encapsulated in PLGA MPs by water-in-oil-in-water double emulsion. ELISAs were used to assess encapsulation and release. Bilateral stent wounds were induced in diabetic and non-diabetic mice, followed by subcutaneous injection of Blank, VEGF, TGFβ2 or VEGF and TGFβ2 MPs near the wound edge (n=3 mice). Wound closure was assessed at days 3, 7 and 10 and flow cytometry was conducted on excised wounds at day 10 for TGFβ2 MP and Blank MP groups.

Results: VEGF and TGFβ2 MPs displayed an initial burst and continuous release over 15 days (Fig.1A). VEGF and TGFβ2 combination showed a trend toward accelerated healing in diabetic mice compared across groups over time (Fig.1C). The combination also displayed significantly accelerated healing over TGFβ2 MPs at day 10 (p=0.017). Interestingly, TGFβ2 MPs trended toward delayed healing over time which aligned with flow cytometry data displaying a trend toward an increased proinflammatory environment (Fig.1D, 1E). There were no significant differences in healing in non-diabetic mice (Fig.1C).

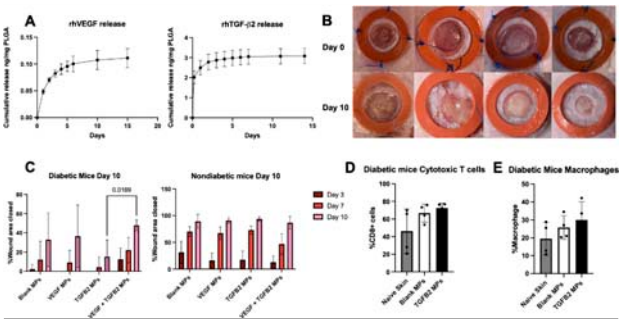


Figure 1: A) Release kinetics for VEGF and TGFβ2 MPs. B) Wound images at Days 0 and 10. C) %wound closure for diabetic and nondiabetic mice. D) Cytotoxic T cells and E) Macrophages in diabetic wounds at day 10.

Conclusion/Significance: TGFβ2 and VEGF combination shows potential to improve diabetic wound healing with increased healing over TGFβ2 at day 10. Future work will assess time to complete healing along with gene expression and immunostaining.

Session 45
Engineering Human Tissues for Translational Impact: Advanced 3D Models, Microphysiological Systems, and AI-enabled Discovery

11-17-2026 @ 8:00 AM - 9:30 AM

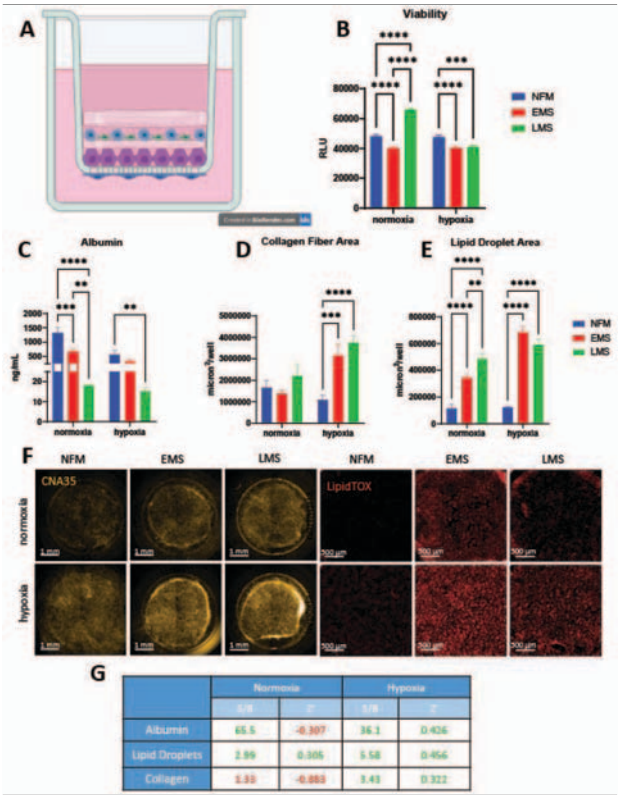
OP-159 - Optimization of a 3D Hepatic Model for Complex Preclinical Screens of Early and Late-Stage MASLD

Lindsey Kirk[1], Seia Comsa[2], Dillon Gavlock[2], Yu-Chi Chen[3], Mark Miedel[2], Marc Ferrer-Alegre[3], Emily Lee[3]

[1]*National Institutes of Health, National Center For Advancing Translational Sciences, Rockville, United States of America*
[2]*University of Pittsburgh, Pittsburgh Liver Research Center, Pittsburgh, United States of America*
[3]*National Center For Advancing Translational Sciences, Rockville, United States of America*

Purpose/Objectives: Metabolic dysfunction-associated steatotic liver disease (MASLD) is a progressive disease spectrum ranging from simple steatosis to metabolic dysfunction-associated steatohepatitis, fibrosis, cirrhosis, and liver failure. Although therapies such as resmetirom and semaglutide have recently been approved as treatments, therapeutic response rates remain limited due to complex phenotypes that vary between hepatic zones. Herein we describe the optimization of a 3D model for high-throughput screening (HTS) of potential therapeutics under early and late MASLD stages in the zone 1 and zone 3 liver. This will allow for efficient evaluation of a large number of potential therapeutic compounds under complex disease conditions, increasing the likelihood of identifying effective treatments.

Methodology: Ninety-six-well polyester inserts were coated with fibronectin and seeded with primary human liver endothelial cells basally and primary human hepatocytes apically, followed by hepatic stellate cells and Kupffer cells. Hyaluronic acid gel covered the constructs (A). Normal fasting media (NFM) contained no supplementary fat, whereas early metabolic syndrome (EMS) media contained 200 µM oleic and 100 µM palmitic acids. Transforming growth factor B and lipopolysaccharide were added to simulate late metabolic syndrome (LMS). Zone-specific conditions were modeled using normoxia (zone 1) or hypoxia (6% O_2; zone 3). After 14 days, constructs were assessed for viability, function, and MASLD markers.



Results: Constructs remained viable under all conditions, while albumin levels decreased significantly under LMS conditions (B-C). Collagen area increased 3.43-fold between NFM and LMS in hypoxic zone-3 conditions (D,F). Total lipid droplet area increased 2.99-fold between NFM and EMS conditions in normoxic and 5.58-fold in hypoxic conditions (E-F). Under zone-3 hypoxic conditions, albumin, collagen, and lipid droplet area all HTS compatible based on signal/background ratios >2 and positive Z' values (G).

Conclusion/Significance: We developed a complex hepatic model representative of MASLD disease progression with HTS-compatible readouts. Additional metrics to be optimized include αSMA, fibroblast activation protein, fibronectin, IL-8, and IL-6. This HTS-compatible model will allow us to screen 42 potential therapeutic compounds, alone and in combination, to efficiently identify clinical candidates for all stages of a complex disease.

OP-160 - A Single-Plate Workflow for Machine Learning-Guided Exercise Optimization in 3D Neuromuscular Junction Tissues

Jacob Fleming, Thomas Leahy, Nelsa Estrella, Hamed Ghazizadeh, Christal Worthen, Greg Luerman, Nicholas Geisse

Curi Bio, Seattle, United States of America

Purpose/Objectives: Models of exercise and atrophy in tissue engineered muscles are critical for therapeutic discovery in neuromuscular indications and for advancing fundamental understanding of skeletal muscle physiology. However, interactions between culture conditions and donor variability make it difficult to identify optimal exercise protocols, and conditions often fail to translate across systems and laboratories. We present a human-in-the-loop optimization workflow combining scalable functional readouts with well-by-well experimental assignment to efficiently identify electrical stimulation parameters that enhance function in a human 3D neuromuscular junction (NMJ) tissue model.

Methodology: Human iPSC-derived myoblasts and motor neurons were co-cultured in 3D hydrogels suspended on flexible posts to generate functional 3D NMJ tissues. Using a commercial platform enabling independently programmable stimulation across a 24-well plate, we sampled four stimulation variables over a 7-day training period: frequency (1 to 40 Hz), block intensity (1 to 10 s), bouts per day (1 to 24), and bout intensity (60 to 360 repeats). A Gaussian process regression model mapped the four-dimensional parameter space and guided subsequent protocol selection.

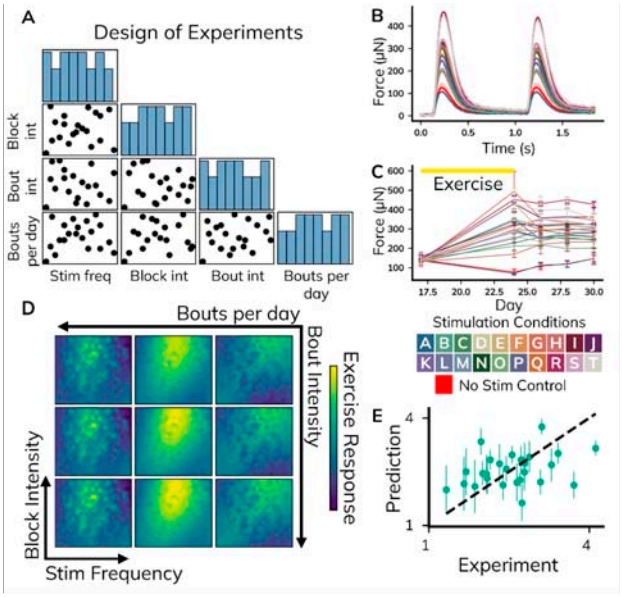


Figure 1. Gaussian process–guided modeling of electrical stimulation parameters optimizes exercise protocols. (A) Sampling across all four parameters using Sobol and Latin hypercube designs. (B) Waveforms and (C) quantified twitch forces range from no improvement to 6.5-fold above unstimulated controls. (D) GP model of the four-dimensional parameter space. (E) Leave-one-out cross-validation demonstrates predictive accuracy for selecting parameters that drive enhanced twitch force.

Results: Sampling across parameter combinations revealed twitch forces ranging from no improvement to 6.5-fold above unstimulated

controls (Figure 1A-C), underscoring the sensitivity of 3D NMJs to stimulation parameters. The Gaussian process regression approach supported rapid identification of effective exercise protocols (Figure 1D-E). Optimized protocols also improved relaxation kinetics following optogenetic NMJ activation, suggestive of enhanced acetylcholinesterase localization and isoform distribution.

Conclusion/Significance: This workflow supports more efficient, reproducible, and physiologically relevant skeletal muscle research. Running all conditions within a single plate eliminates inter-experiment variability while reducing time, cost, and reagent use. This approach removes the need for prior cell line characterization and could be applied to use cases ranging from disuse atrophy to peak exercise adaptation, enabling interrogation of adaptive mechanisms and context-dependent therapeutic efficacy.

OP-161 - A 2.5D platform for high-throughput production of mature and functional human iPSC-derived skeletal muscle cultures

Tamara Rossy, Ritu Raman

Massachusetts Institute of Technology, Mechanical Engineering, Cambridge, United States of America

Purpose/Objectives: Functional in vitro models of human skeletal muscle enable screening for therapies that restore muscle contractility in the context of musculoskeletal disease. Existing models have limitations for high-throughput functional screens. 2D tissues can be manufactured and imaged at high-throughput, but delaminate upon muscle contraction. 3D tissues are compatible with functional readouts, but require low- to medium-throughput fabrication and imaging methods. We have developed a "2.5D" platform enabling high-throughput fabrication and imaging of aligned contractile muscle monolayers on microgrooved hydrogels, and show that this method promotes the maturation of human induced pluripotent stem cell (hiPSC)-derived muscles.

Methodology: Our method leverages 3D nano-printed stamps to pattern microscopic grooves on extracellular matrix (ECM)-mimicking hydrogels (Figure 1A). The grooves guide muscle fiber alignment (Figure 1B), while the soft substrate enables delamination-free contraction. Stamp arrays can pattern a full 96-well plate in a single step, enabling high-throughput functional screens (Figure 1C).

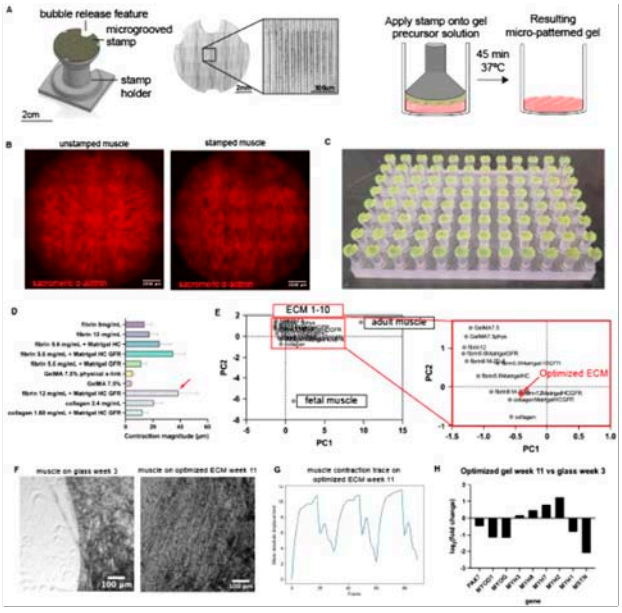


Figure 1.

Results: We measured contractile displacement of the muscles in response to electrical stimulation after 3 weeks on ten different hydrogels (Figure 1D). We found an optimized ECM (fibrin 12 mg/mL + high-concentration, low-growth factor Matrigel GFR, ~0.06 kPa stiffness) which resulted in the largest muscle contraction magnitude. Principal component analysis of RNA-seq transcripts involved in muscle maturation revealed that muscles on all ten ECMs yielded muscle closer to adult than fetal human muscle, and, among those ten, tissues grown on the optimized ECM were the closest to adult muscle in vivo (Figure 1E). While past studies of 2D hiPSC muscle on stiff substrates have been limited to ~2 weeks due to delamination, hiPSC-derived muscle remained adherent and contractile on the optimized ECM for 11 weeks (Figure 1F-G). This enhanced culture timescale enabled further tissue maturation (Figure 1H), including a ~2-fold decrease of early myogenic markers such as MYOD1 and MYOG, and a ~2-fold increase in the adult myosin isoform MYH2.

Conclusion/Significance: We developed a platform to generate mature, contractile hiPSC-derived muscle at high throughput. We are now leveraging this platform to screen how therapeutic interventions (e.g., exercise) impact muscle contractility in healthy and dystrophic states, paving the way for personalized screens of mobility-restoring therapies.

OP-162 - Toward Sex-Informed Afferent Nociceptive Microphysiological Systems via Hormonal Modulation of 3D Neural-Glial Cultures

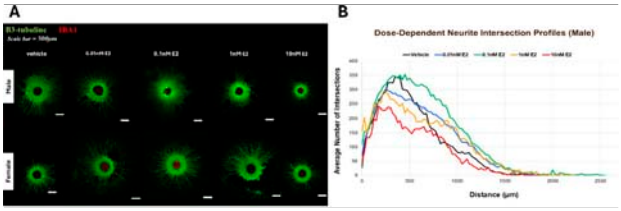
Melika Esmaeili Rad[1], Jared Fink[1], Micheal Moore[1,2]

[1]*Tulane University, Department of Biomedical Engineering, New Orleans, United States of America*
[2]*Tulane University, Brain Institute, New Orleans, United States of America*

Purpose/Objectives: Current preclinical models for evaluating non-opioid analgesics often demonstrate limited physiological relevance and poor predictive translation to clinical outcomes. Microphysiological systems (MPS) offer a promising strategy for bridging the gap between conventional in vitro cultures, animal studies, and clinical evaluation through the development of functional human-relevant tissue circuitry. Our laboratory has been developing afferent nociceptive MPS platforms modeling functional signaling between dorsal root ganglion (DRG) and spinal cord dorsal horn (SCDH) tissues for studying nociceptive transmission and therapeutic modulation. In the current study, we investigate hormonal modulation of neural-glial cultures to support development of sex-informed nociceptive platforms that better capture known sexual dimorphisms in the pathophysiological etiology of chronic pain.

Methodology: Male- and female-derived rat SCDH spheroids were embedded within thick Matrigel matrices to support three-dimensional concentric neurite outgrowth, while male- and female-specific human induced pluripotent stem cell (iPSC)-derived SCDH cultures containing neurons, astrocytes, and microglia were established on planar Matrigel-coated substrates. Cultures were exposed to physiologically relevant concentrations of 17β-estradiol (E2) and dihydrotestosterone (DHT), and hormone-dependent structural responses were evaluated through neurite outgrowth and intersection analyses. Isolated neural-glial culture platforms were used to enable quantitative assessment of neurite organization under controlled hormonal conditions prior to integration into full DRG–SCDH nociceptive circuitry.

Results: Initial studies demonstrated non-linear, dose-dependent modulation of neurite organization under E2 exposure in male rat-derived SCDH cultures, with intermediate concentrations promoting enhanced neurite density, intersection profiles, and extension relative to vehicle and higher-dose conditions (Figure 1). Ongoing studies are expanding these analyses across additional hormonal conditions, male- and female-derived systems, and human-derived cultures. **Figure 1. (A)** Representative neurite outgrowth images of male- and female-derived rat SCDH spheroids exposed to varying E2 concentrations; **(B)** Neurite intersection analysis of male-derived SCDH cultures demonstrating non-linear dose-dependent modulation of neurite organization.



Conclusion/Significance: These findings support the feasibility of incorporating hormonal modulation into afferent nociceptive

MPS platforms and establish a foundation for developing sex-informed human-relevant nociceptive circuitry models capable of capturing sexually dimorphic mechanisms underlying chronic pain and therapeutic response. Incorporation of sex-specific biological factors into engineered nociceptive platforms may improve the physiological relevance and predictive utility of preclinical screening systems for non-opioid analgesics.

OP-163 - Therapeutic Evaluation of CBD-Encapsulated Nanoparticles in Triple-Negative Breast to Brain Metastasis Using a Metastasis-on-a-Chip Device

Jason Scharenberg[1], Emerie Stagner[1], Sanjay Mishra[2], Pratyusha Ghanta[2], Ramesh Ganju[2,3], Aleksander Skardal[1,3]

[1]*The Ohio State University, Biomedical Engineering, Columbus, United States of America*
[2]*The Ohio State University, Medicine - Pathology, Columbus, United States of America*
[3]*The Ohio State University, Comprehensive Cancer Center, Columbus, United States of America*

Purpose/Objectives: Triple-negative breast cancer (TNBC) is an aggressive subtype of breast cancer that exhibits rapid growth and metastasis, including metastasis to the brain. Cannabidiol (CBD) has emerged as a potential inhibitor of tumor growth and metastasis. Nanoparticle-based delivery systems may enhance CBD bioavailability and improve its ability to cross the blood–brain barrier (BBB). To evaluate this, we investigated the anti-metastatic effects of nanoparticle-packaged CBD (NanoCBD) using a bioengineered breast-to-brain metastasis-on-a-chip (MOC) microphysiological system.

Methodology: In the MOC platform, primary human astrocytes and pericytes were encapsulated in a brain-mimetic hydrogel and injected into the device to simulate a simplified healthy brain tissue. Two breast cancer cell lines, the parental MDA-MB-231 and the brain organotropic MDA-MB-231-BrM2-831, were labeled with a lipophilic dye for visualization. These cells were suspended in a 1:1 mixture of astrocyte and pericyte media and perfused through the device for 7 days to assess invasion kinetics. Parallel experiments were conducted with NanoCBD added to the media. To probe potential driver mechanisms, the broad-spectrum matrix metalloproteinase (MMP) inhibitor GM6001 was used as a comparison treatment. Confocal microscopy images were acquired on days 1, 4, and 7 and analyzed using ImageJ. Media was collected on day 7 for downstream assays.

Results: Baseline studies showed both cell lines invaded the brain constructs, with the BrM2-831 clone exhibiting more uniform invasion, fully infiltrating the hydrogel by day 7. Treatment with NanoCBD significantly reduced invasion in both cell lines. ELISA analysis of collected media indicated decreased MMP9 levels following NanoCBD treatment. Use of GM6001 similarly reduced invasion, supporting the hypothesis that NanoCBD may act, at least in part, through MMP inhibition.

Conclusion/Significance: These findings demonstrate that NanoCBD can suppress breast-to-brain metastasis in a physiologically relevant model, potentially via modulation of MMP activity. Nanoparticle delivery may enhance CBD's therapeutic potential by improving bioavailability and BBB penetration. Future work will explore combinatorial strategies with immune cells, such as natural killer (NK) cells and CD8+ T cells, to determine whether NanoCBD can further enhance anti-tumor immune responses and improve outcomes in metastatic TNBC.

Session 46
Scaffolds, Matrices, and Biomaterials (General Session)

11-17-2026 @ 1:30 PM - 3:00 PM

OP-164 - Polypropylene mesh creates heterogeneous force microenvironments that drive divergent fibroblast fates

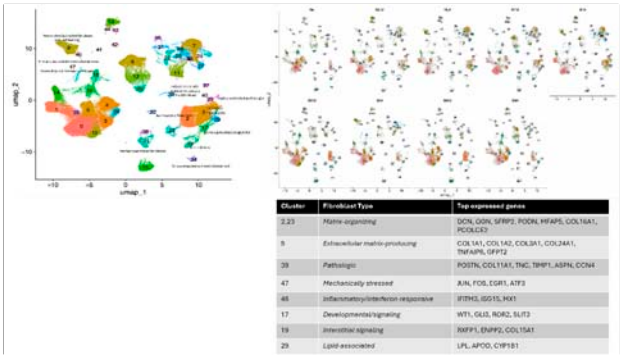
Marrisa Therriault[1,2], Katrina Knight[2,3], Temitope Obisesan[3], Gabrielle King[2], Amanda Artsen[1,2,4], Pamela Moalli[1,2,3]

[1]*University of Pittsburgh, Obgyn, Pittsburgh, United States of America*
[2]*Magee Womens Research Institute, Pittsburgh, United States of America*
[3]*University of Pittsburgh, Bioengineering, Pittsburgh, United States of America*
[4]*University of Pittsburgh, Department of Immunology, Pittsburgh, United States of America*

Purpose/Objectives: Polypropylene meshes used for pelvic organ prolapse repair are associated with both fibrosis and tissue degeneration, yet the cellular mechanisms driving these divergent remodeling responses remain poorly understood. Mechanical loading conditions imposed by implanted biomaterials are increasingly recognized as major regulators of host tissue remodeling. We hypothesized that differential stress distributions generated by mesh would induce distinct fibroblast activation states.

Methodology: Single-cell RNA sequencing was performed on rabbit vagina harvested from 4 surgical groups: sham without hysterectomy (SN), sham with hysterectomy (SH), RestorelleTM implanted under low tension (RL), and RestorelleTM implanted under high tension with wrinkle formation (RT). RT was designed to generate heterogeneous stress distributions with focal regions of elevated mechanical stress adjacent to stress-shielded regions. Tissues were collected at 4 and 12 weeks. Unsupervised clustering, dimensional reduction, and differential gene expression analyses were performed to define fibroblast subpopulations.

Results: Distinct fibroblast subpopulations spanning homeostatic, fibrotic, inflammatory, proliferative, and mechanically activated states were identified. SH tissues demonstrated a relatively limited and transient remodeling response characterized predominantly by homeostatic stromal fibroblasts and early inflammatory remodeling that largely resolved by 12 weeks. In contrast, mesh induced persistent fibroblast diversification that differed according to mechanical loading conditions. Homeostatic stromal fibroblasts (clusters 2 and 23) present in both groups, expressed matrix-organizing and collagen fibrillogenesis genes. RL demonstrated expansion of activated extracellular matrix-producing fibroblasts (cluster 5), indicative of reparative collagen deposition and chronic matrix remodeling. RT was enriched with highly activated pathologic fibroblasts (cluster 39) expressing genes demonstrating persistent myofibroblast activation, and impaired matrix turnover. RT also demonstrated expansion of mechanically stressed fibroblasts (cluster 47) and inflammatory/interferon-responsive fibroblasts (cluster 46), supporting persistent force-responsive stromal activation. Additional fibroblast populations included developmental/signaling fibroblasts, interstitial signaling fibroblasts, and metabolically distinct lipid-associated fibroblasts, suggestive of stress-shielded or mechanically unloaded stromal states.



Conclusion/Significance: Polypropylene mesh implantation induced marked fibroblast diversification into profibrotic, inflammatory, proliferative, and mechanically activated states. Low-tension mesh was associated predominantly with reparative extracellular matrix remodeling, whereas high-tension promoted chronic myofibroblast activation together with stress-responsive and inflammatory fibroblast states. These findings support a mechanobiologic model in which heterogeneous stress distributions drive both fibrosis and matrix degeneration.

OP-165 - Formulation-Dependent Effects of Intestinal dECM on Colorectal Cancer Organoid Chemotherapy Response

Zachary Congress, Nicholas Edenhoffer, Randall Bissette, Shay Soker

Wake Forest University School of Medicine, Wake Forest Institute For Regenerative Medicine, Winston-Salem, United States of America

Purpose/Objectives: Colorectal cancer (CRC) progression and response to therapeutics are strongly influenced by cell interactions with the ECM. Many *in vitro* CRC models fail to recapitulate the complexity of the native microenvironment, which calls into question whether these key interactions in tumor progression are being missed. The objective of this study was to develop a bioprintable model for CRC organoids that incorporate healthy human small-intestine decellularized ECM (dECM) and determine how differences in hydrogel properties influence metabolic activity and chemotherapy response.

Methodology: HCT116 colorectal cancer cells were encapsulated in bioprinted GelMA organoids containing either 0% or 2% (w/v) dECM. Organoids were cultured for seven days and treated with 150 uM 5-fluorouracil (5-FU) or 75 uM oxaliplatin. Metabolic activity was quantified using alamarBlue, measuring fluorescence following a 4-hour incubation. Additional samples were collected for histology and immunofluorescent studies to study ECM distribution, epithelial organization, and proliferation.

Results: Incorporation of dECM produced formulation-dependent effects. Relative to untreated controls, 5-FU survival was 44.6%, 55.8%, 51.4%, and 33% for 6% GelMA, 6% GelMA + 2% dECM, 8% GelMA, and 8% GelMA + 2% dECM, respectively. Oxaliplatin survival in these same groups was 54.2%, 54.8%, 51%, and 17.3%. The highest untreated metabolic activity was observed in the 6% GelMA + 2% dECM group, while the 8% GelMA + 2% dECM group demonstrated the highest sensitivity to both chemotherapeutic agents.

Conclusion/Significance: Preliminary findings imply that the biological impact of intestinal dECM on CRC cells in a 3D printed microenvironment is influenced by the surrounding GelMA environment. When 2% dECM was added to 6% GelMA organoids it was associated with improved cell chemotherapy survival, however when added to 8% GelMA organoids, it was associated with reduced metabolic activity and heightened chemosensitivity. Ongoing histological analyses aim to determine relative ECM distribution, epithelial organization, and proliferation to evaluate the mechanisms underlying this formulation-dependent response to chemotherapy. We aim to discern whether lower metabolic activity corresponds to either cell death or proliferative changes that affected drug response.

OP-166 - In Vitro Degradability and Cytotoxicity of Melt-Electrowritten Polydioxanone Scaffolds

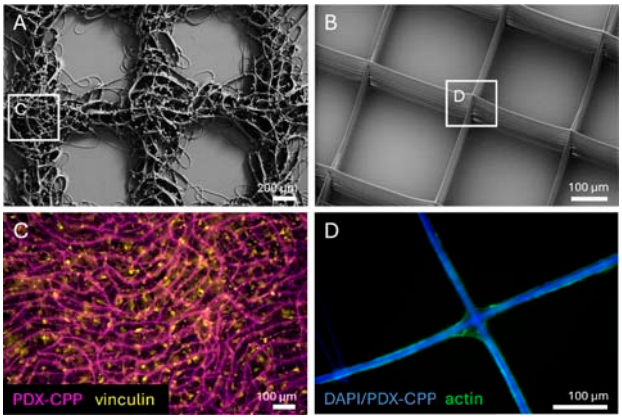
Iman Von Briesen[1,2], Paul Dalton[3], Scarlett Rhinehart[3], Maya Kasteleiner[2], Ramesh Jasti[4]

[1]*University of Oregon, Bioengineering, Eugene, United States of America*
[2]*University of Oregon, Department of Bioengineering, Phil And Knight Campus For Accelerating Scientific Impact, Eugene, United States of America*
[3]*University of Oregon, Department of Bioengineering, Phil And Penny Knight Campus For Accelerating Scientific Impact, Eugene, United States of America*
[4]*University of Oregon, Chemistry, Eugene, United States of America*

Purpose/Objectives: Polydioxanone (PDX) is a clinically proven resorbable polymer, yet its high thermal sensitivity restricts conventional fiber fabrication to a ~150 µm resolution. This work overcomes this by utilizing modified open-source 3D printers for filament Melt Electrowriting (f-MEW). We successfully manufactured sub-cellular (5 µm fibers) PDX scaffolds incorporated with fluorescent [n]cycloparaphenylenes (CPPs) for *in vitro*visualization and evaluated scaffolds' degradation and cytotoxicity.

Methodology: Medical-grade PDX (Poly-Med, USA) was compounded with CPPs and vacuum-molded into 1.75 mm filament. An open-source printer was modified with a grounded printhead and charged collector for f-MEW. To assess thermal processing effects, PDX disks were melted at 119°C for up to 6 h and scaffolds were printed under varying thermal conditions for incubation in standard culture media at 37°C. Material properties were characterized using differential scanning calorimetry, atomic force microscopy, and gel permeation chromatography. Hydrolytic degradation was assessed using mass loss calculations and quasi-static tensile testing. 3T3 fibroblasts were seeded onto PDX scaffolds and metabolic activity (AlamarBlue), cell attachment (DAPI count), focal adhesion formation (vinculin), and cytoskeletal organization (phalloidin) were examined.

Results: Vacuum drying the filament mitigated thermal degradation, extending the stable printing window at 130°C from 2 hours to over 60 hours. At a 1.5 µL/h flow rate and 4.7 kV, f-MEW reliably produced 5±0.5 µm diameter fibers (Figure 1B). Thermal pre-treatment duration increased hydrolytic mass loss by over 400% after 60 days for 6-hour vs. 15-minute pre-treatments. Extrusion rate heavily influenced scaffold mechanics; flow rates of 33.7 and 3.4 µL/h yielded stiffnesses of 170.0±31.0 and 53.8±2.5 MPa, respectively. Tensile strength during hydrolytic degradation decreased more rapidly in scaffolds printed at lower flow rates and higher temperatures. Fibroblasts successfully attached to the constructs, with degraded fibers (Figure 1A) exhibiting pronounced cytoskeletal spreading and pore bridging compared to non-degraded fibers (Figure 1C-D). Figure 1: A) Degraded and B) linear PDX scaffolds. Fluorescent images of cells on C) degraded and D) non-degraded scaffolds.



Conclusion/Significance: This work establishes accessible methodology for fabricating microfiber PDX scaffolds via f-MEW. It further validates that processing parameters can be deliberately leveraged to tune mechanical profiles and resorption kinetics, offering an optimized biomaterial platform for tissue engineering.

OP-167 - Bulk-oxidized Nanocellulose and Perfusable Leaf Model for Endothelialization of Engineered Constructs

Tanya Enderli[1], Kira Scarpignato[1], Zackary Lorton[1], Maryam Young[1], Paul Gatenholm[2], Chris Bashur[3,4]

[1]*Florida Institute of Technology, Melbourne, United States of America*
[2]*CELLHEAL AS, Sandvika, Norway*
[3]*Florida Tech, Melbourne, United States of America*
[4]*Florida Tech, Chemistry And Chemical Engineering, Melbourne, United States of America*

Purpose/Objectives: Alginate-based bioinks can provide mechanical stability for studying tissue vascularization, but cell attachment is limited with these and other hydrogels since extracellular matrix coatings can wash away. We are testing a new bulk oxidized nanocellulose to covalently bind laminin and promote endothelial cell (EC) attachment. Further, a more quantitative understanding of the impact of perfusion on EC response is needed for promoting vascularization in grafts. Thus, we are also utilizing a

leaf-vein inspired model to assess the impact of a range of shear stresses and branch points on ECs within the same sample.

Methodology: Leaf-structure samples were cast from different ratios of nanocellulose/alginate ink using 3D printed molds. Mechanical properties were characterized. Channels were tested with laminin coatings for surface oxidization using sodium periodate, bulk oxidation, or no oxidation (control). Samples were seeded with green fluorescent protein-positive (GFP+) human umbilical vein ECs (HUVECs). After cell attachment, samples were sealed in custom perfusion chambers. Spatial cell density and phenotype are being characterized using confocal microscopy, live/dead stain, and RT-PCR. Expected fluid flow rates and localized shear stresses were simulated using a Comsol® finite element (FE) model. Significance was determined with one-way ANOVA and Tukey.

Results: An 80:20 (v/v) nanocellulose/alginate ratio demonstrated optimal shear-thinning behavior and mechanical toughness for scaffold fabrication (n=6, compression, rheology). Oxidized hydrogels exhibited higher cell attachment and retention over time with oxidized leaf-structures than with no oxidation controls, and the bulk modified samples had the most homogenous cell attachment (n=6). Comsol® FE modeling predicted distinct, localized shear stress regions across the branching side channels within the range found in capillaries and arteries. We are currently utilizing these simulations and initial flow parameters to directly correlate localized shear stress with experimental spatial variations in endothelial cell attachment, viability, and regional growth.

Conclusion/Significance: Bulk oxidized nanocellulose/alginate hydrogels provide the necessary EC retention for testing tissue vascularization. Further, the biomimetic, leaf-inspired platform offers an ink-saving, efficient method to simulate and evaluate the impact of complex fluid dynamics on EC behavior. By combining computational models with initial flow parameters, this model system enables targeted optimization of localized shear stress to ultimately improve engineered tissue vascularization.

OP-168 - Hyaluronic acid-based cryoelectrospun scaffolds to enhance the antifibrotic potential of mesenchymal stem/stromal cells (MSCs)

Paria Baninoe[1], Pujhitha Ramesh[1], Melisa Larsen[2], Susan T. Sharfstein[2], Yubing Xie[1]

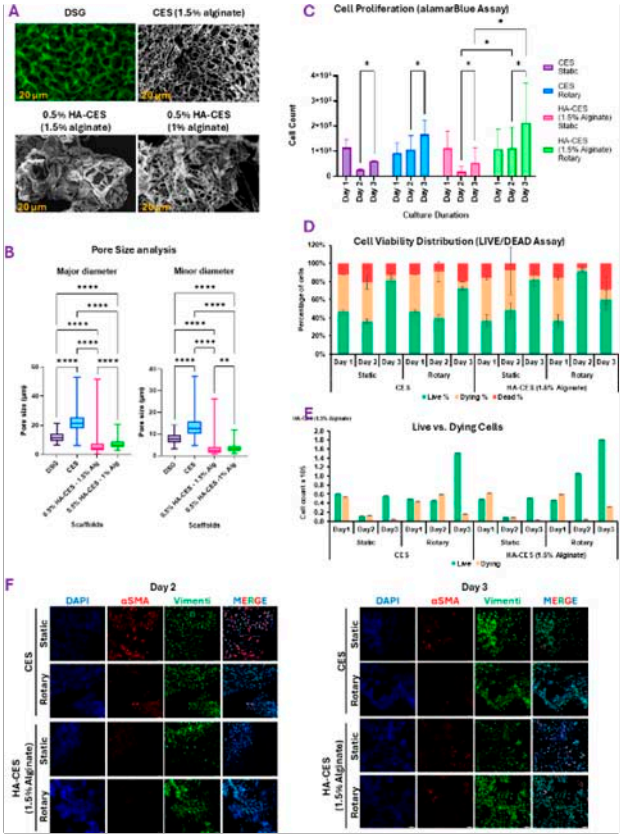
[1]*University at Albany, State University of New York (SUNY), Nanoscale Science And Engineering, Albany, United States of America*
[2]*University at Albany, State University of New York (SUNY), Nanoscale Science And Engineering And The Rna Institute, Albany, United States of America*

Purpose/Objectives: Salivary gland fibrosis is characterized by excessive extracellular matrix (ECM) deposition that leads to gland hypofunction and hyposalivation. Mesenchymal stem cells (MSCs) have demonstrated therapeutic potential through antifibrotic and regenerative effects; however, poor cell retention and survival in vivo, limit their efficacy following transplantation. We previously developed cryoelectrospun scaffolds (CES) that support MSC-like cell stromal phenotype with high cell viability; however, they showed limited antifibrotic effects in vivo. This study examined whether biochemical modification of CES with hyaluronic acid (HA) enhances stromal cell survival and improves their antifibrotic potential for future MSC-based salivary gland regeneration.

Methodology: Scaffold morphology and porous architecture were characterized using scanning electron microscopy (SEM) and ImageJ-based pore size analysis. NIH 3T3 fibroblasts or MSCs were cultured in CES and HA-CES under static and/or rotary culture conditions. Cell proliferation and viability were assessed using alamarBlue and LIVE/DEAD assays, respectively. Mesenchymal- and fibrosis-associated markers, such as vimentin and smooth muscle alpha actin (α-SMA) were evaluated using immunocytochemistry.

Results: SEM of CES and HA-CES showed that scaffolds exhibited honeycomb-like architecture resembling the ECM topography of decellularized salivary gland (Fig. 1A). HA incorporation significantly reduced pore size compared to unmodified CES ($p < 0.01$) (Fig. 1B). Rotary culture over 3 days boosted mesenchymal cell proliferation (Fig. 1C) and viability (Fig. 1D), compared to static culture (Fig. 1E) for both CES and HA-CES. Notably, sustained expression of the mesenchymal marker vimentin was observed in all conditions and reduced expression of the myofibroblast marker α-SMA was observed in rotary cultures compared to static cultures (Fig. 1F).

Figure 1: Cryoelectrospun scaffolds (CES) and HA-CES mimic: (A) ECM topography and (B) pore size of decellularized adult salivary glands (DSG), and (C-E) support viable mesenchymal cell growth, and (F) reduced myofibroblast marker αSMA expression under 3-day static and rotary culture. Scale bar = 40 μm.



Conclusion/Significance: HA incorporation and rotary culture improved mesenchymal cell survival and proliferation, along with reduced myofibroblast-associated marker expression, suggesting that HA inclusion may support a less fibrotic stromal phenotype. This work lays the foundation for future MSC delivery and salivary gland tissue regeneration in vivo.

Session 47
Biofabrication (General Session)

11-17-2026 @ 1:30 PM - 3:00 PM

OP-172 - Microfluidic High-Throughput Fabrication of Synthetic Red Blood Cells

Ashley Onumonu, Sanika Panditrao, Mykel Green

Tulane University, Biomedical Engineering, New Orleans, United States of America

Purpose/Objectives: Global blood shortages disproportionately affect low-income communities, creating an urgent need for scalable blood substitute technologies. Synthetic red blood cells offer a promising solution, but their development is limited by fabrication methods that cannot reliably produce particles with the size and biconcave shape of natural red blood cells at high throughput. Fabrication approaches such as emulsions and electrospinning suffer from low throughput, poor size uniformity, and inconsistent mechanical properties, hindering scalability and clinical translation. To address

this barrier, **we aim to develop a microfluidic platform that fabricates red blood cell-mimicking particles with the shape, size, and function of natural red blood cells.**

Methodology: A photolithography-based microfluidic device will integrate droplet generation, incubation, reagent exchange, and collection (Figure 1). Poly (lactic-co-glycolic acid) (PLGA) in ethyl acetate will be flow-focused with an aqueous phase to generate uniform templates. Templates will be coated by layer-by-layer polyelectrolyte deposition, cross-linked with glutaraldehyde, and exposed to a 2-propanol: Tetrahydrofuran (THF) solution to partially dissolve the PLGA core and induce biconcave collapse.

Results: Ongoing COMSOL simulations will guide channel geometry, flow rate, shear, and residence time. Performance will be defined by continuous production of uniform PLGA templates, stable shell formation, efficient reagent exchange, and reproducible generation of biconcave particles. Particle size, shape, elasticity, deformability, and passage through 3 to 6 μm constrictions will be compared with native red blood cells using SEM, AFM, osmotic ektacytometry, and microfluidic constriction assays.

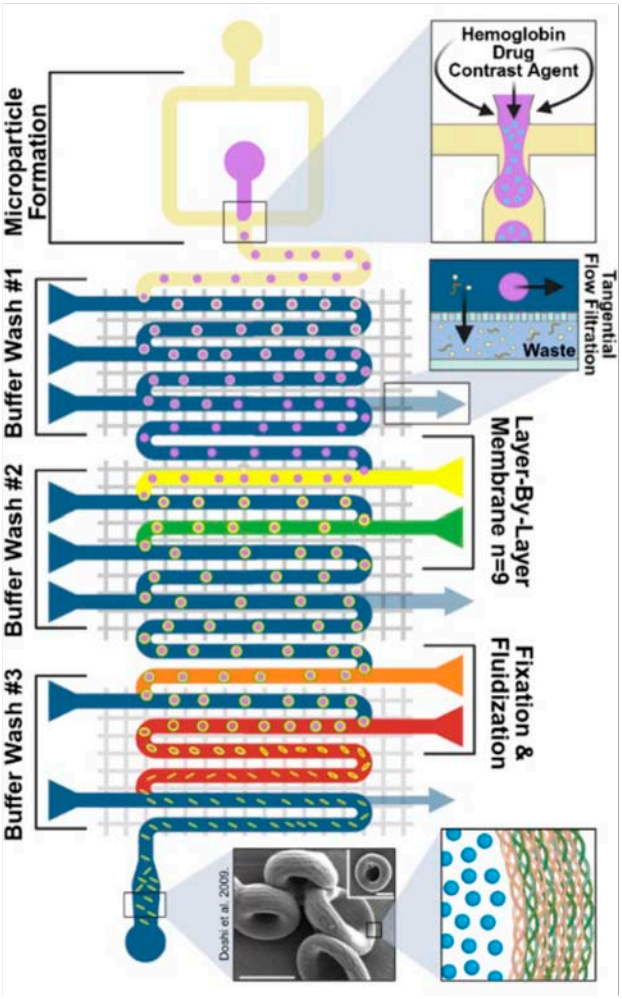


Figure 1. Integrated microfluidic device for high-throughput fabrication of synthetic red blood cells using sequential serpentine channels and on-chip filtration for membrane assembly and shaping.

Conclusion/Significance: This microfluidic platform integrates droplet generation, layer-by-layer shell formation, filtration, and solvent-induced collapse to continuously fabricate red blood cell-mimicking particles with controlled size and biconcave shape. Future work will address PDMS hydrophobicity through surface modification and flow optimization to improve emulsion stability, reproducibility, and throughput.

Session 48
Musculoskeletal (General Session) 2

11-17-2026 @ 1:30 PM - 3:00 PM

OP-175 - Electrically Stimulated Eccentric Contraction Promotes Muscle but not Bone Healing in Composite Musculoskeletal Trauma

Rebecca Sheetz[1], Preston Shake[1], Amelia Ridolfo[1], Avantika Jain[1], Riki Koshimizu[2], Seoyeon Kim[1], Sara Mcbride-Gagyi[3], Koyal Garg[1]

[1]*St Louis University, Biomedical Engineering, St. Louis, United States of America*
[2]*St Louis University, Biology, St. Louis, United States of America*
[3]*Ohio State University, Columbus, United States of America*

Purpose/Objectives: Volumetric muscle loss (VML) injuries rarely occur in isolation, frequently appearing alongside critically sized bone fractures as components of composite injury. Clinicians tend to focus on fracture healing, with many FDA-approved treatments available, while treatments for VML are lacking. The current standard of care for VML injuries lacks standardized rehabilitation protocols. Furthermore, composite trauma presents additional challenges, such as heightened inflammation, and remains particularly understudied in the context of rehabilitation. Therefore, new rehabilitation strategies need to be developed to address these compounding issues.

Methodology: A clinically relevant composite trauma injury involving a critical-sized ($\sim$3.5 mm) segmental bone defect (SBD) in the tibia and a concomitant $\sim$20% VML injury to the adjacent tibialis anterior (TA) muscle was inflicted unilaterally in male Lewis rats ($\sim$3 months old). After three weeks of recovery, animals were subjected to an electrical stimulation-based eccentric contraction training (ECT) protocol previously optimized to improve muscle function, mass, and fiber size following VML injuries. This work aims to investigate whether the optimized ECT protocol could improve recovery from VML and accelerate osteogenesis by providing both mechanical and biochemical cues to healing tissues.

Results: At seven weeks post-injury, composite injured animals that underwent the ECT protocol demonstrated a $\sim$23% improvement in peak isometric torque compared to their untreated counterparts (ANOVA, $p < 0.0001$). Histological analysis revealed that ECT-treated animals had a $\sim$23% increase in type 2B fibers and a simultaneous $\sim$12% decrease in type 2A fibers compared to untreated animals (Interaction, p=0.0004). While untreated muscles showed elevated fibrosis, ECT-treated animals were comparable to uninjured controls (p=0.0195). Fractured tibias were analyzed through microCT and showed no appreciable bone growth at seven weeks within the defect region.

Conclusion/Significance: VML-injured muscle remains responsive to mechanical loading even in the presence of a critical-sized defect in the adjacent tibia, adapting to ECT through neuromuscular remodeling and fiber type transitions. Future studies will examine extended ECT durations and its synergy with biomaterials to influence bone healing outcomes. Developing rehabilitation programs that incorporate ECT may improve long-term functional and quality-of-life outcomes in composite trauma patients.

OP-176 - Apolipoprotein E3 Modulates Motor Endplate Formation and Muscle Force

Daniel Delgado, D. Joshua Cohen, Zvi Schwartz, Michael Mcclure

Virginia Commonwealth University, College of Engineering, Richmond, United States of America

Purpose/Objectives: Each year, approximately 250,000 cases of volumetric muscle loss (VML) occur in the U.S. due to trauma such as gunshot wounds and lacerations. These injuries frequently result in incomplete functional recovery due to denervation and motor endplate fragmentation. Motor endplate regeneration is an important step in restoring functional muscle and begins with the formation of

densely packed acetylcholine receptor (AChR) clusters. In prior VML studies, our lab observed a link between neural connectivity and apolipoprotein E (ApoE), suggesting a potential role in muscle injury response and neuromuscular repair. This study tested the hypothesis that ApoE isoforms regulate motor endplate formation and muscle function.

Methodology: C2C12 myoblasts were seeded on 24-well plates at 10,000 cells/cm^2 in α-MEM supplemented with 10% FBS and 1% P/S. At 100% confluence, cells were treated with recombinant ApoE3 or ApoE4 at 10^{-7}, 10^{-8}, or 10^{-9} M. mRNA was isolated for gene expression analysis via RT-qPCR, targeting myogenic markers (Myod, Myog, Myh1) and synaptic markers (Chrng, Chrne, Musk). The role of Lrp4 on the effect of ApoE3 was examined. AChR cluster morphology was assessed using fluorescent α-bungarotoxin staining in ApoE3 treated myotubes. Male ApoE3 knock-in (KI) and ApoE knockout (KO) mice were compared to male C57BL/6 wild-type controls to investigate differences in muscle force and motor endplate morphology.

Results: In vitro, ApoE3 and ApoE4 treatment did not alter myogenic gene expression but ApoE3 increased Chrng expression and AChR cluster formation in a dose-dependent manner. ApoE3-mediated clustering was partially dependent on Lrp4 signaling, where inhibition of Lrp4 reduced cluster number. In vivo, ApoE3 KI and ApoE KO mice generated the greatest maximal twitch and tetanic muscle force compared to WT controls. ApoE3 KI animals showed increased Chrng expression and enlarged motor endplates, while ApoE KO animals exhibited significantly fewer motor endplates, suggesting a protective role for endogenous ApoE at the neuromuscular junction.

Conclusion/Significance: ApoE3, but not ApoE4, enhanced AChR expression and clustering through a mechanism partially dependent on Lrp4. In vivo, ApoE3 influenced both motor endplate morphology and baseline muscle force. These findings highlight ApoE3 as a potential isoform-specific therapeutic factor for promoting neuromuscular repair in VML and other neurodegenerative disorders.

OP-178 - Energy metabolism differences may drive regenerative versus fibrotic tendon healing responses

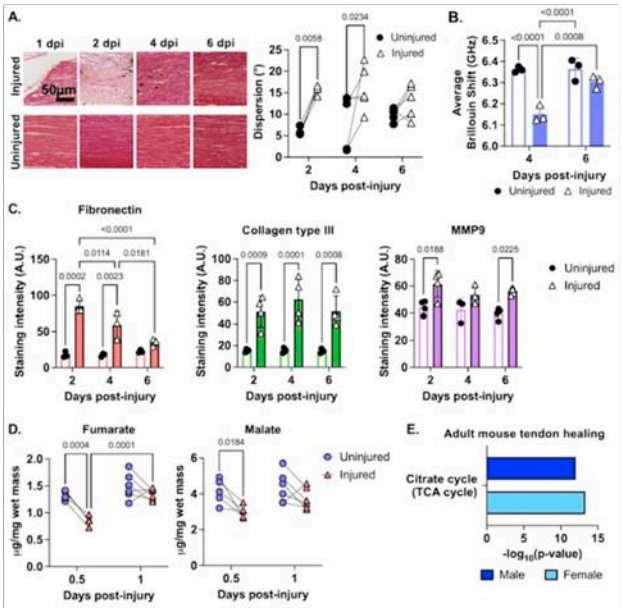
Divya Sivalingam[1], Christoph Hart[1], Nishanth Sunny[2], Giuliano Scarcelli[1], Motomi Enomoto-Iwamoto[3], Catherine Kuo[1,3]

[1]*University of Maryland, Fischell Department of Bioengineering, College Park, United States of America*
[2]*University of Maryland, Department of Animal And Avian Sciences, College Park, United States of America*
[3]*University of Maryland, Department of Orthopaedics, Baltimore, United States of America*

Purpose/Objectives: Adult tendons heal with scar formation and inferior material properties, whereas a prior study showed sheep fetal tendons heal scarlessly. Abnormal metabolism is implicated in adult tendon healing, but mechanisms underlying regenerative fetal tendon healing are unknown. Here, we demonstrate restoration of material properties during fetal healing and examine extracellular matrix (ECM)-associated proteins and metabolism during regeneration versus fibrotic healing. Identification of mechanisms underlying fetal tendon regeneration could inspire therapies that promote adult tendon regeneration.

Methodology: Chick embryo Achilles tendons (AT) were injured *in ovo* at embryo day 14 (contralateral tendons uninjured). Tendons were harvested for metabolomics (biological replicates (N)=6), histology (picrosirius red) and immunohistochemistry (N>=3), and Brillouin microscopy (N=3) at 0.5 to 6 days post-injury (dpi). Histomorphometry was performed using FIJI. Two-way ANOVA with multiple comparisons compared uninjured and injured between healing timepoints. 3-month-old C57BL/6J mice AT were fully transected (contralateral tendons uninjured) and harvested at 4 weeks post-injury for proteomics. KEGG pathway analysis was performed with DAVID.

Results: Collagen alignment and Brillouin shifts (longitudinal elastic moduli) of injured embryo AT matched uninjured AT by 6dpi, consistent with regenerative healing (**Fig. 1A-B**). Fibronectin, collagen type III, and MMP9 levels in injured AT increased, but fibronectin was similar to uninjured by 6dpi (**Fig. 1C**), possibly indicating that ECM remodeling is ongoing at 6dpi. Fumarate and malate were downregulated at 0.5dpi (**Fig. 1D**), but other TCA metabolites were not dysregulated, suggesting embryo tendons do not dysregulate TCA cycle during early phases of healing. In contrast, TCA cycle was upregulated during ECM remodeling of adult mice AT healing (**Fig. 1E**). **Figure: A)** Collagen alignment and **B)** Brillouin shifts of injured chick embryo tendon were similar to uninjured controls by 6dpi. **C)** Fibronectin, collagen type III, and MMP9 were upregulated during embryo healing. **D)** Fumarate and malate levels were lower in injured embryo tendon compared to uninjured. **E)** TCA cycle was upregulated during adult mouse tendon healing.



Conclusion/Significance: Our exciting findings suggest that regenerative and fibrotic tendon healing are metabolically dissimilar. Ongoing studies are investigating these metabolic differences and their role in driving differences in ECM deposition/remodeling in regenerative versus fibrotic healing.

OP-179 - Macrophage-Driven Modulation of Substance P Secretion in Tendon-Derived Cells: A Neuroimmune Mechanism Underlying Tendinopathic Pain

Mariah Turner, Folly Patterson, Blanka Sharma, Brittany Taylor

University of Florida, J. Clayton Pruitt Family Department of Biomedical Engineering, Gainesville, United States of America

Purpose/Objectives: Tendon pain is a hallmark feature of tendinopathy, yet the mechanisms driving pain remain poorly defined. Pain persists despite resolution of inflammation or structural restoration, suggesting that non-steroidal anti-inflammatory drugs and surgical repair may not address the etiology of pain. Substance P (SP) and neurokinin-1 receptor (NK1R) signaling contribute to inflammation and remodeling in multiple tissues. In tendon-derived cells (TDCs), exogenous SP alters proliferation and promotes matrix-degrading remodeling. However, regulation of endogenous SP signaling in pathological conditions and contributions to nociceptive pain remain unclear. This study assessed SP/NK1R expression in TDCs in normal and inflammatory conditions, thereby identifying a potential neuroimmune mechanism contributing to tendon pain.

Methodology: Primary bone marrow- derived macrophages cells and Achilles tendon-derived cells (TDCs) were isolated from female Wistar rats (n = 3, 8-weeks). Macrophages were maintained as unpolarized controls (M0) or polarized to M1 using lipopolysaccharide (5000ng/mL) and interferon gamma (100ng/mL). Conditioned media (CM) was collected from M1 (M1-CM) and M0 (M0-CM). Achilles TDCs were treated with M1-CM, M0-CM, or normal cell

culture media (controls) for up to 72 hours. Metabolic activity was assessed by MTS assay and secreted SP and tumor necrosis factor alpha (TNF-α), were quantified by enzyme-linked immunosorbent assay (ELISA) kits. SP and NK1R expression were evaluated by immunofluorescence. Statistical significance was assessed using two-way ANOVA ($p < 0.05$).

Results: Metabolic activity peaked at 48 hours in control TDCs and declined by 72 hours, while M1-CM-treated TDCs showed a sustained increase over time (Fig 1A). M1-CM significantly increased TNF-α secretion compared to control and M0-CM TDCs (Fig 1B). SP secretion was significantly elevated in M1-CM-treated TDCs at 12, 48, and 72 hours, peaking at 72 hours (Fig 1C). Immunofluorescence confirmed baseline SP/NK1R expression in non-treated TDCs, with SP localized to the cytoplasm and NK1R at the plasma membrane (Fig 1D).

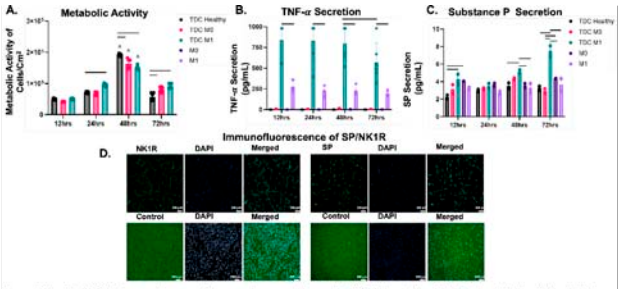


Figure 1. Healthy TDCs that were not exposed to macrophage-condition media (MCM) showed the **(A)** highest metabolic activity at 48 hours, while TDCs exposed to media from naïve macrophages (TDC M0) and M1-polarized macrophages (TDC M1) were higher at 72 hours. TDC M1 had the greatest **(B)** TNF-alpha and **(C)** Substance P protein secretion. **(D)** Expression of the Neurokin-1 Receptor (NR1R) and substance P (SP) on healthy TDCs was also demonstrated with immunofluorescence. Horizontal bars indicate significant differences ($p < 0.05$), and ^ indicates significant differences across time points within a group. Data are mean ± standard deviation. Scale bar = 50 μm.

Conclusion/Significance: These findings demonstrate that TDCs respond to inflammatory macrophage signaling by increasing TNF-α and the pain-related neuropeptide substance P. Sustained substance P production under inflammatory conditions, along with baseline NK1R expression, supports a role for SP/NK1R signaling in tendon neuroimmune crosstalk and suggest a potential mechanism contributing to tendon pain and maladaptive remodeling.

Session 49
Ophthalmologic (General Session)

11-17-2026 @ 1:30 PM - 3:00 PM

OP-182 - Development of an in vitro microphysiological model of the human optic nerve

Narendra Pandala, Zhuo Zhen, Bergen Nordness, Budd Tucker

University of Iowa, Iowa City, United States of America

Purpose/Objectives: The optic nerve is a crucial component of the visual system, transmitting various visual signals from the retina to the brain. The optic nerve is composed of several retinal ganglion cell (RGC) nerve fibers myelinated by oligodendrocytes. This study presents the development of a microfluidic chip to coculture human induced pluripotent stem cell (iPSC) derived RGCs and Oligodendrocyte progenitor cells (OPC) to model the optic nerve in vitro.

Methodology: RGCs are isolated from human retinal organoids (day-40) using CD90 (Thy-1) magnetic beads. OPCs are differentiated from human iPSCs starting with neural induction, followed by oligodendrocyte differentiation. Day 40 OPCs and RGCs are cultured together in a two chambered PDMS based microfluidic device. Immune fluorescence staining was used to characterize different RGC and OPC markers.

Results: Day 40 RGCs were characterized by the expression of BRN3, HuC/D and MAP2. Day 40 OPCs were characterized by expression of O4, Claudin-11, PDGFRA, NG2 and A2B5. The microfluidic device not only facilitates the coculture of RGCs and the maturation of oligodendrocytes but also facilitates the axonal isolation of the RGCs with the potential of myelination from the OPCs.

Conclusion/Significance: We successfully fabricated a PDMS-based microfluidic device capable supporting the coculture of retinal ganglion cells and oligodendrocytes. This serves as a valuable model of the human optic nerve in vitro with the potential to study optic nerve gliomas and also to test different drugs and therapies.

OP-183 - Engineering an Isogenic Inner Blood-Retina Barrier for Disease Modeling and Therapeutic Discovery

Parker Esswein, Ying-Yu Lin, Emily Warren, Sharon Gerecht

Duke University, Biomedical Engineering, Durham, United States of America

Purpose/Objectives: Globally, 1.1 billion people suffer from vision impairment, with 43 million of those afflicted experiencing complete blindness. Retinal vascular diseases (RVDs), the primary contributor to vision reduction and loss, are characterized by compromised inner blood-retina barrier (iBRB) functionality and subsequent vascular leakage. The iBRB is a vascular network containing retinal endothelial cells and pericytes that are tightly associated and regulated via cell-cell surface proteins, maintaining ocular homeostasis. Despite this central role, iBRB dysfunction remains poorly understood. This is due to challenges in accurately modeling the iBRB's biological and functional complexity, including the need for iBRB-specific cells, limiting phenotypic and mechanistic studies. There is thus a critical demand for human-based models that faithfully recapitulate the iBRB to improve cerebrovascular understanding, accelerate countermeasure development, and advance precision health.

Methodology: We developed the first human induced pluripotent stem cell-derived retinal endothelial cells (iRECs) and pericytes (iRPCs) using novel and robust differentiation protocols. Harnessing these cells, soft lithography, and self-assembly, we engineered 3D, multicellular iBRB microphysiological systems (MPS). To model diabetic retinopathy (DR), the leading cause of blindness, we exposed iRECs to hyperglycemia and hypoxia. Genomic, proteomic, and functional assays validated the biological fidelity of the cells and MPS.

Results: The iRECs possessed endothelial, junctional, and retinal markers and physiological barrier properties, while the iRPCs expressed pericyte and retinal markers and functionality, validating their biological accuracy. Using iRECs, we engineered high fidelity iBRB MPS. The iRECs self-assembled into morphologically and phenotypically accurate networks with perfusable lumina that are tightly associated via membrane-bound tight and adherens junction proteins. Exposing iRECs to DR conditions, we demonstrated their sensitivity to disease triggers and recapitulation of clinical presentations, supporting future iBRB dysfunction studies. Integrating iRPCs into the healthy MPS, we observed the formation of luminal iREC networks supported and encapsulated by iRPCs, mimicking iBRB network organization, morphology, and barrier properties.

Conclusion/Significance: We conclude that the iBRB MPS faithfully recapitulate the healthy and diseased iBRB and physiological endothelial-pericyte interactions and permeability, demonstrating their biological fidelity. Our functional, isogenic iBRB MPS can be harnessed as decision-grade tools to investigate iBRB development, elucidate mechanisms underlying RVDs, advance precision medicine, and accelerate therapeutic discovery.

OP-184 - Nano-Ice–Enabled Decellularization and Cryopreservation Preserves Corneal Tissue Ultrastructure and Mechanical Integrity for Lamellar Transplantation and Regenerative Applications

Amy Han[1], Katie Kauffman[2], Ying-Bo Shui[3], Ying Liu[3], Arina Korneva[2], Andrew Huang[3], Xu Han[4]

[1]*CryoCrate LLC, WINSTON SALEM, United States of America*
[2]*Virginia Polytechnic Institute and State University, Biomedical Engineering, Blacksburg, United States of America*
[3]*Washington University, Ophthalmology & Visual Sciences, St. Louis, United States of America*
[4]*Wake Forest Univeristy, Wake Forest Institute of Regenerative Medicine, WINSTON SALEM, United States of America*

Purpose/Objectives: Keratoconus and related corneal ectatic disorders are major causes of visual impairment worldwide and frequently require anterior lamellar transplantation to restore corneal integrity and vision. However, current approaches for stromal decellularization and preservation, including glycerolization and irradiation, often disrupt collagen organization and alter corneal biomechanics, thereby limiting surgical performance and long-term tissue quality. We previously developed DionySol®, a nano-ice–enabled polymer-based preservation platform capable of maintaining stromal transparency and ultrastructure during cryopreservation. In this study, we investigated whether DionySol also preserves biomechanical properties of corneal stroma and supports successful deep anterior lamellar keratoplasty (DALK).

Methodology: Research-exempt human donor corneas obtained from Mid-America Transplant were assigned to three groups: fresh controls, cryopreservation in DionySol for 2 months at –80°C, or cryopreservation in 10% DMSO (n=4/group). Whole corneal buttons underwent inflation testing between 0–50 mmHg using a custom anterior chamber system combined with three-dimensional Digital Image Correlation analysis. Following inflation testing, tissues were sectioned into approximately 2 mm strips and subjected to uniaxial tensile testing until failure. Biomechanical effects associated with tissue swelling were additionally evaluated. For translational validation, GGTA1-knockout pig corneas preserved in DionySol for 2 months were thawed and transplanted into wild-type pigs using a big-bubble/DALK.

Results: Corneas preserved in DionySol demonstrated nonlinear mechanical responses comparable to fresh tissues during inflation testing. Strain distribution remained homogeneous in DionySol-treated corneas, similar to fresh controls, with coefficient of variance values below 1, whereas DMSO-preserved tissues exhibited marked regional variability (COV=4.3), indicating structural discontinuity. Tensile strip testing showed preservation of stromal stiffness in DionySol-treated tissues (5.98 MPa), while DMSO-preserved corneas displayed increased stiffness (17.40 MPa) at 5% extension. In vivo transplantation studies further demonstrated excellent optical clarity and surgical handling of DionySol-preserved grafts, enabling clear visualization of the anterior chamber and precise suture placement without distortion of donor tissue.

Conclusion/Significance: DionySol preserves both stromal ultrastructure and biomechanical integrity while enabling reproducible anterior lamellar transplantation in a preclinical swine model. The biocompatible technology is pracitcally compatible with scalable eye-banking workflows and standard –80°C storage systems, supporting its translational potential as a next-generation platform for long-term preservation of donor stromal tissues for corneal transplantation and regenerative medicine applications.

Session 50
Bioreactors & Organs-On-Chips (General Session)

11-17-2026 @ 1:30 PM - 3:00 PM

OP-187 - Leveraging Computational Fluid Dynamics Simulations for Bioreactor Design to Improve Engineering Cartilage

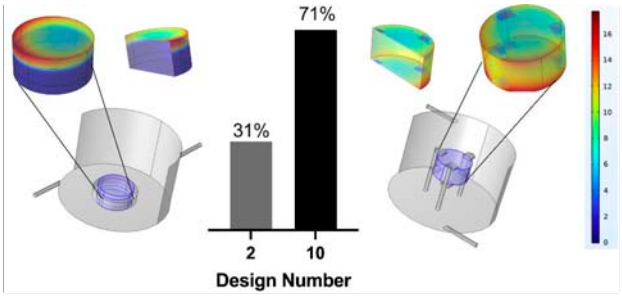
Nima Firouzi[1], Kamal Gautam[1], Bo An Chen[1], Ozan Akkus[1], Jean Welter[1], Harihara Baskaran[2]

[1]*Case Western Reserve University, Cleveland, United States of America*
[2]*Case Western Reserve University, Chemical And Biomolecular Engineering, Clevleland, United States of America*

Purpose/Objectives: Engineering clinically relevant cartilage constructs remains limited by inadequate nutrient transport, particularly in avascular tissues where diffusion dominates. While prior strategies have focused on scaffold design and culture conditions, the role of bioreactor geometry in regulating external nutrient delivery remains underexplored. This study tested the hypothesis that rational optimization of perfusion bioreactor geometry can enhance nutrient transport, cellular metabolism, and extracellular matrix (ECM) formation in engineered cartilage.

Methodology: A computational–experimental framework was developed to optimize perfusion bioreactor design. Ten three-dimensional bioreactor geometries were evaluated in COMSOL using coupled convection–diffusion modeling with Michaelis–Menten glucose consumption kinetics to simulate glucose transport and uptake by human mesenchymal stem cell (hMSC)-seeded cartilage constructs. Glucose uptake efficiency and spatial concentration uniformity were used as design metrics. The highest-performing and lowest-performing designs were fabricated by stereolithographic 3D printing and experimentally validated using hMSC-seeded collagen–glycosaminoglycan scaffolds cultured under perfusion for 25 days in chondrogenic medium. Biochemical, metabolic, histological, and mechanical analyses were performed.

Results: Computational optimization increased predicted glucose uptake efficiency from ~30% in the control design to ~70% in the optimized configuration, with improved glucose uniformity across the construct. Experimentally, the optimized bioreactor demonstrated ~40% higher cumulative glucose uptake and ~20% higher lactate production, indicating enhanced metabolic activity. ECM synthesis was significantly improved, with 165% higher GAG/DNA and ~40% higher hydroxyproline/DNA compared with controls. Histology confirmed substantially greater sulfated glycosaminoglycan deposition, with GAG-positive regions increasing from ~15% in controls to ~35–55% in optimized constructs. Mechanical performance improved markedly, with Young's modulus increasing from ~18 kPa (control) to ~50 kPa (optimized), reflecting superior ECM maturation.



Conclusion/Significance: Bioreactor geometry is a critical determinant of nutrient transport and engineered cartilage quality. Computationally guided reactor optimization led to tissues with substantially enhanced glucose utilization, ECM deposition, and mechanical properties. These findings suggest that bioreactor geometry optimization is underutilized in cartilage tissue engineering and provides a rational framework for improving the manufacture of larger, clinically relevant engineered tissues.

Session 51
Cardiovascular, Angiogenesis, Blood (General Session) 2

11-17-2026 @ 1:30 PM - 3:00 PM

OP-190 - Matrix Stress Relaxation Rewires Endothelial Identity During Atherosclerosis

Shivesh Anand[1,2], Ishita Jain[1,2], Michelle Huang[2,3], Fotis Christakopoulos[2,3], Dipti Tripathi[2,4], Nazish Sayed[2,4], Sarah Heilshorn[2,3], Ngan Huang[1,2]

[1]*Stanford University, Department of Cardiothoracic Surgery, Stanford, United States of America*
[2]*Stanford Cardiovascular Institute, Stanford, United States of America*
[3]*Stanford University, Department of Materials Science And Engineering, Stanford, United States of America*
[4]*Stanford University, Department of Surgery, Stanford, United States of America*

Purpose/Objectives: Atherosclerosis, a chronic cardiovascular disease and the primary cause of coronary artery disease, accounts for nearly 27% of global deaths annually. It is characterized by progressive arterial stiffening and occlusive plaques. Endothelial-to-mesenchymal transition (EndoMT) critically drives this progression, yet the responsible biomechanical signals remain poorly understood.

Specifically, stress relaxation, a key viscoelastic tissue property, is largely understudied. Therefore, this study investigates how stress relaxation cues from the underlying extracellular matrix modulate EndoMT induction and progression.

Methodology: Nanoindentation of healthy and atherosclerotic human carotid artery tissues was performed to validate the physiological relevance of stress relaxation in disease progression. To dissect its role mechanistically, elastin-like protein (ELP) hydrogels crosslinked with aldehyde- (fast-relaxing) or benzaldehyde-modified (slow-relaxing) polyethylene glycol (PEG) were synthesized at two stiffness levels (high and low), yielding four distinct matrix formulations. Primary human coronary artery endothelial cells (HCAECs) were cultured on these ELP–PEG hydrogels to assess dedifferentiation toward mesenchymal phenotypes via immunostaining and qPCR of established EndoMT markers. Single-cell RNA sequencing (scRNA-seq) and time-lapse live-cell imaging have been performed to capture the transcriptomic and morphodynamic changes during this process.

Results: Histological and nanoindentation analyses of atherosclerotic tissue revealed heterogeneous collagen distribution and corresponding biomechanical variability in stiffness and stress relaxation (**Figure 1A-B**). *In vitro* EndoMT of HCAECs was qualitatively confirmed via Transgelin/SM22 protein expression **(Figure 1C)**. Gene expression analysis revealed greater upregulation of EndoMT markers on slow-relaxing hydrogels compared to fast-relaxing ones, whereas stiffness ranges (0.5 versus 3.5 kPa) yielded no significant effect (**Figure 1D**). Furthermore, scRNA-seq mapped a detailed cellular continuum from baseline endothelial through EndoMT states to stabilized mesenchymal populations (**Figure 1E**). Concurrently, time-lapse imaging revealed loss of cobblestone morphology accompanied by progressive cell elongation.

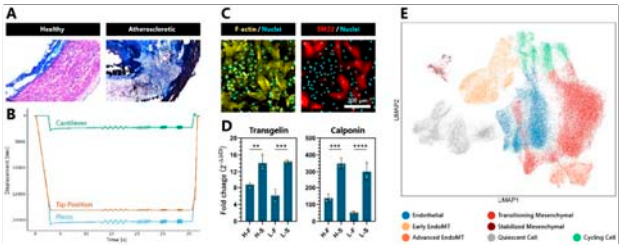


Figure 1. ***(A)*** *Masson's trichrome staining.****(B)*** *Nanoindentation-based stress relaxation quantification.****(C-D)*** *Immunostaining and gene expression of EndoMT markers (H/L: high/low, F/S: fast/slow).* ***(E)*** *scRNA-seq mapping of EndoMT progression.*

Conclusion/Significance: This study demonstrates that slow stress relaxation critically drives EndoMT during atherosclerosis. By investigating this viscoelastic transition at the single-cell level, the current work provides novel mechanobiological insights into stress relaxation as a key biophysical driver of EndoMT and a potential target for cardiovascular regenerative strategies.

OP-191 - OpenVive: a Pumpless Open-Chamber Microfluidic Platform for Perfused Microvascular Beds Supporting 3D Human Tissue Models

Xianyang Li, Ying Wang

Binghamton University, Biomedical Engineering, Binghamton, United States of America

Purpose/Objectives: Functional vascularization remains a major bottleneck in developing physiologically relevant in vitro human tissue models. Although recent advances in organ-on-a-chip and vascularized tissue systems have demonstrated perfused vascular networks and organoid integration in vitro, many platforms still rely on complex pump-and-tubing setups or closed-channel architectures that limit experimental accessibility, scalability, and straightforward tissue manipulation. This study aimed to develop OpenVive, an open-chamber, rocker-driven microfluidic platform capable of supporting perfused human microvascular beds and integrated engineered 3D tissues in vitro.

Methodology: OpenVive was designed as an open-access microfluidic platform incorporating a gravity-driven unidirectional recirculating perfusion system that operates without external pumps or tubing. Human endothelial cells and fibroblasts were co-cultured in fibrin within the tissue chamber to induce self-assembly of microvascular networks (MVNs) under gravity-driven perfusion. MVN perfusability, permeability, and structural maturation were evaluated over 14 days. To assess compatibility with engineered tissues, liver spheroids were incorporated directly onto the vascular bed and analyzed for liver-specific functional activity.

Results: Human endothelial cells and fibroblasts self-assembled into interconnected, perfusable MVNs within the OpenVive platform. The vascular networks remained perfusable for at least 14 days and exhibited progressive structural and barrier maturation, including reduced permeability at later culture stages. Liver spheroids integrated successfully with the vascular bed, and the vascularized microenvironment supported liver-specific functional activity. In addition, the open-access and pumpless design enabled scalable implementation in a multi-unit format compatible with standard well-plate workflows.

Conclusion/Significance: OpenVive establishes an experimentally accessible and scalable platform for coupling perfused human microvascular beds with engineered 3D tissues in vitro. By combining open-chamber accessibility with gravity-driven perfusion and vascularized tissue support, this platform provides a promising foundation for vascularized organoid culture, disease modeling, drug testing, and human-relevant microphysiological systems.

OP-193 - Affinity-controlled delivery systems for phased delivery of VEGF, FGF-2, and PDGF enhance angiogenesis

Justin Svendsen, Chandler Asnes, Samuel Nightheart, Armaan Hajarizadeh, Madeleine Ford, Johnathan O'Hara-Smith, Simon Oh, Robert Guldberg, Marian Hettiaratchi

University of Oregon, Knight Campus For Accelerating Scientific Impact, Eugene, United States of America

Purpose/Objectives: Angiogenesis, the regeneration of blood vessels from existing vascular networks, requires the coordinated secretion of vascular endothelial growth factor (VEGF), fibroblast growth factor-2 (FGF-2), and platelet derived growth factor (PDGF). However, dysregulations in protein secretion can result in poorly revascularized tissues. Our objective was to develop a tunable biomaterial capable of phased protein delivery for enhancing angiogenesis. To achieve this, we applied affibodies, α-helical proteins, as affinity-based epitopes to regulate the release profiles of VEGF, FGF-2, and PDGF from hydrogels.

Methodology: Affibodies were conjugated into 5% (w/v) polyethylene glycol maleimide hydrogels and crosslinked with dithiothreitol. Hydrogels were loaded with 500:1 molar ratios of affibody:protein. Released protein was quantified by enzyme linked immunosorbent assays over 7 days at 37 C. MVFs harvested from epididymal fat pads of 6-month old retired male lewis breeder rats were seeded in 0.3% (w/v) collagen hydrogels. MVFs received either 17.5 pmols of soluble VEGF, FGF-2, and PDGF at day 3 ("simultaneous"), 17.5 pmols VEGF, FGF-2 or PDGF at day 3, 4, and 5 ("sequential"), or 17.5 pmols of VEGF, FGF-2, and PDGF delivered from a transwell multi-affibody conjugated PEG-MAL hydrogel (Fig.1A). At day 7, MVFs were fixed, stained with lectin and anti α-smooth muscle actin, and imaged to quantify vascular network length, branching, and perivascular coverage (Fig.1B). Data normalized to MVFs without growth factors.

Results: Three VEGF-, four PDGF-, and three FGF-2-specific affibodies were identified with K_D's spanning four orders of magnitude (3.07nM-6470nM). Affibody-conjugated hydrogels displayed inverse relationship between protein release and affibody affinity strength. PEG-MAL Optimal treatments showed greater vascular network length and branching as compared to all treatment compositions (Fig.1C-D). MVFs from all treatment compositions showed similar degrees of perivascular coverage (Fig.1E).

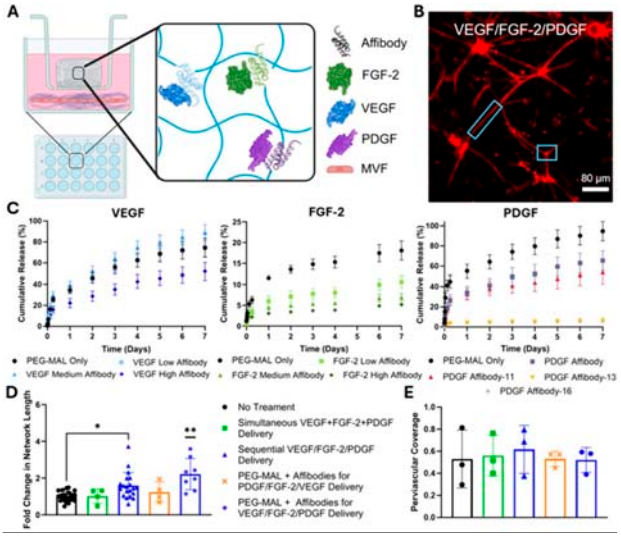


Figure 1. A) Transwell hydrogel schematic. B) Lectin-stained MVFs. C) Controlled Release Assays. MVF D) Network length and E) Perivascular coverage. **p<0.01, *p<0.05.

Conclusion/Significance: We have shown that affibody-conjugated hydrogels tune the presentation of target proteins in accordance to affibody affinity strength and demonstrated the impact of phased VEGF, FGF-2, and PDGF delivery in amplifying angiogenesis. Going forward, we will explore the application of affibodies in modulating the delivery of angiogenic proteins from biologically derived biopolymers.

OP-194 - Modeling Genetic Cardiomyopathies and Arrhythmias in Human 3D Engineered Heart Tissues Using Complementary Genetic and Transient Knockdown Strategies

Ayesha Arefin, Neda Kabi, Thomas Leahy, Ellie Sullivan, Shawn Luttrell, Christal Worthen, Greg Luerman, Nicholas Geisse

Curi Bio, Seattle, United States of America

Purpose/Objectives: Disease-modifying therapies for inherited cardiomyopathies and arrhythmias remain limited, due in part to a shortage of human-relevant models that recapitulate complex functional phenotypes. We established a flexible 3D engineered heart tissue (EHT) platform for modeling distinct cardiac pathologies through complementary approaches: (1) stable genetic mutation to model hypertrophic cardiomyopathy (HCM) via MYBPC3, and (2) rapid, transient siRNA-mediated knockdown to model desmosomal arrhythmia via PKP2.

Methodology: EHTs were fabricated from human iPSC-derived cardiomyocytes on a commercial contractility platform. For HCM modeling, tissues were generated from a commercially available MYBPC3 exon 6 mutant line (MYBPC3e6) and its isogenic corrected control. For arrhythmia modeling, mature wild-type EHTs were treated with PKP2-targeting siRNA, with vehicle-treated and non-targeting siRNA tissues as controls. Functional readouts included twitch force, calcium-dependent inotropy, pacing fidelity, beat-to-beat variability, and histological assessment of fibrotic remodeling.

Results: MYBPC3e6 EHTs exhibited hallmark HCM phenotypes: a 73% increase in twitch force ($p<0.001$), 85% greater inotropic response across 0.5 to 6 mM extracellular calcium ($p<0.01$), impaired pacing fidelity at elevated frequencies, and localized fibrotic lesions positive for α-smooth muscle actin and TGF-β1 in ~20% of tissues. The model also showed disease-appropriate pharmacology, including blunted response to EMD 57033 and normalized beating with mavacamten. PKP2 knockdown EHTs displayed arrhythmic contractile phenotypes, with significantly increased variability in twitch force and twitch period ($p<0.05$), irregular spontaneous beating, and loss of 1 Hz pacing fidelity relative to controls, consistent with impaired excitation-contraction coupling.

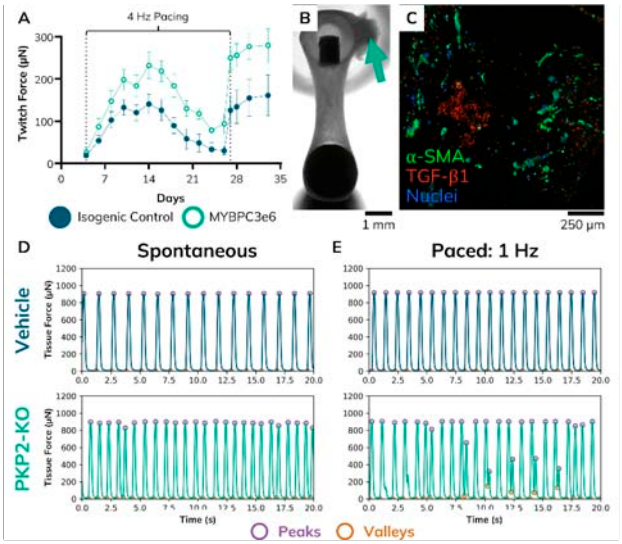


Figure 1. Functional and structural phenotypes in MYBPC3e6 and PKP2 knockdown EHTs. (A) Elevated twitch force in paced MYBPC3e6 EHTs (mean ± SD; n=11-12). (B) Representative fibrotic lesion (arrow) and (C) α-SMA and TGF-β1 staining in MYBPC3e6 tissues. Representative force-time traces show (D) irregular spontaneous beating and (E) loss of 1 Hz pacing fidelity in PKP2 knockdown EHTs.

Conclusion/Significance: Together, these studies demonstrate that 3D EHTs support robust functional modeling of inherited cardiomyopathies and arrhythmias through both stable genetic and rapid siRNA-based perturbation. This dual-modality flexibility, pairing isogenic mutant lines for mechanistic and pharmacological studies with scalable transient knockdown for target triage, establishes a versatile human in vitro platform for mechanistic investigation and preclinical drug discovery across cardiac disease.

Session 52
Imaging And Assessment (General Session)

11-17-2026 @ 1:30 PM - 3:00 PM

OP-195 - Multi-color 19F MRI of infiltrating immune cells and ECM hydrogel implanted into a stroke cavity

Alena Kisel[1], Nadine Didwischus[1], Keith Tang[2], George Hussey[1], Kevin Hitchens[1], Eric Ahrens[2], Mike Modo[1]

[1]*University of Pittsburgh, Pittsburgh, United States of America*
[2]*UC San Diego, San Diego, United States of America*

Purpose/Objectives: The infiltration of immune cells after implantation of an extracellular matrix (ECM) hydrogel in a stroke cavity is essential for its structural remodeling and eventual replacement by *de novo* tissue. To map this dynamic process, ideally both the immune cell infiltration and ECM scaffold are visualized non-invasively over time.

Methodology: Multi-color ^{19}F magnetic resonance imaging (MRI) permits the separate visualization of different perfluorocarbon (PFC) molecules, such as perfluoro-tert-butyl-cyclohexane (PFTBC) and perfluoro-15-crown-5-ether (PFCE). A systemic tail vein injection of PFCE nanoemulsions labelled macrophages during the implantation of PFTBC-labeled ECM hydrogel into the tissue cavities caused by a middle cerebral artery occlusion (MCAo) stroke. PFTBC nanoemulsion is associated within the ECM hydrogel and does not transfer to unlabeled ECM.

Results: The *in vivo* distribution of PFTBC-ECM hydrogel was visualized using ^{19}F MRI and demonstrate complete coverage of the tissue defect 1-day post-implantation, as well as a gradual degradation at days 2, 6, 7, and 14 post-implantation. ^{19}F MRI of PFCE-labeled immune cells displays infiltration into the peri-infarct tissue into the bioscaffold. At 7 days, labeled cells were distributed

throughout the remnants of the scaffold. Over the same time period, conventional ^{1}H T_2-weighted MRI revealed a transformation of the hyperintense tissue cavity into an isointense tissue, suggesting that immune cell-mediated remodeling of the ECM hydrogel implant produced a new tissue. Immunohistochemistry confirmed the degradation of ECM hydrogel at 14 days, as well as the formation of new tissue in the stroke cavity.

Conclusion/Significance: Overall, spatio-temporal mapping using multi-color ^{19}F MRI offers unique insights into the interaction between immune cells and bioscaffolds in tissue regeneration and improves our mechanistic understanding of these processes prior to clinical translation.

OP-196 - Open-source 3D Image Analysis in Python for Mitochondrial Network Analysis

Tarek Klaylat[1], Alain Zhang[2], Derek Rosenzweig[1], Rahul Gawri[1]

[1]*McGill University, Surgery, Montreal, Canada*
[2]*McGill University, Bioengineering, Montreal, Canada*

Purpose/Objectives: Mitochondria play a central regulatory role in connective tissue biology, including the metabolic and functional plasticity of mesenchymal stromal cells (*MSCs*), the progenitors of connective tissue lineages. Mitochondrial networks, through fission and fusion, orchestrate cellular metabolism by modulating energy production pathways to meet bioenergetic demands during differentiation. Furthermore, mitochondrial-derived ATP and reactive oxygen species regulate extracellular matrix (*ECM*) deposition by activating and modulating collagen synthesis pathways. Thus, mitochondrial dynamics integrate metabolic adaptation, lineage specification, and ECM remodeling, ensuring tissue homeostasis and repair in connective tissues. This is crucial for advancing understanding of connective tissue biology and pathophysiology and for developing efficient therapies and tissue engineering applications. In this study, we aim to develop a robust, open-source, automated 3D image analysis pipeline for subcellular organelle-level analysis of mitochondrial network organization.

Methodology: Mitochondria in bone marrow-derived MSCs were stained using MitoTracker™ Red dye following the manufacturer's protocol and imaged using a Zeiss LSM780 confocal microscope. 3D fluorescent confocal z-stack image analysis was performed in exclusively Python using the BioIO, scikit-image, Skan, and napari libraries. Gaussian filtering and Laplacian transform (LoG) were used for pre-processing, producing smooth and denoised images with enhanced features. Global Otsu thresholding was applied before thinning and analyzing with Skan to measure the lengths of skeletonized features.

Results: LoG processing appears to be highly effective at accentuating mitochondrial features from background signal and cellular autofluorescence while sufficiently isolating features such that global Otsu is indistinguishable from adaptive thresholding. Pixel length measurements are automatically converted into physical length scales using image metadata for straightforward data interpretation.

Conclusion/Significance: We have developed a simple workflow for 3D image analysis of mitochondrial networks in Python. Future work aims to refine the pipeline's performance and speed, especially for batch processing. A key feature of this workflow is its low computational cost, enabling CPU-based computation and eliminating hardware limits imposed by GPU acceleration. Future distribution will include a GUI and be delivered either locally or remotely, depending on hosting and data security protocols.

OP-197 - Soφ AI: An Integrated Artificial Intelligence Platform for Accelerating Tissue Engineering and Regenerative Medicine Research and Translation

Mojtaba Javid, Fahimeh Tabatabaei

CLYTE, Ithaca, United States of America

Purpose/Objectives: Tissue engineering and regenerative medicine (TERM) research is often slowed by fragmented workflows, protocol variability, inconsistent image analysis, statistical complexity, and regulatory uncertainty. These barriers reduce reproducibility, delay innovation, and hinder clinical translation. We developed Soφ AI, a specialized biomedical agentic AI platform designed to streamline experimental design, protocol generation, image analysis, statistical interpretation, and translational regulatory planning to accelerate TERM innovation.

Methodology: Soφ, is a multi-agent platform integrating multiple research functions into a unified system for biomedical investigators: (1) The Protocol Engine generates experiment-specific SOPs tailored to user-defined cell lines, biomaterials, and equipment. (2) The Scratch Analyzer applies computer vision to quantify wound closure for in vitro cell migration and wound healing models central to TERM. (3) The Integrated Analytics Engine can perform any statistical test with accuracy, replacing platforms like GraphPad Prism (4) paired with The integrated visualizer engine users are able to visualize any methodology or data. (5) The Regulatory Architect maps FDA pathways and submission guidance for regenerative medicine products. The platform is directly connected to FDA databases and was evaluated across TERM workflows including cell migration assays, biomaterial planning, and translational product development scenarios.

Results: Soφ AI significantly reduced time spent on protocol development, assay analysis, and data interpretation while improving workflow standardization. Custom SOP generation improved experimental adaptability for varying cell lines, reagents, and biomaterials. Automated scratch assay analysis processed up to 100 images per timepoint in seconds with reduced user bias compared to manual methods: ~50x faster and higher accuracy compared to imageJ. Integrated statistical and regulatory tools enhanced decision-making efficiency by reducing dependence on disconnected platforms. Independent study of the reasoning model for the regulatory engine against GPT 4.0, Gemini 3.1 pro, and Opus 4.7, showed only Soφ produces accurate results verified by actual FDA regulators. Collectively, Soφ transformed traditionally labor-intensive research processes into streamlined, reproducible, and translationally aligned workflows.

Conclusion/Significance: Soφ AI represents a novel Agentic research infrastructure for TERM, moving beyond isolated analytical tools toward a comprehensive scientific workflow ecosystem. By improving reproducibility, reducing technical bottlenecks, and integrating translational regulatory strategy, Soφ has the potential to accelerate discovery, and bridge the gap between bench research and clinical application.

OP-198 - A Nanoparticle Dimer-Based Resistive Pulse Sensor for Quantitative Biomolecule Assessment

Jacob Brown[1], Heyi Chen[2], Ge Zhang[1], Jiang Zhe[2]

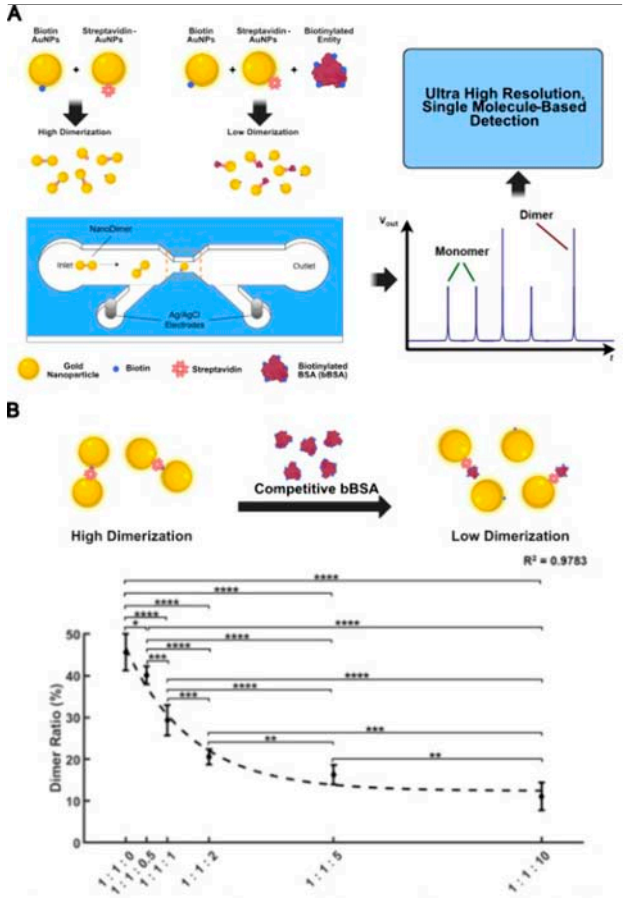
[1]*The University of Akron, Department of Biomedical Engineering, Akron, United States of America*
[2]*University of Akron, Department of Mechanical Engineering, Akron, United States of America*

Purpose/Objectives: Quantitative assessment of secreted biomolecules, including paracrine signaling factors, growth factors, and cytokines, is essential for evaluating the efficacy of cell-based therapies and engineered tissue constructs. Current assessment tools, such as enzyme-linked immunosorbent assay (ELISA), are limited by insufficient sensitivity at physiologically relevant concentrations and require extensive sample processing, constraining their utility for real-time or low-volume biological assessments. Here, we present a label-free microfluidic resistive pulse sensor (RPS) platform that leverages competitive gold nanoparticle (AuNP) dimerization to enable femtomolar-sensitivity quantification of biotinylated biomolecules with minimal sample preparation.

Methodology: Monofunctionalized biotin-AuNPs and streptavidin-AuNPs were engineered to form nano-dimers via the biotin–streptavidin interaction. In the presence of biotinylated target molecules, competitive binding inhibits dimer formation at a rate proportional to target molecule concentration. A microfluidic RPS device with a $2 \times 2 \times 10$ μm sensing channel and an integrated Wheatstone bridge circuit detects nano-monomers and nano-dimers under continuous flow as voltage pulses. The pulses' magnitude and width can then be used to determine the size of each passing particle and, thus, the sample's dimerization ratio (Figure 1A). The dimerization ratio

is then translated into target molecule concentration without fluorescent labels or optical instrumentation.

Results: The platform resolved individual nanoparticles across sizes of 150–400 nm and achieved a limit of detection (LOD) of 0.7606 pg/mL of bBSA (biotinylated bovine serum albumin), demonstrating femtomolar sensitivity across a broad dynamic range (Figure 1B). Quantification was reproducible and required no aptamer engineering or extensive calibration, reducing barriers to routine use in tissue engineering assessment workflows. **Figure 1.** (A) Schematic of RPS-based detection: biotinylated targets competitively inhibit AuNP dimer formation, quantified via voltage pulse analysis. (B) Dimer ratio decreases with increasing bBSA concentration (R^2= 0.9783). ****p<0.0001, ***p<0.001, **p<0.01.



Conclusion/Significance: This nanoparticle dimer-based RPS platform establishes a highly sensitive, label-free, and scalable assessment strategy directly applicable to tissue engineering and regenerative medicine research, including secretome profiling of therapeutic cells, monitoring therapeutic factor release from biomaterial scaffolds, and functional evaluation of engineered cardiac constructs. Future integration with biomaterial platforms will enable real-time, quantitative monitoring of regenerative signaling in vitro, supporting both mechanistic studies and translational assessments.

OP-199 - Decoding Electro-mechano-physiological Rules of Life

Xin Tang[1], Chenyu Liang[1], Yuning Feng[1], Erica Hengartner[2], Abygale Cochrane[1]

[1]*University of Florida, Gainesville, United States of America*
[2]*California Institute of Technology, Gainesville, United States of America*

Purpose/Objectives: Increasing evidence suggests that cells in many biological systems, including but not limited to brain, heart, muscle, and tumor, can modulate their electrical membrane potential (V_m) and apply mechanical forces (F) simultaneously to regulate their key functions and behaviors. Representative key functions and behaviors include proliferation, differentiation, communication, computation, and migration. However, due to the limitation of current technologies to elucidate the coupled biophysical characteristics in cells and tissues, the detailed 3D spatial-temporal dynamics of the electro-mechano-physiological signals in most multi-cellular biological systems remains unknown to date. We believe that this knowledge gap impedes the key physiological understanding of hierarchical multiscale signaling networks in living multicellular systems and the development of targeted bioengineering therapies for diseases such as cancer.

Methodology: To fill this knowledge gap and reveal the general rules of life, we created a wide-field-of-area (FOV) 2D/3D optical interrogation system (**Fig. 1**). Integrated with artificial intelligence (AI/ML) algorithms, our system can accurately visualize and control the electro-mechano-physiological signals in ~100s of cells simultaneously across conditions of in vitro (cultured cancer cells, neurons, stem cells, and cardiomyocytes), ex vivo (tissue slices), and in vivo (zebrafish and mouse).

Results: In this presentation, we will share a couple of examples including interrogation of membrane voltage dynamics and cellular forces of 150,000 neurons on soft-tissue-mimicking substrates *in vitro* or 75,000 neurons *ex vivo* per hour (**Fig. 1**). We apply this integrated experimental-computational framework to (1) identify distinct subtypes of somatosensory neurons, responsible for processing pain, touch, itching, temperature, and proprioception; and (2) accelerate the screening of neurological drug candidates.

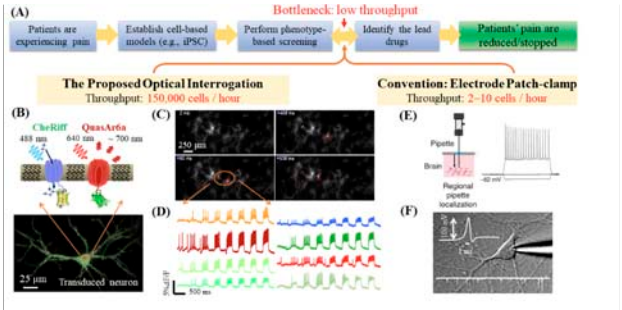


Fig. 1: The all-optical interrogation will advance our knowledge of electro-mechano-physiology of living systems and accelerate personalized drug discovery. (A) An example of application: The bottleneck in drug discovery pipeline is the low throughput. **(B-F)** Our wide-field-of-area (FOV) 2D/3D optical interrogation system accelerates personalized drug discovery by connecting patient-specific genetics/phenotypes to candidate drugs through high-throughput, high-precision, and quantitative optical interrogation. It achieves the measurement of 150,000 cells per hour, comparing to 2-10 cells per hour using conventional electrode-based measurements.

Conclusion/Significance: In summary, our new technologies enable mechanistic study of both electrical and mechanobiological nature of biological systems in a high-throughput, non-invasive, high-speed (> 1kHz), high signal-to-noise ratio, cell-type-specific, and long-term (from milli-seconds to months) manner. Our technologies open the door to decode the basic electro-mechano-physiological rules of life.

OP-200 - Implementation of a Non-Destructive Acoustic Microcarrier Occupancy Assessment in a Rotating Wheel Bioreactor

Jean Welter[1], Jonathan Kenyon[2], Joseph Mansour[3]

[1]*Case Western Reserve University, Center For Modular Manufacturing of Structural Tissues, Cleveland, United States of America*
[2]*Case Western Reserve University, Biology, Cleveland, United States of America*
[3]*Case Western Reserve University, Mechanical And Aerospace Engineering, Cleveland, United States of America*

Purpose/Objectives: Regenerative medicine applications require cell numbers that are impractical to grow in monolayer culture. Using microcarriers as supports in stirred bioreactors can reliably scale up cell expansion. Carrier occupancy is an important parameter

in bioreactor culture that informs decisions on agitation rate, medium exchange rate, or the need to add carriers. Investigators are blind to this parameter without invasive/destructive sampling of the culture. Cell-carrying microcarriers are slightly larger than empty carriers. We previously showed that the method of Hazony (DOI:0.1080/14786430600664130) can be used to compute the average pulse-dispersion length or "grain size" of the material and can quantify size-changes in microcarriers from the empty to the occupied state. We applied this method to an operating bioreactor.

Methodology: Human MSCs were seeded onto Corning Synthemax microcarriers and grown in mini-PBS biotech bioreactors. A 3-D printed holder was used to reproducibly couple an Olympus V205-RM 15 MHz delay-line transducer to the front face of the bioreactor. The holder was positioned so that the US beam cleared the reactor wheel. The rear wall of the chamber served as the reflector. Ultrasound traces were acquired with the reactor spinning at 20-30 RPM using a JSR DRP-500 pulser-receiver and a Keysight MSO-X3054T oscilloscope. Matlab programs were developed to extract the grain size. Samples of the microcarriers were also observed *via* fluorescence microscopy.

Results: We detected a shift in the pulse dispersion length between empty and occupied microcarriers dispersed in medium, in a running bioreactor (Fig.1) which correlated well with occupancy assessed by microscopy. Increases in grain size during growth over 48 hours, and decreasing occupancy under suboptimal culture conditions were detected. Note: "grain size" is an average property of whatever material is in a bioreactor, *i.e.*, culture medium with or without carriers or cells, but does not represent the actual size of individual microcarriers.

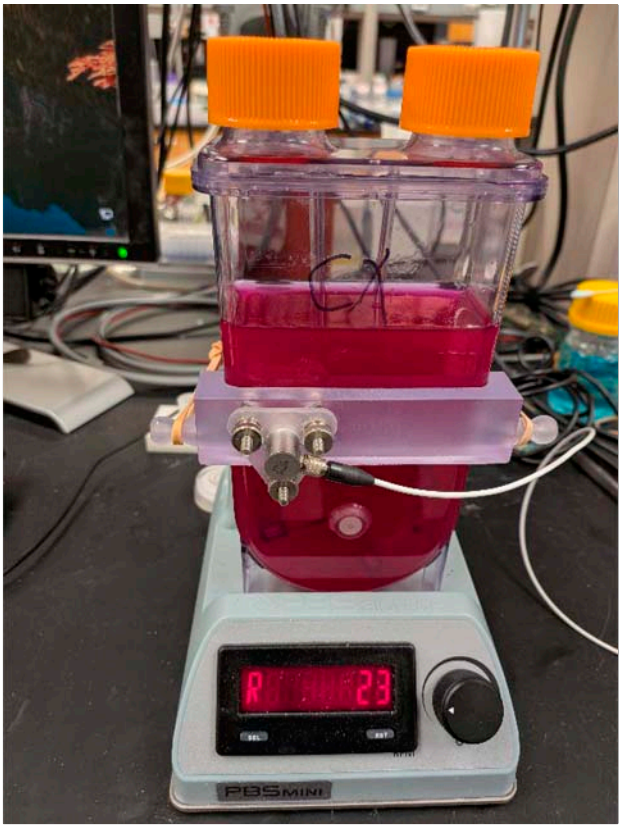


Fig. 1. Custom holder positioning transducer on mini PBS bioreactor.

Conclusion/Significance: These results suggest that pulse dispersion length is a viable, non-destructive approach to monitoring microcarrier occupancy. In this study we were able to probe the microcarrier suspension non-invasively during active bioreactor culture. This has potential for providing real-time actionable feedback on culture conditions.

Session 53
Engineering Immunomodulatory Therapies for Regenerative Medicine

11-18-2026 @ 8:00 AM - 9:30 AM

OP-201 - Neonatal cardiac ECM stabilizes macrophage inflammatory polarization through modulation of the interferon signaling pathway

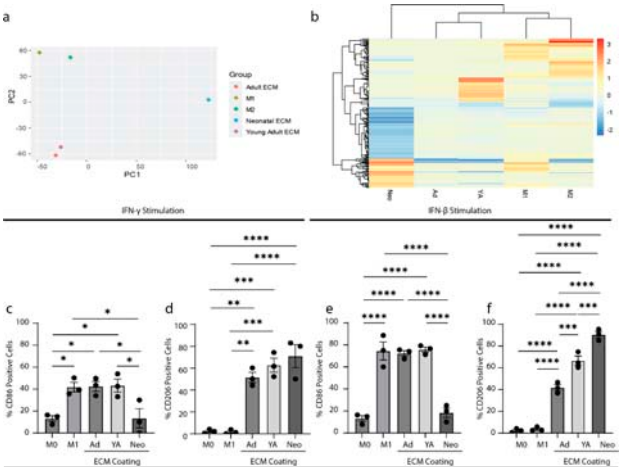
Keely Nugnes[1], Lauren Black[1,2]

[1]*Tufts University, Department of Biomedical Engineering, Medford, United States of America*
[2]*Tufts University School of Medicine, Genetics, Molecular and Cellular Biology, Boston, United States of America*

Purpose/Objectives: Neonatal mammals exhibit robust cardiac reparative capacity that declines rapidly after birth and continues to diminish with age (Porrello et al., 2011). This loss correlates with shifts in macrophage behavior following injury, from pro-regenerative to pro-fibrotic phenotypes (Aurora et al., 2014). We previously showed that macrophages cultured on neonatal cardiac ECM exhibit reduced inflammatory activation and maintain pro-reparative markers even under inflammatory conditions. This study investigates mechanisms underlying macrophage polarization in response to ECM matrikines from different developmental stages.

Methodology: Cardiac ECM from neonatal (P2), adolescent (6 weeks), and adult (16–20 weeks) rats was decellularized and pepsin-digested. ECM peptides (100 μg/cm^2) were adsorbed onto culture plates. Murine RAW 264.7 macrophages were seeded onto ECM-coated or control surfaces. After 24 hours, RNA was collected for sequencing, aligned using STAR (Dobin et al., 2012), and quantified with GFOLD (Feng et al., 2012). Differential expression was analyzed in R and Ingenuity Pathway Analysis. A subset of samples underwent IFN-γ or IFN-β stimulation to assess inflammatory responses.

Results: Principal component and hierarchical clustering revealed clear segregation by ECM presence and age, with neonatal ECM driving the greatest divergence. Gene ontology analysis showed downregulation of viral, immune, and interferon signaling pathways in neonatal ECM conditions. Upon IFN stimulation, macrophages on aged ECM exhibited elevated CD86 expression, resembling M1 polarization, whereas neonatal ECM significantly attenuated CD86. Conversely, CD206 expression was maintained and increased in younger ECM groups under inflammatory conditions. **Figure 1.** Macrophages grown on adult (Ad), adolescent (YA), or neonatal (Neo) ECM coatings underwent RNA sequencing. Gene enrichment analysis included principal component analysis (a) and hierarchical clustering (b), and compared groups to an unstimulated (M0) control. Macrophages grown on ECM coatings were then stimulated with IFN-γ or IFN-β (c–f) and analyzed for their expression of CD86 (c,e) and CD206 (d,f). Significance was determined using a one way ANOVA. * $p < 0.05$, ** $p < 0.01$, *** $p < 0.001$, **** $p < 0.0001$.



Conclusion/Significance: These findings suggest neonatal ECM matrikines suppress interferon-mediated signaling, promoting a pro-

reparative phenotype. This mechanism may contribute to improved neonatal cardiac repair, and ongoing studies aim to validate these effects in vivo.

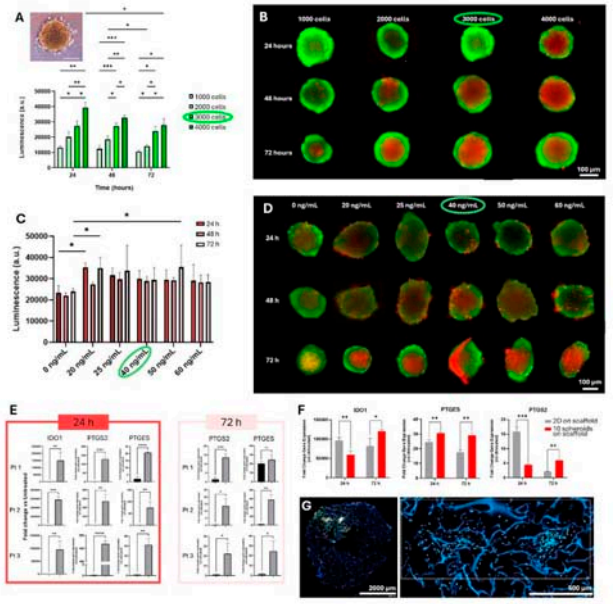
OP-203 - Bioengineering-Powered Cell Therapy: Fat Pad-Derived MSC Spheroids in Collagen Scaffolds as a Enhanced Immunomodulatory Platform for Osteoarthritis

Federica Banche-Niclot[1], Michael Williams[1], Vibha Velur[1], Patrick Mcculloch[2], Francesca Taraballi[1]

[1]*Houston Methodist Research Institute, Center for Musculoskeletal Regeneration, Dept. Orthopedics and Sports Medicine, Houston, United States of America*
[2]*Houston Methodist Hospital, Orthopedics and Sports Medicine, Houston, United States of America*

Purpose/Objectives: Osteoarthritis is a chronic inflammatory joint disease for which MSC-based cell therapy represents a promising regenerative strategy, given their immunosuppressive and regenerative properties. Infrapatellar fat-pad-derived MSCs (FP-MSCs) offer a minimally invasive alternative to standard bone marrow-derived MSCs. Notably, 3D spheroid systems can enhance MSC immunomodulatory capabilities, and biomimetic scaffolds can further potentiate regenerative therapies, enabling spatially controlled delivery. We developed a tissue engineering strategy combining FP-MSC spheroids with a collagen-based porous scaffold to maximize their immunosuppressive activity for advanced osteoarthritis therapy.

Methodology: Individual human FP-MSC spheroids were formed using ultra-low attachment 96-plates, optimized for cell number (1,000-4,000 cells) and culture time (24-72h), and viability assessed via CellTiter-Glo® and Live/Dead assays. MSC phenotype was confirmed by flow cytometry analysis. Inflammation was induced with IFN-γ and TNF-α (40 ng/mL each) for 24h and 72h, and immunomodulatory gene expression (PTGES, PTGS2, IDO1) was assessed by qRT-PCR. Ten spheroids were seeded onto freeze-dried BDDGE-crosslinked collagen scaffolds, evaluating viability and gene expression. Spatial transcriptomic analysis was performed to assess spheroid infiltration and localization of immunomodulatory transcripts throughout the scaffold.



Results: FP-MSCs formed compact spheroids within 24h, remaining viable up to 72 h (Fig.A-B) while retaining MSC identity >99%. An optimal density of 3,000 cells/spheroid was selected as the best compromise between stable viability and limited necrotic core formation. Under inflammatory challenge (Fig.C-D), 3D spheroids consistently showed higher immunosuppressive gene expression compared to 2D culture, with IDO1 virtually undetectable in 2D but robustly induced in 3D, and PTGS2 and PTGES were significantly upregulated (Fig.E). When seeded onto collagen scaffolds, spheroids remained viable and demonstrated a progressive immunosuppressive response over time, with gene expression increasing from 24h to 72h, in contrast to 2D cells on scaffold (Fig.F). Spatial transcriptomic analysis (Fig.G) confirmed spheroid infiltration and localization of immunomodulatory and stemness-related transcripts, including TGFB1 (1,169 counts), PTGS1 (96 counts), and NOTCH2 (3,015), supporting the in-situ immunosuppressive and regenerative activity.

Conclusion/Significance: 3D spheroid culture enhances FP-MSC immunomodulatory capability, and their integration within a collagen scaffold further sustains and prolongs immunosuppressive activity over time. This tissue engineering platform represents a compelling biomimetic strategy for localized immunomodulatory osteoarthritis therapy.

Session 54
Emerging In Vitro and Microphysiological Platforms to Study Human–Microbiome Interactions

11-18-2026 @ 8:00 AM - 9:30 AM

OP-206 - Chaotic bioprinting of a membrane-less intestinal epithelium model for bacteria-host interactions

Mario Álvarez[1,2], Grissel Trujillo-Desantiago[1], Ariel Cantoral-Sánchez[1], Luis Carmona-Ramírez[1], Daniela García-Tijerina[1]

[1]*Tecnológico de Monterrey, Expedition-femsa, MONTERREY, Mexico*
[2]*Tecnológico de Monterrey, Departamento De Mecatrónica, MONTERREY, Mexico*

Purpose/Objectives: Gut microbiota plays a central role in human health and disease, making understanding bacteria–host interactions essential for advancing microbiome research. Early 3D culture systems relied on physical membranes to separate bacteria from intestinal epithelium, limiting the study of bacterial adhesion and invasion. More recent *in vitro* models typically culture either host tissue or bacterial communities in 3D while the counterpart remains in suspension. These approaches often fail to reproduce the spatial organization and dynamic interactions of native tissues, reducing their physiological relevance for studying microbiota–host crosstalk.

Methodology: Here, we fabricated structured cocultures using chaotic bioprinting to generate defined niches where bacteria and mammalian cells coexist without intermixing. Using a printhead with 4 inlets and 3 Kenics static mixer elements, hydrogel constructs with spatially organized layers of *L. rhamnosus*, Caco-2 cells, or their coculture were bioprinted.

Results: We characterized the interplay between them, and the evolution of the coculture over time, using fluorescence microscopy, Live/Dead assays and CFU counting. RT-qPCR was performed to quantify epithelial and barrier-associated gene expression and evaluate bacteria-epithelium interactions. While existing models often struggle to sustain viable mammalian cells and bacteria within the same system over extended periods, quantitative analysis demonstrated that Caco-2 cell viability remained consistently high (>97%) throughout 21 days of coculture. *L. rhamnosus* load increased by

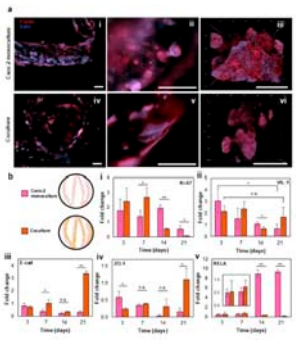


Figure 1. Morphological and molecular characterization of Caco-2 cells in chaotic bioprinted monoculture and coculture constructs. (a) Actin/DAPI staining of Caco-2 cell aggregates within bioprinted monoculture and coculture filaments after long-term culture (Day 21). Cytoskeleton (F-actin) is shown in red and cell nuclei (DAPI) in blue. **(i–iii)** Representative fluorescence micrographs of Caco-2 monoculture constructs showing cellular organization and aggregate morphology at different magnifications, including a three-dimensional reconstruction view. **(iv–vi)** Representative fluorescence micrographs of Caco-2 in coculture constructs showing the morphology and structural organization of epithelial-like cell aggregates at different magnifications, including a three-dimensional reconstruction view. Scale bars: 500 µm. **(b)** Quantification of gene expression through RT-qPCR analysis. Fold changes in (i) Ki-67, (ii) Villin-1 (VIL-1), (iii) E-cadherin (E-cad), (iv) zonula occludens-1 (ZO-1), and (v) RELA. (*p-value < 0.05; **p-value < 0.01; n.s.: non-significant difference).

almost two order of magnitude ($\sim 1\times10^6$ to $\sim 1\times 10^8$ CFU/g) and stabilized over time, showing comparable trends between monoculture and coculture conditions. These results indicate that the constructs support nutrient exchange and long-term stability, maintaining both mammalian cell and bacterial viability without overgrowth or loss of compartmentalization, thereby overcoming a key limitation of existing *in vitro* models.

Conclusion/Significance: Chaotic bioprinting enables the fabrication of a bacteria–host *in vitro* model with defined compartments and perfusable channels. To our knowledge, this is the first report of a one-step, membrane-less, architected gut-like construct integrating both bacterial and mammalian cells. This platform offers a physiologically relevant system to study microbiome-related therapeutics, probiotic and pathogen dynamics, dysbiosis, and host immune responses.

OP-207 - Modeling Gut Metabolite-Driven Aortic Valve Remodeling Using In Vitro and Ex Vivo Tissue Models

Ana Porras

University of Florida, Gainesville, United States of America

Purpose/Objectives: Calcific aortic valve disease (CAVD) is a progressive fibrocalcific disorder with no effective pharmacological therapies. Emerging evidence suggests that gut microbiome-derived metabolites contribute to cardiovascular disease, but their role in valve pathology remains poorly understood. We hypothesized that the gut metabolite trimethylamine-N-oxide (TMAO) promotes early aortic valve remodeling through valvular interstitial cell activation and extracellular matrix dysregulation.To investigate the effects of TMAO across multiple levels of valve complexity, we employed complementary *in vitro* and *ex vivo* models of the aortic valve.

Methodology: Porcine valvular interstitial cells (VICs) were maintained in an engineered culture system that suppresses the spontaneous activation observed on conventional tissue culture plastic, enabling the study of quiescent VIC responses to TMAO. Cells were evaluated for myofibroblastic activation, extracellular matrix production, and oxidative stress. Soluble inhibitor experiments were employed to assess the role of endoplasmic reticulum stress signaling in directing the response to TMAO. To assess tissue-level responses, intact porcine aortic valve leaflets were cultured ex vivo under controlled conditions and exposed to TMAO for 7 days. Gene expression and histological analyses were used to evaluate cellular activation and extracellular matrix remodeling.

Results: In quiescent VICs, TMAO induced myofibroblastic activation, evidenced by increased expression of α-smooth muscle actin and transgelin. TMAO also increased extracellular matrix production and oxidative stress, hallmarks of a profibrotic phenotype. Notably, quiescent VICs were more sensitive to TMAO than conventionally cultured VICs. Pharmacological inhibition of the endoplasmic reticulum stress kinase PERK abolished these responses, implicating ER stress signaling as a key mediator of TMAO-induced VIC activation. To determine whether these cellular responses translated to tissue-level remodeling, intact porcine valve leaflets were exposed to TMAO ex vivo. TMAO increased expression of the myofibroblastic marker ACTA2, the osteogenic marker BMP2, and the matrix remodeling enzymes MMP2 and MMP9. Histological analyses further revealed collagen depletion and disruption of leaflet architecture following TMAO treatment.

Conclusion/Significance: These findings identify TMAO as a potential mediator of early aortic valve remodeling and demonstrate that microbiome-derived metabolites can influence valve biology across both cellular and tissue-level models. Collectively, this work highlights the gut-heart axis as a potential therapeutic target for CAVD.

OP-208 - Establishing oral dysbiosis in an immunocompetent in vitro oral tissue model

Fnu Keerti

University of Massachusetts, Lowell, Biomedical Engineering, Lowell, United States of America

Purpose/Objectives: The present study aims to investigate the interplay between the oral tissue niche, microbiome, and host immune responses using an *in vitro* oral tissue model (OTM) incorporating neutrophils, which are actively recruited during dysbiosis. The study evaluates their role in modulating inflammatory responses following exposure to healthy versus gingivitis-associated microbiomes.

Methodology: Planar scaffolds were fabricated from silk aqueous solution and seeded with primary gingival fibroblasts and epithelial cells to mimic the human oral mucosal barrier. Following maturation and differentiation, human bone marrow–derived polymorphonuclear neutrophils (BM-PMNs) were introduced at densities reflecting oral health and disease conditions, using epithelial cell-to-neutrophil ratios of 1:5 (healthy) and 1:10 (gingivitis). Constructs were exposed to BM-PMNs for 24 h, followed by a second exposure the following day for 3 h, and subsequently challenged with heat-killed (HK) microbiomes derived from healthy and gingivitis individuals for 4 h. Samples were collected post-treatment for assessment of cell viability, gene expression, cytokine profiling, and imaging-based evaluation of neutrophil-specific markers. Statistical analyses were performed using one-way ANOVA with Tukey's multiple comparisons test.

Results: Incorporation of neutrophils into the *in vitro* OTM did not compromise epithelial barrier integrity, as demonstrated by imaging and gene expression analyses. TLR2 and TLR4 expression was increased following neutrophil incorporation, indicating enhanced innate immune activation. Multiplex cytokine profiling revealed modulation of both pro-inflammatory and anti-inflammatory mediators following heat-killed microbiome exposure, with more pronounced responses observed upon neutrophil pre-incubation prior to microbial challenge. Preliminary differences were also observed between healthy- and gingivitis-associated microbiome treatments, suggesting condition-dependent immune responses. These findings suggest that neutrophils contribute to shaping inflammatory responses associated with oral dysbiosis. However, these results are preliminary and require further validation.

Conclusion/Significance: The inclusion of neutrophils in the OTM successfully recapitulates oral inflammatory responses associated with dysbiosis. Further optimization is required to establish a stable and long-term *in vitro* system that more accurately reflects the human oral mucosal environment under disease conditions. This model has potential as a physiologically relevant platform for screening therapeutic interventions and supporting translational preclinical studies.

Session 55
Extracellular Vesicles as Nanomedicine for Musculoskeletal Regeneration and Repair

11-18-2026 @ 8:00 AM - 9:30 AM

OP-210 - EV-Releasing Citrate Scaffolds for Stem Cell Differentiation in Tendon Injury

Anisa Ashraf, Eun Ji Chung

University of Southern California, Biomedical Engineering, Los Angeles, United States of America

Purpose/Objectives: 32 million tendon injuries occur in the United States each year which often result in irreversible damage to the muscle-tendon-bone interface. Current repair strategies fail to restore the complex, integrated transition between these soft and stiff tissues essential for biomechanics and do not support the coordinated regeneration needed across these distinct tissue types. A key gap is modular biomaterials that both 1) recapitulate this complex structure and 2) enable localized delivery of nanomedicine to differentiate tendon resident stem cells and those recruited to sites of injury. Thus, we hypothesize that previously FDA approved citrate biomaterials, with controlled curing, can be utilized as a tunable, multi-composite scaffolds integrating mechanical, biochemical, and extracellular vesicle (EV)-mediated cues to promote region-specific differentiation and improve tendon repair.

Methodology: Methacrylated Poly-(1,8)-octanediol citrate (mPOC) was UV-crosslinked to achieve biomimetic stiffnesses and combined with collagen (0–10% w/w) and hydroxyapatite (0–60% w/w) to provide pro-myogenic/tenogenic and pro-osteogenic signals (1A). Increasing UV exposure significantly increased tensile and

compressive moduli, producing scaffold properties comparable to native tissues (ns vs. tissue; $p < 0.05$ between scaffold groups).

Results: Scaffolds supported cell viability and additionally, mesenchymal stem cells (MSCs) showed improved doubling times on tendon- and bone-mimetic scaffolds, indicating enhanced proliferative capacity (1B). Further, mPOC was cured in PDMS molds into continuous tri-phasic scaffolds which mimicking innate tissue organization and alignment. The mPOC platform supports click chemistry enabled EV delivery, including tenocyte-derived EVs carrying tenomodulin and scleraxis (1C-E) for tenogenesis. EVs were released from scaffolds at an appropriate rate for tendon repair (1F).

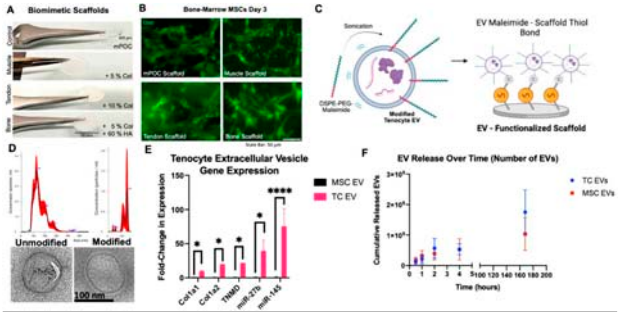


Figure 1. A) Biomimetic scaffolds with B) MSC cultured as shown by Calcein Green live stain on day 3. C) EV - scaffold clicking scheme D) EV characterization by NTA and TEM E) mRNA and microRNA evaluation of tenocyte EVs and F) release from scaffolds over time. (*$p<0.05$, ****$p<0.0001$).

Conclusion/Significance: These findings demonstrate that mPOC scaffolds can integrate mechanical and biochemical signaling, EV-based nanomedicine delivery, and topographical guidance to regulate cell behavior. This platform addresses a critical barrier in interface regeneration and offers a promising strategy for improving functional outcomes in tendon repair through coordinated tissue engineering.

OP-211 - Matrix Microarchitecture Drives Cellular Function and Extracellular Vesicle Proteome in Engineered Tendon Models

Kariman Shama, Zachary Greenberg, Mei He, Brittany Taylor

University of Florida, Gainesville, United States of America

Purpose/Objectives: Tendinopathy is a musculoskeletal disorder characterized by impaired function, altered extracellular matrix organization, and pain. The tendon microenvironment becomes hypercellular, incorporating endogenous and exogenous cell populations that contribute distinct soluble signaling cues. Extracellular vesicles (EVs), cell-secreted nanoparticles that mediate intercellular communication, regulate inflammation, ECM remodeling, and cellular behavior in tissues. However, their role in tendon pathology remains poorly understood. In vitro tendon models provide controlled systems to study early disease mechanisms that are difficult to capture in vivo due to the heterogeneous microenvironment present. Building on our previous findings that EV profiles change in response to nanofibrous microarchitecture, we used biomimetic healthy and diseased tendon models to investigate temporal changes in EV cargo and tendon cell phenotypes.This study aimed to determine how matrix microarchitecture influences cellular behavior and EV cargo in tendon pathology.We hypothesized diseased-mimetic environments would drive distinct EV signatures associated with fibrosis and inflammation, establishing EVs as biomarkers and therapeutic targets.

Methodology: Electrospun polycaprolactone (PCL) scaffolds modeled healthy and diseased tendon microenvironments. Tendon-derived cells were evaluated for proliferation, morphology, and remodeling markers, while EVs isolated from conditioned media LC–MS/MS proteomic analysis. Statistical analyses included ANOVA, ANCOVA, normality testing, and differential protein analysis (FDR < 0.05).

Results: Healthy scaffolds promoted elongated, aligned TDC morphology, whereas diseased scaffolds induced enhanced proliferation and progressive alignment over time. Diseased models exhibited elevated fibronectin and collagen III expression, while collagen I peaked earlier in healthy cultures. EV proteomics revealed disease-associated enrichment of remodeling and inflammatory proteins including annexin-a1 (ANXA1), galectin-1 (LGALS1), Matrix-Metallopeptidase-2 (MMP2), and inhibin-subunit beta-a (INHBA), alongside proteins linked to ECM remodeling and cytoskeletal dynamics (Figure 1).

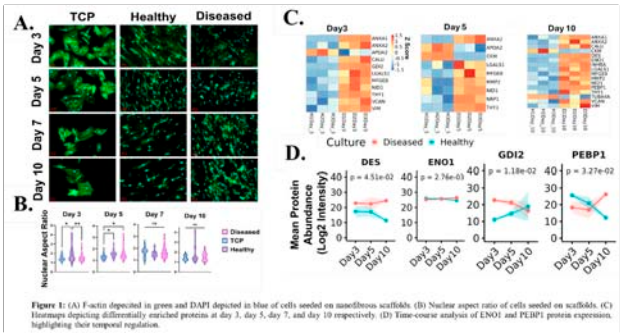


Figure 1: (A) F-actin depicted in green and DAPI depicted in blue of cells seeded on nanofibrous scaffolds. (B) Nuclear aspect ratio of cells seeded on scaffolds. (C) Heatmaps depicting differentially enriched proteins at day 3, day 5, day 7, and day 10 respectively. (D) Time-course analysis of ENO1 and PEBP1 protein expression, highlighting their temporal regulation.

Conclusion/Significance: Diseased tendon microenvironments promoted hypercellularity, fibrotic remodeling, and EV signatures associated with inflammation, matrix remodeling, and metabolic stress. Enrichment of proteins including MMP2, annexins, INHBA, and ENO1 supports roles for EV-mediated remodeling, activin/TGF-β signaling, and glycolytic reprogramming in tendinopathy progression. Together, these findings establish a biomimetic 3D tendon model that recapitulates healthy and diseased microenvironments while demonstrating that EV cargo reflects fibrotic and inflammatory changes, supporting EVs as biomarkers of disease progression and potential antifibrotic therapeutic targets. Future work will evaluate EV functionality through EV administration studies.

OP-212 - Functional Profiling of Cartilage-Derived Matrix-Bound Nanovesicles Reveals Disease-Specific Alterations and Potential for Endogenous Tissue Regeneration

Jiayang Rong[1,2], Catalina Pineda Molina[2,3], Jordyn Mitchell[4], Michael Floren[4], George Hussey[1,2,5]

[1]*University of Pittsburgh, Swanson School of Engineering, Pittsburgh, United States of America*
[2]*University of Pittsburgh, Mcgowan Institute For Regenerative Medicine, Pittsburgh, United States of America*
[3]*University of Pittsburgh, Surgery, Pittsburgh, United States of America*
[4]*AlloSource, Centennial, United States of America*
[5]*University of Pittsburgh, Pathology, Pittsburgh, United States of America*

Purpose/Objectives: Osteoarthritis (OA) is a leading cause of disability, characterized by the progressive cartilage degradation and chronic pain [1, 2]. Current therapies manage symptoms but fail to halt tissue destruction or address the immune imbalance with significant side effects [3-5]. Nevertheless, lack of accurate diagnostic tools for OA remains a significant barrier to early clinical intervention.

Matrix-bound nanovesicles (MBV), a subtype of extracellular vesicles, carry tissue-specific bioactive proteins and microRNA [6], offering potential as both diagnostic biomarkers and regenerative templates. Systemic administration MBV has shown immunomodulatory potential in preclinical arthritis models, promoting tissue repair via effects on cell survival, proliferation, and differentiation [7-9]. However, how the pathological OA alters MBV composition and functional capacity remains poorly characterized.

This study aims to characterize the proteomic divergence between healthy (H-CMBV) and diseased (OA-CMBV) cartilage-derived MBVs and evaluate their functional modulation on chondrocytes.

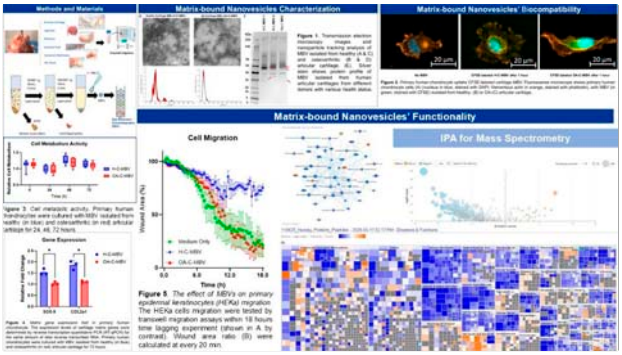
Methodology: Articular cartilage-derived MBV (CMBV) was isolated from different donors' knee of various age/gender and disease status, utilizing ultracentrifugation, nanoparticle analysis and Transmission Electron Microscopy to confirm their presence, size, and purity.

CMBV characterization was performed with mass spectrometry with median normalization based on the total protein intensity.

CMBV uptake. Primary human chondrocytes were treated with CFSE-dyed cartilage MBV for different time points w/wo interleukin-1β (IL-1β), which is a pro-inflammatory cytokine that activates proteinases in catabolism and suppresses cartilage matrix synthesis, leading to cartilage degradation [10, 11]. Then, the cells were stained with Phalloidin and nuclei to be imaged by fluorescence microscope.

MBV as endogenous regenerative medicine. To evaluate MBV natural bioactivity, human articular cartilage explants were cultured ex vivo and treated with allogenic H-CMBVs or OA-CMBVs. MBV penetration into the dense extracellular matrix (ECM) was visualized using ExoGlow™-labeled vesicles. Matrix preservation was quantified via glycosaminoglycans measurement and immunohistochemical staining for MMP13 and type II collagen.

Results: CMBVs exhibit consistent size and morphology across donors and are efficiently internalized by primary human chondrocytes. The identification of OA-specific markers provides a molecular basis for developing sensitive, early-stage diagnostic tools. Furthermore, the loss of "motion inhibition" in OA-CMBVs reflects a pathological shift in maintaining the chondrocyte phenotype.



Conclusion/Significance: MBV divergence enables targeted diagnosis and cartilage regeneration.

Session 57
Dynamic Biophysical Modulation of Tissue Regeneration

11-18-2026 @ 8:00 AM - 9:30 AM

OP-213 - Spatial mapping of TGF-β activation under mechanical load in 3D constructs

Laura Mecchi[1], Tim Welting[2], Marjolein Caron[3], Martin Stoddart[1]

[1]*AO Research Institute Davos, Davos Platz, Switzerland*
[2]*Maastricht University Medical Center, Department of Orthopedic Surgery, Maastricht, Netherlands*
[3]*Maastricht University, Department of Orthopedic Surgery, Maastricht, Netherlands*

Purpose/Objectives: Transforming growth factor beta (TGF-β) is a key growth factor that drives mesenchymal stromal cell (MSC) chondrogenesis. Expressed in latent form, TGF-β must be activated to exert its activity. We have previously shown that TGF-β is mechanically activated in 3D constructs under complex load. Within this study, we demonstrate the key role of interfacial shear in the activation of TGF-β.

Methodology: Cell free polyurethane/ fibrin scaffolds were covered in DMEM containing 50 ng/mL human latent TGF-β1 and subjected to either shear load (0.01 Hz, 0.1 Hz, 1 Hz), compression (10%, 15%, 20%) or left in a free-swelling (FS) state, for 6 hours at which time active TGF-β was measured. For cell containing experiments, scaffolds included 5 million human MSCs (n=3 donors) and were loaded for 22 days in the absence of exogenous TGF-β. Three protocols were applied: P1 (1h of shear at 1 Hz followed by 1h of 20% compression), P2 (simultaneous shear at 1Hz and 20% compression for 2h), P3 (simultaneous shear at 1Hz and 20% compression for 1h) and compared to FS controls. To confirm spatial TGF-β activation, 0.5 million SMAD3 luciferase reporter cells were loaded in the presence of 50 ng/mL latent TGF for 15 minutes with either 20% compression, 0.01 Hz, 0.1 Hz or 1 Hz shear, to map local latent TGF-β activation. Three hours after loading, substrate was added and samples were incubated for 2h before imaging.

Results: Shear mainly activated latent TGF-β1, with activation rising as shear frequency increased. Total TGF-β1 is higher in scaffolds treated with 20% compression, indicating that compression drives TGF-β into the scaffold. In cell experiments, the SOX9/RUNX2 ratio is comparable or higher in all three loaded groups than the positive control. The ratios of chondrocytic marker genes versus fibroblastic marker genes and hypertrophic marker genes in loaded groups are comparable with the positive control. Data from gene expression, glycosaminoglycan analysis and histological staining followed a similar trend. Luciferase spatial mapping demonstrated a shear frequency related activation of TGF-β signaling at the upper surface of the scaffold.

Conclusion/Significance: These data confirm the role of shear in TGF-β activation and its bioavailability.

OP-214 - Scalable Autonomous Microfluidic Oscillator Arrays for Parallelized Generation of Dynamic Cellular Microenvironment

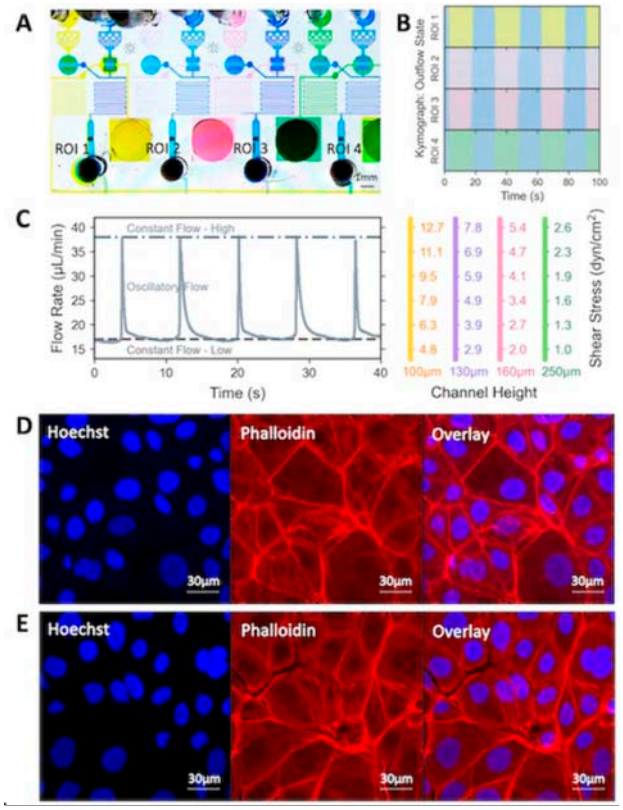
Xiaoqian Wang, Priyan Weerappuli, Julia Vallier, Nhayeon Lee, Sasha Cai Lesher-Pérez

University of Michigan, Ann Arbor, United States of America

Purpose/Objectives: Dynamic mechanical and biochemical cues are critical regulators of cellular behavior, yet their incorporation into in vitro culture systems remains limited by the lack of scalable methods for generating complex temporal stimuli. Conventional liquid-handling approaches are often constrained by cost, footprint, and throughput. Autonomous microfluidic oscillators featuring normally closed (NC) valves offer an alternative for generating dynamic flow environments but have seen limited biological adoption due to fabrication challenges associated with NC valves. Here, we developed scalable oscillator arrays incorporating slightly-open doormat (SOD) valves and used the platform to generate parallelized dynamic in vitro models by exposing human corneal epithelial cells (HCES) to oscillatory shear that mimics the mechanical stimulation associated with eye blinking.

Methodology: Oscillators were fabricated in polydimethylsiloxane (PDMS) using soft lithography. Unlike NC valves, SOD valves eliminate manual selective plasma deactivation during assembly while preserving actuation functionality. Synchronized oscillator arrays generated oscillatory flow stimuli that were applied to HCES for 24 hours in channels of varying heights, producing distinct shear stress conditions under identical flow profiles (Fig C). Constant-flow and static culture conditions served as controls.

Results: SOD oscillators generated stable oscillatory outflows with tunable periods while reducing sensitivity to fabrication variability and improving scalability. Capacitive coupling enabled robust synchronization across multiple oscillators, creating a scalable framework for parallelized generation of dynamic flow environments, including biochemical compositions and shear profiles (Fig A-C). Oscillatory flow was applied to HCES cultured under multiple shear stress conditions (Fig C). Oscillatory stimulation promoted lateral cell spreading across all shear conditions, whereas constant-flow and static controls exhibited increased cell density in taller channels. In addition, oscillatory shear promoted cytoskeletal organization and reduced intercellular gaps compared with constant high-shear conditions (Fig D-E).



(A) Four coupled SOD oscillators integrated on a single chip. (B) Coupled oscillators generate synchronized oscillatory outflows. (C) Oscillatory flow profiles generate distinct shear stress conditions. Representative confocal images of HCES under (D) oscillatory shear, (E) constant high shear.

Conclusion/Significance: SOD oscillators provide a scalable microfluidic platform for recreating physiologically relevant dynamic microenvironments, including blinking-associated mechanical stimulation, and may facilitate development of more biomimetic in vitro tissue models for disease modeling and therapeutic screening.

OP-215 - Glycocalyx remodeling modulates shear mechanotransduction by tuning membrane mechanics and Ca2+ transduction in high grade serous ovarian carcinoma

Salma Abdelgawad, Eric Horst, Hristina Zdravkoska, Chetan Nallani, Srihitha Gadila, Allen Liu, Analisa Difeo, Geeta Mehta

University of Michigan, Ann Arbor, United States of America

Purpose/Objectives: In the dynamic native cellular niche, active biophysical cues, such as fluid shear stress, regulate cell behavior through mechanotransduction. High-grade serous ovarian carcinoma (HGSC) disseminates within the peritoneal cavity where tumor cells experience ascites-associated shear stress. However, the membrane-level parameters that set the "gain" of shear sensing remain poorly defined. The mucin-rich glycocalyx is a targetable mechanically-active polymer layer that may modulate membrane bending and response. We hypothesize that HGSC-associated glycocalyx remodeling alters membrane mechanics to amplify shear-evoked mechanoelectric Ca^{2+} transduction relative to cells of its origin: nontransformed fallopian tube secretory epithelial cells (FTSECs).

Methodology: We combine microfluidic shear stimulation with quantitative membrane biophysics and live mechanotransduction readouts. Mechanosensitivity is quantified by live Ca^{2+} influx imaging under shear. Cytosolic Ca^{2+} is used as a primary mechanosensitivity metric because it is among the earliest intracellular first-responder signals to mechanical stimulation and provides a sensitive, quantitative measure of force-to-signal conversion. Global membrane mechanical strength is quantified by micropipette aspiration measurements (apparent area expansion modulus, K_a), and local surface stiffness is quantified by optical tweezer force calculations (Young's modulus, E). Glycocalyx abundance is assessed by sialic acid lectin flow cytometry with neuraminidase controls. Causality and targetability is tested by active modulation of the surface layer via StcE mucinase (glycocalyx thinning) and orthogonal tuning of membrane stiffness via cholesterol enrichment/depletion.

Results: HGSC cells exhibit a mechanically softened membrane phenotype (32% lower K_a and 20% lower E) relative to FTSECs which result in heightened shear-evoked Ca^{2+} influx (200% higher). Glycocalyx thinning with StcE mucinase partially restores FTSEC-like mechanics and attenuates shear-triggered Ca^{2+} response, consistent with recovery towards non-transformed phenotype. Similarly, pharmacologic membrane stiffening via cholesterol enrichment shifts mechanosensitivity towards FTSEC-like behavior, providing an orthogonal rescue. Consistent with amplified Ca^{2+} responsiveness, proteomics showed upregulated Ca^{2+}-linked membrane signaling candidates in HGSC with up to 39-fold greater expression, including CHRM3 and VGCC-associated subunits (e.g., CACNA2D2, CACNB2), as targetable proteins.

Conclusion/Significance: This work advances active biophysical modulation by identifying a tunable surface property, glycocalyx, that gates membrane mechanics and rapid Ca^{2+} mechanotransduction under shear, providing mechanistic leverage points for disrupting early biophysical drivers of HGSC dissemination.

OP-216 - Development and Validation of a Modular Perfusion Platform for Preconditioning Vascularized 3D Bioprinted Renal Tissue Constructs

Nathan Barney[1], Po-Feng Lee[1], Martin Carrasco[2], Sahar Vakili[2], John Fisher[2], Young Min Ju[1], James Yoo[1], Anthony Atala[1]

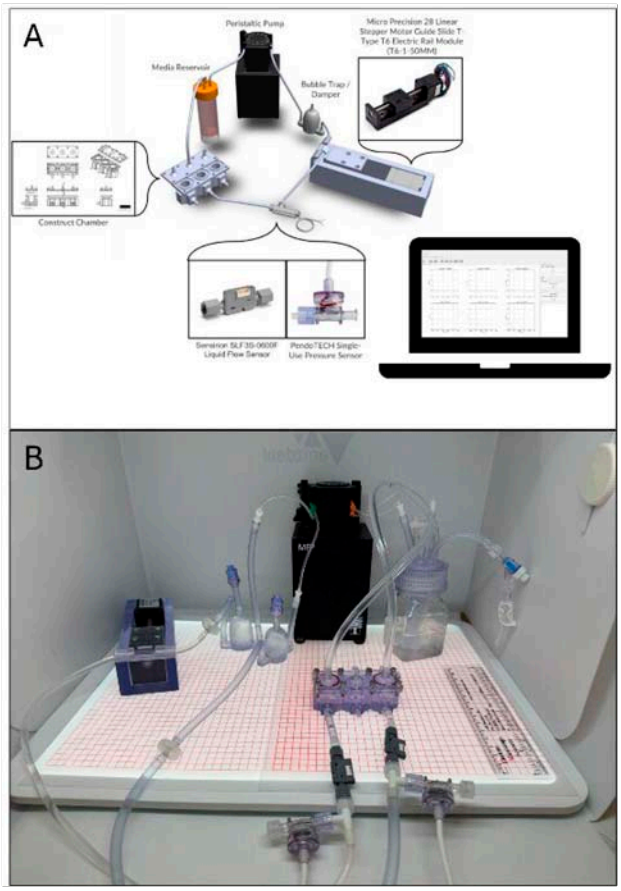
[1]*Wake Forest School of Medicine, Wake Forest Institute For Regenerative Medicine, Winston-Salem, United States of America*
[2]*University of Maryland, Fischell Department of Bioengineering, College Park, United States of America*

Purpose/Objectives: Recent advancements in bioprinting have opened the possibility of producing larger tissue-engineered products with therapeutic precision. We have developed a comprehensive bioprinting strategy to produce vascularized tissue-engineered kidney constructs for surgical implantation. However, a gap remains between printing these constructs and preparing them for implantation. Perfusion bioreactors can address this gap by preconditioning tissue constructs in controlled physiological environments. This study aims to develop a compact, modular perfusion platform that reproducibly delivers monitored flow conditions and evaluate whether these conditions support construct viability and function over time.

Methodology: Wedge-shaped human renal tissue constructs with interconnected channels were bioprinted using a digital light projection (DLP) printer. A cylindrical gyroid construct was assembled from twelve of these wedges to create a standardized porous scaffold. A custom chamber was designed to accommodate cylindrical renal constructs and evenly perfuse them from a bottom inlet to a top outlet. The six-channel bioreactor platform incorporated a Python interface for real-time monitoring of flow, pressure, and temperature, programmable steady and unidirectional pulsatile flow control, and automated data logging. COMSOL Multiphysics modeling was developed to predict the local flow distribution, wall shear stress, and scaffold deformation. Biological validation was performed on the vascularized 3D-bioprinted renal constructs cultured for 7 days under static, steady-flow, or pulsatile-flow conditions. Outcomes included viability imaging, metabolic assays, histology, and immunostaining.

Results: The perfusion bioreactor system maintained the target flow rate and generated a consistent 1 Hz pulsatile waveform with a pulsatility index of 0.71, similar to renal cortex physiology. The computational model showed a uniformly distributed flow throughout the gyroid network, supporting the selected conditions as safe for biological validation. After 7 days, perfused constructs exhibited higher cell viability compared with static controls. Metabolic

activity was also higher in the perfused groups, indicating that both perfusion modes supported constructs more effectively than static conditions.



Conclusion/Significance: These results support that the modular perfusion bioreactor platform with controlled physiological environmental conditions facilitates preconditioning of 3D bioprinted tissue constructs. By combining monitored perfusion, programmable control, automated data capture, and computational modeling, the perfusion bioreactor system links device inputs to cellular-level conditions and guides future optimization of implantation-relevant tissue conditioning.

OP-217 - Differentiation of stem cell-derived airway basal cells and application to bioreactor-based tracheal recellularization

Leo Castiblanco Guzman[1,2], Siba Haykal[2,3], Golnaz Karoubi[1,2]

[1]*University of Toronto, Laboratory Medicine And Pathobiology, Toronto, Canada*
[2]*Latner Thoracic Research Laboratories, Toronto, Canada*
[3]*Yale School of Medicine, Department of Surgery, New Haven, United States of America*

Purpose/Objectives: Normal function of the trachea is dependent on the respiratory epithelium, which removes contaminants through mucociliary clearance. For repair of long segment tracheal defects, transplantation is frequently the only treatment; however, tracheal replacements often fail due to poor epithelial regeneration. While a potential approach for tracheal repair is the use of human induced pluripotent stem cell (hiPSC)-derived airway cells, the development of mucociliary clearance is not well understood. The goal of this work is to characterize the differentiation and transport function of hiPSC-derived airway basal cells (iBCs), and to investigate their potential for tracheal tissue engineering using an ex vivo bioreactor system.

Methodology: iBCs expressing canonical basal cell markers were cultured under air-liquid-interface (ALI) following published protocols for 14, 21, and 28 days. Differentiation was assessed using immunofluorescence staining. Biopsy punches of freshly procured porcine tracheae were used for analysis of native function. Mucociliary clearance function was analyzed using a fluorescent bead tracking assay. Whole porcine tracheae were procured and de-epithelialized using a rotating double-chamber bioreactor. iBCs were seeded into de-epithelialized porcine tracheae and cultured under dynamic ALI. Samples were taken at 3 and 10 days for histological analysis.

Results: iBCs cultured under ALI formed ciliated and goblet cells, as well as tight junctions by day 14, with high ciliation throughout days 14-28. Mucociliary transport displacement and velocity alignment increased from day 14-28 ($\sim$2 um to 7 um, 0.05 to 0.2 respectively). All metrics were 4.5-10 times lower than native tracheal transport. H&E staining revealed the presence of thin epithelium in re-epithelialized tracheae after 3 days of submerged culture. Preliminary results indicate development of a robust epithelial monolayer after an additional 7 days of ALI culture, indicating successful attachment and survival of iBCs on the decellularized tracheal scaffold.

Conclusion/Significance: This work provides insights into the mucociliary properties of hiPSC-derived airway cultures and demonstrates initial maintenance of tracheal epithelium ex vivo, which could serve as platforms for further study of mucociliary clearance development and alignment, as well as a potential tracheal graft for tracheal transplantation.

Session 58
Cardiovascular Tissue Engineering: From Cells, Ecm to AI-driven Organoids

11-18-2026 @ 8:00 AM - 9:30 AM

OP-218 - Spatiotemporal Propagation of Mechanotransductive Signaling in Cardiac Fibroblast Networks Using Dynamic Magnetorheological Elastomers

Ali Lateef[1], Atia Rahman[2], Raysa Rupanti[1], Ryan Zurakowski[1], Elise Corbin[1]

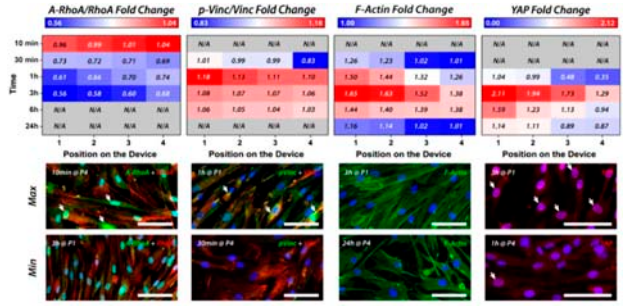
[1]*University of Delaware, Biomedical Engineering, Newark, United States of America*
[2]*University of Delaware, Department of Mechanical Engineering, Newark, United States of America*

Purpose/Objectives: Cardiac fibrosis is a hallmark of heart failure and progressively impairs the heart's contractile function. Following myocardial infarction (MI), remodeling initially occurs near the infarct border zone but can spread into surrounding healthy tissue, ultimately contributing to organ-wide dysfunction. How localized mechanical changes communicate with neighboring cells and the extracellular matrix (ECM) to drive fibrosis progression remains poorly understood. The objective of this study was to develop a dynamic in vitro platform capable of mimicking evolving mechanical injury and to investigate how localized stiffness perturbations propagate mechanotransductive signaling through cardiac fibroblast networks.

Methodology: We developed a magnetorheological elastomer (MRE)-based culture platform capable of reversible, localized stiffness modulation through externally applied magnetic fields. Normal human cardiac fibroblasts (NHCF-Vs) were cultured on fibronectin-coated MRE substrates and exposed to localized stiffening conditions. Mechanotransductive responses were evaluated spatially and temporally at multiple positions and time points. Key signaling markers associated with fibrosis progression, including RhoA activation, vinculin phosphorylation, F-actin remodeling, and YAP nuclear localization, were quantified using fluorescence imaging and image analysis. In parallel, a mathematical model consisting of coupled ordinary differential equations and time-delay elements was developed to characterize signaling kinetics and pathway interactions.

Results: Localized stiffening induced coordinated waves of mechanosensitive activity that propagated outward from the

mechanically perturbed region. RhoA activation occurred rapidly within 10 minutes, followed by vinculin phosphorylation at 1 hour, and both F-actin remodeling and YAP nuclear localization at approximately 3 hours (Fig. 1). Signal intensity progressively decreased with increasing distance from the perturbation site while spreading spatially over time, suggesting the establishment of a spatiotemporal equilibrium. The computational model closely matched experimental trends.



Conclusion/Significance: These findings demonstrate that cardiac fibroblasts rapidly sense and propagate localized mechanical cues through interconnected signaling networks. This dynamic MRE platform provides a powerful tool for studying how evolving mechanical microenvironments influence fibrosis progression and tissue remodeling. Furthermore, integrating experimental and computational approaches may enable predictive modeling of mechanotransduction dynamics in fibrotic disease progression.

OP-219 - Acellular Tissue-Engineered Vascular Grafts with Controlled Heparin and VEGF Biofunctionalization

Yujie Kang[1], Weilue He[2], Feng Zhao[3]

[1]*Texas A&M University, College Station, United States of America*
[2]*Michigan Technological University, Biomedical Engineering, Houghton, United States of America*
[3]*Texas A&M Unniversity, College Station, United States of America*

Purpose/Objectives: Small-diameter (<6 mm) vascular grafts are urgently needed for coronary artery bypass grafting, but current tissue-engineered vascular grafts (TEVGs) are limited by thrombosis and stenosis due to insufficient endothelialization and remodeling. This study aimed to develop a VEGF-loaded acellular extracellular matrix (ECM) TEVG with spatially controlled VEGF delivery to promote rapid endothelialization and favorable immune-mediated remodeling. Photocrosslinkable methacrylated gelatin (GelMA) and methacrylated heparin (HepMA) were incorporated for controlled VEGF immobilization. The pro-endothelialization capacity was evaluated through endothelial cell proliferation and migration assays, while THP-1 monocyte recruitment and differentiation were assessed to determine immunomodulatory effects contributing to graft remodeling.

Methodology: Human dermal fibroblast (hDF)-derived acellular ECM scaffolds were fabricated and functionalized with photocrosslinkable GelMA and HepMA to enable controlled VEGF immobilization. The effects of scaffold modifications on immune responses and endothelialization were evaluated under dynamic culture conditions. THP-1-derived macrophage interactions were assessed by analyzing cell adhesion, morphology, and macrophage polarization markers. Human umbilical vein endothelial cell (HUVEC) attachment, proliferation, and surface coverage were evaluated by immunofluorescence staining and quantitative image analysis to determine the pro-endothelialization capacity of the modified ECM scaffolds.

Results: The TEVG was fabricated by layer-by-layer wrapping of ECM sheets around a mandrel, resulting in a tubular graft with controlled dimensions. VEGF was successfully immobilized within the designed layer, confirming spatial control of growth factor incorporation. VEGF-functionalized ECM significantly enhanced endothelialization, as demonstrated by increased HUVEC proliferation and surface coverage. The VEGF-loaded scaffolds also promoted THP-1 cell recruitment and M2 macrophage polarization, with increased CD68 and CD163 expression. By Day 14, endothelial marker-positive cells exhibited cobblestone-like morphology, indicating enhanced endothelial-like differentiation.

Conclusion/Significance: Overall, this VEGF-functionalized ECM-based TEVGs provide a promising strategy to overcome key limitations of small-diameter vascular grafts by promoting rapid endothelialization and modulating immune responses toward a pro-regenerative phenotype, supporting improved vascular remodeling and long-term graft performance.

OP-220 - Development of a biomimetic biohybrid cardiac patch for mechanical support and in vitro modulation of remodeling processes

Laura Modica De Mohac

Fondazione Ri.MED, Palermo, Italy

Purpose/Objectives: Background: Congestive heart failure affects ~2% people worldwide and continues to rise, with myocardial infarction (MI) contributing substantially to morbidity and healthcare costs. A key driver of CHF progression is left ventricular (LV) pathological remodeling, characterized by dilation, wall thinning, and altered mechanics, typically assessed by imaging and functional analyses. Current pharmacological (ACE inhibitors) and surgical interventions (e.g., Dor, Batista procedures) fail to fully prevent disease progression. Moreover, available cardiac patches: synthetic (Impra ePTFE), pericardial (CardioCel), or ECM-based (CorPatch) do not adequately replicate native myocardial structure and mechanics and fail to mitigate LV dilation. **Objective:** We hypothesize that a biodegradable biohybrid cardiac patch replicating native anisotropic mechanics and incorporating extracellular matrix (ECM) cues can mitigate pathological remodeling by providing mechanical support and promoting cell infiltration and tissue regeneration.

Methodology: Bilayer (BL) patches were fabricated via modified two-stream electrospinning using poly(ester-carbonate urethane) urea (PECUU) and decellularized porcine cardiac ECM. Losartan-loaded PLGA microparticles (BL-MP) were incorporated to modulate remodeling. Patches were characterized by scanning electron microscopy, thickness measurements, and mechanical testing under physiological loading. Degradation and drug release were evaluated under accelerated conditions and via Franz diffusion cells. Cell infiltration potential was assessed using C2C12 cells, analyzing viability, proliferation, and scaffold penetration.

Results: Patches exhibited high thickness homogeneity (~390±7.39μm), minimizing stress concentrations. Microstructural analysis showed aligned fibrous networks with orientation indices of 0.65 (ECM-side) and 0.77 (polymer-side). Mechanical testing confirmed anisotropy (AR 2.18±0.48), closely matching native LV tissue. ECM integration enhanced cell viability, proliferation, and infiltration. Sustained losartan release was achieved over 14 days.

Conclusion/Significance: The biohybrid patch reproduces native LV anisotropy and supports cell infiltration through ECM integration while enabling localized drug delivery. This combined mechanical and biological functionality shows strong potential to mitigate post-MI remodeling. Future work will focus on validation in a chronic MI swine model.

OP-221 - Mechanical History and Substrate Stiffness Shape Integrin-Mediated Endothelial Cell Behavior on Bioactive Hydrogels

Abbey Nkansah, Aashee Budhwani, Elizabeth Cosgriff-Hernandez

The University of Texas at Austin, Austin, United States of America

Purpose/Objectives: We have developed an integrin-targeting hydrogel coating to enhance post-implant endothelialization of synthetic vascular grafts using a collagen-mimetic protein that selectively targets α1β1 and α2β1 integrins. Optimizing this hydrogel requires understanding the temporal regulation of integrin expression and its effects on endothelial cell adhesion, migration, and hemostatic phenotype. The objective of this study is to provide a mechanistic framework for understanding time-dependent changes

in cell behavior based on culture conditions towards designing synthetic conduits with appropriate endothelial cell phenotypes.

Methodology: In this study, cell-releasing hydrogels were used to examine how integrin expression and integrin-mediated cell behavior evolve as endothelial cells transition from stiff TCPS culture conditions to soft hydrogels. To model transanastomotic migration, we also evaluated the effects of culture on vessel-mimetic soft substrates followed by re-seeding onto stiff substrates. These differences in integrin expression profiles were then correlated to focal adhesion formation, proliferation and quiescence, migratory behavior, and hemostatic phenotypes to impart relevance to integrin-mediated transanastamotic migration.

Results: Substrate stiffness and culture duration differentially regulated integrin expression and focal adhesion maturation. While $\alpha1\beta1$ expression remained relatively stable across stiffnesses and timepoints, $\alpha2\beta1$ expression demonstrated clear stiffness- and time-dependent trends, suggesting a more prominent role for $\alpha2\beta1$ in endothelial mechanosensing and mechanical memory. Endothelial cells cultured on stiffer hydrogels exhibited enhanced proliferation, increased migration, and more rapid progression toward confluence compared to cells on softer substrates. Across all substrate conditions, endothelial cells transitioned toward a quiescent phenotype within one week, while nitric oxide production remained consistent regardless of substrate stiffness. Together, these findings support the concept that endothelial mechanical memory influences $\alpha2\beta1$-mediated adhesion and downstream endothelial behavior, with important implications for interpreting in vitro endothelialization studies and designing vascular grafts. These mechanosensitive adaptations were associated with enhanced proliferation and migration, followed by progression toward a more quiescent endothelial phenotype over extended culture.

Conclusion/Significance: Overall, these findings highlight the importance of mechanical history and substrate stiffness in shaping integrin-mediated endothelial behavior and provide mechanistic insight into cellular adaptation during transanastomotic migration.

OP-222 - A Humanized, Drug-Inducible Cytokine Secretion Platform (hDIRECT) for Engineering Pro-Survival Endothelial Cells in Peripheral Artery Disease

Ngan Huang[1], Jaesang Kim[1], Carlos Aldrete[2], Xiaojing Gao[2]

[1]*Stanford University, Department of Cardiothoracic Surgery, Stanford, United States of America*
[2]*Stanford University, Chemical Engineering, Stanford, United States of America*

Purpose/Objectives: Cell therapy with pluripotent stem cell-derived endothelial cells (PSC-ECs) is a promising strategy to restore perfusion in peripheral artery disease (PAD), but the survival of transplanted cells is severely limited by the hypoxic, inflammatory ischemic niche. Local, externally tunable delivery of pro-survival (bFGF) and immunomodulatory (IL-10) factors could improve engraftment, yet existing inducible systems are largely non-human and carry immunogenic risk. The objective is to develop hDIRECT (human Drug-Inducible Regulation of Cytokine Therapy), a fully humanized platform in which engineered cytokines are sequestered ("caged") and activated by ER-retained Renin, with the FDA-approved Renin inhibitor Aliskiren serving as an external OFF switch.

Methodology: Caged IL-10 and ER-retained Renin were expressed in HEK293 cells by transient transfection and by stable lentiviral transduction co-expressing mCherry with puromycin selection. Secreted IL-10 activity was quantified using HEK-Blue/SEAP reporter assays with a 4PL calibration, and Aliskiren dose-response, duration-response, and reversibility were characterized. The construct was then delivered to primary human coronary artery endothelial cells (HCAECs) by lentiviral transduction, with efficiency assessed by mCherry imaging and flow cytometry.

Results: Renin-dependent IL-10 activation was confirmed after transient transfection and in stable HEK293 lines ($\sim$57% mCherry+), which secreted 33.2 $\pm$ 1.1 ng/mL of functional IL-10. Aliskiren suppressed secretion dose-dependently (IC50 $\sim$251 nM) in a duration-dependent, reversible manner, requiring continuous dosing to maintain the OFF state. In HCAECs, transduction efficiency increased with viral dose (18–45% at day 3) and reached 65.8 $\pm$ 3.0% after selection. However, IL-10 secretion and Aliskiren responsiveness remained limited, and transduction combined with prolonged culture induced reduced proliferation and an endothelial-to-mesenchymal transition (EndoMT)-like phenotype, indicating that switch sensitivity and phenotypic maintenance should be improved.

Conclusion/Significance: We established a humanized, drug-tunable cytokine secretion platform and demonstrated robust ON/OFF control of IL-10 in HEK293 cells. Ongoing work optimizes switch sensitivity and mitigates transduction-induced EndoMT in primary and PSC-derived ECs, advancing toward an externally drug-controlled "smart" endothelial cell therapy for PAD.

Session 59
Emerging Biofabrication Technologies

11-18-2026 @ 8:00 AM - 9:30 AM

OP-224 - Lux Chaotic (LuCha) (Bio)Printing: A Light and Chaos Driven Platform for Hierarchically Micro-architected Hydrogel Constructs

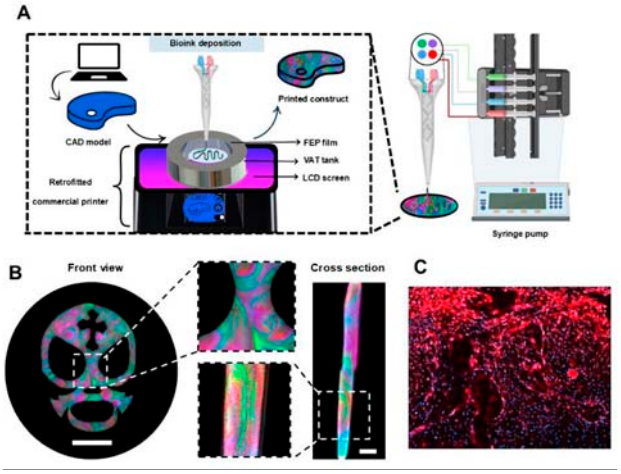
Grissel Trujillo-Desantiago[1,2], Mario Álvarez[2], Victor Sánchez[3], José Romero Orozco[1], Damián Zúñiga-Cárdenas[2]

[1]*Tecnológico de Monterrey, Departamento De Macatrónica, MONTERREY, Mexico*
[2]*Tecnológico de Monterrey, Expedition-femsa, MONTERREY, Mexico*
[3]*Tecnológico de Monterrey, Centro De Biotecnología-femsa, MONTERREY, Mexico*

Purpose/Objectives: Engineering soft materials that simultaneously exhibit defined external geometry and controlled internal microarchitecture remains a central challenge in biofabrication. We introduce Lux Chaotic (LuCha) printing, a fabrication strategy that integrates chaotic advection with light-based photopolymerization to generate hierarchically architected hydrogel constructs in a single-step process.

Methodology: LuCha builds upon chaotic bioprinting principles, where laminar flow through a Kenics static mixer (KSM) deterministically splits and folds input streams into finely multilayered microarchitectures. These structured inks are deposited as droplets or continuous patterns onto a cooled substrate, where their internal organization is preserved by spatially controlled crosslinking via digital light projection (Fig1A). This coupling enables independent yet simultaneous control over microscale architecture and macroscale geometry.

Results: We evaluated the influence of deposition modalities (droplet, spiral, and random) and printhead configurations (varying number of inlets and mixing elements) on structural features. Droplet-based deposition most effectively preserved internal lamellar features and exhibited higher reproducibility than spiral and random deposition. All deposition strategies yielded striation thickness distributions characterized by a high frequency of $\sim$100 μm striations near the theoretical mean, and a long tail of lower-frequency, thicker striations. Increasing mixer complexity (i.e., adding more inlets or static mixing elements) enhanced structural resolution, enabling tunable microarchitectures with controlled length scales. LuCha is compatible with photocrosslinkable GelMA bioinks (5% w/v), enabling the fabrication of cell-laden constructs, and supports multimaterial integration, including the incorporation of fugitive inks to generate internal void channels and surfaces. Time-resolved analyses confirmed efficient removal of sacrificial components, yielding porous, channel-rich constructs that enhance mass transport. Bioprinting experiments with myoblasts demonstrated extended culture (>30 days) with high viability (>95%), guided alignment along microarchitected patterns, and volumetric muscle-like tissue organization facilitated by internal porosity (Fig1C).



Conclusion/Significance: Results establish LuCha printing as a versatile and accessible platform for fabricating hierarchically organized soft materials. Bridging chaotic microstructuring with light-defined shaping, LuCha expands the design space for tissue engineering and advanced functional biomaterials.

OP-225 - Tomographic Volumetric Bioprinting for 3D Organs-on-Chips

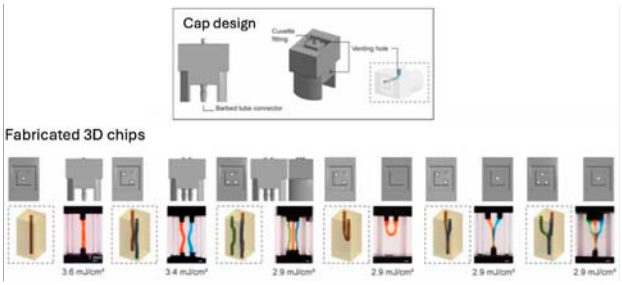
Christophe Moser[1], Riccardo Rizzo[1], Felix Wechsler[1], Viola Sgarminato[2]

[1]*Ecole Polytechnique Fédérale de Lausanne (EPFL), Institute of Electrical And Microengineering (iem), Lausanne, Switzerland*
[2]*Politecnico di Torino, Dipartimento Di Ingegneria Meccanica E Aerospaziale (dimeas), Torino, Italy*

Purpose/Objectives: Tomographic Volumetric Additive Manufacturing (TVAM) is an emerging optical 3D printing technology [1] that fabricates centimeter-scale structures by projecting 2D light patterns into a rotating photosensitive resin. TVAM enables true volumetric fabrication of complex freeform geometries with high speed.This capability is particularly promising for organ-on-chip (OoC) technologies, which are currently limited by soft lithography to rigid and mainly planar or 2.5D architectures. Here, we demonstrate how TVAM can enable soft, fully 3D OoC systems with biomimetic vascular networks and physiologically relevant microenvironments. To address the challenge of printing in complex optical environments, we employ Dr.TVAM,[2] an open-source simulation and optimization framework.

Methodology: We use Dr.TVAM to simulate and optimize volumetric printing inside pre-assembled microfluidic devices. The framework models light propagation through refractive and partially occluding environments to compute optimized projection patterns for accurate 3D fabrication. Structures are printed directly around embedded components such as inlet and outlet interfaces. Dr.TVAM compensates for optical distortions during fabrication. This approach enables the fabrication of enclosed, perfusable microvascular networks inside flat microfluidic platforms compatible with standard microscopy and biological workflows.

Results: Using Dr.TVAM-enabled optimization, we fabricated complex 3D perfusable microfluidic architectures directly inside pre-assembled devices. Overprinting enabled interconnected vascular-like networks around light-occluding inlet/outlet structures while preserving geometric fidelity and fluidic continuity. The fabricated systems demonstrate: embedded perfusable 3D vascular architectures in soft biomaterials, i leakage-free and contamination-free operation within enclosed microfluidic devices, These results highlight the ability of TVAM to create physiologically relevant 3D tissue microarchitectures that are difficult to achieve using conventional soft lithography or layer-based fabrication.



Conclusion/Significance: This work demonstrates that TVAM provides a transformative route toward truly 3D organ-on-chip systems. By overcoming the geometric limitations of conventional microfabrication, TVAM enables soft, biomimetic, and perfusable microphysiological platforms that better reproduce native tissue architecture. Combined with Dr.TVAM and overprinting strategies, this approach enables rapid fabrication within complex microfluidic environments and opens new opportunities for tissue engineering, disease modeling, drug screening, and personalized medicine. [1l] Bernal P. N et al *Volumetric Bioprinting of Complex Living-Tissue Constructs within Seconds,* Advanced Materials, 2019. [2] Wechsler, F. et al *Inverse Rendering for Tomographic Volumetric Additive Manufacturing.* ACM Trans. Graph. 2024

OP-226 - Biofabrication of an in situ hypoxia-delivery scaffold for hyaline cartilage regeneration

Denise Murgia[1], Francesca Romano[1], Riccardo Gottardi[2], Roberto Di Gesù[1]

[1]*Ri.MED Foundation, Musculoskeletal Tissue Engineering (mste) Lab., Palermo, Italy*
[2]*University of Pennsylvania, Philadelphia, United States of America*

Purpose/Objectives: Osteoarthritis (OA) is a debilitating joint condition affecting millions of people worldwide, triggering painful chondral defects (CDs) that ultimately compromise the overarching patients' quality of life. Currently, several reconstructive cartilage techniques (RCTs) (i.e.: matrix-assisted autologous chondrocytes implantation has been developed to overcome the total joint replacement limitations in the treatment of CDs. However, there is no consensus on the effectiveness of RCTs in the long term, as they do not provide adequate pro-regenerative stimuli to ensure complete CDs healing.

Methodology: In this study, we describe the biofabrication of an innovative scaffold capable to promote the CDs healing by delivering pro-regenerative hypoxic cues at the cellular/tissue level, to be used during RCTs. The scaffold is composed of a gelatin methacrylate (GelMA) matrix doped with hypoxic seeds of GelMA functionalized with a fluorinated oxadiazole (GelOXA), which ensures the delivery of hypoxic cues to human articular chondrocytes (hACs) embedded within the scaffold.

Results: We found that the GelMA/GelOXA scaffold preserved hACs viability, maintained their native phenotype, and significantly improved the production of type II collagen. Besides, we observed a reduction in type I and type X collagen, characteristic of unhealthy cartilage. These findings pave the way for the regeneration of healthy, hyaline-like cartilage, by delivering hypoxic cues even under normoxic conditions.

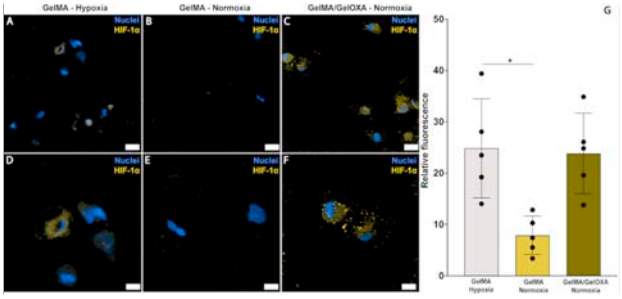


Figure. Expression of HIF-1a, key factor in hypoxia-related cellular response, in differente experimental conditions

Conclusion/Significance: The GelMA/GelOXA scaffold's ability to deliver healing signals directly to the injury site holds great potential for treating OA and related CDs, and has the potential to revolutionize the field of cartilage repair and regenerative medicine

OP-227 - Fabrication of microvessels in high-swelling hydrogels

Rishabh Singh[1], Krish Patel[1], John Slater[2]

[1]*University of Delaware, Biomedical Engineering, Newark, United States of America*
[2]*University of Delaware, Biomedical Engineering And Materials Science And Engineering, Newark, United States of America*

Purpose/Objectives: Successfully integrate functional and perfusable channels within high swelling synthetic hydrogels to serve as a microphysiological model of vascular endothelium.

Methodology: The proteolytically-degradable PEG-diacrylate macromer, PEG-PQ-PEG (PEG-PQ), and the integrin-ligating mono-acrylated macromer, PEG-RGDS (RGDS), used in this study were synthesized as previously described. Hydrogel formulations used in this study contained either 5% weight/volume (w/v) PEGDA or 5% w/v PEG-PQ, 2.1 mM RGDS and were photo-crosslinked using lithium phenyl-2,4,6-trimethylbenzoylphosphinate at 3.0 mg/mL via exposure to broad spectrum UV (wavelength: 365 nm, intensity: 10 mW/cm^2) for 1 min. The human brain microvascular endothelial cell line (hCMEC/D3) was used to form the vascular network. The vascularized hydrogel was cultured under rocker driven flow for up-to seven days before immunofluorescent analysis.

Results: When using conventional confined devices, 5% PEGPQ (high swelling) results in closure of channel after 24 hours and in a decrease in channel diameter in 5% PEGDA (low swelling), but no significant change in diameter of molded channels is observed in both hydrogels when using unconfined devices. We are able to now seed the open channels with endothelial cells and culture them till a robust lumen with low permeability is formed.

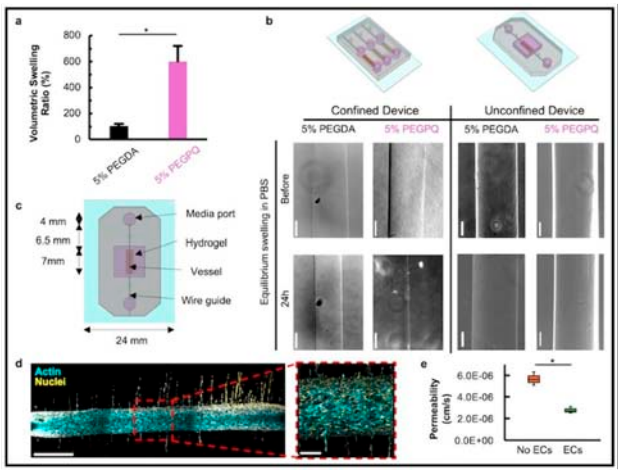


Figure 1. a) Mean volumetric swelling ratio of free-standing gels measured after hydration (*p <0.05 as determined by the Student's t test). b) Images of molded channels immediately after hydration and following equilibrium swelling after 24h using confined and unconfined device respectively (scale bar, 100 μm). c) Schematic depicting the geometry of proposed unconfined device. d) Immunofluorescent staining of microvessel cultured on unconfined device for seven days (scale bar, 500 μm) with inset showing high resolution details of actin fiber alignment (scale bar, 100 μm). e) Quantification of diffusive permeability of vessels with or without ECs using 10 kDa fluorescent dextran (*p <0.05 as determined by the Student's t test).

Conclusion/Significance: We solved the challenge by developing a novel unconfined housing that allows the hydrogel to freely swell upon hydration while maintaining the initial diameter of the molded channel. This bio-fabrication technique opens the possibility to vascularize synthetic hydrogels without compromising on its tunability to enable a wide range of previously inaccessible biomedical applications.

Session 60
Skin, Wound Healing, and Inflammation (General Session) 2

11-18-2026 @ 11:00 AM - 12:30 PM

OP-228 - Interrogating the Impact of Oxygen-Generating Scaffold on Host Cell Remodeling and Immune Cell Infiltration

Cameron Crouse[1], Taylor Lansberry[1], Irayme Labrada[1], Kevin Conklin[1], Aljae Lewis[1], Cherie Stabler[2]

[1]*University of Florida, J. Crayton Pruitt Family Department of Biomedical Engineering, Gainesville, United States of America*
[2]*University of Florida, Diabetes Institute, Gainesville, United States of America*

Purpose/Objectives: Hypoxia dramatically impairs transplanted cellular function and viability, limiting tissue engineering and regenerative medicine outcomes. One approach to address this limitation is the use of oxygen-generating biomaterials (OGBs). In our laboratory, we have created an OGB by encapsulating calcium peroxide within PDMS and 3D-printed it into a macroporous scaffold. While this local oxygen supports the transplanted cells, it is unclear if it alters tissue remodeling, as oxygen tension can be a key parameter in host infiltration and vascularization. To systematically investigate this, we implanted OGB scaffolds and measured their temporal impacts on vascularization via lectin imaging, cellular composition via flow cytometry, and global host responses via histology.

Methodology: OGB scaffolds were generated via reverse casting of polydimethylsiloxane (PDMS, liquid RTV, 4:1 Part A:B) with or without oxygen-generating microbeads (30% volume: volume, 1:1 CaO_2: PDMS) in a sacrificial polyvinyl alcohol mold. OGB and PDMS-only scaffolds were implanted subcutaneously or into the fat pad of C57BL/6 mice and explanted at days 3 and 14.

Results: Flow cytometric analysis of host cell infiltration showed no significant impact of local oxygenation on global immune cell infiltration, vascular cell presence, or on T cell or macrophage infiltration at either time point. The duration of implantation did have an effect, with higher immune cells, T cells, macrophages, and vascular cells observed in the transplant environment on day 14 compared to day 3 ($p = 0.0169$ for vascular cells, $p < 0.0001$ for all other cells) **(Fig. 1A-D)**. Visualization of vascular infiltration revealed patent

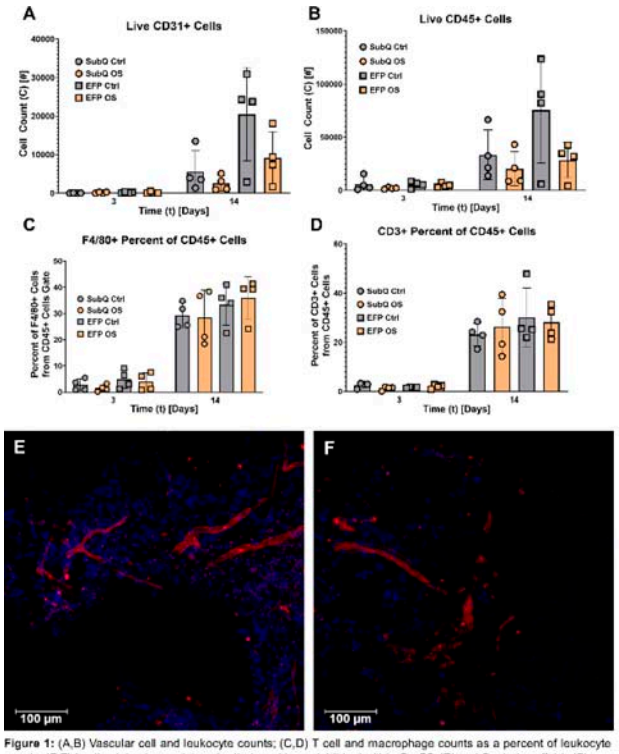


Figure 1: (A,B) Vascular cell and leukocyte counts; (C,D) T cell and macrophage counts as a percent of leukocyte counts; (E,F) Lectin-stained vasculature (red) alongside nuclei (blue) within OxySS (E) and Control scaffolds (F).

vasculature for both OGB and control implants **(Fig. 1E, F)**, indicating robust neovascularization despite supplemental oxygenation. Assessment of histological outcomes is ongoing.

Conclusion/Significance: Characterizing the impacts of local oxygenation on host responses further supports the benefits of OGM in supporting enhanced survival of transplanted cells and tissues. Future work will extend this study to longer time periods to fully capture the temporal effects of these implants.

OP-229 - Mitigating interferon-γ induced inflammation with a bacterial serine protease encapsulated in a polyelectrolyte nanocomplex

Promita Bhattacharjee[1], Pratik Patel[1], Vinaya Gedi[1], Francisco Duarte[1], Kieran Mcgourty[1,2], Sarah Hudson[1,2]

[1]*UNIVERSITY OF LIMERICK, Chemical Science, LIMERICK, Ireland*
[2]*SSPC, Research Ireland's Centre for Pharmaceuticals, Bernal Institute, Limerick, Ireland*

Purpose/Objectives: Inflammatory bowel diseases (IBD), including Crohn's disease and ulcerative colitis, contribute substantially to morbidity in Western populations and are becoming increasingly prevalent in developing regions. This work highlights the potential of enzymatic therapies, such as serine proteases streptococcal C5a peptidase (ScpA), along with simple manufacturable formulations, for the sustainable development of patient-centred drug products to treat inflammatory diseases.

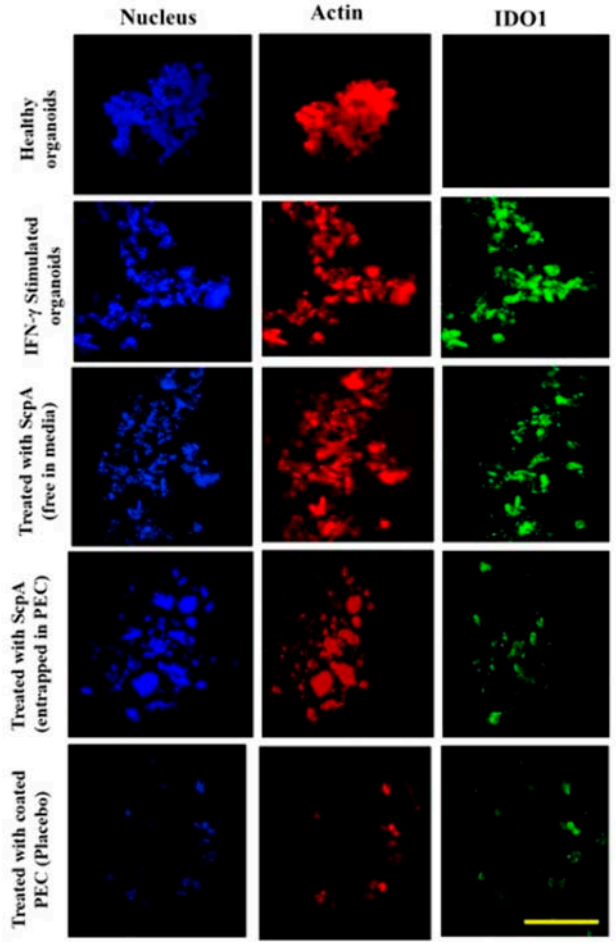


Fig. 1. Expression of inflamed positive (green; expression increased in inflammation: Recombinant Anti-Indoleamine 2, 3-dioxygenase antibody; IDO1, red: actin, blue: nucleus) marker Scale bar=1mm.

Methodology: Anionic polyelectrolyte complex (PECs) comprised of hyaluronic acid and chitosan in an optimum mass mixing ratio, coated with acid resistant pH-dependent polymer, Eudragit S100® were designed to load ScpA, optimizing enzyme encapsulation. Mean hydrodynamic diameter and polydispersity index of PEC dispersions were measured. Association efficiency and loading of ScpA in PECs were determined by using size exclusion chromatography. Proteolysis studies in different condition (gastric and intestinal) were performed to study activity of ScpA to mimic *in vivo* condition. Healthy human intestinal organoids (HIOs) were generated from iPSCs (protocol Stem Cell Technology). Inflamed HIOs were developed by treating healthy HIOs with IFN-γ. ScpA was delivered (free form and from PECs) to inflamed HIOs to restore health. The morphology, barrier function and gene expression of healthy, inflamed, and ScpA treated HIOs were investigated.

Results: Surface charge on the PECs reversed upon coating with Eudragit, as expected, suggesting a coating of negatively polymer on the positively charge PECs. The size of the coated PEC is 765.8nm±9.23 nm. PEC coated with Eudragit®S-100 was found to protect ScpA from degradation by pepsin and to protect the protease in fasted state simulated intestinal fluid. Morphology and integrity of barrier function test revealed that integrity of the cellular barrier in organoids was compromised in samples treated with IFN-γ. Treatment with ScpA, free or associated with the anionic PECs, successfully restored barrier function of organoids. Immunofluorescence (Fig.1) and gene expression analysis of accepted biomarkers of IBD pathogenesis consistently indicated that treatment with ScpA markedly reduced the inflammation in organoids.

Conclusion/Significance: The promising results with ScpA highlight its potential as a valuable addition IBD treatment, warranting further clinical evaluation.

OP-230 - Green injectable self-healing hydrogel from modified pectin and gelatin for chronic wound treatment

Alice Zoso[1], Francesca Tivano[1], Cutietta Giuseppe[1], Pochettino Elisa[1], Sophia Khan[2], Stephan Schandl[3], Santin Matteo[4], Monica Boffito[1], Irene Carmagnola[1], Valeria Chiono[1]

[1]*Politecnico di Torino, Dept. of Mechanical and Aerospace Engineering, Torino, Italy*
[2]*Tissue Click, Brighton, United Kingdom*
[3]*University of Siegen, Siegen, Germany*
[4]*University of Brighton, Brighton, United Kingdom*

Purpose/Objectives: Chronic wounds affect nearly 2% of the global population, impairing quality of life, and representing a major healthcare burden. They are characterized by persistent inflammation, infection, and impaired extracellular matrix remodelling, delaying healing and limiting the efficacy of conventional dressings. Injectable hydrogels can adapt to wound geometries and enable localized therapeutic delivery. Here, we developed a green, self-healing injectable hydrogel composed of oxidized pectin (OPec) and carbohydrazide-modified gelatin (G-CDH), designed for rapid in situ crosslinking and controlled drug release in chronic wound environments.

Methodology: OPec was synthesized by periodate oxidation of citrus pectin (2.5 and 5 mol.% oxidation), while G-CDH was prepared via carbodiimide-mediated coupling. Two hydrogel compositions were selected: OPec_2.5/G-CDH (70:30% w/w) and OPec_5/G-CDH (50:50% w/w). Network structure and release properties were investigated using fluorescein-dextran (4 and 70 kDa), along with water absorption and weight loss properties in phosphate buffered saline (PBS). Injectability through G27–G30 needles was analysed in 3D-printed wound phantoms. Litmus was loaded for real-time pH monitoring, then validated in PBS at pH 5, 7, and 9. Antimicrobial and antioxidant agents were loaded into hydrogels directly or through nanocarriers (e.g., dendrons) and their release was tested. Cytocompatibility was assessed using Human Umbilical Vein Endothelial Cells (HUVECs) and Human Dermal Fibroblasts (HDFs).

Results: OPec_2.5/G-CDH and OPec_5/G-CDH hydrogels exhibited rapid gelation with a crosslinking degree of ~70 mol%. Rheological analysis confirmed shear-thinning behaviour and rapid structural recovery. Dendron loading did not alter the storage modulus G' (~28 Pa and ~20 Pa for OPec_2.5/G-CDH and OPec_5/G-CDH, respectively), while it accelerated the crosslinking kinetics. Injection tests confirmed homogeneous filling of wound phantom channels. Water absorption and weight loss studies showed faster degradation/dissolution of OPec_2.5/G-CDH hydrogel within 14 days, whereas the OPec_5/G-CDH hydrogel remained stable over the same period. Fluorescein dextran diffusion tests showed size-dependent permeability, while litmus-loaded hydrogels enabled real-time pH monitoring through colour changes at pH 5, 7, and 9. Cytocompatibility assays confirmed high cell viability with all cell lines tested. Controlled release of the agents was confirmed.

Conclusion/Significance: OPec/G-CDH hydrogels demonstrated promising physicochemical and biological properties for use as a multifunctional platform for minimally-invasive drug delivery in chronic wound treatment. INJECTHEAL (101177924) is acknowledged.

OP-231 - In silico and In vitro Evaluation of Vitamin C–Loaded Chitosan Nanocarriers for Early Burn Wound Stabilization, Infection Control, and Tissue Repair

David Raguindin[1], Amy Qiao[1], Monique Bion[2], Victor De Souza Lima[2], Ryan Clark[3], Jessica De Novais[2], Ryan Cilsick[1], John Newby[4], Helena Zomer[2]

[1]*Edgewood Junior Senior High School, Science Department, Merritt Island, United States of America*
[2]*University of Florida, Physiological Sciences, Gainesville, United States of America*
[3]*University of Florida, J. Crayton Pruitt Family Department of Biomedical Engineering, Gainesville, United States of America*
[4]*Eastern Florida State College, Melbourne, United States of America*

Purpose/Objectives: Sepsis contributes to over 350,000 deaths annually in the US and millions worldwide. Many cases originate from contaminated burn wounds where infections escalate rapidly, causing dysregulated inflammation and tissue damage. Currently, there is a lack of pre-hospital burn stabilization treatments in developing countries. The objective of this study was to evaluate Vitamin-C and Poloxamer-188 (P188) loaded chitosan nanocarriers for the promotion of human mesenchymal stem cell (MSCs) healing, macrophage immunomodulation, and Pseudomonas aeruginosa (PAO1) biofilm disruption.

Methodology: First, vitamin-C-loaded chitosan nanocarriers were synthesized using ionic gelation and evaluated by dynamic light scattering. Effects of nanocarriers on PAO1 were determined via serial dilution inhibition assay and molecular docking simulations. MSCs were treated with nanocarriers to assess cell viability (MTT) and in-vitro wound healing (scratch assay). Targets for protein and gene expression evaluation were assessed in a human mRNA dataset GSE236713 using GEO2R ($p < 0.05$, $|\log FC| > 1$) and KEGG pathway analysis. Then, pilot ELISA and RT-qPCR were conducted on LPS-stimulated, RAW264.7 macrophage cells to determine potential anti-inflammatory effects.

Results: The nanocarriers measured ~420 nm in diameter, with a polydispersity index of 0.03. Molecular docking indicated P188 disrupts lipid transport in PAO1, increasing bacterial susceptibility. At 1.0 mg/mL, the solution inhibited 73% of PAO1 over 24 hours, reducing the bacteria's ability to form biofilms ($n=3$-4, $p < 0.001$). Treatment of MSCs with nanocarriers was not cytotoxic ($n=4$, $p < 0.001$) and in vitro wounds closed 88% vs 19% in non-treated controls ($n=12$, $p < 0.001$) after 24h. In silico analysis revealed TNF and related genes as central drivers of the sepsis inflammatory response; then, protein and gene expression analysis indicated that nanocarriers dampened inflammatory pathways, including TNF-α and PTGS2, suggesting a possible role in immune modulation.

Conclusion/Significance: This multi-action treatment reduces cellular damage and biofilm formation, with the potential for bridging the critical gap in care between the emergency site and the hospital. By developing an affordable, fast-acting antimicrobial and wound-healing nanocarrier solution, the treatment will have strong potential for applications in low-resource settings.

Session 61
Challenges in Clinical Applications of Cancer Organoids

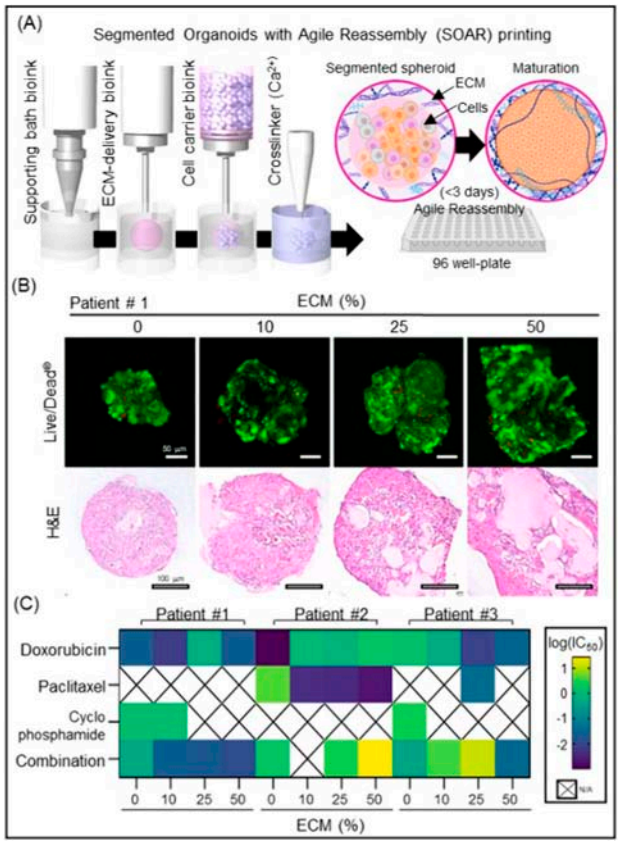
11-18-2026 @ 11:00 AM - 12:30 PM

OP-233 - Segmented Organoid Reassembly for Stiffness-Dependent Drug Response Stratification in Patient-Derived Breast Cancer Models

Wonwoo Jeong[1], Dongju Kim[2], Nadeem Wajih[1], Hyun-Wook Kang[3], Marissa Howard-Mcnatt[4], Konstantinos Ioannis Votanopoulos[4], Shay Soker[1], Sang Jin Lee[1]

[1]*Wake Forest Institute for Regenerative Medicine, Winston-Salem, United States of America*
[2]*The Catholic University of Korea, Department of Surgery, Daejeon St. Mary's Hospital, Daejeon, Korea, Republic of*
[3]*Ulsan National Institute of Science and Technology, Ulju-gun, Korea, Republic of*
[4]*Wake Forest Baptist Medical Center, Winston-Salem, United States of America*

Purpose/Objectives: Clinical translation of patient-derived cancer organoids is limited by variable biopsy-derived cell yield, slow organoid formation, and inconsistent fabrication methods for ex vivo drug testing. In addition, biopsy processing and enzymatic dissociation can disrupt native basement membrane (BM)-associated extracellular matrix (ECM) structures and cell-ECM interactions, removing critical tumor microenvironment (TME) cues that regulate tumor stiffness, aggressiveness, and therapeutic response. Here, we



developed Segmented Organoids with Agile Reassembly (SOAR) printing as a 96-well platform for BM stiffness-guided fabrication and therapeutic stratification of patient-derived breast cancer organoids.

Methodology: MDA-MB-231 spheroids were used to optimize SOAR printing parameters, including the alginate-based supporting bath bioink, cell-carrier bioink, and Matrigel-based matrix bioink. After establishing reproducible spheroid formation and cell-matrix co-localization, patient-derived breast cancer cells were fabricated into organoids using the optimized SOAR printing. Matrigel concentration was adjusted as a biofabrication strategy to tune BM-associated ECM stiffness. Organoids were evaluated by morphology, viability, histology, cytokeratin 14/cytokeratin 19 organization, stiffness-associated matrix remodeling, and drug-response testing. Doxorubicin, paclitaxel, cyclophosphamide, and doxorubicin plus paclitaxel were tested using dose-response analysis, half-maximal inhibitory concentration (IC_{50}), and integrated viability-drug exposure (IVDE).

Results: MDA-MB-231 spheroid optimization confirmed controllable spheroid formation, reproducible cell-matrix co-localization, and consistent printing in a 96-well format (**Fig.A**). Increasing BM-associated ECM stiffness reduced spheroid sensitivity to tested chemotherapies, supporting matrix-dependent drug-response testing. Using these parameters, SOAR printing generated patient-derived breast cancer organoids within 7 days. Organoids retained epithelial organization, with CK14-positive basal-like cells localized mainly at the periphery and CK19-positive luminal epithelial cells distributed internally, while matrix tuning induced patient-dependent desmoplasia-like morphology (**Fig.B**). Drug testing revealed patient-specific response stratification (**Fig.C**). Patient #2 showed increased resistance across all tested drugs under higher stiffness conditions, including a 1.71-fold increase in IVDE for doxorubicin. In contrast, Patient #3 showed increased doxorubicin sensitivity but reduced response to combination therapy, with a 1.91-fold increase in IVDE.

Conclusion/Significance: SOAR printing provides a standardized and scalable strategy to fabricate patient-derived breast cancer organoids while reconstructing BM-associated ECM stiffness lost during biopsy processing and cell isolation. By integrating BM-mimetic matrix tuning with quantitative drug-response metrics, this platform supports clinically relevant tumor modeling and ex vivo therapeutic stratification for personalized oncology screening.

OP-234 - Regulatory perspectives on clinical applications for cancer organoids

Steven Bauer

Wake Forest Institute for Regenerative Medicine, Regulatory Science Affairs, Winston-Salem, United States of America

Purpose/Objectives: This talk will summarize regulatory perspectives on use of cancer organoids for clinical applications. The talk will familiarize audience members with different possible mechanisms of regulatory oversight that can be pursued by stakeholders who are developing tumor organoid models for drug screening, for drug sensitivity testing, and for other preclinical or non-clinical research. Mechanisms for interaction with the FDA to obtain FDA input or to engage in FDA approval pathways will be discussed.

Methodology: Applicable regulatory pathways relevant to FDA were researched in available guidance documents and through presentation materials and discussions with current and recent FDA employees.

Results: Ex-vivo clinical diagnostic organoid testing for specific patients falls under the category of a Laboratory Determined test and remains primarily under the oversight of the Centers for Medicare & Medicaid Services (CMS) through Clinical Laboratory Improvement Amendments (CLIA) certification. If a stakeholder is interested in commercialization of drug sensitivity testing, several pathways could be utilized including development of a tumor organoid model as a companion diagnostic for a tumor treatment drug or biologic. A stakeholder could also develop an organoid drug sensitivity testing application as a classical diagnostic device under various FDA pathways such as an IDE or PMA. If a stakeholder was interested in developing a tumor organoid system as a New Alternative Method to replace animal testing, various pathways for FDA oversight such as the ISTAND program for Drug Development Tools are available. For all of these pathways, fitness for purpose and context of use are important considerations for establishing the suitability, reproducibility, and regulatory acceptance of a particular tumor organoid model.

Conclusion/Significance: Tumor organoids have tremendous potential to refine cancer treatment, to speed development of novel cancer therapies, and to replace or refine animal testing during drug development. Increased stakeholder understanding of regulatory perspectives and timely engagement with regulatory authorities will facilitate development and use of these models, allowing stakeholders to harness their potential as efficiently as possible.

OP-237 - Bioprinted Bladder Cancer Organoids for Predicting Chemotherapy Response and Novel Drug Screening

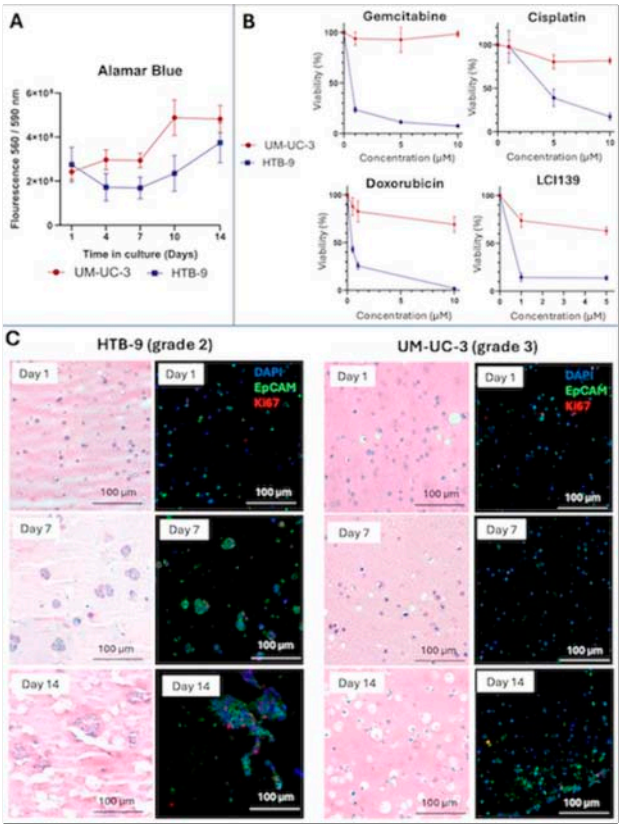
Randall Bissette[1,2], Zachary Congress[2], Gemma Nomdedeu-Sancho[2], Nadeem Wajih[2], Krishnaiah Maddeboina[3], Shay Soker[2]

[1]*Wake Forest University School of Medicine, Department of Urology, Winston-Salem, United States of America*
[2]*Wake Forest University School of Medicine, Wake Forest Institute For Regenerative Medicine, Winston-Salem, United States of America*
[3]*Atrium Health Levine Cancer Center, Charlotte, United States of America*

Purpose/Objectives: Bladder cancer is the fifth most common cancer nationwide, causing 17,000 deaths annually. Its genetic heterogeneity causes treatment resistance with low response rates. Organoids better replicate tumor microenvironments compared to 2D culture, enabling improvement in drug development and screening. We generated bioprinted gelMA-based bladder cancer organoids to model muscle-invasive bladder cancer using cell lines of different grades.

Methodology: HTB-9 (grade 2) and UM-UC-3 (grade 3) bladder cancer cells were resuspended in 8% GelMA-based hydrogel (bioink) at a density of 10^6 cells/mL, and in 10μL drops were crosslinked by UV exposure to form the organoids. Organoids were treated with cisplatin (1-10μM), doxorubicin, (0.5-10 μM), gemcitabine (1-10 μM), and a small-molecule inhibitor LCI39 (1-5 μM) for 72 hours. Cell viability was determined by Alamar blue assay. H&E and immunostaining for EpCAM, and Ki67 were performed to assess cellular organization and demonstrate proliferation patterns of cells within the organoids.

Results: Different grades of bladder cancer cells showed distinct proliferation dynamics and progression markers within the organoids. Untreated Grade 2 cells demonstrated early viability loss with late proliferation. Histologically they showed decreasing cell density during early culture, followed by later growth of cell clusters with concentrated proliferation markers. In contrast, grade 3 cells demonstrated minimal loss of viability on Alamar blue. Histologically, they showed negligible loss of cell density and did not form clusters. Chemotherapies revealed a grade-dependent tumor response (n=5) with grade 2 versus grade 3 viability reduction as follows: Cisplatin, 2% versus 2% at 1μM ($p>0.05$), 61% versus 20% at 5μM ($p<0.001$), 83% versus 18% at 10μM ($p<0.0001$); Doxorubicin, 57% versus 12% at 0.5μM ($p<0.001$), 74% versus 17% at 1μM ($p<0.001$), 98% versus 31% at 10μM ($p<0.0001$); Gemcitabine, 76% versus 6% at 1μM ($p<0.0001$), 89% versus 7% at 5μM ($p<0.001$), 93% versus 1% at 10μM ($p<0.0001$); LCI139, 85% versus 26% at 1μM ($p<0.0001$), 86% versus 37% at 5μM ($p<0.0001$). **Figures. 1.** Untreated viability. **2.** Chemotherapy responses. **3.** H&E and IHC



Conclusion/Significance: Bioprinting of tumor organoids represents a reproducible and consistent technology for testing and response prediction of anti-cancer drugs that can be adapted to different grades and sets groundwork for strategies to improve patient outcomes.

Session 62
Gene Editing for Tissue Engineering and Regenerative Medicine

11-18-2026 @ 11:00 AM - 12:30 PM

OP-238 - CRISPR Based Upregulation of Transcription Factors in Goat BMSC for Temporomandibular Joint Regeneration

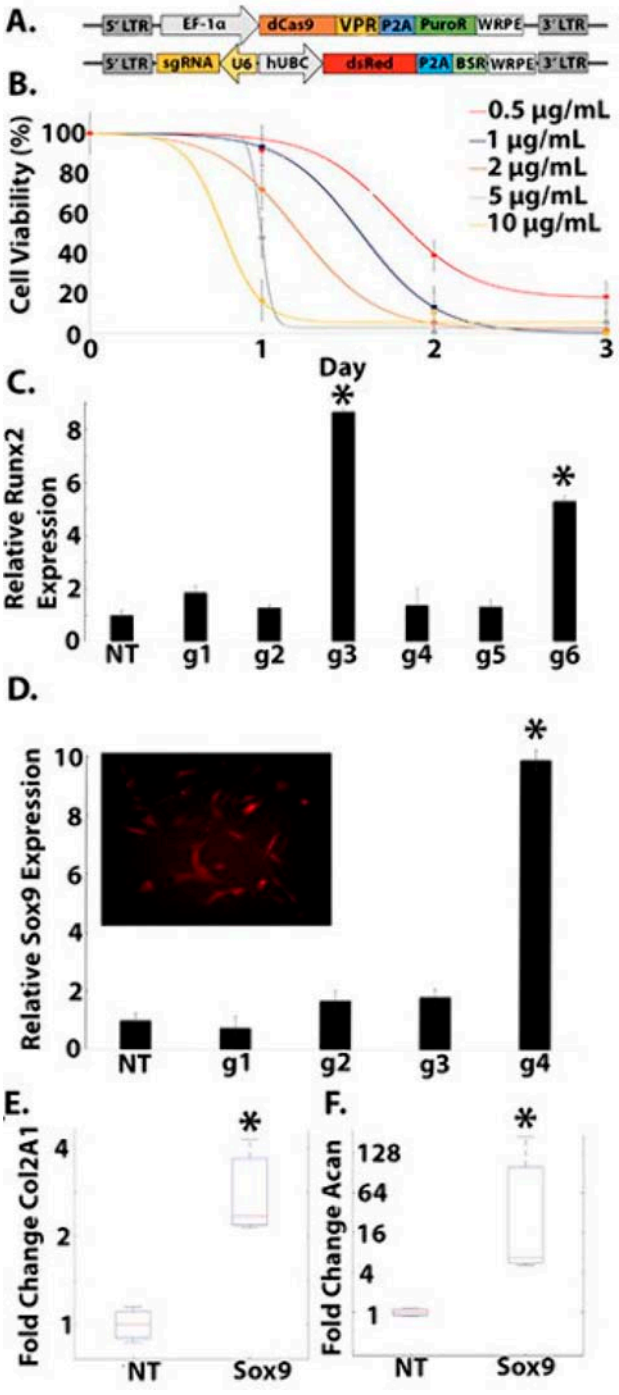
Joshua Stover, Alejandro Almarza

University of Pittsburgh, Pittsburgh, United States of America

Purpose/Objectives: Temporomandibular joint (TMJ) disorders (TMDs) are the second most common musculoskeletal pain disorder with greater than 25% of cases requiring surgical intervention. Currently, no FDA approved allograft alternatives to total joint replacement exist. Here, we investigate CRISPR epigneome editing of goat BMSCs as a TMJ regeneration strategy

Methodology: First, CRISPR epigenome editing constructs that express 1) dCas9-VPR-PuroR or 2) gRNAs targeting the Runx2 or Sox9 promoter or a non-target gRNA were created (**Figure 1A**) and lentivral vectors produced. Next, puromycin dosage for VPR expressing cells selection was determined by goat BMSCs culture in puromycin supplemented media and cell viability measurement. Gene expression of Sox9 and Runx2 was determined via RT-qPCR of BMSCs 7 days after co-transduction with VPR and gRNA lentiviral vectors. In separate experiments, expression of Col2A1 and ACAN were measured via RT-qPCR 7 days after Sox9 lentiviral vector transduction.

Results: 1 μg/mL was demonstrated to be the minimum effective puromycin dose for BMSCs selection (**Figure 1B**). Transduction efficiency of BMSC with gRNA vectors was high(90%, **Figure 1D inset**). BMSCs transduced with gRNAs targeting the Runx2 promotor region exhibited significantly higher expression ($p<0.05$) of Runx2 when compared to nontarget (NT) controls, with guide g3 exhibiting the highest upregulation of Runx2 expression (8.68 ± 0.17 fold) (**Figure 1C**). Similarly, BMSCs transduced with gRNAs targeting the Sox9 promotor region exhibited significantly higher expression ($p<0.05$) of Sox9, when compared to NT controls (**Figure 1D**). BSMCs transduced with guide g4 exhibited the highest upregulation of Sox9 expression(10.27 ± 0.34 fold). In separate experiments, BMSCs transduced with Sox9 g4 exhibited significant upregulationof Col2A1(**Figure 1E**) and ACAN (**Figure 1F**). **Figure 1. A).** Vector map of dCAS9-VPR-PuroR (top) and sgRNA-dsRed lentiviral vectors (bottom). **B).** Goat BMSC puromycin kill curve. Epigenome editing of BMSCs upregulates **C).** Runx2 and **D).** Sox9 expression. **Inset:** BMSCs expressing gRNA vectors. Epigenome editing of Sox9 upregules **E).** Col2A1 and **F).** ACAN expression. *=$p<0.05$ compare to NT.



Conclusion/Significance: These results demonstrate that CRISPR epigenome editing can be utilized to upregulate expression of key

transcription factors that regulate BMSC osteogenic and chondrogenic differentiation and suggests this approach may be utilized in therapeutic strategies for TMJ regeneration.

OP-239 - ZNF865 (BLST) CRISPR Gene Modulation Regulates DNA Repair Pathways and Senescence and Promotes Recovery from Induced DNA Damage

Jonah Holbrook[1], Christian Lewis[1], Hunter Levis[2], Brian Diekman[3], Robby Bowles[1]

[1]*University of Utah, Biomedical Engineering, Salt Lake City, United States of America*
[2]*University of Pennsylvania, Orthopedics, Philadelphia, United States of America*
[3]*University of North Carolina, Chapel Hill, Lampe Joint Department of Biomedical Engineering, Durham, United States of America*

Purpose/Objectives: DNA damage accumulation contributes to aging and degenerative diseases through endogenous and exogenous stressors. Our lab has recently shown that human nucleus pulposus cells (hNPCs) from degenerative discs display elevated DNA damage and senescence. Because cellular senescence is closely linked to DNA repair dysfunction, we investigated the role of ZNF865 (BLST) in DNA repair pathways, demonstrating that CRISPRa of BLST rescues degenerative cells from a senescent state and returns DNA damage levels to a healthy baseline. Further, we demonstrate BLST's ability to protect from low-pH induced DNA damage, highlighting BLST's potential as both a preventative and regenerative therapeutic for age-related diseases.

Methodology: Human IVD samples were obtained from deidentified trauma (n=5) or microdiscectomy patients (n=8). RNA sequencing was performed following CRISPRa-mediated BLST upregulation or non-target control treatment. Alkaline comet assays quantified DNA damage in healthy and degenerative hNPCs. Additional healthy hNPCs were transduced with a lentiviral BLST transgenic vector and cultured in media ranging from physiologic to acidic pH. DNA damage and cell proliferation were assessed across treatment groups.

Results: RNA sequencing identified senescence and DNA repair mechanisms as significantly differentially expressed pathways. Baseline levels of DNA damage are significantly elevated in degenerative hNPCs relative to healthy. CRISPRa BLST upregulation in degenerative hNPCs shows significantly decreased levels of DNA damage and senescent staining relative to non-target control, and no significant differences relative to healthy. Unmodified hNPCs cultured in low pH media showed a significant increase in DNA damage and decrease in proliferation ($p<.05$). Cells treated with the EFS-BLST ZNF865 transgenic vector showed no significant differences in DNA damage and proliferation across pH cultures.

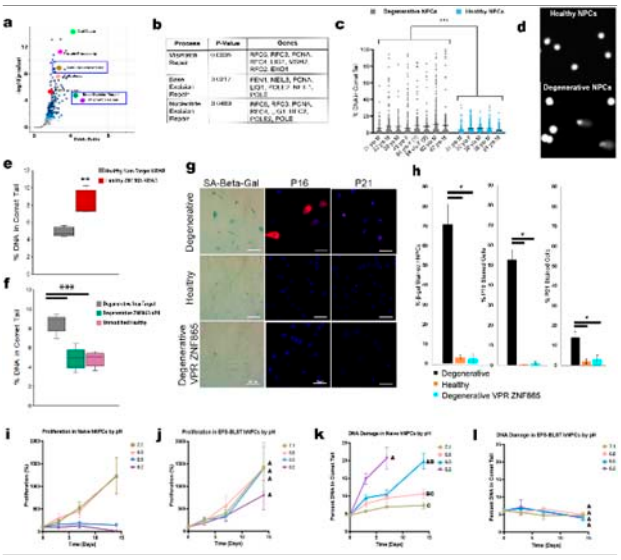


Figure 1. ZNF865 Regulates Cell Senescence and DNA Repair and Promotes Recovery from Induced DNA Damage.

Conclusion/Significance: This work demonstrates that CRISPRa BLST upregulation reverses senescence and returns degenerative hNP cells to healthy baseline levels of DNA damage. Additionally, BLST upregulation protects from DNA damage accumulation and proliferative decreases in hNPCs in low pH. Overall, this research elucidates BLST's involvement in DNA damage pathways and suggests that BLST upregulation could be used as a regenerative therapy for degenerative disc disease and other conditions related to senescence and DNA damage.

OP-241 - CRISPRa and LNP mRNA Delivery of ZNF865 (BLST) Regulates Cell Cycle, Proliferation, and ECM Deposition

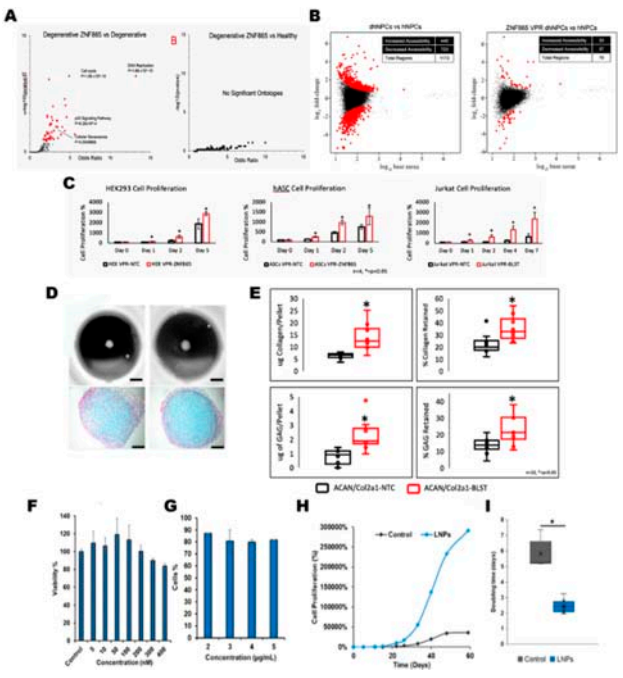
Jonah Holbrook[1], Hunter Levis[2], Cansu Tunc[3], Christian Lewis[1], Jake Polaski[4], Jay Gertz[4], Hamid Ghandehari[3], Robby Bowles[1]

[1]*University of Utah, Biomedical Engineering, Salt Lake City, United States of America*
[2]*University of Pennsylvania, Orthopedics, Philadelphia, United States of America*
[3]*University of Utah, Molecular Pharmaceutics, Salt Lake City, United States of America*
[4]*University of Utah, Huntsman Cancer Institute, Salt Lake City, United States of America*

Purpose/Objectives: Low back pain is the world's leading cause of years lived with disability, and as such, creates a tremendous economic burden of over $100 billion in the United States annually. The leading cause of low back pain is degenerative disc disease (DDD), accounting for 40% of all instances. The gene ZNF865 (BLST) has recently been identified by our lab as a regulator of cell cycle and senescence with involvement in intervertebral disc degeneration; Here, we investigate CRISPRa and LNP mRNA delivery of BLST to increase cell proliferative capacity and ECM deposition and provide insight into its use as a potential regenerative therapeutic for DDD.

Methodology: Human IVD samples were obtained from deidentified trauma (n=5) or microdiscectomy patients (n=8) and nucleus pulposus (hNP) cells were isolated. RNA sequencing and ATAC sequencing were performed following CRISPRa-mediated BLST upregulation or non-target control treatment. Cell lines with CRISPRa upregulation of ACAN and Col2a1 with and without additional ZNF865 upregulation were developed. Cells were pelleted and gross size, collagen, and aggrecan deposition were quantified. A LNP encapsulating BLST mRNA was developed and efficiency, viability, and resulting cell proliferation were quantified.

Results: (a) RNA sequencing identified senescence and cell cycle as significantly differentially expressed pathways in CRISPRa BLST



upregulated hNP cells, while no significant gene ontologies were observed between CRISPRa BLST and healthy hNP cells. **(b)** ATAC sequencing demonstrated a 94% reduction in differential chromatin sites when comparing CRISPRa BLST to degenerative vs. healthy hNP cells. **(c)** Various cell lines treated with CRISPRa BLST upregulation resulted in significant increases in cell proliferation. **(d,e)** CRISPRa BLST upregulation yielded significantly increased aggrecan and collagen II production in pellet cultures. **(f)** Viability, **(g)** EGFP-positive cell percentage, **(h)** proliferation rates, and **(i)** doubling time of human degenerative hNP cells with LNP treatment. Cells treated with BLST mRNA LNP demonstrate significant increases in proliferation rate.

Conclusion/Significance: This work demonstrates that CRISPRa and LNP mRNA BLST upregulation return degenerative hNP cells to a healthy state, as characterized by RNASeq and ATAC Seq. Overall, this research elucidates BLST's ability to increase ECM deposition and cell proliferation, highlighting its potential use as a regenerative therapeutic for DDD.

Session 63
Stem Cell Signaling in Tissue Engineering and Regenerative Medicine: From In Vitro to In Vivo

11-18-2026 @ 11:00 AM - 12:30 PM

OP-244 - Immunosuppressive Characteristics of Placental-Derived Stem Cells

Bita Nickkholgh[1], Tiana Stewart[1], Courtney Campagna[2], Jennie Smith[1], Elisabeth Willard[1], Mitchell Stockinger[1], Anthony Atala[2], Steven Bauer[3], Stephen Sawyer[2]

[1]*Wake Forest Institute for Regenerative Medicine, Translational Core, Winston-Salem, United States of America*
[2]*Wake Forest Institute for Regenerative Medicine, Winston Salem, United States of America*
[3]*Wake Forest Institute for Regenerative Medicine, Regulatory Science Affairs, Winston-Salem, United States of America*

Purpose/Objectives: Placental-derived stem cells (PLSCs) represent a promising cell source for regenerative medicine due to their multipotency and potential immunomodulatory properties. Similar to mesenchymal stem cells (MSCs), PLSCs are hypothesized to suppress lymphocyte proliferation and reduce inflammatory cytokine activation, suggesting their potential applications in immune-mediated disorders, transplantation, and tissue repair. The objective of this study is to quantify the immunosuppressive properties of PLSCs and benchmark their potency against bone marrow-derived MSCs and five FDA-approved immunosuppressive drugs: Dexamethasone, Cyclosporine, Tacrolimus, Rapamycin, and Mycophenolic Acid.

Methodology: PLSCs were isolated from full-term placentas and enriched for CD117 expression using MACSQuant® TYTO® (Miltenyi Biotec) cell sorting. Sorted cell populations were expanded and cryopreserved to establish both master and working cell banks. Immunomodulatory effects were assessed using mixed lymphocyte reaction (MLR) assays in one- and two-way formats. Peripheral blood mononuclear cells (PBMNCs) from unrelated donors were co-cultured with PLSCs, bone marrow-derived MSCs, or immunosuppressive drugs. Viability, proliferation, and proinflammatory cytokines (IFN-γ, TNF-α) were quantified by flow cytometry.

Results: MLR assays demonstrated that PLSCs exhibited immunosuppressive effects comparable to MSCs. Inhibition of proinflammatory cytokine expression was similar between groups, with 28.6% inhibition observed for PLSCs and 28.2% for MSCs, with no significant difference between the two cell types. In addition, preliminary dose-response studies demonstrated that a ratio of 1 PLSC to 20 PBMNCs was sufficient to significantly suppress lymphocyte proliferation. Ongoing studies are further evaluating the dose-dependent effects of PLSCs on CD4+ and CD8+ peripheral blood mononuclear cell proliferation and cytokine expression. These effects are being benchmarked against serial dilution of the selected immunosuppressive drugs to further characterize the relative potency of PLSC-mediated immunosuppression.

Conclusion/Significance: These findings indicate that PLSCs exhibit immunosuppressive properties comparable to MSCs, supporting their potential as a safe, allogenic cell source for regenerative medicine and immune-modulatory therapeutic applications.

Session 64
Clinical and Engineering Perspectives for Using Stem Cells to Grow New Vessels

11-18-2026 @ 11:00 AM - 12:30 PM

OP-248 - Investigating the Pro-angiogenic Effects of MSCs on HUVECs in 2D and 3D Environments

Rabina Lamichhane, Emma Barna, Ge Zhang

The University of Akron, Department of Biomedical Engineering, Akron, United States of America

Purpose/Objectives: Pre-vascularization of engineered constructs through endothelial–stromal cell co-culture enhances vascular network formation, improving post-implantation cell survival and long-term functionality for cardiac repair. Human Mesenchymal Stem Cells (hMSCs) possess pro-angiogenic potential through paracrine-mediated regulation of endothelial cell (EC) migration, proliferation, stabilization, and vascular maturation. However, the optimal conditions for hMSC/HUVEC (Human Umbilical Vein Endothelial Cells) co-cultures, including cell ratio, cell seeding order and culture conditions remain poorly established. This study investigates these conditions through direct contact hMSC/HUVEC co-culture in 2D and 3D spheroid models and evaluate the role of hMSCs in promoting endothelial angiogenesis and vasculogenic network formation in vitro.

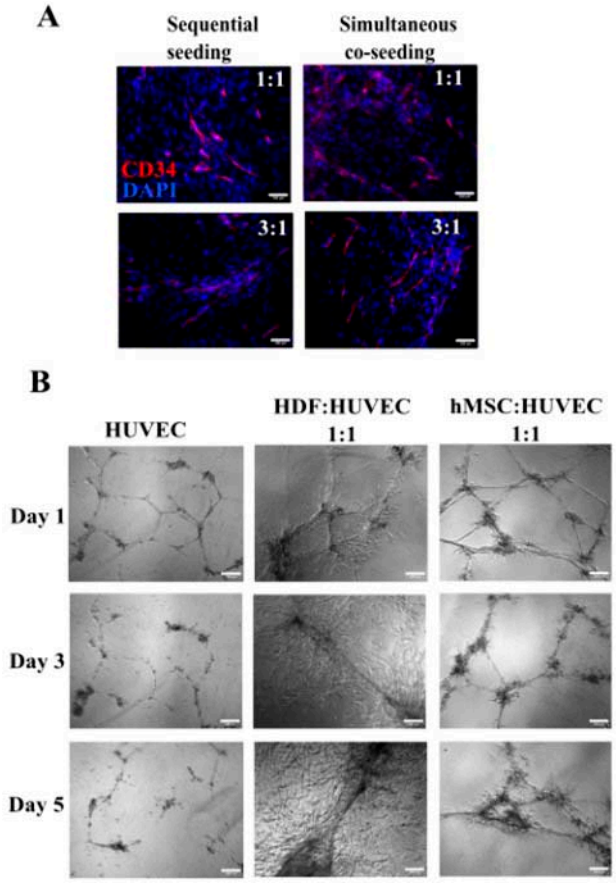


Figure 1. A) CD34 staining performed on hMSC/HUVEC co-culture seeded on tissue culture plate without Matrigel **B)** Brightfield images of HUVEC network on Matrigel after addition of HDF or hMSCs, Scale bar= 100μm(A), 200μm(B)

Methodology: HUVEC/hMSC co-cultures, alongside Human Dermal Fibroblasts (HDF/HUVEC) co-culture, were evaluated in Matrigel-coated or non-coated wells as mixed cell suspensions or spheroids at varying cell ratios and seeding orders to observe the network formation. Additionally, hMSCs were added to pre-formed

HUVEC networks on Matrigel to evaluate the influence of supporting cell incorporation on network stabilization. Tubular network formation was assessed by CD34 immunostaining. Spheroid diameter and sprouting behavior were quantitatively analyzed, while endothelial sprouting was characterized by von Willebrand factor (vWF) immunostaining and confocal microscopy.

Results: Under non-Matrigel condition, hMSC/HUVEC formed longer endothelial networks when hMSC proportion was higher across sequential and simultaneous co-seeding conditions (**Figure 1**). In 3D culture, hMSC/HUVEC spheroids displayed dense and radial interconnected sprouting. HUVEC networks remained stable when hMSCs at same proportion were introduced to the network following 24 h of initial network formation.

Conclusion/Significance: Distinct differences in endothelial network formation and sprouting behavior were observed between fibroblast/HUVEC and hMSC/HUVEC co-cultures under both 2D and 3D conditions. Heterocellular spheroids composed of HUVECs, and stromal support cells were successfully fabricated. Ongoing studies are focused on elucidating hMSC–HUVEC crosstalk within vascular networks and evaluating long-term network stability. Insights gained from this work may contribute to improved vascular network maturation, lumen formation, and functional vascularization strategies for cardiac tissue engineering and repair.

OP-250 - In Vitro Extended Culture for Vascular Network Formation within 3D Printed Scaffolds

Kevin Conklin[1], Robert Accolla[1], Cherie Stabler[2]

[1]*University of Florida, J. Crayton Pruitt Family Department of Biomedical Engineering, Gainesville, United States of America*
[2]*University of Florida, J Crayton Pruitt Family Department of Biomedical Engineering, Gainesville, United States of America*

Purpose/Objectives: Engineered vascular beds are a potential approach to scale engineered tissues, fabricated through the self-assembly of vascular cells within a hydrogel to form an interconnected 3D vessel network. Their clinical use is hindered by 1) substantial hydrogel compaction during the remodeling process, causing network collapse and reduction in scale, and 2) the fragility of the hydrogel, limiting transferability. Our lab has previously developed a 3D printed PDMS scaffold which has mitigated these issues and has been shown to support early network formation. As fully connected vascular networks take several weeks to develop and that prolonged culture enhances vessel perfusion after implantation, we sought to utilize the scaffold to generate mature vessel networks over a 3-week period.

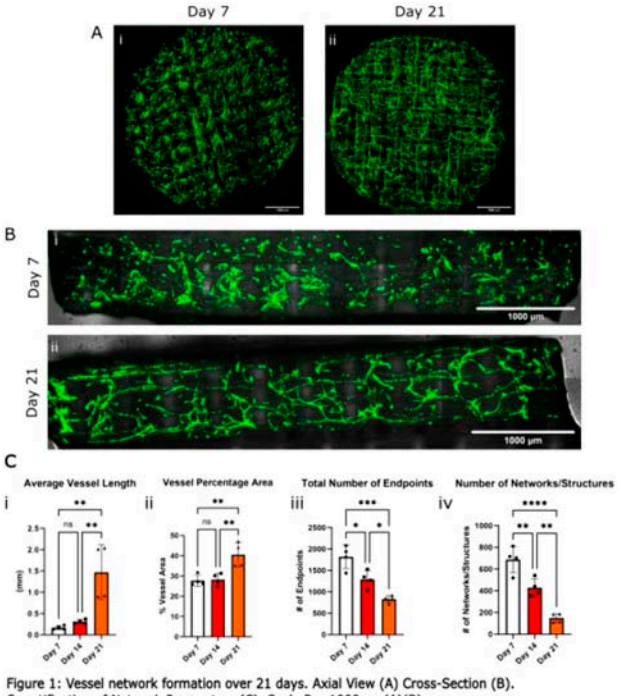


Figure 1: Vessel network formation over 21 days. Axial View (A) Cross-Section (B). Quantification of Network Parameters (C) Scale Bar 1000um (A)(B)

Methodology: A PDMS (Momentive PDMS, 4:1; Part A:B) mixture was loaded into a sacrificial 3D printed PVA mold, where a reverse cast method was used to fabricate the 3D printed master scaffold, and a biopsy punch used to fabricate 5mm diameter scaffolds. A 1:1 ratio of GFP-HUVECs/NHLFs at 3.0 x 10^6 ECs/mL were suspended in fibrin gel, seeded into the scaffolds, and cultured for 7, 14, and 21 days. Fixed scaffolds were imaged on their axial plane and cross-sections. Image stacks were z-projected to create 2D representative images and analyzed with Angiotool and a custom Matlab script.

Results: Connected networks developed over 21 days, extending full scaffold length and thickness (Fig 1 A-B). Analysis of the axial plane scaffold images showed significantly different increases in average vessel length and vessel percentage area, and significantly different decreases in number of endpoints and networks/structures, on day 21 compared to both day 7 and 14 (Fig 1C). Figure 1: Vessel Network Formation over 21 days.

Conclusion/Significance: We have demonstrated that the PDMS scaffold enables the development of clinically scalable, 3D interconnected vascular networks by mitigating hydrogel compaction and supporting extended culture. This platform enables vascular bed formation capable of supporting larger tissue constructs, overcoming limitations of thin or sheet-like networks that require stacking to achieve comparable thickness. Together, this platform advances vascular tissue engineering strategies for functionally scalable constructs for regenerative medicine.

OP-251 - Beyond Diffusion: Why Flap-Scale Tissue Engineering Requires Microsurgical Vascular Anastomoses

Ramon Llull[1,2], Adam Katz[2]

[1]*Wake Forest University, Plastic Surgery, Winston-Salem, United States of America*
[2]*Atrium Health Wake Forest Baptist, Department of Plastic And Reconstructive Surgery, Winston-Salem, United States of America*

Purpose/Objectives: Large-volume engineered tissues remain constrained by a central translational problem: the inability to establish rapid, homogeneous, and durable perfusion at clinically relevant scales. The objective of this article is to explore the conceptual feasibility of in vivo vasculogenic therapies by defining the recipient-flap contact surface area that may be sufficient and necessary to promote incipient inosculation and efficient capillary reconnection across the graft interface.

Methodology: To address this question, the discussion is framed within regenerative microsurgery and contrasts ex vivo and in vivo vasculogenic strategies while emphasizing their shared hemodynamic limitations. Ex vivo approaches can generate preformed vascular architecture but remain dependent on timely integration with the host circulation after implantation. In vivo strategies promote vascular ingrowth from the recipient bed, yet their effectiveness is ultimately constrained by the limited conductance of surface capillary exchange.

Results: A simplified quantitative model based on subcutaneous adipose capillary density, physiological capillary flow, and Poiseuille scaling demonstrates that the recipient interface required to sustain flap-level perfusion would far exceed realistic reconstructive dimensions. Direct comparison with the flow carried by a single 2 mm pedicle-level vessel further highlights the marked hemodynamic superiority of centralized vascular inflow over recipient-surface perfusion alone.

Conclusion/Significance: The analysis therefore supports a central conclusion: successful translation of flap-scale engineered tissues will likely require microsurgical vascular integration and the generation of centralized, suturable vascular conduits capable of reproducing the architecture and conductance of native perforator-based flap perfusion.

Session 65
Musculoskeletal (General Session) 3

11-18-2026 @ 11:00 AM - 12:30 PM

OP-253 - NIR-Activated, Oxygen Vacancy TiO2 Nanohoneycomb Structure on Titanium Enables Rapid Biofilm Eradication and Osteoimmune Driven Osseointegration

Kelvin Yeung, Can Ai, Yizhou Zhu

The University of Hong Kong, Hong Kong, Hong Kong PRC

Purpose/Objectives: Orthopedic implant–associated infections remain difficult to treat because biofilm-encased bacteria tolerate antibiotics and host clearance, yet aggressive antibacterial strategies can compromise bone healing. To address both challenges with a simple, additive-free approach, we developed agent-free hydrogenated TiO_2 nanohoneycomb surfaces (H-NCs) directly fabricated on titanium. Hydrogenation introduces oxygen vacancies that broaden light absorption into the near-infrared (NIR) range, enabling on-demand reactive oxygen species (ROS) generation with mild photothermal heating for rapid biofilm disruption. In parallel, the 90-nm honeycomb topography is designed to modulate macrophage polarization, establishing a pro-regenerative osteoimmune microenvironment that supports osteogenesis and stable bone–implant integration.

Methodology: TiO_2 nanohoneycombs were fabricated on titanium via polystyrene-sphere templating and calcination, followed by hydrogen plasma treatment to introduce oxygen vacancies. This treatment narrows the TiO_2 bandgap and enables NIR activation without changing the titanium bulk chemistry or incorporating antibiotics/metal ions. Antibacterial performance (including *Staphylococcus aureus* biofilm removal) was assessed under brief NIR irradiation *in vitro*and in an implant-associated infection model *in vivo*. Macrophage polarization and osteogenic responses were evaluated to determine osteoimmunomodulatory effects and bone–implant integration, alongside standard biosafety testing.

Results: Upon 15 minutes of NIR exposure, H-NCs achieved rapid, agent-free killing of *S. aureus* (99.94% *in vitro*) and markedly reduced bacterial burden *in vivo* (91.58%). Beyond antibacterial activity, the nanohoneycomb surface shifted macrophages toward a pro-healing phenotype, creating an immune milieu that enhanced osteogenic responses and improved bone-to-implant integration. Together, these findings demonstrate a single, scalable surface modification that delivers on-demand antibiofilm function while actively supporting osseointegration, without exogenous antimicrobial loading.

Conclusion/Significance: H-NCs provide an antibiotic-free, NIR-triggered strategy that couples rapid antibiofilm action with osteoimmunomodulation to promote osseointegration. By avoiding drug loading and relying on a straightforward, scalable surface process, this platform is well positioned for translation to infection-resistant orthopedic implants and broader tissue-engineering interfaces where regeneration and infection control must be achieved simultaneously.

OP-254 - An Adhesive Hydrogel Enabling Suture-Free Cell Delivery Across Osteochondral Tissues

Dominique Pioletti[1], Peyman Karami[2], Robin Martin[3], Alexis Laurent[4], Virginie Philippe[3], Lee Laurent-Applegate[5]

[1]*EPFL, Laboratory of Biomechanical Orthopedics, Lausanne, Switzerland*
[2]*University of Fribourg, Faculty of Science And Medicine, Fribourg, Switzerland*
[3]*University of Fribourg, Department of Orthopedic Surgery And Traumatology, Fribourg, Switzerland*
[4]*LAM Biotechnologies SA, Manufacturing Department, Epalinges, Switzerland*
[5]*University of Lausanne, Cell Therapy Unit, Lausanne, Switzerland*

Purpose/Objectives: Failure at the repair–host interface significantly limits cartilage and osteochondral regeneration, as insufficient fixation compromises tissue integration prior to extracellular matrix formation. Existing methods, such as sutures, press-fit constructs, and fibrin glues, fail to provide durable adhesion across both cartilage and subchondral bone while remaining compatible with cell delivery. This study aimed to evaluate the adhesive, mechanical, and translational performance of MechaGel, a novel light-activated injectable hydrogel designed for simultaneous cell delivery and suture-free fixation in osteochondral repair.

Methodology: MechaGel hydrogels containing 5–20 wt% polymer were photocured and characterized for bulk mechanical properties and lap-shear strength. Tensile adhesion was specifically assessed on human cartilage, subchondral plates, and cancellous bone, with performance benchmarked against fibrin glue. The study systematically evaluated the effects of polymer concentration, sterilization processes, and batch-to-batch variability. Furthermore, ex vivo human tibial plateau models were utilized to examine hydrogel–tissue contact under both dry and wet conditions and to analyze precursor penetration into cancellous bone defects.

Results: MechaGel exhibited tunable cohesive and adhesive properties with minimal batch variability. Notably, adhesion strength consistently surpassed that of fibrin glue by approximately fivefold across all tested osteochondral tissues. While sterilization significantly impacted mechanical performance, it resulted in a comparatively smaller reduction in adhesive strength relative to bulk stiffness. Additionally, polymer concentration effectively controlled hydrogel infiltration into cancellous bone, allowing for either localized confinement or partial tissue penetration based on specific application requirements.

Conclusion/Significance: These findings confirm that MechaGel offers reproducible, quantifiable fixation for osteochondral tissues, validating its potential as a suture-free adhesive platform for cell delivery and cartilage repair. By addressing critical limitations in current fixation strategies, this system represents a promising translational biomaterial capable of enhancing integration and stability in regenerative orthopedic therapies.

OP-255 - Bone Morphogenetic Protein-2 Delivery from Hydroxyapatite-Binding Fusion Proteins for Enhancing Bone Allograft Efficacy

Malvika Singhal[1,2,3], Marian Hettiaratchi[1,2,3], Caroline Foskett[1,4]

[1]*University of Oregon, Knight Campus For Accelerating Scientific Impact, Eugene, United States of America*
[2]*University of Oregon, Department of Chemistry And Biochemistry, Eugene, United States of America*
[3]*Institute of Molecular Biology, Department of Biology, Eugene, United States of America*
[4]*University of Oregon, Department of Human Physiology, Eugene, United States of America*

Purpose/Objectives: Robust bone repair relies on interactions between numerous cells, proteins, and extracellular matrix molecules (ECM). In critically-sized bone fractures, which do not heal without intervention, these interactions are disturbed, leading to inhibited expression of osteogenic proteins, such as bone morphogenetic protein-2 (BMP-2). Current treatments such as decellularized bone cannot mimic critical effects of BMP-2 signaling. To localize BMP-2 within bone allografts and introduce osteoinductivity, we developed a fusion protein library containing a peptide sequence that binds to hydroxyapatite (HAp), the mineral component of bone allograft (EEEEEEEDGEA, SVSVSVK, or KNFQRSH), a flexible or rigid peptide linker, and an affibody engineered to bind specifically to BMP-2.

Methodology: Micro-bicinchoninic acid assay revealed neither the affibody nor the SVSVSVK and KNFQRSH peptides were retained on HAp pellets, while all fusion proteins and the E7DGEA peptide were retained on HAp pellets (Fig. 1A). After 48 hours, fusion proteins containing the SVSVSVK binding domain demonstrated the highest surface retention. BMP-2 was loaded onto HAp pellets containing fusion proteins and the BMP-2 affibody. Enzyme-linked immunosorbent assay (ELISA) showed HAp pellets with the BMP-2-specific affibody loaded more BMP-2 than all other groups except the KNFQRSH rigid linker fusion protein (Fig. 1B). ELISA revealed all fusion proteins demonstrated moderate BMP-2 release that was faster than release from pellets with affibodies but slower than release from pellets without any fusion protein or affibody (Fig.

1C) over 2 weeks, demonstrating that the fusion protein can slow BMP-2 release from the HAp pellets.

Results:

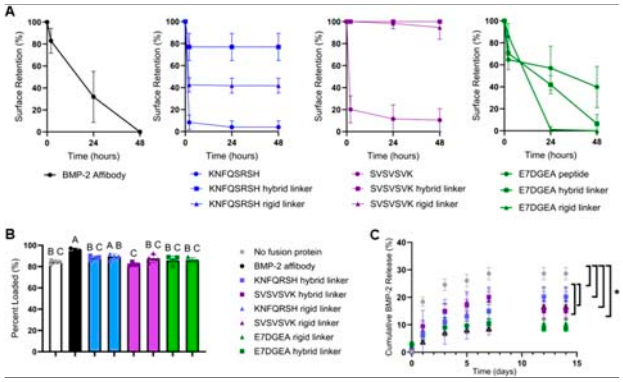


Figure 1. A) Percent surface retention of fusion proteins on Hap pellets over 48 hours. B) BMP-2 retained on HAp pellets treated with different fusion proteins. C) Cumulative BMP-2 release from HAp pellets over two weeks. For panels A,C, 2-way ANOVA and for panel B, 1-way ANOVA with Tukey correction, $\alpha = 0.05$ was performed across all groups.

Conclusion/Significance: Moving forward, we will evaluate the effect of HAp-binding fusion proteins on BMP-2 delivery and mineralization in an *in vivo*rat bone injury model treated with bone allografts. This is the next step toward creating a clinical treatment strategy that combines bone allografts with the potent osteogenic activity of BMP-2.

OP-256 - Impact of Transforming Growth Factor-β3 and Bioprinted Collagen Compliance for Fibrocartilage Differentiation

Emily Matheson[1], Alexander Caballero-Espinosa[1], Diya Pillai Babu[1], Shirin Changizi[1], Nashaita Patrawalla[1], Vipuil Kishore[1], Chris Bashur[2]

[1]*Florida Institute of Technology, Melbourne, United States of America*
[2]*Florida Tech, Chemistry And Chemical Engineering, Melbourne, United States of America*

Purpose/Objectives: We are developing bioprinted gradient sleeves to aid in anterior cruciate ligament graft integration at the bone-fibrocartilage-ligament interface. However, there are questions about whether chondrogenic factors would diffuse to other segments and how important sleeve microenvironment is for fibrocartilage differentiation of endogenously recruited mesenchymal stem cells (MSCs). This study aims to determine *in vitro* the impact of both spatio-temporal availability of transforming growth factor-β3 (TGF-β3) and collagen hydrogels compliance on MSC differentiation.

Methodology: A hydrogel with two sides, one incorporating TGF-β3, was printed on a magnet and cross-linked. The bio-ink consisted of methacrylated collagen, streptavidin Magnesphere® paramagnetic particles, xanthan gum, and TGF-β3. The hydrogel and TGF-β3 release were characterized. MSCs were seeded on hydrogels and stained with DAPI and phalloidin. Constructs with exogenous TGF-β3 were tested to decouple release from compliance differences. The presence of fibrochondrogenic markers (PCR) and hydrogel compliance (mechanical tester) are being studied.

Results: SEM and optical coherence microscopy (OCM) images showed clean interfaces between two connected hydrogels. ELISA showed TGF-β3 release through 3 days, with lower release at 5 days. There was higher release from 20ng/ml vs. 10ng/ml hydrogels (n=3), with the majority of loaded TGF-β3 released from the (∼0.035mL) hydrogels. MSCs attached and spread on hydrogels at 7 days. Preliminary RT-PCR results showed expression of chondrogenic markers SOX9 and Aggrecan (n=2). Images indicate that sample-sides that were more compliant, and contained TGF-β3, had lower cell attachment than stiffer control sides (n=6). Additionally, control sides connected to TGF-β3-containing hydrogels had higher cell attachment than control only samples, suggesting that TGF-β3 diffuses to impact adjacent cell proliferation. There also appeared to be morphological differences (cell area and aspect ratio) between conditions that are being quantified.

Conclusion/Significance: Overall, this study validated a 3D-printed model to study growth factor localization. Bulk TGF-β3 incorporation provided release through 5 days, with evidence its diffusion impacted MSCs. Results also indicate that changes in bioprinted hydrogel compliance also impact MSC attachment and morphology. Characterizing the impacts on MSC differentiation to fibrocartilage cells is ongoing. These studies will aid in optimizing gradient printed ligament sleeves for promoting spatially-localized differentiation of MSCs.

Session 66
Tissue Engineering Models of The Nervous System

11-18-2026 @ 11:00 AM - 12:30 PM

OP-257 - A Microfiber Scaffold Platform for Glioblastoma Invasion Studies and Therapeutic Screening

Maya Kasteleiner[1], Charlotte Olds[1], Patrick Hall[1], Joshua Kupfer[1], Ievgenii Liashenko[1], Paul Dalton[2], Gabriella Lindberg[1]

[1]*Knight Campus, University of Oregon, Bioengineering, Eugene, United States of America*
[2]*University of Oregon, Knight Campus, Eugene, United States of America*

Purpose/Objectives: Glioblastoma multiforme (GBM) is a highly aggressive brain malignancy characterized by diffuse invasion along anisotropic white matter tracts. *In vitro* models of this cancer often fail to recapitulate aligned extracellular cues that guide tumor migration, limiting their predictive accuracy for anti-migratory drug screening. This study presents a 3D-printed GBM platform combining melt electrowritten (MEW) microfibers with hydrogel matrices to reproduce white matter tract-like guidance cues *in vitro.*

Methodology: Aligned poly(ε-caprolactone) (PCL) scaffolds were fabricated using MEW (PC12, 64°C, 0.38 bar, 22G nozzle, 1.5 mm collector distance, 4 kV, 500 mm/min collector speed) to generate highly aligned microfibers with controlled bridging architectures that enhance scaffold stability and cell attachment. To create a hybrid 3D matrix, MEW scaffolds were embedded within Matrigel (9 mg/mL), producing a microenvironment combining haptotactic cues with extracellular matrix support. U87-MG glioblastoma spheroids generated in V-bottom plates were cultured on these constructs to evaluate fiber-guided invasion and migration.

Results: Substrate anisotropy strongly regulated GBM invasion, with aligned MEW fibers inducing long-range directional migration absent in isotropic 2D and 3D systems. MEW microfiber scaffolds significantly increased maximum migration distance after 7 days compared to aligned electrospun (ES) meshes (ES: 1.02±0.06 mm; MEW: 3.84±0.69 mm; $p<0.0001$). While hydrogel-only matrices restricted invasion, incorporation of aligned MEW fibers within Matrigel significantly increased migration distance (Matrigel: 0.51±0.15 mm; Matrigel+MEW: 2.57±0.34 mm; $p=0.0003$) and invaded area (Matrigel: 0.82±0.57 mm^2; Matrigel+MEW: 22.14±6.41 mm^2; $p<0.0166$). Migration alignment correlated with substrate anisotropy, with the highest alignment observed on MEW scaffolds (alignment index on TCP: 0.12±0.12; Matrigel: 0.14±0.11; ES: 0.31±0.10; MEW: 0.63±0.12; Matrigel+MEW: 0.34±0.15).

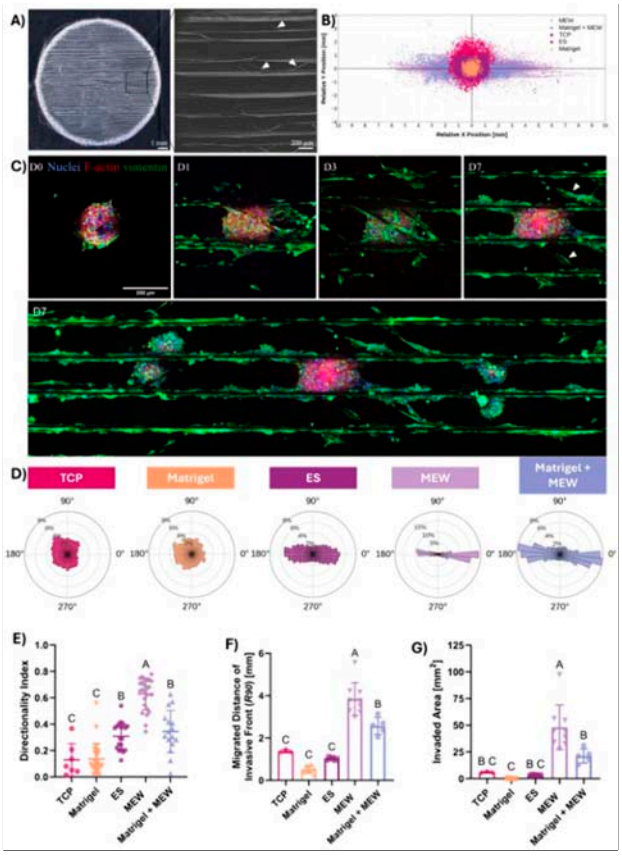


Figure-legend: Fiber-guided GBM migration. (A) MEW scaffold with bridging fibers (triangles). (B) Cell distribution relative to substrate topography. (C) Confocal images of GBM migration along MEW fibers. Cell directionality (D) increases with substrate anisotropy (E). Maximum migration distance (F) and invaded area (G) increase on anisotropic substrates.

Conclusion/Significance: This work establishes a biomimetic and tunable *in vitro* platform for studying GBM invasion within physiologically relevant anisotropic microenvironments. By integrating oriented microfibers within hydrogel matrices, this platform enables controlled investigation of long-range tumor migration and provides a predictive system for evaluating anti-migratory therapeutics in an engineered tumor microenvironment.

OP-258 - Developing microphysiological platforms to understand the healthy and diseased nervous system

Christina Tringides

Rice University, Houston, United States of America

Purpose/Objectives: Biomaterial scaffolds have emerged as a tool to build 3D cultures of cells which better resemble biological systems, while advancements in bioelectronics have enabled the modulation of cell proliferation, differentiation, and migration. Often, the same materials and processing techniques from the electronics industry are used to interface with the nervous system. As the materials used for electronics are often mechanically stiff and brittle, they offer limited interfaces with the nervous system and have minimal conformability or contact with the underlying tissues. Further, this mechanical modulus mismatch leads to irreversible tissue damage.

Methodology: I'll describe our work in mechanically and electrically supportive hydrogels, designed to have the same mechanical modulus and also viscoelasticity as neural tissue. Electrical conductivity is achieved by create conductive hydrogel composites, and incorporating low amount of carbon nanomaterials into a hydrogel matrix. By tuning the materials processing techniques, we introduce highly porous networks with electrical percolation. The mechanical and electrical properties of these material can be carefully tuned and used to modulate the growth and differentiation of neural progenitor cells (NPCs) *in vitro*.

Results: When seeded into the bulk 3D hydrogels, the neurite networks form dense networks that span the entire volume of the materials, and the NPCs can differentiate into astrocytes and oligodendrocytes. With increasing hydrogel viscoelasticity and conductivity, we observe the formation of denser neurite networks and a higher degree of myelination. In addition to bulk hydrogels, we combine our materials with micropatterned elastomeric materials to create hybrid materials technologies for *in vitro* applications. We then explore different techniques to integrate hydrogels into the PDMS microstructures, such that the hydrogel can facilitate neurons to form 3D networks while still confined by the PDMS. This platform is compatible with various methods to assess neuronal functionality (e.g. high-density multielectrode array electrical recordings), and can be used to understand the effect(s) of hydrogel properties on the resulting neuronal networks for >100 days in culture.

Conclusion/Significance: Both described biomaterial platforms can support the growth of neuronal cells for over multiple months, and could facilitate the development of biohybrid electronic devices to understand neuronal development and disease, such as demyelinating disorders.

OP-259 - Complementary Photocrosslinked and Dynamic HA Bioinks for Architected 3D Scaffolds

Rounak Pokharel[1], Nic Leipzig[2]

[1]*University of Akron, Chemical Engineering, Akron, United States of America*
[2]*University of Akron, Department of Chemical, Biomolecular, and Corrosion Engineering, Akron, United States of America*

Purpose/Objectives: Spinal cord injury (SCI) repair requires biomaterial scaffolds that are both biologically relevant and structurally configurable, yet most hyaluronic acid (HA)-based systems rely on a single crosslinking strategy that limits accessible scaffold formats. Here, we compare two HA bioinks: a photocrosslinkable GelMA/methacrylated HA (MeHA) system for permanent architected constructs and an aldehyde-HA/gelatin (A-HA/Gel) system with dynamic Schiff base crosslinking, to determine how crosslinking modes and scaffold architecture influence scaffold format and neural fate for SCI repair applications.

Methodology: Photocrosslinkable GelMA/methacrylated HA (MeHA; 5%/2% w/v, 0.1% LAP) and dynamically crosslinked aldehyde-HA/gelatin (A-HA/Gel; 2%/4% w/v) formulations were prepared and fabricated into bulk or 3D constructs. GelMA/MeHA was fabricated as UV-crosslinked bulk disks and extrusion-printed UV-crosslinked geometries including 3 mm cylindrical, 5 mm square, and 14 mm petal-shaped constructs. A-HA/Gel was fabricated as dynamically crosslinked injectable and 3D constructs. Construct morphology and initial cytocompatibility were assessed by quantitative viability analysis. Ongoing work will assess scaffold architecture effects on VSCP-derived motor neuron differentiation.

Results: GelMA/MeHA enabled reproducible UV-crosslinked bulk and printed 3D geometries, including cylindrical, square, and petal constructs, while A-HA/Gel formed bulk and printed 3D constructs through dynamic Schiff base crosslinking. Across all tested scaffold formats, including UV-crosslinked GelMA/MeHA, bulk, and printed cylindrical, square, and petal geometries, and A-HA/Gel constructs. Quantitative viability analysis showed high viability across all groups, supporting the general cytocompatibility of permanent and dynamic HA scaffold formats. Together, these data establish a complementary HA scaffold platform spanning multiple geometries and crosslinking modes for architected 3D scaffold design.

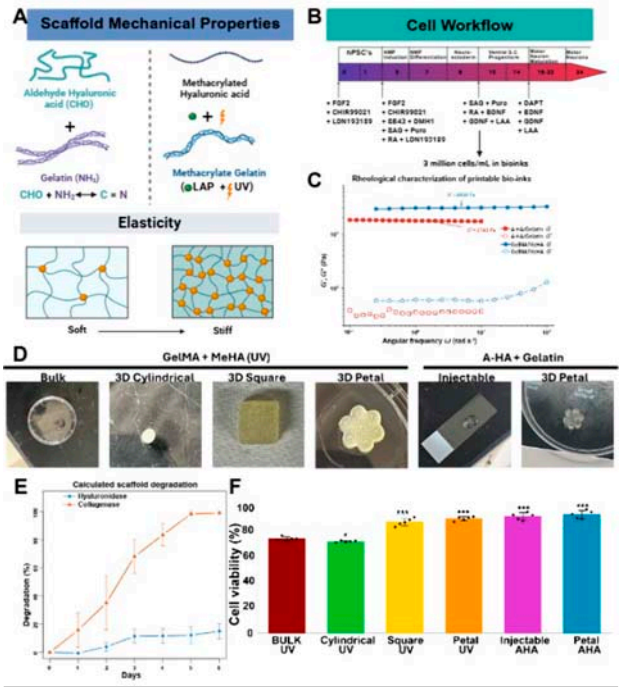


Figure. (A) Schematic of dynamic Schiff base crosslinking in aldehyde-HA/gelatin and photocrosslinking in GelMA/MeHA. (B) Workflow for differentiation of hPSCs into ventral spinal cord progenitors (VSCPs). (C) Rheological characterization of both bioinks. (D) Representative bulk and 3D scaffold geometries fabricated from both formulations. (E) Enzymatic degradation of GelMA/MeHA scaffolds. (F) Cell viability across scaffold formats, demonstrating cytocompatibility (* $p<0.05$, ***$p<0.001$).

Conclusion/Significance: These results establish complementary HA scaffold modalities that combine geometric versatility with distinct crosslinking behaviors while maintaining 3D cytocompatibility. This platform provides a foundation for ongoing studies examining how scaffold architecture and matrix dynamics influence neural organization in SCI repair.

OP-260 - Microphysiological Model of Sensory-Innervated Lung Epithelium for Investigating Respiratory Viral Neurotropism

Jared Fink[1], Michael Moore[1], Mark Mondrinos[1], Ethan Byrne[1], Omar Cepeda Torres[2], Swaminathan Rajaraman[2], Giovanni Piedimonte[3]

[1]*Tulane University, Department of Biomedical Engineering, New Orleans, United States of America*
[2]*University of Central Florida, Department of Materials Science And Engineering, Orlando, United States of America*
[3]*Tulane University School of Medicine, Biochemistry And Molecular Biology, New Orleans, United States of America*

Purpose/Objectives: Respiratory infections with pathogens such as respiratory syncytial virus (RSV) have been implicated in chronic conditions, like asthma, with potential neural sequelae. We previously demonstrated direct infection of peripheral nerves by RSV-induced neuropathy, but a more physiologically-relevant model is needed to elucidate the mechanisms of viral neurotropism. Here, we present a proof-of-concept microphysiological system (MPS) of sensory-innervated lung epithelium to enable the study of these processes. Desired design criteria were to enable placement of a neural spheroid above an electrode and to support axonal growth toward an epithelial monolayer cultured at an air-liquid interface (ALI). Our objective is to establish the feasibility of this novel sensory nerve-to-lung epithelium MPS to study RSV neurotropism.

Methodology: Our method used stereolithography-fabricated molds to produce multi-chambered chips that allow seeding spheroids beneath small airway epithelial cells (SAEC) cultured at an ALI (Figure 1A). These chips possess features such as a microfluidic trapping mechanism that keeps peripheral neurons in place (Figure 1B), an ALI for epithelial cells (Figure 1C), and separate media channels. The devices are designed to interface with a planar multiple electrode array (MEA) that was fabricated using photolithography. Cell types relevant for respiratory pathophysiology were cultured, including H441 lung epithelial cells, human SAEC, and neural-glial spheroids.

Results: The trapping mechanism effectively facilitated the consistent placement of spheroids at the location of an electrode to be used for electrophysiology. Peripheral neurons exhibited robust neurite outgrowth after 14 days. Lung epithelial cell types remained viable when cultured at ALI. In co-culture, neurites grew through the central channel from the neural spheroid into the membrane of the H441 layer.

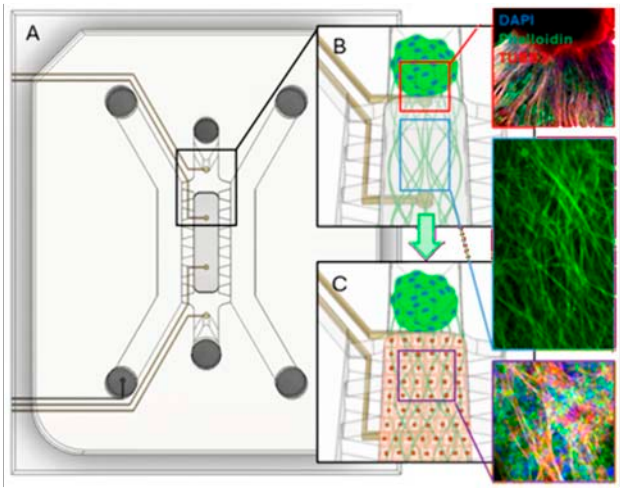


Figure 1.Innervated-Lung-Epithelium MPS. A) PDMS device bonded to MEA. B) Spheroid is trapped and axons extend. C) Axons (red) grow into membrane where lung epithelial cells (green) are cultured at ALI.

Conclusion/Significance: This MPS supported the co-culture of sensory neurons with lung epithelial cells at an ALI. The use of a 3D printer and MEA fabrication methods position this MPS as a cost-effective and adaptable model system. Next steps include optimizing the co-culture of SAEC with human induced pluripotent stem cell-derived nociceptor spheroids and scaling up to multiple wells.

OP-261 - Human Brain Organoids Bridge Spaceflight and Neurodegeneration Research on the International Space Station

Livia Nascimento[1], Maria Balaguer[1], Andrelia Carmona[1], Nicholas Behnke[1], Pinar Mesci[2], Jana Stoudemire[1], Jim Mossman[1], Scott Noggle[3], Paula Grisanti[3]

[1]*National Stem Cell Foundation, San Diego, United States of America*
[2]*Axiom Space, Houston, United States of America*
[3]*National Stem Cell Foundation, Louisville, United States of America*

Purpose/Objectives: Long-duration spaceflight presents significant challenges to brain health. Spaceflight induces cephalad fluid shifts, alters protein clearance, and promotes neuroinflammation, factors that together may accelerate brain aging and neurodegenerative processes. Previous missions using cortical and dopaminergic brain organoids aboard the International Space Station (ISS) demonstrated altered developmental trajectories, including reduced proliferation and accelerated neuronal maturation in low-Earth orbit compared to ground controls. These missions revealed how microgravity influences human neural fate and maturation.

Methodology: Building upon these findings, we developed a novel cholinergic brain organoid platform modeling familial Alzheimer's disease (AD) using induced pluripotent stem cell (iPSC) lines carrying PSEN1 and APP mutations. Cholinergic neuronal degeneration represents one of the earliest and most prominent pathological hallmarks of AD and is strongly associated with cognitive decline and memory impairment. The establishment of disease-relevant cholinergic organoids therefore provides a translational platform to investigate neurodegenerative mechanisms in the context of spaceflight and evaluate future neuroprotective strategies.

Results: Current ground-based characterization includes electrophysiological assessment using multielectrode array (MEA) recordings, immunofluorescence analyses to evaluate cellular identity and disease-associated phenotypes, and ongoing transcriptomic profiling to define molecular signatures associated with neuronal maturation and AD pathology.

Conclusion/Significance: Beyond astronaut health applications, this work contributes to the growing field of in-space biomanufacturing by integrating stem cell-derived human disease models with low-Earth orbit research platforms, supporting the development of therapeutic strategies with potential benefits for both space exploration and terrestrial neurodegenerative disease research.

RAPID FIRE PRESENTATION ABSTRACTS

Session 1
3D Printing Advances in Musculoskeletal Tissue Engineering

11-15-2026 @ 1:00 PM - 2:30 PM

RF-001 - Multilayer Biomimetic Scaffold for Cartilage Regeneration: In Vitro Morphological and Cellular Evaluation

Christian Buckley[1], Hugues Mondesert[2], Sarah Berndt[2], Marine Delcros[2], Antoine Turzi[1]

[1]*RegenLab USA, Jersey City, United States of America*
[2]*RegenLab SA, Le Mont-sur-Lausaunne, Switzerland*

Purpose/Objectives: Tissue regeneration benefits from materials that can mimic the complex native tissue architecture. This study aimed to perform *in vitro* morphological characterization of a biomimetic multilayer scaffold and to evaluate the cellular behavior and chondrogenic differentiation potential of human bone marrow–derived mesenchymal stem cells (hBM-MSCs). Cellular activity was assessed in the scaffold's middle cartilage layer by seeding cells within the core scaffold under different culture conditions: differentiation medium, platelet-rich plasma (PRP), and PRP combined with hyaluronic acid (PRP-HA).

Methodology: Multilayer scaffolds were fabricated using a combination of electrospinning, fused deposition modeling (FDM), and hydrogel deposition. Constructs were crosslinked, incubated, and freeze-dried following a proprietary protocol. Scaffold morphology and mechanical properties were evaluated using scanning electron microscopy (SEM) and compression testing. hBM-MSCs were seeded onto scaffolds and cell viability and proliferation were assessed using Live/Dead assays. Chondrogenic differentiation was evaluated by Alcian Blue staining, glycosaminoglycan (GAG) quantification, immunostaining (SOX9, aggrecan).

Results: The multilayer scaffolds exhibited a well-defined porous architecture, robust structural integrity, and stability for over 30 days under in vitro conditions, with no evidence of layer delamination, supporting their suitability for cartilage tissue engineering. hBM-MSCs demonstrated high viability, adhesion, proliferation and differentiation within the scaffold core. The addition of PRP and PRP-HA significantly improved cell adhesion/proliferation and improved the differentiation capacity of hBM-MSCs in the scaffold.

Conclusion/Significance: This biomimetic multilayer scaffold provides a supportive microenvironment for MSC recruitment, viability, and differentiation. The addition of PRP, particularly in combination with hyaluronic acid, enhances chondrogenic outcomes, highlighting its potential for cartilage regeneration applications.

Session 2
Emerging Bioengineering and Gene-based Strategies for Wound Healing and Tissue Regeneration

11-15-2026 @ 1:00 PM - 2:30 PM

RF-002 - Antimicrobial peptide-loaded violet phosphorene-based photothermal composite hydrogel combined with CRISPR/Cas9 targeting mecA for eradication of MRSA-infected wounds

Qingfang Zhao[1], Yuan Chi[2], Jinfei Hou[1]

[1]*The First Affiliated Hospital, Zhejiang University School of Medicine, Hangzhou, Hangzhou, China*
[2]*Zhejiang University, Hangzhou, China*

Purpose/Objectives: To design a multifunctional composite hydrogel composed of violet phosphorene (VP) nanosheets, an AMP (HNP 4), and a CRISPR/Cas9 system targeting *mecA*, and to evaluate its antibacterial efficacy against MRSA in vitro and in an infected wound model.

Methodology: VP nanosheets were synthesized by liquid exfoliation. The CRISPR/Cas9 ribonucleoprotein (RNP) targeting the *mecA* gene was complexed with cationic liposomes. VP, RNP and HNP 4 were co-encapsulated into a thermosensitive Pluronic F127/gelatin hydrogel. In vitro, MRSA (ATCC 43300) was treated with different formulations. Gene editing efficiency was assessed by PCR and Sanger sequencing. MIC of oxacillin was measured. Bacterial viability and morphology were examined by colony counting and SEM. In vivo, a full-thickness dorsal skin wound infected with MRSA (10^7 CFU) was established in C57 mice. Wounds were treated with the composite hydrogel followed by 808 nm NIR irradiation (1.0 W/cm^2, 10 min). Wound closure and bacterial burden were evaluated on days 3, 7 and 14; inflammation (IL-6, TNF-α,ROS), and histology (H&E, Masson) were evaluated on days 7 and 14.

Results: In vitro, the VP-CRISPR-AMP+NIR group achieved a 5.5-log reduction of MRSA compared to controls. PCR/Sanger sequencing confirmed disruption of *mecA* in >40% of surviving colonies, leading to a 32-fold reduction in oxacillin MIC. SEM revealed severe membrane disruption. In vivo, the combination therapy accelerated wound healing (closure rate 98% at day 14), reduced bacterial load by 4.0-log, and decreased ROS and IL-6/TNF-α levels. Histology showed enhanced collagen deposition and angiogenesis.

Conclusion/Significance: The HNP 4-loaded VP-based photothermal hydrogel together with CRISPR/Cas9 targeting *mecA* effectively eradicates MRSA, reverses antibiotic resistance, and promotes infected wound healing. This platform provides a novel "genetic-physical-chemical" triple-therapy strategy against drug-resistant wound infections.

Session 3
Harnessing the Power of Microgravity to Accelerate Breakthroughs in Regenerative Medicine

11-15-2026 @ 1:00 PM - 2:30 PM

RF-003 - Development of an ISS-Compatible Tissue-Engineered Neuromuscular Co-Culture Platform

Hayleigh Kahn, Eileen Su, Derek Hwang, Lisa Larkin

University of Michigan, Molecular And Integrative Physiology, Ann Arbor, United States of America

Purpose/Objectives: Sarcopenia is the age-related loss of skeletal muscle mass and function. There is limited understanding of and a lack of intervention to address sarcopenia, despite societal costs. Astronauts have shown similar muscle atrophy after 17 days in microgravity. Thus, microgravity may provide an accelerated environment to study underlying mechanisms of sarcopenia. Microgravity and aging appear to disrupt the neuromuscular junction (NMJ) structure and reactive oxidative species (ROS) activity, altering muscle function. We plan to investigate these disruptions in microgravity aboard the International Space Station (ISS) using a nerve-muscle co-culture system. Our goals are: (1) fabricate viable co-cultures of skeletal muscle units (hSMUs), engineered neural conduits (hENCs), and motor neurons (MNs) and (2) develop a protocol adjusting for obstacles faced on the ISS.

Methodology: Human skeletal muscle myoblasts (Lonza) and human bone marrow mesenchymal stromal cells (RoosterBio) were used to construct hSMUs and hENCs. Applied StemCell's human induced pluripotent stem cells were used to proliferate and network MNs within hENCs. Co-culture viability was determined by assessing force production. We developed one media suitable for maintenance of all tissue types in co-culture (3-D Media) and adjusted feeding protocols to address: limited media storage, storage temperature, and inability to do 100% media exchanges. Here we present a protocol that will work on the ISS given the existing limitations.

Results: Co-culture viability is optimal when hSMUs and hENCs are fabricated on 60 mm plates and co-cultured for 5 days prior to transfer to the Space Tango bioreactor. 3-D Media included 91% DMEM, 7% HS, 1% ABAM, 1% Dex, 1uL/mL ITSX, 0.72 uL/mL Ascorbic Acid, 1% N2, with 2.8 mL per well, stored at 4 degrees prior to use for feeding. Optimal feeding frequency with 80 % partial media exchange was every 2 days.

Conclusion/Significance: We are able to fabricate viable co-cultures made of hSMUs, hENCs, and IPSC-MNs with functional NMJs, and developed a protocol adjusting for the differences limitations on the ISS. The co-cultures are prepared for launch into the

microgravity environment on the ISS and ready to examine the underlying mechanisms of sarcopenia.

Session 4
Quantitative Non-Invasive Imaging for Regulatory-Ready Engineered Tissues and Human-Relevant Models

11-15-2026 @ 1:00 PM - 2:30 PM

RF-004 - Early Adaptive Responses to Trastuzumab in Bioprinted HER2+ Tumor Aggregates Assessed by Optical Coherence Tomography

Elizabeth Mcdonough[1], Margarida Barroso[2], David Corr[1]

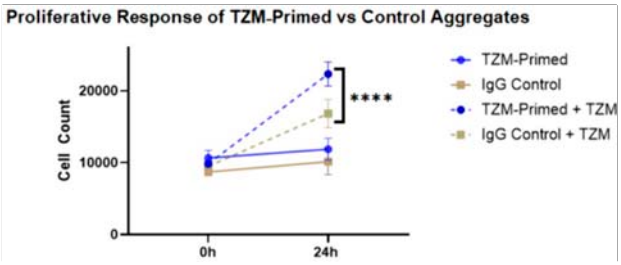
[1]*Rensselaer Polytechnic Institute, Biomedical Engineering, Troy, United States of America*
[2]*Albany Medical College, Albany, United States of America*

Purpose/Objectives: HER2-positive breast cancer accounts for ~20% of invasive cases and remains associated with poor prognosis despite targeted therapy. Trastuzumab (TZM) improves outcomes, yet resistance develops in many initially responsive patients. Early adaptive changes preceding resistance are difficult to capture in 2D systems. This work uses 3D bioprinted tumor aggregates and Optical Coherence Tomography (OCT) to characterize proliferative responses following short-term TZM exposure.

Methodology: HER2-positive AU565 cells were primed for 24 h with 20 μg/mL TZM or human IgG (control) prior to bioprinting into 3D microcapsules wherein the cells self-assemble to form dense spherical aggregates over the course of 20 days, and the developing aggregates were imaged longitudinally using spectral-domain OCT. On Day 20, aggregates received a 50 μg/mL TZM bolus, with follow-up imaging at 24 h. OCT volumes were processed in Imaris to quantify cell counts and density. Statistical comparisons used two-way ANOVA with Tukey post-hoc tests ($\alpha = 0.05$).

Results: Longitudinal OCT imaging revealed differences in growth dynamics between primed and non-primed aggregates. Across the culture period, TZM-primed aggregates exhibited higher cell counts and greater cell density than IgG controls, with divergence most pronounced by Day 21. Following bolus TZM treatment, both groups increased in cell number at 24 h, but the magnitude differed substantially. Two-way ANOVA showed significant effects of time, condition, and their interaction ($p < 0.0001$). Tukey post-hoc tests confirmed that TZM-primed aggregates exhibited the greatest 24-hour proliferative increase following TZM exposure compared to all other groups ($p < 0.0001$), while no baseline differences were observed at 0 h. These findings indicate that short-term TZM priming enhances subsequent proliferative recovery, consistent with an early adaptive phenotype.

Figure. OCT-derived cell counts at 0 h and 24 h for IgG control, TZM-primed, IgG + TZM, and TZM-primed + TZM aggregates. Error bars represent SD. A significant difference at 24 h between TZM-primed + TZM and IgG + TZM is indicated (****, $p < 0.0001$).



Conclusion/Significance: This work demonstrates the utility of OCT for label-free, longitudinal assessment of 3D tumor models and shows that brief TZM exposure can shift HER2+ cell aggregates toward a rebound-prone phenotype. These early adaptive responses may contribute to acquired resistance and highlight the need to evaluate imaging-dose effects in therapeutic planning.

Session 6
Rapid Fire Session

11-15-2026 @ 2:30 PM - 4:00 PM

RF-005 - Evaluating the pathophysiology of a rare CEP290 variant in patient-derived iPSCs and retinal organoids

Erin Burnight, Cathryn Cranston, Benjamin Brophy, Robert Mullins, Edwin Stone, Budd Tucker

University of Iowa, Iowa City, United States of America

Purpose/Objectives: In a survey of 1000 consecutive families clinically diagnosed with an inherited retinal disease, we identified a disease-causing genotype in 76%. of these, ~9% were diagnosed with one of a group of retinal diseases [Leber congenital amaurosis (LCA), Severe Early Childhood Onset Retinal Dystrophy (SECORD), or Early Childhood Onset Retinal Dystrophy (ECORD)] characterized by visual dysfunction before their fourth birthday. The largest contributor (20%) in this cohort were disease causing variants in the cilia-associated gene *CEP290*. The purpose of this study was to evaluate the pathophysiology of a rare disease-causing *CEP290*variant, Arg151Ter, in patient-derived cells.

Methodology: We designed CRISPR-Cas9 reagents to edit the Arg151Ter locus in iPSCs from a compound heterozygous patient carrying the Arg151Ter variant on one allele and the most common disease-causing IVS26 variant on the other allele. We verified editing via RFLP and NGS sequencing in single cell clones. We confirmed pluripotency via hPSC ScoreCard™ Analysis and karyotyping. Patient derived iPSCs were differentiated into retinal organoids via EB formation in microcavities using Elplasia 12K flasks (Corning), and our previously described 3D differentiation protocol.

Results: We evaluated six ssODN-mediated editing strategies using *Bst*BI RFLP analysis and NGS sequencing on bulk DNA isolated from CRISPR-Cas9 treated cells. We observed Arg151Ter correction from four of the six approaches (7.85% - 19.50% of variant allele reads carried the repair edit). We evaluated single cell clones and observed correct *Bst*BI digestion products in ten of twenty-eight clones (35.71%). Patient retinal organoids differentiated to 180 days developed normally with clearly defined lamination and brush boarders. No obvious signs of degeneration were observed.

Conclusion/Significance: We have successfully edited the Arg151Ter variant in patient-derived iPSCs. Disease lines differentiated normally without obvious signs of degeneration. Isogenic controls are being used to investigate the phenotype.

Session 10
Advances in Decellularization and Recellularization of Complex Tissues

11-15-2026 @ 2:30 PM - 4:00 PM

RF-007 - Development and characterization of a decellularized human trabecular bone scaffold for tissue engineering applications

Gemma Izzo[1], Antonio Menini[1], Chiara Sorrentino[1], Veronica Romano[1], Anna Maria Sacco[1], Giulia Ricci[2], Daria Nurzynska[3], De Giovanni Roberto[1], Franca Di Meglio[1], Clotilde Castaldo[1]

[1]*University of Naples Federico II, Public Health, Naples, Italy*
[2]*University of Campania Luigi Vanvitelli, Experimental Medicine, Caserta, Italy*
[3]*University of Salerno, Medicine, Surgery And Dentistry, Baronissi, Italy*

Purpose/Objectives: The extracellular matrix (ECM) represents a fundamental constituent of tissues, providing structural support and biochemical signals that regulate cellular activity. In bone, the ECM accounts for most of the tissue volume, surrounds and sustains resident cells, contributes to mechanical strength and rigidity,

preserves the native three-dimensional architecture necessary for proper skeletal function. Although synthetic biomaterials have advanced considerably, they remain limited in their ability to reproduce the biochemical complexity, structural heterogeneity, and functional properties of native bone ECM. Consequently, naturally derived decellularized matrices have emerged as promising scaffolds for bone tissue engineering, regenerative medicine, and orthopedic research. This study describes a reliable and reproducible method for generating decellularized ECM (d-ECM) from human trabecular bone for applications in tissue engineering and orthopedic research.

Methodology: Bone specimens obtained from the humeral heads of patients undergoing orthopedic surgery (n=8) were decalcified using a 14% EDTA solution, then trimmed and decellularized through treatment with sodium dodecyl sulfate (SDS), Triton X-100, and antibiotics under constant agitation. Decellularization efficacy was assessed by histological analysis and quantification of residual double-stranded DNA (dsDNA) while preservation of matrix architecture and biochemical composition were evaluated using SEM, histochemical staining, immunohistochemistry, and quantitative assays. Biocompatibility was tested in vitro using human adipose-derived mesenchymal stromal cells (hADMSCs) obtained from patients undergoing abdominoplasty (n=16). Cells were seeded onto d-ECM scaffolds to assess the ability of d-ECM to support cell viability, using the Trypan Blue Exclusion assay and the CellTiter-Glo luminescence assay, and differentiation, using real-time PCR.

Results: Complete removal of cell nuclei in Hematoxylin-Eosin staining and low residual dsDNA levels (30.6±2.14 ng/mg) demonstrated effective decellularization. Masson, Mallory, and Van Gieson staining, together with immunohistochemistry and specific quantitative assays, confirmed preservation of the three-dimensional architecture and key ECM proteins. Furthermore, the viability of hADMSCs exceeding 90% and their expression of osteogenic differentiation markers, including OPN, OCN, BSP, RUNX2, and COL1A1, indicated the excellent cytocompatibility of bone d-ECM scaffolds.

Conclusion/Significance: The evidence from this study demonstrates that the proposed protocol produces cytocompatible human trabecular bone d-ECM with preserved structure and intact biochemical components, thus supporting its potential application in bone reconstruction, regenerative therapies, and translational orthopedic research.

Session 13
Musculoskeletal Microphysiological Systems and New Alternative Models: Development to Application

11-16-2026 @ 8:00 AM - 9:30 AM

RF-009 - Tenocytes Morphology and Metabolism Differs with Respect to Age and Microstructure in Biomimetic Tendon Models

Harrison Broadaway[1], Emily Brown[1], Roni Saffar[1], Brittany Taylor[1,2]

[1]*University of Florida, Biomedical Engineering, Gainesville, United States of America*
[2]*University of Florida, Pharmacology And Therapeutics, Gainesville, United States of America*

Purpose/Objectives: Mechanically sensitive tenocytes rely upon aligned extracellular matrices (ECM) and cyclic loading to maintain homeostasis. However, overuse and overloading promote diseased phenotypes characterized by ECM disorganization, fibrosis, and degeneration, further influencing cellular disfunction. Furthermore, aging alters biomechanical responsiveness and tissue maintenance, confounding relationships between microstructure, load, and cellular phenotypes. The influence of ECM alignment and loading on tendon health is evident, though difficult to mimic *in vitro* due to poorly understood, complex biomechanical relationships. Therefore, biomimetic scaffold models mimicking healthy and diseased tendon are needed to decouple tenocyte responses from the complex microenvironments and elucidate influences of microstructure, load, and age on tenocyte phenotypes.

Methodology: Polycaprolactone solutions were electrospun at 150 and 550 rotations per minute to fabricate unaligned-diseased and aligned-healthy scaffolds that mimic tendinous ECMs. Primary Achilles tendon-derived cells (TDCs) from 4- or 15-month Wistar rats were seeded on tissue culture polystyrene (TCP) or scaffolds and cultured for 3 days. Immunofluorescent staining and metabolic analyses were performed immediately (T0), 24- (T24), 48- (T48), or 72-hours (T72) following media change. Samples were stained for F-actin (Phalloidin) and nuclei (DAPI). Cytoskeletal alignment and nuclear aspect ratio (NAR) were quantified via a custom Matlab code and CellProfiler, respectively. Metabolism was assessed via MTS assays normalized to cell counts obtained in Zen Blue. Statistical analyses ($p<0.05$) were run in GraphPad.

Results: Cells adhered and proliferated across substrates (Fig. 1A), while cells on scaffolds had increased nuclear elongation relative to cells on TCP (Fig. 1C). Cytoskeletal organization was increased on aligned scaffolds relative to unaligned counterparts (Fig. 1D). 15-month TDCs had increased nuclear elongation and cytoskeletal alignment relative to 4-month counterparts, suggesting age-associated morphological differences (Fig. 1C-D; statistics not shown). Metabolic activity was generally reduced for cells on scaffolds compared to TCP controls, with only 4-month cells showing significance between scaffold alignments (Fig. 1B), which may be attributed to reduced age-associated biomechanical responsiveness.

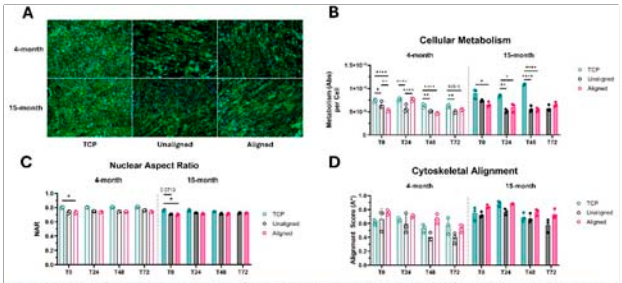


Figure 1. Tendon-derived cells (TCDs) **(A)** express unique cytoskeletal morphology on scaffolds relative to TCPs (Images displayed at T0; F-actin = green, nuclei = blue). Furthermore, TDCs had **(B)** decreased metabolism and **(C)** increased nuclear elongation on scaffolds relative to TCPs. **(D)** TDCs were more elongated on aligned scaffold groups relative to unaligned counterparts. 15-month TCPs at T72 were excluded from analyses due to a lack of cytoskeletal deposition, likely due to cells becoming overgrown and dying off. Data is displayed as mean ± SD. ($p^* < 0.05$, $p^{**} < 0.01$, $p^{****} < 0.0001$)

Conclusion/Significance: Age- and microstructure-dependent responses suggest biomimetic tendon models are suitable to model healthy and diseased biomechanical stimuli at various simulated ages. Delineating between microstructural-, mechanical-, and age-dependent influences is critical in elucidating pathways and mechanisms prevalent to healthy tendon maintenance and disease progression.

Session 14
Engineering Dynamic Microenvironments to Direct Cell Signaling, Stem Cell Fate, and Function

11-16-2026 @ 8:00 AM - 9:30 AM

RF-011 - Proteolytically Engineering a Biomimetic Cardiac Hydrogel Model for Evaluating Mesenchymal Stem Cell Survival in the Injured Heart

Jacob Brown[1], Emma Barna[1], Rabina Lamichhane[1], Joseph Ketchum[1,2], Faith Campbell[1], Ashley Wong[1], Ge Zhang[1]

[1]*The University of Akron, Department of Biomedical Engineering, Akron, United States of America*
[2]*University of Akron, Biomedical Engineering, Akron, United States of America*

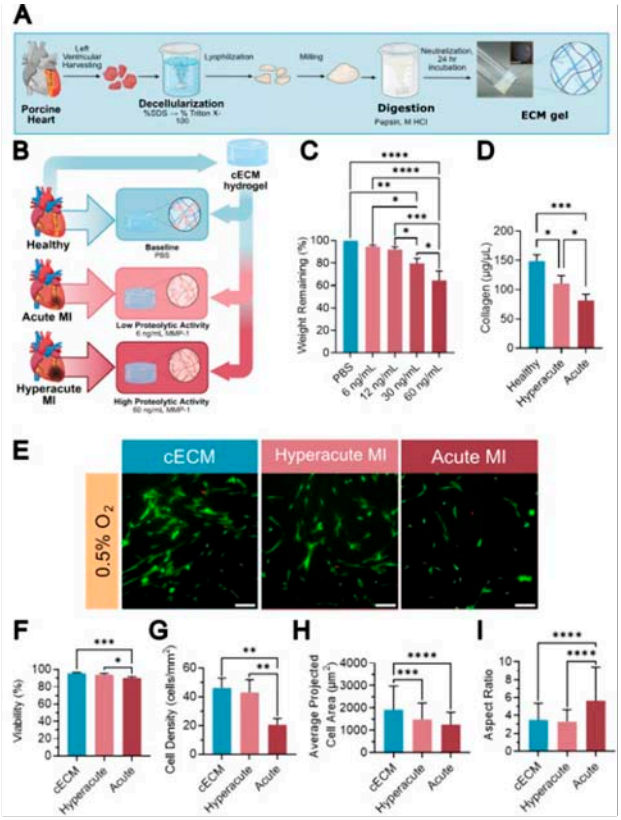
Purpose/Objectives: Mesenchymal stem cell (MSC)-based cardiac cell therapy is a promising approach for treating myocardial infarction and improving cardiac function. However, the low survival rate of transplanted MSCs is a key challenge in achieving consistent clinical outcomes. Although MSC-based therapies show promise, most studies are in vivo, limiting controlled assessment of the impact of individual stressors. Porcine myocardial-derived hydrogel is an attractive biomimetic platform that

closely recapitulates the cardiac extracellular environment. In this study, we aim to develop an in vitro platform to investigate how the proteolytically remodeled cardiac extracellular matrix (cECM) and extreme hypoxia impair therapeutic MSC survival and function.

Methodology: cECM was fabricated according to previously established methods, and cECM hydrogels were created via incubation with 6 to 60 ng/mL MMP-1. MSCs were cultured under extreme hypoxia (0.5% O_2), on proteolytically engineered cECM to assess how each condition affects MSC survival and function. Cell viability, cell density, and morphology were assessed across conditions and their combinations.

Results: cECM hydrogels were manufactured and proteolytically engineered. MMP-1 treatment produced dose-dependent reductions in weight and collagen content. The combination of proteolytic cECM and extreme hypoxia resulted in a significant reduction in MSC viability and cell density, as well as the expression of a smaller and more elongated MSC phenotype.

Figure 1. (A) [G(Z1] Schematic depicting the fabrication of cECM. **(B)** Schematic depicting fabrication of proteolytically engineered cECM hydrogels. Characterization of proteolytically engineered cECM hydrogels in terms of **(C)** weight remaining and **(D)** collagen content. **(E)** Representative live/dead images of MSCs on proteolytically engineered cECM hydrogels under extreme hypoxia at Day 3 with quantitative measurements of **(F)** viability, **(G)** cell density, **(H)** cell area, and **(I)** aspect ratio. Green = live, red = dead. *p<0.05, **p<0.01, ***p<0.001, ****p<0.0001.



Conclusion/Significance: We have successfully created a proteolytically engineered cECM platform to model MSC engraftment in the post-infarct environment. Our findings suggest that therapeutic MSC fate is negatively affected by the combination of proteolytically altered ECM and extreme hypoxia at the treatment site. Future work will identify the mechanistic pathway underlying these functional changes. This platform can be used to better understand the factors underlying low clinical MSC survival rates.

Session 15
Biophysical and Biomaterial Strategies to Modulate Wound Healing

11-16-2026 @ 8:00 AM - 9:30 AM

RF-012 - Controlled Release of VEGF and PDGF Using Affibody-Conjugated Hydrogel Microparticles

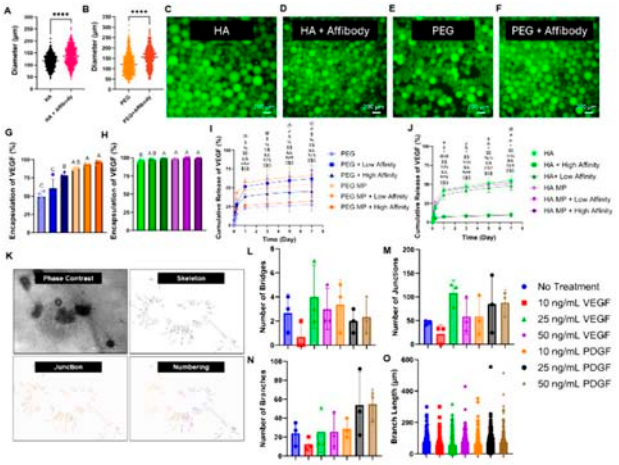
Juan Garcia

University of Oregon, Bioengineering, Eugene, United States of America

Purpose/Objectives: Vascularization is crucial for tissue repair and requires coordinated growth factor presentation. Vascular-endothelial growth factor (VEGF) promotes endothelial sprouting, while platelet-derived growth factor (PDGF) supports vessel-stabilization and maturation. Because these are opposing cues, simultaneous VEGF/PDGF delivery can inhibit angiogenesis. Systems that can temporally-control growth factor presentation may better support vascular-network-formation. Our lab has developed affibody-conjugated-hydrogels that enable affinity-controlled growth factor release. Here, we investigated whether affibody-conjugated-hydrogels and hydrogel microparticles (HMPs) can temporally control VEGF and PDGF delivery and promote angiogenic sprouting in a mesenchymal-stromal cell/endothelial cell spheroid model.

Methodology: HMPs were fabricated using 8-arm poly(ethylene-glycol)-norbornene (PEG-Nor) or hyaluronic acid-norbornene (HA-Nor). VEGF- or PDGF-specific affibodies containing a C-terminal cysteine were expressed in E. coli, purified by metal-affinity and size-exclusion chromatography, and conjugated to HA- or PEG-Nor-polymers using Irgacure-2959 and UV light (1 min,10 mW/cm2). Affibody-conjugated-polymers were crosslinked with dithiothreitol and lithium phenyl-2,4,6-trimethylbenzoylphosphinate (UV, 5 min, 30 mW/cm2) in a water-in-oil emulsion to form HMPs. HMPs were loaded with 100 ng VEGF or PDGF. Protein release was quantified by enzyme-linked-immunosorbent-assay over 7 days. To evaluate angiogenic response, human mesenchymal-stomal-cells (MSCs) and human-umbilical-vein-endothelial-cells (HUVECs) were expanded to ~80% confluency, mixed at a 3:1-MSC:HUVEC ratio, and seeded at 300,000 cells-per-well in AggreWells to generate 300 spheroids containing approximately 1000 cells-each. Spheroids were embedded in collagen/fibrin gels, and treated with 10, 25, or 50 ng/mL VEGF or PDGF. Sprout-number and length were quantified using ImageJ-Analyze-Skeleton (Fig. 1K).

Results: HMPs had mean diameters of 100–150 µm (Fig. 1A, 1B), and HA-Nor-hydrogels and HMPs encapsulated >90% of GF (Fig. 1H). HA- and PEG-based systems demonstrated affinity-dependent VEGF and PDGF release, with high-affinity-affibodies releasing less protein than low-affinity affibodies (Fig. 1I, 1J). In spheroid cultures, branch-length was not significantly different from no-treatment-control (Fig. 1M). 25 and 50 ng/mL PDGF increased branch number (Fig.



1N), while 25 ng/mL of VEGF produced the highest number of junctions (Fig. 1L) and most bridging between spheroids (Fig. 1O).

Conclusion/Significance: Overall, affibody-conjugated HMPs provide a promising platform for temporally controlling growth factor presentation for the initiation of angiogenesis. Future work includes optimizing VEGF and PDGF timing to enhance vessel formation and maturation in the MSC/HUVEC spheroids.

Session 20
Development of Stimuli-Responsive Implants for Musculoskeletal Tissue Engineering

11-16-2026 @ 1:30 PM - 3:00 PM

RF-014 - Photosoftening Macroporous Hydrogels: Single-Chemistry In Situ Pore Formation and Dynamic Stiffness Control for 3D Mechanobiology

Golnaz Navidi[1], Ben Canter[2], Ella Morris[1], Teresa Rapp[1]

[1]*University of Oregon, Chemistry And Biochemistry, Eugene, United States of America*
[2]*University of Oregon, Biology, Eugene, United States of America*

Purpose/Objectives: Hydrogel scaffolds for 3D cell culture face an inherent tension between stiffness and confinement: stiffness is tuned by tightening the polymer mesh into the 5–100 nm range, which physically cages cells (10–20 μm) regardless of bulk modulus and restricts spreading, protrusion, and migration. Macroporous architectures relieve this confinement, but existing strategies (porogen leaching or granular assembly) preclude in situ cell encapsulation and yield static mechanical properties once formed. We sought a single chemistry that delivers in situ macropore formation, simultaneous cell encapsulation, and user-controlled dynamic softening on demand.

Methodology: We synthesized RuTetrazine, a photocleavable ruthenium(II) polypyridyl-based crosslinker bearing two tetrazine moieties for bioorthogonal inverse electron-demand Diels–Alder (iEDDA) reactivity with norbornene. Mixed with norbornene-modified hyaluronic acid (NorHA), RuTetrazine crosslinks the network through iEDDA click chemistry while liberating N_2 gas. In sufficiently dense networks the N_2 is trapped during gelation, nucleating macropores in situ. Tunable softening was achieved by co-formulating with a photostable di-tetrazine crosslinker. Mechanical properties were characterized by photorheology; pore architecture was quantified by confocal microscopy. Cytocompatibility of RuTetrazine was assessed in normal human dermal fibroblasts (NHDFs) and human mesenchymal stromal cells (hMSCs) by WST-8, Ames mutagenicity, and CellROX oxidative-stress assays. Cellular response to photosoftening and pore formation was monitored by cytoskeleton staining in NHDFs and hMSCs encapsulated in macroporous NorHA-RuTetrazine hydrogels.

Results: RuTetrazine–NorHA hydrogels achieved tunable initial storage moduli from 1.5 to ~10 kPa and tunable photosoftening of 60–87% by varying the RuTetrazine:DiTet ratio. Macropore size was independently controlled through polymer concentration (with an average of 175, 85, and 55 μm diameter for 1, 2, and 3 wt%; $p<0.0001$). RuTetrazine was non-mutagenic, induced no measurable ROS, and supported >80% viability across all formulations before and after photosoftening. Encapsulated fibroblasts localized at macropore boundaries; upon photosoftening, cell surface area increased ~6-fold (~1,100 to ~6,500 μm^2, $p<0.0001$) by Day 10, while non-irradiated controls remained rounded.

Conclusion/Significance: This platform integrates macroporosity and dynamic mechanical softening into a single cytocompatible click chemistry, decoupling physical confinement from bulk stiffness. This material enables 3D mechanobiology and dynamic cell-fate studies inaccessible to conventional nanoporous photosoftening systems, with applications for modeling dynamic extracellular matrix remodeling in development, fibrosis, and cancer progression.

Session 21
Cardiovascular, Angiogenesis, Blood (General Session)

11-16-2026 @ 1:30 PM - 3:00 PM

RF-015 - Graphene as a Dual-Function Nanomaterial Platform for Enhanced Hydroxyurea Therapy in Sickle Cell Disease

Phoebe Hu[1], Yun Hu[2]

[1]*Covenant Healthcare College of Medicine at Central Michigan University, Mt. Pleasant, United States of America*
[2]*Michigan Technological University, Materials Science And Engineering, Houghton, United States of America*

Purpose/Objectives: Sickle cell disease (SCD) is one of the most prevalent inherited blood disorders worldwide, causing a wide variety of symptoms from anemia and frequent infections to debilitating pain crises. Hydroxyurea remains the standard pharmacologic treatment for SCD, with its therapeutic benefit largely attributed to the generation of nitroxide radical intermediates that promote fetal hemoglobin production. Because radicals contain one or more unpaired electrons, their formation and reactivity are strongly influenced by their intrinsic stability. Graphene, a nanomaterial renowned for its unique π-conjugated structure, is hypothesized to leverage this principle of radical stabilization to enhance hydroxyurea activation and improve its therapeutic efficacy. This study investigates graphene as a multifunctional platform for promoting hydroxyurea activation while also serving as a drug delivery vehicle for long-term SCD management.

Methodology: Density functional theory (DFT) calculations were performed to evaluate the interactions between hydroxyurea and graphene. Multiple graphene binding sites were examined to determine their effects on hydroxyurea stability and nitroxide radical formation. The electronic properties of graphene were analyzed to assess its ability to stabilize radical intermediates through electron delocalization across its extended π-conjugated structure.

Results: Computational modeling demonstrated favorable interactions between hydroxyurea and graphene. Specifically, replacing the hydrogen atom on the hydroxyl-bearing nitrogen of hydroxyurea with a graphene sheet increased the propensity for nitroxide radical generation. These findings suggest that graphene stabilizes radical intermediates, thereby facilitating hydroxyurea activation. In addition, graphene conjugation may prolong hydroxyurea retention relative to the free drug, supporting its potential utility as a drug delivery platform.

Conclusion/Significance: These findings identify graphene as a promising dual-function platform for hydroxyurea-based therapy. By promoting nitroxide radical formation while simultaneously enabling drug delivery, graphene may improve the therapeutic performance of hydroxyurea for the treatment of SCD. More broadly, this work demonstrates the potential of nanomaterial-based approaches to modulate drug activation mechanisms and advance next-generation therapeutic strategies for hematologic diseases.

Session 22
Emerging Advances in Microphysiological Platforms to Study Disease

11-16-2026 @ 1:30 PM - 3:00 PM

RF-016 - 3D Model of Adipocyte Hypertrophy-Induced Atrial Dysfunction for Therapeutic Screening

Lara Celebi[1], Pinar Zorlutuna[2]

[1]*University of Notre Dame, Aerospace And Mechanical Engineering, South Bend, United States of America*
[2]*University of Notre Dame, South Bend, United States of America*

Purpose/Objectives: Cardiovascular disease remains the leading cause of obesity-related mortality, driven in part by epicardial adipose tissue dysfunction. In obesity, epicardial adipose tissue undergoes hypertrophy and adopts a proinflammatory, metabolically disruptive phenotype that promotes myocardial dysfunction.

However, the lack of epicardial adipose tissue in small animal models has restricted mechanistic insight. We developed a human-derived, 3D bioprinted hypertrophic adipocyte-hiPSC-derived atrial cardiomyocyte model to study adipocyte hypertrophy-induced atrial dysfunction and evaluate metformin as a therapeutic candidate.

Methodology: Human adipose-derived stem cells were encapsulated in GelMA-collagen type I hydrogel and bioprinted into hollow cylindrical constructs using a CELLINK BioX6 bioprinter. Constructs were differentiated into adipocytes and treated with palmitic acid-containing media to induce a hypertrophic obese phenotype. Adipocyte function was assessed by lipid droplet analysis, glucose uptake, basal lipolysis, insulin receptor activation, ELISA, and cytokine array. DiPS 1016 SevA hiPSCs were differentiated into atrial cardiomyocytes and characterized by MLC2A, cardiac troponin T, and sarcomeric alpha-actinin expression. Atrial cardiomyocytes were then bioprinted into lean or hypertrophic adipocyte constructs. After five days, contractile function was quantified by bright-field video analysis, and insulin receptor activation, Connexin43 expression, lipid accumulation, and stress markers were evaluated by immunostaining and western blotting. To assess therapeutic response, constructs were treated with 2 mM metformin for 48 hours.

Results: Hypertrophic adipocytes exhibited increased lipid droplet size, basal lipolysis, proinflammatory cytokine secretion, altered adipokine profiles, and reduced insulin receptor expression compared with lean adipocytes. Conditioned media from hypertrophic adipocytes impaired mitochondrial respiration, glycolytic capacity, and ATP production in atrial cardiomyocytes. In direct 3D coculture, hypertrophic adipocytes disrupted calcium handling and contractile function, reduced gap junction expression, increased intracellular lipid accumulation, induced endoplasmic reticulum stress, and impaired insulin receptor phosphorylation. Metformin restored beating velocity, reduced beat-to-beat variability, enhanced insulin receptor activation, and increased AMPK phosphorylation.

Conclusion/Significance: This human-derived 3D model recapitulates key features of obesity-induced atrial dysfunction and provides a physiologically relevant platform for mechanistic studies and therapeutic screening. The findings demonstrate that metformin can partially reverse pathological effects of adipocyte hypertrophy on atrial cardiomyocytes, supporting engineered tissue models as tools to advance targeted therapies for obesity-related cardiovascular disease.

Session 25
Sex Hormone Influence on Tissue Engineering and Regenerative Medicine

11-16-2026 @ 3:05 PM - 4:35 PM

RF-017 - Local Immunotuning Patches (LIPs) Reveal Sex-Dependent Inflammatory Dynamics During Full-Thickness Wound Healing

Giulia Zaffaroni[1,2], Julia Enterria-Rosales[3], Wendy Silva[3], Federica Banche-Niclot[2], Richard Willson[4], Francesca Taraballi[2], Bruna Corradetti[3]

[1]*University of Houston, Biomedical Engineering, Houston, United States of America*
[2]*Houston Methodist Research Institute, Center For Musculoskeletal Regeneration, Dept. Orthopedics And Sports Medicine, Houston, United States of America*
[3]*Baylor College of Medicine, Center For Precision Environmental Health, Houston, United States of America*
[4]*University of Houston, Chemical And Biomolecular Engineering, Houston, United States of America*

Purpose/Objectives: Chronic wounds in metabolically dysfunctional patients exhibit dysregulated macrophage-mediated healing. Because wound repair is sexually dimorphic, this study evaluated how a Local Immunomodulatory Patch (LIP), consisting of collagen functionalized with mannose to target macrophage mannose receptors (MRC1/CD206), modulates local and systemic immunity compared with unfunctionalized collagen in a high-fat diet (HFD) mouse model, and whether these responses differ by biological sex.

Methodology: Full-thickness excisional wounds in HFD male and female mice received LIP or unfunctionalized collagen control patches. Healing and inflammation were assessed via longitudinal luminol-based IVIS imaging (local oxidative burden, days 1–21), day 1 wound qPCR (inflammatory and pro-regenerative transcriptional profiles), and day 3 terminal hematology (systemic immune status).

Results:

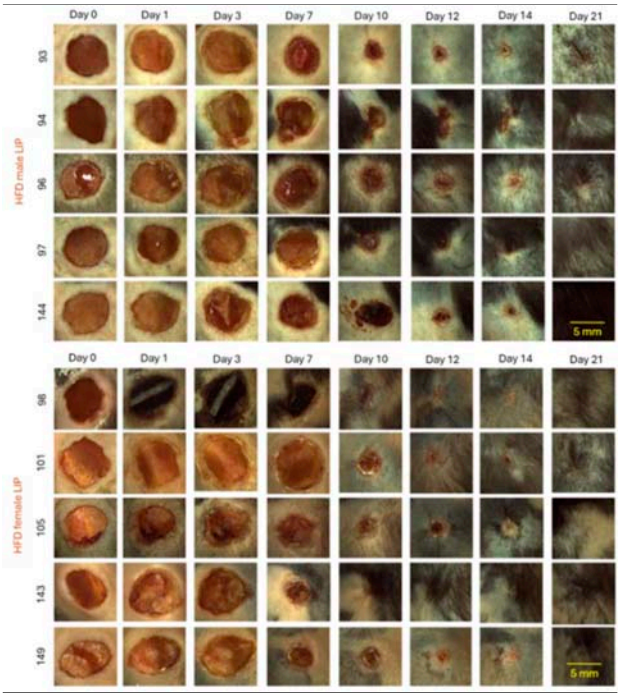


Figure 1. Representative wound images from male and female HFD mice treated with unfunctionalized collagen or LIP, illustrating sex-dependent differences in early local inflammatory burden and progressive inflammatory resolution across the 21-day healing period. LIP attenuated early local inflammatory intensity relative to controls, most prominently in females. Conversely, LIP-treated males exhibited higher early local luminol signal than females within the same treatment group. Day 1 qPCR demonstrated that LIP permitted requisite acute inflammation while concurrently engaging repair-associated pathways; LIP-treated males showed significantly higher TGF-β, IL-1β, and TNF-α expression than females. Day 3 hematology revealed that LIP-treated males mounted a stronger systemic leukocyte and neutrophil response than collagen-treated males, whereas females maintained lower overall systemic inflammatory activation with less pronounced treatment-dependent differences. Inflammatory signals in all groups progressively resolved by days 14–21.

Conclusion/Significance: LIP coordinates early immune activation with progressive inflammatory resolution under metabolic stress without suppressing the acute phase necessary for repair. The host response to LIP is markedly sex-dependent: males exhibit robust early local and systemic inflammation alongside concurrent repair-associated signaling, while females demonstrate attenuated local inflammatory burden and a more regulated systemic baseline. These divergent trajectories demonstrate that pooling sexes without stratification obscures biologically meaningful differences in immune activation and resolution kinetics, identifying both sex and metabolic status as essential covariates in preclinical LIP and broader biomaterial research.

Session 27
Advanced Biomaterials for Controlled Drug Release and Immune Modulation

11-16-2026 @ 3:05 PM - 4:35 PM

RF-018 - Improving Immunoprotective Cell Surface Engineering Using Branched PEG Architectures

Damea Pham[1], Cherie Stabler[1,2], Allison Bayer[2]

[1]*University of Florida, J Crayton Pruitt Family Department of Biomedical Engineering, Gainesville, United States of America*
[2]*University of Florida, Diabetes Institute, Gainesville, United States of America*

Purpose/Objectives: Cellular therapies hold significant promise; however, clinical translation is limited by immune-mediated recognition and rejection. To decrease reliance on systemic immunosuppression, researchers have explored the use of biomaterials. Polymer cell-surface grafting using poly(ethylene) glycol (PEG) decreases cell rejection in preclinical models; however, how PEG exerts this effect and the role of polymer architecture in governing immune protection remain poorly defined. One parameter of interest is PEG architecture, as increased PEG branching can increase steric hindrance and potentially decrease cell-surface immunogenicity. Here, we leveraged an vitro immune screening platform to investigate the capacity of linear and Y-shaped PEG architectures to mask cell-surface proteins and dampen CD8+ T cell activation.

Methodology: Murine cells were derivatized with linear or Y-shaped mPEG-NHS by incubation for one hour in a 4mM PEG-DPBS solution (pH 7.8). PEG-mediated inhibition of antibody binding to CD3, CD45, T cell receptor, and Major Histocompatibility Complex I (MHC-I) was assessed via flow cytometry. To evaluate impacts of PEG cell grafting on immunogenicity, PEGylated cells were then co-cultured with antigen-specific naïve OT-I CD8+ T cells for 6 hours. Early activation of OT-I CD8+ T cells via CD69+Nur77+ was detected via flow cytometry.

Results: PEGylation globally reduced antibody binding across all tested surface epitopes, with varying degrees of suppression. Compared with linear PEG, Y-PEG decreased CD3 and TCR recognition but increased MHC-I detection. Utilizing an antigen-specific mixed lymphocyte reaction, PEGylated mOVA stimulators globally reduced activation of OT-I CD8+ T cell responders, measured via CD69+Nur77+ co-expression. Compared with linear PEG, CD8+ T cells cultured with Y-PEG-grafted cells showed decreased co-expression of CD69 and Nur77, indicating enhanced suppression of early T cell activation.

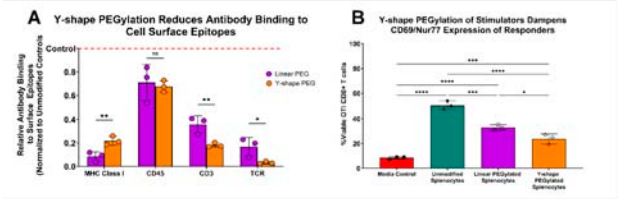


Figure 1. Branched PEGylation results in (A) enhanced epitope masking, leading to (B) enhanced suppression of T cell activation

Conclusion/Significance: These findings demonstrate that PEGylation establishes a steric barrier that limits recognition of cell-surface markers. Polymer architecture significantly influences immune shielding, with Y-shaped PEG providing greater epitope masking and stronger attenuation of early T cell activation than linear PEG. Collectively, these results provide mechanistic insight into how PEG structure modulates immune recognition and support the development of branched PEG conformations to improve immunoprotective cell-surface engineering.

Session 31
Biofabrication Technologies for Organoid Engineering

11-16-2026 @ 3:05 PM - 4:35 PM

RF-020 - Dissecting Solid Tumor Invasion Through Systematic Variation of Fibrillar Matrix Architecture In Vitro

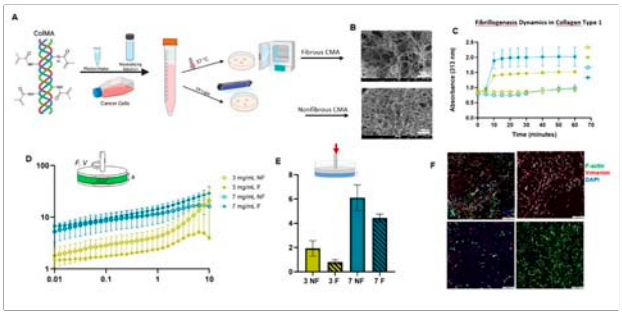
Ayda Sadat Pourmostafa[1], Mohaddeseh Mohammadi[2], Hasan Erbil Abaci[3], Leila Donyaparastlivari[2], Deniz Ornek[3], Amir K Miri[2]

[1]*New Jersey Institute of Technology, Newark, United States of America*
[2]*New Jersey Institute of Technology, Biomedical Engineering, Newark, United States of America*
[3]*Columbia University, Biomedical Engineering, New York, United States of America*

Purpose/Objectives: The tumor microenvironment (TME) provides critical biophysical cues that regulate cancer progression and invasion. During metastasis, extracellular matrix (ECM) remodeling alters collagen organization and tissue mechanics, influencing cancer cell behavior. Although collagen I is a key regulator of migration, invasion, and mechanotransduction, the specific role of collagen fibrillar architecture remains poorly understood. Here, we developed a 3D collagen-based platform with engineered fibrous and non-fibrous architectures to investigate how collagen fibrillogenesis regulates breast cancer cell behavior and ECM remodeling.

Methodology: Methacrylated collagen (CMA) hydrogels were engineered to generate either fibrous matrices through thermal self-assembly or non-fibrous matrices through direct photocrosslinking. Fibrillogenesis was confirmed using turbidity assays. Matrix architecture and mechanics were characterized by scanning electron microscopy (SEM), and rheological testing. MDA-MB-231 breast cancer cells were encapsulated at 1×10^6 cells/mL and cultured for 14 days. Cell viability, proliferation, morphology, migration, and ECM remodeling were assessed using Live/Dead staining, phalloidin/DAPI staining, confocal microscopy, and ImageJ-based analysis. Expression of matrix remodeling genes, including MMPs, LOX, and TGM2, was evaluated to quantify tumor-associated ECM remodeling.

Results: Turbidity analysis demonstrated successful collagen fibrillogenesis in thermally assembled hydrogels, whereas photocrosslinked hydrogels remained non-fibrillar. SEM and reflectance imaging confirmed distinct microarchitectures, with dense collagen fiber networks present only in fibrous matrices (A-C). Rheological and indentation measurements confirmed that increasing collagen concentration from 3 to 7 mg/mL increased matrix stiffness, whereas fibrillar hydrogels exhibited reduced elastic modulus and enhanced viscoelastic relaxation relative to non-fibrillar matrices (D-E). Over time, fibrous hydrogels exhibited increased fiber density, collagen deposition, and matrix stiffening, indicating active tumor-mediated remodeling. MDA-MB-231 cells cultured within fibrous matrices displayed enhanced spreading, elongated morphology, cytoskeletal organization, and significantly greater spheroid migration compared with cells in non-fibrous matrices (F). In contrast, cells in non-fibrous hydrogels remained predominantly rounded with limited matrix interaction. Increased expression of matrix-remodeling markers further confirmed elevated invasive activity within fibrous environments.



Conclusion/Significance: Our findings demonstrate that collagen microstructure, independent of matrix composition, is a key determinant of breast cancer remodeling and invasive behavior. By recapitulating tumor-associated fibrous architectures, this platform enables mechanistic investigation of the invasion–metastasis cascade and offers a physiologically relevant system for evaluating ECM-targeted therapies.

Session 32
Lymphatic Engineering and Regeneration

11-16-2026 @ 5:05 PM - 6:35 PM

RF-021 - Detecting Differences in Lymphatic Junction Morphology in a Lymphatic-on-a-Chip Model with a Novel Quantitative Analysis Pipeline

Stephen Larson[1], Annabelle Feller[2], Catherine Whittington[1]

[1]*Worcester Polytechnic Institute, Biomedical Engineering, Worcester, United States of America*
[2]*DeCalifornia State Polytechnic University Humboldt, Chemistry And Biochemistry, Arcata, United States of America*

Purpose/Objectives: Lymphatic vasculature enables tissue homeostasis by controlling fluid drainage via lymphatic endothelial cell (LEC) junctions. With button-like junctions, fluid passes easily into lymphatic vessels. Fibrosis causes vessel dysfunction with more zipper-like junctions that inhibit fluid uptake. Fibrotic mechanisms that influence junction morphology remain unclear, so we need to quantify changes in junction morphology and correlate them with lymphatic function (e.g., permeability). We addressed that gap by leveraging our newly developed analysis pipeline of LEC junction morphology to evaluate vessel integrity under fibrotic/inflamed conditions within a microfluidic chip.

Methodology: We used a lymphatic-on-a-chip platform to model lymphatic vessels in fibrotic tissue with and without tumor necrosis factor (TNF)-α (inflammatory factor). Methacrylated type I collagen gel with ruthenium/sodium persulfate photoinitiators and photo-crosslinking were leveraged to mimic acute (1 kPa) and chronic fibrosis (6 kPa). Human dermal LECs were seeded within collagen channels in the chip, treated with TNF-α (20 ng/mL; 24 hours), and stained for confocal microscopy of VE-cadherin (junction protein). A new automated image analysis pipeline (MATLAB, ImageJ/FIJI, CellProfiler™) was used to quantify button- or zipper-like morphologies by sectioning cells and measuring junction skeletal endpoints and object size (measures of junction fragmentation) and junction thickness based on VE-cadherin signal. We also measured permeability of 40 kDa fluorescently labeled dextran through acellular collagen gels within the device.

Results: The pipeline quantified differences in junction morphology between inflamed (TNF-α, button) and non-inflamed (no TNF-α, zipper) conditions in 1 and 6 kPa gels. Across stiffness conditions, more zipper-like junctions were observed with less junction fragmentation (decreased endpoints; increased object size) and decreased junction width. When demonstrating feasibility for future correlation of junction morphology and function, fluorescence intensity decreased with distance in both gels, but stiff gels exhibited a slightly steeper decline in intensity.

Conclusion/Significance: Our pipeline produces a comprehensive analysis to quantify differences in LEC junction morphology and detect subsequent vessel dysfunction. When combined with preliminary permeability studies, results demonstrate our ability to evaluate vascular integrity under fibrotic/inflamed conditions within a lymphatic-on-a-chip model. Moreover, this work provides a foundation for futures studies of mechanisms driving lymphatic function in fibrotic diseases.

Session 33
Extracellular Vesicles for Regenerative Medicine, Drug Delivery, and Cell-Free Therapies

11-16-2026 @ 5:05 PM - 6:35 PM

RF-022 - Hydrogel stiffness influences cancerous matrix-bound nanovesicle production and subsequent cell behavior

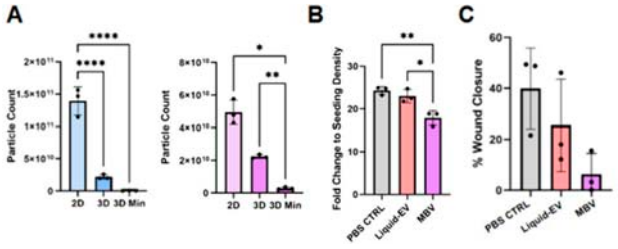
Ivan Chavez, Catherine Zhu, Marley Dewey

University of California Santa Barbara, Bioengineering, Santa Barbara, United States of America

Purpose/Objectives: The extracellular matrix (ECM) has been identified as an influential component of the microtumor environment, affecting cell behavior through both mechanical and biomolecular signals. Recently, a new subtype of extracellular vesicle (EV) known as matrix-bound nanovesicles (MBVs) was discovered residing in the ECM; however, their role in cancer is still poorly understood. Given the roles of both the ECM and EVs in cancer, we sought to characterize how ECM stiffness influences EV production and how MBVs impact cancer progression.

Methodology: MG-63 and SAOS-2 osteosarcoma cells were cultured on 2D (tissue culture plastic), soft 3D (collagen hydrogel), and stiff 3D (hydroxyapatite collagen hydrogel) culture conditions for 15 days, after which liquid-EVs were isolated from conditioned culture medium and MBVs from digested ECM and gels. We then characterized their size, yield, surface markers, protein cargo, and functional outcomes on healthy cells (stem cells, fibroblasts).

Results: MBV and liquid-EV protein concentrations were dependent on culture conditions, and MBVs were enriched in different surface proteins compared to liquid-EVs (CD81, CD63, ALIX). Both EV types were the same size regardless of culture conditions; however, culture conditions altered EV yields, with stiff 3D gels yielding the fewest EVs. We also found that cancerous MBVs negatively impacted stem cell viability, whereas liquid-EVs did not, and MBVs inhibited wound closure in fibroblasts. We plan to present forthcoming data on proteomic analyses, as well as function differences of EVs from different culture conditions. (A) MBV yield from SAOS-2 cells (blue) and MG-63 (purple), 3D (soft gels) and 3D Min (stiff gels). (B) Fold increase in MSC metabolic activity (Alamarblue) after exposure to EVs after 3 days (1E6 EVs/well). (C) Percent wound closure of lung fibroblasts after 24hr treatment with 1E8 EVs/well. Data presented as mean+/-standard deviation (n=3, significance $p<0.05$).



Conclusion/Significance: Our findings suggest that MBVs are a distinct type of EV, culture conditions influence resulting EV yields, and MBVs have different functional impacts on healthy cells. This indicates MBVs within the ECM may influence cancer progression and cell function distinctly from other EV types.

Session 35
Musculoskeletal (General Session) 1

11-16-2026 @ 5:05 PM - 6:35 PM

RF-024 - Affinity-based protein delivery for bone regeneration using affibody-functionalized polyethylene glycol-maleimide microparticles

Andy Huang[1,2], Joseph Qualtier[2], Marian Hettiaratchi[1,2,3]

[1]*University of Oregon, Bioengineering, Eugene, United States of America*
[2]*University of Oregon, Knight Campus For Accelerating Scientific Impact, Eugene, United States of America*
[3]*University of Oregon, Chemistry And Biochemistry, Eugene, United States of America*

Purpose/Objectives: Bone regeneration after traumatic injury relies on the coordinated release of signaling proteins but is often impaired by dysregulation of the healing cascade. Effective healing requires sustained release of osteogenic cues like bone

morphogenetic protein-2 (BMP-2). Current clinical strategies deliver recombinant BMP-2 with a collagen sponge but often fail to successfully heal delayed- or non-union fractures due to burst release. Here we aim to use an affinity-based approach with engineered protein binders, known as affibodies, that can specifically bind BMP-2 with variable affinity to control release from affibody-functionalized polyethylene glycol (PEG) hydrogels.

Methodology: PEG microparticles (PEGMPs) were fabricated via batch emulsion. Affibody-functionalized 4-arm PEG-maleimide was emulsified in mineral oil and crosslinked with dithiothreitol to form PEGMPs. Affibody-functionalized PEGMPs (Aff-PEGMPs) were loaded with BMP-2 and incubated in 10% fetal bovine serum (in saline). Samples were periodically collected for protein quantification via enzyme-linked immunosorbent assay and compared to BMP-2 release from a bulk PEG hydrogel. Successful affibody functionalization was verified via fluorescent imaging of fluorescein-tagged affibodies on PEGMPs.

Results: Fluorescent imaging verified successful affibody incorporation, where only Aff-PEGMPs exhibited fluorescence compared to non-functionalized PEGMPs (Figure 1A). Protein release rates were inversely correlated with affibody density, where 500x molar excess affibody PEGMPs demonstrated the slowest release and 100x molar excess affibody PEGMPs demonstrated faster release, similar to what was observed with bulk PEG hydrogels (Figure 1B). All affibody-containing PEGMPs released BMP-2 more slowly than PEGMPs without affibodies, regardless of hydrogel morphology.

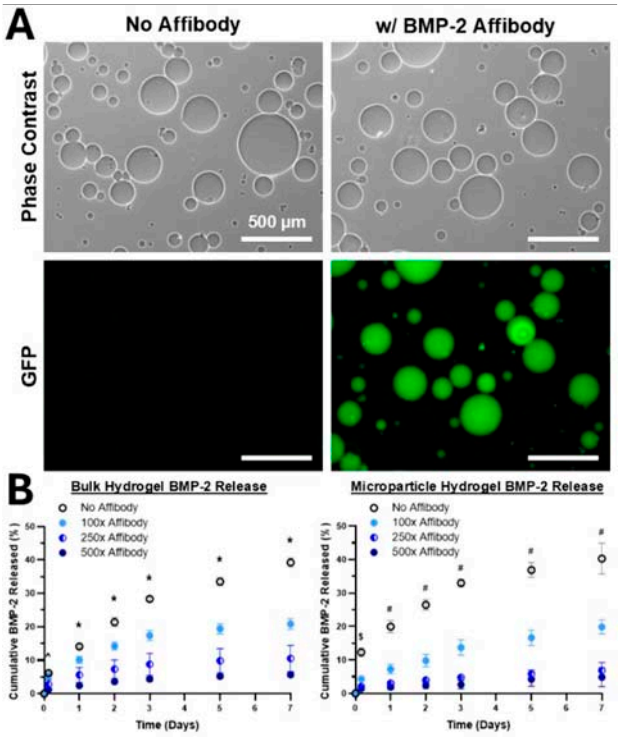


Figure 1. **A**) PEGMPs with and without fluorescein-tagged BMP-2 affibody and **B**) controlled BMP-2 release from bulk hydrogel and PEGMPs at varying affibody concentrations (100x, 250x, and 500x molar excess to 100ng of BMP-2). Symbols indicate significance from a two-way ANOVA ($p<0.05$): ^ No Affibody vs 250x or 500x Affibody groups, * all groups, $ No Affibody vs all Affibody groups, # all groups except 250x vs 500x Affibody.

Conclusion/Significance: This work demonstrates the first-time affibodies have been used to modulate protein delivery from an injectable PEG-based platform. Future work will focus on demonstrating the efficacy our platform and the bioactivity of the factors released through osteogenic differentiation of human mesenchymal stem cells.

Session 36
Advancing MPS as New Approach Methods (NAMS)

11-16-2026 @ 5:05 PM - 6:35 PM

RF-025 - Engineering a microphysiological system (MPS) to assess the impacts of inflammation on human cytotoxic T cell (CTL) invasion into 3D pancreatic tissue niches

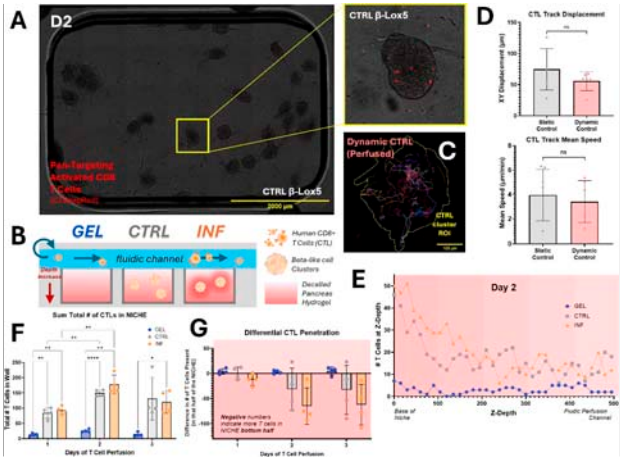
Sierra Jackson[1], Madgalena Samojlik[2], Min Du[2], Aidan Fernandez[2], Cherie Stabler[2,3]

[1]*University of Florida, Biomedical Engineering, Gainesville, United States of America*
[2]*University of Florida, J Crayton Pruitt Family Department of Biomedical Engineering, Gainesville, United States of America*
[3]*University of Florida, Diabetes Institute, Gainesville, United States of America*

Purpose/Objectives: In many human autoimmune conditions, large amalgamations of cytotoxic T cells (CTLs) are identified proximally to sites of target cell loss, potentially driving disease progression. While CTLs have the capacity to kill target cells, we still lack an extensive understanding of the temporal drivers of this CTL tissue invasion.

Methodology: To interrogate the temporal impacts of cell load and inflammation on CTL infiltration into 3D pancreatic-tissues, we generated serial 3D niches in an MPS (ibidi, 3D Luer) containing decellularized pancreas hydrogel. We then loaded this ECM with beta-cell-like clusters that were pre-treated, or not, with an inflammatory cocktail (A-B). Human CTLs were continuously perfused within the MPS at 1-3 dynes/cm^2 using a peristaltic pump. The inclusion of solubilized dextran (70kDa, 3%) to the media enabled continuous perfusion of viable (>50%) T cells over 48hrs.

Results: Over 3d of continuous perfusion, CTLs were present in all MPS niches, exhibiting the migration of CTLs from perfusion into the ECM niche (A, F); TrackMate analysis of CTL migration via timelapse confocal images found the migration behavior metrics of speed and displacement consistent between CTLs perfused or added atop the niche (C, D). Global assessment of CTL invasion revealed that cell load, with or without inflammation, significantly contributed to CTL recruitment (F). Furthermore, cell presence resulted in deeper infiltration into tissue niches (E, G). [LEGEND] (**A**) Tile-scan and zoomed vignette of control clusters with recruited, previously-circulated CTLs (D2, confocal, 10x) (**B**) MPS side-view highlighting serial niches (**C**) Total CTL tracks on a dynamically perfused control cluster (D2, confocal, 20x) (**D**) Migration parameters for CTL displacement and mean speed on dynamically perfused clusters (**E**) Representative CTL invasion into niche (N=1) (**F**) Sum total of invaded CTLs over time (n=4, N=1) (**G**) Differential CTL penetration into niche (n=4, N=1).



Conclusion/Significance: This approach establishes the feasibility of a translational benchtop platform for exploring CTL recruitment in the pancreas using novel immune cell circulation

techniques. Initial studies support the contributions of cell load and inflammation in promoting CTL tissue invasion. Future studies seek to leverage the technology to further investigate the contributions of antigen-specificity on T cell invasion, retention, and target killing.

Session 39
Stem Cells & Cell Therapies & Developmental Biology and Cell Signaling (General Session)

11-17-2026 @ 8:00 AM - 9:30 AM

RF-027 - A proteomic overview of low-dose Chlorpyrifos toxicity in equine adipose tissue-derived multipotent stromal/stem cells

Ernesto Miranda-Morales, Mandi Lopez, Aiyanna Mcgowan, Colette Rainey

Louisiana State University School of Veterinary Medicine, Veterinary Clinical Sciences, Baton Rouge, United States of America

Purpose/Objectives: Studies measuring the effect of Chlorpyrifos (CPF) on progenitor cells from grazing horses are limited. This study measured protein expression levels following acute exposure of equine adipose tissue-derived multipotent stromal/stem cells (ASCs) to CPF.

Methodology: Cells were revitalized and subcultured to P2. At 80% confluence, stromal medium was replaced with unmodified medium (control), 0.057, 0.14, or 1.4 μM CPF for 24-hours. Peptides were obtained using tandem mass tag labeling liquid chromatography-mass spectrometry. Raw data was processed with MaxQuant and UniProt. Proteins were identified at a false discovery rate (FDR) < 1% and ProteinProphet for assigning probabilities. Differential protein abundances between control and CPF-treated groups and between CPF treatment groups were quantified (P_{adj}< 0.05, $|\log_2 FC| \geq 0.58$) and annotated using Gene Ontology (GO).

Results: 34 proteins were abundantly high, while 63 were low. In total, 97 were differentially abundant. Five proteins demonstrated differential abundance at all three CPF concentrations. Following verification, 41 proteins were significantly modified. Biological processes for the highly abundant proteins included double-strand break repair, associated in all three treatment groups (0.057, 0.14, and 1.4 μM CPF) via BRCC3 (P_{adj} = 0.003, 0.0003, and 0.003, respectively), mitochondrial function, and gene regulation. GO enrichment cluster analysis identified low abundance proteins including the biological processes of actin cytoskeleton organization and actin filament-based movement and the molecular function of microfilament motor activity.

Conclusion/Significance: Modification to the horse ASC proteome following low-dose CPF toxicity may be impacting cellular stress and injury via cytoskeletal structure, mitochondrial function, and gene regulation.

RF-028 - Hematopoietic Stem Cell Aging in a 3D In Vitro Bone Marrow-Mimetic Model

Truc Dinh, Charlotte Stevens, Connor George, Dallin Jacobs, Nathan Bribiesca, Aidan Gilchrist

University of California, Davis, Biomedical Engineering, Davis, United States of America

Purpose/Objectives: The bone marrow (BM) microenvironment regulates hematopoietic stem and progenitor cells (HSPCs), which give rise to blood and immune cells. With aging, the BM undergoes significant changes in stiffness that are linked to HSPC dysfunction. However, interactions between these altered mechanical cues and HSPCs are poorly understood, limiting our ability to predict HSPC behavior in vivo and the development of therapies tailored to older patients. To address this, we present an *in vitro* 3D model that incorporates mechanical properties of the aging BM. Our BM-mimetic model consists of HSPCs encapsulated in polyisocyanopeptide (PIC), a fibrous hydrogel that dissociates at low temperatures. This property enables non-enzymatic recovery of HSPCs for downstream applications, preserving critical surface markers involved in mechanosensing.

Methodology: Low molecular weight (LMW, 295 kg/mol) and medium molecular weight (MMW, 476 kg/mol) PIC contain 1% GRGDS. Mechanical properties of PIC were characterized using a rheometer at a 1% strain and a 1 $rad*s^{-1}$ frequency. Human induced pluripotent stem cells were differentiated into HSPCs before resuspension in PIC at 1 * 10^6 $cells*mL^{-1}$. The system was cultured in StemSpanII supplemented with recombinant human SCF, TPO, IL-6, and Flt3-Ligand at 100 $ng*mL^{-1}$ each.

Results: The storage moduli range of 0.2 wt% PIC covers the stiffness of a young rhesus macaque BM sample (~50 Pa) (Fig. 1A). HSPCs in 0.5 wt% MMW PIC formed smaller, compact clusters (Fig. 1B) whereas those in LMW PIC were more disperse and had cells with visible protrusions. Both 0.5 wt% LMW and MMW PIC maintained HSPCs and other progenitors over 7 days (Fig. 1C).

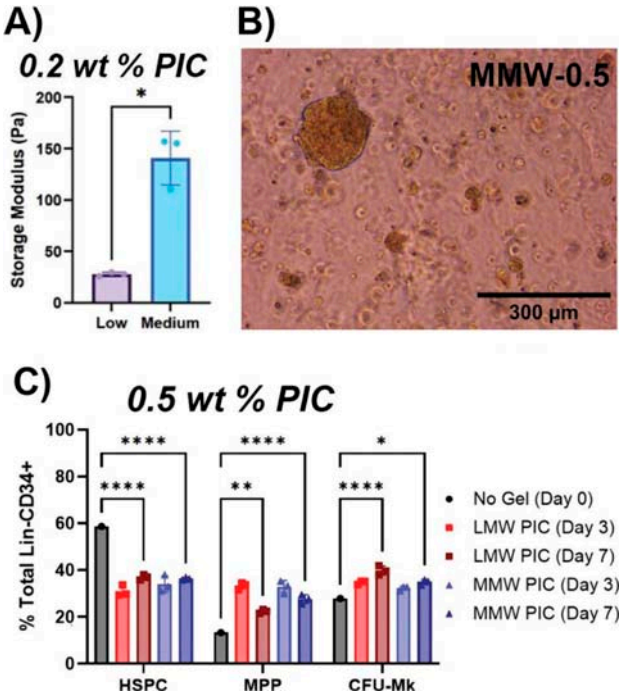


Figure 1. A) Stiffnesses of 0.2 wt% PIC. B) HSPCs in LMW-0.5 PIC by Day 14. C) Changes in HSPC differentiation over 7 days. * p≤0.05, ** p≤0.01, *** p≤0.001, **** p≤0.0001

Conclusion/Significance: We developed an *in vitro* 3D niche that models aged BM by controlling hydrogel mechanical properties while maintaining constant binding ligand density. HSPCs cultured in our hydrogels maintained multipotency, self-renewal, and proliferative capacity, demonstrating the feasibility of our model. Incorporation of intrinsic and extrinsic aging factors enables our platform to reveal new mechanobiological targets and guide the development of therapies to slow hematopoietic aging.

Session 41
Dental & Craniofacial (General Session)

11-17-2026 @ 8:00 AM - 9:30 AM

RF-029 - Phytocystatin CaneCPI-5 modulates the osteoimmune microenvironment to enhance scaffold-mediated osteogenic differentiation and bone repair

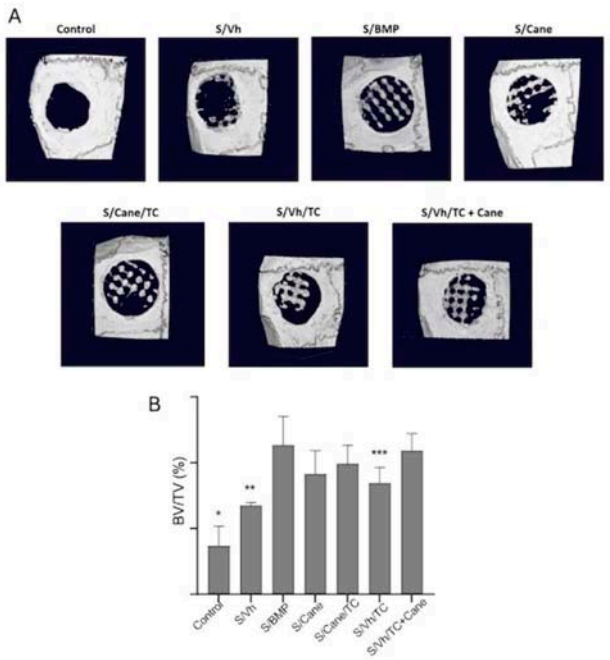
Maria Lopes[1], Luan Faria[1], Camyla Nascimento[1], Felippe Marega[2], Eduardo Backes[2], Carlos Rossa Jr[1], Flavio Da Silva[3], Joni Cirelli[1]

[1]*School of Dentistry at Araraquara, Sao Paulo State University, UNESP, Diagnosis And Surgery, Araraquara-SP, Brazil*
[2]*Federal University of São Carlos, UFSCAR, Materials Engineering, São Carlos, Brazil*
[3]*Federal University of São Carlos, UFSCAR, Genetics And Evolution, São Carlos, Brazil*

Purpose/Objectives: Phytocystatins have emerged as promising bioactive molecules due to their immunomodulatory and matrix-regulatory properties; however, their effects on osteogenic differentiation and bone repair remain insufficiently explored. This study investigated the effects of the phytocystatin CaneCPI-5 on the osteogenic differentiation of bone marrow stem cells (BMSCs) and its potential to enhance bone regeneration when combined with scaffolds and cell therapy.

Methodology: In vitro, BMSCs were treated with different concentrations of phytocystatin under basal and osteogenic conditions. Cell viability was assessed by Alamar Blue assay, osteogenic differentiation was evaluated by RT-qPCR analysis of osteogenic markers, alkaline phosphatase activity, and Alizarin Red staining for matrix mineralization. To better mimic the in vivo microenvironment, where multiple cell types coexist, 3D cultures were also evaluated under co-culture conditions of BMSCs and bone marrow-derived macrophages (BMDMs). For the in vivo study, critical-size calvarial defects were created in mice and treated with 3D-printed PCL scaffolds combined with GelMA hydrogel, CaneCPI-5, BMP-2, and/or BMSC cell therapy. Bone regeneration was evaluated after 42 days by micro-computed tomography and immunohistochemical analysis of Runx2, osteopontin, and osteocalcin expression.

Results: In vitro, CaneCPI-5 at higher concentrations enhanced osteogenic gene expression and promoted increased ALP activity and mineralized matrix deposition without compromising cell viability. 3D co-culture models of BMSCs and BMDMs showed increased mineralized nodule formation in groups containing CaneCPI-5 incorporated into the GelMA hydrogel compared with control groups. Quantitative analysis demonstrated greater mineralized matrix deposition under co-culture conditions, suggesting a synergistic effect between both cell types on osteogenesis ($p<0.05$). Furthermore, multiplex analysis of 3D culture BMSC lysates demonstrated that pretreatment with CaneCPI-5 significantly increased VEGF, IGF-1, and OPN production compared with the other experimental groups. In vivo, pretreatment of BMSCs with CaneCPI-5 increased bone formation compared with non-pretreated cell therapy, achieving values comparable to those of BMP-2 treatment. The immunohistochemistry results corroborated the micro-CT data ($p<0.05$, One-way-ANOVA, Tukey).



Legend-(A) Representative images of the three-dimensional reconstruction. **(B)** Percentage of bone volume assessed by microCT (ANOVA/Tukey, $p \leq 0.05$).

Conclusion/Significance: Collectively, in vitro and in vivo findings demonstrate that CaneCPI-5 modulates osteogenic differentiation and supports bone regeneration by creating a favorable microenvironment for matrix deposition and tissue maturation.

Session 42
Strategies for Regeneration of the Nervous System

11-17-2026 @ 8:00 AM - 9:30 AM

RF-030 - A Robust Rat Optic Nerve Crush Model for Testing Neuroregenerative Therapy

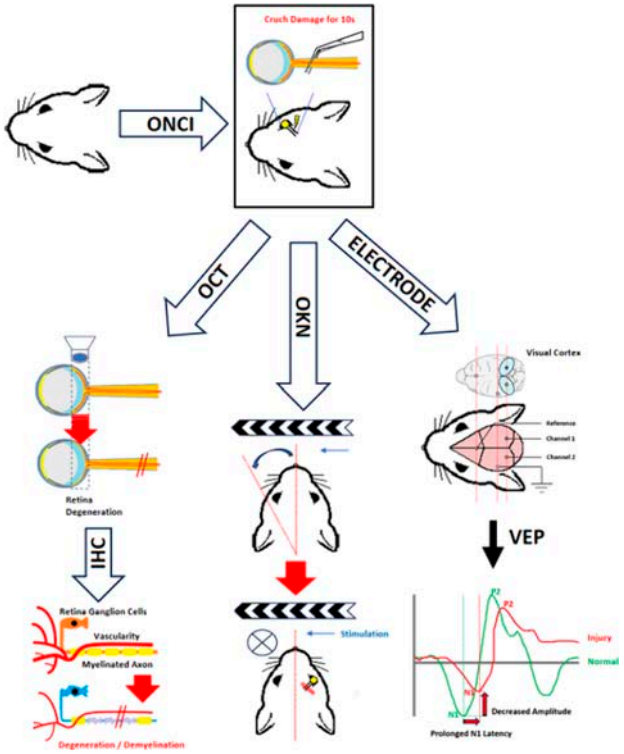
Qingqi Li[1,2], Eric Marrotte[1,2,3], Brent Roeder[1,2], Vy Vuong[1,2], Brendyn Miller[1,2], Yalcin Kulahci[1,2], Robert Hampson[1,2], J. William Vaughan[1,2], Anthony Atala[1,2], Shay Soker[1,2]

[1]*Wake Forest Institute for Regenerative Medicine, Winston-Salem, United States of America*
[2]*Wake Forest University School of Medicine, WinstonSalem, United States of America*
[3]*Department of Neurology, Wake Forest University School of Medicine, WinstonSalem, United States of America*

Purpose/Objectives: Eye injuries in the United States result in over 50,000 cases of permanent vision loss annually, with incidence varying by etiology. Because the optic nerve lacks intrinsic regenerative capacity, therapeutic options remain limited. Placental-derived stem cells (PSCs), initially identified by Wake Forest Institute for Regenerative Medicine (WFIRM) faculty, exhibit multipotency, including neuronal differentiation, positioning them as promising candidates for optic nerve repair. This study aims to establish reproducible protocols to evaluate PSC efficacy in promoting optic nerve regeneration.

Methodology: Optic nerve crush injury was induced using Dumont crossover forceps. During surgery, electrodes were implanted over the visual cortex and interfaced with a BlackRock electrophysiology system for visual evoked potential (VEP) acquisition and MATLAB based analysis. Retinal morphology was assessed via Optical Coherence Tomography (OCT), and visual function evaluated using Optokinetic Nystagmus (OKN). Immunohistochemistry (IHC) employed βIII-tubulin and neurofilament (NF) for neuronal and axonal labeling, while VE-cadherin assessed vascular junction integrity. Luxol Fast Blue staining quantified myelin integrity within the optic nerve.

Results: A reproducible rat optic nerve injury model was successfully established and validated using visual evoked potentials (VEP), which consistently demonstrated N1 latency prolongation and



amplitude reduction. Optimization of OCT and OKN protocols is currently underway. Histological analysis revealed significant reductions in neuronal density, vascularity, and myelination within injured optic nerves and retinas.

Conclusion/Significance: We successfully developed a reproducible optic nerve injury model with integrated functional and structural assessments using VEP, OCT, and histology. These findings provide a robust platform for investigating PSC based therapies aimed at restoring vision following optic nerve damage.

RF-031 - Grafting of Hyaluronic Acid Thin Films onto Polyimide-Based Neural Implants

David Frey, Ander Switalla, Felix Deku, Max Tenenbaum, Jaisel Sappal, Marian Hettiaratchi

University of Oregon - Phil & Penny Knight Campus for Accelerating Scientific Impact, Bioengineering, Eugene, United States of America

Purpose/Objectives: Microelectrode arrays (MEAs) are powerful tools for the treatment of neurological diseases. Reliable signaling between MEAs and neural tissue remains limited due to inflammation-mediated fibrotic encapsulation of the device. Hydrogel coatings can soften device-tissue interfaces, serve as therapeutic delivery platforms, and modulate cell behavior. Hydrogel coatings have depended on non-covalent interactions to adhere to the device, but film shearing during implantation may result in delamination. While Polyethylene glycol-based (PEG) coatings can reduce immune cell reactions and fibrotic encapsulation, growing evidence of anti-PEG immunity limits their long-term application. Hyaluronic acid (HA) is an intrinsic component of brain tissue and helps regulate cell behavior. HA has been explored as an anti-fouling coating but there is little work on covalent attachment of HA onto neural devices. We present a method for the covalent attachment of HA coatings onto polyimide-based neural devices.

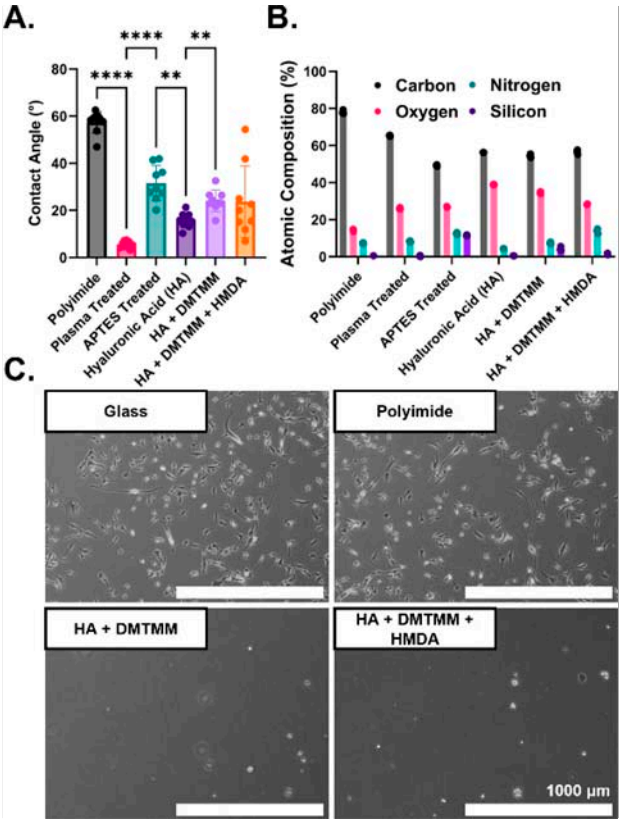


Fig 1. **A)** Water contact angle of functionalized polyimide surfaces (n=9, * $p < 0.01$ One-way ANOVA Brown-Forsythe and Welch test). **B)** Atomic composition from XPS analysis, 3 test sites per sample. **C)** U-87s on coated coverslips, day 4.

Methodology: Polyimide (PI) was spin coated on glass coverslips, cured at 350 °C, activated under O_2-plasma exposure then functionalized with primary amines via vapor deposition of (3-Aminopropyl)triethoxysilane (APTES). 8 w/v% HA was spin coated on amine-functionalized polyimide. To conjugate HA onto the APTES and crosslink with adjacent HA chains, a mixture of 0.5 M 4-(4,6-Dimethoxy-1,3,5-triazin-2-yl)-4-methylmorpholin-4-ium chloride (DMTMM) and 0.25 M hexamethylenediamine (HMDA) was applied to the film overnight. Surface functionalization was evaluated via contact angle measurements, X-ray photoelectron spectroscopy (XPS), and atomic force microscopy. Human astrocytoma cells (U-87 MG) were cultured on HA thin films and evaluated for cell adherence and spreading over 4 days.

Results: Surface characterization suggests successful grafting of HA onto the surface (**Fig. 1A & 1B**). Astrocytoma cells cultured on HA films were found to be less adherent than on glass or polyimide, suggesting that the HA film can be used as an anti-fouling coating (**Fig. 1C).**

Conclusion/Significance: Grafted HA thin films are promising for mitigating cell-interface interactions and will be evaluated chronically *in vivo*for mitigating glial encapsulation of implanted neural probes.

Session 43
Respiratory, Urologic & Gastrointestinal (General Session)

11-17-2026 @ 8:00 AM - 9:30 AM

RF-032 - Mouse Thyroid Cartilage as a Model of Cartilage Regeneration

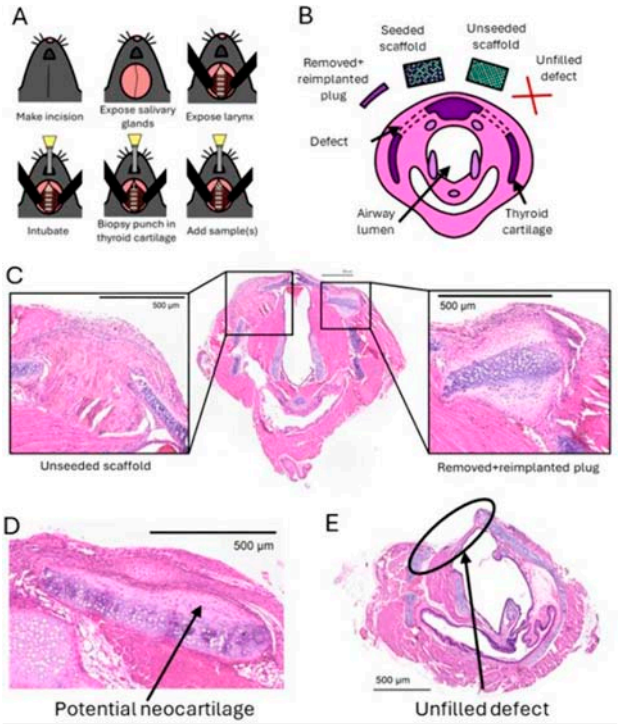
Rayna Schoenberger[1,2], Isabella Lopez[1,2], Yasmine Dahleh[3], Eiman Bandora[1,4,5,6], Hagar Kenawy[1], Dana Ragbirsingh[1], Hannah Bonelli[1,2], Kenji Yeoh[2], Riccardo Gottardi[1,2]

[1]*Children's Hospital of Philadelphia, Otolaryngology, Philadelphia, United States of America*
[2]*University of Pennsylvania, Bioengineering, Philadelphia, United States of America*
[3]*Temple University, Bioengineering, Philadelphia, United States of America*
[4]*Tel Aviv Medical Center, Department of Otolaryngology, Head And Neck Surgery, Tel Aviv, Israel*
[5]*Tel Aviv University, The Gray Faculty of Medical And Health Sciences, Tel Aviv, Israel*
[6]*The Children's Hospital of Philadelphia, Surgery, Philadelphia, United States of America*

Purpose/Objectives: Current laryngotracheal reconstruction surgeries harvest rib cartilage as a graft for airway expansion, increasing surgical time and risk. There is a critical need for off-the-shelf biomaterials for airway cartilage repair, yet current research relies heavily on slow and expensive large animal models with limited genetically engineered variants for mechanistic studies. Our objectives are to develop and characterize a model of mouse thyroid cartilage as a platform for cartilage repair research for use in the airway and beyond. We hypothesize this model would also allow for large and rapid cartilage regeneration studies in wild-type and genetically engineered mice.

Methodology: Fig. 1A) The mouse laryngotracheal complex was exposed through cutting one or both sides of the thyroid cartilage with a 1mm biopsy punch. **Fig. 1B)** The thyroid cartilage plug was then 1) removed, 2) removed and reimplanted, or 3) replaced with a cell-seeded or unseeded scaffold. The larynx was harvested three weeks later, embedded, and histologically or immuno-stained for morphological or cellular differences.

Results: Fig. 1C) H&E stains demonstrate that removed and reimplanted thyroid cartilage plugs produced robust appositional, direction-agnostic neocartilage growth, potentially derived from the perichondrium, while unseeded scaffolds did not integrate into the thyroid cartilage. Notably, this growth is largely restricted to the plugs and not adjacent defect edges. **Fig. 1D)** This neocartilage growth is observed in mice up to 32 weeks of age. **Fig. 1E)** The defects do not fill within three weeks.



Conclusion/Significance: Our data indicate that mouse thyroid cartilage is capable of hosting critically-sized defects at three weeks, and unseeded scaffold controls demonstrate limited cartilage integration. Furthermore, the mouse thyroid cartilage perichondrium may be potentially regenerative, and reimplanted plugs are capable of robust appositional neocartilage formation. Ongoing research is investigating why neocartilage formation is observed primarily in removed and reimplanted plugs through *in vivo* aSMA^{+} progenitor cell quantification, *ex vivo* perichondrium cultures, and new ECM tracking. This simple mouse cartilage defect model may also be utilized for non-airway cartilage regeneration research due to its accessibility, large surface area, and exposure to cyclical mechanical forces, though the presence of a perichondrium is not reflective of articular cartilage.

Session 44
Skin, Wound Healing, and Inflammation (General Session) 1

11-17-2026 @ 8:00 AM - 9:30 AM

RF-034 - Development of A Wound Care Treatment with Stem Cell-derived Specific Mimetic Peptides for Combat Burn Injuries

Young Min Ju, Abdulkadir Kabasakal, Sunil George, Olivia Clemensen, Denethia Green, Erika Billman, Ji Hyun Kim, Sang Jin Lee, Bill Vaughan, Anthony Atala, James Yoo

Wake Forest School of Medicine, Wake Forest Institute For Regenerative Medicine, Winston-Salem, United States of America

Purpose/Objectives: Burn injuries, prevalent in battlefield trauma caused by flames and blasts, necessitate early necrotic tissue excision and rapid wound coverage for improved survival. Split-thickness autologous and allografts are standard treatments, but they face limitations such as donor site issues, morbidity, and rejection risks. We previously developed a novel therapeutic option using a tailored combination of multiple factors (i.e., CMFs, conditioned media factors) derived from human placental stem cell (HPSC)-conditioned media for wound-healing therapy. In this study, we investigate the effectiveness of factor-specific mimetic peptides in wound therapy compared to CMF. These peptides offer advantages such as lower immunogenicity, low-cost production, and enhanced stability from long-term delivery formulations. Our study aims to investigate the therapeutic effectiveness of mimetic peptides compared with CMF in a large animal preclinical model.

Methodology: Toward this goal, we developed an alginate-gelatin-based wound patch technology. This technology incorporates CMF derived from HPSCs and synthetic growth factor-mimetic peptides, which are highly expressed proteins identified in the secretome of stem cell culture-conditioned media (ANG-1, FGF-7, Follistatin, HGF, IL-6, Insulin, TGFβ-1, uPAR, and VEGF). Nine recombinant protein cocktails and mimetic peptide cocktails were examined and evaluated *in vitro*. We then applied the wound patch containing the cocktails in a full-thickness skin wound defect model in pigs. Wound closure and histological examination were performed to evaluate cellular proliferation, re-epithelialization, tissue formation, and angiogenesis.

Results: The results demonstrated that the mimetic peptide cocktail promotes the proliferation and migration of skin and vascular cells *in vitro*. The treatment of CMFs and mimetic peptide groups significantly accelerated wound closure, tissue formation, and mature re-epithelialization *in vivo*. Furthermore, both CMFs and mimetic peptide-treated groups demonstrated increased formation of mature vessels and basket-weave collagen networks, which are phenotypically similar to native skin tissue.

Conclusion/Significance: This study demonstrates that growth factor mimetic peptides can serve as a viable and effective alternative to stem cell-derived CMFs for promoting wound healing. These findings indicate that the factor-specific mimetic peptide treatment may be a promising therapeutic option for combat burn injuries.

RF-035 - A Multicellular In Vitro System to Investigate the Effects of Carbon Nanoparticle-Containing Scaffolds on Inflammation and Vascularization in Wound Healing

Ruth Harper, Kirin Loughrey, Madhu Dhar

Tissue Engineering and Regenerative Medicine, Large Animal Clinical Sciences, College of Veterinary Medicine, The University of Tennessee, Knoxville, Knoxville, TN, United States of America, Knoxville, United States of America

Purpose/Objectives: Wound healing mechanisms involve interactions among diverse cell types, resulting in a complex microenvironment. Multicellular in vitro models such as co-culture systems can enable examination of intercellular and intracellular signaling, better reflecting in vivo dynamics. We aim to simulate the wound microenvironment using human mesenchymal stem cells (hMSCs), THP-1-derived macrophages, and umbilical vein endothelial cells. This platform will be used to assess the therapeutic potential of carbon nanoparticle-containing scaffolds (CNCS) in wound healing outcomes. We hypothesize that, by virtue of their immunomodulatory function, hMSCs will drive macrophage polarization from M1 to M2 subtypes, and that carbon nanoparticles will support or enhance this immunomodulatory response.

Methodology: THP-1 monocytes were differentiated into macrophage-like cells using phorbol 12-myristate 13-acetate (PMA). Dose-dependent effects on pan-macrophage marker CD14 expression were monitored following differentiation. Lipopolysaccharide and IFN- were used to polarize differentiated cells toward an M1 state, while IL-4 and IL-13 were used to polarize toward an M2 state, and they were verified via immunofluorescence (IF). In addition, hMSCs were cultured in two media, DMEM-F12 and RPMI-1640, for 48 hours and assessed using DiI labeling and vimentin staining. Next, THP-1 monocytes and hMSCs were co-cultured at various seeding densities for 48 hours to assess cellular responses using IF for F-actin and macrophage markers CD68 and CD206.

Results: PMA concentration influenced the expression of the CD14 in a dose-dependent manner. 25 µg/mL PMA – treated cells were positive for CD14, whereas cells treated with 1 x 10^{6}-fold higher concentration showed no expression. In DMEM-F12 and RPMI-1640 media conditions, the hMSCs showed similar growth with vimentin expression, and co-cultures formed a confluent hMSC layer with THP-1 monocytes loosely localizing and attaching to hMSCs. The findings also demonstrated that co-culture of THP-1 monocytes and hMSCs resulted in expression of the M2 marker CD206, suggesting an immunomodulatory effect of hMSCs on macrophage activation.

Conclusion/Significance: We established a multicellular in vitro system to understand inflammation and vascularization during wound healing. This platform will enable us to better evaluate how CNCS influences immunoregulation, macrophage polarization, and vascularization when integrated into the system.

Session 45
Engineering Human Tissues for Translational Impact: Advanced 3D Models, Microphysiological Systems, and AI-Enabled Discovery

11-17-2026 @ 8:00 AM - 9:30 AM

RF-036 - A Microfluidic Skin-on-Chip Platform Integrating Extended Viability, Tissue Complexity, and Tensile Homeostasis

Qiong June Cao, Chengyu Feng, Jing Chen

HiComp Microtech, San Diego, United States of America

Purpose/Objectives: Reconstructed skin models are inherently limited in physiological complexity, while traditional explant cultures suffer rapid viability loss (typically 7–14 days) and stress-relaxed mechanical states that alter cellular behavior. We aimed to establish a microfluidic skin-on-chip platform integrating three key features: extended viability, native tissue complexity, and tensile homeostasis.

Methodology: A microfluidic device incorporating an integrated pumping system was developed to enable continuous medium perfusion, and an engineered tensioning ring was implemented to preserve physiological tension across the explant. Full-thickness human skin explants were maintained for 21 days under different culture conditions, including static Petri dish, Petri dish under rocking agitation, chip under rocking agitation, and chip under active perfusion. Tissue viability was quantified by lactate dehydrogenase (LDH) activity in conditioned medium collected daily, and tissue integrity was monitored via visual observation and histological analysis. Various chip design is tested to further optimize the system.

Results: No skin dislocation or detachment was observed in any condition over 21 days, confirming stable tissue mounting across all platforms. Cumulative LDH activity in conditioned medium from the perfused chip was significantly lower than that from static Petri dish controls, indicating superior tissue viability sustained over 3 weeks. Notably, neither rocking condition yielded viability improvement over static culture, demonstrating that active perfusion, rather than passive fluid mixing, is the principal mechanism preserving explant integrity.

Conclusion/Significance: This study establishes a microfluidic skin-on-chip platform that overcomes the longstanding viability barrier of human skin explant culture. By extending functional culture beyond 3 weeks while preserving native tissue complexity and physiological tension, the platform unlocks experimental capabilities previously inaccessible with conventional models, including chronic dosing, repeat-exposure toxicology, immune-mediated disease modeling, and long-term regenerative studies. More broadly, it offers a translationally relevant, human-based alternative to animal testing, aligning with regulatory momentum toward New Approach Methodologies (NAMs) in pharmaceutical, cosmetic, and biomedical research.

Session 46
Scaffolds, Matrices, and Biomaterials (General Session)

11-17-2026 @ 1:30 PM - 3:00 PM

RF-037 - Precision-Engineered Porous Gelatin Scaffolds Designed to Reduce the Foreign Body Response and Promote Vascularization

Louis Chen[1], Le Zhen[2], Buddy Ratner[3]

[1]*University of Washington, Molecular Engineering And Bioengineering, Seattle, United States of America*
[2]*University of Washington, Chemical Engineering, Seattle, United States of America*
[3]*University of Washington, Bioengineering, Seattle, United States of America*

Purpose/Objectives: The long-term performance of implantable medical scaffolds is limited by the body's foreign body reaction (FBR), in which inflammatory responses can lead to dense, avascular scar tissue layer encapsulating the device. Previous studies have found that materials with uniform, interconnected spherical pores of 40 μm reduced fibrosis and improved vascularized healing. In this study, we hypothesized that a biocompatible, biodegradable gelatin-based scaffold with a uniform, interconnected 40 μm porous structure could enhance cell attachment and support tissue integration during scaffold degradation, compared with non-porous and 100 um materials.

Methodology: The gelatin scaffolds were chemically cross-linked with carbodiimide (EDC-NHS) at varying concentrations to regulate the in vitro degradation rate over 2 months (with in vivo degradation is generally considered approximately twice as fast as in vitro degradation). The gelatin materials with defined cross-linking density were fabricated as non-porous, 40 μm, and 100 μm scaffolds, and evaluated according to ISO10993 cytotoxicity standards and Limulus amebocyte lysate (LAL) endotoxin assay prior to in vitro HUVECs (Human Umbilical Vein Endothelial Cells) seeding.

Results: In situ implant-cell interactions demonstrated that the 40 μm gelatin scaffolds enhanced cell attachments compared with non-porous and 100 μm scaffolds after 7 days of incubation. Implants encapsulated with cells will be harvested in 45 days for analysis, including SEM and H&E staining, to provide preliminary insights into cell structural integrity and cellular organization following partial scaffold degradation.

Conclusion/Significance: In summary, this study evaluates cell-implant integration and cellular organization during progressive degradation of non-porous, 40 μm, and 100 μm porous gelatin scaffolds with controlled in vitro degradation rates.

RF-038 - Functionalized Poly(2-oxazoline) Hydrogels with Tunable Ligand Presentation for Cardiac Patch Applications

I-Yin Cheng[1], Kelly Mint[2], Matthew Mail[1], Shirin Nour[1], Ren Jie Phang[3], Shiang Yong Lim[3], Andrea O'connor[1], Kristian Kempe[2], Daniel Heath[1]

[1]*The University of Melbourne, Biomedical Engineering, Melbourne, Australia*
[2]*Monash University, Monash Institute of Pharmaceutical Sciences, Melbourne, Australia*
[3]*St Vincent's Institute of Medical Research, O'brien Institute Department, Melbourne, Australia*

Purpose/Objectives: Engineering cardiac patches by combining biomaterials, cells, and bioactive molecules offers a viable strategy for treating ischemic heart disease and replacing lost cardiomyocytes. However, poor cell survival and integration remain significant barriers. This work aimed to develop a poly(2-methyl-2-oxazoline) (PMeOx) hydrogel platform with controlled nanoscale ligand clustering to enhance cell adhesion, spreading, contractility, and ultimately suitability for cardiac patch applications.

Methodology: We synthesized hydrophilic PMeOx polymers with 20% norbornene functionalization and conjugated varying amounts of short peptide (CGGGRGDS) for biofunctionality via the thiol-ene click reaction. We also developed new photopolymerization conditions to crosslink these polymers into hydrogels using di-thiol crosslinkers, thereby minimizing unwanted norbornene homopolymerization. RGD-functionalized PMeOx hydrogels were fabricated with either randomly dispersed or nanoclustered ligand distributions at defined global ligand densities. Cell culture with human dermal fibroblasts and human induced pluripotent stem cell-derived cardiomyocytes (iPSC-CMs) were used to demonstrate different biofunctionality.

Results: Our synthetic biomaterials strategy yielded PMeOx hydrogels with precise control over ligand cluster density, spatial nanopatterning, and ligand type. The resulting materials were engineered to achieve tunable stiffness in the 3-111 kPa range, comparable with soft tissues, and the thiol-ene click reaction made the polymers amenable to complex scaffold formation via photopolymerization through digital light processing printing. RGD-functionalized PMeOx hydrogels effectively regulated fibroblast and iPSC-

CM spreading, which peaked at a global ligand density of 15 mM, and nanoclustered RGD distributions enhanced cell spreading compared with randomly distributed ligands (Fig 1).

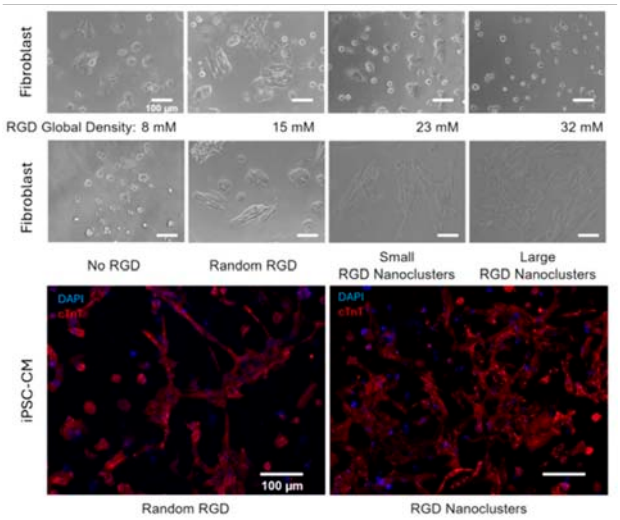


Figure 1. Fibroblasts and iPSC-CMs exhibited enhanced spreading on RGD-functionalized PMeOx hydrogels with nanoclustered RGD distributions compared with randomly distributed RGD. Spreading response determined optimal global and local RGD densities.

Conclusion/Significance: PMeOx hydrogels enable robust tuning of physical and biochemical properties, offering a versatile alternative to the conventional FDA-approved material, polyethylene glycol. Our approach establishes a method of generating hydrogels that limits unwanted norbornene homopolymerization, provides a straightforward strategy to control ligand patterning in three-dimensional environments, and demonstrates its improved performance compared to standard biofunctional hydrogels with random ligand distribution.

Session 48
Musculoskeletal (General Session) 2

11-17-2026 @ 1:30 PM - 3:00 PM

RF-040 - Fibro-Adipogenic Progenitor-Mediated Angiogenesis Reduces Adipogenesis in a 3D Co-Culture Model

Christian Mendiondo, Eric Brey, Christopher Rathbone

The University of Texas at San Antonio, Department of Biomedical Engineering And Chemical Engineering, San Antonio, United States of America

Purpose/Objectives: Fibro-adipogenic progenitors (FAPs) are muscle-resident mesenchymal stem cells located in the interstitial space between muscle fibers and are critical for skeletal muscle homeostasis and regeneration. Although FAPs are often in close proximity to capillaries within muscle, few studies have investigated interactions between FAPs and microvessels. We have recently demonstrated that FAPs co-cultured with microvascular fragments (MVFs) from adipose tissue localize to vessels and significantly enhance vascular network development. However, it has yet to be determined whether interactions between FAPs and microvessels reciprocally influence brown/beige adipogenesis, which has previously been associated with improved regenerative outcomes after muscle injury. Therefore, the objective of the present study was to determine how establishing the FAP-microvessel niche influences downstream adipogenic capacity and localization.

Methodology: Cells were isolated from the hindlimb skeletal muscles of Lewis rats and subjected to magnetic-activated cell sorting (MACS) to obtain an enriched population of FAPs expressing PDGFRα and SCA-1. FAPs were co-cultured with MVFs in 3D fibrin hydrogels and cultured under standard growth media (GM) or brown adipogenic media (BAM) conditions for 18 days. Hydrogels were fixed with 4% paraformaldehyde and stained with Griffonia Simplicifolia lectin I and BODIPY to visualize vascular networks and lipids, respectively, using a Leica SP8 confocal microscope.

Results: MVFs alone and FAP + MVF co-cultures in GM form robust vascular networks at Day 18, while FAPs alone, as expected, do not form vessels. Minimal adipogenesis was observed in all groups cultured in GM. Although MVFs and FAPs alone cultured under BAM conditions develop a high density of lipid-loaded adipocytes, FAP + MVF co-cultures in BAM form vascular networks with fewer lipids that appear more localized to vessels.

Conclusion/Significance: Overall, these results indicate that FAP-mediated development of MVF networks is associated with reduced adipogenic capacity, suggesting a possible relationship between vascularization and FAP adipogenesis. Ongoing and future studies will (1) determine how FAP concentration and the extent of vascular network development influence adipocyte content, localization, and phenotype (brown vs. white) and (2) investigate the mechanisms underlying FAP-vessel crosstalk.

Session 49
Ophthalmologic (General Session)

11-17-2026 @ 1:30 PM - 3:00 PM

RF-041 - An Insulin-like Growth Factor-1 Sustained Release Strategy Preserves Retinal Tissue and Function in the rd10 Mouse Model of Retinal Degeneration

Sophia Lu[1], Jonathan Labriola[2], Margaret Ho[3], Harry Chin[1], Hong Cui[3], Lia Huo[3], Diane Lee[3], Lacrimioara Comanita[4], Valerie Wallace[4], Molly Shoichet[1]

[1]*University of Toronto, Chemical Engineering & Applied Chemistry, Toronto, Canada*
[2]*Synakis Corp., Toronto, Canada*
[3]*University of Toronto, Toronto, Canada*
[4]*Toronto Western Hospital, Toronto, Canada*

Purpose/Objectives: Retinitis pigmentosa is a heterogeneous condition involving progressive photoreceptor degeneration, leading to blindness. Insulin-like growth factor 1 (IGF-1) is a pleiotropic hormone that exerts neuroprotective effects and has potential as a gene-agnostic therapeutic. However, barriers to its clinical translation include poor pharmacokinetics and off-target effects. Here, we present an IGF-1 sustained release (I-SR) strategy for local delivery to the retina.

Methodology: SH3-IGF-1 fusion protein was expressed to leverage the sub-micromolar interactions between the SH3 domain and a weak binding peptide (WBP) for controlled release. The delivery vehicle uses ketone-modified hyaluronan (HAK) polymers immobilized with WBP via oxime chemistry and covalently crosslinked with a 4-arm PEG. SH3-IGF-1 was loaded into I-SR at 1:300 molar eq. SH3-IGF-1: WBP. *In vitro* sustained release of SH3-IGF-1 from I-SR was evaluated over 7 days. We then used the *rd10* retinal degenerative mouse model to evaluate the efficacy of I-SR *in vivo*. *Rd10* mice were divided into 4 cohorts: I-SR, IGF-1 bolus in PBS, and SR vehicle and PBS controls. The mice were intravitreally injected at post-natal day 18-20, and immunohistochemistry was used to assess photoreceptor cell death at 1-week post-injection, and electroretinography (ERG) to assess functional retinal preservation at 2- and 3-weeks post-injection.

Results: *In vitro* release with I-SR demonstrated a significant reduction in SH3-IGF-1 diffusivity compared to unmodified HAK with therapeutic levels released over 7 days. *Rd10* mice injected with I-SR showed preserved outer nuclear layer (ONL) thickness and suppressed cell death compared to untreated controls and bolus at 7 days post-injection. Functional responses measured by ERG of photoreceptors (a-wave) and bipolar cells (b-wave) were improved in the I-SR cohort. In SR vehicle and I-SR groups, there was a non-significant loss of a- and b-wave amplitudes at 2-weeks post-injection compared to untreated. Only the I-SR cohort showed a significant level of a- and b-wave functional preservation compared to the PBS injected cohort at 2-weeks post-injection.

Conclusion/Significance: I-SR suppresses cell death and preserves retinal function in the *rd10* model. Future work will investigate I-SR in larger animal models with eyes that have greater clinically relevant anatomy and advance the delivery strategy by extending the duration of IGF-1 release.

Session 52
Imaging and Assessment (General Session)

11-17-2026 @ 1:30 PM - 3:00 PM

RF-044 - Deep Learning and Imaging Approaches for Improved In Vitro Assessment of MSC Functionality in 2D and 3D Systems

Emine Berfu Ozmen[1,2], Steven Newby[2], David Keffer[3], Madhu Dhar[2]

[1]*The University of Tennessee, Knoxville, Genome Science And Technology, The Bredesen Center For Interdisciplinary Research And Graduate Education, Knoxville, United States of America*
[2]*The University of Tennessee, Knoxville, Tissue Engineering And Regenerative Medicine, Large Animal Clinical Sciences, College of Veterinary Medicine, Knoxville, United States of America*
[3]*The University of Tennessee, Knoxville, Material Science And Engineering, Knoxville, United States of America*

Purpose/Objectives: Understanding cellular responses and evaluating functional properties using emerging in vitro systems accelerates progress and deepens understanding of tissue engineering constructs. These assessments support the development and characterization of biomaterials and stem cells, ultimately improving constructs and establishing a tissue-specific, biomimetic environment. In our study, we aim to understand mesenchymal stem cell (MSC) functionality in 2D and 3D systems for Achilles tendon regeneration by examining morphological changes in response to chemical and mechanical stimuli. Cells are segmented using a machine-learning tool for morphological identification, and MSC functions are interpreted based on protein expression profiles.

Methodology: We isolated MSCs from rabbit Achilles tendons (RtMSCs), characterized them, and assessed their tenogenic differentiation in 2D using TGFβ3. We further developed a 3D poly(lactic-co-glycolic acid) (PLGA)/graphene oxide (GO) nanocomposite scaffold and seeded with RtMSCs. The cells' morphological changes during differentiation and their response to the 3D-printed scaffold were evaluated with phalloidin staining by immunofluorescence (IF) from 1 to 96 hours and from 1 to 36 hours, respectively. Cells were segmented using the deep-learning tool CellPose 2.0, and morphologies were quantified using ImageJ/Fiji. Morphological changes in both 2D and 3D environments were analyzed using principal component analysis (PCA) in MATLAB. Furthermore, to link the morphological findings to function, tenocyte-specific protein expressions were assessed by IF.

Results: RtMSCs showed substantial differentiation potential, with more elongated morphologies and alignment. On the scaffold, they exhibited high viability and mechanotransduction-mediated morphological changes. CellPose with 'human-in-the-loop' training eased cell segmentation in both environments, and its integration with ImageJ/Fiji enabled the extraction of quantitative morphological measurements. We observed significant morphological changes at 48 and 24 hours under TGFβ3 induction and with the 3D scaffold, respectively. Morphological changes correlated with the expression of tenocyte markers such as Tenomodulin and SCX, confirming differentiation and, thus, the cell lineage.

Conclusion/Significance: We established an in vitro method that includes a machine-learning tool to assess MSC responses to biological and mechanical cues. We linked morphological changes in 2D and 3D environments to cell function. This approach will help us understand and predict function in vitro, lay the foundation for more in vitro systems.

RF-045 - Development of Fibroblast-Specific DNA Aptamers for Applications in Regenerative Medicine

Av Thanusha[1], Jean Welter[2], Rodrigo Somoza[1]

[1]*Case Western Reserve University, Biology, Cleveland, United States of America*
[2]*Case Western Reserve University, Center For Modular Manufacturing of Structural Tissues, Cleveland, United States of America*

Purpose/Objectives: Fibroblasts play a critical role in tissue repair, fibrosis, and regenerative medicine, making their selective identification and targeting essential for both diagnostic and therapeutic applications. DNA aptamers—short, single-stranded oligonucleotides—offer high specificity, low immunogenicity, and chemical versatility, positioning them as promising alternatives to antibodies. The objective of this study is to initiate the development of DNA aptamers that selectively bind to human fibroblast cells using the cell-SELEX (Systematic Evolution of Ligands by Exponential Enrichment) strategy.

Methodology: A single-stranded DNA library containing a randomized 18-nucleotide region flanked by constant primer-binding sequences was used to initiate the cell-SELEX process. Positive selection was performed using cultured human fibroblast cells. Six iterative rounds of selection were completed, each consisting of incubation with target cells, washing to remove unbound sequences, elution of bound aptamers, and PCR amplification. Single-stranded DNA pools were regenerated for subsequent rounds. Binding enrichment was evaluated by flow cytometry after selecting rounds to assess the cellular binding affinity of the evolving aptamer pools.

Results: Across six rounds of selection, progressive enrichment of fibroblast-binding DNA sequences was observed. Flow cytometry analysis conducted during the second selection round demonstrated approximately 40% cell-binding affinity, indicating early and measurable enrichment of fibroblast-specific aptamer candidates (Figure 1). Successful amplification and recovery of DNA pools were achieved throughout all selection rounds, supporting the robustness of the SELEX workflow.

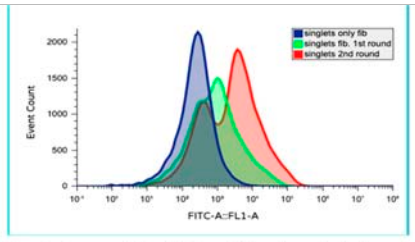


Figure 1: Flow cytometry was used to verify the specificity and quantity of aptamer binding after the second-round selection.

Conclusion/Significance: This study successfully establishes the early-stage development of DNA aptamers with affinity for human fibroblast cells. The observed binding detected by flow cytometry as early as the second selection round suggests effective enrichment of target-specific sequences. Subsequent studies will involve sequencing of the enriched aptamer pools to identify predominant sequences, followed by a comprehensive evaluation of their binding affinity and specificity. These fibroblast-targeting aptamers have potential applications in skin tissue engineering and regenerative medicine.

Session 53
Engineering Immunomodulatory Therapies for Regenerative Medicine

11-18-2026 @ 8:00 AM - 9:30 AM

RF-046 - Substrate topography and composition drive macrophage crosstalk with muscle and bone in vitro

Joshua Vanderpool[1], Liam Aranda-Michel[2], Krista Habing[1], Karina Nakayama[1]

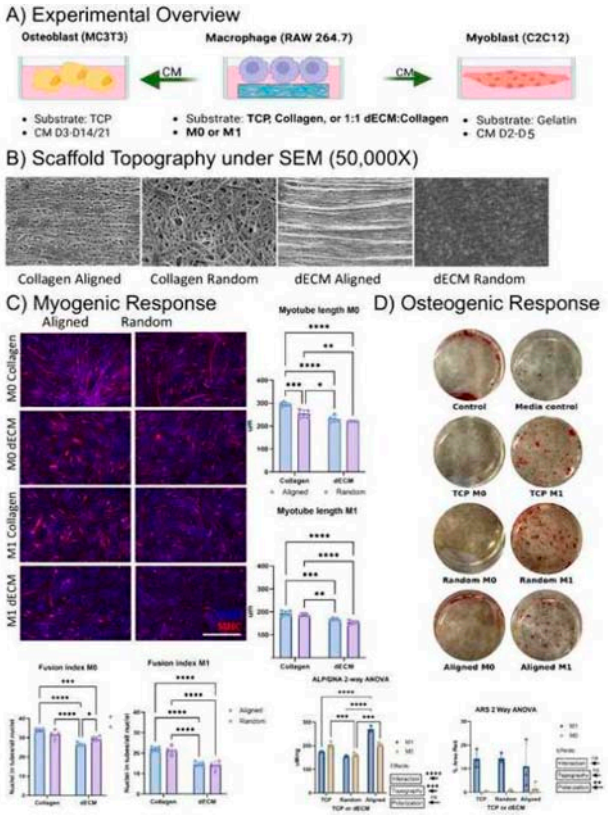
[1]*Oregon Health and Sciences University, Biomedical Engineering, Portland, United States of America*
[2]*Massachusetts Institute of Technology, Cambridge, United States of America*

Purpose/Objectives: An estimated 5 million composite lower extremity injuries occur annually, often involving severe bone fractures coupled with volumetric muscle damage. These injuries frequently lead to long-term disability, with approximately 20% nonunion rates and permanent functional deficits in strength and mobility. A prolonged and dysregulated immune response is central to poor healing outcomes in both bone and muscle. Specifically, macrophages which are dynamic and highly secretory cells, have emerged as a key regulator of regenerative success. Current preclinical regenerative approaches use engineered scaffolds that not only replace lost tissue, but also modulate the immune response and macrophage behavior after injury, but the secretory effects of scaffold-induced macrophage phenotype have not been investigated.

Methodology: RAW 264.7 macrophages were cultured on scaffolds composed of collagen or a 1:1 collagen:decellularized mouse muscle extracellular matrix (dECM) with either random or aligned fibrillar topography and either polarized to be pro-inflammatory (M1) or unpolarized. Macrophage conditioned media (CM) was applied to differentiating myoblasts and pre-osteoblasts. Macrophage phenotype was assessed by iNOS and CD206 staining, myogenesis by myosin heavy chain staining at day 3, and osteogenesis by alkaline phosphatase activity (ALP, day 13) and mineralization staining (day 24).

Results: Myoblasts treated with CM from unpolarized macrophages cultured on aligned Collagen scaffolds formed significantly larger, more multinucleated myotubes compared to aligned dECM and randomly patterned scaffolds. However, when treated with CM from M1 macrophages on aligned and random topographies there was no significant difference in myogenesis outcomes. CM form M1 macrophages caused a decrease in myotube maturity, more so with CM from dECM scaffolds. ALP activity at day 11 trended higher in osteoblasts treated with aligned scaffold-derived media, which was consistent with Mineralization at day 24.

Figure Legend: A) Experimental Overview B) Topography of scaffolds C) Representative Myogenesis. 2-way ANOVA with piecewise comparisons, effects not reported. D) Representative mineralization images. 2-Way ANOVA with comparisons within topography.



Conclusion/Significance: These findings demonstrate that scaffold composition and topography influence macrophage secretory profiles in an inflammation-dependent manner, modifying the pro-regenerative effects on both bone and muscle cells. Ongoing studies aim to validate these findings using primary cells and to characterize the bioactive components of the CM.

Session 54
Emerging In Vitro and Microphysiological Platforms to Study Human–Microbiome Interactions

11-18-2026 @ 8:00 AM - 9:30 AM

RF-047 - Investigating probiotic treatment to dampen oral inflammation within tissue model

Grace Callen[1], Miryam Adelfio[1], Anyelo Diaz[1], Hatice Hasturk[2], Xuesong He[2], Chiara Ghezzi[1]

[1]*UMass Lowell, Biomedical Engineering, Lowell, United States of America*
[2]*The ADA Forsyth Institute, Somerville, United States of America*

Purpose/Objectives: This study leverages a physiologically relevant, long-term *in vitro* oral tissue model (OTM) platform to investigate the mechanistic role of probiotics in modulating oral epithelial and microbial pathophysiology through integrated analyses of epithelial viability, gene expression, cytokine networks, biofilm formation, and 16S rRNA sequencing.

Methodology: OTMs are gingiva replicas populated with human gingival stromal and epithelial cells. Whole human subgingival plaque samples from gingivitis patients were inoculated into the OTM gingival sulcus, establishing a complex biofilm that mimics *in vivo*diversity. The first seven days of OTM culture were in a static regime, followed by 15 days of a dynamic regime in artificial saliva. Treated OTMs received clinically relevant bi-daily doses of a lyophilized probiotic blend of *Lactobacillus rhamnosus* and *Bifidobacterium longum* in phosphate-buffered saline; untreated OTMs served as controls. Host–probiotic interactions were evaluated through epithelial viability, gene expression, and cytokine network response. Microbiome-probiotic interactions were evaluated using qualitative analysis of biofilm formation via scanning electron and confocal laser scanning microscopy, and 16S rRNA sequencing to profile changes in microbial composition and diversity in response to treatments. Statistical analyses used Student's *t*-test, two-way repeated measures ANOVA, and Bonferroni post hoc correction.

Results: Probiotic treatment did not affect OTM cellular viability or epithelial barrier integrity, as demonstrated by maintenance of cell number and claudin-1 transmembrane protein expression. Further gene expression analysis is expected to reveal whether probiotic treatment maintains or enhances epithelial differentiation. Cytokine network analysis revealed shifts to homeostatic signaling pathways following probiotic treatment. Expected biofilm formation was observed, while 16S rRNA sequencing revealed probiotic-induced modulation of community composition, marked by changes in Socransky's bacterial complexes. In parallel, metabolic fluctuations were characterized using a cell culture analyzer, revealing changes in nutrient utilization, acidification, and other bioenergetic parameters in response to probiotic treatment.

Conclusion/Significance: Integration of multimodal host–microbiome endpoints strengthens the translational relevance of the OTM and supports the future development of clinically applicable probiotic strategies to maintain oral epithelial homeostasis and prevent dysbiosis-associated disease. Future studies will focus on elucidating probiotic effects by comparing their impact in healthy versus diseased states.

Session 58
Cardiovascular Tissue Engineering: From Cells, Ecm to AI-driven Organoids

11-18-2026 @ 8:00 AM - 9:30 AM

RF-049 - Physiological mechanical conditioning enhances the maturation and three-dimensional structural organization of fully biological human cardiac bioconstructs in vitro

Antonio Menini[1], Chiara Sorrentino[1], Gemma Izzo[1], Anna Maria Sacco[1], Veronica Romano[1], Franca Di Meglio[1], Giulia Ricci[2], Daria Nurzynska[3], Fabrizio Schonauer[1], Clotilde Castaldo[1]

[1]*University of Naples Federico II, Public Health, Naples, Italy*
[2]*University of Campania Luigi Vanvitelli, Experimental Medicine, Caserta, Italy*
[3]*University of Salerno, Medicine, Pharmacy And Dentistry, Baronissi, Italy*

Purpose/Objectives: Ischemic necrosis results in myocardial injury that affects both the cellular components and the extracellular matrix (ECM). The ECM represents the major portion of the noncellular compartment of tissues and provides a finely tuned combination of mechanical support and biochemical signals that regulate cell behavior. Therefore, effective restoration of myocardial structure and function requires the replacement of both cellular and extracellular elements. Although the composition and properties of the ECM are tissue-specific, the limited availability of donor organs and the high incidence of ischemic heart disease have intensified the search for alternative biological scaffolds capable of reproducing the native cardiac environment. In this context, we developed fully biological cardiac constructs based on decellularized human skin (d-HuSk) scaffolds repopulated with human adipose-derived mesenchymal stromal cells (hADMSCs). We hypothesized that the intrinsic elasticity of the dermal matrix could be exploited through cyclic mechanical stimulation to enhance construct maturation.

Methodology: To test this hypothesis, three-dimensional d-HuSk scaffolds were generated, seeded with hADMSCs, and cultured under static conditions for one week to allow cell attachment and adaptation. The constructs were then transferred to a cyclic stretch bioreactor and subjected to 10% strain at a frequency of 2 Hz for seven days. The effects of mechanical stimulation on cell engraftment, distribution, alignment, and differentiation were evaluated through histological, immunohistochemical, and gene expression analyses. Constructs maintained under static conditions for two weeks served as controls.

Results: Histological analysis revealed that hADMSCs engrafted onto scaffold surface under both conditions. However, dynamically stimulated constructs showed enhanced cell migration into deeper regions of the dermal matrix. Moreover, only these bioconstructs exhibited a well-organized cellular alignment, predominantly oriented across the direction of stretch. Gene expression profiling demonstrated upregulation of markers associated with multiple cardiac lineages, including cardiomyocytes, smooth muscle, endothelial, and mesenchymal cells (e.g., MEF2C, ACTC1, CX43, TBX3/5, GATA6, ACTA2, ETS1, CD90, CD105), indicating improved maturation.

Conclusion/Significance: Overall, these findings demonstrate that d-HuSk is a promising substitute for cardiac ECM and that physiological mechanical stimulation significantly enhances the structural organization and maturation of fully biological and potentially autologous bioconstructs, supporting their potential application in cardiac tissue engineering.

Session 59
Emerging Biofabrication Technologies

11-18-2026 @ 8:00 AM - 9:30 AM

RF-050 - Confirmation of Tethered Ligand Dose on Bone and Microvascular Tissue Engineered Scaffolds for Craniomaxillofacial (CMF) Regeneration

Joshua Alexander[1], Aaron Gillespie[2], Xianrui Zhu[3], Matthew Becker[3], David Dean[1,2,4]

[1]*University of Wisconsin-Madison, Biomedical Engineering, Madison, United States of America*
[2]*The Ohio State University, Material Science And Engineering, Columbus, United States of America*
[3]*Duke University, Chemistry, Durham, United States of America*
[4]*The Ohio State University, Plastic And Reconstructive Surgery, Columbus, United States of America*

Purpose/Objectives: During normal healing, cytokines induce cell attachment, proliferation, and differentiation. While the use of some freely circulating cytokines are FDA-approved, such as bone morphogenetic protein 2 (BMP2) for intervertebral fusion, side effects such as inflammation, heterotopic bone formation, and cancer have been observed.

Methodology: To avoid these adverse outcomes, our group has been investigating the tethering (conjugation) of BMP2 and other ligands to 3D-printed bone scaffolds at controlled surface concentrations. More recently, we also began tethering angiogenic growth factors to micro-patterned hydrogels that will accept blood from nearby arteries and be wrapped around the bone graft to provide perfusion upon implantation.

Results: Our polymer bone scaffolds are composed of poly(propylene fumarate-co-propylene succinate) (PPFPS) which is resorbable and non-toxic in vivo. PPFPS has previously demonstrated good printability but its ability to be functionalized with osteogenic peptides has yet to be verified. We present here a study that used X-ray photoelectron spectroscopy (XPS) to verify the successful attachment of beta fibroblastic growth factor (bFGF), a cell attachment motif (RGD), and BMP2 to PPFPS thin films (Figure 1A). For microvasculature biofabrication, we use chaotic printing of gelatin methacryloyl and sodium alginate (GelMA/SA) composite hydrogels to produce hierarchically branching channels (30–150 μm diameter). We functionalize these microvascular appendage sheets (MAS) with platelet-derived growth factor (PDGF) and vascular endothelial growth factor (VEGF) ligands to support endothelial cell growth and organization. To measure dose, we labeled ligands with fluorescein isothiocyanate (FITC) and have successfully confirmed a linear relationship between fluorescence intensity and ligand concentration in the MAS (Figure 1B).

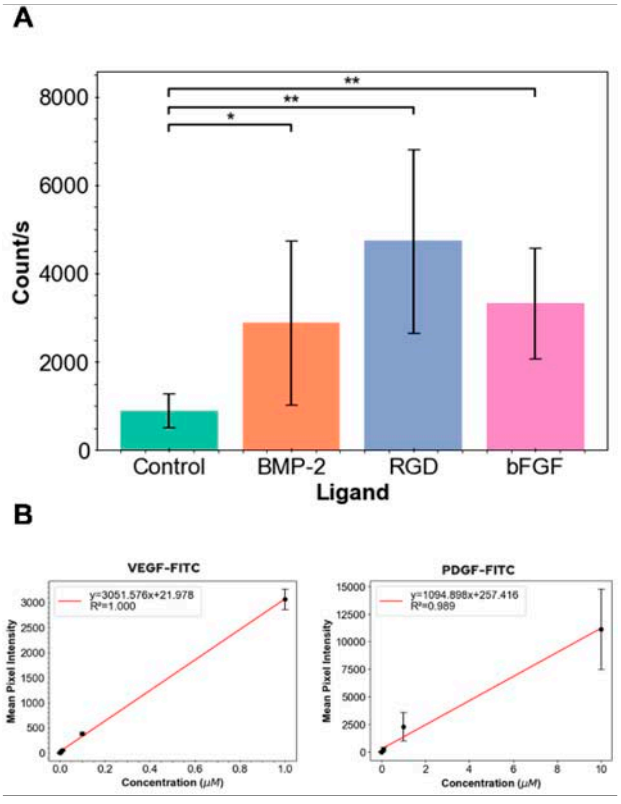


Figure 1. (A) Amide peak area of conjugated peptides on PPFPS (*$p<0.05$; **$p<0.01$) (n=5) (B) Fluorescence intensity of VEGF-FITC (left) and PDGF-FITC (right) with respect to concentration (n=3). Error bars represent standard deviation.

Conclusion/Significance: For both the tissue engineered bone grafts and the biofabricated MAS grafts, we can control surface presentation (dose) by modifying conjugation parameters such as UV irradiance and initial peptide concentration. In the future, we will perform in vitro testing to see if ligand concentration affects bone marrow-derived human mesenchymal stem cell (BM-hMSCs) behavior on PPFPS scaffolds or pericyte and endothelial cell behavior within a MAS.

Session 63
Stem Cell Signaling in Tissue Engineering and Regenerative Medicine: From In Vitro to In Vivo

11-18-2026 @ 11:00 AM - 12:30 PM

RF-053 - MSC-Driven Vascularization in UBM Hydrogel: A Dual-Role Strategy for Implantable Tissue-Engineered Devices

Paula Marin[1,2], Scott Johnson[1], Gavin Schmit[3], Paul Walter[3], Burak Ozdoganlar[3], George Hussey[1,2,4]

[1]*University of Pittsburgh School of Medicine, Mcgowan Institute For Regenerative Medicine, Pittsburgh, United States of America*
[2]*University of Pittsburgh School of Medicine, Department of Surgery, Pittsburgh, United States of America*
[3]*Carnegie Mellon University, Department of Mechanical Engineering, Pittsburgh, United States of America*
[4]*University of Pittsburgh, Department of Bioengineering, Pittsburgh, United States of America*

Purpose/Objectives: Insufficient vascularization remains the primary cause of cell death and functional failure in implantable tissue-engineered devices. Mesenchymal stem cells (MSCs) are an attractive transplantable payload due to their regenerative and immunomodulatory properties; however, their survival post-implantation depends on rapid vascular integration. Urinary bladder matrix (UBM) hydrogel offers a biologically active scaffold whose heparan sulfate glycosaminoglycan chains sequester and sustainably release heparin-binding growth factors, making it an ideal carrier for vascularization strategies. MSCs natively express perivascular markers (PDGFRβ, NG2) and can functionally substitute for pericytes by wrapping around nascent endothelial tubes and suppressing vessel regression — reducing the number of cell types required in a clinically translatable device. This study evaluates a dual-role MSC strategy combined with HUVEC co-culture and a multi-growth factor cocktail within UBM hydrogel to drive stable, patent vascular network formation in vitro for implantable constructs.

Methodology: HUVECs and MSCs were cultured alone or in combination within UBM hydrogel formulations enriched with exogenous growth factors. Constructs were assessed at day 7 (early network formation) and day 14 (maturity and stability); readouts included CD31 (endothelial identity), α-SMA (perivascular stabilization), Ki67 (proliferation), and cleaved caspase-3 (apoptosis).

Results: The in vitro HUVEC + MSC (5:1 ratio) + VEGF-A/bFGF/PDGF-BB construct yielded robust $CD31^{+}/\alpha\text{-}SMA^{+}$ co-staining at day 14, consistent with MSC-stabilized mature vessel structures. Cleaved caspase-3 signal was markedly reduced, indicating significantly improved construct viability under vascularized conditions. Confocal imaging confirmed patent lumen formation as the primary go/no-go criterion beyond CD31 positivity.

Conclusion/Significance: MSCs within UBM hydrogel serve a dual function as both the transplantable stromal payload and perivascular stabilizers of HUVEC-driven vascular networks, reducing device complexity without sacrificing vascular maturity. Sequential VEGF-A/bFGF/PDGF-BB delivery within the UBM matrix establishes patent, stable lumens at day 14 — meeting the critical in vitro benchmark required before advancing to immunocompromised in vivo models.

Session 65
Musculoskeletal (General Session) 3

11-18-2026 @ 11:00 AM - 12:30 PM

RF-054 - Microvascular Fragments Improve Myogenesis in Tissue Engineered Skeletal Muscle

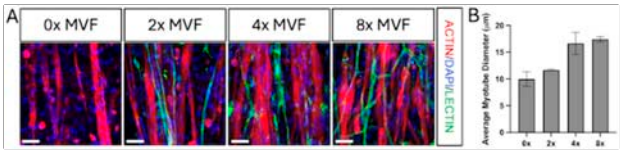
Felipe Morales Gonzalez, Christopher Rathbone

The University of Texas at San Antonio, Department of Biomedical Engineering And Chemical Engineering, San Antonio, United States of America

Purpose/Objectives: The incorporation of adipose-derived microvascular fragments (MVFs) is an effective way to vascularize tissue engineered skeletal muscle (TE-SkM). The purpose of this study was to determine if changing the concentration of MVFs could improve the myogenesis in TE-SkM. Varying concentrations of MVFs in a TE-SkM model were investigated for the optimization of myogenesis and angiogenesis.

Methodology: Satellite cells (SCs) were isolated from hindlimb muscles of Lewis rats, and MVFs were isolated from subcutaneous, inguinal and epididymal adipose tissue. 3D TE-SkM made in a fibrin hydrogel were cultured for 21 days using isolated SCs with varying concentrations of MVFs. Upon fixation, constructs were permeabilized and stained using DAPI to detect nuclei, F-Actin to visualize cytoskeletal structures, and Lectin to visualize microvessels. To further evaluate MVFs effect on myogenesis, conditioned media from MVF cultures were added to satellite cell cultures for 5 days, after which time myogenesis was quantified.

Results: There is a positive relationship between myotube diameter with respect to increased MVF density in the TE-SkM (**Figure 1.B**) with the higher density of MVFs having the highest increase in myotube development. In a 2D environment, exposure to conditioned media collected from varying densities of MVFs showed improvements in the myogenic capacity of SCs. Although differences in myotube diameter are not observed in 2D as seen in 3D, myotube count increases in SCs groups that received conditioned media from higher densities of MVFs compared to lower densities or no conditioned media at all. **Figure 1. A)** Confocal imaging of TE-SkM at varying MVF densities. Scale bar: 50 μm. **B)** Average myotube diameter measured in TE-SkM constructs.



Conclusion/Significance: Increasing the density of MVFs in TE-SkM construct results in an increased level of myogenesis. Preliminary results indicate that the improved myogenesis occurs through the secretion of pro-myogenic factors by MVFs.

Session 66
Tissue Engineering Models of The Nervous System

11-18-2026 @ 11:00 AM - 12:30 PM

RF-055 - A 3D Human Blood Brain Barrier Organoid Platform to model cytokine-mediated neurovascular injury

Ananya Datta, Isaac Atkins, John Clegg

University of Oklahoma, Norman, Biomedical Enginnering, Norman, United States of America

Purpose/Objectives: Blood brain barrier (BBB) dysfunction is a hallmark of stroke which contributes to secondary neuroinflammation, vascular instability, and neuronal injury. Inflammatory cytokines including Interleukin-1 beta (IL-1β) and tumor necrosis factor-alpha (TNF-α) are upregulated post-stroke; disrupting BBB integrity by altering tight junction organization and inducing endothelial activation. Existing endothelial monoculture BBB models fail to capture neurovascular unit interactions essential for barrier integrity and recovery after stroke-associated insults. To address this technical gap, we evaluated a human multicellular 3D BBB organoid platform under stroke-relevant cytokine exposures. We hypothesized that TNF-α and IL-1β would produce cytokine-specific changes in BBB tight junction, zona occludens-1 (ZO-1) expression; reflecting distinct inflammatory effects on endothelial barrier regulation.

Methodology: 3D BBB organoids were generated using a 1:1:1 ratio of human brain microvascular endothelial cells, primary human astrocytes, and human pericytes. Post 48h of formation, spheroids were treated with IL-1β (10-25ng/ml) and TNF-α (20-50ng/ml) for 24h to model stroke-like conditions. Organoids were then fixed and immunostained for ZO-1. Confocal microscopy and ImageJ

quantification assessed neurovascular cell marker expression, and cytokine-dependent changes in ZO-1 mean fluorescence intensity (MFI).

Results:

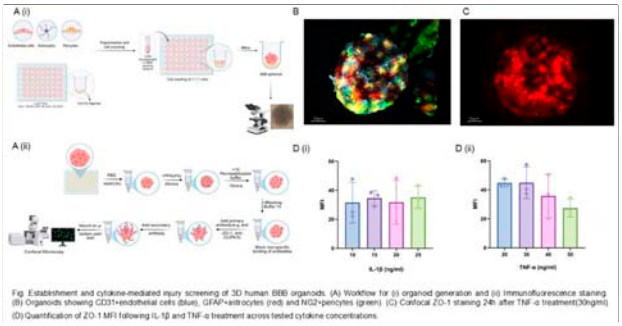


Fig. Establishment and cytokine-mediated injury screening of 3D human BBB organoids. (A) Workflow for (i) organoid generation and (ii) Immunofluorescence staining. (B) Organoids showing CD31+endothelial cells (blue), GFAP+astrocytes (red) and NG2+pericytes (green). (C) Confocal ZO-1 staining 24h after TNF-α treatment(30ng/ml) (D) Quantification of ZO-1 MFI following IL-1β and TNF-α treatment across tested cytokine concentrations.

The 3D BBB organoids formed reproducibly. Immunofluorescence confirmed $CD31^+$ endothelial cells, $GFAP^+$ astrocytes, and $NG2^+$ pericytes, supporting formation of a human multicellular BBB organoid platform. Post 24h cytokine exposure, IL-1β treated organoids showed variable ZO-1 expression without a consistent concentration-dependent trend. TNF-α treated organoids showed a slight reduction in ZO-1 MFI from 44.81 (20ng/ml) to 27.40 (50ng/ml), corresponding to a $\sim$40% decrease; however, this change was not statistically significant. This suggests TNF-α as a candidate inflammatory condition for modelling post-stroke BBB injury. Fig. Establishment and cytokine-mediated injury screening of 3D human BBB organoids. (A) Workflow for (i) Organoid generation and (ii) Immunofluorescence staining. (B) Organoids showing $CD31^+$endothelial cells (blue), $GFAP^+$astrocytes (red) and $NG2^+$pericytes (green). (C) Confocal ZO-1 staining 24h after TNF-α treatment(30ng/ml) (D) Quantification of ZO-1 MFI following IL-1β and TNF-α treatment across tested cytokine concentrations.

Conclusion/Significance: This work establishes a human multicellular 3D organoid platform for modelling cytokine-mediated neurovascular injury. By integrating endothelial cells, astrocytes and pericytes, this platform enables evaluation of BBB injury-associated responses and guides future studies investigating neurovascular repair mechanisms.

KEYNOTE PRESENTATION ABSTRACTS

Session 11
Advancing Women's Health through Inclusive Innovation

11-16-2026 @ 8:00 AM - 9:30 AM

KP-001 - Macrophage-Targeted Nanoparticle-in-Microparticle Therapy Mitigates Inflammation and Pain Following Post-Traumatic Osteoarthritis

Paul Sagoe[1], Kaixiang Zhang[1], William Eghan[1], Maddie Olson[2], Era Jain[1]

[1]*Syracuse University, Biomedical and Chemical Engineering, Syracuse, United States of America*
[2]*Syracuse University, Biology, Syracuse, United States of America*

Purpose/Objectives: Post-traumatic osteoarthritis (PTOA) is a progressive joint disease that frequently develops following anterior cruciate ligament (ACL) injury and is driven in part by persistent inflammation. Synovial macrophages play a central role in disease progression by promoting inflammatory signaling, cartilage degradation, and pain. Current therapies primarily address symptoms and have limited ability to modify disease progression. The objective of this study was to develop and evaluate a macrophage-targeting nanoparticle-in-microparticle (NiM) drug delivery system for sustained local delivery of zoledronic acid to modulate joint inflammation and improve outcomes following ACL injury.

Methodology: A non-invasive mouse model of ACL rupture was used to induce PTOA. Following injury, mice received intra-articular injections of saline, free zoledronic acid, or zoledronic acid-loaded NiM particles. Biodistribution and joint retention were assessed using fluorescent imaging. Immune responses were evaluated by flow cytometry with emphasis on macrophage phenotypes. Pain-related behavior was measured using the von Frey assay, and gait function was assessed by footprint analysis over a seven-week period. Histological and micro-computed tomography analyses were performed to evaluate disease progression.

Results: NiM particles demonstrated prolonged retention within the injured joint, remaining detectable for up to 35 days, whereas free dye was largely cleared within 7 days. Flow cytometric analysis revealed that NiM treatment reduced the proportion of pro-inflammatory CD86+ macrophages while increasing CD206+ macrophages associated with inflammation resolution. These immunomodulatory effects translated into functional improvements. NiM-treated mice exhibited significantly higher paw withdrawal thresholds, indicating reduced pain sensitivity, and maintained more stable gait patterns compared with saline- and free-drug-treated controls throughout the study period. Histological and microCT analyses are currently underway.

Conclusion/Significance: This study demonstrates that macrophage-targeting NiM particles provide sustained intra-articular drug delivery, promote a shift toward a less inflammatory joint microenvironment, and improve pain- and mobility-related outcomes following ACL injury. These findings support the potential of immunomodulatory biomaterial-based therapies as disease-modifying interventions for the early treatment of PTOA.

Session 18
From in Silico Design to Precision Recovery: AI and Biofabrication in Tissue Regeneration

11-16-2026 @ 1:30 PM - 3:00 PM

KP-002 - Engineering Precision Recovery: A Multiscale Digital Twin to Accelerate Biomaterial Design for Volumetric Muscle Loss

George Christ[1], Shayn Peirce-Cottler[2], Silvia Blemker[2]

[1]*University of Virginia, Biomedical Engineering and Orthopaedic Surgery, Charlottesville, United States of America*
[2]*University of Virginia, Biomedical Engineering, Charlottesville, United States of America*

Purpose/Objectives: Volumetric muscle loss (VML) injuries overwhelm intrinsic regeneration and leave warfighters and civilians with permanent functional and cosmetic deficits that have withstood clinical progress for three decades. The barrier is no longer a shortage of candidate therapies; it is the complexity of the combinatorial biomaterial design space (e.g., 5 tunable hydrogel parameters yield >3,000 formulations) that empirical experimentation cannot efficiently solve, and with no consideration of inter-patient biology. Our long-term goal is to build a digital-twin (DT) framework that predicts the recovery trajectory of individual VML injuries: from cell-scale dynamics to whole muscle force, while identifying biomaterial formulations for maximum functional recovery.

Methodology: The proposed DT will couple four components: (i) an agent-based model (ABM) representing satellite stem cells, M1/M2 macrophages, neutrophils, fibroblasts, FAPs, myofibroblasts, endothelial cells, and the cytokine milieu (TGF-β, HGF, IGF, VEGF, IL-6, IL-10, TNFα) within an evolving biomaterial/extracellular matrix environment; (ii) a finite-element model (FEM) incorporating emergent tissue-level properties (myofiber size/number/location, collagen, modulus, innervation, vascularization, pennation angle) to compute muscle force; (iii) AI/ML surrogates that evaluate parameter space orders of magnitude faster than the mechanistic models; and (iv) eventually, subject-specific architectural inputs (MRI, ultrasound, laser-microendoscopic sarcomere length, dynamometry) acquired non-invasively in humans.

Results: Each methodological component has published traction. Specifically our ABMs: 1) reproduced macrophage and satellite-cell dynamics after muscle injury and identified the satellite cell microenvironment as the dominant determinant of failed VML regeneration; 2) a multiscale machine-learning framework predicts individual muscle disease progression; 3) coupled in situ/in silico studies resolved lateral force transmission as a contributor to post-VML force production; 4) Hyaluronic acid-based hydrogels achieve approximately 90% long-term functional recovery in preclinical rat VML models. Pilot data in healthy humans demonstrated that the integrated imaging pipeline predicted measured tibialis-anterior torque via dynamometry.

Conclusion/Significance: Integrating experimentally validated, multiscale mechanistic models with subject-specific imaging and AI/ML acceleration will move VML care from empirical trial-and-error toward engineered, personalized, impairment-based therapeutics. To our knowledge this represents the most comprehensive computational foundation purpose-built for designing precision therapies to enable musculoskeletal regeneration following VML injury and repair: an approach that may have applications to other unmet medical needs.

KP-003 - Virtual Mechanical Testing of Fracture Healing with Digital Twins

Hannah Dailey

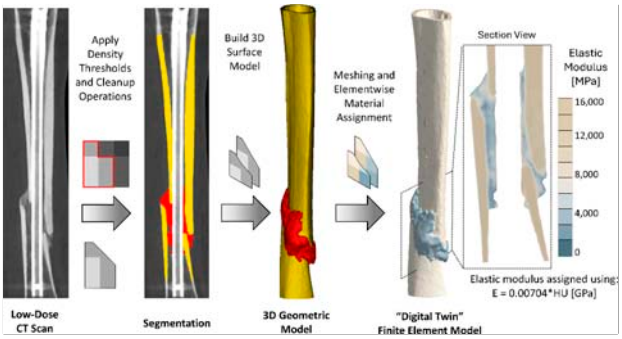
Lehigh University, Mechanical Engineering & Mechanics, Bethlehem, United States of America

Purpose/Objectives: Traditionally, bone mechanical properties have been obtained through cadaver testing in humans or postmortem testing in animal models. In clinical studies, direct mechanical testing is impossible, and the lack of objective measures of biomechanical outcomes has contributed to large sample size requirements and inconclusive findings. Addressing these challenges requires a new approach: the use of *digital twins* to produce mechanical biomarkers for bone.

Methodology: This invited talk will establish the development of image-based digital twins (subject-specific finite element models) for assessment of bone fracture healing outcomes. These procedures begin with processing computed tomography (CT) images to reconstruct 3D models of bone and fracture callus. After meshing and material properties assignment, the resulting models are subjected to virtual torsion testing, a noninvasive computational analog of the gold-standard postmortem biomechanical testing used in animal studies. Results from the torsion test of the fractured bone are normalized to a virtual reconstruction of the patient's own intact bone, resulting in a bone healing score that ranges from 0% (no healing) to

100% or more (mechanical healing on par with the intact bone due to the formation of bridging callus).

Results: Case studies will show how digital twin analysis can be leveraged in a clinical context to detect poor healing outliers (delayed unions and impending nonunions) and to capture the depressed fracture healing response in patients with comorbidities. Mechanical analysis of established nonunions and limb salvage cases will show how digital twins can be used to measure the progress of mechanical healing longitudinally along a continuum that could be used for prognosis to guide clinical care. Figure 1 – Workflow for creating a digital twin to measure healing of a fractured tibia.



Conclusion/Significance: Digital twin are poised to transform clinical care in orthopaedic trauma and musculoskeletal regeneration by providing quantitative outcomes measures (biomarkers) that enable early, evidence-based decision-making for high-risk patients.

Session 36
Advancing MPS as New Approach Methods (NAMS)

11-16-2026 @ 5:05 PM - 6:35 PM

KP-005 - Next-Generation Multi-Organ Microphysiological Systems for Disease Modeling and the Realization of Digital Twins

Aakash Patel[1], Kaveena Autar[1], Walker Hagan[1], Sarah Noureddine[1], Mridu Malik[1], Gaurav Srivastava[2], Hannah Hanson[1], Xiufang Guo[2], Christopher Mcaleer[1], Christopher Long[1], Rocky Brighton[1], James Hickman[1]

[1]*Hesperos, Orlando, United States of America*
[2]*University of Central Florida, Orlando, United States of America*

Purpose/Objectives: Traditional preclinical drug development relies heavily on animal models that frequently fail to accurately translate to human physiological responses, contributing to immense financial burdens from clinical trial failures. Recognizing these shortcomings, recent regulatory milestones, notably the FDA Modernization Act 2.0, actively encourage the adoption of New Approach Methodologies (NAMs). To bridge this translational gap, functional, multi-organ microphysiological systems (MPS) have been established.

Methodology: Hesperos's Human-on-a-Chip® platform operates in a pumpless, serum-free environment, utilizing human induced pluripotent stem cell (iPSC)-derived tissues or primary cells to reliably emulate complex human disease states. Our clinically relevant capabilities include key active organ modules (cardiac, hepatic), specialized central and peripheral nervous system components, neuromuscular junction (NMJ) models, and barrier tissues (blood-brain barrier, GI tract). These can be investigated individually or combined into a multi-organ device. Crucially, these systems utilize non-destructive functional readouts such as microelectrode arrays for electrical activity, and cantilevers for mechanical contractility, allowing for continuous, longitudinal monitoring of cellular health and phenotypic responses over several weeks.

Results: These interconnected systems enable the simultaneous assessment of absorption, distribution, metabolism, and excretion (ADME), alongside therapeutic efficacy and off-target toxicity. Demonstrating immediate clinical relevance, our platform has successfully advanced multiple therapeutics to the Investigational New Drug (IND) stage. The culmination of these capabilities is the realization of predictive digital twins. First, a malaria digital twin dynamically evaluates systemic efficacy and off-target toxicities of antimalarials. Second, an opioid overdose model integrates autonomic neuronal respiratory control with skeletal muscle, liver, and cardiac modules to successfully replicate opioid-induced suppression and subsequent naloxone rescue.

Conclusion/Significance: By combining phenotypic disease modeling with pharmacokinetic/pharmacodynamic (PK/PD) digital simulation, the MPS platform transcends traditional *in vitro* testing. These predictive digital twins significantly de-risk the pharmaceutical pipeline by identifying toxicities and efficacy hurdles earlier in development. As these capabilities expand, they offer a robust framework for the precise prediction of clinical *in vivo* outcomes and the rapid evaluation of next-generation therapies. Furthermore, by utilizing patient-specific iPSCs, this NAM paves the way for personalized medicine, enabling the creation of individualized digital twins to evaluate patient-specific responses and support targeted clinical trial design for rare diseases.

Session 49
Ophthalmologic (General Session)

11-17-2026 @ 1:30 PM - 3:00 PM

KP-006 - RPE State Remodeling in AMD: Implications for Engineering iPSC-RPE for Cell Replacement

Michael Farkas

State University of New York at Buffalo, Ophthalmology, Buffalo, United States of America

Purpose/Objectives: Age-related macular degeneration is commonly viewed as a disease of retinal pigment epithelium dysfunction and loss, supporting the rationale for RPE cell replacement using stem cell-derived RPE. However, successful transplantation may require more than generation of cells expressing canonical RPE markers. The AMD host environment is a chronically remodeled tissue state shaped by oxidative stress, inflammation, lipid dysregulation, extracellular matrix remodeling, and regional vulnerability. The purpose of this study was to define how native RPE state changes during AMD progression and how these changes may inform engineering criteria for iPSC-RPE cell replacement.

Methodology: We integrated stage-resolved human donor RPE transcriptomic analyses with iPSC-RPE epigenetic data. Macular versus peripheral RPE expression patterns were compared across normal donor tissue and AMD stages, including intermediate AMD, advanced preatrophic AMD, and geographic atrophy. Coding and long noncoding RNA programs were analyzed to define regional RPE state architecture and disease-associated remodeling. iPSC-RPE epigenetic remodeling data were evaluated to determine how stem cell-derived RPE differentiation aligns with adult donor RPE states relevant to transplantation.

Results: Normal human RPE exhibited broad macula–periphery transcriptional specialization involving both coding genes and lncRNAs. Across AMD progression, this regional architecture became compressed, with disproportionate remodeling of lncRNA-associated programs and emergence of disease-associated transcriptional signatures. Shared regional genes retained their directionality, indicating that AMD does not simply invert regional identity, but instead narrows and remodels normal RPE state architecture. In GA, regional transcriptional differences partially re-emerged. In parallel, iPSC-RPE analyses demonstrated acquisition of RPE-associated identity during differentiation, while retaining differences from adult donor RPE.

Conclusion/Significance: These findings support a model in which RPE replacement for AMD involves a three-state challenge: transplanted cells begin in an engineered iPSC-RPE state, must approximate adult regional RPE identity, and must survive within an AMD-remodeled host environment. This framework suggests that AMD cell therapy should be evaluated not only by conventional RPE markers, pigmentation, polarity, and phagocytosis, but also by state fitness: the ability of engineered RPE to acquire adult-like regional programs, maintain epithelial and metabolic homeostasis, and resist AMD-associated stress remodeling. Thus, RPE replacement for AMD should be viewed as a problem of cell-state engineering, not simply cell substitution.

POSTER PRESENTATION ABSTRACTS

POSTER SESSION 1

11-15-2026 @ 6:30 PM - 8:30 PM

A01 - Engineering a Hyaluronan-based Bioink for 3D Bioprinting of Cardiac Tissue

Shumaim Barooj[1], Jaci Bliley[2], Adam Feinberg[2], Molly Shoichet[3]

[1]*University of Toronto, Chemical Engineering And Applied Chemistry, Toronto, Canada*
[2]*Carnegie Mellon University, Biomedical Engineering, Pittsburgh, United States of America*
[3]*University of Toronto, Institute of Biomedical Engineering, Toronto, Canada*

Purpose/Objectives: Three-dimensional (3D) bioprinting enables fabrication of cell-laden constructs that better recapitulate native tissue architecture than 2D culture, particularly for human pluripotent stem cell–derived cardiomyocytes (hPSC-CMs). However, many current bioinks fail to balance print fidelity with cytocompatibility, limiting structural stability and stem cell viability. To address this, I aim to engineer a hydrogel-based bioink to encapsulate cells for the 3D bioprinting with high shape fidelity and resolution. Previously, the Shoichet lab developed a hyaluronan (HA)-based hydrogels using an oxime click-crosslinking system. HA is an excellent candidate for bioink because it is abundant in the extracellular matrix, permissive to cell migration, and has tunable mechanical properties. My goal is to design a stem cell–supportive HA bioink that promotes encapsulation, alignment, and functional maturation within 3D-printed constructs.

Methodology: The HA was chemically modified with aldehyde groups to enable gelation and characterized using ^{1}H NMR and gel permeation chromatography. Bioprinting was performed using a FRESH support bath to allow high-resolution printing of soft hydrogels without deformation. The crosslinker was incorporated into the support bath, while the base polymer and cells were loaded into the syringe. The bioink encapsulated hPSC-CMs with cardiac fibroblasts to enhance survival and maturation. Cell viability was assessed using LIVE/DEAD staining, and functional performance was evaluated via calcium transient imaging and electrical simulation.

Results: The optimized HA hydrogel exhibited shear-thinning behavior, rapid gelation, and minimal swelling. In contrast, fibrin-based cardiac constructs compacted within a day, resulting in loss of shape, whereas HA-based cardiac constructs preserved shape fidelity over 28 days. Near-instant gelation enabled layer-by-layer printing, achieving a printing ratio of 1.1 with the HA-based bioink as seen in Figure 1.

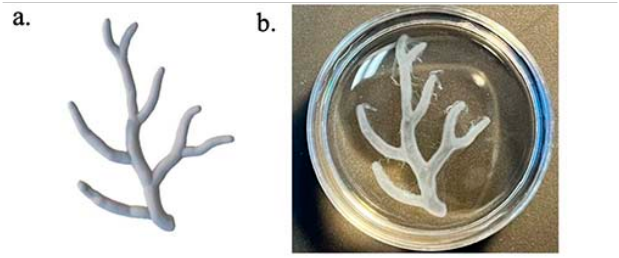


Figure 1. Template of a hollow coronary artery printed with HA-based bioink. (a) Computational design of the construct with dimensions of 31 mm × 26 mm × 6 mm. (b) Physical construct printed with an HA-based bioink.

Conclusion/Significance: Our innovative HA-based bioink, crosslinked via oxime chemistry, enables the fabrication of 3D constructs with mechanical properties suitable for bioprinting while sustaining viable cells. This hydrogel supports the formation of robust and self-supporting 3D-printed constructs. By combining the structural fidelity of HA-oxime hydrogels with the biological cues required for cardiac function, this platform advances the development of functional tissue constructs. The success of this system highlights its potential applicability to other tissue systems, broadening its impact in the field of tissue-engineered biomaterials.

A03 - Embedded Cell-Strand Bioprinting for Self-Actuating 4D Tissue Morphogenesis

Aixiang Ding[1,2], Ana Filipa Cunha[1,3], Eben Alsberg[1,2,4]

[1]*University of Illinois Chicago, Biomedical Engineering, Chicago, United States of America*
[2]*Jesse Brown Veterans Affairs Medical Center, Chicago, United States of America*
[3]*University of Aveiro, Aveiro, Portugal*
[4]*University of Illinois Chicago, Orthopaedic Surgery, Pharmacology And Regenerative Medicine, And Mechanical & Industrial Engineering, Chicago, United States of America*

Purpose/Objectives: Engineering biomimetic tissues with complex three-dimensional (3D) architectures remains a major challenge in tissue engineering. Four-dimensional (4D) bioprinting offers a promising strategy for generating such architectures through programmed shape transformation, particularly through cell-based actuation systems that exhibit excellent cytocompatibility and physiologically relevant morphogenesis. This study aimed to develop a self-actuating embedded cell-strand bioprinting platform that harnesses intrinsic cell contractile forces (CCFs) to drive programmable tissue morphogenesis without requiring external stimuli.

Methodology: Two oxidized and methacrylated alginate (OMA)-based bioinks with distinct degradation profiles were developed, including a slow-degrading bioink for printing mechanically compliant base constructs and a fast-degrading bioink for embedded high-density cell-strand printing. Embedded cell strands were printed within the base hydrogel constructs through extrusion-based bioprinting. Rheological, mechanical, swelling, and degradation properties of the bioinks and hydrogels were characterized. Shape transformation behavior, morphing kinetics, and tissue formation were evaluated during long-term culture in expansion and differentiation media. Mechanistic insights into the morphogenesis process were investigated through comprehensive cellular viability, proliferation, organization, and histological analyses throughout the culture period.

Results: The developed bioinks exhibited suitable shear-thinning and self-healing properties for extrusion and embedded bioprinting. The slow-degrading matrix underwent substantial softening after culture while maintaining long-term structural stability, whereas the fast-degrading matrix rapidly degraded to generate biomaterial-free cell strands with enhanced cell-cell interactions. Strong localized CCFs generated within the embedded cell strands induced autonomous morphogenesis, enabling controlled bending, folding, twisting, helixing, and formation of complex curvature architectures without external stimulation. Mechanistic studies revealed that progressively enhanced cell proliferation, cell-cell interactions, and cellular alignment amplified collective CCF generation over time, thereby driving continuous morphogenesis and formation of tissue constructs with complex and well-defined architectures. Furthermore, stem cell-laden constructs cultured under tissue-specific differentiation conditions supported the formation of engineered tissues with defined curved geometries and morphologically matured structures.

Conclusion/Significance: This study establishes a self-actuating 4D cell-strand bioprinting strategy that leverages intrinsic cellular contractility to achieve autonomous tissue morphogenesis. The platform provides a biomimetic and cytocompatible approach for engineering dynamically evolving tissue architectures and holds strong potential for applications in morphogenetic tissue engineering, disease modeling, and regenerative medicine.

A04 - Additive manufacturing of collagen-based bioelectronics for soft and bioactive tissue interfaces

Tianran Liu[1], Jae Park[1], Somtochukwu Okafor[1], Sandra Montgomery[1], Anna Goestenkors[1], Barbara Semar[2], Riley Alvarez[1], Cayleigh O'hare[1], Yuqing Wu[1], Justin Yu[1], Cielo Vargas Espinoza[2], Alexandra Rutz[1]

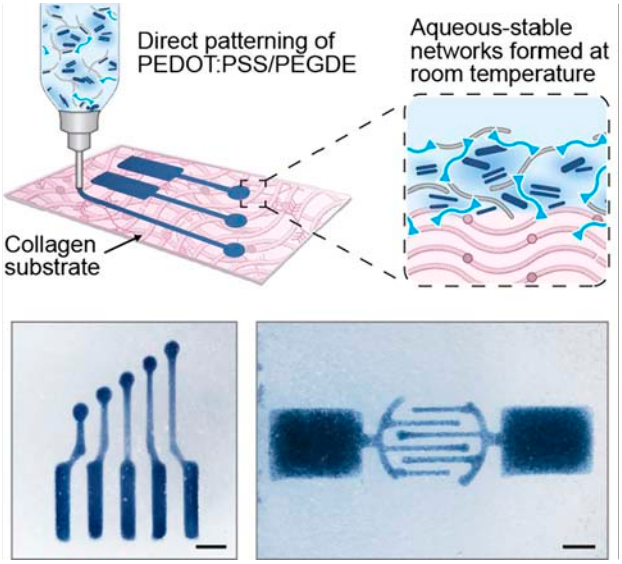
[1]*Washington University in St.Louis, Biomedical Engineering, St Louis, United States of America*
[2]*Washington University in St.Louis, Department of Mechanical Engineering and Materials Science, St Louis, United States of America*

Purpose/Objectives: Bioelectronic devices offer powerful capabilities for monitoring and modulating biological systems, but are

often limited by electronic materials that poorly match the mechanical and biochemical properties of native tissues. Efforts to incorporate extracellular matrix (ECM)-derived biomaterials, such as collagen, are severely constrained by existing approaches for integrating functional electronic components. This work aimed to develop an additive manufacturing strategy that enables fabrication of bioelectronic interfaces directly on collagen substrates under conditions compatible with bioactive biomaterials.

Methodology: To facilitate room-temperature electrode patterning, dispersions of the conducting polymer poly(3,4-ethylenedioxythiophene):poly(styrene sulfonate) (PEDOT:PSS) were formulated with varying concentrations (1–15 v/v%) of poly(ethylene glycol) diglycidyl ether (PEGDE). Gelation kinetics, rheological properties, and printability were evaluated to enable direct extrusion printing onto solvent-cast collagen films. To assess device stability, electrical conductivity and electrochemical performance were characterized during 7 days of physiological incubation. A sacrificial patterning strategy utilizing 3D-printed cacao butter was developed to spatially control collagen encapsulation around printed electrodes. Cytocompatibility was evaluated using primary human cells cultured on both collagen and electrode regions for up to 14 days.

Results: PEDOT:PSS/PEGDE formulations enabled direct extrusion printing of conductive electrode patterns on collagen substrates while maintaining compatibility with mild fabrication conditions. Printed PEDOT:PSS/PEGDE on collagen exhibited high conductivity (up to 2788 S m^{-1}) and stable electrochemical performance during 7 days of physiological incubation. The sacrificial cacao butter strategy enabled selective patterning of collagen encapsulation while preserving device functionality. Primary human cells adhered and proliferated on both collagen and electrode regions, forming a confluent monolayer spanning the entire interface and maintained high viability (>95%) for 14 days. Together, these results establish a platform that combines the biological advantages of ECM-derived materials with the functional capabilities of conducting polymer bioelectronics.



Conclusion/Significance: This work establishes an additive manufacturing framework for integrating conducting polymer electronics with collagen-based biomaterials to create soft, bioactive bioelectronic interfaces. By combining ECM-derived substrates with extrusion-printed conducting polymer electrodes, this approach addresses a critical challenge in bioelectronic device biointegration and provides a versatile platform for tissue-engineered models, biosensing applications, and future implantable bioelectronic systems.

A05 - A Sensor-Integrated, Closed-Loop Bioreactor System for Preconditioning Bladder Constructs

Young Min Ju[1], Brendyn Miller[1], Chancen Law[2], Damir Kantimerov[1], Po-Feng Lee[1], Adit Mehta[1], James Yoo[1], Anthony Atala[1]

[1]*Wake Forest School of Medicine, Wake Forest Institute For Regenerative Medicine, Winston-Salem, United States of America*
[2]*Harvard University, Boston, United States of America*

Purpose/Objectives: Ballistic pelvic trauma involving multiple organs, including the bladder, is particularly challenging due to a high immediate mortality and associated complications. We previously demonstrated that tissue-engineered bladders can be used to augment bladder anatomy and function. In tissue engineering, bioreactors are often used to precondition and mature tissue-engineered constructs prior to implantation to improve their clinical outcome. In particular, bladder bioreactors have been developed to replicate the complex mechanical loading conditions experienced by bladder tissue during normal filling and voiding. However, these systems only partially provide the physiological environment and lack integrated sensory feedback mechanisms. The objective of this study was to develop a biomimetic bioreactor capable of replicating functional filling and voiding cycles using an automated, closed-loop control system with continuous flow and pressure monitoring.

Methodology: To develop a bladder bioreactor system, pressure and flow sensors, a peristaltic pump, and a pre-programmed microcontroller were used to implement closed-loop control. For flow/pressure validation testing, we applied stable pressure cycles ranging from 0 to 10 mmHg at a controlled flow rate of 1.5 mL/min, corresponding to the physiological normal bladder filling and voiding cycle. To validate the system biologically, tissue-engineered bladder constructs were prepared and placed into the bioreactor system. The porcine bladder was selected as the inflatable substrate for this experiment. At the end of the experiment, samples were collected and processed for viability, metabolic activity, and gene expression.

Results: Benchtop testing confirmed stable, repeatable pressure cycles of 0–10 mmHg with consistent flow rates of ±1.5 mL/min over 5 days. Cell viability was maintained in both groups. Dynamically conditioned constructs exhibited significantly higher metabolic activity as compared to static controls ($p<0.05$). Gene expression analysis revealed upregulation of COL1A1, ELN, and UPK2 in dynamically conditioned constructs, indicative of early extracellular matrix remodeling and urothelial differentiation.

Conclusion/Significance: This study presents a novel sensor-integrated bladder bioreactor capable of delivering physiologically relevant low-pressure filling and voiding cycles. Sensor-integrated bladder bioreactors enable continuous monitoring of the tissue construct's health and overcome current deficiencies in replicating the physiological tissue environment and function, thus improving the clinical outcome after bladder tissue reconstruction.

A06 - Multi-functional Solid 3D Organ Bioreactor with real-time monitoring for Regenerative Medicine Applications

Young Min Ju[1], Po-Feng Lee[1], Adit Mehta[1], Nathan Barney[1], Eric Renteria[1], Frank Marini[1], Ji Hyun Kim[1], Tracy Criswell[1], Thomas Shupe[1], Anthony Atala[1], Joshua Hunsberger[2], Metin Gurcan[3], Shay Soker[1], James Yoo[1]

[1]*Wake Forest School of Medicine, Wake Forest Institute For Regenerative Medicine, Winston-Salem, United States of America*
[2]*RegenMed Development Organization (ReMDO), Winston-Salem, United States of America*
[3]*Wake Forest School of Medicine, Center For Artificial Intelligence, Winston-Salem, United States of America*

Purpose/Objectives: Solid organ injuries are seen at a significantly high incidence in critically injured military and civilian patients and are associated with increased mortality. Regenerative medicine is emerging as a potential solution for restoring damaged organ function and is rapidly transitioning from the research phase to the clinical phase. Many cell-based tissue-engineered products require tissue-specific bioreactors for preconditioning and maturation; however, clinically usable organ-specific bioreactors are unavailable, and many bioreactors are custom-made, creating regulatory and manufacturing challenges. This study aimed to develop a standardized, self-contained, and modular bioreactor platform that enables a scalable, automated process for the clinical manufacturing of solid 3D organ constructs.

Methodology: We developed a solid 3D organ-specific bioreactor prototype, consisting of a rotatable and pressurizable organ enclosure to fit and stabilize organs in different shapes or sizes. This enclosure also minimizes stress concentration from the gravity influence during whole organ perfusion. The constant-pressure motion was carried out by integrating the flow pump, flow rate sensor, pressure sensor, and PID (proportional–integral–derivative) controller to minimize the delay or overshoot of the flow rate, which could lead to damage to the microstructure of the organ. Validation tests under constant pressure and constant-flowrate perfusion modes were conducted using a decellularized porcine kidney to confirm the functionality and reliability of the bioreactor.

Results: The results showed the solid 3D bioreactor system's proper operation with quantitative data displayed by the integrated sensors. Under the PID-controlled flow, we were able to perfuse multiple organs with one gear pump simultaneously, and the pressure of the renal artery during perfusion was successfully maintained for 48 hours without a flow rate overshoot observed. The design of the rotatable and pressurizable organ enclosure improved the organ circulation as evidenced by the dye perfusion experiment. The module was successfully used for porcine kidney conditioning to maintain scaffold integrity.

Conclusion/Significance: The multi-functional perfusion bioreactor has been successfully validated and may be used as a standard tool for biomanufacturing tissue-engineered solid 3D organ constructs, and the perfusion system can be applied to other perfusion-based tissue bioreactors.

A11 - Tailored biomaterial therapies for concomitant muscle and bone repair

Koyal Garg[1], Kevin Sekerak[2], Rebecca Sheetz[3], Riki Koshimizu[2], Avantika Jain[3], Amelia Ridolfo[3], Jamshid Tadiwala[2], Sonja Gurbani[1], Ken Bertram[1], Sara Mcbride-Gagyi[1]

[1]*Saint Louis University, Biomedical Engineering, Saint Louis, United States of America*
[2]*School of Science and Engineering, Saint Louis University, Biomedical Engineering, Saint Louis, United States of America*
[3]*St Louis University, Biomedical Engineering, St. Louis, United States of America*

Purpose/Objectives: Extremity trauma frequency involves both muscle and bone damage. To address these injuries, we have developed a clinically relevant composite trauma model involving a segmental bone defect (SBD) of the tibia and concomitant volumetric muscle loss (VML) of the adjacent tibialis anterior (TA) muscle. Additionally, we have developed biosponge scaffolds with varying mechanical and physical properties for muscle (MUSponge) and bone (OSSponge) repair. To further enhance their regenerative potential, MUSponges and OSSponges were chemically conjugated with key growth factors for tissue repair and seeded with placental stem cells (PSCs).

Methodology: Male Lewis rats (10-12 weeks old) were subjected to unilateral SBD to the tibia ($\sim$3.5 mm) and a $\sim$20% defect in the TA muscle (n=6/group). After 4 weeks of recovery, peak isometric torque was determined, and tissue was collected for analysis. To treat these injuries, biosponge scaffolds composed of gelatin, collagen, and laminin were prepared with low (MUSponge) or high (OSSponge) concentrations of ECM proteins and chemical cross-linkers (i.e., EDC/NHS). Furthermore, the MUSponge and OSSponges were chemically conjugated with 1 µg of insulin-like growth factor (IGF)-1 and bone morphogenetic protein (BMP)-2, respectively. PSCs were seeded at a density of 500,000 cells/disk, and their secretome was analyzed.

Results: Relative to uninjured controls, the VML+SBD injured limbs showed a 39% deficit in TA muscle mass and a 46% deficit in peak isometric torque (t-test, $p<0.05$). The tibia was found unbridged. The MUSponge scaffold showed a heterogeneous pore structure with lower Young's modulus and distinct swelling kinetics, relative to OSSponges. While IGF-1 showed a burst-release profile over 3 days, BMP-2 showed a sustained-release profile with greater sequestration within the OSSponges. PSCs released higher levels of IL-1a, FGF-basic, and IL-1b on MUSPonges but greater levels of IL-17A and Osteopontin on the OSSponges after 48 hours of culture.

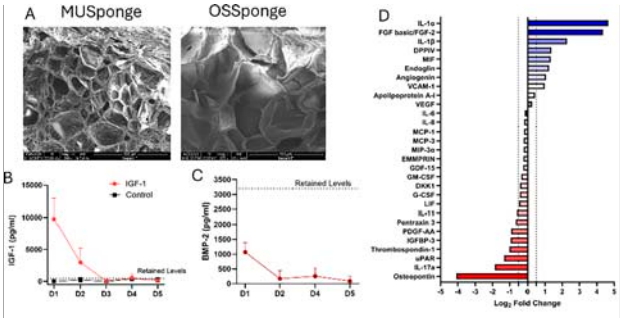


Figure: (A) Scanning electron micrographs of MUSponges and OSSponges show differences in pore network. The release kinetics of MUSponge conjugated (B) IGF-1 and OSSponge conjugated (C) BMP-2 is shown on days 1-5. (D) PSCs seeded on MUSponges and OSSponges show distinct secretory profiles with higher FGF-basic on MUSponges and greater Osteopontin on OSSponges.

Conclusion/Significance: We have successfully developed tailored therapies with distinct biophysical and biochemical properties to simultaneously repair muscle and bone in a clinically relevant rodent model of composite trauma. Ongoing studies are investigating the therapeutic potential of these therapies *in vivo*.

A13 - Systemic stressors increase joint senescence burden

Nikhil Bagchi, Elise Gray-Gaillard, Lexi Rindone, Jennifer Elisseeff

Johns Hopkins University, Baltimore, United States of America

Purpose/Objectives: Osteoarthritis (OA) is a chronic disease of the joints that affects over 500 million people worldwide. Our lab and others have found that senescent cells (SnCs) accumulate in the joint with OA, and their clearance had positive effects on joint structure and pain. However, OA still does not have any disease-modifying therapeutics commercially available. Of note, joint damage has been established in clinic as a poor predictor of arthralgia (joint pain). This discordance between patient pain and radiographic signs of OA highlights an undiscovered mechanism by which systemic conditions in the body may influence joint biology and pain. In this study, we leverage two clinically relevant murine models to determine the effects of distal inflammatory stimuli on SnCs in the joint.

Methodology: Anterior Cruciate Ligament Transection (ACLT) was performed on wildtype mice to induce post-traumatic osteoarthritis (mice without surgery served as controls). Subsequently, mice were given a subcutaneous injection of B16-F10 metastatic melanoma cancer cells into the right flank (mice without tumor inoculation served as controls). Four weeks after ACLT, right hindlimb joints were processed for histology. Immunofluorescence staining (IF) of p16 (a commonly used senescence marker) was performed on joint sections. In a separate experiment, mice were subjected to volumetric muscle loss (VML) surgery in quadriceps muscle with polycaprolactone particle (PCL) implantation. At week 6 following VML, uninjured joints were harvested, processed, and stained for p16.

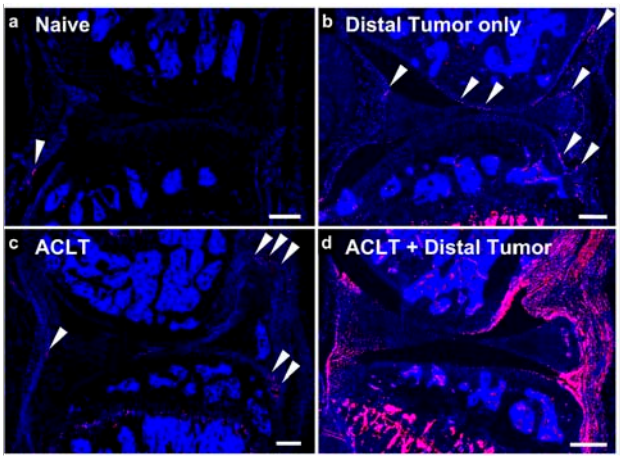


Figure 1. Distal tumor increases p16+ cells (red) in joints. **A.** No injury or tumor. **B.** Distal tumor without ACLT injury **C.** ACLT injury without tumor. **D.** ACLT with distal tumor. Scale bar: 200 µm

Results: In both ACLT and non-ACLT injured mice, we observed an increase in $p16^+$ cells in the joint with the distal tumor inoculation, especially in the synovium (**Fig. 1**). The VML-PCL implant induced senescence in the uninjured joint relative to naïve controls.

Conclusion/Significance: Taken together, these results indicate a previously unrecognized axis of systemic stressors-local senescence induction in the joint. With increasing importance placed on precision medicine in today's age, these observations reframe understanding of the mechanisms by which systemic perturbations may influence joint pathology.

A15 - High-throughput functional neurotoxicity screening using human iPSC-derived brain region-specific neural spheroid models

Yining Wang, Jiajing Zhang, Ruili Huang, Emily Lee, Marc Ferrer-Alegre

National Center For Advancing Translational Sciences, Rockville, United States of America

Purpose/Objectives: Neurotoxicity accounts for approximately 25% of safety failures in drug development and around 16% of post-marketing safety withdrawals, underscoring the need for more predictive preclinical neurotoxicity models. Because brain function arises from coordinated neural network activity rather than individual neurons, current *in vitro* assays may not detect effects on neuronal functional network connectivity in a high-throughput manner and may not adequately capture drug responses in different brain regions. To address these limitations, we developed a high-throughput, 384-well 3D neural spheroid platform that enables multiplexed assessment of neurotoxicity by measuring cell viability and functional network activity. We hypothesize that network-level functional readouts improve the sensitivity of detecting adverse effects and that brain region–specific spheroids reveal differential neurotoxic responses.

Methodology: Brain region-specific spheroids were assembled from human induced pluripotent stem cell (hiPSC)-derived neurons and glial cells in defined ratios to model distinct brain regions. After three weeks, spheroids exhibit spontaneous, synchronized network activities measured using fluorescent calcium imaging. Region-specific spheroids display distinct calcium oscillation patterns, reflecting neural subtype specific differences in activity. Utilizing prefrontal cortex (PFC)-like and ventral tegmental area (VTA)-like spheroids, we screened a library of 126 compounds, including drugs targeting the nervous system and other organs, as well as environmental chemicals and food additives, to represent a broad range of neurotoxicity liabilities.

Results: Our preliminary results show that, at the same drug concentrations and dosing durations, the functional readout based on neural calcium oscillations identifies more than twice as many neurotoxic hits compared to cell viability assays, indicating greater sensitivity to neurotoxic effects. Additionally, distinct responses to certain compounds were observed between PFC- and VTA-like spheroids. Select compounds are being further evaluated in dose–response studies to confirm neurotoxic effects and assay reproducibility. Additional studies will provide mechanistic insights into the differential network connectivity and biological processes perturbed in brain region-specific spheroids. This data will also support the development of *in silico* models for virtual screening and neurotoxicity prediction.

Conclusion/Significance: This study validates an integrated use of in vitro/in silico NAMs with functional 3D neural spheroids, with potential to improve early identification of neurotoxic compounds in preclinical drug discovery.

A17 - Engineering an outer retinal graft for autologous cell replacement

Laura Bohrer[1], Nicholas Stone[1], Martin Hermann[2], Mariah Leidinger[1], Adam Goeken[1], Katayoun Varzavand[1], Jens Kiilgaard[2], Robert Mullins[1], Edwin Stone[1], Budd Tucker[1]

[1]*Institute for Vision Research, University of Iowa, Ophthalmology And Visual Sciences, Iowa City, United States of America*
[2]*University of Copenhagen, Department of Ophthalmology, Rigshospitalet, Copenhagen, Denmark*

Purpose/Objectives: Induced pluripotent stem cells (iPSCs) provide the opportunity to derive differentiated tissues from patients with inherited retinal diseases and use these models to study disease mechanisms and test therapeutics. However, current protocols often fail to accurately recapitulate the cellular organization present in the native tissue. The purpose of this study was to engineer a human model system that accurately recapitulates the outer retinal unit for disease modeling and transplantation.

Methodology: Polycaprolactone (PCL) scaffolds were printed on glass slides using ultra-high resolution two-photon lithography. Patient-derived iPSCs were generated via Sendai virus reprogramming of dermal fibroblasts. IPSC-derived RPE were plated onto PCL scaffolds. Retinal organoids were derived using a stepwise 3D differentiation protocol using cGMP-compliant reagents and dissociated with papain and layered on RPE. Subretinal injection of ICG in pigs resulted in loss of photoreceptors by 1-month and were used for transplantation studies.

Results: To generate a construct that closely mimics the outer retinal unit, a PCL scaffold was designed and fabricated using two-photon lithography. The final design was an elongated octagon with a continuous wall surrounding its perimeter that was canted to enable maneuverability within the vitreous cavity. The floor was positioned 60μm below the top of the perimeter wall to house a monolayer of RPE cells beneath multiple rows of photoreceptor cells. To promote consistent loading, a device that surrounded the scaffold was fabricated. Upon reaching confluence, RPE cells pigmented and formed tight junctions as indicated by ZO-1 staining. Retinal organoids containing photoreceptor precursor cells expressing OTX2, ARR3, NRL, and recoverin were generated. Photoreceptor precursor cells were enriched using a partial dissociation strategy and loaded onto monolayers of RPE, giving rise to a multilayered outer retinal construct. Subretinal transplantation of 3D retinal grafts using a custom tool was performed in the immunosuppressed ICG pig model of retinitis pigmentosa. One week after transplantation, the graft lay flat next to the Bruch's membrane.

Conclusion/Significance: We have successfully developed an outer retinal microphysiologic system containing a monolayer of iPSC-derived RPE and photoreceptor cells. This construct will be invaluable for study of disease pathology and development of drug, gene, and cell-based therapeutics to treat retinal degenerative blindness.

A20 - Chemical and Biochemical Properties of novel hydrolyzed collagen

Bradley Rodier, Jonathan Velasco, Fahimeh Tabatabaei, Nina Bionda

Rochal Technologies, Sanara Medtech subsidiary, San Antonio, United States of America

Purpose/Objectives: This study investigated the chemical and biochemical properties of a low-molecular-weight bovine hydrolyzed collagen used extensively in surgical wound management. The primary goal was to identify lot-to-lot chemical similarities within this complex system. Identifying these baselines will allow researchers to develop more targeted approaches, enhancing the efficacy of future products.

Methodology: Multiple techniques were utilized for analysis **O-phthaldialdehyde assay -** For evaluating degree of hydrolysis the o-phthaldialdehyde (OPA) assay was used to quantify free α-amino groups. **LC-MS –** In order to determine Mw as well as peptide sequence tandem LC-MS was used. Chromatographic separation was performed using a Dionex UltiMate3000 UHPLC. Mw distribution was determined and peptides and associated proteins were detected by Uniprot accession numbers based on fragment weight. **FTIR -** The chemical structure of the powder was analyzed by Fourier-transform infrared spectroscopy with attenuated total reflection. **pH –** The pH of the dissolved collagen was taken to ascertain how the powder would influence a moist environment. Hydrolyzed collagen was reconstituted in phosphate-buffered saline (PBS) following ISO 10993-12 guidelines. PBS alone was used as a control.

Results: Analysis of this hydrolyzed collagen demonstrated highly consistent properties across multiple fabricated lots. The powder exhibited a peptide molecular weight range of 500–3000

[Da], which included di- and tripeptides, and an average degree of hydrolysis yielding 400 nmol/mL of free amines. FTIR spectra maintained a consistent signature across all tested lots, displaying the expected amide bond peaks. The collagen also remained slightly acidic, with the pH decreasing from 5.96 to 5.81 over 24 hours compared to PBS control. Furthermore, LC-MS identified over 2,500 unique peptide sequences, 105 of which were conserved across all samples regardless of their bovine source.

Conclusion/Significance: In conclusion, this study demonstrated that the bovine hydrolyzed collagen product maintains highly conserved properties across multiple lots—a crucial consistency for medical devices used in surgical wound management. Moving forward, isolating these common peptide sequences will allow researchers to explore how specific peptides directly drive the healing process, paving the way for more targeted therapies.

A22 - A Dual Affinity Fusion Protein for Localized Bone Morphogenetic Protein-2 (BMP-2) Delivery from Collagen Sponges

Malvika Singhal[1,2,3], Marian Hettiaratchi[1,2,3]

[1]*University of Oregon, Knight Campus For Accelerating Scientific Impact, Eugene, United States of America*
[2]*University of Oregon, Department of Chemistry and Biochemistry, Eugene, United States of America*
[3]*Institute of Molecular Biology, Department of Biology, Eugene, United States of America*

Purpose/Objectives: Bone morphogenetic protein 2 (BMP-2) is critical for bone regeneration, as it mediates the osteogenic differentiation of mesenchymal stromal cells and osteoprogenitor cells, which actively participate in bone formation. Current treatments for critical bone defects deliver supraphysiological BMP-2 doses in a collagen sponge to overcome the short half-life of BMP-2. However, BMP-2 binds weakly to collagen, leading to its rapid release and abnormal bone growth, which contributes to swelling and pain. The goal of this project is to develop and characterize a dual affinity fusion protein that binds to BMP- and collagen to localize BMP-2 within a collagen sponge delivered to the site of bone injury. We developed a fusion protein consisting of a 7 amino acid peptide, TKKTLRT, engineered to bind specifically to collagen and a 58 amino acid domain called an affibody engineered to bind specifically to BMP-2. TKKTLRT anchors the fusion protein to the collagen sponge, while the affibody enables local BMP-2 retention within the implantation site.

Methodology: We characterized the affinity of the affibody domain for BMP-2 to be 11 nM using biolayer interferometry (BLI) and the affinity of the fusion protein to collagen to be 360 nM using a custom collagen enzyme-linked immunosorbent assay (Fig 1A). Fluorescent fusion protein was retained on collagen sponges for 24 hours (Fig 1B). We confirmed binding interactions between the fusion protein and BMP-2 and then that complex to collagen using BLI (Fig 1C).

Results:

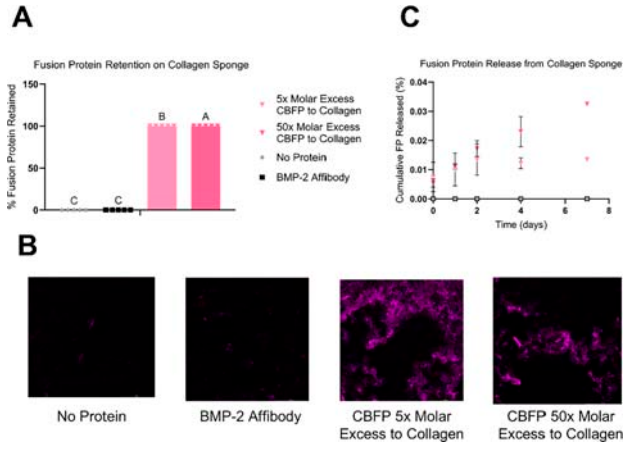


Figure 1. A) Dose response curve of fusion protein binding to collagen. B) Fluorescence images of collagen sponge with or without fusion protein after 1 day of incubation at 37°C. C) Sequential association of fusion protein to BMP-2 followed by collagen on a biolayer interferometer.

Conclusion/Significance: Our engineered dual affinity fusion protein binds to both BMP-2 and collagen sponge and can be retained on a collagen sponge over time. Next, we will evaluate the effect of the fusion protein on BMP-2 delivery from collagen sponges and on BMP-2-mediated mineralization of collagen sponges *in vivo*. Overall, we aim to enhance the ability of clinical collagen biomaterials to locally deliver BMP-2 to large bone defects.

A23 - A Tough, Click-Functional Nanofibrous Block Copolymer Scaffold for Cell-Free Bone Regeneration

Tongqing Zhou, Rafael Cavalcante, Peter Ma

University of Michigan, School of Dentistry, Ann Arbor, United States of America

Purpose/Objectives: Tissue engineering is a rapidly expanding multidisciplinary field, with multiple recent market analyses projecting the global market to reach roughly $35–56 billion by 2032. Meeting this growing demand requires scaffold materials that combine interconnected porosity, mechanical durability, extracellular-matrix-like nanostructure, biodegradability, and stable presentation of bioactive signals. However, high porosity for tissue ingrowth and bioactive modification often compromises scaffold strength, creating a need for stronger and chemically reactive base materials. Here, we develop a new poly(L-lactide) (PLLA)-based block copolymer scaffold that integrates nanofibrous morphology, enhanced mechanical performance, tunable degradation, and covalent peptide presentation for cell-free bone regeneration.

Methodology: A norbornene-functional PLLA-based block copolymer, poly(spiro-lactic-co-lactic acid)-block-poly(l-lactic acid) (PSLA-b-PLLA), was synthesized through a two-step ring-opening polymerization strategy. Polymer composition was optimized to control nanofiber formation, mechanical properties, and peptide conjugation density. Three-dimensional porous nanofibrous scaffolds were fabricated using thermally induced phase separation combined with porogen leaching. Bioactive peptide conjugation was achieved through an efficient click chemistry, and scaffold performance was evaluated using mechanical property characterization, degradation studies, and a mouse critical-sized calvarial defect model.

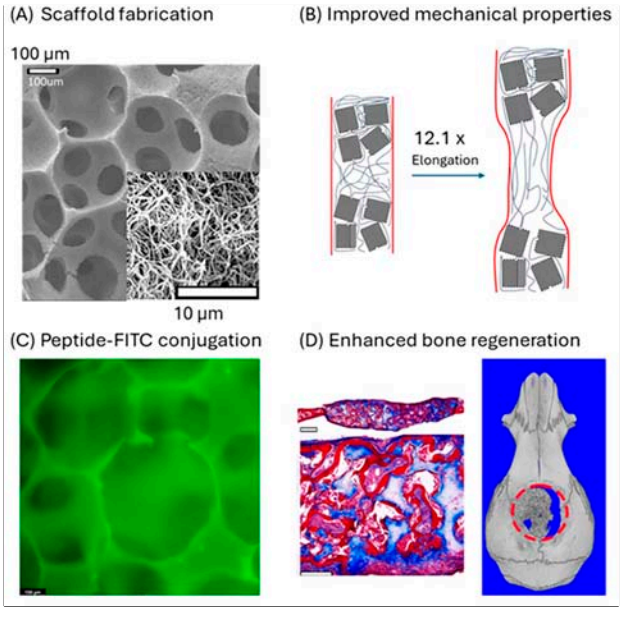


Figure 1. PSLA-b-PLLA combines nanofibrous architecture, enhanced toughness, peptide conjugation, and improved bone regeneration.

Results: PSLA-b-PLLA preserved the nanofibrous architecture of PLLA while enabling stable peptide conjugation. Optimized PSLA-b-PLLA achieved 1.2-fold tensile modulus, 12.1-fold strain at break, 2.1-fold ultimate strength, and 35.1-fold toughness compared with PLLA

nanofibrous films. The selected composition formed 3D porous scaffolds comparable to PLLA but degraded faster over 8 weeks. P24-conjugated PSLA-b-PLLA significantly enhanced bone regeneration in mouse critical-sized calvarial defects, producing 3.6-fold greater bone volume than unconjugated controls after 8 weeks, with increased mature bone formation, vascularization, and osteogenic activity.

Conclusion/Significance: This work establishes PSLA-b-PLLA as a scaffold platform that overcomes key limitations of conventional PLLA by combining ECM-like nanofibrous structure, superior toughness, accelerated degradation, and covalent biomolecular signaling. The tunable chemistry and mechanics of PSLA-b-PLLA suggest broad potential for bone and other tissue engineering applications.

A24 - In Vitro Evaluation of Hydrolyzed Collagen Surgical Powder on Human Keratinocytes Migration and Proliferation

Tiffany Sanchez[1], Sergio Medina[1], Nina Bionda[2], Fahimeh Tabatabaei[2]

[1]*Rochal Technologies, R&D division of Sanara MedTech, San Antonio, United States of America*
[2]*Sanara MedTech, Rochal Technologies, R&d Division of Sanara Medtech, San Antonio, United States of America*

Purpose/Objectives: Successful epithelial wound repair requires coordinated keratinocyte migration and proliferation to restore skin barrier integrity following tissue injury. Hydrolyzed collagen-derived peptides have been investigated for their role in modulating cellular behaviors associated with tissue repair. The purpose of this study was to evaluate the effects of a hydrolyzed type I collagen product, on human keratinocyte migration and proliferation in vitro.

Methodology: Experiments were performed using HaCaT human keratinocytes cultured under serum-free conditions. Keratinocytes migration was evaluated using a scratch-wound assay following treatment with hydrolyzed collagen (CellerateRX® Surgical Powder; Sanara MedTech) at concentrations of 0.3 mg/mL and 3 mg/mL. Migration into the wound region was quantified after 6 hours. Keratinocytes proliferation was assessed using the AlamarBlue assay following both short-duration (2-minute) exposure and continuous exposure for up to 48 hours across concentrations ranging from 0.03 to 30 mg/mL.

Results: Hydrolyzed collagen treatment significantly increased keratinocyte migration compared to untreated serum-free controls. Enhanced migration was observed at both 0.3 mg/mL and 3 mg/mL concentrations. Short-duration exposure resulted in increased keratinocytes proliferation after 24 hours, particularly at 3 mg/mL and 30 mg/mL. Continuous exposure demonstrated increased keratinocytes proliferation over 48 hours, with the largest response in cell viability observed at higher concentrations. No reduction in cell viability was observed across the tested concentrations.

Conclusion/Significance: These *in vit*ro findings demonstrate that hydrolyzed collagen-derived peptides can positively influence keratinocytes migration and proliferation. The observed enhancement of epithelial cell activity supports the potential role of this product as a biomaterial adjunct to support early wound healing responses. Further preclinical and clinical studies are warranted to evaluate the translational relevance of these findings in surgical wound healing applications.

A25 - Physical Characterization of a hydrolyzed type I collagen: Particle Size Distribution, Surface Coverage, and Aqueous Solubility

Jonathan Velasco, Fahimeh Tabatabaei, Nina Bionda

Rochal Technologies, a Sanara MedTech Company, San Antonio, United States of America

Purpose/Objectives: Effective wound management materials should provide uniform wound bed coverage, predictable handling characteristics, and reproducible physicochemical behavior to support consistent clinical performance. Material properties such as particle size distribution, dispersibility, and aqueous interaction can influence surface contact, application uniformity, and interaction with the local wound environment. This study aimed to evaluate key physical characteristics of a surgical powder across multiple production lots to better characterize performance-related material attributes.

Methodology: Particle size distribution of the hydrolyzed collagen powder (CellerateRX® surgical powder; SanaraMedtech) was characterized using microscopic particle count and sieve analysis according to USP <788> and USP <786>. Surface coverage was assessed using a simulated wound model consisting of a leveled, grid-patterned surface (1 cm^2 units). A defined mass (1 g) was applied as a light dusting to evaluate dispersive coverage. Total coverage area was calculated by summing grid units occupied by material and normalized to applied mass (g/cm^2). Aqueous solubility was evaluated via turbidity following dispersion in distilled water at 40 °C (1.5–2.0 g/mL). Samples were vortexed, gently mixed, and analyzed by absorbance at 600 nm using a microplate reader. Measurements were performed in triplicate and normalized to water controls.

Results: Particle size analysis demonstrated that the hydrolyzed collagen powder consisted predominantly of fine particles, with particles <150 µm representing the largest population (~ 686,800 particles/g). Sieve analysis confirmed that most powder mass was distributed between 75 and 150 µm, with 44.4%, 28.5%, and 21.6% retained on the 100, 140, and 200 mesh screens, respectively. Surface coverage testing demonstrated high dispersibility, with 1 g covering an average of 210 cm^2. Mass-to-area ratios were consistent across lots (0.0047 ± 0.0005 g/cm^2), indicating minimal inter-lot variability. Solubility testing demonstrated concentration-dependent turbidity behavior. Complete solubility was observed at 1.5 mg/mL (absorbance <0.05), whereas higher concentrations showed progressively increased turbidity, indicating partial or incomplete solubilization ($p < 0.05$ across groups).

Conclusion/Significance: Hydrolyzed collagen powder demonstrates controlled particle size distribution, efficient surface coverage, and reproducible solubility under tested conditions. These attributes support predictable handling, consistent application, and manufacturing reliability. These findings provide physicochemical characterization relevant to product handling and performance in regenerative wound care applications.

A30 - Investigating the Paracrine Effects of Multipotent Stem Cell Secretomes Using 2D and 3D Human Cardiac Models

Olivia Latham[1], Josh Maxwell[2]

[1]*Wake Forest Institute for Regenerative Medicine, Winston-Salem, United States of America*
[2]*Wake Forest Institute of Regenerative Medicine, Winston-Salem, United States of America*

Purpose/Objectives: Congenital heart disease (CHD) is the most common birth defect affecting 9 in 1,000 live births. CHD patients with right ventricle (RV) involvement often develop progressive RV failure (RVF) characterized by cardiac myocyte hypertrophy, decreased microvascular density, and interstitial myocardial fibrosis. Current treatments cannot restore RV function or prevent progression into RVF. Stem/progenitor cell-based therapies represent a novel approach to address unmet clinical needs of pediatric CHD patients with cardiac dysfunction. Stem/progenitor cell-secreted paracrine factors can elicit innate cardiac reparative processes; however, the precise mechanisms by which the secretome modulates cardiac cell functions remain unknown. We evaluated the reparative potential of conditioned media (CdM) prepared from human bone marrow-derived mesenchymal stromal cells (hMSCs), human cardiac-derived c-kit positive cells (hCPCs), or human placental-derived stem cells (hPLSCs) on cardiac cell function using 2D and 3D models.

Methodology: Following CdM treatments, proliferation, migration, and tube formation assays characterized the effects of multipotent stem/progenitor cell secretomes on human cardiac ventricular fibroblast (hcFB-V) proliferation and migration and human cardiac microvascular endothelial cell (hcMVEC) angiogenic capacity. To better recapitulate the *in vivo* microenvironment, we developed a novel 3D *in vitro* human cardiac spheroid (hCS) model comprised of human induced pluripotent stem cell-derived cardiac myocytes

(hiPSC-CMs), hcFB-Vs, and hcMVECs. Additionally, TGF-β1 was used to induce cellular dysfunction in hcFB-Vs and hCSs.

Results: All three CdM treatments enhanced hcFB-V proliferation and migration (percent confluence and number of migratory cells) compared to untreated cells (± TGF-β1) and improved hcMVEC angiogenic potential by increasing tube formation (number of new branch points). Taken together, these results indicate that multipotent stem/progenitor cell secretomes promote hcFB-V proliferation and migration and hcMVEC angiogenesis, all of which are key cardiac reparative processes. TGF-β1-treated hCSs exhibited abnormal contractility, potentially correlating with clinical observations of increased susceptibility to arrhythmogenesis seen in RVF.

Conclusion/Significance: Our findings provide insight into the underlying functional mechanisms of the reparative benefits of multipotent stem/progenitor cell secretomes. This research bridges the gap between 2D and 3D *in vitro* modeling, thereby providing a framework to optimize cell-based therapies for RVF, ultimately advancing cardiac regenerative medicine for pediatric patients.

POSTER SESSION 2

11-16-2026 @ 6:35 PM - 8:00 PM

B01 - Nano-Ice–Enabled and Glycocalyx-Mediated Biocompatible Cryopreservation Preserves Skin, Eyelid, Corneal, and Retinal Tissues and NK Cells for Regenerative Medicine Applications

Xu Han[1], Ying-Bo Shui[2], Ying Liu[2], Wenxuan Zhou[1], Hongmin Sun[3], Xunlei Kang[4], Joanne Konstantopoulos[5], Rebecca Sappington[5], Andrew Huang[2]

[1]*Wake Forest University, Wake Forest Institute of Regenerative Medicine, WINSTON SALEM, United States of America*
[2]*Washington University, Ophthalmology & Visual Sciences, St. Louis, United States of America*
[3]*Univ. of Missouri, Department of Medicine, Columbia, United States of America*
[4]*Univ. of Missouri, Precision Medicine Center, Columbia, United States of America*
[5]*Wake Forest University, Department of Biochemistry, Winston Salem, United States of America*

Purpose/Objectives: Current cryopreservation technologies frequently rely on toxic permeating cryoprotectants and often fail to preserve multicellular tissue integrity and cellular functionality after thawing. These limitations are particularly significant for engineered tissues, immune cell therapies, ocular tissues, eyelid preservation, and skin banking applications. OdinSol®, a first-in-class biocompatible cryopreservation platform, was developed to preserve tissues and cells through glycocalyx-mediated suppression of damaging hexagonal ice formation while enabling nano-scale cubic ice formation. In this study, we evaluated the translational applicability of OdinSol across multiple regenerative systems, including natural killer (NK) cells, skin, eyelids, corneal limbal tissues, and retinal pigment epithelial (RPE) tissues. The objective was to determine whether OdinSol preserves viability, tissue ultrastructure, and functional recovery.

Methodology: Human and porcine tissues and cellular systems were cryopreserved at –80°C using OdinSol and compared with conventional glycerol- or DMSO-based preservation approaches. Human corneal limbal tissues and retinal pigment epithelial tissues were evaluated for post-thaw epithelial integrity, tissue architecture, and structural preservation. Human and porcine skin and porcine eyelids underwent histological and ultrastructural analyses following long-term storage. NK cell cryopreservation studies assessed post-thaw viability, migratory capacity, and cytotoxicity. Tissue morphology and ultrastructure were characterized using histology, immunofluorescence imaging, and transmission electron microscopy. Functional recovery was further evaluated through either in vivo transplantation studies or immunohistochemical analyses depending on the tissue system.

Results: OdinSol demonstrated broad cryopreservation efficacy across immune, epithelial, and multicellular tissue systems. Cryopreserved NK cells exhibited improved post-thaw migration capability and cytotoxicity in vivo. Human and porcine skin tissues preserved in OdinSol were successfully transplanted for wound healing. Porcine eyelid tissues similarly demonstrated preservation of cell viability and tissue ultrastructure. Corneal limbal tissues cryopreserved with OdinSol maintained proliferation and differentiation capability and cured limbal stem cell defficiecny after transplantation. Retinal pigment epithelial tissues also demonstrated preserved epithelial morphology.

Conclusion/Significance: OdinSol represents a nano-ice–enabled biocompatible cryopreservation platform capable of preserving diverse cellular and tissue systems while minimizing structural and functional damage associated with conventional cryopreservation. Successful preservation demonstrates the broad translational potential of this glycocalyx-mediated preservation strategy. The platform is compatible with scalable –80°C biobanking workflows and supports future applications in regenerative medicine, immunotherapy, tissue engineering, ophthalmology, and transplantation.

B02 - Embedded Printing and Template Stamping-Based Lung Model for Air–Liquid Interface Epithelial Culture with Perfusable Microchannels

Jooyoung Lee, Hyungseok Lee

Kangwon National University, Chuncheon, Korea, Republic of

Purpose/Objectives: Conventional lung in vitro models often fail to simultaneously reproduce epithelial curvature, air exposure, and basal nutrient supply, which are key features of the native lung microenvironment. This study aimed to develop a lung epithelial model designed for air–liquid interface (ALI) culture by integrating template stamping to create alveolar-like surface geometry and embedded sacrificial printing to generate perfusable microchannels.

Methodology: A GelMA/glycerol-based support bath was optimized as a permanent hydrogel matrix for embedded printing. Gelatin was used as a thermoresponsive sacrificial ink that could be removed at 37°C, enabling the formation of hollow microchannels. The bath and sacrificial ink were evaluated through rheological characterization and printability tests to identify printing conditions suitable for filament support, shape retention, and channel fidelity. In parallel, template stamping was used to fabricate curved or hemispherical features on the bath surface to mimic alveolar-like geometry. A549 lung epithelial cells were seeded onto the upper surface of the GelMA/glycerol bath and initially cultured under submerged conditions to promote cell attachment. After sacrificial ink removal, the constructs were maintained under ALI culture by supplying medium through the embedded basal channels while exposing the apical epithelial surface to air. Cell viability, metabolic activity, epithelial morphology, mucus-associated staining, junctional marker expression, and barrier-related permeability were evaluated.

Results: The GelMA/glycerol bath exhibited tunable viscoelasticity, shear-thinning behavior, and self-recovery, enabling stable support of embedded sacrificial filaments. A 6% gelatin sacrificial ink and GelMA/glycerol bath supported continuous channel formation with improved filament fidelity and circularity. The stamped bath substrates provided defined curved epithelial culture regions, while the embedded channels enabled basal medium supply during ALI culture. Compared with channel-free constructs, perfusable channel-containing models supported improved long-term epithelial maintenance, higher metabolic activity, stronger mucus-associated staining, and clearer epithelial junction formation, as indicated by markers such as ZO-1 and MUC5AC.

Conclusion/Significance: This study demonstrates a hybrid fabrication strategy that combines embedded printing and template stamping to construct a more physiologically relevant lung epithelial model. By integrating alveolar-mimetic surface geometry, ALI exposure, and perfusable basal channels, this platform may provide a useful tissue-engineered model for studying lung epithelial barrier maturation, mucus-related function, and future drug response evaluation.

B05 - From Bench to Chip: High-Fidelity 3D Bioprinting of Human-Relevant Microphysiological Systems

Shreyas Gaikwad[1], Sam Belden[1], Ting-Yu Lu[2], Rahul Roy[3], Volodymyr Kuzmenko[4], Shaochen Chen[2], Wei Zhu[3]

[1]*Cellink, Woburn, United States of America*
[2]*University of California San Diego, San Diego, United States of America*
[3]*Cellink, San Diego, United States of America*
[4]*Cellink, Gothenburg, Sweden*

Purpose/Objectives: To use next generation bioprinting technologies for developing a human-relevant liver and a placental model. The models were used for evaluating drug metabolism, transfer, and toxicity under physiologically realistic conditions.

Methodology: Using Digital Light Processing (DLP), a high-fidelity liver platform was constructed within a modular PEG-norbornene hydrogel engineered to support cell-driven matrix remodeling. iPSC-derived hepatocytes and endothelial cells were spatially organized into lobule-inspired architectures, and microfluidic perfusion was incorporated to promote functional maturation. Test compounds were administered via the perfusion system and evaluated by tracking metabolic function, cell viability, and tissue-level responses over time. In parallel, extrusion bioprinting was used to construct placenta model with precise cellular organization. Trophoblasts, endothelial cells, and stromal components were arranged within biomimetic bioinks to reproduce maternal-fetal interfaces. The resulting cell-laden placental membranes were incorporated into a microfluidic platform with distinct maternal and fetal channels, enabling controlled perfusion and real-time compound exposure.

Results: The DLP-bioprinted liver platform demonstrated strong functional performance across multiple readouts. Robust CYP450 enzymatic activity was achieved alongside sustained albumin production and urea synthesis, confirming long-term viability and metabolic stability under continuous perfusion. Transcriptomic profiling revealed gene expression profiles closely aligned with primary human hepatocytes, and benchmarking against established clinical hepatotoxicants confirmed superior predictive accuracy over conventional 2D and animal-based systems. Drug compounds introduced through the perfusion system produced dose-dependent changes in metabolic function and cell viability that closely mirrored known in vivo hepatotoxicity profiles. The extrusion-bioprinted placental model similarly performed well, with the spatially organized maternal-fetal interface maintaining structural integrity and defined cellular organization throughout testing. Barrier integrity measurements confirmed the formation of a tight, physiologically representative membrane, and drug transport studies under controlled perfusion yielded quantifiable, reproducible transfer rates consistent with known clinical placental data. Dose-dependent changes in barrier integrity and cell viability enabled reliable early detection of placental toxicity, validating the model as a sensitive and human-relevant system for assessing compound transfer and safety.

Conclusion/Significance: Together, these reproducible and scalable bioprinted NAMs integrated with organ-on-chip technology provide a sophisticated framework for studying drug transfer and safety.

B07 - Development of a Speaker-Based Vibratory Bioreactor for Vocal Fold Tissue Engineering

Mohaddeseh Mohammadi[1], Amir K Miri[1], Richart Ng[2], Daniel Li[1]

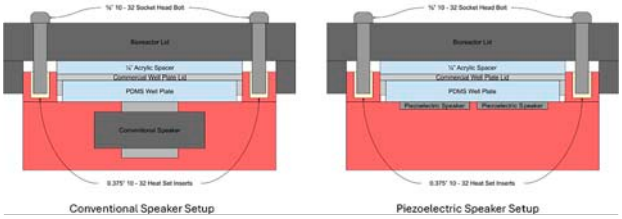
[1]*New Jersey Institute of Technology, Biomedical Engineering, Newark, United States of America*
[2]*New Jersey Institute of Technology, Mechanical Engineering, Newark, United States of America*

Purpose/Objectives: The purpose of this study was to design, fabricate, and characterize a speaker-based vibratory bioreactor system for the application of controlled phonatory-like mechanical stimulation to vocal fold fibroblasts encapsulated in GelMA hydrogels. Specifically, this work aimed to compare the vibrational output and biological efficacy of two actuator systems: a conventional speaker and a piezoelectric speaker.

Methodology: HVOX vocal fold fibroblasts were encapsulated in 5% (w/v) GelMA hydrogels and cultured within custom PDMS well plates fabricated to maximize flexibility and vibration propagation. A vibratory bioreactor system comprising a DC power supply, a signal amplifier, and laptop-based tone-generation software was used to deliver controlled mechanical stimulation via two speaker configurations: a conventional speaker and a piezoelectric speaker. Both systems operated at 200 Hz with a cyclic stimulation regimen of 2 hours on and 1 hour off for 3 days. An orbital shaker set to 900 rpm served as a low-frequency reference condition. Bioreactor characterization was performed using laser Doppler velocimetry (LDV) to quantify vibration velocity distribution across all well positions at both 100 Hz and 200 Hz. Following culture, samples were assessed via immunofluorescence staining to evaluate cytoskeletal organization and mechanobiological response across stimulation conditions.

Results: LDV characterization confirmed vibrational output across well plate for both speakers. The conventional speaker produced velocity amplitudes of 0.21-1.38 mm/s at 200 Hz and 0.30-2.72 mm/s at 100 Hz, with spatial heterogeneity across the plate. The piezoelectric speaker amplitudes range from 0.25 to 1.60 mm/s at 200 Hz and 0.29 to 3.82 mm/s at 100 Hz, with higher peak velocities in central well positions. Immunofluorescence staining revealed distinct morphological differences across conditions. Static cultures showed disorganized actin architecture in fibroblasts. Orbital shaker stimulation increased elongation and cytoskeletal organization. Conventional speaker produced moderate improvements in cell elongation and actin fiber alignment. Piezoelectric speaker elicited the most pronounced mechanobiological response, and highly elongated spindle-shaped cells with well-organized, directionally aligned actin fibers distributed throughout the scaffold.

Figure 1a:Construction of the bioreactor



Conclusion/Significance: This study demonstrates the successful design of a vibratory bioreactor capable of delivering controlled stimulation to engineered vocal fold constructs in vitro.

B08 - Fully passive working heart loading system as simple inserts for scalable Heart Slice culture

Joern Huelsmann[1], Abhijeet Kumar[1], Sairam Pasam[1], Aboubakr Salama[1], Kamal Abou Farraj[1], Angel Moctezuma Ramirez[2], Mir Timo Nazari Shafti[1], Emmanuel Camors[1], Rose Mathew[1], Rebecca Liu[1], Sara Taha[1], Riham Abouleisa[1], Tamer Mohamed[1]

[1]*Baylor College of Medicine, Center For Cardiac Engineering And Regenerative Therapeutics (cert), Houston, United States of America*
[2]*Texas Heart Institute at Baylor College of Medicine, Center For Preclinical Surgical & Interventional Research, Houston, United States of America*

Purpose/Objectives: The Heart Slice technology enables the use of native human myocardium for translational medicine, addressing the longstanding disconnect between preclinical models and clinical trials in predicting cardiotoxicity. Despite its promise, maintaining cardiac physiology ex vivo remains technically demanding and commonly requires sophisticated technology for mechanical stimulation and functional readouts, limiting applications to low-throughput lab research.

Methodology: To address these challenges, we developed fully passive inserts for culture plates to provide physiological

contractions resistance within a mechanical environment that mimics a working heart. We compared their operational modes in culture: 1) No Load, 2) Preloaded, 3) Inotropy, and 4) Pre-+ Afterload - to assess their effect on porcine heart slice physiology. Therefore, contractions were assessed optically. The critical functional markers Connexin 43 (Intercalated Discs), alpha actinin (Sarcomeres), Ryonidin 2 Receptor, and Junctophilin 2 (Dyad Structure) were assessed by IF staining and confocal microscopy of whole fixated slices.

Results: In all modes, contractions were composed of a phase of fast force generation and a plateau phase, similar to the phases of pressure generation and ejection in the heart. While mode 1), what only counters artificial shrinking, measured contractile force did not exceed ~5 kPa and ceased rapidly, mode 2 showed to increase the force and sustain contractility over time. The continuous beating modes 3) vs. 4) could mimic and contrast inotropy vs. the Frank Starling mechanism with contractile forces ranging at ~10 vs. ~25 kPa. Additionally, continuous contractions in mode 3 and 4 and showed a period of increasing force over time, indicating the presence of the Anrep Effect as well. Physiological loading was confirmed by confocal microscopy, showing preserved structures for sarcomeres, intercalated discs, and dyads in culture under mechanical stimulation in mode 4.

Conclusion/Significance: The mechanical environment of our inserts successfully preserved the myocardial physiology in ex-vivo culture. Moreover, all loading states and modes of performance of a working heart could be reflected and are made available for translational research in a simple platform that can be scaled up to high-throughput applications. Additionally, it may be used as platform to advance the culture and monitoring of engineered myocardial constructs.

B11 - Engineering Human Donor Derived Germinal Center-like Organoids (GCLOs) for studying Immune Response to Vaccination

Bhumi Suthar[1], Suresh Pallikkuth[2], Ashutosh Agarwal[1]

[1]*University of Miami, Biomedical Engineering, MIAMI, United States of America*
[2]*University of Miami, Microbiology And Immunology, MIAMI, United States of America*

Purpose/Objectives: Germinal centers (GCs) are transient microanatomical structures that coordinate humoral immune response through dynamic interactions between antigen presenting cells, T follicular helper cells, and B cells. Despite their central importance to immune protection, GC human biology remains difficult to interrogate due to significant inter-species variability, limited experimental accessibility to primary human tissues, and high interindividual variability. We developed a human immune culture platform that supports spontaneous multicellular organization of human peripheral blood mononuclear cells derived primary CD19+ B cells, memory CD4+ T cells, and monocyte derived Dendritic Cells into Germinal Center-like Organoids (GCLOs) that self-organize into stable clusters that exhibit stimulus and donor dependent differences in cellular composition and function.

Methodology: This study included deidentified PBMC samples from six healthy adult donors, who received seasonal influenza vaccination, comprising three older (A1, A2, A3) and three younger (Y1, Y2, Y3) individuals. Primary monocytes were isolated from PBMC and differentiated to yield monocyte derived dendritic cells (moDCs), which were then co-cultured with memory CD4+ T cells, and total CD19+ B cells in fibronectin suspension.

Results: We observed emergence of GC-like T and B cell subsets, functional IgG output, and appearance of plasmablast-like populations. Across stimulation conditions, we observed distinct and reproducible immune cell organization and population. The distinct cellular and functional phenotypes across stimulation conditions highlight the platform's sensitivity to physiological cues. We used the Fluzone lots corresponding to the same influenza season in which each donor was vaccinated. Donor's clinical titers and responsiveness to vaccine was mirrored by the platform's IgG concentration. Vaccine stimulation elicited the most inter-donor variability, underscoring the importance of examining immune responses at the individual level. The IgG accumulation along with UMAP-derived cellular compositions illustrate a tight correspondence between platform and clinical outcomes.

Conclusion/Significance: Overall, the platform supports cognate B cell – T cell interactions, plasmablast differentiation and antibody secretion over a clinically relevant time frame. Human GCLOs enable a framework for studying donor-specific secondary humoral responses, probing age-associated immune decline, capturing and predicting human-specific vaccine responses and immune heterogeneity.

B13 - From Action Potentials to Organoids: A Unified Optical Platform for Multi-Modality Safety Pharmacology in Human iPSC Models

Thomas Leahy, Christos Michas, Kevin Gray, Arjun Acharya, Travis Moerk, Jacob Fleming, Nelsa Estrella, Christal Worthen, Greg Luerman, Nicholas Geisse

Curi Bio, Seattle, United States of America

Purpose/Objectives: Safety pharmacology increasingly demands human-relevant functional data spanning multiple organ systems and tissue architectures, yet most microphysiological platforms are optimized for a single modality or format. Here, we demonstrate a high-throughput workflow capturing voltage, calcium, and contractility readouts across 2D monolayers and 3D engineered tissues, spanning cardiac, skeletal muscle, and CNS models on a single instrument.

Methodology: A single optical instrument acquired functional readouts across four hiPSC-derived systems: (1) 2D cardiomyocyte monolayers profiled by voltage imaging across an 8-point half-log dose curve (0.05 to 100 μM) of flecainide, amiodarone, and quinidine, with four-parameter logistic fits; (2) 96-well 3D engineered heart tissues (EHTs) profiled for contractility responses to mavacamten, omecamtiv mecarbil, and verapamil at doses up to 5 μM; (3) 96-well 3D engineered muscle tissues (EMTs) for longitudinal, parallel quantification of transgene expression and contractility across MOIs for 10 myotropic AAV capsids; and (4) 384-well CNS-3D brain organoids profiled by calcium imaging during acute and repeat-dose exposures to rotenone, 4-AP, MK-801, and muscimol across seven-point half-log dilutions.

Results: Voltage imaging in cardiomyocyte monolayers yielded sigmoidal concentration-response relationships (all $R^2 > 0.95$), with IC_{50} values of 4.96, 0.84, and 0.41 μM for flecainide, amiodarone, and quinidine. In EHTs, mavacamten produced ~85% twitch-force inhibition at 5 μM, verapamil abolished spontaneous contractility by 5 μM, and omecamtiv mecarbil elicited >5-fold increases in twitch force. In EMTs, the most efficiently expressed AAV capsids induced dose-dependent functional impairment at elevated MOIs, including contractile force reduction to ~25% of controls and loss of calcium signaling. In brain organoids, calcium imaging captured mechanism-consistent responses to all four neuroactive compounds (Figure 1), with reversible muscimol responses across repeated dose-washout cycles demonstrating longitudinal capability.

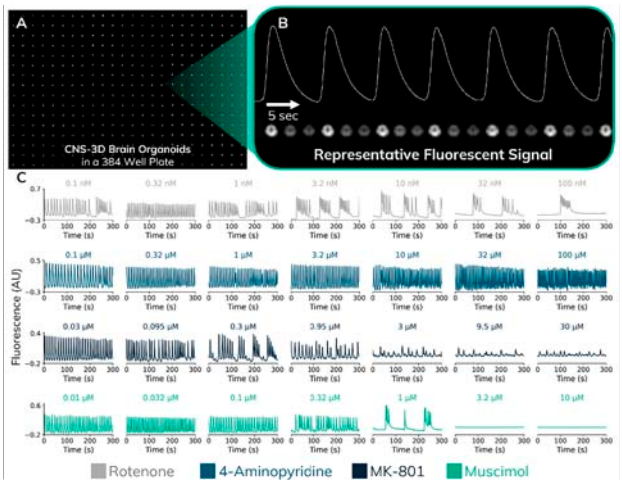


Figure 1. High-throughput calcium imaging of CNS-3D Brain Organoids. (A–B) Representative fluorescence images and corresponding calcium transient waveform. (C) Calcium activity profiles measured 30 minutes after compound dosing.

Conclusion/Significance: A single optical platform supports multi-modality functional profiling across 2D and 3D hiPSC models from 96- to 384-well formats. This unified workflow streamlines safety pharmacology by enabling dose-response characterization, mechanism-consistent functional signatures, and longitudinal repeat-dose studies, reducing instrumentation fragmentation and offering a scalable foundation for safety and efficacy assessment.

B16 - Custom Three-Dimensional Printed Grafts Restore Mandibulofacial Critical-Size Bone Defects in a Miniature Swine Model

Mandi Lopez, Mariano Carossino, Aiyanna Mcgowan

Louisiana State University School of Veterinary Medicine, Baton Rouge, United States of America

Purpose/Objectives: Bony mandibulofacial reconstruction is challenged by insufficient autologous graft material, harvest morbidity, and complex anatomy. The study goal was to evaluate healing of zygomatic and mandibular critical bony defects following implantation of custom three-dimensional (3D) printed β-tricalcium phosphate (βTCP) grafts in a porcine model.

Methodology: Following IACUC approval, grafts were generated from preoperative computed tomography (CT) scan models. They were stabilized within full thickness zygomatic (right) and mandibular angle (left) osteotomies of 8 adult male Yucatan swine with prebent titanium ladder and mandibular reconstruction plates, respectively. Males were used for comparison to previous work. Preoperatively and immediately, 3, and 6 months postoperatively, CT imaging was performed. Implant new bone deposition was objectively evaluated with light microscopy (H&E, Masson's trichrome) and micro-computed tomography (μCT). Mechanical properties of explants and non-implanted grafts were quantified from single cycle to failure compressive load testing.

Results: Implants were stable and integrated into parent bone as evident on longitudinal CT models. Histologic analysis confirmed implant integration and vascularization with minimal pathology. Native bone and implant bone volume, trabecular volume and their ratio were similar after 6 months. The material properties of explant graft were higher than non-implanted grafts. Custom 3-D printed β-TCP mandibular angle and zygoma grafts integrate into and assume native bone microstructure and material properties increase 6 months after implantation. Results are limited to the study animal model, test product, and outcome measures.

Conclusion/Significance: Three-dimensional printing of custom implants that integrate into native bone will expand current treatment options for critical-size mandibulofacial bone defects.

B19 - Hybrid tissue-engineered construct for bone regeneration based on the omental flap and osteogenic cell spheroids

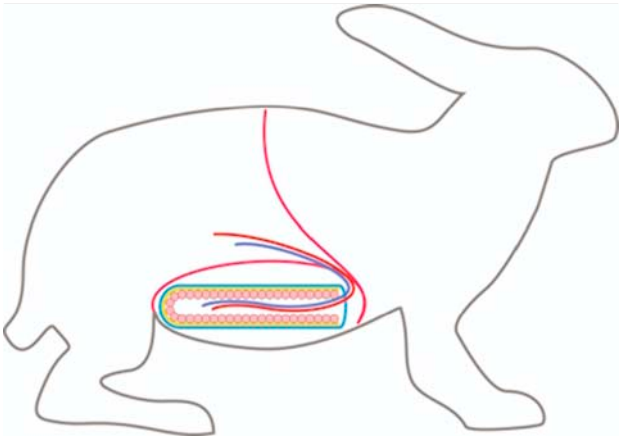
Alexey Kovalev

N.N. Priorov National Medical Research Center of Traumatology and Orthopedics of the Russian Ministry of Health, Moscow, Russia, Moscow, Russian Federation

Purpose/Objectives: To design, assemble, and evaluate in a rabbit model a hybrid bone tissue-engineered construct consisting of an omental flap combined with osteogenic cell spheroids.

Methodology: Osteogenic cell spheroids were generated from autologous periosteal cell cultures using 3D Petri Dish® agarose microwell technology. Partially demineralized bone matrix (PDBM) powder was added to create biocomposite spheroids. An omental flap, harvested via laparotomy using the right gastroepiploic vessels, was brought out through the abdominal wall into the subcutaneous space and wrapped around an electrospun tube. Cell spheroids were placed between folds of the omentum using applicator tubes, and PDBM powder was applied to the surface. The rolled construct, the "omental bioreactor," was placed into a subcutaneous celluloid membrane container. The construct was analyzed using histochemical methods and micro-CT.

Results: The omentum integrated with the cell spheroids and responded to the osteoinductive stimulus of PDBM. The construct expanded to fill the container. The spheroids remained viable and showed strong regenerative activity. Within the omental bioreactor, osteoid formation, mineralized matrix, actively remodeling bone and cartilage tissue, blood vessels, trabecular bone structures, marrow-like spaces, and early bone marrow formation were observed. Micro-CT imaging revealed radiopaque mineralized areas forming nodules, islands, and bridging networks. Figure: The hybrid tissue-engineered construct in the subcutaneous space of a rabbit.



Conclusion/Significance: Poor vascularization hinders the clinical use of tissue-engineered bone constructs. A key challenge in modern orthopedics is the treatment of segmental bone defects caused by high-energy trauma. Standard approaches, including bone grafting, the induced membrane technique, and distraction osteogenesis, have limited effectiveness. Bone tissue engineering using the omental flap is a complex but promising strategy for managing such defects. The omental flap scaffold supported spheroids and PDBM. The bioreactor created a highly osteogenic environment for bone formation and remodeling. Rapid ossification in omental tissue following abdominal injury may contribute to the regenerative response. A key factor in the construct's performance was the protective celluloid membrane, which maintained structural integrity. The construct has its own vascular supply and shows potential for transplantation and bone reconstruction.

B21 - Development of Decellularized ECM-based 3D Bioprinted Muscle Constructs with Dual Growth Factors Delivery for Repairing Volumetric Muscle Loss (VML) Injury

Young Min Ju, Olivia Clemensen, Furman Wall, Erika Billman, Siyuan Li, Ji Hyun Kim, James Yoo

Wake Forest School of Medicine, Wake Forest Institute For Regenerative Medicine, Winston-Salem, United States of America

Purpose/Objectives: The reconstruction of extensive muscle loss caused by traumatic injury or tumor ablation presents significant clinical challenges due to the limited treatment options available, including allogenic tissue rejection and donor/host muscle transplantation. To overcome these critical obstacles, we propose developing and evaluating a cell-free functionalized bioink composed of decellularized muscle extracellular matrix (dmECM) with uniformly sized ($\sim$50 μm) decellularized muscle fiber fragments (dMFFs). The primary objective of this study is to facilitate *in situ* muscle tissue regeneration by utilizing a dECM bioink containing dMFFs, myogenic factor (IGF-I), and angiogenic factor (VEGF) to promote the functional recovery of extensive muscle loss.

Methodology: To prepare dmECM, we treated pig thigh muscle tissue with solutions at various concentrations, including Triton-X, sodium dodecyl sulfate (SDS), and DNase. Methacrylated-dmECM (dmECM-MA) was obtained by protein digestion, dissolving in acetic acid, adjusting the pH to 8-9, adding methacrylic anhydride, precipitating, and dialyzing. For dMFFs, pig thigh muscle tissue was obtained and cryosectioned at 50 μm. We performed printability tests with different concentrations of dECM-MA bioink mixed with dMFFs and conducted *in vitro* cell characterizations. The

morphology of the printed dMFFs-dmECM constructs was assessed to ensure the preservation of dMFF size and uniform distribution within the printed patterns.

Results: We successfully obtained dmECM biomaterials with complete removal of cellular components and intact tissue-specific ECMs. We prepared the photo-crosslinkable dmECM bioink and confirmed the formation of a white-colored hydrogel from the UV-treated dmECM-MA. Subsequently, we established a successful bioprinting protocol for fabricating transplantable muscle constructs using dMFF-laden dmECM-based bioink and a gelatin-based sacrificial bioink.

Conclusion/Significance: Acellular 3D bioprinted functionalized muscle dMFFs-dmECM with a dual growth factor delivery system facilitated muscle cell migration, proliferation, and angiogenic properties. This approach can accelerate and enhance muscle tissue regeneration, thereby facilitating functional recovery from significant muscle loss.

B23 - Optimization of myokine secretion from tissue-engineered skeletal muscle by electrical stimulation

Toshia Fujisato

Osaka Institute of Technology, Biomedical Engineering, Osaka, Japan

Purpose/Objectives: Skeletal muscles are mainly responsible for maintaining and changing body posture and locomotion. Besides that, skeletal muscle produces a variety of cytokines and peptides called myokines, including interleukin-6 (IL-6), brain-derived neurotrophic factor (BDNF), leukemia inhibitory factor (LIF), irisin, and acidic, cysteine-rich secreted protein (SPARC). All of these are associated with metabolic changes, tissue regeneration and repair, and the maintenance of healthy bodily functions. In our previous study, tissue-engineered skeletal muscle (TEM) was cultured under various electrical and mechanical stimuli to examine its contractility and IL-6 production. In this study, the optimal electrical stimulation conditions for enhancing myokine secretion was studied.

Methodology: Two artificial tendons were introduced at each end of the TEM; the two tendons were fixed with stainless steel pins 12 mm apart before cell seeding. C2C12 myoblasts embedded in cold collagen solution were seeded between and on the surface of the two tendons After gelation at 37°C, constructs were cultured in growth medium of high glucose DMEM with 10% FBS for 2 days, followed by differentiation medium of high glucose DMEM with 7% horse serum for 2 weeks. TEM was stimulated with electric pulse stimulation (ES) of various voltage and frequency for 1 hr/day for 1 week. After ES culture, contractility was measured with a strain transducer and the amount of myokine produced in the medium and in the constructs was measured with an EIA Assay Kit.

Results: The isometric twitch force of the TEM cultured with ES was remarkably higher than that of without stimulation. In addition, significant increases of myokine of IL-6 secretion were observed under both 10V, 20Hz and 20V, 20 Hz compared with the non-stimulated control group, with no significant difference between these conditions.

Conclusion/Significance: These results suggest that both voltage and frequency influence myokine secretion from TEM, and appropriate electrical stimulation conditions may effectively enhance myokine secretion. These findings may contribute to the development of in vitro exercise models using TEM.

B24 - Driving Functional Maturity in MSC-Seeded Collagen Ligaments Through Physioxic Preconditioning

Tarek Klaylat[1], Zhiqiu Ye[2], Showan Nazhat[2], Derek Rosenzweig[1], Rahul Gawri[3,4]

[1]*McGill University, Surgery, Montreal, Canada*
[2]*McGill University, Mining & Materials Engineering, Montreal, Canada*
[3]*University of Toronto, Surgery, Toronto, Canada*
[4]*University Health Network, Schroeder Arthritis Institute, Toronto, Canada*

Purpose/Objectives: Ligament injuries are among the most prevalent musculoskeletal injuries, with limited intrinsic healing capacity due to biomechanical constraints, hypovascularization, and hypocellularity. Ligament reconstruction surgery is associated with failure, complications, and a frequent need for revision. Implantable cell-seeded bioengineered ligament grafts offer a promising alternative. However, the optimal combination of cell source, scaffold architecture, and culture microenvironment remains challenging. Human bone marrow-derived mesenchymal stromal cells ***(hBM-MSCs)*** exhibit promising ligamentogenic potential. Aligned dense collagen gels ***(ADCGs)*** that mimic native tissue architecture and composition can be tuned to optimize mechanical properties. Another critical factor is the mismatch between standard *in vitro* culture conditions and the physiological ligament microenvironment, which is characterized by relative hypoxia (tissue physioxia) and limited nutrient supply. This study aimed to develop bioengineered ligament grafts by maturing hBM-MSC-seeded ADCGs under near-physiological oxygen tensions and glucose concentrations, thereby recapitulating the intra-articular environment, and to evaluate the impact of these conditions on graft development and functionality.

Methodology: hBM-MSCs were differentiated for 10 days in ligamentogenic media at three oxygen tensions: atmospheric ***(20% O_2)***, intravenous ***(5% O_2)***, and intraarticular ***(2% O_2)***. After priming, cells were embedded in collagen gels and compacted via gel aspiration-ejection with our uniquely configured liquid handler. Constructs were matured for 21 days under the same oxygen conditions. Cell viability and metabolic activity were assessed using Live/Dead and Alamar Blue assays. Scaffold architecture was examined by scanning electron microscopy. Immunofluorescence staining was performed to evaluate ligamentogenic marker expression, and mechanical properties were assessed by uniaxial tensile testing.

Results: Live/Dead assays showed high cell viability across all culture conditions, with increased cell spreading and alignment over time. SEM confirmed highly aligned collagen fibres in all groups, with matrix remodelling under physioxia. Immunofluorescence analysis showed higher expression of ligamentogenic markers under physioxia (5% and 2% O_2). Tensile testing indicated significantly enhanced mechanical properties under physioxia compared with as-made counterparts and with those matured under 20% O_2.

Conclusion/Significance: These findings underscore the critical role of oxygen tension in regulating functional mechanical maturation in ligament tissue engineering and suggest that physiologically relevant culture conditions may enhance the development of bioengineered ligament grafts.

B26 - Stimulating endogenous neurogenesis improves tissue regeneration after ECM hydrogel implantation in stroke

Alena Kisel[1], Nadine Didwischus[1], George Hussey[2], Kylie Wishneski[1], Joe Inzano[1], Mackenzie Mills[1], Mike Modo[1]

[1]*University of Pittsburgh, Pittsburgh, United States of America*
[2]*University of Pittsburgh School of Medicine, Mcgowan Institute For Regenerative Medicine, Pittsburgh, United States of America*

Purpose/Objectives: An ischemic stroke results in the loss of neural tissue and the formation of a cavity. Implantation of extracellular matrix (ECM) hydrogels into this cavity can promote brain tissue regeneration. Neurogenesis plays a critical role by supplying neural progenitor cells (NPCs) that repopulate the scaffold. However, the extent of NPC infiltration remains insufficient to restore neuronal density to levels comparable to native tissue. We hypothesized that enhancing neurogenesis with the growth factor betacellulin (BTC) would increase neuronal density in newly formed tissue.

Methodology: In a rat model of middle cerebral artery occlusion, ECM hydrogel was implanted 14 days post-stroke. An osmotic pump delivered BTC continuously into the lateral ventricle for 14 days following ECM implantation, after which brains were perfusion-fixed for histological analysis.

Results: BTC treatment markedly amplified $SOX2^+$ neural progenitors in the subventricular zone (SVZ). Specifically, BTC significantly increased the numbers of Type A (proliferating NPCs), Type B1 (quiescent neural stem cells), Type B2 (proliferating neural stem cells), and Type C (transit-amplifying cells). The relative proportion

of Type C cells was increased, whereas Type B2 cells decreased, revealing a shift in the dynamics of the neurogenic process. Within the scaffold, $SOX2^+$ progenitors increased by 36%. Because NPCs were continuously generated and recruited during the treatment period and hence not all these cells are counted as mature neurons. Nevertheless, by 14 days post-implantation, neuronal (NeuN+ cells) density within the scaffold increased fourfold.

Conclusion/Significance: These findings demonstrate that stimulation of endogenous neurogenesis significantly enhances NPC recruitment into ECM bioscaffolds, ultimately increasing neuronal density in *de novo* tissue and improving the process of brain tissue regeneration.

B28 - Reweaving the trabecular meshwork: electrospun scaffolds for glaucoma treatment

Abigail Christie, Carl Sheridan, Neeru Vallabh, Lucy Bosworth

University of Liverpool, Eye And Vision Science, Liverpool, United Kingdom

Purpose/Objectives: Glaucoma can result from dysfunction of the trabecular meshwork, leading to impaired fluid drainage, increased intraocular pressure, and vision loss. Minimally invasive glaucoma surgery (MIGS) can help lower intraocular pressure by improving aqueous humour drainage, but current devices bypass the diseased TM, rather than restoring its original function. This project aims to develop a cell-loaded, electrospun scaffold that can be delivered into the iridocorneal angle and then assessed ex vivo by Human Organ-Cultured Anterior Segment (HOCAS) as a novel glaucoma treatment.

Methodology: Scaffolds were fabricated by electrospinning poly(ε-caprolactone) at a concentration of 12% w/v in 1,1,1,3,3,3-hexafluoroisopropanol. Scaffolds were oxygen plasma treated to improve surface hydrophilicity and scaffold morphology, structure, wettability, and mechanical properties were assessed using scanning electron microscopy, X-ray computed tomography, contact angle analysis, tensile testing, and atomic force microscopy. Preliminary biological performance was evaluated by culturing transformed NTM5 cells and primary human TM cells on the scaffold for up to 14 days. Cell attachment, viability, infiltration, extracellular matrix deposition, and phagocytic function were assessed. Ongoing work involves adapting this scaffold for minimally invasive delivery, optimizing scaffolding placement, assessing cell viability on delivered scaffolds, and functional integration ex vivo via the Human Organ-Cultured Anterior Segment (HOCAS).

Results: Electrospun fiber scaffolds successfully mimicked human TM structure. Oxygen plasma treatment improved surface hydrophilicity without disrupting fiber morphology or bulk scaffold mechanics. Both NTM5 and primary human TM cells attached to the scaffold and remained viable for up to 14 days. Cultured cells deposited TM-relevant extracellular matrix proteins, including fibronectin and collagen IV, and retained phagocytic activity, supporting the scaffold as a biologically permissive substrate for TM cell function.

Conclusion/Significance: These proof-of-concept data support electrospun PCL scaffolds as a candidate platform for biological MIGS development. This approach could provide the first regenerative, tissue-engineered strategy for early glaucoma intervention and offers a translational framework for testing cell-loaded scaffold delivery in clinically relevant eye models.

B29 - Development of engineered retinal organoids to model inherited retinal diseases and test concomitant AAV based gene therapies

Shradha Darira, Erin Burnight, Dalyz Ochoa, Allison Wright, Robert Mullins, Budd Tucker, Edwin Stone

University of Iowa, Iowa City, United States of America

Purpose/Objectives: Approximately 1 in 3450 people worldwide are affected by inherited retinal diseases. Different genetic mutations manifest as different molecular and pathophysiological phenotypes. In vitro models serve as valuable tools to understand these diverse molecular mechanisms and evaluate the efficacy of restorative gene therapies. This study presents the use of human induced pluripotent stem cell (iPSC) derived retinal organoids to model patients with MAK and CLN3 mutations and the correction of these mutations using AAV based gene therapies. Mutations in the MAK gene are associated with a form of retinitis pigmentosa (RP) and mutations in the CLN3 gene are associated with Bechet's disease.

Methodology: Patient specific iPSCs were derived from the dermal fibroblasts of different patients with molecularly confirmed mutations in the MAK and CLN3 genes respectively. These iPSCs were differentiated into retinal organoids using our previously published protocols. Immunofluorescence staining was used to characterize the morphological changes at different time points (40, 80, 120 and 160 days) in the differentiation process. The retinal organoids were then transduced with cGMP grade icap9 AAV9 MAK and icap9 AAV6 CLN3 vectors containing full length MAK and CLN3 cDNA transcripts. The efficacy of these vectors in reversing the observed phenotype was evaluated.

Results: Mutations in the MAK gene were found to be associated with an elongated length of primary cilia and mutations in the CLN3 gene were found to be associated with increased autofluorescence attributed to enlarged lysosomes. Transduction by the viral vectors rescued these phenotypes as determined by immunostaining using Acetylated Tubulin and Lysosomal-Associated Membrane Protein-1 (LAMP1) antibodies respectively.

Conclusion/Significance: We were successfully able to generate retinal organoids from patient derived iPSCs with MAK and CLN3 mutations and subsequently use AAV based gene therapy strategies to correct these mutations. This approach may reliably be extrapolated to other inherited retinal diseases.

B30 - Development of an in vitro neurovascular model using bioengineering to evaluate pathophysiological aspects of diabetic retinopathy

Rafaela Campos De Menezes[1], Luiza De Paula[1], Marlos E Silva[2], Marize Valadares[1], Artur Silva[3]

[1]*Federal University of Goiás, Pharmaceutical Sciences, Goiânia, Brazil*
[2]*Federal University of Goiás, Goiânia, Brazil*
[3]*Federal University of Goiás, Pharmaceutical Bioengineering, Goiânia, Brazil*

Purpose/Objectives: To use human corneal stromal stem cells (hCSSCs) as a cellular source for generating retinal neuronal progenitors and to establish an in vitro model of diabetic retinopathy (DR) reproducing the neuronal and endothelial compartments under mimetic conditions of hyperglycemia.

Methodology: hCSSCs were cultured in low-adhesion plates for three days to form spheroids, which were subsequently transferred to Matrigel-coated plates and maintained for an additional 11 days in differentiation medium. Neuronal biomarkers were assessed by immunofluorescence on days 0, 3, and 14. Endothelial cells of the human umbilical vein (HUVECs) were cultured in monolayers in diabetic medium (33 mM glucose, IL-6, and TNF-α), and evaluated for MTT and LDH assay, tube formation, transwell migration, and ICAM-1 expression. The model was established through co-culture in a transwell system. For that, the viability window of the neuronal progenitors in the insert was initially defined, evaluated by the Live/Dead assay for up to 35 days, and a medium formulation compatible with both cell types was also developed. For model construction, hCSSCs were differentiated in the apical compartment and, after 14 days, HUVECs were seeded in the basolateral compartment. The model was maintained for eight days in harmonized medium and evaluated by cell Live/Dead assay.

Results: hCSSCs showed morphological changes and increased expression of β3-tubulin, BRN3A, and NeuN, reduced in Pax6 after differentiation. HUVECs showed no cytotoxicity in diabetic medium but exhibited endothelial dysfunction with reduced tube formation, increased migration, and ICAM-1 overexpression. Neuronal progenitors in the transwell insert remained viable between 21 and 28 days of culture, providing at least a seven-day window for DR induction.

HUVECs remained viable after the removal of retinoic acid from the neuronal medium formulation. After all harmonizations, the model remained viable with both compartments intact.

Conclusion/Significance: hCSSCs have demonstrated potential for differentiation into retinal neuronal phenotypes, while HUVECs in diabetic medium reproduced key features of endothelial dysfunction in the early stages of DR. The results support the integration of neuronal progenitors derived from hCSSCs with HUVECs to construct a neurovascular model for investigating DR pathophysiology and screening new therapeutic approaches.

B35 - Development of Silk Fibroin-Based Bioabsorbable Vascular Grafts with a Gradient Structure

Yasumoto Nakazawa[1], Shuhei Tara[2], Yohei Kamei[1], Tamaki Nishigaya[1], Takashi Tanaka[3], Kazumi Shimada[3], Satoshi Somamoto[4], Shingo Kawabata[4], Shota Akioka[1]

[1]*Tokyo University of Agriculture and Technology, Biotechnology And Life Science, Tokyo, Japan*
[2]*Nippon Medical School, Cardiovascular Medicine, Tokyo, Japan*
[3]*Tokyo University of Agriculture and Technology, Veterinary Medicine, Tokyo, Japan*
[4]*Sanyo Chemical Industries Ltd, Kyoto, Japan*

Purpose/Objectives: Small-diameter vascular grafts remain difficult to clinically apply because of thrombosis, restenosis, and poor long-term patency. Bioabsorbable vascular grafts (BVGs) are expected to overcome these limitations by promoting vascular tissue regeneration; however, rapid degradation can reduce graft strength, whereas delayed degradation may induce stenosis. In this study, a novel BVG material with a gradient structure was developed using slowly degradable silk fibroin (SF) and rapidly degradable Silk-Elastin® (SELP). By gradually changing the SF/SELP composition ratio from the lumen side to the outer layer, the graft was designed to balance mechanical durability and controlled biodegradation while promoting physiological vascular tissue regeneration. The effects of the gradient structure on degradability, compliance, and vascular tissue regeneration were evaluated.

Methodology: SF and SELP solutions were electrospun to fabricate Gradient, non-gradient, Blend, and SF tubes. The Gradient tube was produced by gradually changing the SF/SELP ratio from the lumen to the outer layer. Degradability was evaluated using elastase solution. Compliance values were measured under 80–120 mmHg according to ISO 7198-2016. Gradient sheets were implanted into rat abdominal aortas for 4 weeks followed by EVG staining.

Results: The inner lumen side of the Gradient structure showed the highest degradability (86.5 ± 0.9%), whereas the outer layer exhibited slower degradation (61.1 ± 2.3%), confirming successful control of biodegradation behavior across the graft wall. Histological analysis after 4 weeks of rat abdominal aorta implantation demonstrated vascular tissue regeneration without stenosis or occlusion, including regeneration of elastic-like tissue layers. Compliance testing showed that all grafts tolerated pressurization without rupture, and compliance values increased in the order of SF < Blend < non-gradient < Gradient tube. The Gradient tube exhibited compliance comparable to or greater than that of autologous vessels (∼4.5%), indicating improved expandability and mechanical compatibility with native vessels.

Conclusion/Significance: The SF/SELP Gradient tube demonstrated controlled degradability, improved compliance, and enhanced vascular tissue regeneration. The gradient structure effectively improved expandability and may reduce postoperative complications such as thrombosis and aneurysm formation, suggesting strong potential for small-diameter vascular graft applications.

Acknowledgements: This work was supported by JSPS KAKENHI Grant Numbers JP24K03277 and JP23KK0202.

B36 - Hyaluronic Acid–Coated Poly(ε-Caprolactone) Composite Scaffolds for Controlled Protein Delivery in Skeletal Muscle Regeneration

Diana Flores Barnett[1], Alycia Galindo[1], Ievgenii Liashenko[1], Paul Dalton[1], Marian Hettiaratchi[1,2], Kelly O'Neill[1]

[1]*University of Oregon, Department of Bioengineering, Phil And Knight Campus For Accelerating Scientific Impact, Eugene, United States of America*
[2]*University of Oregon, Chemistry And Biochemistry, Eugene, United States of America*

Purpose/Objectives: Skeletal muscle is a highly organized tissue that loses its ability to fully regenerate following traumatic injuries such as volumetric muscle loss (VML). Current treatments include autologous muscle grafts but are highly invasive and often fail to restore function. Therefore, tissue engineered scaffolds can be used to provide structural support by providing biochemical and biophysical cues to restore anisotropic muscular architecture and function. Our overall goal was to develop a hyaluronic acid (HA) hydrogel coated poly(E-caprolactone) (PCL) composite scaffold to guide anisotropic cellular alignment and serve as a platform for controlled protein delivery. We hypothesized that by combining alignment properties of a fiber-based scaffold with biomimetic properties of HA hydrogels, we could enhance myoblast attachment and alignment.

Methodology: We previously optimized our hydrazone-crosslinked HA hydrogel using design of experiments (DOE) to obtain an optimal gelation time, compressive modulus, and degradation rate. In this study, we further modified HA with norbornene to enable functionalization with the fibronectin-derived arginine-glycine-aspartic acid (RGD) peptide to promote cellular attachment. We then fabricated melt electrowritten PCL fiber scaffolds to guide myoblast alignment. The fibers were spaced 150 μm apart in the x-direction and 500 μm apart in the y-direction with varying diameters (10, 20, and 30 μm) and total scaffold height of 200 μm. Scaffolds were embedded between equal volumes of HA polymer solutions. Once crosslinking was complete, C2C12 murine myoblasts were seeded onto non-coated, HA-coated, and HA-RGD-coated scaffolds. Cells were further differentiated and stained to evaluate myoblast attachment and myotube formation via confocal imaging.

Results: While fluorescence and myotube directionality analysis showed all scaffolds supported myoblast alignment, HA-RGD coated scaffolds containing 20 μm fibers showed significantly higher cellular attachment and myotube formation (Figure 1A-B). However, alpha-actinin staining suggests that myotubes were not fully mature due to lack of sarcomeric striations indicated by the white arrow (Figure 1C).

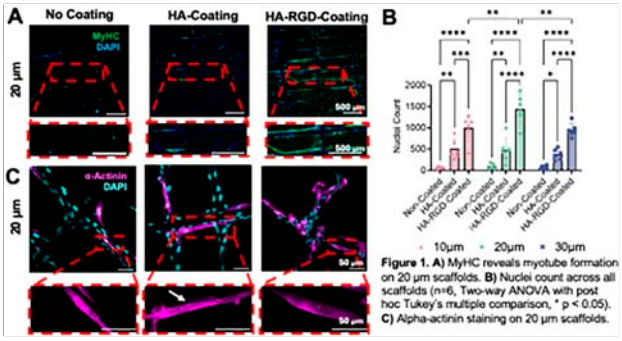


Figure 1. A) MyHC reveals myotube formation on 20 μm scaffolds. **B)** Nuclei count across all scaffolds (n=6, Two-way ANOVA with post hoc Tukey's multiple comparison, * $p < 0.05$). **C)** Alpha-actinin staining on 20 μm scaffolds.

Conclusion/Significance: Our work successfully combines structural and biomimetic components into a scaffold that promotes myoblast attachment, alignment, and differentiation. In ongoing work, we are incorporating affinity-based protein binders (affibodies) for sustained protein delivery to aid in mature myotube formation, advancing this platform toward functional skeletal muscle regeneration.

B37 - Gelatin methacryloyl hydrogel for on-demand therapeutic release in protease-rich microenvironments

Yuhang Huang[1], Chau-Minh Phan[2], Lyndon Jones[2], Evelyn Yim[1]

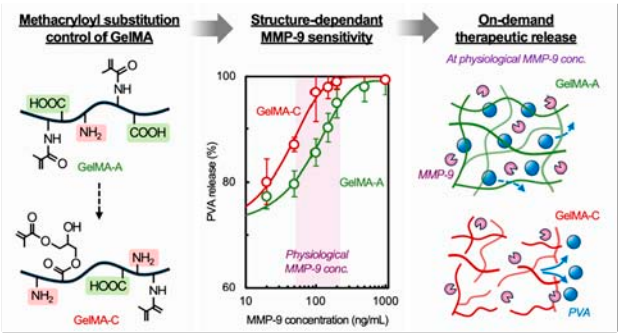
[1]*University of Waterloo, Department of Chemical Engineering, Waterloo, Canada*
[2]*University of Waterloo, School of Optometry, Waterloo, Canada*

Purpose/Objectives: Enzymatically degradable motifs within hydrogels allow disease-elevated enzymes to degrade the network

and enable "on-demand" therapeutic release. Gelatin methacryloyl (GelMA) hydrogels contain matrix metalloproteinase (MMP)-cleavable sequences; however, triggering release requires enzyme concentrations above clinically observed levels. Formulation strategies that enhance enzyme sensitivity are often accompanied by changes in bulk mechanical properties. This study investigated whether group-selective methacrylation of GelMA could improve triggered release within physiological MMP ranges while maintaining comparable mechanical properties.

Methodology: GelMA were synthesized by varying degree of substitution (number of methacryoyls normalized to amino groups) and the group targeted for methacryloyl substitution. Hydrogels were formed from 20 wt% GelMA and 0.5 wt% LAP under 405 nm irradiation (600 mW·cm^{-2}, 60 s). Release of poly(vinyl alcohol) (MW 85 kDa) was quantified in PBS at 37°C over 24 h under 0–2000 ng mL^{-1} MMP-9. Baseline release was defined as cumulative release without the presence of MMP-9, and the trigger concentration, c^*, was defined as the MMP-9 concentration at which release transitioned from a diffusion-dominated baseline to a degradation-accelerated increase. Data are reported as mean ± SD (n = 3 gels per condition).

Results: For GelMA-A with methacryloyls substituting amino groups and with substitution degree of 74 ± 2%, baseline release was 71 ± 3% and c^* = 146 ± 13 ngṡmL^{-1}. At a similar degree of substitution, GelMA-C with 76% of the methacryloyls from substituting amino to carboxyl groups maintained baseline (75 ± 4%) while reducing c^* to 72 ± 6 ngṡmL^{-1}. Increasing number of preserved amino groups did not significantly alter shear storage modulus ≈ 55–57 kPa, but increased partition coefficient of negatively charged bovine serum albumin from 0.69 ± 0.07 to 0.82 ± 0.08.



Conclusion/Significance: Group-selective functionalization enables independent control of enzyme-triggered release and bulk mechanical properties in GelMA hydrogels. While stiffness remained governed by the degree of substitution, critical enzyme concentration to trigger degradational release correlated with the number of preserved amino groups. Increased protein partitioning in GelMA-C supports electrostatically mediated enzyme accumulation as a mechanism for enhanced sensitivity, providing a strategy to responsive therapeutic delivery in protease-elevated microenvironments.

B47 - In Vitro Evaluation of Collagen Deposition by Human Dermal Fibroblasts Following Exposure to Hydrolyzed Type I Collagen Powder

Sergio Medina[1], Tiffany Sanchez[1], Fahimeh Tabatabaei[2], Nina Bionda[1]

[1]*Rochal Technologies, R&D division of Sanara MedTech, San Antonio, United States of America*
[2]*Sanara MedTech, Rochal Technologies, R&d Division of Sanara Medtech, San Antonio, United States of America*

Purpose/Objectives: Successful surgical healing depends on restoration of tissue integrity, largely driven by fibroblast-mediated extracellular matrix production and collagen deposition. Hydrolyzed collagen peptides may act as bioactive signals influencing extracellular matrix turnover and fibroblast activity. This study aimed to quantify time dependent changes in collagen deposition by human dermal fibroblasts following exposure to a hydrolyzed type I collagen using a colorimetric collagen detection assay.

Methodology: Primary human dermal fibroblasts were seeded into 48-well plates and allowed to adhere overnight prior to treatment. Cells were assigned to one of two conditions: exposure to hydrolyzed type I collagen powder (CellerateRX® Surgical Powder, Sanara MedTech; 30 mg/mL) in serum free media for 2 minutes followed by media replacement, or untreated controls maintained in serum free media. Experiments were performed in six replicate wells per condition and assessed at 2, 5, and 7 days post-treatment across three independent plates using a Sirius Red–based total collagen detection assay. Data was normalized to untreated control values for each time point.

Results: Quantitative analysis revealed time-dependent differences in collagen deposition between treatment and control groups. No statistically significant differences were observed at day 2. By day 5, fibroblasts exposed to hydrolyzed collagen demonstrated a statistically significant increase in collagen deposition compared to untreated controls. At day 7, collagen deposition levels showed a slight, non-significant decrease relative to day 5 but remained significantly elevated compared with control cultures.

Conclusion/Significance: Brief *in vitro* exposure of human dermal fibroblasts to hydrolyzed type I collagen resulted in a time dependent increase in collagen deposition, with measurable effects emerging by day 5 and stabilizing by day 7, consistent with physiologic wound healing kinetics and fibroblast activation dynamics. These findings support the potential role of collagen derived peptides in modulating fibroblast mediated extracellular matrix synthesis under controlled laboratory conditions. While limited to an *in vitro* model, the results provide mechanistic insight into collagen-driven tissue repair processes and support further evaluation in *in vivo* wound management systems.

B48 - LAL-Based In Vitro Endotoxin Testing for Medical Devices: A Comprehensive Overview

Preethi Sivaswaamy Mohana, Fahimeh Tabatabaei, Nina Bionda

Rochal Technologies, R&d Division of Sanara Medtech, San Antonio, United States of America

Purpose/Objectives: Endotoxins are complex lipopolysaccharides (LPS) present in the outer membrane of gram-negative bacteria and are known to induce severe inflammatory responses, making their detection critical for ensuring the safety of medical devices. This study provides a comprehensive overview of current endotoxin testing methodologies, with a focus on *in vitro* Limulus Amebocyte Lysate (LAL) based approaches.

Methodology: A literature-based overview of compendial and review sources was synthesized, focusing on the three stablished LAL formats including gel clot (qualitative), turbidimetric (kinetic turbidity), and chromogenic (quantitative EU/mL) assays and on their application to medical devices. This review also considered current practice patterns, including cartridge-based chromogenic testing designed for automated, high-throughput testing.

Results: The literature consistently shows that LAL testing is sensitive, reliable, and standardized for endotoxin detection, with chromogenic and kinetic chromogenic formats offering the strongest quantitative performance and automation potential for routine device testing. Cartridge-based chromogenic LAL systems generate results using standard curves derived from known endotoxin concentrations and demonstrate suitability for both in-process and final product testing. System validity is confirmed through positive product control (PPC) recovery and standard curve linearity. However, all LAL methods remain limited to endotoxin detection and do not identify non-endotoxin pyrogens, which can require complementary assessments such as Monocyte activation test (MAT) or rabbit pyrogen testing (RPT) in select cases.

Conclusion/Significance: Overall, LAL-based *in vitro* endotoxin testing remains the regulatory and scientific standard for demonstrating endotoxin control in medical devices. LAL assays provide rapid, sensitive, quantitative detection, but require robust validation to address interference and endotoxin masking and ensure reliable results.

B51 - Dose-Dependent Effects of Collagenous Peptides on Healing Critical Bone Defects

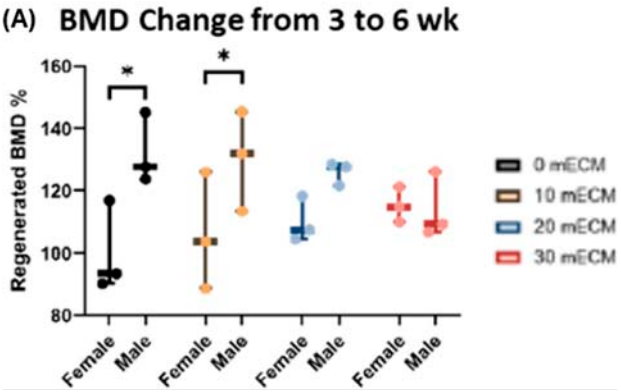
Victoria Garza[1], Opemipo Sanyaolu[2], Gabriela Cervantes Gonzales[2], Rena Bizios[2], Teja Guda[2], Alisa Isaac[2,3]

[1]*UT San Antonio, Biomedical Engineering, San Antonio, United States of America*
[2]*UT San Antonio, San Antonio, United States of America*
[3]*St. Mary's University, San Antonio, United States of America*

Purpose/Objectives: Recent studies suggest potential in leveraging molecules released from damaged cells following tissue injury, called damage-associated molecular patterns (DAMPs), due to their ability to activate the innate-immune system, initiate wound healing, and influence cellular behavior. This work seeks to replicate the effect of DAMPs by fabricating extracellular matrix motifs (mECMs) from rat tail collagen I, and exploring their effect on stromal cell behavior, bone regeneration, and bone mineral density.

Methodology: For in-vitro studies, mECMs were presented to 2D and 3D cultured rat fibroblasts at 0, 10, 20, or 30% v/v. Fibroblasts were then fixed and stained to analyze proliferation and cellular morphology. In-vivo, hydrogels (at the 4 doses of mECMs) were implanted in 2 mm-sized female and male mouse calvarial defects, then allowed to heal for 3 or 6 weeks. Isolated samples were then evaluated through microCT analysis of bone regeneration.

Results: Fibroblasts exposed to mECMs in 2D-culture depicted morphological changes after 24-hours, including a decrease in nuclei area and increased cellular elongation in higher percentage mECM groups compared to control groups, indicating a potential transition into a myofibroblast phenotype. Moreover, a similar trend was observed in the decrease in fibroblast proliferation in both 2D and 3D cultures as mECM percentage increased. In-vivo, bone growth was observed across all groups from week 3 to week 6. By week 6, dose-dependent effects on bone growth and opposite trends on BMD between males and females as mECM percentage increased.



(A) BMD changes showed that high mECM doses improved continued densification in females from 3 to 6 weeks.

Conclusion/Significance: In-vitro findings depict that mECMs influence the behavior of stromal cells in a dose-dependent manner. mECMs were also observed to have a positive effect on bone regeneration, especially in terms of bone density, which continually improved in female mice. Lastly, at early timepoints females and males had very similar bone regeneration (both volume and BMD), but over time at 6 weeks the females with 30% mECMs had similar bone quality and quantity as males (with no mECM exposure). This suggests that mECMs can play an important role in leveraging sex-based differences in regeneration in bone engraftment.

B54 - Mechanosensitive PIEZO1/PEZO-1 Signaling Regulates Lysosomal Remodeling and Autophagic Adaptation During Stress

Manizheh Sarikhani, Kathryn R. Deleo, Adam Bohnert

Louisiana State University, Biological Science, Baton Rouge, United States of America

Purpose/Objectives: Ever since life began, organisms have encountered mechanical forces and adapted by evolving ways to sense and respond to mechanical stress. The mechanosensitive channel PIEZO1 mediates calcium transport across membranes in response to mechanical cues. While this is well-known to influence downstream cell behavior, how this signaling interacts with quality-control machinery within cells to recalibrate cell health and homeostasis, particularly in response to stressors, is poorly understood. Here, we report that the mechanosensitive channel PIEZO1/PEZO-1 supports high autophagic activity in the nematode *Caenorhabditis elegans* by promoting the remodeling of lysosomes into interconnected tubular networks, which we previously showed enhance cargo degradation.

Methodology: As part of a genetic screen, we identified a loss-of-function mutation in *C. elegans pezo-1* that impaired age-associated clearance of protein aggregates and organelles.

Results: Notably, *pezo-1* mutants showed defective tubular lysosome (TL) induction under multiple physiological conditions that stimulate lysosomal remodeling, including osmotic stress, aging, and starvation. Loss of *pezo-1* additionally decreased lifespan and healthspan. Our data suggest that PEZO-1 functions upstream of lysosomal adaptation pathways, as disruption of *pezo-1* prevented the induction of key lysosomal membrane proteins associated with TL formation and reduced activation of the autophagy-promoting transcription factor HLH-30/TFEB.

Conclusion/Significance: Together, these findings reveal a previously unrecognized role for mechanosensitive PIEZO1 in regulating lysosomal plasticity and autophagic capacity, pathways essential for stress adaptation and renewal in cell health and homeostasis.

B56 - Disease-Mimicking 3D Hydrogels to Study Sex Differences in Valvular Fibrosis

Nafeesah Ibrahim[1], Lysmarie Rios[2], Kristyn Masters[3]

[1]*University of Colorado Boulder, Boulder, United States of America*
[2]*University of Wisconsin-Madison, Madison, United States of America*
[3]*University of Colorado Anschutz, Aurora, United States of America*

Purpose/Objectives: Calcific aortic valve disease (CAVD) is characterized by progressive extracellular matrix (ECM) remodeling and aberrant activation of valvular interstitial cells (VICs). While changes in matrix composition and stiffness are hallmarks of disease progression, their role in regulating sex-specific mechanobiological responses remains poorly understood. This study investigates how ECM composition and mechanics influence VIC inflammatory signaling and extracellular matrix remodelling.

Methodology: Biomimetic hydrogel platforms composed of gelatin methacrylate (GelMA) and collagen type I were engineered to recapitulate early and late-stage valvular ECM environments with defined differences in total collagen content. Male and female porcine VICs were encapsulated within these 3D matrices and stimulated with transforming growth factor-beta (TGF-β1), a pro-fibrotic signaling factor. Responses were compared across matrix conditions and biological sex, where inflammatory signaling was quantified via cytokine secretion while differences in ECM production was investigated using immunostaining methods.

Results: The results show that sex and extracellular matrix disease stage shape how valvular interstitial cells respond to profibrotic stimulation. In the inflammatory data, male VICs were more responsive to increased collagen content than female VICs. TGF-β1 significantly suppressed IL-8 secretion in males, especially in the higher-collagen disease model, while females showed little change across matrix conditions or treatment. Fibrotic gene expression also showed sex-specific patterns. Male VICs had higher baseline activation of ACTA2 and FN1, suggesting a more activated state without stimulation. In contrast, female VICs showed greater TGF-β1-induced upregulation of fibrotic genes. COL1A1 increased from early- to late-stage matrix conditions in both sexes. Matrix production imaging further showed stage- and sex-dependent remodeling. Overall, the data suggest that ECM composition and TGF-β1 interact differently in male and female VICs, producing distinct inflammatory, fibrotic, and matrix synthesis programs.

Conclusion/Significance: These findings demonstrate that ECM composition and mechanics actively govern VIC mechanobiological responses in a sex-specific manner. The selective suppression of inflammation by TGF-β1 in male VICs, particularly in matrices with

higher collagen content, highlights a coupling between biochemical signaling and the extracellular matrix. This work underscores the importance of integrating matrix properties and biological sex in engineered models of cardiovascular disease and provides insight into early mechanobiological drivers of CAVD progression for therapeutic applications.

B59 - Optimal PEGylation of Cell Penetrating Peptide Nanoparticles Increases Transfection Efficiency and Stability in Serum Conditions

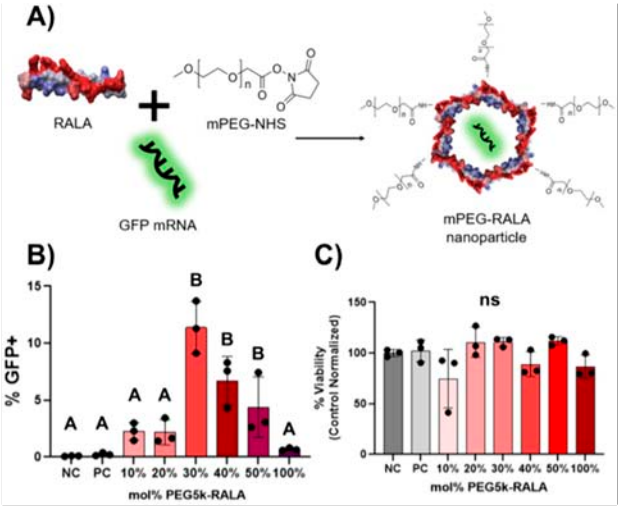
Benjamin Childs, Josh Graham, Jose-Gabriel Castro, Tomas Gonzalez Fernandez

Lehigh University, Bioengineering, Bethlehem, United States of America

Purpose/Objectives: The use of Clustered Regularly Interspaced Short Palindromic Repeats (CRISPR) allows for highly precise and tunable gene editing. Achieving effective CRISPR delivery in physiological conditions remains a challenge for clinical translation. Previously, we optimized the arginine-alanine-leucine-alanine (RALA) cell penetrating peptide (CPP) for CRISPR delivery with commercially competitive efficiency and low cytotoxicity. However, CPPs are vulnerable to degradative enzymes, preventing transfection *in vitro* under physiological serum conditions. Methoxy Polyethylene glycol (mPEG) modifications (PEGylation) have been found to increase serum stability and improve biodistribution. The objective of this study is to optimize PEGylation of RALA nanoparticles to improve stability and CRISPR efficiency in serum conditions.

Methodology: PEGylation of RALA was achieved using NHS-amine chemistry. The N-hydroxysuccinimide (NHS) ester reacted with the primary amine at the N-terminus of RALA, forming a stable amide linkage with mPEG-RALA as the final product. Serum transfections with mPEG-RALA nanoparticles were conducted using GFP mRNA and delivered to primary rat mesenchymal stem cells cultured in 10% FBS. Transfection efficiency was assessed using flow cytometry and viability using alamarBlue.

Results: To identify the optimal mPEG-RALA conjugate, transfections were performed with mPEG at differing molecular weights. $mPEG_{5k}$-RALA achieved the highest serum shielding capabilities, so further optimization of molar ratio of $mPEG_{5k}$-RALA:RALA was conducted. 30% $mPEG_{5k}$-RALA achieved 11.38% ± 2.30 transfection efficiency in serum **(Fig. 1A)**, in comparison to 0.25% ± 0.13 by unmodified RALA. Furthermore, metabolic activity measured by alamarBlue confirmed that the delivery of PEGylated RALA nanoparticles did not significantly compromise cell viability **(Fig. 1B)**. **Figure 1**. A) Formulation of mPEG-RALA nanoparticles. B) Transfection efficiency by mol% mPEG5k-RALA in serum. B) Viability of transfected cells by alamarBlue. A & B are significantly different ($p < 0.05$) by one-way ANOVA and Tukey. ns = not significant.



Conclusion/Significance: Current approaches in nanoparticle-based CRISPR delivery fail to acknowledge the importance of serum stability. Previously, PEGylation had not been applied to CPP-based CRISPR vectors such as RALA. This study revealed mPEG-RALA increases serum delivery efficiency by 46-fold. The optimal conjugate for serum delivery was found to be 30% mPEG5k-RALA. Overall, PEGylation improves nanoparticle serum stability and transfection efficiency, essential for the clinical translation of CRISPR gene therapy.

POSTER SESSION 3

11-17-2026 @ 5:45 PM - 7:15 PM

C02 - Fabrication of a 3D Bioprinted Peripheral Nerve Model via Sequential Hydrogel Printing and a Spheroid Patterning

Minkyoung Lee[1], Hyungseok Lee[1,2]

[1]*Kangwon National University, Department of Smart Health Science And Technology, Kangwon National University, Republic If Korea, Chuncheon-si, Korea, Republic of*
[2]*Kangwon National University, Department of Mechanical Convergence Engineering, Kangwon National University, Republic of Korea, Chuncheon-si, Korea, Republic of*

Purpose/Objectives: Peripheral nerves are distributed throughout the body and play essential roles in motor, sensory, and autonomic functions. When peripheral nerves are damaged by disease or trauma, signal transmission between nerve cells can be disrupted, leading to the loss or impairment of major functions. Autologous nerve grafting is regarded as the clinical gold standard for peripheral nerve repair. However, its application is limited by donor site morbidity and limited graft availability. Therefore, in vitro peripheral nerve models are needed for nerve regeneration studies and the development of therapeutic strategies. In this study, we fabricated a 3D bioprinted peripheral nerve model by creating a hydrogel-based 3D environment using single-nozzle bioprinting and patterning neural cell-laden spheroids within the construct.

Methodology: The peripheral nerve model was fabricated through a sequential single-nozzle printing process. A stiff bioink was first printed to form a guidance frame designed to define the construct geometry and provide contact guidance for neurite outgrowth. The inner region of the guidance frame was then filled with a Schwann cell-laden soft hydrogel to create a neurite growth region. Subsequently, neuron-laden spheroids were printed at predefined positions within the hydrogel-filled region.

Results: Rheological analysis confirmed that the bioinks exhibited printability and structural stability for extrusion-based bioprinting. Based on these properties, a 3D peripheral nerve model composed of a printed guidance frame, a hydrogel-filled growth region, and patterned spheroids was successfully fabricated through a sequential printing process. Microscopic and cell tracker-based imaging confirmed that neuron-laden spheroids with controlled diameters were spatially patterned within the construct, creating a controllable structure for subsequent evaluation of neurite outgrowth directionality. Live/dead and proliferation assays further showed that the hydrogel environment supported the viability and growth of both neurons and Schwann cells. In addition, comparison of neuronal morphology and neurite extension in hydrogels with neural growth-promoting cues, such as NGF and laminin, demonstrated that the bioactive hydrogel region provided a favorable microenvironment for neuronal growth.

Conclusion/Significance: These results suggest that the proposed printing strategy may be useful for developing 3D in vitro peripheral nerve models with controllable cellular arrangement.

C03 - Patient-Derived Organoids as a Platform for Preclinical Validation of Multitargeted Kinase Inhibitors (MKIs): LCI 139 MKI Overcomes the Lung Cancer Chemoresistance

Nadeem Wajih[1], Sara Muhiczukic[1], Krishnaiah Maddeboina[2], Rajeev Dhupar[3], Donald Durden[2], Konstantinos Votanopoulos[3], Eleftherios Makris[3], Shay Soker[1]

[1]*Wake Forest University School of Medicine, Wake Forest Institute For Regenerative Medicine, Winston-Salem, United States of America*
[2]*Atrium Health Levine Cancer Center, Charlotte, United States of America*
[3]*Wake Forest University School of Medicine, winston salem, United States of America*

Purpose/Objectives: The purpose of the present study is to evaluate computationally designed multitargeted kinase inhibitor LCI 139 (PI3K–CDK4/6–CDK9–AURKA/B) for its ability to induce synthetic lethality in patient-derived lung cancer organoids.

Methodology: Lung cancer specimens were collected under IRB approval. Lung cancer organoids (LCO) were generated using unsorted tumor cell suspensions in a PEPGEL and characterized by immunofluorescence for established lung cancer markers (TTF-1, Ki67, P63, Claudin-4, PDL-1, and desmoglein) and H&E. LCOs were treated with LCI 139 (0.25–1.0 μM), single-target drugs (1 μM), and chemotherapeutics (gemcitabine, pemetrexed, and cisplatin; 5 μM) for 72 hours. Cytotoxicity was assessed via metabolic activity assays; apoptosis via Annexin V binding and caspase 3/7/8 activity; and mechanistic pathways were confirmed by immunoblotting for phospho-CDK9, AURKA/B, pAkt, MCL-1, and pRNA polymerase II.

Results: LCI 139 demonstrated dose-dependent inhibition of lung cancer organoid (n=6) viability, with a 29% reduction at 0.25 μM ($p<0.05$), 50% at 0.5 μM, and 58% at 1 μM ($p<0.0001$). To evaluate the therapeutic advantage of LCI139 targeting key oncogenic pathways, we assessed and compared its efficacy with single-target therapies at equimolar concentrations (1 μM). Post 72 hrs. of treatment, LCI139 reduced viability by 77% ($p < 0.0001$) compared to single agents: 19% (AURKAi) $p<0.05$, 20% (AURKBi) $p<0.005$, 38% (PI3Ki) $p<0.0001$, 12% (CDK4/6i) $p < 0.43$, and 42% (CDK9i) $< p<0.0001$. Furthermore, patient-matched normal lung organoids showed minimal sensitivity to LCI 139 treatment, suggesting that LCI 139 is more effective against lung cancer with minimal cytotoxicity. Mechanistically, LCI 139 (1 μM) increased both caspase-3/7 18-fold ($p < 0.0001$) and caspase 8 activity 2-fold ($p < 0.02$), indicating both canonical and non-canonical caspase-dependent apoptosis. Annexin V binding confirmed apoptosis in LCI139-treated cancer organoids. Immunoblotting showed reduced expression of pAkt, retinoblastoma, RNA polymerase II, MCL-1, cMyc, and p53, suggesting cell cycle arrest and apoptosis.

Conclusion/Significance: LCI139 shows stronger anti-tumor effects than a single-target drugs in patient-derived lung cancer organoids. Our data support the use of cancer organoid models for drug development and highlight the potential of multitargeted kinase inhibitors to overcome chemotherapeutic resistance. Our findings also support further evaluation of LCI 139 as a potential therapeutic candidate for lung cancer.

C05 - "The Role of Melt Electrowriting Microtextile Pore Size in Cell Seeding and Confluence"

David Dean[1,2,3], Tanya Djemal[3], Javier Vazquez-Armendariz[4]

[1]*The Ohio State University, Plastic And Reconstructive Surgery, Columbus, United States of America*
[2]*The Ohio State University, Material Science And Engineering, Columbus, United States of America*
[3]*University of Wisconsin-Madison, Biomedical Engineering, Madison, United States of America*
[4]*The Ohio State University, Integrated Systems Engineering, Columbus, United States of America*

Purpose/Objectives: Melt electrowriting (MEW) is a novel technology that can be used to print 200 nanometer-150 μm polymer fibers. A MEW printer pushes a melted polymer through an electrically charged needle towards a collector with the opposite charge. The electrical field causes polymer fibers to form. Most regenerative medicine research using MEW has used biocompatible and resorbable polycaprolactone (PCL) fibers in the 5-25 μm range. This study reports the printing of highly accurate single layer microtextiles with 50 – 250 μm pores. This creates an unprecedented opportunity to produce confluent sheets of cells that are accessible from either side of the microtextile. Once confluent, these microtextiles of the same type of cells can be stacked as can layers of two cell types to bring about tissue function. Vascular layers may be interleaved. FDM printing of PCL with 150 μm or thicker fibers can add strength, facilitating handling and cell culture, and facilitate suturing microtextiles together or to adjacent host tissue on implantation. We have also demonstrated the creation of MEW microtextiles with defect-fitting curving surfaces.

Methodology: We hypothesize that smaller pore size would reduce time to confluence. To test that we fabricated 6 × 6 mm microtextiles with 5.6 μm (±1.5) PCL fibers in square pores of 50, 100, 150, or 250 μm surrounding an "X". 1×10^5 L929 (mouse fibroblast) cells were seeded on each scaffold. Cell metabolic activity and immunocytochemistry assays were taken on days 1, 3, 5, and 7. Standard Live/Dead cytotoxicity assays were taken on days 1 and 3 for all pore geometries. FDM boundary fibers of 450.3 μm (±20.5) were added to facilitate handling.

Results: Figure 1 shows that smaller pore geometries promote cell seeding efficiency and more rapid progression towards confluence. Analysis is ongoing. However, scaffolds with 50 μm pores exhibited significant ($p < 0.001$) improvement over 100 μm pores.

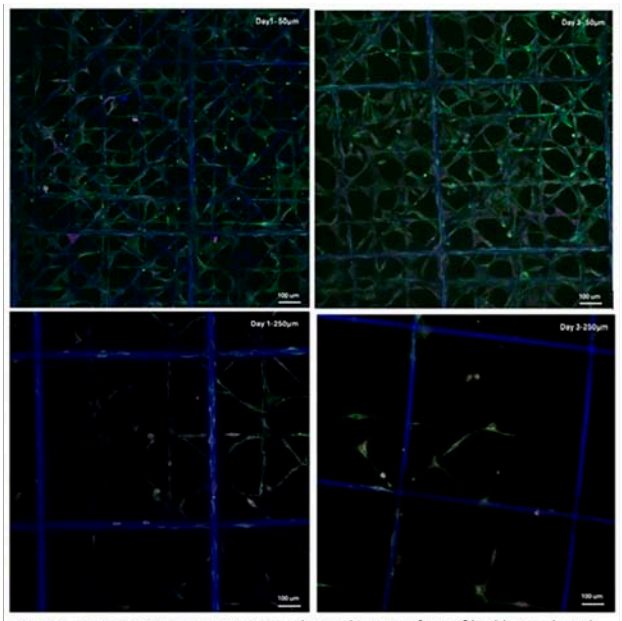


Figure 1. Representative 20× immunocytochemical images of L929 fibroblasts cultured on MEW microtextile scaffolds with 50, 100, 150, and 250 μm pore sizes at Days 1 and 3. (Key: DAPI (blue), F-actin (green), and vinculin (magenta). Scale bar = 100 μm.).

Conclusion/Significance: Achieving accurate, regular, sub-250 μm pores required development of novel MEW biofabrication methods that we will present. Those novel MEW pore geometries appear to enhance cell attachment and accelerate progression to confluence leading to the formation of stackable living cell membranes (i.e., sheets of cells).

C11 - Integrating multimaterial chaotic bioprinting with 3D-printed millifluidic organ-on-chip systems to engineer and sustain perfused, microarchitected tumor niches

Mario Álvarez[1,2], Grissel Trujillo-Desantiago[1], Mariana García-Ortega[2]

[1]*Tecnológico de Monterrey, Departamento De Mecatrónica, MONTERREY, Mexico*
[2]*Tecnológico de Monterrey, Expedition-femsa, MONTERREY, Mexico*

Purpose/Objectives: Recreating the complexity of tumor microenvironments *in vitro* remains a central biofabrication challenge. Achieving precise spatial organization of multiple cell types while enabling dynamic culture conditions is critical to capture key features of tumor progression, stromal interaction, and therapeutic response. Here, we present an integrated platform that combines

multimaterial chaotic bioprinting with culture in 3D-printed millifluidic chips to engineer and sustain perfused, microarchitected tumor-on-chip niches.

Methodology: Chaotic bioprinting was enabled by the coextrusion of multiple (bio)inks through a Kenics static mixer printhead, generating hydrogel filaments with finely controlled multilayered architectures (Fig.1A). By incorporating sacrificial inks, we created longitudinal microchannels that function as prevascularization, enhancing mass transport and enabling the culture of densely populated constructs. This approach allowed the spatial organization of breast tumor spheroids (derived from MDA-MB-231 cells), stromal (fibroblasts), and immune (macrophages) cells within well-defined microenvironments (Fig.1B). These engineered tumor constructs were integrated into resin-based 3D-printed millifluidic chips designed to support continuous perfusion under controlled hydrodynamic conditions (Fig.1C).

Results: Flow characterization demonstrated that filament-packed chambers promoted plug-flow–like behavior, reducing velocity gradients and enabling stable nutrient delivery across the tissue. This dynamic environment supported long-term culture and facilitated the establishment of physiologically relevant gradients. Using this platform, we recapitulated breast cancer niches of increasing complexity, including mono-, co-, and triculture systems. Constructs maintained high viability (>90%) during 4-week perfusion, while tumor spheroids exhibited sustained metabolic activity and interplay with surrounding stromal and immune components. Dynamic culture induced functional changes, including modulation of proliferation (Ki-67 expression), mesenchymal transition (vimentin expression), and angiogenic signaling (VEGF expression), demonstrating the effect of perfusion and cellular composition on tumor behavior. Real-time metabolic monitoring further reveals stable glucose consumption profiles, indicating the establishment of steady-state conditions under continuous flow (Fig1.D). In addition, material cytotoxicity effects on cellular proliferation (associated with using different 3D-printing resins) highlight the importance of device cytocompatibility in long-term cancer modeling.

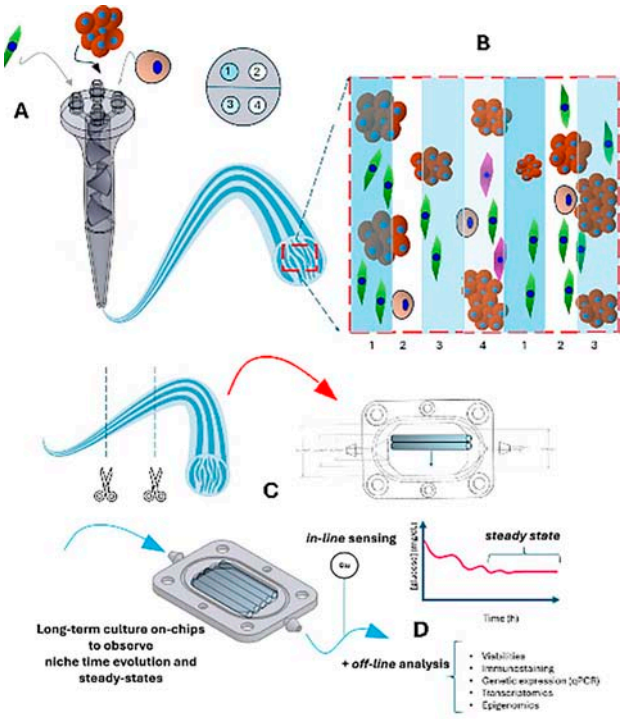


Figure 1. Engineering of perfused, microarchitected tumor niches via chaotic bioprinting and culture within millifluidic organ-on-chip integration. (A) Multimaterial chaotic bioprinting using a Kenics static mixer printhead enables the coextrusion of multiple bioinks containing tumor spheroids, stromal cells, and immune cells, generating hydrogel filaments with controlled multilayered architectures and embedded sacrificial domains. (B) Resulting filaments exhibit finely organized lamellar microstructures with spatially defined cellular compartments and longitudinal microchannels formed after removal of the sacrificial phase, mimicking prevascular features and enabling enhanced mass transport. (C) Bioprinted filaments are sectioned and integrated into 3D-printed millifluidic chips, where dense packing of the constructs supports controlled perfusion and long-term culture under plug-flow–like conditions. (D) The integrated platform enables continuous in-line monitoring of metabolic activity (e.g., glucose consumption) and the establishment of steady-state conditions, while allowing downstream off-line analyses, including viability assays, immunostaining, gene expression (qPCR), and transcriptomic or epigenomic profiling.

Conclusion/Significance: This work establishes an accessible strategy to engineer perfused tumor microenvironments with controlled architecture and dynamics. The platform provides a robust foundation for studying tumor–stroma–immune interactions and offers new opportunities for drug testing and mechanistic investigations in physiologically relevant cancer models.

C12 - Development of a Modular Bioreactor for High-Throughput Simulation of Endothelial Injury During Organ Transplantation

Christophe Kwizera[1,2], Ernesto Curty Da Costa[2], Fernanda Mesquita[2], Camila Hochman-Mendez[2]

[1]*Rice University, Mechanical Engineering, Houston, United States of America*
[2]*Texas Heart Institute at Baylor College of Medicine, Department of Surgery, Houston, United States of America*

Purpose/Objectives: Ischemia–reperfusion injury remains a major contributor to endothelial dysfunction, vascular permeability, inflammation, and primary graft dysfunction (PGD) following transplantation. Most in vitro models fail to reproduce physiologically relevant hemodynamic forces, while ex vivo organ perfusion (EVOP) is costly, technically complex, and limited in throughput. To address this gap, we developed a tunable in vitro bioreactor that enables controlled modeling of endothelial responses under different transplant regimens.

Methodology: The bioreactor integrates commercial microfluidic slides with a custom microcontroller-driven pulsatile pump that generates user-defined shear stress profiles. Inline flow and pressure sensors provide feedback for closed-loop regulation of flow rate, pulsatility, and waveform patterns. Low-volume tubing minimizes media consumption, while the ability to perfuse up to four slides in series increases experimental throughput and cell yield. The portable design, combined with a forced-air motor-cooling system, supports operation under normothermic conditions and a range of hypothermic settings to model different transplant protocols. A wireless interface enables remote programming and real-time monitoring. To simulate traditional static cold storage (SCS), human lung microvascular endothelial cells (HLMVECs) are cultured for 16 hours at 4°C without flow. In parallel, cells are exposed to flow at 4°C, 22°C, and 37°C to model EVOP-like conditions. Endothelial injury is assessed through membrane disruption and morphological changes, including cell elongation, alignment, disarray, and loss of cell-cell contact.

Results: Our system successfully generates programmable steady and pulsatile flow regimes in a compact, sterile-compatible configuration suitable for endothelial cell culture studies. Its modular design allows simultaneous perfusion of multiple microfluidic slides for higher-throughput studies of endothelial responses to physical stressors. Under EVOP conditions, cells align and elongate in the direction of flow. Under SCS, HLMVECs show dynamic changes in morphology, with membrane disarray and weakened cell-cell interaction.

Conclusion/Significance: This bioreactor provides a tunable and accessible platform to study endothelial responses to combined temperature-driven and hemodynamic stresses during transplantation. By bridging static culture systems and complex ex vivo perfusion models, it offers a practical tool to investigate mechanisms and evaluate transplant modalities to reduce PGD.

C14 - RCAN1.4 Modulated Differentiated Thyroid Cancer Cell Invasion and Natural Killer Cell Intervention in a Thyroid to Lung Metastasis-on-a-chip Model System

Jason Scharenberg[1], Tilak Khanal[2], Marco Rodriguez[1], Matthew Ringel[2], Aleksander Skardal[1,2]

[1]*The Ohio State University, Biomedical Engineering, Columbus, United States of America*
[2]*The Ohio State University, Comprehensive Cancer Center, Columbus, United States of America*

Purpose/Objectives: Differentiated thyroid cancer is a treatable form of thyroid cancer that accounts for about 90% of thyroid cancer diagnoses. These treatments include lumpectomies, radiation treatment among others. RCAN1.4 suppresses metastasis in cells where expression is normal. When expression is lost, risk of metastasis increases. Under the right conditions, natural killer (NK) cells can target cancer cells and clear them from tissue. Here we utilize a thyroid cancer metastasis-on-a-chip (MOC) model to assess the role of RCAN1.4 in thyroid cancer metastasis into a 3D lung construct, followed by treatment with NK-92 cells.

Methodology: The target lung constructs are comprised of normal human lung fibroblasts and normal human bronchial epithelial cells suspended in a collagen and hyaluronic acid-based hydrogel. Two fluorescently tagged thyroid cancer cell lines, each with RCAN1.4 knockdown and scramble clones, (hth74 and FTC236) were perfused through the device for 5 days to allow invasion into the lung construct to take hold. The lipophilic dyed NK-92 cell line was then perfused through the device for 7 days. Evaluation of cancer invasion and NK-92 cancer cell killing was completed using confocal imaging on days 1, 5, 6, 9, and 12. ELISAs will be used to evaluate cancer cell biomarkers and NK-92 cell effector function through secreted cytokines.

Results: Studies completed in the MOC platform showed that all five cell types engrafted on the interface of the hydrogel lung construct. The htht74 KD was the only cell line that invaded into the construct, albeit non-uniformly. Treatment with the NK92 cells showed targeting and clearing of all the cell types and invasion into the constructs for the trials with the hth74 KD cells. ELISA analysis of the media showed positive results for NK-92 cell effector function.

Conclusion/Significance: These findings align partially with previous research on the RCAN1.4 modulation. Previous research utilized a more basic system using cell lines rather than the primary cells that this system used. Differing results show that there is more to explore with this system/gene modulation. The addition of the NK-92 cells in this system showed positive cancer cell targeting and killing.

C17 - An Improved Manufacturing Method for Infusible Extracellular Matrix Materials to Enable Clinical Translation and Further Material Development

Michael Nguyen[1,2], Emma Zelus[3,4], Benjamin Lieberman[1,5], Quincy Lyons[1,2], Maria Karkanitsa[1,2], Colin Luo[1,2], Carlos Munoz[2], Pedro Cabrales[2], Karen Christman[1,2]

[1]*Sanford Consortium for Regenerative Medicine, La Jolla, United States of America*
[2]*UC San Diego, Shu Chien-gene Lay Department of Bioengineering, LA JOLLA, United States of America*
[3]*University of California, San Diego, Shu Chien-gene Lay Department of Bioengineering, La Jolla, United States of America*
[4]*Sanford Stem Cell Institute, La Jolla, United States of America*
[5]*University of California, San Diego, Division of Pulmonary And Critical Care And Sleep Medicine, La Jolla, United States of America*

Purpose/Objectives: Infusible extracellular matrix (iECM) demonstrates promise for treating inflamed tissues in conditions including myocardial infarction (MI) and multiple organ dysfunction syndrome (MODS). Following intravascular delivery, iECM reduces vascular permeability and presents immunomodulatory and pro-reparative signals, improving cardiac function and survival in animal models of MI and MODS, respectively. However, aspects inherent to iECM manufacturing steps, centrifugation, dialysis/lyophilization, and filtration (C-D-F), limit clinical translation due to limited output and potential for human handling associated contamination. To address this, we developed a method for manufacturing iECM utilizing depth filtration and tangential flow filtration (DF-TFF), increasing output and aligning the process with good manufacturing practices.

Methodology: To produce iECM through C-D-F and DF-TFF, 1g of digested cardiac ECM was fractionated through centrifugation and membrane filtration or depth filtration and concentrated through dialysis/lyophilization or TFF. iECM material properties were characterized according to protein/peptide characteristics, biochemical properties, and hemocompatibility. To assess DF-TFF scalability, 4g of digested ECM were processed using the DF-TFF method. Retention and bioactivity of iECM of both methods was evaluated in a mouse model of MODS and a rat model of MI. Finally, iECM was made from decellularized lung, skeletal muscle, aorta, and kidney to assess DF-TFF's use outside of cardiac ECM.

Results: In all material property metrics, DF-TFF iECM was comparable to C-D-F iECM, producing an equivalent product with decreased manufacturing time (70 versus 264 hours). Both C-D-F and DF-TFF iECM were able to reduce vascular permeability and inflammation in MODS. DF-TFF enabled increased concentration, which was necessary for maximum retention in male rats post MI. DF-TFF enabled increased scale, with the 4X production scale resulting in equivalent material. Finally, DF-TFF iECM from alternative tissues retained tissue specific properties, demonstrating DF-TFF's potential outside of cardiac iECM.

Conclusion/Significance: DF-TFF enables increased iECM production while requiring less time and human handling than iECM made with the C-D-F method. Both methods yielded material with equivalent material properties, hemocompatibility, and immunomodulatory and pro-reparative effects in MODS. This optimized protocol can efficiently produce large amounts of iECM, enabling further testing in new models of disease, preclinical large animal models, and human clinical trials.

C20 - Strontium-Functionalized Mesoporous Bioactive Glass Cryogels Promote Bone Regeneration in Osteoporotic Craniofacial Defects: A Translational Approach

Yu-Chen Kuo[1], Chia-Hsuan Tsai[2], Chien-Tzung Chen[2], Hsiu-Mei Lin[3], Chih-Hao Chen[1]

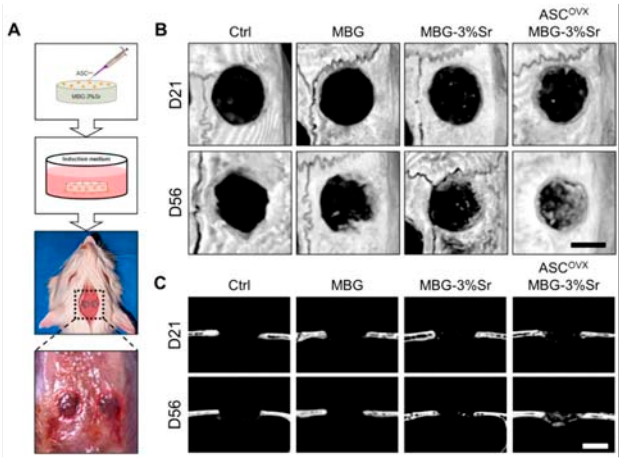
[1]*Chang Gung Memorial Hospital, Keelung, Department of Plastic And Reconstructive Surgery, Keelung, Taiwan*
[2]*Chang Gung Memorial Hospital, Linkou, Department of Plastic And Reconstructive Surgery, Taoyuan, Taiwan*
[3]*National Taiwan Ocean University, Department of Bioscience And Biotechnology, Keelung, Taiwan*

Purpose/Objectives: Functional reconstruction of craniofacial bone defects in osteoporotic individuals remains a formidable clinical challenge due to systemic hormonal disruption and the inherent "cellular fatigue" of resident mesenchymal stem cells. Although Strontium (Sr) is a potent dual-action therapeutic agent, its clinical utility is hindered by the cardiovascular risks associated with systemic administration. This study proposes a synergistic "nano-bio" coupling strategy: a macroporous gelatin-based cryogel scaffold incorporating strontium-doped nanostructured mesoporous bioactive glass (nMBG@Sr) and adipose-derived stem cells from ovariectomized rats (ASC^{OVX}) to rescue impaired bone healing in the osteoporotic microenvironment.

Methodology: nMBG@Sr nanoparticles were synthesized via a template-assisted sol-gel method and characterized using HR-TEM, XRD, and BET analysis. The G/nMBG@Sr cryogels were engineered through a sub-zero cryogelation technique, ensuring an interconnected macroporous architecture. We evaluated the localized Sr^{2+} release kinetics via ICP-MS and assessed the cytocompatibility and osteoinductive potential of the constructs *in vitro*. Molecular mechanisms were elucidated through the expression of Runx2, Osteocalcin (OCN), and β-catenin. Finally, 5-mm critical-sized calvarial defects in an ovariectomized rat model were utilized to validate *in vivo* bone regeneration via longitudinal micro-CT morphometry and histological analysis.

Results: The nMBG@Sr nanoparticles enable sustained Sr^{2+} release within the cryogel matrix. This localized ionic stimulus successfully "rescued" the impaired proliferative and osteogenic capacity of ASC^{OVX}. *In vitro* assays demonstrated significant upregulation of Runx2 and OCN, orchestrated by the nuclear translocation of β-catenin, confirming the activation of canonical Wnt signaling pathway. *In vivo*, the G/nMBG@Sr+ASC^{OVX} construct achieved superior therapeutic outcomes compared to acellular G/nMBG or G controls, characterized by accelerated centripetal bone bridging,

significantly higher bone mineral density (BMD), and robust collagen matrix maturation within the craniofacial defect.



*(A) ASC^{OVX} seeded into**G/nMBG@Sr cryogel scaffolds**, followed by implantation into**5-mm parietal bone defects** in OVX rats.**(B) Longitudinal 3D micro-CT**displaying temporal progression of bone healing.**(C) Cross-sectional micro-CT morphometry** The synergistic group achieved superior cortical restoration and higher mineral density.*

Conclusion/Significance: The localized delivery of Sr via a mesoporous nanocarrier-integrated cryogel synergizes with ASC^{OVX} overcome osteoporosis-induced healing impairment. By providing an interconnected macroporous niche and targeted ionic modulation, this platform offers a translatable, precision-medicine strategy for the reconstruction of critical-sized craniofacial defects in osteoporotic population.

C26 - tUnabLe smarT biomateRiAl for CARTilage REGENERAtion (ultracart regenera)

Denise Murgia[1], Francesca Romano[1], Riccardo Gottardi[2], Roberto Di Gesù[1]

[1]*Ri.MED Foundation, Musculoskeletal Tissue Engineering (mste) Lab., Palermo, Italy*
[2]*University of Pennsylvania, Philadelphia, United States of America*

Purpose/Objectives: Rheumatoid Arthritis (RA) and Osteoarthritis (OA) are among the most prevalent musculoskeletal disorders, leading to progressive degradation of articular cartilage and joint dysfunction[1]. Matrix-Assisted Autologous Chondrocyte Implantation (MACI) represents a promising approach for cartilage repair; however, post-surgical rehabilitation often fails to reproduce the optimal mechanical environment necessary for effective regeneration[2]. To address this limitation, we developed a smart scaffold capable of delivering localized, tunable mechanical stimuli to human articular chondrocytes (hACs), integrating mechanobiological and biomaterial engineering principles.

Methodology: Magneto-responsive, piezoelectric scaffolds were fabricated from aligned electrospun poly(vinylidene fluoride–trifluoroethylene) (PVDF-TrFE) fibers alone or incorporating Fe_3O_4 magnetic nanoparticles (MNPs). The aligned structure conferred mechanical anisotropy, while MNPs enabled remote activation via external magnetic fields. After hAC seeding, daily magnetic stimulation for up to 14 days mimicked physiological loading, activating the piezoelectric response and generating localized electromechanical cues.

Results: MNPs were successfully integrated within the polymer fibers, enabling the fabrication of PVDF and PVDF–Fe_3O_4 matrices. The scaffolds showed reproducible deformation under magnetic actuation and high biocompatibility. Stimulated constructs exhibited enhanced deposition of type II collagen and a higher type II/type X collagen ratio, indicating a stable chondrogenic phenotype and reduced hypertrophy. These outcomes align with previous evidence that electromagnetic and electrical cues can modulate cartilage metabolism and promote regenerative signaling[3]. Our results suggest that combined mechanical and piezoelectric stimulation supports hyaline cartilage formation and improves chondrocyte function.

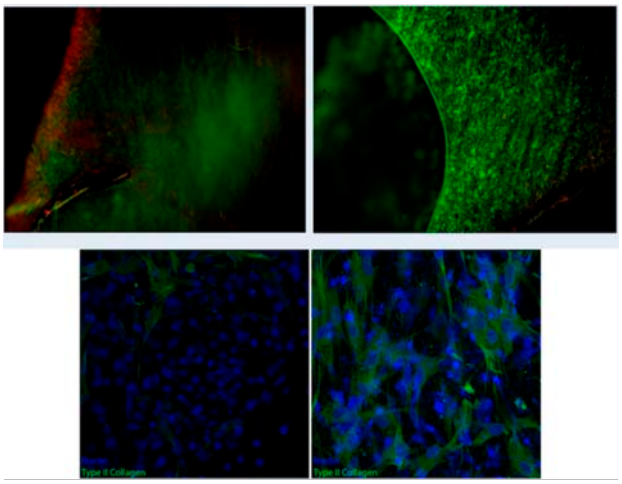


Figure: Live/dead of PVDF (upper left) and PVDF-Fe_3O_4 (upper right). Type II collagen deposition in ECM of PVDF (lower left) and PVDF-Fe_3O_4 (lower right).

Conclusion/Significance: This multifunctional scaffold provides controlled electromechanical cues to embedded chondrocytes, effectively reproducing joint-like stimuli and promoting cartilage regeneration. The approach offers a promising advancement toward personalized and functionally effective treatments for chondral defects. **References** Ostrowska et al., 2018, Reumatologia. Seok-Jung et al., 2009, J. Med. Case Rep. Ongaro et al., 2011, Bioelectromagnetics **Acknowledgment** This work was supported by the ON Foundation (CH), starting grant n° 22-006/2022.

C29 - A Synthetic Colloidal Aggregates-Embedded Hydrogel for Sustained Release of Antifibrotic Therapeutics

Xiang Olivia Li[1], Jojo Peng[2], Quinton Sirianni[3], Mark Hamer[4], Fabio Rossi[4], Molly Shoichet[1]

[1]*University of Toronto, Department of Chemical Engineering And Applied Chemistry, Toronto, Canada*
[2]*University of Toronto, Institute of Biomedical Engineering, Toronto, Canada*
[3]*University of Toronto, Department of Chemistry, Toronto, Canada*
[4]*University of British Columbia, School of Biomedical Engineering, Vancouver, Canada*

Purpose/Objectives: Colloidal drug aggregates are a promising drug delivery platform due to their ultra-high drug loading. However, stabilizers are usually required in physiological conditions, and only a limited number of colloid aggregators have been successfully formulated. This study uses computationally guided drug modification to stabilize nintedanib colloidal aggregates for sustained delivery. To target fibrotic scarring associated with spinal cord injury repair, we propose an in-situ depot for localized, controlled antifibrotic release while minimizing off-target toxicity.

Methodology: This study employs a random forest-based colloidal aggregates model[5] to design nintedanib analogs as colloidal aggregates with hydrophobic, aromatic, or electronegative nonpharmacological cores. Analogs were synthesized using a robust three-step synthesis approach, and have been confirmed to preserve the binding with their native targrts. These analogs self-aggregate into amorphous nanoparticles detected via dynamic light scattering. Stability of formed nanoparticles was assessed by screening various stabilizers, including small molecule co-aggregators, proteins, and lipids, for size distribution over 7 days *in vitro*. Antifibrotic activity was evaluated *in vitro* using a mouse embryonic fibroblast model, and stable colloidal aggregates were embedded in a hydrogel to assess their sustained release profile over 7 days.

Results: A novel and robust three step synthesis approach generated the full library of nintedanib analogs. Modifying nintedanib with hydrophobic or electronegative nonpharmacological cores significantly lowered the critical aggregation concentration in aCSF from 44.83 μM to 1.29 μM. The stability of colloidal aggregates is intrinsic to their physiochemical properties: π-π stacking, hydrogen bonding or van der Waals interactions; increased intermolecular interactions introduced by chemical modifications resulted in more stable nanoparticles formation. While unmodified nintedanib colloidal aggregates precipitated after 2 hours at 37°C, analogs remained stable for up to 7 days when co-formulated with small molecule dye. Embedding these colloidal aggregates in a hydrogel enabled sustained release of small molecules over 7 days.

Conclusion/Significance: In conclusion, chemical modification of nintedanib enabled sustained release of antifibrotic molecules for 7 days from a colloidal aggregates-embedded hydrogel. These findings highlight the potential of a colloidal aggregates-based platform for drug delivery, paving the way for improved formulations in drug optimization and controlled drug delivery.

C31 - 3D Neural Tissue Construct Multimodal Stimulation and Recording Capacities

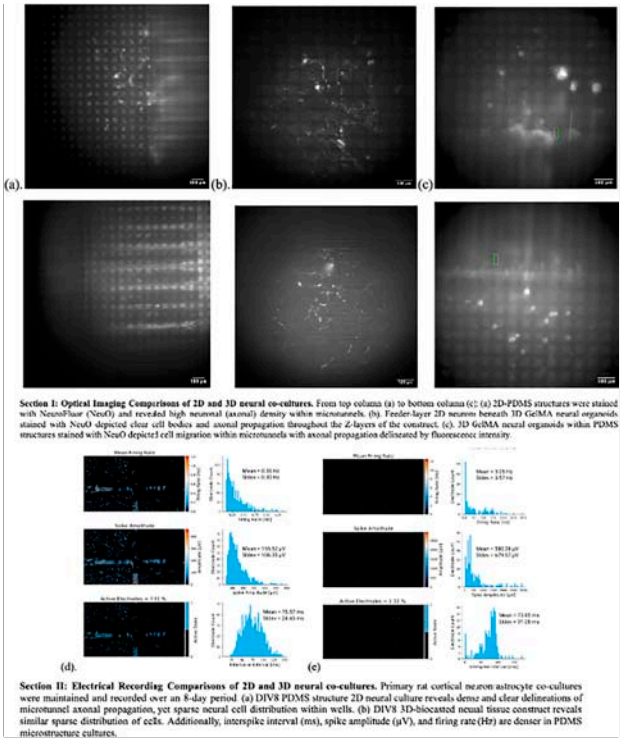
Lauren Gomes[1], Kasun Pathirage[2], Nathaniel Renegar[3], Amal Shabazz[1], John Fisher[1], Timothy Horiuchi[2], Pamela Abshire[3]

[1]*University of Maryland, Fischell Department of Bioengineering, College Park, United States of America*
[2]*University of Maryland, Electrical & Computer Engineering, College Park, United States of America*
[3]*Stonybrook University, Electrical & Computer Engineering, Stony Brook, United States of America*

Purpose/Objectives: Countless neurological disorders lack effective treatments due to mechanistic gaps in understanding neuronal network processing. The cerebral cortex mediates higher-order cognitive functions through action potential propagation between cortical neurons, inducing structural and functional changes, yet mechanisms underlying selective neuronal strengthening and rewiring remain unclear. To investigate these processes, polydimethylsiloxane (PDMS) microstructures fabricated atop high-definition microelectrode array (HD-MEA) chips confine neurons and axonal projections to active regions for studying neuron interactions. However, electrical stimulation and recording are limited by hardware electrical artifact, while optical paradigms have primarily been studied in 2D despite native neural processing relying on complex 3D cytoarchitecture. Thus, we developed a tri-combinatorial approach to fabricate 3D neural organoid constructs within PDMS microtunnel structures. Our objectives are to (1) characterize electrical and optical inputs/outputs and (2) determine how stimulation paradigms induce network-level changes, the purpose being to articulate how 3D biofabricated neural tissue constructs emulate plastic network dynamics.

Methodology: MaxWell Biosystems (MXWB) 2D-HD-MEA chips contained either photolithography-manufactured polydimethylsiloxane (PDMS) microstructures with large-well pockets, or left blank for basic constructs for comparison. Organoids were co-cultured Primary Rat Neurons & Astrocytes (E18/E19, respectively, from Gibco), with 1 astrocyte:8 neurons. Chips underwent routine electrical activity and network scans 2x/week via MXWB Scope. Tissue constructs were biocasted by synthesizing 5% (w/v) gelatin methacrylate (GelMA) via stepwise methacrylation of PBS-dissolved Type A porcine gelatin, 1-week dialyzation, and LAP photoinitiator crosslinking via UV. ~280,000 cells/100 μL droplet organoids were cast and UV-cured within PDMS-2D-HD-MEA pockets. Neurofluor imaging verified neuron-specific encapsulation and preliminary optical recording capacities. Voltron2-Cre and ChR2 combinatorial viral transfection enabled optical recording and stimulation, respectively, on our group's custom digital-micromirror-device optical rig for further analysis.

Results: Our data suggests that PDMS structures containing organoids both on top of a feeder layer in 2D and without a feeder layer in 2D can be optically recorded with clear axonal propagation depicted in microtunnels. Electrical recordings also depict clear readouts of dense network actvity concentrated within microtunnels and pockets, as a platform for targeted stimulation.



Section I: Optical Imaging Comparisons of 2D and 3D neural co-cultures. From top column (a) to bottom column (c): (a) 2D-PDMS structures were stained with NeuroFluor (NeuO) and revealed high neuronal (axonal) density within microtunnels. (b). Feeder-layer 2D neurons beneath 3D GelMA neural organoids stained with NeuO depicted clear cell bodies and axonal propagation throughout the Z-layers of the construct. (c). 3D GelMA neural organoids within PDMS structures stained with NeuO depicted cell migration within microtunnels with axonal propagation delineated by fluorescence intensity.

Section II: Electrical Recording Comparisons of 2D and 3D neural co-cultures. Primary rat cortical neuron astrocyte co-cultures were maintained and recorded over an 8-day period. (a) DIV8 PDMS structure 2D neural culture reveals dense and clear delineations of microtunnel axonal propagation, yet sparse neural cell distribution within wells. (b) DIV8 3D-biocasted neural tissue construct reveals similar sparse distribution of cells. Additionally, interspike interval (ms), spike amplitude (μV), and firing rate (Hz) are denser in PDMS microstructure cultures.

Conclusion/Significance: PDMS-3D-biocasting for neural network modeling shows significantly higher spike amplitude differences, as 3D GelMA environment successfully propagates neuronal signaling, serving as a robust model.

C34 - Physicochemical and Functional Characterization of Modified Alginate Microbeads Encapsulating Corneal Stromal Cells for Retinal Neurovascular Disorders Treatment

Luiza De Paula[1], Pietra Mota[1], Maria Clara Silva[1], Gabriel Ribeiro[1], Rafaela Campos De Menezes[1], Marize Valadares[1], Artur Silva[2]

[1]*Federal University of Goiás, Pharmaceutical Sciences, Goiânia, Brazil*
[2]*Federal University of Goiás, Pharmaceutical Bioengineering, Goiânia, Brazil*

Purpose/Objectives: Diabetic retinopathy is a leading cause of irreversible visual impairment worldwide, and human corneal stromal cell (hCSCs) based therapies have emerged as promising regenerative approaches for retinal repair. Biomaterial-assisted encapsulation systems may improve cell retention, viability, and paracrine activity after administration. This study aimed to characterize sodium alginate-based microbeads containing hCSCs and evaluate their physicochemical behavior and neuroprotective secretory profile for potential application in diabetic retinopathy treatment.

Methodology: Microbeads were produced using 2.5% sodium alginate (SA) alone or combined with 0.1% hyaluronic acid (SA+HA), 0.1% bovine gelatin (SA+BG), or 0.1% bovine corneal hydrogel (SA+CH). hCSCs were encapsulated at 5×10^7 cells/mL. Automated extrusion was performed using a 1 mL syringe fitted with a 30G needle at 0.040 mL/min into a 0.9% calcium chloride crosslinking solution. Physicochemical analyses included swelling, degradation/weight loss over seven days, encapsulation efficiency, and mean diameter. Enzyme-linked immunosorbent assay (ELISA) quantified SERPIN F1 (also known as Pigment Epithelium-Derived Factor - PEDF), ciliary neurotrophic factor (CNTF), brain-derived neurotrophic factor (BDNF), and beta-nerve growth factor (β-NGF) secretion.

Results: All formulations generated homogeneous spherical microbeads with successful hCSCs encapsulation. SA+HA demonstrated the best overall physicochemical performance, showing reduced degradation (~15–16% weight loss) and high encapsulation efficiency (~96–102%) compared to SA alone, which exhibited greater swelling (~26%) and lower encapsulation efficiency (~68–78%). SA+HA also produced smaller and more homogeneous

microbeads (~590–620 μm), whereas SA+BG presented the largest mean diameters (~780–820 μm). ELISA analysis demonstrated enhanced secretion of neuroprotective factors in modified formulations. SA+HA showed the highest SERPIN and CNTF concentrations, reaching approximately 24 μg/mL and 9.5 ng/mL, respectively in a group of 112 beads. β-NGF secretion was also increased in SA+HA groups, with concentrations above 1.0 pg/mL in the same samples. BDNF levels were detected at lower concentrations across groups, while SA+BG generally showed reduced neurotrophic factor detection.

Conclusion/Significance: Modified alginate formulations, particularly SA+HA, improved microbead stability, encapsulation efficiency, and neuroprotective factor secretion. These findings support the use of hyaluronic acid-enriched alginate microbeads as a promising minimally invasive platform for hCSCs delivery in retinal regenerative therapies targeting diabetic retinopathy.

C35 - Turbidity Sensing for Controlled Dissociation of Retinal Organoids

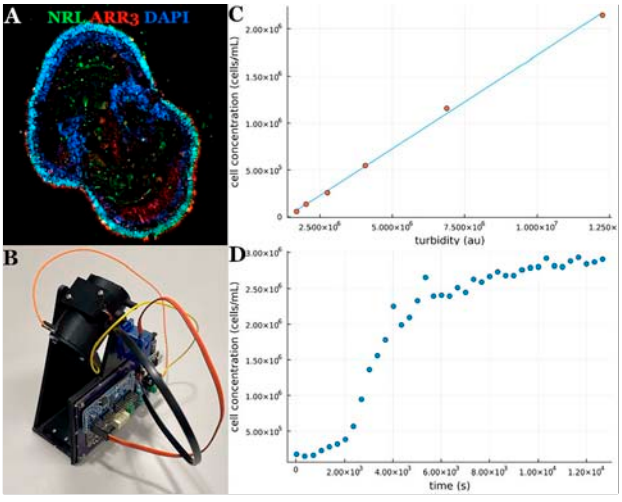
Nicholas Stone, Laura Bohrer, Budd Tucker

University of Iowa, Institute For Vision Research, Iowa City, United States of America

Purpose/Objectives: While patient stem cell derived retinal organoids (ROs) are an ideal source of cells for photoreceptor replacement therapies, techniques are needed for purifying photoreceptors needed for transplant from other cells which make up ROs. As we have shown previously, given that photoreceptors are on the outermost layer of ROs (Fig 1A), partial dissociation can be used to purify photoreceptors for transplant. However, as different batches of ROs can dissociate at different rates, methods for monitoring the dissociation rate of ROs will be useful for maximizing the purity and recovery of photoreceptors. To address this need, we have developed a system for continuous monitoring of RO dissociation via turbidity measurement.

Methodology: Dissociations were performed by placing ~5-10 ROs in a dissociation buffer made up of 36 U/mL papain (Worthington) in EBSS supplemented with DNAse I (Worthington). This mixture was loaded in a 2mL glass scintillation vial which in turn was inserted into our dissociation device. As shown in Figure 1B, our system consists of a sample holder capable of repeatedly inverting the RO vial to promote mixing, as well as a LED lamp and photodetector mounted perpendicular to each other. During dissociation, mixing was occasionally paused, allowing ROs to settle into the cap of the scintillation vial. The lamp was then turned on, and the amount of light scattered by suspended cells measured using the photodetector, allowing for the measurement of the concentration of liberated cells, and therefore the dissociation rate.

Results: As shown in Figure 1C, scattered light intensity measured by the photodetector changed linearly with cell concentration over a useful range of cell concentrations. In Figure 1D, we show that our system can measure cell concentration in real time during RO dissociation.



Conclusion/Significance: We have demonstrated that turbidity measurement can be used for continuous monitoring of RO dissociation rate. We believe that compared to constant duration dissociations, dissociating to the same point on a cell concentration curve will generate more uniform cell populations for transplant.

C38 - Optimizing Ring Frequency in Esophageal Grafts: Finite Element Analysis for Enhanced Structural Support and Stability

Laura Modica De Mohac, Federica Cosentino

Fondazione RiMED, Palermo, Italy

Purpose/Objectives: Background: Esophageal strictures are characterized by a reduction of the esophagous lumen diameter. Standard treatment for benign esophageal strictures is endoscopic dilation, which, despite being effective, can lead to perforation and relapse due to hyperplastic tissue response. **Objectives:** Our goal is to design a **stent-less biohybrid graft** that provides mechanical stability and minimizes the risk of relapse and migration using finite element model.

Methodology: Methods: The graft is a **multi-layered structure** organized as follows: 1) an internal ring-like structure to confer mechanical resistance to buckling, kinking and migration; 2) a polymeric layer for mechanical support. Rings were spaced at 1 -3- 5 mm interval along a 100 mm-long graft. These concentric rings are hypothesized to play a crucial structural role by providing an outward radial force capable of expanding the lumen of an organ affected by stenosis. The geometry was modeled in Solidworks and meshed (~35k S4 quadrilateral shell elements). The graft includes an inner layer of PCL and outer layer Tecoflex85A, with linear elastic and isotropic material properties. Simulations were performed using Abaqus/Explicit. To mimic physiological esophageal loading, a simulated food bolus (8.3 mm diameter, 0.5 mm thickness sphere) was introduced. Buckling performance was assessed by applying axial displacement (10%, 15%, 20%).

Results: The 3-mm ring spacing configuration showed the highest mechanical stability. Von Mises stress decreased from **1.4 MPa (1-mm)** to **0.6 MPa (5-mm)** as ring spacing increased. Similarly, radial displacement increased from **0.48 mm (1-mm)** to **1.15 mm (5-mm)** during buckling, confirming superior resistance of the 3-mm design to food-passage-induced compression.

Conclusion/Significance: Conclusion: FEM analysis indicates that tight ring spacing (3-mm) provides optimal radial support and structural integrity, effectively limiting buckling and potential graft migration. Future validation will include ex vivo and in vivo studies to compare FEM predictions with experimental performance under physiological conditions.

C42 - Fibronectin tethering as a shear-thinning bio-annealing strategy for granular hydrogels

Ethan Nicklow[1], Olivia Ernst[1], Donald R. Griffin[1], Chris Highley[2]

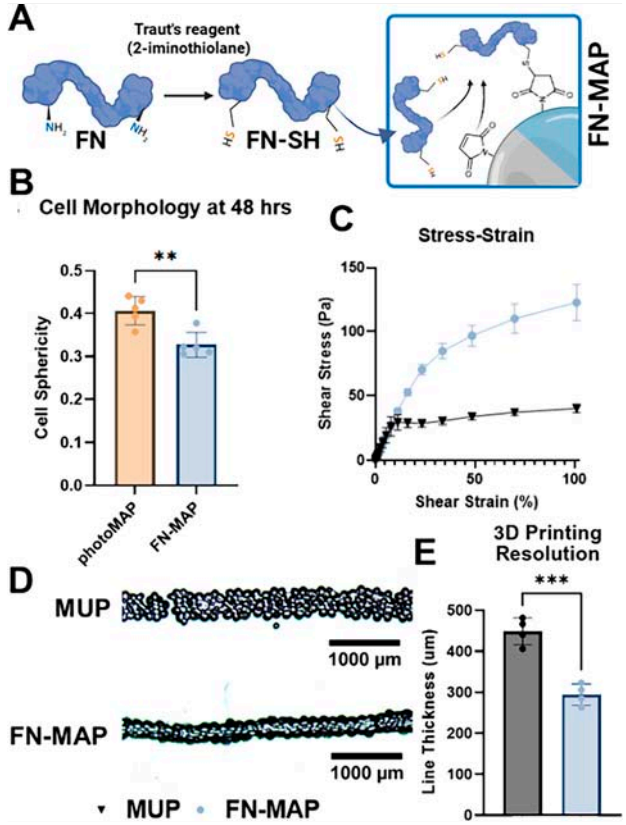
[1]*University of Virginia, Biomedical Engineering, Charlottesville, United States of America*
[2]*University of Virginia, Biomedical Engineering And Chemical Engineering, Charlottesville, United States of America*

Purpose/Objectives: Granular hydrogels are injectable biomaterials comprised of hydrogel microparticles that enable rapid cell infiltration. Microporous annealed particle (MAP) scaffolds feature covalent interparticle crosslinks that confer greater stability than jammed scaffolds, which rely solely on interparticle friction. Various annealing strategies, including covalent photo-crosslinking and reversible guest-host chemistries, combined with tethered cell-adhesion ligands, modulate scaffold stability and bioactivity to mimic the extracellular matrix (ECM). A common ligand, RGD, is a binding motif derived from fibronectin (FN), a multifunctional ECM protein essential in cell-ECM interactions, ECM assembly, and tissue regeneration. Here, we present FN-coated MAP scaffolds (FN-MAP) as a strategy to simultaneously incorporate bioactivity and ECM-inspired annealing.

Methodology: PEG-based microparticles were fabricated via step emulsification and internally crosslinked through thiol-maleimide reactions. FN was modified with 2-iminothiolane to increase thiol content and conjugated to microparticles with excess maleimides. FN-MAP scaffolds were characterized via parallel-plate rheology to

assess mechanical properties and self-healing under cyclic strain. Printability was evaluated using an extrusion-based 3D bioprinter. Human lung fibroblasts (HLFs) were cultured in FN-MAP to assess viability and morphology, and a murine diabetic wound model was used to evaluate *in vivo* stability and bioactivity.

Results: FN-MAP exhibited significantly increased yield strength and strain compared to jammed scaffolds and recovered more effectively than covalently crosslinked scaffolds after repeated high strain. These properties supported greater print stability and resolution in extrusion bioprinting relative to jammed particles. HLFs cultured in FN-MAP spread and elongate more than those in RGD-functionalized scaffolds while maintaining similarly high viability. FN-MAP accelerated epidermal wound closure in a diabetic mouse model with comparable endothelial cell infiltration to covalently crosslinked controls. A) Modification and conjugation of FN (FN-MAP). FN-MAP decreases fibroblast sphericity B) and increases scaffold strength C). D-E) FN-MAP allows for higher resolution 3D printing.



Conclusion/Significance: FN-MAP represents a novel approach for enhancing mechanical stability and bioactivity in granular hydrogel scaffolds without exogenous linkers or heterogeneous microparticle populations. FN coating enables interparticle crosslinking and bioactivity, improving fibroblast spreading and accelerating wound closure in a challenging regenerative environment. This biologically inspired, single-component design avoids high complexity while offering strong potential for clinical application in soft tissue repair and regeneration.

C43 - Single-cell transcriptomic profiling identifies tension-dependent macrophage remodeling states following polypropylene mesh implantation for pelvic organ prolapse repair

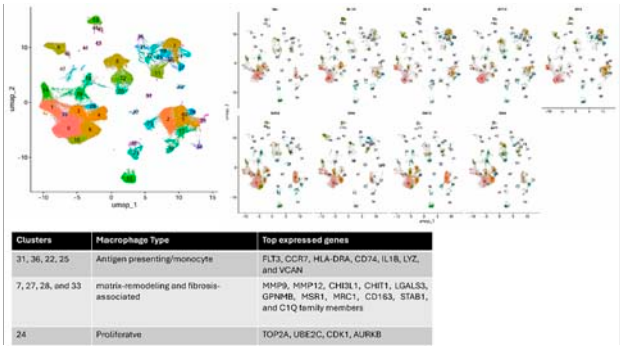
Marrisa Therriault[1,2], Tianjiao Chu[1], Katrina Knight[1,3], Pamela Moalli[1,2,3]

[1]*Magee Womens Research Institute, Pittsburgh, United States of America*
[2]*University of Pittsburgh, Obgyn, Pittsburgh, United States of America*
[3]*University of Pittsburgh, Bioengineering, Pittsburgh, United States of America*

Purpose/Objectives: Polypropylene mesh implanted for pelvic organ prolapse (POP) repair is associated with complications including pain, fibrosis, and vaginal degeneration. While prior studies have demonstrated that mesh deformation, pore collapse, and wrinkling alter tissue integration and increase mesh burden, the cellular mechanisms driving maladaptive remodeling remain poorly understood. In particular, the macrophage response to mechanical environments following implantation has not been characterized longitudinally at single-cell resolution. We therefore performed single-cell RNA sequencing (scRNA-seq) to define macrophage phenotypic heterogeneity and mechanobiologic remodeling programs at the mesh–tissue interface in a rabbit lumbar colpopexy model.

Methodology: Parous rabbits underwent lumbarcolpopexy with implantation of Restorelle polypropylene mesh under low-tension (RL) or high-tension/wrinkled (RT) conditions, or sham/no mesh controls. Mesh–tissue complexes were harvested at 4 and 12-weeks following implantation. Single-cell suspensions were generated using enzymatic digestion and processed using 10X Genomics. Dimensional reduction, clustering, and differential gene expression analyses were performed using Seurat in R.

Results: scRNA-seq identified 47 transcriptionally distinct cellular clusters within the mesh–tissue interface. A discrete myeloid/macrophage compartment consisting of clusters listed in Figure 1 formed a contiguous transcriptional manifold suggestive of activation and remodeling states. High-tension/wrinkled mesh conditions (RT), particularly at 12-weeks, demonstrated visual enrichment of remodeling macrophage states compared to low-tension conditions (RL). These populations localized to transcriptional regions associated with extracellular matrix turnover, chronic foreign body remodeling, phagocytic activation, oxidative stress adaptation, and wound-healing fibrosis. Cross-talk between macrophages and activated fibroblast populations was suggested by coordinated expression of profibrotic and matrix-remodeling mediators including TGFBI, FN1, POSTN, and MMP family members. In addition, an epithelial-associated cluster expressing KRT16 together with mesenchymal/remodeling markers including POSTN, COL1A1, COL3A1, FN1, ACTA2, VIM, and SNAI1 suggested the presence of an epithelial remodeling or epithelial-to-mesenchymal transition-like program in response to mesh implantation.



Clusters	Macrophage Type	Top expressed genes
31, 36, 22, 25	Antigen presenting/monocyte	FLT3, CCR7, HLA-DRA, CD74, IL1B, LYZ, and VCAN
7, 27, 28, and 33	matrix-remodeling and fibrosis-associated	MMP9, MMP12, CHI3L1, CHIT1, LGALS3, GPNMB, MSR1, MRC1, CD163, STAB1, and C1Q family members
24	Proliferative	TOP2A, UBE2C, CDK1, AURKB

Conclusion/Significance: Polypropylene mesh implantation induces mechanically regulated macrophage remodeling programs that extend beyond the traditional M1/M2 paradigm. High-tension mesh deformation was associated with expansion of macrophage states linked to chronic inflammation, matrix remodeling and fibrosis, consistent with maladaptive foreign body remodeling and stress shielding. The data further support coordinated macrophage–fibroblast interactions and identify candidate epithelial remodeling populations that may contribute to mesh exposure and vaginal tissue degeneration.

C45 - Integration of PEGDA Microgels into Cardiac ECM Granular Hydrogels for Enhanced Mechanical Stability

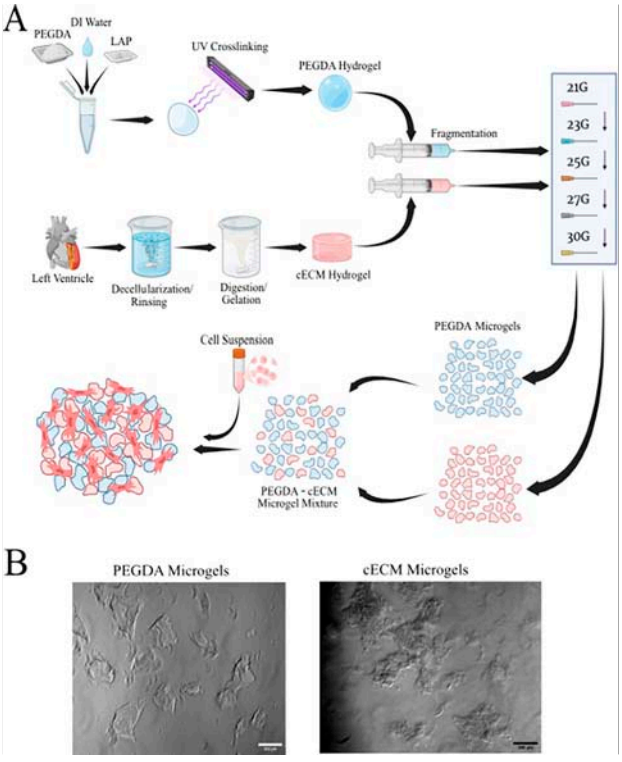
Joseph Ketchum[1], Rabina Lamichhane[2], Emma Barna[2,3], Jacob Brown[2], Ge Zhang[2]

[1]*University of Akron, Department of Biomedical Engineering, Akron, United States of America*
[2]*The University of Akron, Department of Biomedical Engineering, Akron, United States of America*
[3]*University of Akron, Biomedical Engineering, Akron, United States of America*

Purpose/Objectives: Natural hydrogels such as cardiac extracellular matrix (cECM), which is synthesized from the decellularized porcine myocardium, are already used clinically to treat damaged cardiac tissue following myocardial infarction. cECM is rich in bioactive components which make a natural scaffold for the recellularization of the hydrogel that can modulate inflammation, revascularization, and can help regenerate tissues of the heart. One major limitation of cECM hydrogel is retention *in vivo*. cECM hydrogel is mechanically weak and fails under long-term stress. Conversely, Poly-ethylene glycol diacrylate (PEGDA) forms a highly tunable, non-immunogenic, relatively stiff hydrogel scaffold. In this study, we aim to synthesize a granular hydrogel that possesses the mechanical tunability of PEGDA to increase the stiffness of the composite while preserving the available bioactive components of the cECM.

Methodology: Bulk PEGDA hydrogels were prepared at varying polymer concentrations to tune the mechanical properties, which were quantified using rheometry. cECM hydrogels were prepared from decellularized porcine cardiac tissue using an established protocol. PEGDA and cECM microgels were formed independently via extrusion fragmentation. PEGDA microgels were analyzed in ImageJ for their shape and size distributions relative to their bulk mechanical properties. PEGDA and cECM microgels were combined with a cell suspension, where cell–microgel interactions served as biological crosslinkers to form a granular hydrogel.

Results: PEGDA and cECM microgels were successfully fabricated with comparable size and morphology following fragmentation, allowing uniform mixing within the granular hydrogel (Figure 1). The incorporation of PEGDA microgels increased the stiffness of the composite material without disrupting cECM's biochemical features. Figure 1. A) PEGDA-cECM granular hydrogel synthesis schematics. B) PEGDA and cECM microgel images showcasing their similarity.



Conclusion/Significance: In this study we successfully synthesized a cECM PEGDA granular hydrogel with cell microgel based crosslinking. This work demonstrates that integrating PEGDA microgels into cECM based granular hydrogels provide greater, tunable, mechanical properties while maintaining the bioactive microenvironment essential for cardiac tissue repair. Future work will involve granular material testing, further cytocompatibility and functionality studies and perhaps *in vivo*testing. The resulting hybrid material offers a highly modifiable balance between hydrogel strength and bioactivity which will provide greater functionality of cECM hydrogels for myocardial regeneration.

C46 - Collagen Sponge Scaffold for Skeletal Muscle Fabricated using Oriented Mold

Toshiki Fujiwara[1], Tatsuya Kitagawa[2], Kazuya Sawada[3], Toshia Fujisato[1]

[1]*Osaka Institute of Technology, Biomedical Engineering, Osaka, Japan*
[2]*PGS HOME CO., Ltd, Osaka, Japan*
[3]*Osaka Seikei Collage, Life Design, Osaka, Japan*

Purpose/Objectives: Skeletal muscle may be resected as a result of treatment for malignant bone or soft tissue tumors, or following an accident. However, effective treatments for skeletal muscle have not yet been established. Consequently, such patients are often forced to spend the rest of their lives with impaired activities of daily living. Tissue engineering offers a promising strategy for volumetric muscle loss. To achieve this, one approach involves arranging skeletal muscle cells axially as a living tissue. In this study, we fabricated oriented collagen sponges using an acrylic mold with aligned grooves.

Methodology: An acrylic mold featuring semi-elliptical convex grooves (width/depth (W/D): 400 μm/400 μm and 400 μm/800 μm) was fabricated using a stereolithography 3D printer (Form3, Formlabs, USA). A 3 mg/mL collagen solution was poured into the acrylic mold, frozen at -80°C, and then freeze-dried. Subsequently, the sample was cross-linked using EDC/NHS and freeze-dried again to obtain a collagen sponge. To investigate surface properties and pore distribution, the morphology of the scaffold was analyzed using a scanning electron microscope (SEM).

Results: SEM images of the sponge surface and cross-section are shown. The widths of the collagen sponges fabricated using semi-elliptical molds with aspect ratios of 400 μm/400 μm and 400 μm/800 μm were 558 ± 59 μm and 593 ± 48 μm, respectively. Their depths were 114 ± 8 μm and 210 ± 13 μm, respectively. The orientation of the grooves in each sponge was the same as that of the mold. It was confirmed that the width of the sponge grooves provided sufficient space for cell adhesion. Furthermore, the depth of the grooves is considered sufficient for cells to obtain nutrients through diffusion.

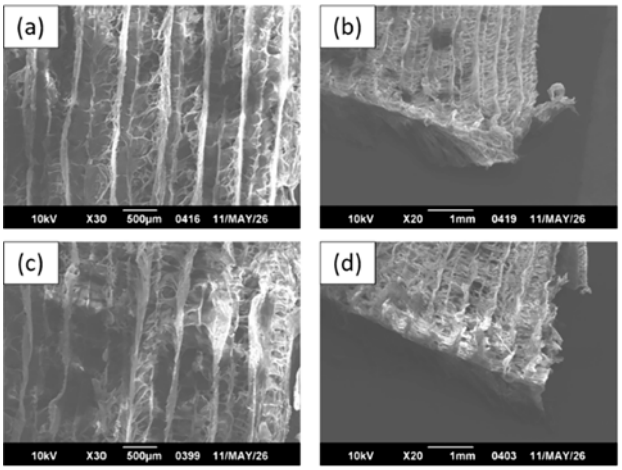


Fig. Shape Observation (SEM)
(a)W0.4 D0.4 Surface (b)W0.4 D0.4 Cross Section
(c)W0.4 D0.8 Surface (d)W0.4 D0.8 Cross Section

Conclusion/Significance: The resulting oriented collagen sponge is considered a suitable scaffold for skeletal muscle tissue. It can also be applied to other types of oriented tissues.

C53 - Differential In Vitro Macrophage Responses to Collagen-Based Biomaterials in Surgical Wound Healing

Fahimeh Tabatabaei, Nina Bionda

Sanara MedTech, Rochal Technologies, R&d Division of Sanara Medtech, San Antonio, United States of America

Purpose/Objectives: Macrophage behavior is a critical determinant of surgical wound healing outcomes. Collagen-based surgical wound products differ in source, processing, and structural organization, which may alter immune-cell interactions and downstream tissue repair responses. This study comparatively evaluated macrophage proliferation and morphology in response to hydrolyzed collagen, native collagen, and ECM-derived biomaterials to better understand how biomaterial presentation modulates inflammatory and reparative phenotypes relevant to acute surgical wound healing.

Methodology: RAW 264.7 macrophages were cultured as unstimulated (M0) or lipopolysaccharide-stimulated pro-inflammatory (M1) cells. Cells were exposed to hydrolyzed bovine type I collagen (CellerateRX® Surgical Powder), native bovine type I collagen (Medifil® II collagen particles), or porcine placental-derived ECM (InnovaMatrix® PD) at 5 mg/mL for 24-48 hours. Macrophage proliferation was quantified using PicoGreen® DNA assays and normalized to untreated controls. Morphological responses were evaluated after fluorescent staining of actin cytoskeleton and nuclei using fluorescence microscopy to assess cell spreading, elongation, and structural organization.

Results: Distinct macrophage response profiles were observed across biomaterial classes. Hydrolyzed collagen selectively increased proliferation of M0 macrophages without notable enhancement of M1 proliferation. Morphologically, hydrolyzed collagen maintained predominantly rounded M0-like cells while inducing a subset of elongated spindle-like morphologies associated with reparative phenotypes, even under inflammatory conditions. ECM-derived material increased proliferation in both M0 and M1 populations and produced heterogeneous morphologies without evident M2-like structures in inflammatory cultures. Native collagen demonstrated minimal effects on proliferation but induced spread, irregular morphologies in unstimulated M0 cultures resembling LPS-activated macrophages.

Conclusion/Significance: These *in vitro*findings suggest that collagen source, processing, ECM composition, and fibrillar structure differentially regulate macrophage-material interactions. Hydrolyzed collagen demonstrated a macrophage interaction profile potentially favorable for balanced immune engagement without prolonged inflammatory activation. These mechanistic findings support the importance of biomaterial design in regulating immune responses and advancing translational strategies for surgical wound repair and regenerative medicine.

C54 - A Bioengineered Interwoven Extracellular Matrix for Diabetic Wound Healing

Archita Sharma, Dhavan Sharma, Feng Zhao

Texas A&M Unniversity, College Station, United States of America

Purpose/Objectives: Chronic wounds, such as diabetic ulcers, remain a major clinical challenge due to persistent inflammation, impaired angiogenesis, and delayed re-epithelialization. Current therapies, including commercial acellular dermal matrices (ADMs), are limited by donor scarcity, high cost, inconsistent mechanical properties, and potential adverse immune responses. This study aimed to develop a donor-independent, fully biological, and biomimetic interwoven extracellular matrix (iECM) scaffold that recapitulates native dermal ECM composition, architecture, and mechanical properties to promote regenerative wound healing.

Methodology: iECM was fabricated by decellularizing human dermal fibroblast (hDF)-derived cell sheets. The structural, biochemical, and mechanical properties of iECM were characterized using imaging, ECM composition analysis, tensile testing, and atomic force microscopy (AFM). Immunomodulatory effects were evaluated using THP-1 macrophages through marker expression and cytokine profiling. The therapeutic efficacy of iECM was assessed in a full-thickness excisional diabetic rat wound model. An in vitro migration model was further used to investigate iECM-mediated cellular migration, myofibroblast activation, and matrix remodeling mechanisms.

Results: The resulting iECM preserved native ECM proteins and growth factors while forming self-reinforced, submicron-scale interwoven ECM fiber networks resembling native dermal architecture. iECM exhibited enhanced mechanical integrity with a Young's modulus of ~4 MPa, within the range of native dermis (3–18 MPa), and demonstrated region-specific mechanical heterogeneity and multilayer folding capability. In vitro immune assessment showed that iECM promoted macrophage polarization toward an anti-inflammatory M2-like phenotype, with reduced pro-inflammatory marker expression and cytokine secretion. In diabetic rats, a single iECM application improved wound closure (~80%), reduced inflammation and scarring, enhanced angiogenesis and granulation tissue formation, and accelerated re-epithelialization. Mechanistically, iECM guided directional cellular migration, promoted organized F-actin arrangement, spatially regulated transient α-SMA expression, and enhanced aligned collagen deposition, supporting structured tissue remodeling.

Conclusion/Significance: The biomimetic architecture of iECM provides structural and biochemical cues that modulate the chronic wound microenvironment by regulating immune responses, directional cell migration, and matrix remodeling. This donor-independent, completely biological iECM platform overcomes key limitations of conventional ADMs and represents a promising next-generation regenerative therapy for chronic diabetic wound healing.

C56 - Effect of Immunophenotype and Sex on the In Vitro Behavior of Feline Adipose-Derived Multipotent Stem Cells Following Continuous Culture or Cryopreservation

Aiyanna Mcgowan[1], Mandi J. Lopez[2], Ernesto Miranda-Morales[2], Thi Hong Tham Phan[1,3], Wendy Wolfson[2], Marilyn Dietrich[4]

[1]*Louisiana State University School of Veterinary Medicine, Veterinary Clinical Sciences, Baton Rouge, United States of America*
[2]*Louisiana State University, School of Veterinary Medicine, Veterinary Clinical Sciences, Baton Rouge, United States of America*
[3]*Laboratory for Equine and Comparative Orthopedic Research, Veterinary Clinical Sciences Department, School of Veterinary Medicine, Lsu, Baton Rouge, United States of America*
[4]*Louisiana State University School of Veterinary Medicine, Pathobiological Sciences, Baton Rouge, United States of America*

Purpose/Objectives: Adipose tissue-derived multipotent stem cells (ASCs) are an option for feline cell-based regenerative therapies. Cryopreservation required to store and transport cells can impact behaviors. This study was designed to evaluate how cryopreservation, sex, and immunophenotype affect ASC characteristics.

Methodology: ASCs isolated from adipose tissue of male (n=6) and female (n=6) feline gonads were cultured in stromal medium until passage(P) 1. Next, ½ was cryopreserved (CR) while ½ was continuously cultured (CC). At 80% confluence, ½ of each was maintained in unsorted continuous culture (UCC) and ½ was sorted into two immunophenotypes: CD44+, CD105+, MHCII+ (MHCII+) and CD44+, CD105+, MHCII- (MHCII-). For all cohorts, P3 cell proliferation was assessed via resazurin reduction, multipotentiality via colony forming unit (CFU) assays, and following differentiation, fibroblastic (F), osteoblastic (Ob), and adipocytic (Ad) gene expression via qPCR.

Results: Most cells had an MHCII- immunophenotype. Unsorted cultures had higher proliferation overall. Immunophenotyped CR male cells typically had higher proliferation than female cells. Male UCC and MHCII- cells had higher CFU-F than MHCII+. Unsorted CC and MHCII- had higher CFU-Ob percentages than MHCII+. The highest CFU-Ad percentages were with CC MHCII- cells. Cryopreserved UCC and CR MHCII- cells had higher CFU-Ad percentages than MHCII+ cells. Osteoblastic gene expression was greater in all CR cohorts, and highest in the UCC cohort. Male MHCII- cells had the highest adipogenic gene expression.

Conclusion/Significance: These results suggest that cryopreservation does not significantly reduce proliferation and increases expression of some differentiation-associated genes. Sex-associated differences were also evident among ASC immunophenotypes.

C58 - Prediction of Bone Marrow Functional Output from Immunophenotype and Genotype in a Sickle Cell Disease Mouse Model

Erin Schwarzbach, Madison Aliff, Mykel Green

Tulane, Biomedical Engineering, New Orleans, United States of America

Purpose/Objectives: Sickle cell disease (SCD) disturbs the hematopoietic stem cell (HSC) niche and bone marrow microenvironment, leading to reduced bone marrow functional output. Colony-forming unit (CFU) assays remain the gold standard for measuring this output yet are typically endpoint assays and time-intensive. We aim to develop a machine learning framework that predicts CFU yield and lineage composition from fluorescence-activated cell sorting (FACS) derived immunophenotypic features, physiological metadata, and genotype in the Townes humanized SCD mouse model (HbAA, HbAS, HbSS), enabling a non-destructive assessment of the marrow functional reserve.

Methodology: Age- and sex-matched Townes mice across three genotypes were used. Long-term HSCs (LT-HSC; $Lin^{-}Sca1^{+}cKit^{+}CD150^{+}CD48^{-}$) were isolated by FACS. CFU assays were performed with colony scoring at day 14. FACS-derived features, including LT-HSC frequency and LSK abundance, along with genotype and physiological covariates served as model inputs. Supervised machine learning approaches including regularized regression and ensemble tree-based models were trained to predict total CFU output and lineage-specific colony composition. Model performance was evaluated by cross-validation, and feature importance analysis identifying the strongest biological predictors.

Results: Genotype-dependent differences in CFU output are confirmed across HbAA, HbAS, and HbSS animals, consistent with published reports of stemness exhaustion in HbSS mice. Model development and full cross-genotype validation are ongoing.

Conclusion/Significance: This work establishes a predictive model linking bone marrow cell composition to functional output in the context of SCD, with the HbAS (sickle cell trait) genotype included as a historically understudied intermediate group. When validated, this framework could inform pre-transplant HSC assessment, gene therapy candidate screening, and broader efforts to predict marrow reserve from flow cytometry data alone, reducing reliance on time consuming endpoint assays.

C62 - Stimuli-Responsive CRISPR Delivery via Protease-Sensitive Functionalized 3D-Printed Scaffolds

Chiebuka Okpara[1], Juan Azmitia Delgado[1], E. Thomas Pashuck[1], Lesley Chow[1,2], Tomas Gonzalez Fernandez[1]

[1]*Lehigh University, Bioengineering, Bethlehem, United States of America*
[2]*Lehigh University, Materials Science And Engineering, Bethlehem, United States of America*

Purpose/Objectives: Effective gene editing for regenerative medicine requires a fundamentally different delivery paradigm distinct from that used for monogenic diseases. Unlike single-gene correction strategies, regenerative applications must synchronize editing activity with dynamic biological processes, as uncontrolled CRISPR release risks off-target editing and immunogenicity. Stimuli-responsive delivery systems offer a promising solution by enabling autonomous CRISPR release in response to physiological cues present in the native microenvironment. The dynamic proteolytic microenvironment characteristic of chronic inflammatory conditions such as osteoarthritis offers endogenous triggers for self-regulating systems capable of controlled CRISPR release in musculoskeletal tissues. Therefore, the objective of this work is to develop a protease-responsive delivery platform in which CRISPR-loaded nanoparticles are conjugated to scaffolds via a protease-sensitive peptide, enabling localized and temporally controlled gene editing.

Methodology: *Biomaterial fabrication*: Inks were prepared by dissolving poly(caprolactone) (PCL) in hexafluoroisopropanol and solvent-casting into 3D-printed scaffolds. The scaffolds were treated with 2-chloroethylamine hydrochloride to functionalize the surface and characterized with attenuated total reflectance Fourier transform infrared (ATR-FTIR). A protease-sensitive peptide (KRVKRRLLMETGGGC), modified with biotin (biotin-peptide) or Cyanine-3 (Cy3-peptide) was grafted to the scaffold surface using tris(2-carboxyethyl)phosphine hydrochloride in 2-N-morpholino-ethanesulfonic acid. Peptide presentation was verified by fluorescence microscopy. *Nanoparticle grafting*: Fluorescently labelled Cas9-gRNA ribonucleoprotein complex-loaded biotinylated cell penetrating nanoparticles (biotin-SGESGSGWEARLARALARALARHLARALARALRACEA) were conjugated to biotin-functionalized scaffolds via an avidin bridge linker. The coupling reaction was confirmed with fluorescence microscopy. *Release kinetics*: Scaffolds were incubated in a collagenase solution for 7 days. Cy3 was used as a fluorescent reporter to quantify enzyme-driven release kinetics.

Results: ATR-FTIR confirmed the presence of an alkyl halide functional peak near 800 cm^{-1} following aminolysis of the PCL scaffolds. Increased fluorescence intensity was observed in functionalized scaffolds compared with non-functionalized controls, indicating successful CRISPR-loaded nanoparticle grafting. Release studies showed increased Cy3 release from surface-functionalized scaffolds in collagenase compared to a non-collagenase control, confirming protease-trigger release.

Conclusion/Significance: This strategy localizes CRISPR-loaded nanoparticles onto PCL surfaces via a protease-sensitive peptide, enabling selective nanoparticle release in response to proteolytic activity, thereby providing a stimuli-responsive delivery of gene editing cargos. Ongoing and future work focuses on on-demand CRISPR delivery to osteoarthritic chondrocytes to promote cartilage tissue regeneration.

C64 - Vaginal matrix-bound nanovesicles induce pro-regenerative function in human vaginal fibroblasts

Joshua Montano[1], Morgan Egnot[2], Marrisa Therriault[3], Pamela Moalli[3,4], Amrita Sahu[5], Amanda Artsen[3]

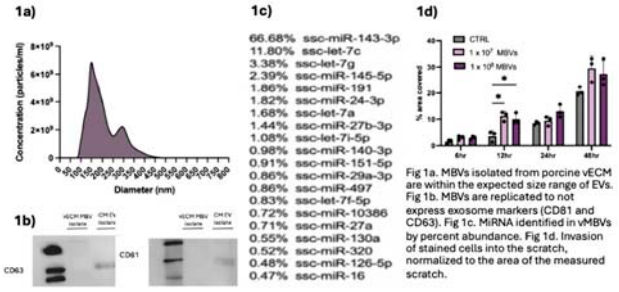
[1]*University of Pittsburgh School of Medicine, Department of Pharmacology And Chemical Biology, Lothrop St, United States of America*
[2]*University of Pittsburgh School of Medicine, Department of Bioengineering, Pittsburgh, United States of America*
[3]*Magee Womens Research Institute, Pittsburgh, United States of America*
[4]*University of Pittsburgh, Obgyn, Pittsburgh, United States of America*
[5]*University of Pittsburgh School of Medicine, Department of Physical Medicine And Rehabilitation, Pittsburgh, United States of America*

Purpose/Objectives: ECM derived from porcine tissue can attenuate the deleterious foreign body response to polypropylene mesh, but its regenerative capacity is not well understood. We hypothesize that vaginal extracellular matrix (vECM) provides regenerative benefit through its matrix-bound nanovesicles (vMBV).

Methodology: vMBVs were isolated from decellularized porcine vECM by collagenase digestion and ultracentrifugation, then resuspended in PBS or TRIzol for miRNA extraction and sequencing. Secreted EVs from human vaginal fibroblast (HVF) conditioned media were isolated as a control. Nanoparticle tracker analysis characterized particle size and concentration. vMBV and EV lysates were probed for exosome surface markers CD81 and CD63 using western blot. A scratch assay was performed on HVF monolayers before treatment with 1.0 x 107 or 1.0 x 108 vMBVs over 6-48 hours. Percent area covered was measured by thresholding crystal violet stained cell bodies within the scratch area defined by the region of interest (ROI), normalized by the total area of the ROI.

Results: vMBVs concentration was 3.93 x 1012 particles/ml with a mode of 149.5 ± 9.3 nm. As reported from intestine and bladder, vMBVs lacked common EV markers (CD81 and CD63), compared

to EVs from conditioned media. Sequencing of vMBV miRNA indicates that 67% of all miRNA cargo are miR-143-3p and 12% are ssc-let-7g. 6 of the most abundant miRNAs are also abundant in bladder or intestinal MBVs and 14 were uniquely enriched in vMBVs. vMBVs at both concentrations significantly increased closed wound area at 12 hours after scratch assay.



Conclusion/Significance: vMBVs exhibit similar size and surface marker characteristics as MBVs from other organs and contain miR-143-3p as more than half of the miRNA present, which has been shown to decrease SMAD2/3 signaling and attenuate fibrosis. This uniquely situates vMBVs as a therapeutic benefit to prevent mesh complications and promote vaginal healing.

C66 - Identification And Characterization of Hair-Matrix-Derived Vesicles

Peyton Leyendecker[1,2], George Hussey[1,2,3,4]

[1]*University of Pittsburgh Swanson School of Engineering, Department of Bioengineering, Pittsburgh, United States of America*
[2]*McGowan Institute for Regenerative Medicine, Pittsburgh, United States of America*
[3]*University of Pittsburgh School of Medicine, Department of Surgery, Pittsburgh, United States of America*
[4]*University of Pittsburgh School of Medicine, Department of Pathology, Pittsburgh, United States of America*

Purpose/Objectives: Extracellular vesicles (EVs) are increasingly recognized as promising biologics for regenerative medicine due to their role in cell communication and tissue repair. Yet, keratinous tissues, like hair, have been largely overlooked as a source of these vesicles. Here, we identify and characterize a novel, naturally occurring class of keratin-associated nanovesicles embedded within hair. Notably, hair is an abundant, renewable, and sustainable resource, positioning these vesicles as an environmentally friendly and scalable platform for future applications. These vesicles—which have not been intentionally studied—are shown to be present across species, with a distinct composition and biological effect on cells.

Methodology: Keratin-based tissues were enzymatically digested and processed via ultracentrifugation to isolate nanovesicle-sized particles (<200 nm). Nanoparticle tracking analysis and electron microscopy confirmed vesicle morphology and size distribution. Techniques like SDS-PAGE, lipidomics, and RNA isolation were used to characterize the molecular content of the vesicles. Functional bioassays evaluated the effects of these keratin-tissue-derived nanovesicles on various cell types, including dermal fibroblasts and epidermal keratinocytes.

Results: Keratin tissue-derived nanovesicles were consistently isolated from diverse sources of hair and were found to contain a distinct cargo profile and makeup compared to established EV populations, such as matrix-bound nanovesicles (MBVs) and exosomes. Additionally, functional assays revealed that these vesicles elicit unique cellular responses, underscoring their specialized biological role.

Conclusion/Significance: This work introduces a new class of EV with distinct origin, molecular composition, and biological function. The discovery of these keratin-associated nanovesicles not only expands our understanding of vesicle diversity within various tissue sources but also provides a new, naturally sourced tool for therapeutic innovation. Derived from hair—a renewable and abundant tissue—these vesicles could serve as a platform for the development of more environmentally sustainable bioactive materials and regenerative therapies, with potential applications in skin, hair, and beyond.

C68 - Multi-Stain Quantitative Histochemistry for Decellularization Assessment: A Dose-Response Study in Human Uterine Myometrium

Elena Wenger[1], Zelalem Ayalew[2], Guillermo Ameer[1], Taneka Jones[2]

[1]*Northwestern University, Biomedical Engineering, Evanston, United States of America*
[2]*Lehigh University, Bethlehem, United States of America*

Purpose/Objectives: Decellularized extracellular matrix (ECM) from human myometrium is a promising substrate for uterine hydrogels and scaffolds in regenerative engineering, requiring quantitative assessment of decellularization quality. Current consensus standards recommend complementary characterization attributes, but standard color deconvolution methodology does not address combined stains like Masson's Trichrome with Elastic van Gieson (TRI-EVG) that visualize multiple ECM components. This study develops a multi-stain color deconvolution framework with custom vectors for combined stains, demonstrated through a dose-response study of sodium deoxycholate (SDC) treated human myometrium.

Methodology: Human myometrium tissue was treated with 1%, 2%, or 4% SDC and native controls. ECM and cellular content were characterized by color-deconvolution-based image analysis of hematoxylin and eosin, Alcian Blue, and TRI-EVG stained sections. Custom deconvolution vectors resolved collagen and muscle channels in TRI-EVG sections, absent a standard preset. Signal was expressed as a percentage of native tissue. Lyophilized tissue was milled to powder, weighed, and assayed for residual dsDNA by Picogreen fluorescence. Values were normalized to dry tissue mass.

Results: Residual dsDNA was non-monotonic across SDC concentrations. Native: 68.3, 1%: 0.2, 2%: 25.8, 4%: 4.4 ng/mg dry tissue. All treatment groups met the ≤50 ng dsDNA per mg dry tissue benchmark, yet 2% SDC retained over 100-fold more dsDNA than 1% or 4%. TRI-EVG muscle area mirrored the dsDNA pattern, with 1.9% and 2.6% of native muscle area retained at 1% and 4%, respectively, but 40.6% retained at 2%. Alcian Blue staining of the 2% group clustered with native rather than with other treatment groups. Collagen area was preserved at 2% and 4% SDC (within 10% of native), with a transient increase at 1%.

Conclusion/Significance: Three quantitative histochemical readouts and dsDNA quantification converged on dose-dependent variation in cellular clearance, with 2% SDC retaining substantially more residual cellular content than 1% or 4%. While dsDNA quantification or any single readout of residual cellular content alone would have identified 1% SDC as the most decellularized condition, integrated multi-readout assessment including custom vector definition surfaced concurrent ECM changes informing the selection of 4% SDC as the operating concentration. This approach establishes multi-readout characterization for human myometrium decellularization, where regenerative engineering approaches remain limited.